



QA: NA

November 2003

Technical Basis Document No. 5: In-Drift Chemical Environment

Revision 1

Prepared for:
U.S. Department of Energy
Office of Civilian Radioactive Waste Management
Office of Repository Development
1551 Hillshire Drive
Las Vegas, Nevada 89134-6321

Prepared by:
Bechtel SAIC Company, LLC
1180 Town Center Drive
Las Vegas, Nevada 89144

Under Contract Number
DE-AC28-01RW12101

CONTENTS

	Page
1. INTRODUCTION	1-1
1.1 OBJECTIVE AND SCOPE.....	1-3
1.2 SUMMARY OF THERMAL REGIMES AFFECTING THE IN-DRIFT CHEMICAL ENVIRONMENT.....	1-4
1.3 ORGANIZATION OF THE REPORT	1-5
1.4 NOTE REGARDING THE STATUS OF SUPPORTING TECHNICAL INFORMATION	1-6
2. EVOLUTION OF NEAR-FIELD TEMPERATURE, HUMIDITY, AND SEEPAGE CONDITIONS.....	2-1
2.1 CONCEPTUAL UNDERSTANDING OF IN-DRIFT TEMPERATURE, HUMIDITY, AND SEEPAGE.....	2-1
2.1.1 Conceptual Understanding of Ambient Seepage.....	2-1
2.1.2 Conceptual Understanding of the Evolution of In-Drift Temperature and Humidity	2-3
2.1.3 Conceptual Understanding of Thermal Seepage.....	2-5
2.2 TECHNICAL BASIS FOR CONCEPTUAL UNDERSTANDING OF IN- DRIFT TEMPERATURE, HUMIDITY, AND SEEPAGE.....	2-6
2.2.1 Technical Basis for Ambient Seepage.....	2-6
2.2.2 Technical Basis for Thermal-Hydrologic Processes from Field Thermal Tests	2-7
2.2.3 Technical Basis for Thermal Seepage.....	2-12
2.3 PROCESS MODEL DEVELOPMENT AND RESULTS.....	2-15
2.3.1 Model Results for Ambient Seepage.....	2-15
2.3.2 Model Results for In-Drift Temperature and Relative Humidity.....	2-18
2.3.3 Model Results for Thermal Seepage	2-25
2.4 SUMMARY OF BOUNDARY CONDITIONS IMPORTANT TO IN-DRIFT CHEMICAL MODELS.....	2-28
3. EVOLUTION OF NEAR-FIELD WATER AND GAS CHEMISTRY IN THE NEAR-FIELD HOST ROCK	3-1
3.1 CONCEPTUAL UNDERSTANDING OF THE EVOLUTION OF NEAR- FIELD WATER AND GAS CHEMISTRY.....	3-1
3.2 TECHNICAL BASIS FOR UNDERSTANDING AMBIENT AND THERMALLY ALTERED NEAR-FIELD CHEMISTRY	3-4
3.2.1 Initial Pore-Water Chemistry	3-5
3.2.2 The Drift Scale Test and Supporting Laboratory and Field Investigations	3-7
3.3 THERMAL-HYDROLOGIC-CHEMICAL PROCESS MODEL DEVELOPMENT AND RESULTS	3-15
3.3.1 Drift Scale Test Thermal-Hydrologic-Chemical Model	3-15
3.3.2 Thermal-Hydrologic-Chemical Seepage Model Results.....	3-24

CONTENTS (Continued)

	Page
3.4 SUMMARY OF BOUNDARY CONDITIONS IMPORTANT TO IN-DRIFT CHEMICAL MODELS.....	3-31
4. EVOLUTION OF IN-DRIFT WATER AND GAS CHEMISTRY	4-1
4.1 SEEPAGE EVAPORATION	4-5
4.1.1 Conceptual Understanding	4-5
4.1.2 Technical Basis	4-5
4.1.3 Abstraction of Thermal-Hydrologic-Chemical Seepage Model Results for Use in Engineered Barrier System Chemistry Models	4-10
4.1.4 Seepage Scenario Process Model Results	4-14
4.1.5 Effects of Introduced Materials on Seepage.....	4-22
4.1.6 Seepage Scenario Summary	4-24
4.2. DUST DELIQUESCENCE.....	4-24
4.2.1 Conceptual Understanding	4-24
4.2.2 Technical Basis	4-25
4.2.3 Deliquescence Analysis Results.....	4-25
4.2.4 Deliquescence Scenario Summary	4-34
4.3 IMPLEMENTATION IN TOTAL SYSTEM PERFORMANCE ASSESSMENT	4-34
4.4 PHYSICAL AND CHEMICAL ENVIRONMENT MODEL VALIDATION SUMMARY	4-35
4.4.1 Thermal-Hydrologic-Chemical Seepage Abstraction Compared with Thermal-Hydrologic-Chemical Model Output.....	4-35
4.4.2 Evaporation of Sierra Nevada Spring Water to Brine.....	4-36
4.4.3 Deliquescence Point Comparison.....	4-38
4.4.4 Chromium Speciation.....	4-39
4.5 RELATION OF PROCESS MODEL RESULTS TO CORROSION TESTING CHEMISTRIES.....	4-41
5. SUMMARY	5-1
6. REFERENCES	6-1
6.1 DOCUMENTS CITED	6-1
6.2 DATA, LISTED BY DATA TRACKING NUMBER.....	6-6
APPENDIX A — CREDIBLE RANGE OF BRINE WATER CHEMISTRY AND CONSISTENCY BETWEEN CORROSION TESTING ENVIRONMENTS AND MODELS (RESPONSE TO CLST 1.01, TSPA I 3.12, TSPA I 3.13, AND GEN 1.01 (COMMENTS 50, 113, 118, 122, AND 124))	A-1
APPENDIX B — UNCERTAINTY AND VARIABILITY IN THE NEAR-FIELD GEOCHEMICAL ENVIRONMENT (RESPONSE TO ENFE 1.05, TSPA I 3.09, AND GEN 1.01 (COMMENTS 81, 93, 98, 104, AND 110)).....	B-1

CONTENTS (Continued)

	Page
APPENDIX C — EVALUATION OF TRACE ELEMENTS AND FLUORIDE (RESPONSE TO ENFE 2.04).....	C-1
APPENDIX D — IN-DRIFT GEOCHEMICAL DATA AND MODEL UNCERTAINTIES (RESPONSE TO ENFE 2.05).....	D-1
APPENDIX E — THE RANGE OF LOCAL CHEMISTRY CONDITIONS AT THE DRIP SHIELD AND WASTE PACKAGE SURFACES (RESPONSE TO ENFE 2.06).....	E-1
APPENDIX F — MODELING OF SALT INTERACTIONS AT LOW RELATIVE HUMIDITY (RESPONSE TO ENFE 2.09 AND ENFE 2.15).....	F-1
APPENDIX G — RANGE OF WATER COMPOSITIONS THAT COULD CONTACT THE DRIP SHIELD OR WASTE PACKAGE SURFACES (RESPONSE TO ENFE 2.10).....	G-1
APPENDIX H — KINETICS OF CHEMICAL PROCESSES (RESPONSE TO ENFE 2.11).....	H-1
APPENDIX I — THE IMPACTS OF DUST DEPOSITION ON THE SALT ANALYSES (RESPONSE TO ENFE 2.13).....	I-1
APPENDIX J — ANALYSIS OF LABORATORY SOLUTION OF INTRODUCED MATERIALS (RESPONSE TO ENFE 2.14).....	J-1
APPENDIX K — ASSESSMENT OF DATA UNCERTAINTY AND DOCUMENTATION OF DATA USED TO CALIBRATE MODELS AND SUPPORT MODEL PREDICTIONS (RESPONSE TO ENFE 2.17 AND GEN 1.01 (COMMENTS 47 AND 109))	K-1
APPENDIX L — MULTISCALE THERMAL-HYDROLOGIC MODEL (RESPONSE TO TEF 2.04)	L-1

INTENTIONALLY LEFT BLANK

FIGURES

	Page
1-1. Components of the Postclosure Technical Basis for the License Application	1-1
2-1. Phenomena and Processes Affecting Drift Seepage	2-2
2-2. Thermal-Hydrologic Processes at the Drift Scale.....	2-4
2-3. Three-Dimensional Perspective of the As-Built Borehole Configuration of the Drift Scale Test	2-9
2-4. Total Power and Representative Drift-Wall Temperature (TC-19) during the Drift Scale Test Heating Phase	2-10
2-5. Temporal Evolution of Temperature at Selected Borehole Sensors, in Horizontal Temperature Boreholes that Traverse the Drift Scale Test.....	2-11
2-6. Change in Matrix Liquid Saturation from Preheating Conditions, at the End of the Heating Phase.....	2-13
2-7. Change in Measured Apparent Fracture Air-Permeability during the Heating Phase of the Drift Scale Test.....	2-14
2-8. Mean Seepage Percentage as a Function of Capillary-Strength Parameter and Mean Permeability for a Percolation Flux of 1, 10, 50, 200, 400, 600, 800, and 1,000 mm/yr	2-17
2-9. Complementary Cumulative Distribution Function for Peak Temperature on the Drift Wall and on the Waste Packages Plotted for the Mean, Upper, and Lower Infiltration-Flux Cases	2-21
2-10. Complementary Cumulative Distribution Functions for the Time when Boiling at the Drift Wall Ceases and for the Maximum Lateral Extent of the Boiling-Point Isotherm	2-22
2-11. Range of Waste Package Temperature and Relative Humidity Histories	2-24
2-12. Seepage Percentage for Tptpmn Submodel and Reference Thermal Mode and Tenfold Percolation Flux	2-26
2-13. Alternative Model for Comparison to the Thermal-Hydrologic Seepage Model	2-27
2-14. Thermal-Hydrologic-Mechanical Model Results	2-29
3-1. Fracture–Matrix Interface, Showing the Relation between Thermal-Hydrologic Processes and Geochemical Processes.....	3-3
3-2. Piper Plot of Water Compositions from Repository Units	3-6
3-3. Uranium Concentration and $^{234}\text{U}/^{238}\text{U}$ Activity Ratios in Drift Scale Test Samples Plotted versus Collection Date	3-10
3-4. Strontium Isotope Ratio Compositions of Water Samples Collected from Drift Scale Test Boreholes Compared to Compositions of Pore Water, Rock, Calcite, and Grout	3-12
3-5. Measured Activities of ^{14}C in CO_2 from Gas Collected in Several Hydrology Boreholes over Most of the Heating Phase of the Drift Scale Test	3-13
3-6. Two-Dimensional Numerical Mesh for the Drift Scale Test Thermal-Hydrologic-Chemical Model	3-16
3-7. Modeled CO_2 Concentrations in Fractures after Three Years of Heating	3-19
3-8. Modeled CO_2 Concentrations in Fractures and Matrix Compared to Measured Values from Boreholes (Corrected for Vapor Condensation)	3-20

FIGURES (Continued)

	Page
3-9. Measured and Modeled pH (in fractures) for Samples Collected from Borehole Interval 60-3, Located below the Heaters.....	3-21
3-10. Volume Percent Change in Amorphous Silica Abundance in Fractures.....	3-22
3-11. Volume Percent Change in Calcite Abundance in Fractures.....	3-23
3-12. Key Findings of the Thermal-Hydrologic-Chemical Seepage Model.....	3-25
3-13. Incoming Seepage Composition for W0 at the Drift Crown (Fracture Water, Top, Front, Node 4).....	3-26
3-14. Incoming Seepage Composition for W4 at the Drift Crown (Fracture Water, Top, Front, Node 4).....	3-27
3-15. Incoming Seepage Composition for W5 at the Drift Crown (Fracture Water, Top, Front, Node 4).....	3-27
3-16. Incoming Seepage Composition for W6 at the Drift Crown (Fracture Water, Top, Front, Node 4).....	3-28
3-17. Incoming Seepage Composition for W7 at the Drift Crown (Fracture Water, Top, Front, Node 4).....	3-28
3-18. $p\text{CO}_2$ Concentration in the Drift, the Near-Drift Environment, and in the Invert through Time.....	3-29
3-19. Thermal-Hydrologic-Chemical Simulation (Tptpl in Fractures at 2,400 Years—W0): Contour Plot of Modeled Liquid Saturation and Temperature (a) and Permeability Change (b).....	3-30
3-20. Temperature History for the Drift Crown, the Host Rock above the Crown from Where Water Compositions Were Obtained, and the Waste Package Surface, from the THC Seepage Model.....	3-31
4-1. Simplified Chemical Divide Diagram Based on Evaporative Concentration of Dilute Starting Waters to Form a Suite of Naturally Occurring Lake Waters.....	4-2
4-2. Deliquescence and Evaporation Processes.....	4-3
4-3. Engineered Barrier System Environment Water Chemistry Scenarios for Total System Performance Assessment for the License Application for Localized Corrosion on the Waste Package and Drip Shield.....	4-4
4-4. Experimental Relationship between Borehole Temperature and Volumetric Water Content for Borehole 79 during the Drift Scale Test over a 2-Year Period during Heating.....	4-5
4-5. Predicted versus Measured Br^- , Cl^- , and SO_4^{2-} Concentrations from Evaporation of Inagua Seawater.....	4-9
4-6. Flow Diagram Showing Some of the Precipitated Minerals and Chemical Divides That Are Associated with Each of the 11 Seepage Bins.....	4-12
4-7. Bin 7 Aqueous Composition Evaporation Predictions versus Relative Humidity at 70°C and a $p\text{CO}_2$ of 10^{-3} bar.....	4-15
4-8. Bin 7 Mineral Precipitation Evaporation Predictions versus Relative Humidity at 70°C and a $p\text{CO}_2$ of 10^{-3} bar.....	4-16
4-9. Range of pH versus Relative Humidity for the Seepage Evaporation Lookup Tables Representing Bins 3 through 11 (at Three Temperatures and Three $p\text{CO}_2$ Values).....	4-17

FIGURES (Continued)

	Page
4-10. Range of Cl ⁻ Molality versus Relative Humidity for the Seepage Evaporation Lookup Tables Representing Bins 3 through 11 (at Three Temperatures and Three pCO ₂ Values).....	4-18
4-11. Range of F ⁻ Molality versus Relative Humidity for the Seepage Evaporation Lookup Tables Representing Bins 3 through 11 (at Three Temperatures and Three pCO ₂ Values).....	4-19
4-12. Range of Ionic Strength versus Relative Humidity for the Seepage Evaporation Lookup Tables Representing Bins 3 through 11 (at Three Temperatures and Three pCO ₂ Values).....	4-20
4-13. Range of Cl ⁻ /NO ₃ ⁻ Molal Ratios for the Seepage Evaporation Lookup Tables Representing Bins 3 through 11 (at Three Temperatures and Three pCO ₂ Values).....	4-21
4-14. Bin History Maps Showing Bin Occurrence for Crown Seepage and Invert Wicking Locations.....	4-22
4-15. Bin 5 Aqueous Composition Evaporation Predictions versus Relative Humidity at 70°C and 10 ⁻³ CO ₂ Fugacity.....	4-27
4-16. Bin 5 Mineral Precipitation Evaporation Predictions versus Relative Humidity at 70°C and 10 ⁻³ CO ₂ Fugacity.....	4-28
4-17. Range of Cl ⁻ /NO ₃ ⁻ Molal Ratios versus Relative Humidity for the Dust Leachate Lookup Tables Representing Bins 1 through 6.....	4-29
4-18. Preliminary Range of Cl ⁻ /NO ₃ ⁻ Molal Ratios versus Relative Humidity at 140°C for the Dust Leachate Lookup Tables Representing Bins 1 through 6.....	4-30
4-19. Comparison of THC Seepage pH with Abstraction Results for W5 (Base of Invert Front, Node 4 Matrix Water).....	4-36
4-20. Results of Evaporation of Typical Sierra Nevada Spring Water at 25°C in Equilibrium with Atmospheric pCO ₂ at 10 ^{-3.5} atm.....	4-37
4-21. Calculated Results of Evaporation of Typical Sierra Nevada Spring Water at 25°C in Equilibrium with Atmospheric pCO ₂ at 10 ^{-3.5} atm.....	4-38
4-22. EQ3/6 Calculated Chromium Concentrations in Equilibrium with Cr(OH) ₃ (am) Compared to Nonlinear Least-Squares Regression by Rai et al.	4-40

INTENTIONALLY LEFT BLANK

TABLES

	Page
1-1. List of Appendices and the KTI Agreements They Address	1-6
2-1. Peak Drift-Wall and Waste-Package Temperatures over All Waste Packages Simulated, for the Lower, Mean, and Upper Infiltration-Flux Cases	2-20
2-2. Duration of Above-Boiling Temperature in the Host Rock at the Drift Wall, for the Lower, Mean, and Upper Infiltration-Flux Cases	2-21
2-3. Maximum Lateral Extent of the Boiling-Point Isotherm (96°C for the Repository Elevation) for the Lower, Mean, and Upper Infiltration-Flux Cases.....	2-23
3-1. Input Pore-Water Compositions	3-8
4-1. Model Uncertainty in Selected Output Parameters.....	4-6
4-2. Maximum Differences between Predictions and Measurements for pH, Ionic Strength, Cl^- , NO_3^- , and the $\text{Cl}^-/\text{NO}_3^-$ Ratio	4-7
4-3. Model Predictions of Equilibrium Relative Humidity for Saturated Aqueous Solutions in Contact with an Excess of Solid-Phase Salts.....	4-8
4-4. Frequency and Compositions of the 11 Binned Input Waters	4-13
4-5. Starting Water Composition Scenario Probability (W0 to W7) and Time Integrated Bin Probability (Norm %) of Occurrence for Any Given Crown Seepage Bin for the 20,000-Year Simulation Period.....	4-14
4-6. Corrosion Rates for Stainless Steel Type 316L	4-23
4-7. Absolute (Percent Relative) Differential Effect of Stainless Steel Type 316L Dissolution in Bin 11 Seepage Water at 100 and 98 Percent Relative Humidity.....	4-24
4-8. Total EQ3NR Equilibrated Aqueous Elemental Compositions for the Six Median Waters Selected to Represent the Dust Leachate Bins	4-26
4-9. Percentage of Dust Leachate Waters in Each Bin	4-27
4-10. Deliquescence Points and Anion Chemistry of Evolved Dust-Associated Waters for the Six Bin Chemistries Shown on Table 4-8	4-31
4-11. Comparisons of Relative Humidity Values for Equilibrium Deliquescence Points of Selected Salts between EQ3/6 (Version 8.0–data0.ypf Pitzer Database) and Experimental Data	4-39
4-12. General Classification of the Brine Types that Could Be in Contact with Drip Shields and Waste Packages and the Probabilities of Contact	4-42
4-13. Drift Crown Seepage Water Limiting Compositions and Probabilities of Their Formation, the Associated Brine Type, and the Corresponding Corrosion Test Solutions	4-45
4-14. Brines from Dust Deposited on the Waste Packages Including Bromide, the Probabilities of Their Formation, the Associated Brine Type, and the Corresponding Corrosion Test Solutions.....	4-46
4-15. Target Composition of Standard Test Media Based on Evaporative Concentration of a Dilute Carbonate Type Water.....	4-47

INTENTIONALLY LEFT BLANK

ACRONYMS AND ABBREVIATIONS

BSW	basic saturated water
BWR	boiling water reactor
DOE	U.S. Department of Energy
DST	Drift Scale Test
ECRB	Enhanced Characterization of the Repository Block
EPA	U.S. Environmental Protection Agency
ESF	Exploratory Studies Facility
KTI	Key Technical Issue
LA	license application
MSTHM	multiscale thermal-hydrologic model
NRC	U.S. Nuclear Regulatory Commission
PWR	pressurized water reactor
SAW	simulated acidic water
SCW	simulated concentrated water
SDW	simulated dilute water
SSW	simulated saturated water
THC	thermal-hydrologic-chemical
TSPA	total system performance assessment
TSPA-LA	total system performance assessment for the license application

INTENTIONALLY LEFT BLANK

1. INTRODUCTION

This report provides an integrated discussion of the in-drift chemical environment and responds to issues raised by the U.S. Nuclear Regulatory Commission (NRC) related to the chemical environment on the surfaces of the waste package and drip shield. In general, the issues raised by the NRC concern the need for adequate description of features and processes affecting this environment, including treatment of uncertainty and the need for corrosion testing at conditions consistent with the environmental conditions predicted for the repository.

This technical basis document provides a summary of the conceptual understanding of the chemical environments likely to exist in the Yucca Mountain repository after the permanent closure of the facility. This document is one in a series of technical basis documents prepared for each component of the Yucca Mountain repository system relevant to predicting the likely postclosure performance. The other components are illustrated in Figure 1-1.

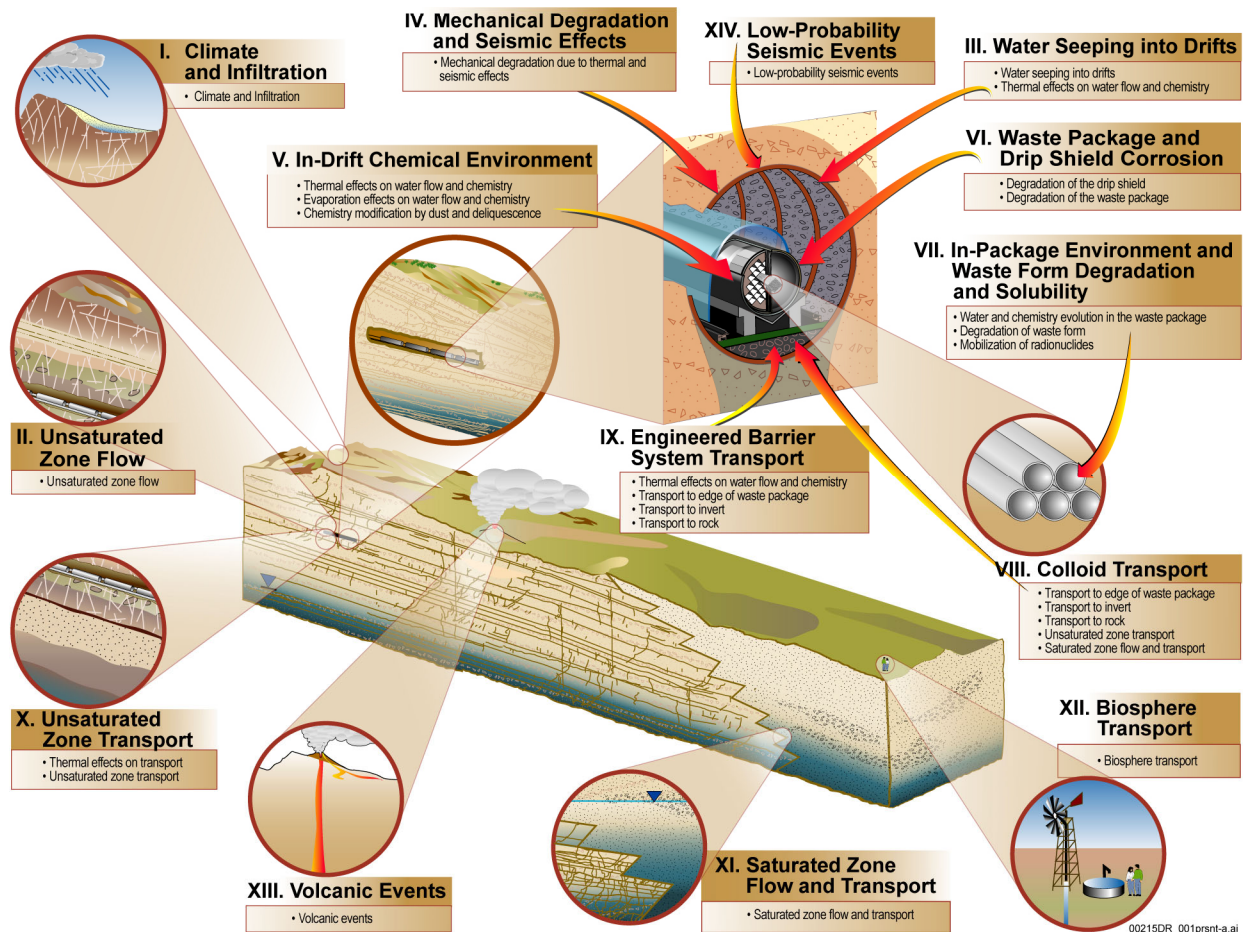


Figure 1-1. Components of the Postclosure Technical Basis for the License Application

The information presented in this document and the associated references form an outline of the ongoing development of the postclosure performance assessment to be included in the license application (LA). This information is also used to respond to open Key Technical Issue (KTI) agreements made between the NRC and the U.S. Department of Energy (DOE). The DOE

responses to individual KTI agreements are provided as appendices to this overview of the processes that affect the evolution of the in-drift chemical environment. This context allows for more direct discussions of the relevance of the agreements, as they relate to postclosure performance.

Appendices to this document are designed to allow for a transparent and direct response to each KTI agreement. Each appendix addresses one or more of the agreements. If agreements apply to similar aspects of the in-drift chemical environment, they are grouped in a single appendix. In some cases, appendices provide detailed discussions of data, analyses, or information related to the further conceptual understanding presented in this technical basis document. In other cases, the appendices provide information that is related to the technical basis document information but at a level of detail that relates more to the uncertainty in a particular data set or feature, event, or process that is less relevant to the overall technical basis. In these cases, the appendices reference the relevant section of the technical basis document to put the particular KTI agreement into context, but the technical basis document does not reference the appendices.

This technical basis document and appendices are responsive to agreements made between the DOE and the NRC during Technical Exchange and Management Meetings on Evolution of the Near-Field Environment (Reamer 2001), Thermal Effects on Flow (Reamer and Williams 2001), Total System Performance Assessment and Integration (Reamer and Gil 2001), and Container Life and Source Term (Reamer and Williams 2000). Most of the agreements were based on questions that NRC staff developed after reviewing site recommendation support documents and DOE presentations at the technical exchanges. The agreements, in general, required the DOE to present additional information, conduct further testing, perform sensitivity or validation exercises for models, or provide justification for assumptions used in the *Yucca Mountain Site Suitability Evaluation* (DOE 2002a). Since those technical exchanges, additional analyses and testing necessary to meet the agreements have been conducted. The appendices present the additional information that forms the technical basis for addressing the intent of the KTI agreements.

This document presents a summary and synthesis of the detailed current technical information presented in the analyses and model reports and other technical products that are used as the basis for the description of the in-drift chemical environment and the incorporation of these environments into the postclosure performance assessment. Several analyses, model reports, and other technical products (some of which are drafts in progress, as discussed in Section 1.4) support this summary:

- *Thermal Testing Measurements Report* (BSC 2002a)
- *Multiscale Thermohydrologic Model Report* (BSC 2003a)
- *Drift-Scale Coupled Processes (DST and TH Seepage) Models* (BSC 2003b)
- *Drift-Scale Coupled Processes (DST and THC Seepage) Models* (BSC 2003c)
- *In-Drift Precipitates/Salts Model* (BSC 2003d)
- *Engineered Barrier System: Physical and Chemical Environment Model* (BSC 2003e)

- *Thermal Tests Thermal-Hydrological Analyses/Model Report* (BSC 2001a)
- *Ventilation Model and Analysis Report* (BSC 2003f)
- *Environment on the Surfaces of Drip Shield and Waste Package Outer Barrier* (BSC 2003g)
- *Drift Scale THM Model* (BSC 2003h)
- *UZ Flow Models and Submodels* (BSC 2003i)
- *Seepage Model for PA Including Drift Collapse* (BSC 2003j)
- *In-Drift Natural Convection and Condensation Model Report* (BSC 2003k)
- *In Situ Field Testing of Processes* (BSC 2001b).

1.1 OBJECTIVE AND SCOPE

The objective of this report is to present an integrated conceptual and predictive basis for modeling the in-drift chemical environment, along with a broad base of supporting information. The report links corrosion performance of the drip shield and waste package materials, with the chemical evolution of the in-drift environment, constrained by thermal-hydrologic and thermal-hydrologic-chemical processes in the host rock. This approach is summarized in the following main points:

1. Boundary conditions of the in-drift chemical environment are established by thermal-hydrologic and thermal-hydrologic-chemical processes in the host rock. The thermal-hydrologic and thermal-hydrologic-chemical processes are represented by simulation models discussed in Sections 2 and 3, respectively. The models are supported by in situ field testing, and include treatment of spatial variability and important sources of predictive uncertainty.
2. Evolution of the chemical environment on the surfaces of the drip shield and waste package is represented for the total system performance assessment (TSPA) by using the drift-wall boundary conditions, with models for deliquescence of dust deposits on the waste package and evaporative concentration of potential seepage water contacting the drip shield or waste package (Section 4). These models are supported by laboratory and field testing and by technical information from published chemical literature.
3. Chemical test conditions used by the corrosion-testing program are compared with the range of predicted chemical conditions on the surfaces of the drip shield and waste package (Section 4.5).
4. This report does not consider potential effects of seismic events, which may affect unsaturated zone thermal-hydrology and which may, in turn impact the in-drift chemical environment. Seismic effects, including any potential impact on the in-drift

chemical environment, will be addressed in the technical basis document on low-probability seismic events.

5. This report includes appendices that specifically address 16 KTI agreements that relate to the evolution of the in-drift chemical environment.

The conceptual and predictive basis presented here is integrated with the framework for the LA. The processes described in this report will affect waste isolation performance by controlling the chemical environment for the drip shield and waste package, and will be operative throughout the repository in a sequence that extends throughout the postclosure regulatory period.

The processes and models included in this technical basis document are those used to represent and evaluate the environmental conditions within the drifts. The environment then determines other aspects of repository performance, including corrosion of drip shields and waste packages (to be described in a technical basis document on waste package and drip shield corrosion) and the transport of any released radionuclides away from the drifts (to be described in the technical basis document on unsaturated zone transport). The likelihood of seepage into emplacement drifts (especially during the period of above-boiling host-rock temperature, to be described in the technical basis document on water seeping into drifts), a potential source of water whose evolution is a primary concern of this report, is discussed to the extent necessary here. This report describes the chemical characteristics of that seepage, and its evolution in the drift environment.

1.2 SUMMARY OF THERMAL REGIMES AFFECTING THE IN-DRIFT CHEMICAL ENVIRONMENT

For expository purposes and for the TSPA abstractions, the thermal evolution of the emplacement drifts is sequenced into three regimes based on the drift wall and waste package surface temperatures:

- **Dryout: Drift Wall Temperature Greater Than the Boiling Point of Water**—At the time of permanent closure, the drift-wall rock will be significantly dried out by at least 50 years of forced ventilation, and the emplacement drifts will be dry. After closure, temperatures in the emplacement drifts will increase for a few tens or hundreds of years, depending on local thermal loading. Throughout most of the repository, drift-wall temperatures will be greater than boiling (nominally 100°C), but relative humidity will be low, and seepage of liquid water into drift openings will not occur because of the vaporization barrier effect, combined with the capillary barrier, so the drifts will remain dry (as described in the technical basis document on water seeping into drifts), and no aqueous phase corrosion on the waste package or drip shield surfaces due to seepage is expected. Waste package surface temperatures will be as much as 20°C higher than the nearby drift-wall temperatures (BSC 2003a); however, depending on the surface temperature and relative humidity conditions, the existence of liquid-phase water on the waste package or drip shield is possible due to the presence of a dust or salt deposit. In the presence of such a deposit, a thin-film liquid phase can be established at a higher temperature and lower relative humidity than otherwise possible. Thus, formation of deliquescence brines in the absence of seepage may occur, and corrosion of the waste

package and the drip shield is considered in the context of these solutions (as discussed in the technical basis document on waste package and drip shield corrosion).

- **Transition: Drift Wall Temperature at or below the Boiling Point of Water**—Seepage into the drifts will become possible as the waste package cools, as the temperature of the drift wall drops below the boiling point of water, and while the waste package surface temperature is at or above the boiling point of the seepage water. During this period, the capillary diversion barrier will inhibit seepage (similar to ambient conditions; see the technical basis document on water seeping into drifts), and the drip shields will prevent seepage from contacting the waste packages. The waste package and drip shield surface temperatures will be higher than the drift-wall temperature, so seepage water will tend to evaporate if it contacts drip shields or waste packages, evolving into either carbonate- or sulfate-type brines. As in the dryout regime, formation of deliquescent brines could also occur in this regime. All of these conditions are incorporated probabilistically in the in-drift chemical environment abstraction for TSPA.
- **Low Temperature: Waste Package Temperature Less Than the Boiling Point of the Water**—As the waste package cools to a temperature below the boiling point of water, the in-drift relative humidity will increase, so evaporated solutions cannot be as concentrated. With further cooling, the temperature will drop to below the threshold for localized corrosion for the repository-relevant environments. This threshold temperature is a function of the presence of beneficial ions, such as nitrates and sulfates.

1.3 ORGANIZATION OF THE REPORT

This report begins with a discussion of the thermal-hydrologic models and supporting data that permit prediction of temperature and humidity in the host rock and in the emplacement drifts (Section 2). Seepage during the period of above-boiling host-rock temperatures (thermal seepage) and after cooling (ambient seepage) will also be discussed. This is followed by a discussion of the thermal-hydrologic-chemical models and data that permit prediction of the chemical evolution of liquid water in the near-field host rock, which could potentially seep into the emplacement drifts (Section 3). The thermal-hydrologic-chemical framework is consistent with the thermal-hydrologic and seepage process descriptions in Section 2. Section 4 then describes the thermal-chemical evolution of seepage water and dust within the drifts, emphasizing changes in the chemical environment that could affect corrosion performance of engineered barrier materials. The manner in which the process models for in-drift chemistry are implemented in the TSPA (i.e., as abstractions) to provide inputs for the probabilistic models representing corrosion is briefly discussed in Section 4.3. A discussion of the relation of the process model results to corrosion testing chemistries is provided in Section 4.5. KTI agreements associated with this report are included in the appendices, as described in Table 1-1.

Table 1-1. List of Appendices and the KTI Agreements They Address

Appendix	Appendix Title	Key Technical Issues Addressed
A	Credible Range of Brine Water Chemistry and Consistency between Corrosion Testing Environments and Models	CLST 1.01, TSPAI 3.12, TSPAI 3.13, and GEN 1.01 (Comments 50, 113, 118, 122, and 124)
B	Uncertainty and Variability in the Near-Field Geochemical Environment	ENFE 1.05, TSPAI 3.09 and GEN 1.01 (Comments 81, 93, 98, 104, and 110)
C	Evaluation of Trace Elements and Fluoride	ENFE 2.04
D	In-Drift Geochemical Data and Model Uncertainties	ENFE 2.05
E	The Range of Local Chemistry Conditions at the Drip Shield and Waste Package Surfaces	ENFE 2.06
F	Modeling of Salt Interactions at Low Relative Humidity	ENFE 2.09 and ENFE 2.15
G	Range of Water Compositions that Could Contact the Drip Shield or Waste Package Surfaces	ENFE 2.10
H	Kinetics of Chemical Processes	ENFE 2.11
I	The Impacts of Dust Deposition on Salt Analysis	ENFE 2.13
J	Analysis of Laboratory Solutions of Introduced Materials	ENFE 2.14
K	Assessment of Data Uncertainty and Documentation of Data Used to Calibrate Models and Support Model Predictions	ENFE 2.17 and GEN 1.01 (Comments 47, and 109)
L	Multiscale Thermal-Hydrologic Model	TEF 2.04

1.4 NOTE REGARDING THE STATUS OF SUPPORTING TECHNICAL INFORMATION

This document was prepared using the most current information available at the time of its development. This technical basis document and its appendices providing KTI agreement responses that were prepared using preliminary or draft information, reflect the status of the Yucca Mountain Project's scientific and design bases at the time of submittal. In some cases, the development involved the use of draft analysis and model reports and other draft references whose contents may change with time. Information that evolves through subsequent revisions of the analysis and model reports and other references will be reflected in the LA as the approved analyses of record at the time of LA submittal. Consequently, the project will not routinely update either this technical basis document or its KTI agreement appendices to reflect changes in the supporting references prior to submittal of the LA.

2. EVOLUTION OF NEAR-FIELD TEMPERATURE, HUMIDITY, AND SEEPAGE CONDITIONS

The in-drift chemical environment depends on physical conditions (principally temperature, relative humidity, and potential seepage of liquid water into the drifts) determined by the near-field host rock. This section begins with a discussion of present-day ambient conditions and processes, including seepage, and then describes the predicted evolution of these thermal-hydrologic conditions and processes after permanent closure. Prior to excavation, ambient conditions in the host rock will involve stable temperature, high humidity (approaching 100 percent relative humidity), and natural percolation of liquid water flux from the ground surface through the host rock to the water table. These ambient conditions represent the state of the host rock during site characterization (before excavation or thermal testing) and after thousands of years when the emplaced waste has cooled to the point when heat is no longer added in the drift.

Extensive observation, testing, and modeling of ambient conditions and processes at Yucca Mountain have been performed and documented. The resulting unsaturated zone flow model describes present-day movement of water, including the effects of spatially variable surface infiltration processes, layered geometry of rock units at Yucca Mountain, and geologic faults. The unsaturated zone flow model has been extended to predict the percolation flux in the host rock for future flow conditions after permanent closure (BSC 2003i, Section 6.6.3). Confidence in the unsaturated zone flow model is supported by quantitative and qualitative comparisons to many observations and data from the site, such as measurements in boreholes and on core samples, the distribution of Cl^- in unsaturated zone waters, and the occurrence of natural and anthropogenic isotopes (BSC 2003i, Sections 6.2 through 6.5 and Section 7).

The in-drift chemical environment will depend on the temperature, humidity, and potential seepage determined by the response of the host rock. The remaining parts of this section describe the conceptual understanding of host-rock processes (Section 2.1), the available and relevant laboratory and field test data (Section 2.2), and the models that have been developed to represent future conditions and processes during the postclosure regulatory period, supported by those data (Section 2.3).

2.1 CONCEPTUAL UNDERSTANDING OF IN-DRIFT TEMPERATURE, HUMIDITY, AND SEEPAGE

2.1.1 Conceptual Understanding of Ambient Seepage

Unsaturated flow of liquid water in geologic media is controlled by capillary forces, similar to the forces that retain water in sponges or within cracks or pores that form in solid materials. The welded tuff host rock at Yucca Mountain includes two types of porosity: namely, the micropores of the rock matrix and the macropores represented by fractures and cavities. Water is held tightly in the relatively impermeable microporosity and less tightly in the more transmissive fractures. When water drainage occurs in the rock, the mobile water moves almost entirely through the fractures.

Water enters the unsaturated zone from above as net infiltration, then drains or percolates downward through the host rock under the impetus of gravity, principally through the fractures and to a lesser extent through the relatively impermeable rock matrix. This water is under capillary tension; it can flow through fine pores and fractures but resists flowing into larger openings. When the percolation encounters an opening such as an emplacement drift, it resists seeping into the opening; this effect is called the capillary barrier effect (BSC 2003I, Section 6.3.1).

Underground openings in unsaturated rock have a tendency to divert water around them because of the capillary barrier effect, as illustrated in Figure 2-1. The barrier effect leads to a local saturation buildup in the host rock immediately above and adjacent to the drift opening. If capillary and permeability properties of the fracture network in this region are sufficient, some or all of the incident percolation is diverted around the drift. Locally, however, the saturation may increase and capillarity may decrease such that water can enter the drift as seepage (BSC 2003I, Section 6.3.1). The conditions for occurrence of seepage have been investigated by extensive underground field testing at Yucca Mountain.

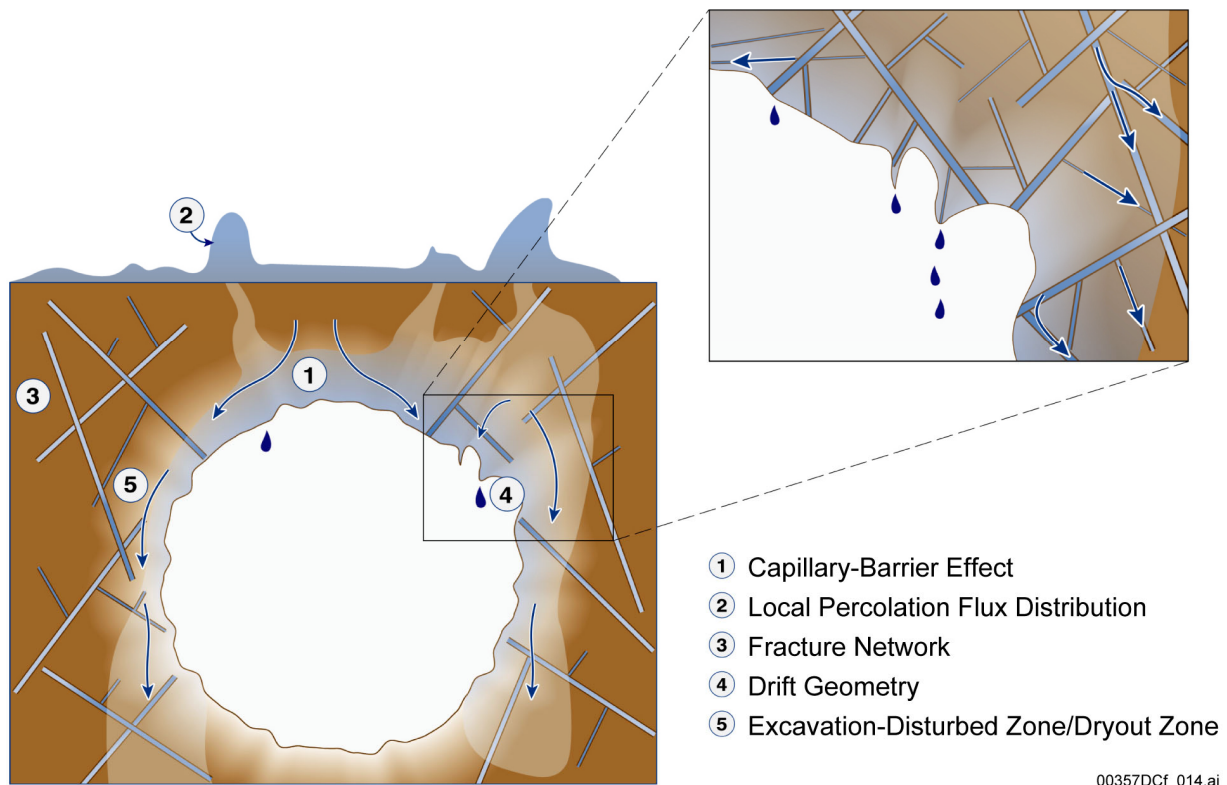


Figure 2-1. Phenomena and Processes Affecting Drift Seepage

Seepage is defined as the movement of liquid water into an underground opening and does not include movement of water vapor or condensation within openings. Seepage flux is the rate of seepage per unit flow area. Seepage percentage is defined as the ratio of the seepage flux to the percolation flux in the host rock. The seepage threshold is a critical percolation flux below which seepage in the opening is unlikely to occur. As described in the following sections, field tests have demonstrated the existence of a seepage threshold in the host rock. Where seepage

occurs, the water: evaporates, follows the inclined rough wall of the opening as flow in a thin film, or forms a drop that grows and eventually detaches (Or and Ghezzehei 2000). The former two possible mechanisms do not transport chemical species to the surfaces of the drip shield or waste package and are not considered further here. The latter mechanism is considered drift seepage.

For an emplacement drift of a given shape, the seepage threshold and the amount of seepage once this threshold is exceeded depend on the local flow conditions in the near field (Figure 2-1). These conditions are mainly influenced by the local percolation flux reaching the opening and by the local hydrologic properties of the host rock (principally the capillary strength and relative permeability of the fracture network) (BSC 2003l, Section 6.3.1). Small-scale heterogeneity of hydrologic properties (i.e., fracture characteristics) increases the likelihood of seepage (Birkholzer et al. 1999). Effects from small-scale heterogeneity are included in the field data sets that have been used to calibrate the ambient seepage model (BSC 2003l, Section 6.4.1.1). In addition, intermediate-scale and mountain-scale variability in hydrologic properties and flow paths within Yucca Mountain produces spatial variability in the percolation flux, which is accommodated through the estimation of flow focusing (BSC 2003l, Section 6.3.1). The drift-opening cross-sectional shape and size also affect seepage as described by Philip et al. (1989). Uncertainty and variability in local hydrologic properties and percolation flux, as well as long-term changes in drift size and shape, are addressed in the seepage models for the TSPA (Section 2.3.1).

2.1.2 Conceptual Understanding of the Evolution of In-Drift Temperature and Humidity

The heat output from the spent nuclear fuel and high-level radioactive waste will decline continuously due to radioactive decay. Waste package heat output will be at a maximum during the preclosure period (nominally 50 years), but the emplacement drifts will be ventilated to remove most of the heat (BSC 2003f, Section 6.6). Waste package temperatures will be elevated, and some packages may approach 100°C immediately after emplacement (subject to control by ventilation). However, the warming of ventilation air will ensure that preclosure conditions are dry (e.g., less than 20 percent relative humidity), especially where in-drift temperatures are greatest (BSC 2003f, Section 6.9).

At permanent closure, ventilation will cease and the drift-wall rock temperature will be well below boiling but will increase sharply within a few decades (BSC 2003a, Section 6.3.1). The maximum postclosure temperature of a waste package at any location will be determined by the history of heat output, the resistance to dissipation of heat in the host rock, heat transfer from the waste package to the drift wall, and the relationship to other nearby heat sources. Stated differently, at a great distance the host rock will remain at near-ambient temperature, and natural transfer of heat to such a distance will produce a temperature gradient. The cumulative effect of that gradient will determine the temperature at the drift wall, and the efficiency of heat transfer from the waste package to the drift wall (by conduction, buoyant convection, and thermal radiation, all of which are addressed in process models) will determine the waste package temperature. Hence, the host-rock response will control the waste package temperature.

Heating of the host rock will produce the greatest movement of moisture and liquid water after permanent closure (DOE 2002b, Section 4.2.2). Much of the heat will be transported away from

the drifts by thermal conduction through the rock. A portion of the heat will be transported as latent heat by water that vaporizes near the drift and condenses in cooler rock farther away. These processes are depicted in Figure 2-2, which represents the conceptual understanding of thermal-hydrologic processes occurring around a drift as derived from the Single Heater Test and the Drift Scale Test (DST).

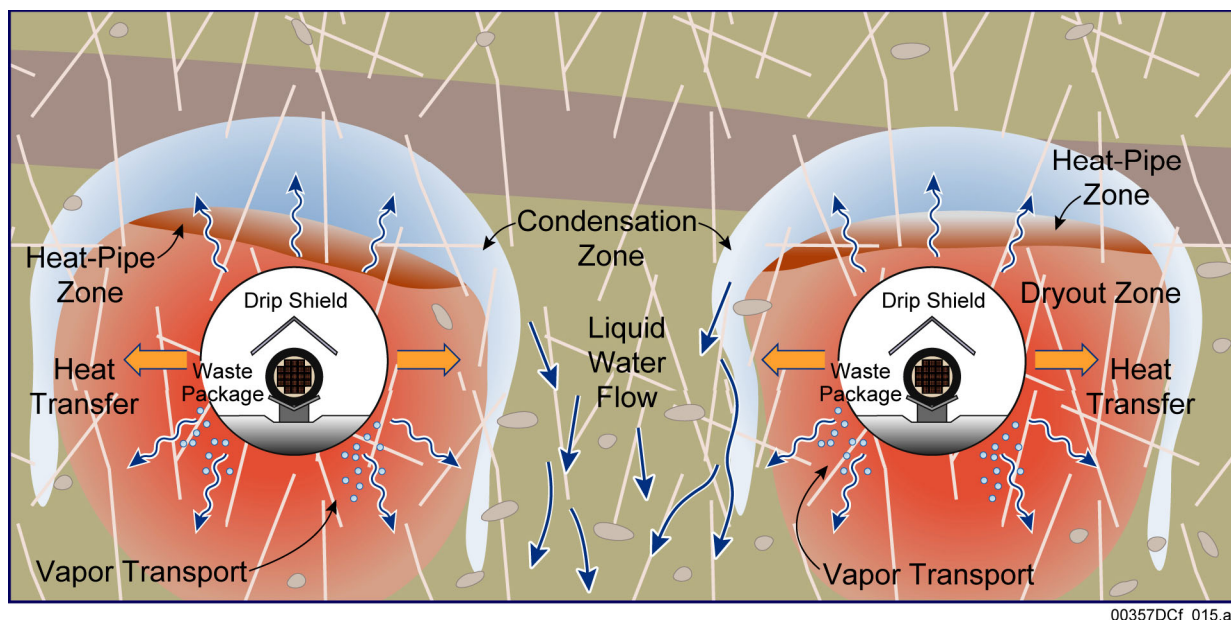


Figure 2-2. Thermal-Hydrologic Processes at the Drift Scale

Given the projected heat output of the waste and the host-rock characteristics, the near-field host rock will be heated to above-boiling temperatures (i.e., greater than 96°C at the repository elevation) for several centuries (BSC 2003a, Section 6.3.1). Where temperatures exceed boiling, substantially all of the water will be evaporated from the rock (dryout zone in Figure 2-2). For the current repository design concept, the dryout zone will extend to a distance of approximately 5 to 10 m from the drift wall (BSC 2003b, Sections 6.2.2 and 6.2.3). The duration and extent of dryout will depend on the history of local heat generation, the percolation flux in the host rock, and host-rock properties, such as thermal conductivity. Thermal evolution of a particular waste package will also depend on its location in the repository layout (i.e., whether it is near the center or the edge). As the waste heat output decreases with time, the dryout zone will eventually shrink back to the drift wall, cooling to below-boiling temperatures. Waste package temperatures will follow the evolution of the local drift-wall temperature but will be as much as 10°C to 20°C warmer because of thermal resistance across the drip shield and the in-drift air spaces. This temperature difference will approach zero at later times as the heat output declines.

Figure 2-2 shows how water vapor that is evaporated from the above-boiling dryout zone condenses farther away. This controls the relative humidity on the waste package surfaces, for the following reason: relative humidity will be very close to 100 percent where the condensation occurs (always true for condensation). Water vapor is readily dispersed in the gas phase of the host rock, so the water vapor fraction in the gas phase varies little over the few meters from the drift wall to the location of condensation. Accordingly, if the in-drift temperatures (e.g., on the

waste package and the drift wall) are greater than boiling, then those surfaces will be above their dew point temperatures. Thus, the condensation of water vapor in the host rock and the difference in temperature compared to the waste package determine the evolution of dew point temperatures on the waste package and drip shield surfaces. The extent of the condensate zone depicted in Figure 2-2 is schematic only, and the amount of mobile condensate water above the drift at any time is limited to that present in fractures.

Thermally driven movement of water will be most important when the host rock forms a dryout zone at above-boiling temperature. In the rock at the outer margin of the dryout zone, water vapor will coexist with liquid condensate (Pruess et al. 1990, p. 1,235) (Figure 2-2). Reflux will occur if the condensate flows back toward the dryout zone under gravity, but the condensate water may also drain away from the dryout zone and be removed from further consideration as potential seepage. Reflux activity has been observed during thermal testing at Yucca Mountain, and occurs only when and where the rock temperature is at boiling (BSC 2003b, Section 7). These phenomena are discussed further in the next section.

Another potential mechanism for moisture transport involves migration of some vapor back into the emplacement drifts, where it could be transported along the open drifts. Along a particular emplacement drift, it is likely that vapor will be produced mainly in the region of the drift where the rock temperature is above boiling and that condensation will occur in cooler portions of the drift (e.g., at the ends where there are no waste packages). From mass and energy balance considerations, it can be shown that during the dryout period and for locations where there is a dryout zone and the drift wall temperature is above boiling the latent heat associated with the water available for evaporation is small compared with the amount of heat available to evaporate it. This means that the thermal evolution of any particular waste package may tend to be dominated by the transport of its own internally generated heat to the drift wall. Condensation effects associated with large-scale variations in temperature and humidity within the emplacement drifts are currently under investigation.

2.1.3 Conceptual Understanding of Thermal Seepage

Thermal seepage for temperatures at or above boiling will be prevented by vigorous boiling in the hot, dry rock of the dryout zone (BSC 2003b, Section 6.2.1.1.2). The zone (Figure 2-2) will form a vaporization barrier that prevents thermal seepage by completely evaporating any liquid water that enters the zone from above, before it reaches the drift wall. Thermal seepage is unlikely because of this evaporation barrier, as long as above-boiling temperatures persist. In addition, the intensity of reflux activity is directly related to heat output, which will be strongest early in the thermal evolution when the dryout zone has its greatest extent. By the time the host rock cools and the dryout zone shrinks, the magnitude of the reflux activity will be attenuated because the heat output of the repository will have decayed.

Relatively large liquid fluxes (compared with the natural percolation flux) may impinge on the dryout zone because of reflux, possibly associated with episodic reflux events. Such episodic events have been observed (BSC 2001a, Section 6.2.4.1) for test conditions similar to the repository host rock, and the capability to simulate such events is discussed in Section 2.3.2. Liquid flow in the dryout zone will be prevented by the vaporization barrier; moreover, the capillary barrier (Section 2.1.1) will also be effective, even at elevated temperatures. It is

reasonable to use the same conceptual basis for the capillary barrier at elevated temperature that was developed for ambient seepage (BSC 2003b, Section 6.2.1.1.2). The thermal-hydrologic seepage model discussed in Section 2.3.3 further describes the vaporization barrier.

2.2 TECHNICAL BASIS FOR CONCEPTUAL UNDERSTANDING OF IN-DRIFT TEMPERATURE, HUMIDITY, AND SEEPAGE

This section reviews the available technical information and data that pertain to the thermal-hydrologic processes that control in-drift temperature and humidity and the potential for water seepage into drifts at ambient conditions and during the thermal period.

2.2.1 Technical Basis for Ambient Seepage

Data for understanding ambient seepage comes from niche studies and the systematic borehole testing program conducted in the Exploratory Studies Facility (ESF) at Yucca Mountain since 1997. Measured data include air permeabilities and seepage rates from active injection tests conducted at several locations in the ESF and the Enhanced Characterization of the Repository Block (ECRB) Cross-Drift. These tests investigated seepage behavior in the middle nonlithophysal and lower lithophysal host-rock units. Test methods were refined to investigate seepage threshold effects, film flow of water on the drift wall, evaporation, and other effects. Multiple test locations in the nonlithophysal and lithophysal units were used to sample variability. The test results have been analyzed to develop seepage-relevant, model-related effective parameters on the drift scale (Section 2.3.1). Further description and analysis of active seepage and air-permeability tests performed in the niches and ECRB Cross-Drift are provided in the technical basis document addressing water seeping into drifts, which also describes analysis of geochemical indications of past seepage conditions and describes the passive moisture monitoring program and its results.

Niche Studies—Short drifts (ranging from 6.3 m to 15.0 m in length) were constructed for seepage niche studies. Air-injection tests were conducted in several 1-ft (0.3-m) packed-off borehole intervals above the niches, before and after excavation, to measure permeability and evaluate changes from excavation. After niche construction, liquid-release tests were conducted by injecting water at specified rates into intervals of the same boreholes to investigate the potential for water seepage into the openings (BSC 2003m, Section 6.5.1). Seepage water was collected in trays and quantified.

Systematic Hydrologic Characterization—A second study, referred to as the systematic borehole testing program, was initiated in 2000 to complement the niche tests. Air-injection and liquid-release tests were conducted in slant boreholes above the ECRB Cross-Drift. Like the niche studies, seepage water was collected and quantified.

Results from the testing confirmed the existence of a seepage threshold, which is the largest value of the percolation flux in the host rock, for which seepage into repository-type drift openings does not occur.

Air-Permeability Testing—Air permeability is used in the representation of spatial variability in seepage modeling, and in the evaluation of excavation effects. The tests were performed in packed-off borehole intervals using constant-rate air injection.

Lithophysal Cavities—Direct observations of calcite and opal in lithophysal cavities can be used to estimate long-term seepage rates into these small openings (BSC 2002b, Section 6.10.1). From an understanding of the mechanism for calcite precipitation, seepage into lithophysal cavities can be estimated from calcite-deposition data. The analysis of calcite and opal precipitation data shows that not all lithophysal cavities encountered seepage, and seepage flux derived from mineral deposits is a very small fraction of percolation flux.

Passive Monitoring of Drifts at Yucca Mountain—When drift openings at Yucca Mountain are closed to ventilation, the humidity increases rapidly and evaporation is attenuated so that it could be possible to directly observe seepage. Bulkheads have been installed in the Cross-Drift (lower lithophysal) and Alcove 7 (middle nonlithophysal) specifically to facilitate passive observation of seepage. These tests are still in progress but so far have confirmed that the wall rock at ambient conditions becomes substantially wetter without ventilation. Water has been observed to form as condensation in these tests, when artificial heat sources are present in unventilated areas. Indications of water droplets falling on the floor have been observed and samples of water have been collected.

Overall, there have been few, if any, indications of seepage into these openings after heat sources have been removed, and if seepage has occurred, the amounts are probably small compared to the background percolation flux.

Archaeological Analogs—Studies of how the capillary barrier effect performs over thousands of years have shown that water percolating through rock and soil is prevented from entering tombs and other archaeological structures that have existed under unsaturated conditions (Stuckless 2000). Survival of artifacts or lack of deposits such as calcite is attributed to capillary diversion of water around the constructed openings. Also, film flow along the inner walls of such openings has been identified. These observations provide additional confidence that seepage into repository emplacement drifts will be prevented by capillary barrier effects.

2.2.2 Technical Basis for Thermal-Hydrologic Processes from Field Thermal Tests

Field thermal testing during site characterization has greatly aided development and validation of thermal-hydrologic models used to calculate the repository performance of thermal-hydrologic processes at Yucca Mountain. The program has included, in chronological order, the Large Block Test (conducted at the surface near Yucca Mountain), the Single Heater Test, and the DST (BSC 2002a, Sections 6.1, 6.2, and 6.3 for further details). These tests have supported significant advances in thermal-hydrology, accompanied by advances in the associated models. The Single Heater Test was performed prior to the DST in the same rock mass to prove test methods and provide preliminary data. The results are encompassed by the DST, so the Single Heater Test will not be discussed further in this report.

In contrast to the Single Heater Test and DST, which are located deep down in the Exploratory Studies Facility in an area of very small percolation, the Large Block Test is a block of fractured rock at the ground surface just southeast of Yucca Mountain. During heating of the block, a few intense rainfall events caused significant influx of water at the top of the block, which percolated downward to the boiling region. The water was able to penetrate into the above-boiling region and cool part of it to below boiling for a few hours. In the weeks that followed the initial

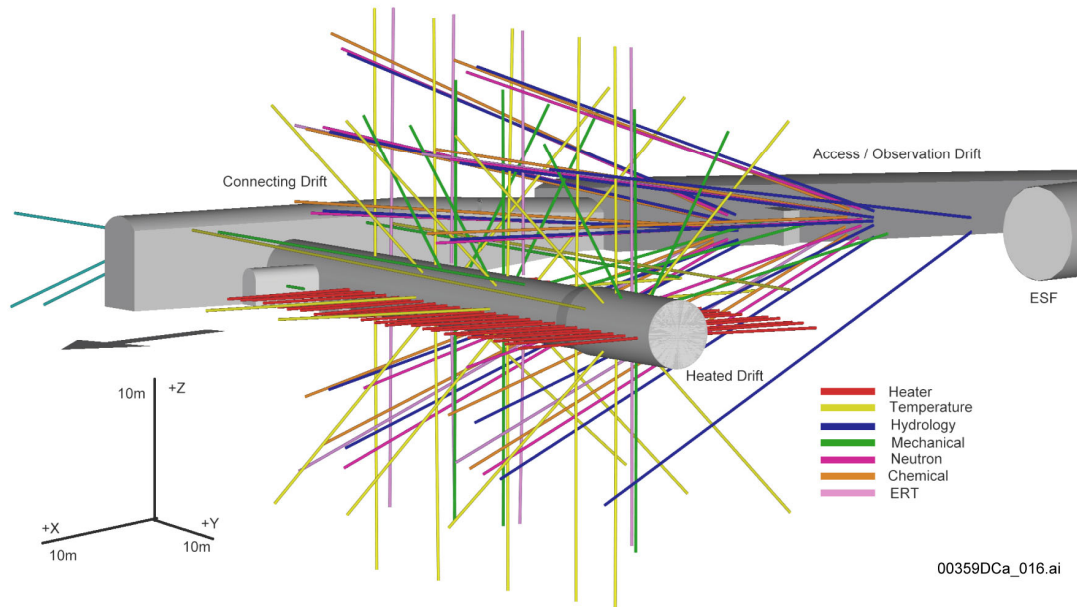
rainfall, temperature measurements showed episodic flow of water back into the boiling region. It was demonstrated that large conductive fractures connected the top of the block with the heater horizon, thereby providing a fast path for water fluxes of large magnitude. Such conditions are not representative of hydraulic connections deep underground at Yucca Mountain; also, the Large Block Test was surrounded by an impermeable membrane that trapped fracture water in the block. As a confidence-building exercise, Mukhopadhyay and Tsang (2002, Section 5) accurately modeled the Large Block Test response to transient water influx using a process model similar to the thermal-hydrologic seepage model.

Much of the discussion in this report is based on understanding gained from the DST. The main purpose of the test is to support more in-depth understanding of thermally driven coupled processes anticipated in the host rock surrounding the repository. The DST is probably the largest in situ heater test ever performed in a fractured rock environment, and results from the DST encompass those obtained from the earlier tests. The test area is located in one of the side alcoves of the ESF in the middle nonlithophysal tuff. Figure 2-3 shows a three-dimensional perspective of the DST with heaters and many of the instrumented boreholes for measuring thermal, hydrologic, mechanical, and chemical processes. The DST centers around the heated drift, which has a 47.5-m-long heated section isolated by a thermally insulated bulkhead. Approximately 200,000 m³ of rock were heated during the test, monitored by more than 3,000 sensors of different types. Heating was provided by nine canister heaters (i.e., simulated waste packages) within the heated drift as well as 50 borehole heaters placed in horizontal boreholes that extend horizontally from the heated drift. The dimensions of the heated drift and canister heaters are similar to the current design concept for waste emplacement drifts. All the DST heaters were operated from December 1997 until January 2002. The test is presently in a 4-year cooldown period. The power utilization and representative drift-wall temperature histories are shown in Figure 2-4.

Measurements during the heating and cooling phases of the DST are divided into two categories: continuous monitoring and active, periodic testing. The DST test block has been instrumented with thousands of sensors to monitor thermal, mechanical, hydrologic, and chemical processes. Humidity, temperature, and pressure sensors were installed in 12 of the hydrologic boreholes for passive monitoring. These same boreholes are also used for periodic air-permeability testing to track saturation changes associated with condensation zones in the test block. The boreholes are also used for collection of water (if present) and gas sampling for chemical and isotopic analysis. Finally, neutron logging, electrical resistivity tomography, and crosshole radar tomography have been carried out at appropriate time intervals throughout the heater test to probe changes in the moisture that is present predominantly in the rock matrix.

Temperature histories from two near-horizontal boreholes are shown in Figure 2-5. Borehole 160 extends horizontally from the heated drift, and borehole 59 emanates subhorizontally from the observation drift toward the heated drift. Each trace on the figure represents a different temperature sensor. These plots were selected from the many available to show model–data agreements; the model predictions shown are discussed in Section 2.3.2. General model–data agreement in temperature histories indicates correct selection of values for thermal parameters such as the thermal conductivity. The leveling-off of temperature at the hottest sensors (near the heaters) after 24 months was caused by power adjustments intended to stabilize the near-field temperature at 200°C. Each of the curves (both the measured data and

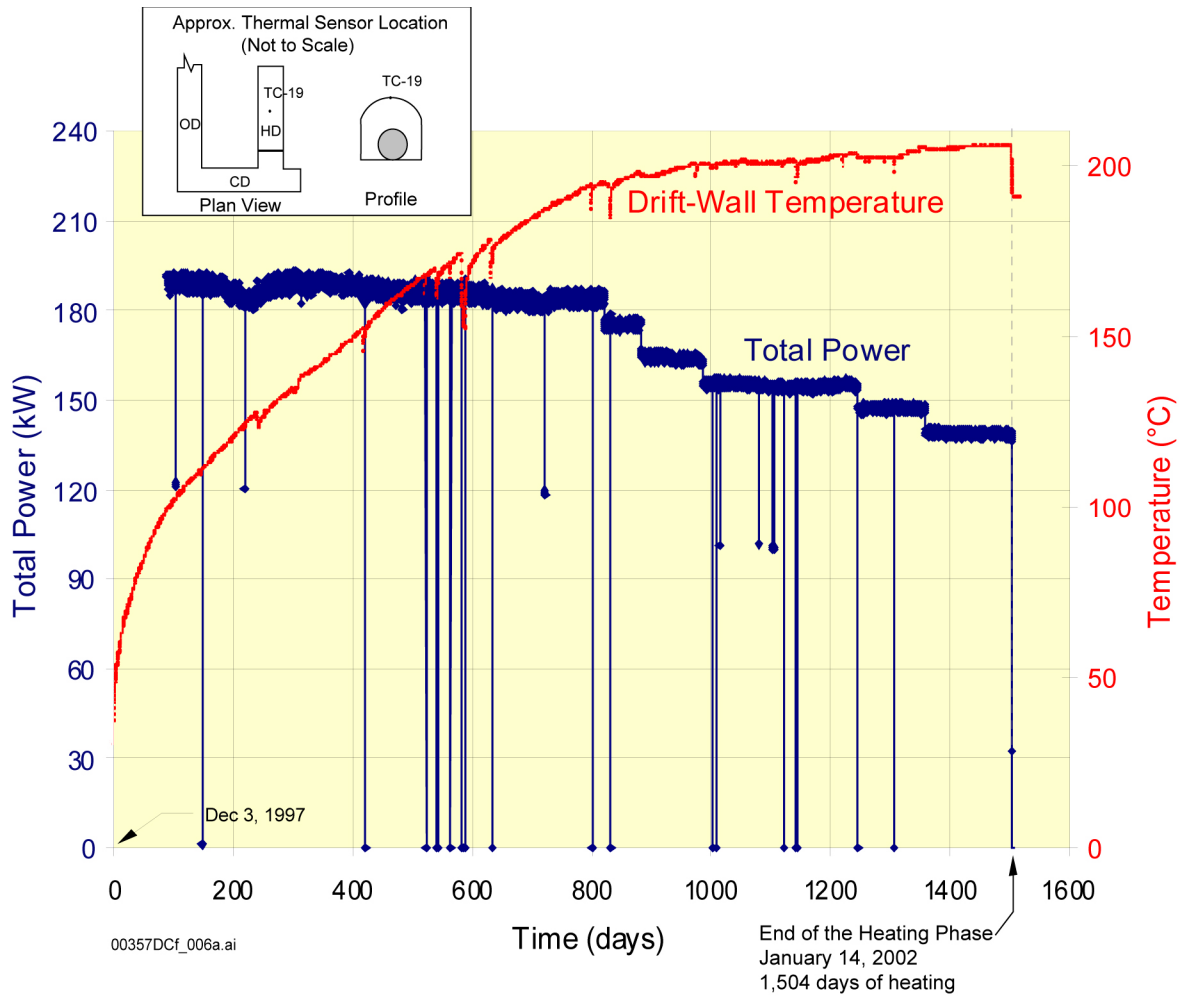
calculated results) that passes through boiling tends to flatten somewhat as it does so. This occurred because of reflux activity at the margin of the expanding dryout zone (BSC 2003b, Section 7.4.4.1.2), and the correspondence builds confidence in model predictions of reflux behavior.



Source: BSC 2003b, Figure 7.2.1-2.

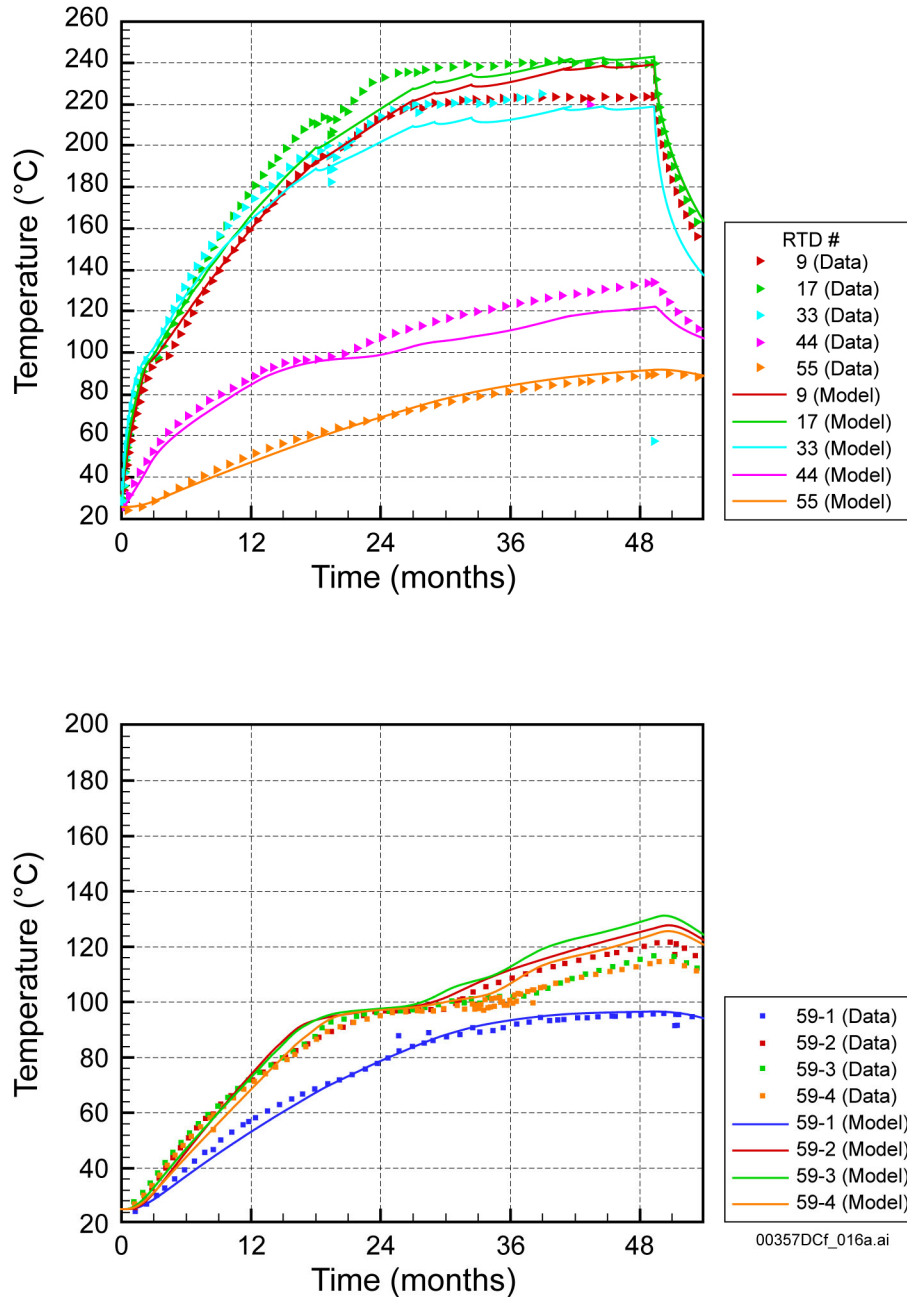
NOTE: ERT = electrical resistance tomography.

Figure 2-3. Three-Dimensional Perspective of the As-Built Borehole Configuration of the Drift Scale Test



Source: BSC 2002a, Figure 6.3.1.1-1.

Figure 2-4. Total Power and Representative Drift-Wall Temperature (TC-19) during the Drift Scale Test Heating Phase



Source: BSC 2003b, Figure 7.4.3.1-3.

NOTE: Top: Borehole 160 (horizontal). Bottom: Borehole 59 (subhorizontal, above and perpendicular to the heated drift).

Figure 2-5. Temporal Evolution of Temperature at Selected Borehole Sensors, in Horizontal Temperature Boreholes that Traverse the Drift Scale Test

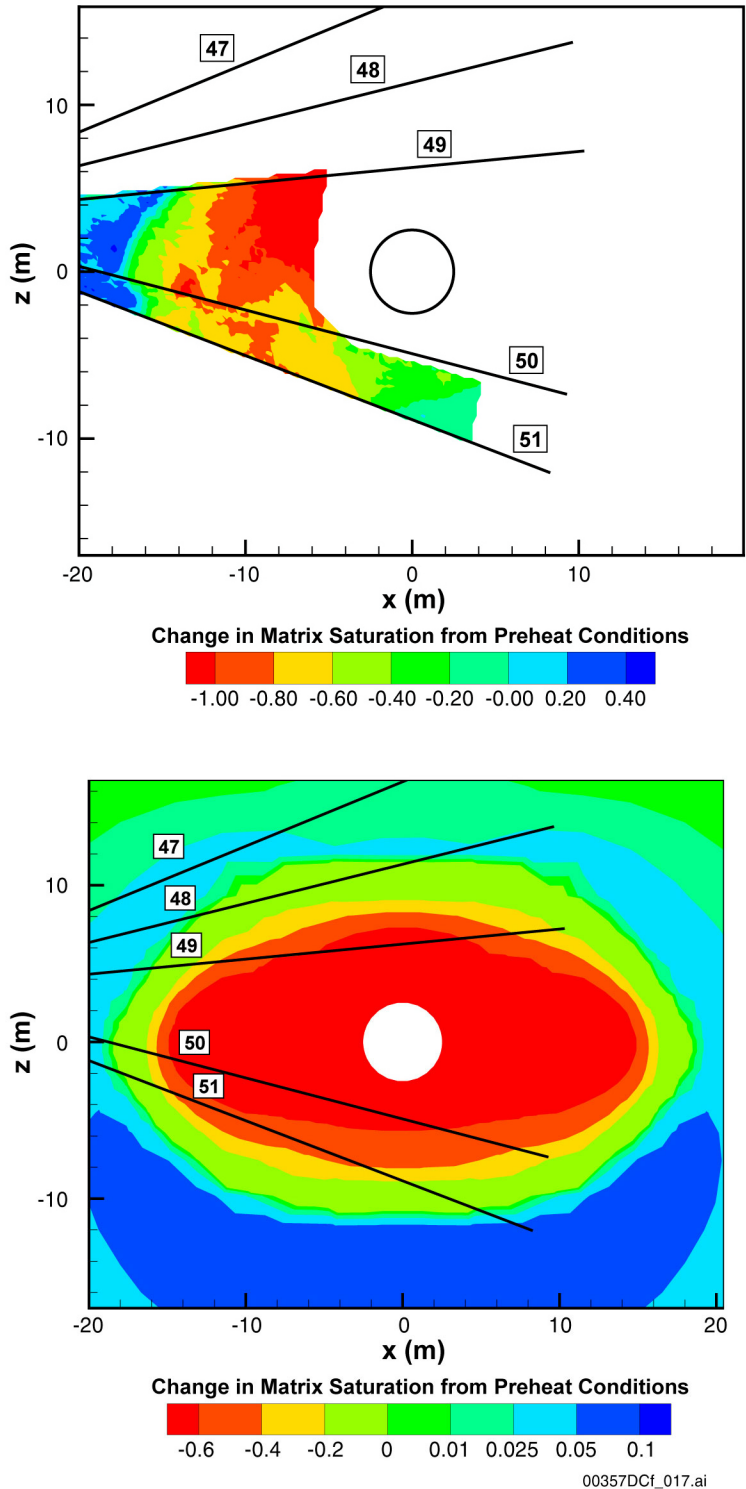
Expansion of the dryout zone was also tracked using geophysical methods. An example from using ground-penetrating radar is shown in Figure 2-6. Ground-penetrating radar investigates the total water content between boreholes (limited by borehole geometry), which is dominated by the matrix liquid saturation. The results are compared with a thermal-hydrologic simulation of the DST corresponding to the end of the heating period (the associated model is discussed in Section 2.3.2). The ground-penetrating radar cross section confirms the geometry and extent of dryout. Model–data comparisons, such as the one shown in Figure 2-6, which portrays moisture conditions rather than temperature alone, are an important confidence-building step for thermal-hydrologic models.

From the DST results, it has also been possible to interpret changes in fracture air-permeability that are associated with condensation. Over all of the permeability test intervals for which data are presented in Figure 2-7, there is an immediate, consistent trend of air-permeability decrease from a combination of saturation buildup from condensation and fracture closure from thermal-mechanical effects. The relative contribution from each is evaluated by *Drift Scale THM Model* (BSC 2003h, Figures 7.4.3-3 and 7.4.3-4), which documents and validates coupled thermal-hydrologic-mechanical process models. The observed decrease in permeability is followed by a stabilization or increase, showing that saturation decreased as a result of the extending drying front. Differences between the observed and simulated trends in air-permeability are attributed to the additional effect of thermal-hydrologic-mechanical fracture closure.

2.2.3 Technical Basis for Thermal Seepage

The thermal load in the DST produced boiling and subsequent condensation of water, with maximum near-field rock temperature greater than 200°C. With such intense thermal-hydrologic processes occurring, the DST data provide the basis for validation of repository-predictive models through observed temperature and saturation changes. Because of concern over vapor losses through the bulkhead of the heated drift (BSC 2003b, Section 7.3.4), the DST results are not used as direct evidence for a totally effective vaporization barrier, even though no seepage of water into the heated drift has been observed. Rather, investigation of other observed responses from the DST and associated model-data comparisons are used to establish confidence in thermal-hydrologic simulation capability. The simulation capability is then used to simulate thermal seepage as well as other responses to repository heating. Thermal loading in the repository will be less intense, applied over a much longer duration, and the resulting temperatures will be lower than in the DST.

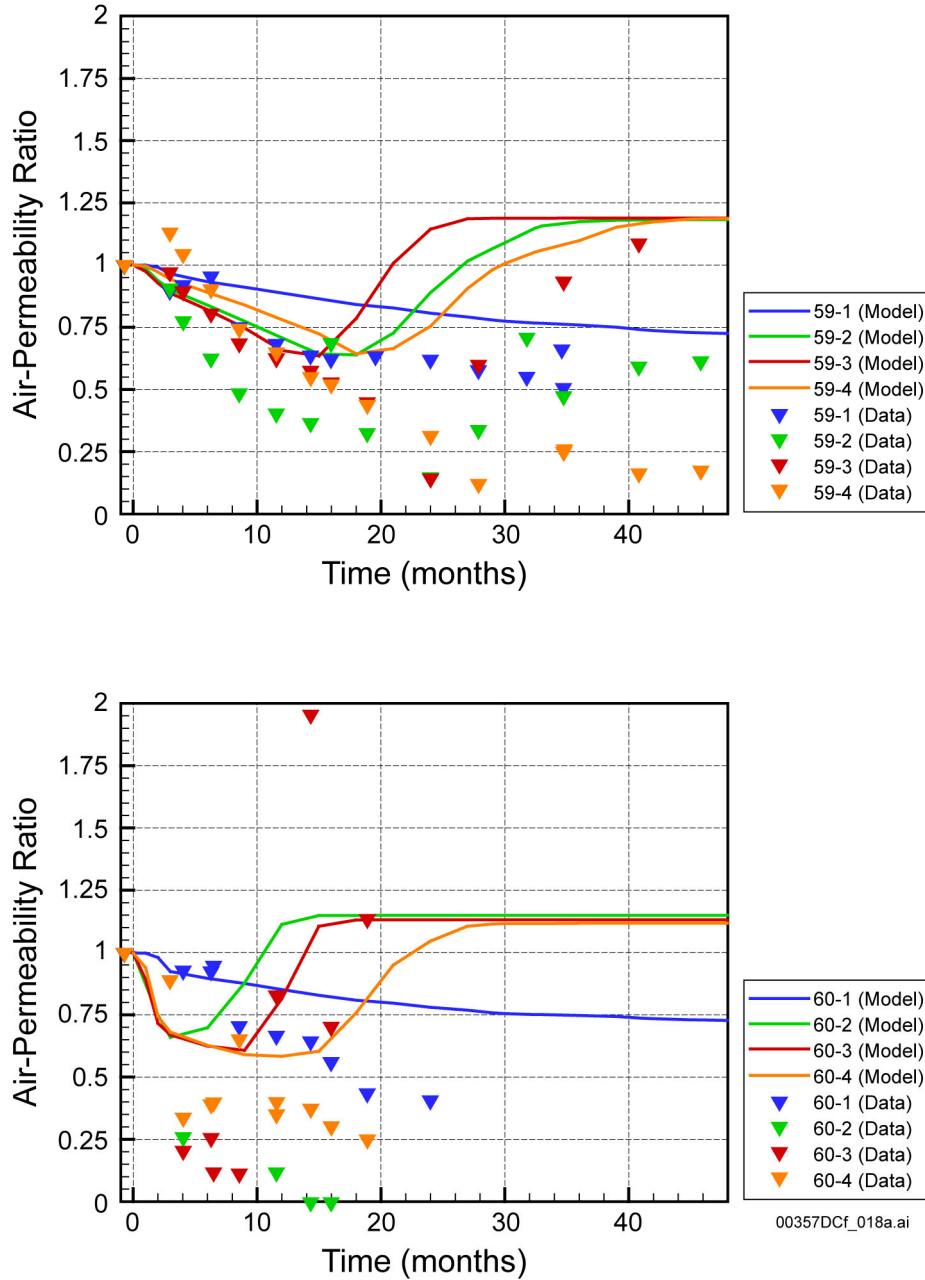
There are three general approaches to indirect validation of the thermal seepage vaporization barrier model. First, the capability to predict overall thermal-hydrologic behavior for the DST provides model confidence in thermal seepage predictions. Second, the conceptual model for thermal seepage is similar to the conceptual model applied to ambient seepage prediction (Sections 2.1.1 and 2.2.3) with similar key properties (permeability and fracture capillary strength). Third, to gain additional confidence in the nonequilibrium continuum model used to represent thermal seepage for TSPA, an alternative conceptual model for thermal seepage in discrete fractures is introduced in Section 2.3.3, confirming that seepage is highly unlikely when the host-rock temperature is above boiling.



Source: BSC 2003b, Figure 7.4.3.2-3.

NOTE: Top: measured ground-penetrating radar response in boreholes 49 to 51 (January 2002 near the end of heating). Bottom: simulated results at end of the heating phase.

Figure 2-6. Change in Matrix Liquid Saturation from Preheating Conditions, at the End of the Heating Phase



Source: BSC 2003b, Figure 7.4.3.3-2.

NOTE: Boreholes are subhorizontal, oriented from the observation drift toward the heated drift: (top) Borehole 59 (above the heated drift); (bottom) Borehole 60 (below).

Figure 2-7. Change in Measured Apparent Fracture Air-Permeability during the Heating Phase of the Drift Scale Test

Further use of information from the DST provides another reason why thermal seepage will not occur. Observations from the DST (see Section 4, Figure 4-4) showed that the rock matrix dries out when the temperature crosses through boiling over a narrow temperature range of only a few degrees. These observations are based on borehole neutron log measurements, which are less influenced by loss of vapor through the DST bulkhead than seepage into the heated drift. The abrupt decrease in volumetric water content observed at boiling conditions ensures the matrix will be very dry in the dryout zone. Liquid water that penetrates the dryout zone will not only be evaporated by heat conducted through the fracture walls (as represented in the alternative model mentioned above) but will also be imbibed into the dry matrix by powerful capillary gradients. Once in the matrix, the water will slow down, and evaporation becomes more certain. Further discussion of thermal seepage and its technical basis is provided in the technical basis document addressing water seeping into drifts.

2.3 PROCESS MODEL DEVELOPMENT AND RESULTS

2.3.1 Model Results for Ambient Seepage

The following discussion provides an overview of the seepage calibration model, the seepage model for TSPA, and the abstraction model for drift seepage. An alternative discrete-fracture model for ambient seepage is also briefly discussed. More detailed discussion of ambient seepage modeling is provided in the technical basis document addressing water seeping into drifts.

The general approach followed to analyze data from seepage tests and to develop a defensible predictive seepage model is a calibration approach that relies directly on observed seepage-rate data from active tests, which inherently contain information about the relevant features and processes. In other words, the test data (drift-scale seepage rates) are similar to the measure of interest for repository performance predictions.

The following paragraphs describe the development of the process and abstraction models used to make predictive seepage calculations for TSPA.

Conceptual and Numerical Seepage Models—The drift-scale numerical seepage models are heterogeneous continuum models, calibrated to drift-scale seepage test observations. The model grids have been configured to represent the underground openings where the tests were performed. Water flow or seepage occurs predominantly through or from fractures. Accordingly, and given the density of fractures and their orientation characteristics, a three-dimensional heterogeneous fracture continuum model is an appropriate conceptualization to analyze liquid-release tests and to predict seepage into emplacement drifts (BSC 2003m, Section 6.3.2).

The numerical process model used for reproducing seepage-rate data from liquid-release tests and to predict seepage into waste emplacement drifts solves the Richards equation (Richards 1931) for saturated–unsaturated flow through porous materials. The van Genuchten–Mualem constitutive relations (van Genuchten 1980) are used to describe the capillary pressure and relative liquid permeability in the fracture continuum as a function of liquid saturation. This approach captures the main driving forces (gravity, viscous, and capillary forces) and phenomena (phase interference) relevant for modeling unsaturated flow and seepage in a geologic medium.

To appropriately include heterogeneity, the spatial structure of the air-permeability data was used to generate geostatistical realizations of a spatially correlated permeability field. The permeability fields were mapped onto a numerical grid representing an appropriate section of the host rock around the injection interval, including the underground opening. Evaporation from the drift surface during seepage tests was accounted for in the numerical approach.

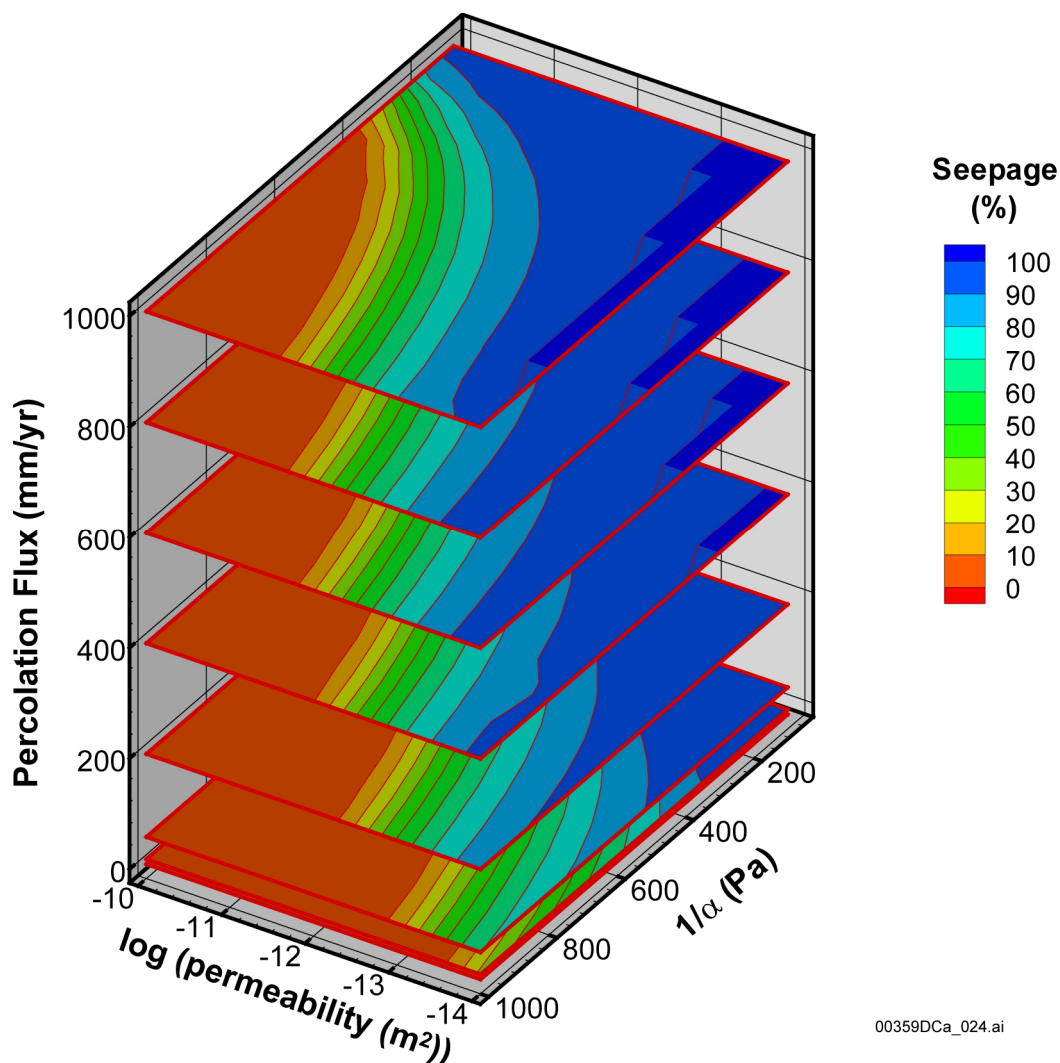
Model Calibration and Validation—The model is calibrated against seepage-rate data from the numerous liquid-release tests conducted in the middle nonlithophysal zone and the lower lithophysal zone. Eighty-one liquid-release test events conducted in Niches 3, 4, and 5 and in the systematic testing area of the ECRB Cross-Drift were available to support the seepage model.

Measured seepage-rate data from 22 liquid-release tests were used to calibrate the seepage calibration model and to estimate the seepage-relevant, model-related van Genuchten capillary-strength parameter $1/\alpha$. Remaining seepage-rate data were either used for further comparison with the seepage calibration model or they were redundant or otherwise unsuited for use. The capillary-strength parameter was determined by calibrating the model against multiple tests using different liquid-release rates. The seepage calibration model was validated against tests conducted both above and below the seepage threshold (i.e., tests that produced seepage as well as those that did not).

Prediction of Ambient Seepage and Abstraction for Total System Performance Assessment—The seepage model for performance assessment was developed based on the seepage calibration model to predict average seepage into a section of a waste emplacement drift under ambient conditions (BSC 2003j). Isothermal flow simulations were performed for wide ranges of key parameters: permeability, capillary-strength parameter, and percolation flux.

The predictive seepage model for performance assessment is a three-dimensional drift-scale model representing a repository emplacement drift. It uses a stochastic, heterogeneous continuum representation of the fractured host rock. Applying a percolation flux at the top of the model, the steady-state seepage flux is obtained. The seepage percentage (the ratio of seepage flux to percolation flux) directly indicates the flow diversion capability of the capillary barrier at the drift wall surface.

To build the abstraction used for TSPA, the calculation was repeated for many different parameter combinations and different realizations of the underlying stochastic permeability field. A lookup table (depicted graphically in Figure 2-8) was generated whereby the seepage percentage is expressed over ranges of the key independent parameters: permeability (k), capillary-strength parameter ($1/\alpha$), and percolation flux. For use in TSPA, each of the independent variables (k , $1/\alpha$, flux) is sampled from an uncertainty distribution based on site data, and the seepage percentage is read directly from the lookup table (BSC 2003j, Section 6.3). Figure 2-8 shows that the seepage percentage is large for small capillary strength, small permeability, and large percolation flux. For some combinations, seepage may be as high as 100 percent (i.e., there is no flow diversion at the drift wall and all the incident percolation flux seeps into the drift). In contrast, for many cases there is no seepage at all (i.e., the percolation flux is below the seepage threshold for the parameters given, and all the incident percolation flux is diverted around the drift). More detailed discussion of seepage modeling and abstraction is provided in the technical basis document addressing water seeping into drifts.



Source: BSC 2003j, Figure 6-8.

Figure 2-8. Mean Seepage Percentage as a Function of Capillary-Strength Parameter and Mean Permeability for a Percolation Flux of 1, 10, 50, 200, 400, 600, 800, and 1,000 mm/yr

Seepage and Drift Degradation—Various drift degradation models have been developed for the nonlithophysal and lithophysal host-rock units (BSC 2001c; BSC 2003n). Degradation in the nonlithophysal host rock is primarily controlled by geologic structure (i.e., the nature of fracturing). Rockfall into repository openings in the nonlithophysal rock will be relatively minor even for low-probability seismic ground motions and strongly reduced rock mass strength properties. Flow and seepage calculations were performed for selected representative drift profiles to examine the impact of changes in drift shape on seepage. The simulation results indicate that minor rockfall and correspondingly minor drift shape changes lead to limited effects on seepage for all degradation cases expected to occur in the middle nonlithophysal zone.

The lithophysal host rock is comparatively weaker so that strong seismic events or reduction in strength properties may lead to collapse of drift openings. Collapsed drifts will approximately double in size and accumulate rubble, which eventually may fill the drift and support the roof, preventing further collapse. Although filled with rubble, a capillary barrier will still be effective

because the rubble and will contain large scattered voids. Also, for partial collapse situations an air gap will exist between the rubble and the roof. To simulate drift collapse effects in the lithophysal host rock, a worst-case drift profile was selected to represent the drift collapse scenarios depicted in *Drift Degradation Analysis* (BSC 2003n). Comparison of seepage simulation results from the nondegraded drift scenario indicates a moderate increase in seepage percentage, caused by the larger opening size and by the nonzero capillary strength used within the collapsed drift. Most of the percolation flux is still diverted around the collapsed drift over most of the considered parameter range; actual seepage fluxes, however, are increased because of the larger footprint of the collapsed drift. The simulated effects of drift degradations on seepage are incorporated in the abstraction approach for TSPA. Additional discussion of seepage into degraded drift openings is provided in the technical basis documents addressing water seeping into drifts and low-probability seismic events.

Implementation of the Ambient Seepage Abstraction in TSPA—To illustrate how ambient seepage behavior will be represented in TSPA system-model implementation, a probabilistic seepage calculation was conducted following the abstraction method described in *Abstraction of Drift Seepage* (BSC 2003l, Section 6.8). Summary results indicate the importance of the capillary barrier to seepage, for example, for drifts located in the lower lithophysal tuff (the most extensive unit of the repository) under likely future climate conditions, the mean seepage percentage will be about 8 percent during the glacial transition climate. This means that on average 92 percent of the incident percolation flux will be diverted around the emplacement drifts. Note that this calculation result will not be used directly in TSPA; the seepage component in the TSPA simulations will conduct a similar seepage calculation embedded in the Monte Carlo simulation procedure.

2.3.2 Model Results for In-Drift Temperature and Relative Humidity

The following discussion summarizes the model-data comparisons that form the basis for confidence in thermal-hydrologic models used to interpret the DST. The discussion then describes the closely related thermal-hydrologic model (multiscale model) used to predict the evolution of temperature and relative humidity in the host rock and within repository emplacement drifts for TSPA.

Validation of Predictive Model Capability Based on the Drift Scale Test—Comparison of measured and simulated results for the DST is first presented for temperature (Figure 2-5) for which many thousands of measurements have been made. The agreement is good, both qualitatively (Figure 2-5) and quantitatively as shown by statistical measures for goodness-of-fit. The temperature profiles and temperature history plots show similar reflux behavior (deflections near 100°C in Figure 2-5) in measured and simulated responses, providing confidence that thermal-hydrologic coupling is understood and represented in the model. The mean difference between measured and simulated temperatures at more than 1,700 temperature sensors in the DST does not exceed 2 percent of the maximum rock temperature, and the root-mean-square difference is less than 6 percent. This establishes that the modeling framework for the DST thermal-hydrologic model successfully incorporates the relevant thermal-hydrologic processes (BSC 2003b, Section 7.5), as does the thermal-hydrologic seepage model (based on the same conceptual understanding).

In addition to temperature measurements, thermal-hydrologic processes are also monitored by tracking the time-varying location of the dryout zone and the associated condensation front in response to heating. For the DST, the dryout zone and condensation front were tracked using geophysical methods that respond to liquid saturation changes in the matrix, and by periodic air-injection tests that respond to liquid saturation changes in the fractures. Qualitative agreement has been obtained between observed trends in the geophysical images of permeability tests, and simulation results (Figure 2-6). As discussed in Section 2.2.2, because the DST thermal-hydrologic model does not account for thermal-hydrologic-mechanical effects, some differences remain between simulated and measured trends in air-permeability. To provide additional confidence, the simulated fracture-saturation results were also compared to the location and timing of water collection from several packed-off borehole intervals (BSC 2003b, Section 7.4.3.3). It was shown that water collection data correspond well with the predicted locations of high saturation from the model. This, and the overall good agreement of temperature and matrix saturation data, provides confidence that the model accurately represents the relevant thermal-hydrologic processes of moisture redistribution.

As mentioned previously, the DST is one of three heater tests of different scales and geometry that have been conducted at Yucca Mountain. The successful modeling analyses performed for the Single Heater Test and the Large Block Test provide additional confidence in the capability to predict thermal-hydrologic conditions for the repository (Tsang and Birkholzer 1999; BSC 2001a; Mukhopadhyay and Tsang 2002).

Finally, the many geochemical measurements conducted in the DST (Section 3.3) also contribute to confidence in the DST thermal-hydrologic model. The simulation model for analyzing the thermal-hydrologic-chemical processes in the DST fundamentally depends on thorough understanding of the water and gas flow thermal-hydrologic processes. Thus the agreement between measured chemical data and results from the DST thermal-hydrologic-chemical model (Section 3.3) provide additional confidence because the models share similar concepts and thermal-hydrologic rock properties.

Multiscale Model—The purpose of the multiscale thermal-hydrologic model (MSTHM) is to predict the evolution of thermal-hydrologic conditions in the repository emplacement drifts and in the adjoining host rock (BSC 2003a). The fundamental concept in the MSTHM is that results from two-dimensional drift-scale thermal-hydrologic models can be combined with other models that account for mountain-scale heating, and local effects arising from the variability in heat output of adjacent waste packages, to produce more accurate predictions of in-drift conditions. The MSTHM approach was motivated by the need for a modeling tool that simultaneously accounts for processes occurring at a scale of a few tens of centimeters around individual waste packages and emplacement drifts and also at the mountain scale. A single numerical model (even using embedded grids) was not selected to do this because of computational effort.

The approach is conceptually similar to embedding numerical models at different scales, but uses a different approach based on processing of calculated differences between the constituent models. Conceptually, the approach is simple. Thermal-hydrologic behavior is simulated for a typical waste package using a two-dimensional drift cross-section model for a variety of thermal loading conditions representing different locations throughout the repository (e.g., center versus edge locations). The conceptual model and numerical formulation is very similar to the DST

thermal-hydrologic model discussed above. The model represents thermal conduction and convective processes in the rock, and thermal conduction, convection, and radiation in the drift openings. These two-dimensional thermal-hydrologic results are then modified to account for three-dimensional heat flow at the mountain scale and at the drift scale. The MSTHM framework includes several types of waste packages containing waste forms with different heat output characteristics, accounts for the manner in which the emplacement drifts will be ventilated during the preclosure period, and addresses variation of heat-removal efficiency by ventilation as a function of time and distance along each emplacement drift. Propagation of parametric uncertainty in the MSTHM is accomplished using calculations that address uncertainty on host-rock thermal conductivity and percolation flux. In the calculations presented below, three distributions of percolation flux variation are used (lower, mean, and upper) to represent uncertainty on present-day and future infiltration conditions at the site.

The MSTHM calculates the temperature, relative humidity, fracture and matrix liquid saturations, evaporation rate, and liquid- and gas-phase fluxes for key locations within the emplacement drift and in the host rock. This approach implements the controls on temperature and relative humidity in the drifts discussed in Section 2.1.2. Validation of the MSTHM was achieved by comparison to available results from other mountain-scale thermal-hydrologic models representing the repository, and by using the same conceptual and numerical tools to simulate field thermal tests including the Large Block Test and the DST (BSC 2003a, Section 7; BSC 2001a, Section 6).

Summary of the Range of Thermal-Hydrologic Conditions for the Total System Performance Assessment for License Application Base Case—The ranges of peak drift-wall and waste-package temperatures, estimated from MSTHM results for all waste packages in the repository, are shown in Table 2-1. The ranges for duration of above-boiling temperatures at the drift wall are tabulated in Table 2-2. The same information is shown as complementary cumulative distributions in Figures 2-9 and 2-10.

Table 2-1. Peak Drift-Wall and Waste-Package Temperatures over All Waste Packages Simulated, for the Lower, Mean, and Upper Infiltration-Flux Cases

Infiltration-flux case	Peak drift-wall temperature (°C)			Peak waste-package temperature (°C)		
	Coolest	Median	Hottest	Coolest	Median	Hottest
Lower	106	135	155	116	156	183
Mean	105	133	144	116	153	172
Upper	99	132	143	109	152	171

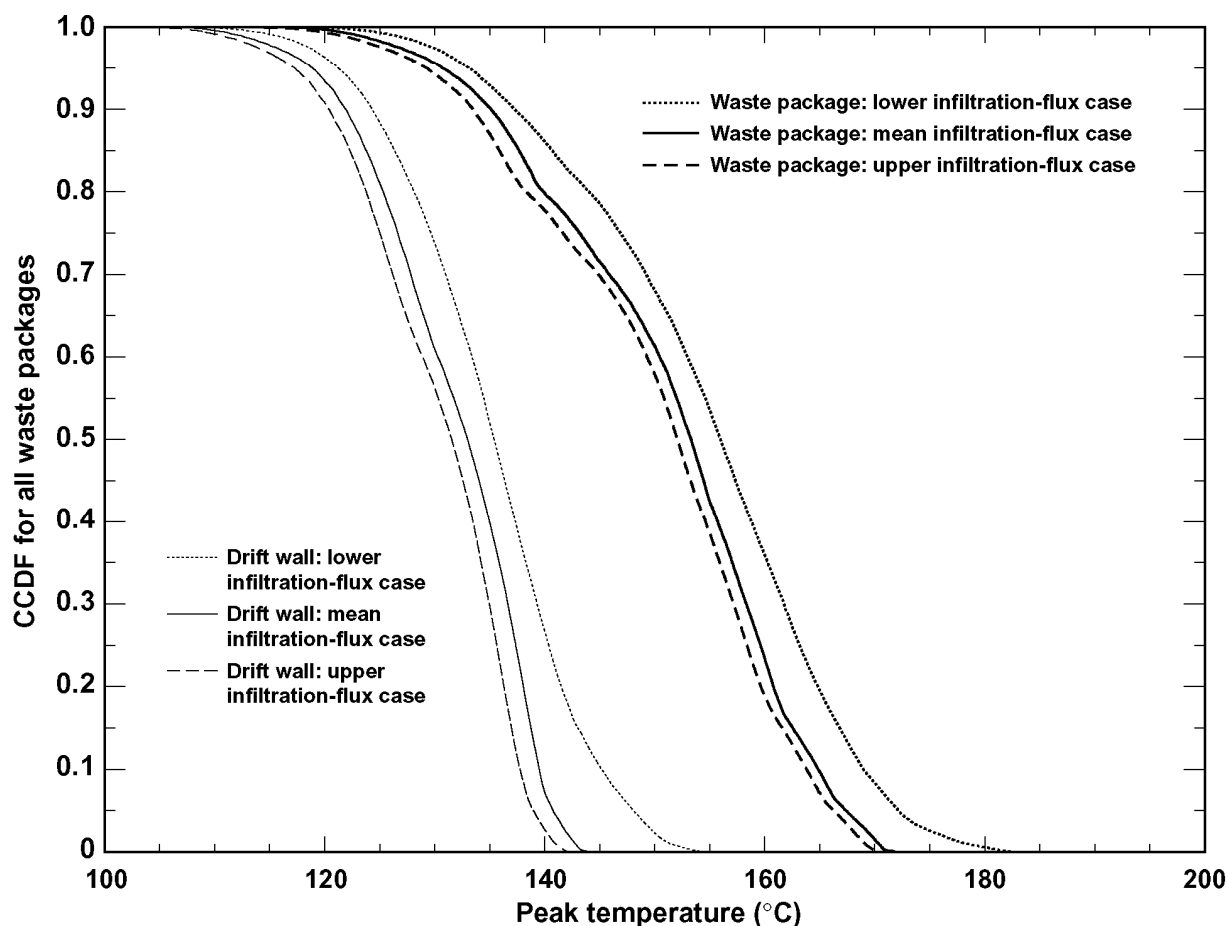
Source: BSC 2003a, Table 6.3-4.

Table 2-2. Duration of Above-Boiling Temperature in the Host Rock at the Drift Wall, for the Lower, Mean, and Upper Infiltration-Flux Cases

Infiltration-flux case	Time when Boiling at the Drift Wall Ceases (years)						
	Shortest	10th percentile	30th percentile	Median	70th percentile	90th percentile	Longest
Lower	130	350	631	860	1123	1453	1735
Mean	127	298	536	721	871	1007	1356
Upper	98	268	472	644	769	887	1163

Source: BSC 2003a, Table 6.3-5.

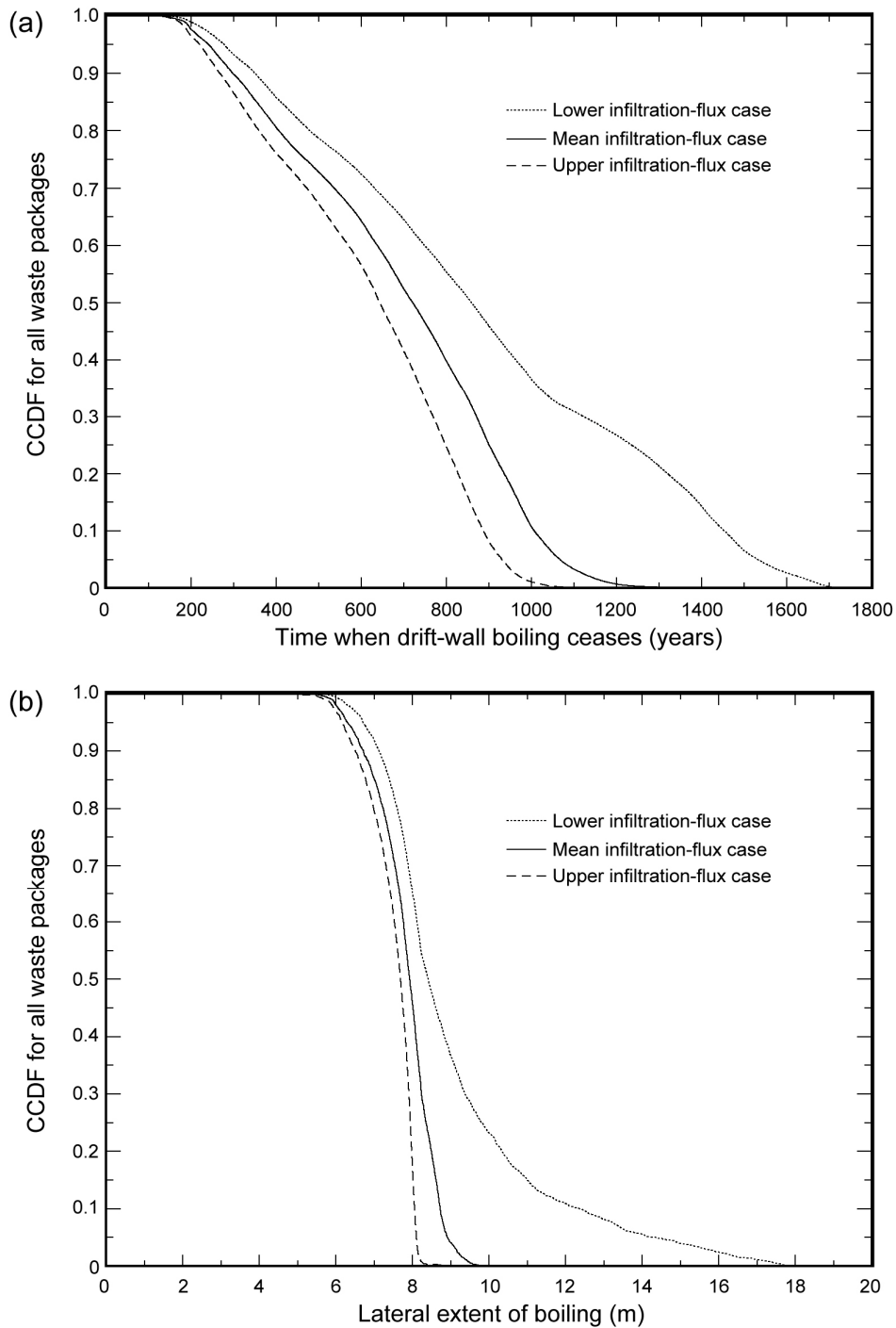
NOTE: Time starts at waste emplacement, with closure at 50 years.



Source: BSC 2003a, Figure 6.3-2.

NOTE: CCDF – complementary cumulative distribution function.

Figure 2-9. Complementary Cumulative Distribution Function for Peak Temperature on the Drift Wall and on the Waste Packages Plotted for the Mean, Upper, and Lower Infiltration-Flux Cases



00357DC_011.ai

Source: BSC 2003a, Figure 6.3-4.

NOTE: (a) The time when boiling at the drift wall ceases; (b) the maximum lateral extent of the boiling-point isotherm (96°C) are plotted for the mean, upper, and lower infiltration-flux cases. The lateral extent of the boiling-point isotherm is measured from the center of the emplacement drift. CCDF – complementary cumulative distribution function.

Figure 2-10. Complementary Cumulative Distribution Functions for the Time when Boiling at the Drift Wall Ceases and for the Maximum Lateral Extent of the Boiling-Point Isotherm

In Figure 2-11 the ranges for temperature and relative humidity histories are plotted with separate groupings for commercial spent nuclear fuel and defense high-level radioactive waste packages. The peak temperatures are 182.9°C and 169.2°C for the hottest commercial spent nuclear fuel and defense high-level radioactive waste packages, respectively. The peak temperatures are 114.3°C and 108.6°C for the coolest commercial spent nuclear fuel and defense high-level radioactive waste packages, respectively. Table 2-2 shows that duration of above-boiling temperatures in the host rock ranges from approximately 98 to 1,735 years. These results are computed using the mean thermal conductivity and, therefore, emphasize the variability associated with repository location and waste package heat output, as well as infiltration.

Additional MSTHM calculations have shown that the combined influence of percolation-flux uncertainty and thermal-conductivity uncertainty results in peak waste-package temperatures ranging from approximately 100°C to 200°C. It was also found that the combined influence of percolation-flux uncertainty and thermal-conductivity uncertainty results in a range of 70 to 2,700 years for the duration of above-boiling temperatures in the host rock.

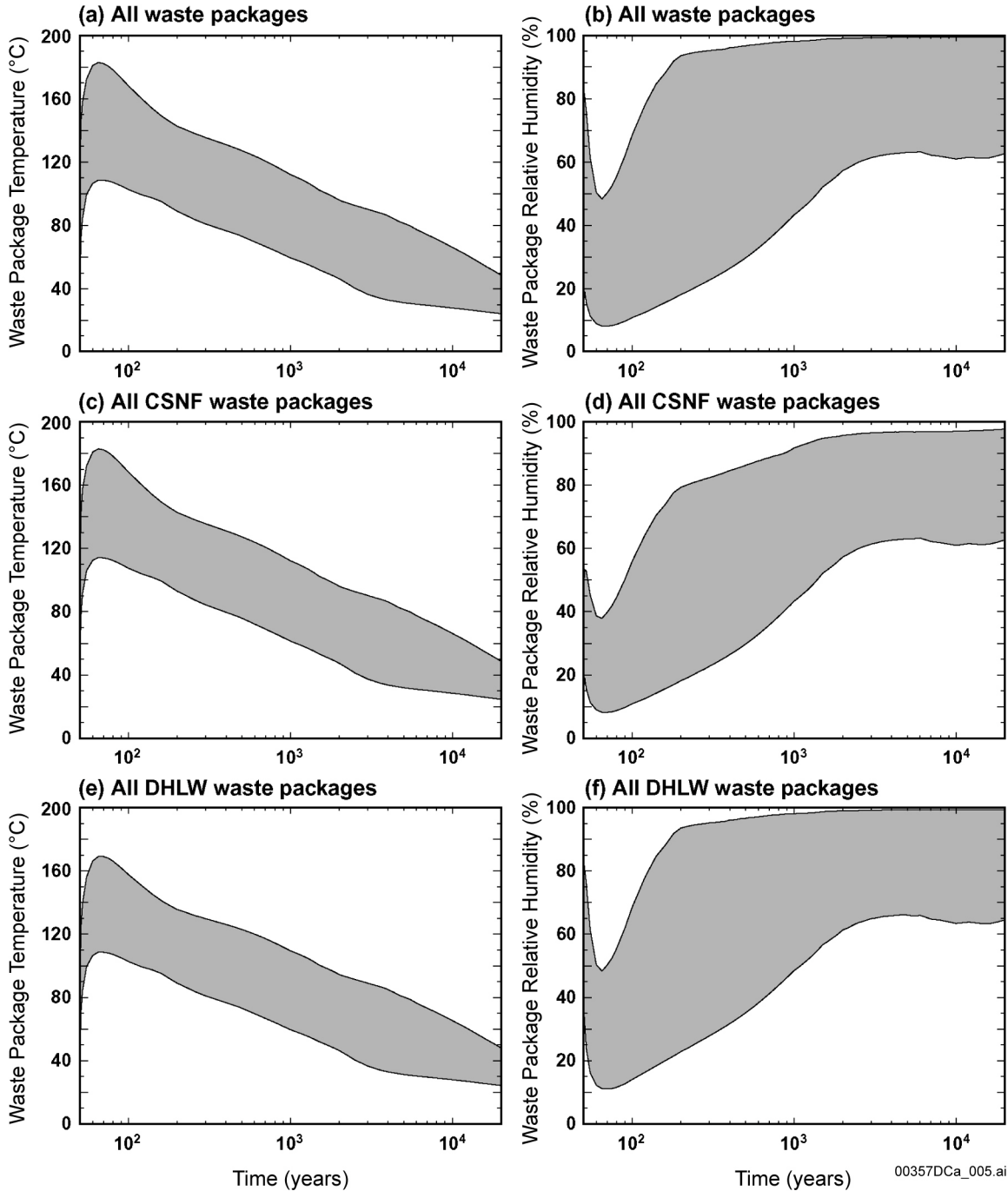
The maximum extent of the dryout zone (defined as the distance from the drift center to the 96°C isotherm in the host rock) is tabulated in Table 2-3 and plotted as a complementary cumulative distribution in Figure 2-10. Over all three infiltration flux conditions, the maximum lateral extent of boiling ranges from 5.1 to 17.8 m with a median extent of 7.9 m. The lateral extent of boiling will always be much smaller than the spacing between emplacement drifts (81 m). The majority of the host rock between emplacement drifts will remain below the boiling point, thereby enabling condensate and percolation flux to drain between emplacement drifts. Because of this drainage, the thermal-hydrologic model predicts that the accumulation of condensate above the emplacement drifts will have limited spatial extent.

Table 2-3. Maximum Lateral Extent of the Boiling-Point Isotherm (96°C for the Repository Elevation) for the Lower, Mean, and Upper Infiltration-Flux Cases

Infiltration-flux case	Maximum Lateral Extent of Boiling ($T > 96^{\circ}\text{C}$)						
	(m)						
	Least	10th percentile	30th percentile	Median	70th percentile	90th percentile	Greatest
Lower	5.6	7.1	7.9	8.4	9.4	12.3	17.8
Mean	5.3	6.7	7.5	7.9	8.2	8.7	9.9
Upper	5.1	6.5	7.3	7.7	7.9	8.1	9.0

Source: BSC 2003a, Table 6.3.6.

NOTE: The lateral extent of the boiling-point isotherm is measured from the center of the emplacement drift.



Source: BSC 2003a, Figure 6.3-33.

NOTE: For all waste packages (a and b), for all commercial spent nuclear fuel waste packages (c and d), and for all defense high-level radioactive waste waste packages (e and f). The ranges include the lower, mean, and upper infiltration-flux cases and use the mean values of thermal conductivity for all model layer units, including the host-rock units.

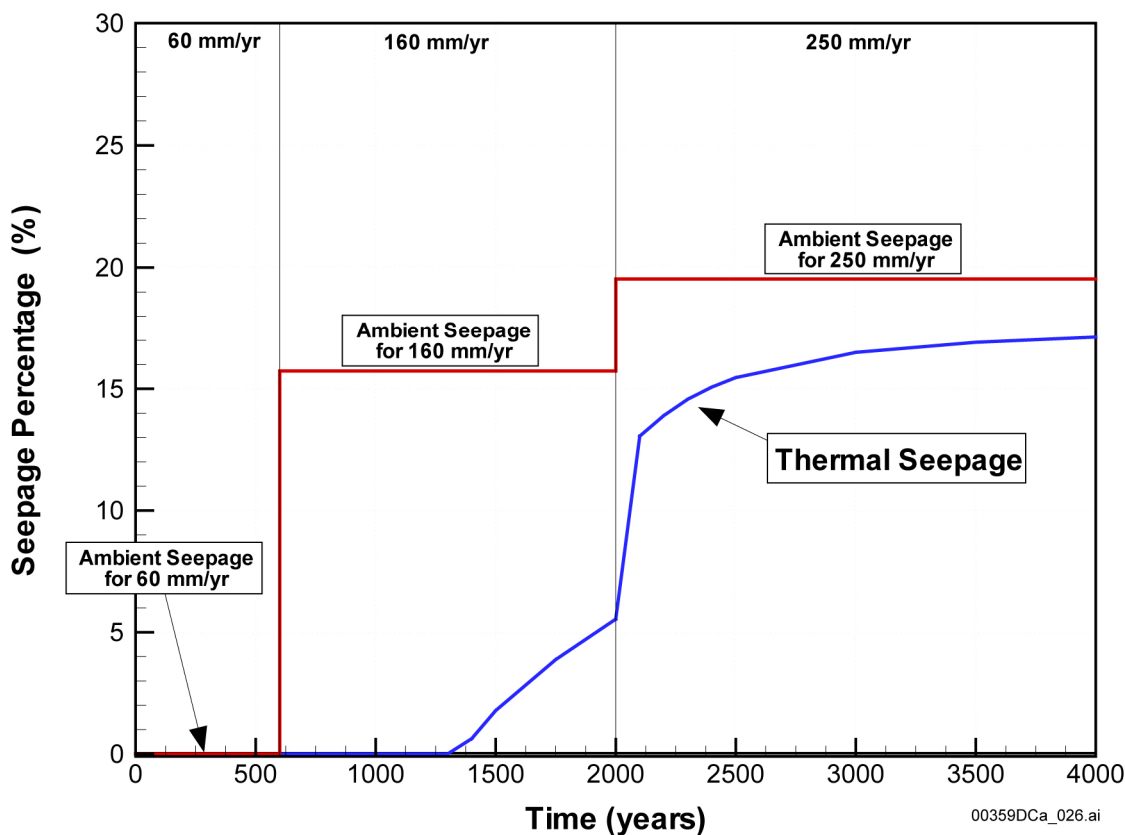
Figure 2-11. Range of Waste Package Temperature and Relative Humidity Histories

2.3.3 Model Results for Thermal Seepage

The thermal-hydrologic seepage model was developed to evaluate the coupled thermal-hydrologic processes and their impact on seepage into repository drifts. The following discussion is taken from *Drift-Scale Coupled Processes (DST and TH Seepage) Models* (BSC 2003b). The drift-scale thermal-hydrologic seepage model combines the two barriers that may prevent seepage into drifts at elevated temperatures: the capillary barrier, which is independent of the thermal conditions; and the vaporization barrier, which is in effect while the host-rock temperature is above boiling (nominally 100°C). While incorporating the conceptual framework for ambient seepage, the thermal-hydrologic seepage model accounts for all important flow and energy transport processes in response to heating, including the movement of gas and liquid phases, transport of latent and sensible heat, phase transitions between liquid and vapor, and vapor pressure lowering due to capillarity. In the thermal-hydrologic seepage model the fractured rock is treated as a dual-permeability domain, accounting for the fractures and the rock matrix as two separate, overlapping continua. A stochastic continuum model is implemented for fractures near the drift that considers the small-scale variability of permeability to account for flow channeling, and the capillary-strength parameter close to the drift wall is derived from the properties provided by the calibration against seepage-rate data (BSC 2003b, Section 4.3).

The predicted thermal-hydrologic conditions are strongly driven by the thermal load placed into the drifts and by the local percolation flux. In general, thermal seepage is possible only when liquid water penetrates the dryout zone, and arrives at the drift wall, and saturation at the drift wall exceeds a given threshold value defined by the capillary barrier effect. Modeling results consistently demonstrate that the magnitude of liquid flux associated with heat-pipe activity, causing increased downward flux from the condensation zone towards the drifts, is strongest during the first few hundred years after closure when rock temperature is highest and the vaporization barrier is most effective. Even if the background natural percolation flux is increased with flow channeling caused by fracture heterogeneity, water cannot penetrate far into the superheated rock. Thus, the potential for thermal seepage is small. Much of the vaporized water condenses outside around the dryout zone and drains away from the drift. At the time when temperature in the rock near the drift wall returns to below-boiling conditions, the magnitude of liquid flux associated with reflux activity is decreased because the waste heat output is decreased, and fractures start rewetting at the drift wall. In addition, the capillary barrier effect will continue to reduce or prevent seepage into the drift.

Transient seepage rates were explicitly calculated by the thermal-hydrologic seepage model to directly quantify the potential for seepage during the period when the drift-wall temperature will be above boiling. These transient seepage rates are compared with results from ambient (steady-state) simulations to evaluate the vaporization barrier. Example results (Figure 2-12) illustrate the time dependence of the thermal seepage model. Note that the ambient seepage percentage is zero for the background percolation rate of 60 mm/yr, which is 10 times the average present-day mean infiltration rate (BSC 2003i, Section 6.1.4). In other words, even without heating of the repository, the capillary barrier at the drift wall is predicted to be completely effective during the first 600 years after waste emplacement. This provides additional confidence, as two barriers independently impede seepage.



Source: BSC 2003b, Figure 6.2.2.2-7b.

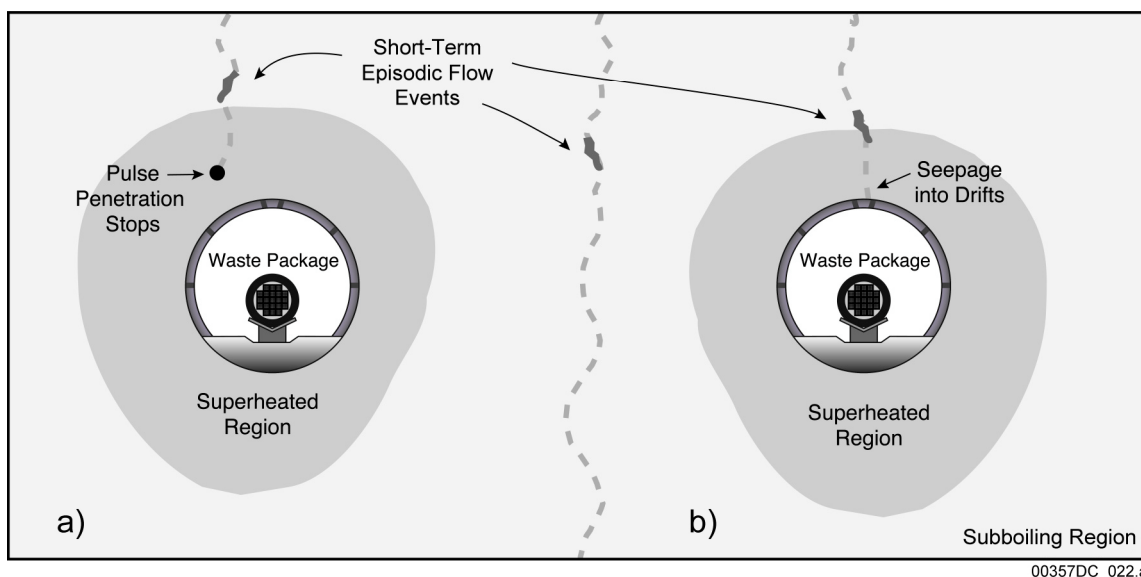
Figure 2-12. Seepage Percentage for Tptpmn Submodel and Reference Thermal Mode and Tenfold Percolation Flux

Different simulation cases studied with the thermal-hydrologic seepage model have produced several important observations common to all cases (BSC 2003b, Sections 6.2.4 and 8.1):

- Thermal seepage was never observed in simulation runs where the respective ambient seepage was zero.
- Thermal seepage never occurred during the period of above-boiling temperatures in the rock close to the emplacement drifts.
- In simulation cases where ambient seepage was obtained, thermal seepage was initiated at several hundred to a few thousand years after rock temperature has returned below boiling.
- Thermal-seepage rates were always smaller than the respective ambient reference values. The ambient seepage values provide an upper limit for thermal seepage.

Alternative Model Used to Test the Thermal-Hydrologic Seepage Model—Predictions from the thermal-hydrologic seepage model regarding effectiveness of the vaporization barrier were tested by comparison with an alternative conceptual model of water flow in the superheated rock environment (BSC 2003b, Section 6.3). In this alternative model (Figure 2-13), the downward

flux from the condensation zone towards the above-boiling dryout zone is conceptualized to form episodic preferential-flow events. The effectiveness of the vaporization barrier was then tested for extreme conditions where downward flux is faster and larger compared to the average flux. A semianalytical solution (Birkholzer 2003) was used to represent the nonequilibrium flow process of episodic, fingering fracture flow in a superheated medium. With this solution, the maximum penetration distance into the superheated rock was determined for specific episodic flow events and thermal conditions, and the amount of water arriving at the drift wall was calculated. It was shown that finger flow is not likely to penetrate through the superheated rock during the first several hundred years of heating, when rock temperature is high and boiling conditions exist in a sufficiently large region above the drifts. Only later, when the boiling zone is small and the impact of vaporization is limited, can channelized water arrive at the drift wall (where it is still subject to diversion around the opening by the capillary barrier effect). For further discussion of this alternative model, see the technical basis document on water seeping into drifts.



Source: BSC 2003b, Figure 6.3-1.

NOTE: (a) Schematic of conceptual model for finger flow in a vertical fracture above a drift with heat conduction from the adjacent rock; (b) episodic finger flow in unsaturated fractured rock in the vicinity of waste emplacement drifts.

Figure 2-13. Alternative Model for Comparison to the Thermal-Hydrologic Seepage Model

Thermal-Hydrologic-Mechanical Effects on Seepage—A drift-scale thermal-hydrologic-mechanical model (BSC 2003h) was developed to assess the magnitude and distribution of stress-induced changes in hydrologic properties and to analyze the impact of such changes on the percolation flux in the rock mass around a repository drift. Thermally induced changes in the stress field will act upon pre-existing fractures, with the result of changing the hydrologic properties of the rock mass and the potential for thermal seepage.

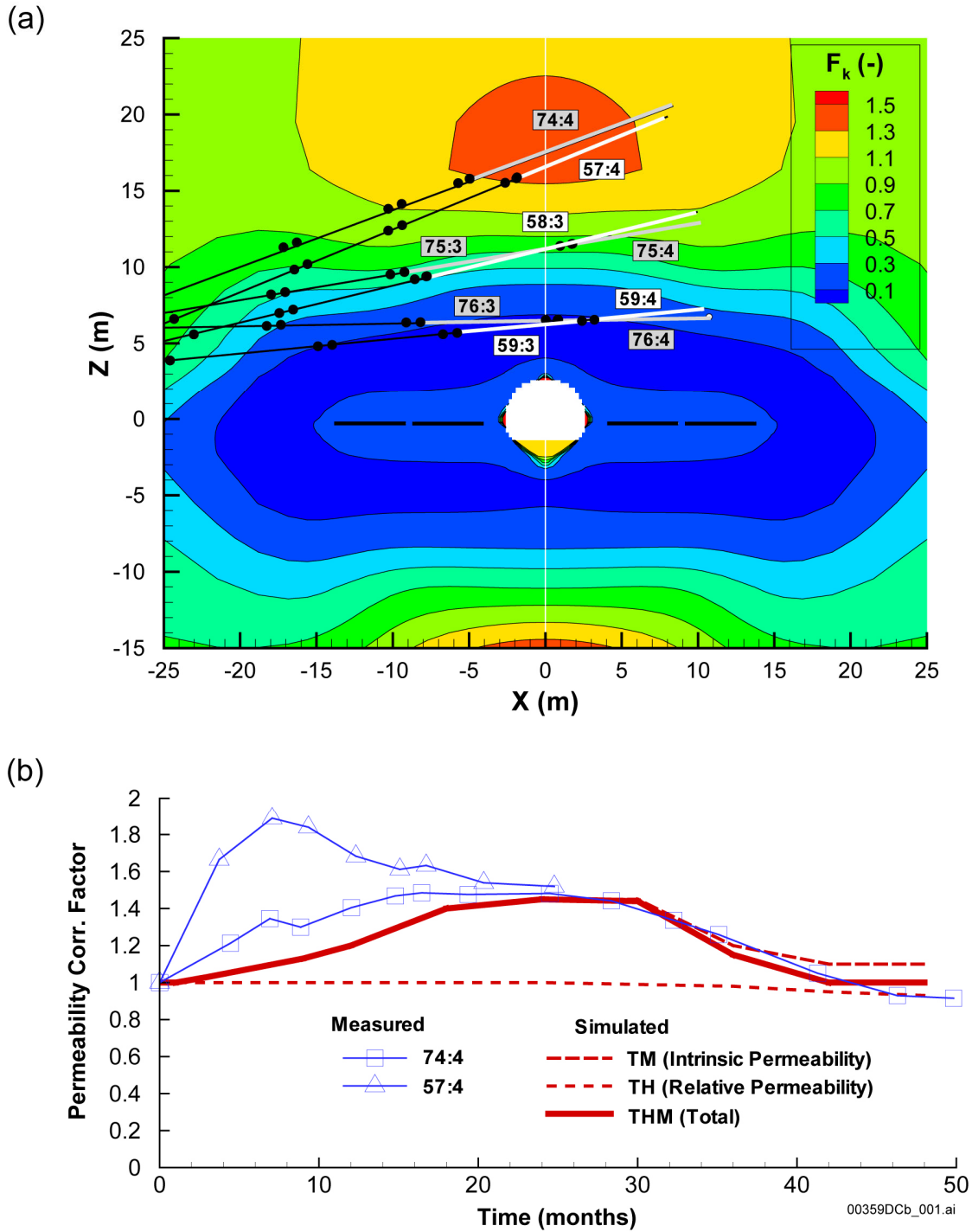
The modeling framework for the thermal-hydrologic-mechanical processes is similar to the thermal-hydrologic seepage model described above. However, the thermal-hydrologic-mechanical simulations concentrate on the thermally induced stress changes and resulting impact on the flow field and host-rock properties. The model was validated by comparison with rock mass displacement data (for thermal-mechanical processes) and air-permeability data (for hydrologic-mechanical processes) measured during the heating phase of the DST (BSC 2003h, Section 7). Figure 2-14(a) shows predicted changes in air permeability (a seepage-relevant parameter) as a result of both thermal expansion and saturation changes (dryout and condensation effects) during the DST test. The favorable comparison with measured air permeabilities shown in Figure 2-14(b) provides confidence that the model predictions can be used to assess property changes induced by coupled thermal, hydrologic, and mechanical processes on seepage.

Simulations of thermal-hydrologic-mechanical effects for the nonlithophysal Ttpmn and lithophysal Ttpll units (BSC 2003h, Sections 6.5 and 6.6) generally show a decrease in vertical permeability as a result of temperature-induced stresses near the drift openings, while the horizontal permeabilities remain essentially unchanged from initial postexcavation values. These anisotropic property changes suggest that flow would be more readily diverted around the drifts, decreasing the potential for seepage. This result was also obtained in a comparison of fully coupled thermal-hydrologic-mechanical simulations with thermal-hydrologic simulations (in which the stress-induced property changes were neglected). The reduction in vertical permeability appeared to give rise to less water reaching the drift wall, decreasing the potential for seepage.

2.4 SUMMARY OF BOUNDARY CONDITIONS IMPORTANT TO IN-DRIFT CHEMICAL MODELS

The discussion above provides process model results and corroborative modeling of tests and experiments that provide primary boundary conditions to the in-drift chemical models discussed in Section 4. The model results presented above provide two primary pieces of information for use in in-drift chemistry analyses. First, the thermal conditions at the drift wall when seepage is predicted to enter the drifts (i.e., when temperature is less than 100°C), along with the timing of when seepage is expected to flow through the drift wall (see Figure 2-12). Second, the quantitative prediction of in-drift temperatures and relative humidities through time (see Figure 2-11).

This information, when coupled with the results from Section 3 (i.e., the predicted composition of seepage at the drift wall through time), allows for the prediction of the evaporated seepage chemistries discussed in Section 4.1. Figure 2-11 shows the environmental boundary conditions in the drift that drive the formation of brines from deliquescent salts present in dusts on the waste packages (Section 4.2).



Source: BSC 2003h, Figures 7.4.3-2b and 7.4.3-3.

NOTE: (a) Simulated changes in absolute air permeability caused by the combined effect of moisture redistribution and stress-induced changes in intrinsic permeability at the DST after 12 months of heating, expressed in terms of permeability correction factor ($F_k = k/k_i$); (b) an example of a comparison to measured data. TM – thermal-mechanical; TH – thermal-hydrologic; THM – thermal-hydrologic-mechanical.

Figure 2-14. Thermal-Hydrologic-Mechanical Model Results

INTENTIONALLY LEFT BLANK

3. EVOLUTION OF NEAR-FIELD WATER AND GAS CHEMISTRY IN THE NEAR-FIELD HOST ROCK

The evolution of water and gas chemistry in the near-field host rock controls the composition of potential seepage water and the associated gas-phase composition in the emplacement drifts. Thermal-hydrologic-chemical coupled processes in the host rock relate the transport of heat, gas, and liquid water, with chemical speciation, dissolution, and precipitation reactions, and potential changes in hydrologic properties. The following sections describe the conceptual model, technical basis, and process model results for predicting thermal-hydrologic-chemical processes in the near field. More detailed information can be found in *Drift-Scale Coupled Processes (DST and THC Seepage) Models* (BSC 2003c). The results of this process model become a principal boundary condition (i.e., the composition of seepage at the drift wall) to the model that predicts the chemical evolution of seepage in the drift (see Section 4.1).

3.1 CONCEPTUAL UNDERSTANDING OF THE EVOLUTION OF NEAR-FIELD WATER AND GAS CHEMISTRY

The geologic setting at Yucca Mountain has been extensively studied using surface outcrop studies, borehole investigations, and the ESF. The stratigraphy at Yucca Mountain is generally described in terms of the lithologic characteristics of the rock units. Comprehensive models of the stratigraphy and geologic structure (BSC 2002c), mineralogy (BSC 2002d), and other rock properties (BSC 2003o) have been prepared to summarize the state of knowledge for site characteristics. Thermal-hydrologic-chemical models developed to examine flow and transport at Yucca Mountain use the derived hydrogeologic stratigraphy based on the degree of welding and hydrologic properties of the lithostratigraphic units. This information has been used, where appropriate, in the formulation of predictive models.

Matrix pore-water composition is an important input to the coupled chemical process models for the host rock (see Sections 3.3.1 and 3.3.2). *Drift-Scale Coupled Processes (DST and THC Seepage) Models* (BSC 2003c, Section 6.2.2.1) discusses the conceptual model for initial pore-water and pore-gas chemistry used in THC seepage modeling. The conceptual model presented in this report to explain the aqueous chemistry and background $^{36}\text{Cl}/\text{Cl}$ isotopic ratios in the ESF holds that percolating water passes mostly through the rock matrix of the Paintbrush nonwelded (PTn) hydrogeologic unit. The PTn unit corresponds to the lithostratigraphic units from the top of the Tiva Canyon Tuff crystal-poor member vitric zone moderately welded subzone (Tpcpv2) to the bottom of the Topopah Spring crystal-rich member vitric zone moderately welded subzone (Tptrv2). After passing through the PTn the percolating water reverts to fracture-dominated flow in the Topopah Spring welded (TSw) hydrogeologic unit. The TSw unit corresponds to the lithostratigraphic units from the top of the Topopah Spring Tuff crystal-rich member vitric zone densely welded subzone (Tptrv1) to the bottom of the Topopah Spring Tuff crystal-poor member vitric zone densely welded subzone (Tptpv3). The TSw includes the repository host-rock intervals: the Topopah Spring Tuff upper lithophysal (Ttpul), middle nonlithophysal (Ttpmn), lower lithophysal (Ttpll), and lower nonlithophysal (Ttpln) units. The high matrix permeability and low fracture frequency within the nonwelded units comprising the PTn tend to homogenize flow and the composition of through-going waters. Thus the water that enters the TSw host rock has already acquired the chemical characteristics of matrix pore water from the PTn unit. As discussed by Levy et al. (1997, pp. 907 to 908), this seems to be true everywhere

except near large structural discontinuities in the PTn (i.e., faults in which percolating water passes more quickly through the PTn). Analyses of PTn pore waters, pore waters from the top of the TSw, and many Cl^- analyses of pore waters from the TSw host-rock units are consistent with this interpretation (Sonnenthal and Bodvarsson 1999, pp. 140 to 141).

Matrix pore waters from the TSw and PTn have higher concentrations of anions and cations than perched waters above the PTn, which is consistent with the concept that the pore waters have flowed through the PTn matrix. Perched water is not observed in the host-rock intervals, and fracture water is very scarce compared to matrix pore water, so it is reasonable to regard the initial composition of fracture waters to be the same as that in the rock matrix in all hydrogeologic units. At or near the ground surface, there are additional geochemical and transport processes, such as evapotranspiration and biologically mediated reactions, that are not modeled explicitly but can be accounted for in the boundary conditions used for modeling coupled processes in the host rock hundreds of meters below.

Thermal-Hydrologic-Chemical Processes—The chemical evolution of waters, gases, and minerals is intimately coupled to the thermal-hydrologic processes (i.e., boiling, condensation, and drainage) discussed in Section 2. The distribution of liquid water determines where mineral dissolution and precipitation can occur and where there can be direct interaction (via diffusion) between matrix pore waters and fracture waters. Figures 2-2 and 3-1 show relationships between thermal-hydrologic and geochemical processes in the zones of boiling, condensation, and drainage in the rock mass around the emplacement drifts.

The effects of thermal-hydrologic processes on water chemistry depend on the intrinsic characteristics of the dissolved species and the types of chemical reactions in which they are involved. Conservative species (i.e., nonreactive and nonvolatile) such as Cl^- become concentrated in waters undergoing vaporization or boiling, but are essentially absent from the vapor condensing in the fractures. Therefore, the concentrations of conservative species in condensate waters are determined by the extent of mixing with background fracture waters and matrix pore waters. In addition, concentrations of aqueous species such as Ca^{2+} are also affected by mineral dissolution or precipitation reactions and by exchange or alteration reactions involving zeolites, clays, or feldspars.

Retrograde calcite solubility (less soluble at higher temperature), and prograde solubilities of other minerals such as silica (more soluble at higher temperatures) cause differences in the distribution of calcite and siliceous phases (Figure 3-1). Precipitation of amorphous silica or a similar phase tends to be confined to a narrower zone where evaporative concentration exceeds the solubility. In contrast, calcite tends to precipitate at elevated temperature and where CO_2 has exsolved and tends to dissolve where there is lower pH. Alteration of feldspars to clays and zeolites tends to be most rapid in the boiling zone because of increased solubility (as well as having higher dissolution and precipitation rates) at higher temperatures (Lasaga 1998, p. 66).

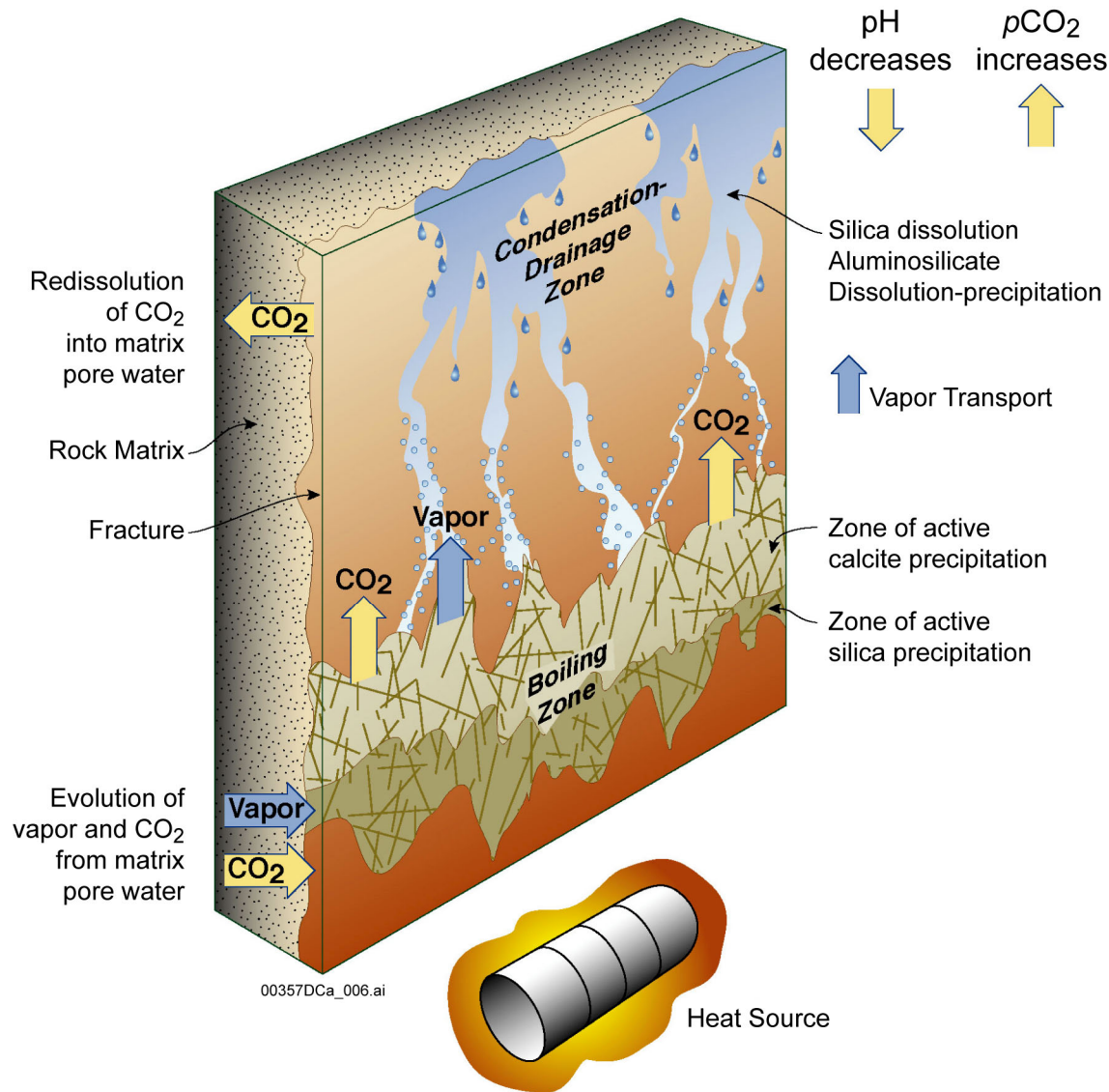


Figure 3-1. Fracture–Matrix Interface, Showing the Relation between Thermal-Hydrologic Processes and Geochemical Processes

When chemical species are transported in fracture waters at rates greater than the rate of equilibration with the rock matrix, the result is disequilibrium between waters in fractures and matrix. The disequilibrium can change the prevailing mineral assemblage and lead to differences in reaction rates. Because the system is unsaturated and undergoes boiling, the transport of gaseous species is important. The separate yet interacting processes in the fractures and the rock matrix involve geochemical, hydrologic, and thermal processes that are incorporated in a dual-permeability modeling approach. In this approach, each location in the model is represented by both matrix and fracture grid blocks, each with its own pressure and temperature, liquid saturation, water and gas chemistry, and mineralogy.

An aspect of the chemical system that is particularly important to simulation of thermal testing and repository heating is the exsolution (i.e., dissolution) of CO₂ from liquid water as temperature increases. Where boiling occurs, exsolution of CO₂ causes a local increase in pH.

Where vapor enriched in CO₂ is transported and condenses, there is a decrease in pH. The extent to which the pH is shifted depends on the rate of mineral–water reactions that can buffer the change. Because the diffusivities of gaseous species are several orders of magnitude greater than those of aqueous species, and because the advective transport of gases is more rapid than that of liquids in the environment, the region where CO₂ exsolution affects water and gas chemistry will be larger than the region affected by the transport of aqueous species.

Effects of Infiltration and Climate Changes—Early in the thermal evolution of the repository (dryout regime described in Section 1), the chemistry of the host rock around the emplacement drifts will be strongly influenced by the chemistry of ambient fracture and matrix pore water, affected by boiling, condensation, and mineral–water–gas reactions. Once the peak rock temperatures have subsided (transition and low-temperature regimes), natural percolation flux will mix with the condensate above the drifts and eventually rewet the dryout zone. The composition of the percolating waters (before mixing) could be similar to that presently found in the host rock as matrix pore water, or it could be more dilute reflecting wetter climates. Future changes in the percolation flux will also affect the extent of mineral precipitation and dissolution, because of dilution effects and changes in the fluxes of dissolved species to the near field.

Hydrologic Property Changes in Fractures and Matrix—Mineral precipitation and dissolution in the fractures and matrix have the potential to modify the porosity, permeability, and unsaturated hydrologic properties of the host rock. Because the molar volumes of minerals created by hydrolysis reactions (e.g., feldspars reacting with water to form zeolites or clays) are commonly greater than the molar volumes of the reactant minerals, the reactions lead to porosity reduction. The extent of mineral–water reaction is controlled by the surface areas of the mineral phases in contact with water, which is sensitive to heterogeneity in the distribution of minerals in the fractures. Therefore, changes in porosity and permeability may also be heterogeneously distributed. Other factors that could lead to heterogeneity in property changes are the distribution of liquid saturation in fractures and the proportion of fractures having actively flowing water.

3.2 TECHNICAL BASIS FOR UNDERSTANDING AMBIENT AND THERMALLY ALTERED NEAR-FIELD CHEMISTRY

The technical basis for thermal-hydrologic-chemical modeling includes mathematical process descriptions, parameterized using site-specific measurements in addition to chemical constants and data supported by the chemical literature (e.g., thermodynamic and kinetic constants, and diffusion coefficients). Site characteristics that have been investigated and used for model development include the initial water and gas chemistry, initial mineralogy, mineral volume fractions, reactive surface areas, and boundary conditions. Further confidence in model predictions is obtained from laboratory and field-testing to refine and validate the methodology and test various combinations of uncertain input data. This section discusses the rationale for the choices of initial water compositions, which are found to be important inputs, followed by the comparison of various model predictions to observations from the DST.

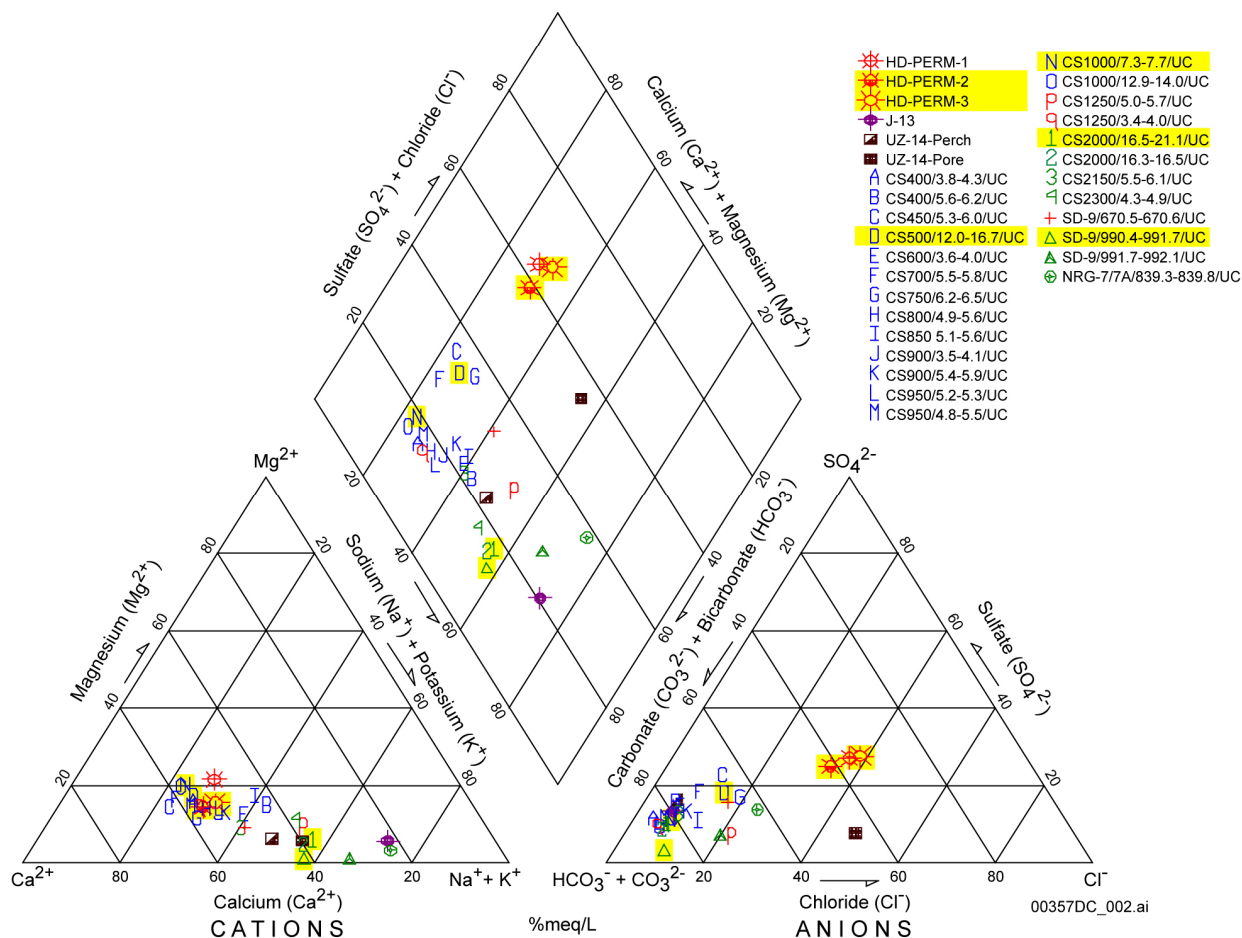
3.2.1 Initial Pore-Water Chemistry

The initial composition for matrix pore water could be selected from pore-water chemistry in the unsaturated zone at or above the repository horizon, perched water, or the saturated zone. Perched waters are generally more dilute than unsaturated zone pore waters. Isotopic compositions ($^{36}\text{Cl}/\text{Cl}$, $^{18}\text{O}/^{16}\text{O}$, D/H, ^{14}C as percent modern carbon) and Cl^- concentrations of the perched waters suggest that they have a large proportion of late Pleistocene–early Holocene water (Levy et al. 1997, p. 906; Sonnenthal and Bodvarsson 1999, pp. 107 to 108). The saturated zone waters are also more dilute than pore waters, and neither saturated zone waters nor perched waters reflect calculated CO_2 partial pressures consistent with CO_2 concentrations in gas measured in the unsaturated zone in repository units. The saturated zone and perched-water compositions like J-13 water are, therefore, deemed poor candidates as initial input water compositions. Preference is given, instead, to actual pore waters from unsaturated rocks within or above the repository units.

During the initial stages of thermal-hydrologic-chemical model development for the DST, a few pore-water samples were ultracentrifuged from core samples that originated in the middle nonlithophysal unit (Tptpmn) near the DST. Nearly complete chemical analyses were obtained for three samples (HD-PERM-1, HD-PERM-2, and HD-PERM-3) using core from one general location yielding similar water compositions. Two of these analyses were composited for use as an input water composition in the model. More recently, additional pore-water samples from the repository host-rock units have been obtained from core collected in the Cross-Drift and in boreholes SD-9 and NRG-7/7A. These water compositions are discussed in detail below.

Measured compositions for the more recent series of matrix pore waters are depicted on a Piper diagram in Figure 3-2 along with the HD-PERM samples, perched waters, pore water from similar depths (base of the nonlithophysal Tptpln unit) in borehole UZ-14, and groundwater from well J-13. This figure summarizes characteristics for waters from the site and suggests a wide range of potential initial water compositions. The HD-PERM samples lie at one endpoint of the range (calcium-sulfate-chloride-type waters), and groundwater from well J-13 defines another endpoint (sodium-bicarbonate type). Figure 3-2 also shows that samples from deeper units tend to exhibit higher Na^+ (plus K^+) concentrations relative to Ca^{2+} (plus Mg^{2+}) and a higher proportion of total aqueous carbonate (relative to Cl^- and SO_4^{2-}) compared to shallower waters (see also Yang et al. 1996, p. 13). These trends are probably caused by the hydrolysis of volcanic glass and feldspars and exchange reactions with zeolites below the host-rock units (e.g., BSC 2002b; Vaniman et al. 2001).

Differences in the proportions of the various cations and anions (i.e., ratios not concentrations) have an important influence on the types of evaporated solutions or brines that could develop as a result of evaporation or boiling (BSC 2003d, Section 6). Should these waters seep onto the surface of a hot waste package or drip shield, the composition of the resulting brine can affect the initiation of corrosion and corrosion rates (BSC 2003e). Therefore, the selection of input water compositions for thermal-hydrologic-chemical modeling should take into account the end-brine compositions of these waters and the natural variability of pore-water compositions in the host-rock units (Figure 3-2).



Source: BSC 2003c, Figure 6.2-4.

NOTE: Samples labeled HD-PERM are pore waters from the Tptpmn unit in Alcove 5 of the ESF. Sample identifiers starting with CS represent pore waters from the Cross-Drift, listed in order of increasing distance (feet) into the drift (down stratigraphy), with labels reflecting lithostratigraphic units as follows: Tptpul (capitals A-O), Tptpmn (lower case p-q), and Tptpll (numbers 1-4). Sample identifiers starting with SD-9 and NRG-7 represent pore waters from boreholes with the same names and show the sampling interval in feet from the ground surface. The first SD-9 sample at 670 ft is from the base of the Tptpul; the others are from the Tptpll. The NRG-7 sample is from the Tptpmn. Highlighted samples were chosen for this study (see text).

Figure 3-2. Piper Plot of Water Compositions from Repository Units

The following samples represent the range of compositions and are assigned arbitrary identifiers (W0, W5, etc.):

- W0: HD-PERM water from the Tptpmn unit in Alcove 5. This is an average composition (from Samples HD-PERM-2 and HD-PERM-3). The HD-PERM samples plot higher than other pore waters on the diamond-shaped area in Figure 3-2, bounding the range of compositions in the calcium-sulfate-chloride field.
- W5: Sample CS-1000/7.3-7.7/UC from the base of the Tptpul lithostratigraphic unit in the Cross-Drift. This sample was selected because it exhibits one of the highest $(Ca^{2+} + Mg^{2+})/(Na^{+} + K^{+})$ ratios of the cross-drift samples and better charge balance than other samples with high $(Ca^{2+} + Mg^{2+})/(Na^{+} + K^{+})$ ratios.

- W4: Sample CS-2000/16.5-21.1/UC from the Tptpll lithostratigraphic unit in the cross-drift. This sample exhibits the lowest $(Ca^{2+} + Mg^{2+})/(Na^{+} + K^{+})$ ratio of the cross-drift samples and better charge balance than other samples of similar composition. It also contains a higher F^{-} concentration than the other samples.
- W6: Sample SD-9/990.4-991.7 from the Tptpll lithostratigraphic unit in borehole SD-9. This sample exhibits a low $(Ca^{2+} + Mg^{2+})/(Na^{+} + K^{+})$ ratio nearly identical to that of W4 but a better charge balance than W4 and a higher NO_3^{-} concentration compared to most other samples.
- W7: Sample CS500/12.0-16.7 from the Tptpul lithostratigraphic unit in the cross-drift. This sample plots between the HD-PERM waters and W5 on Figure 3-2, further capturing the variability of water compositions.

Compositions of the waters are given in Table 3-1.

3.2.2 The Drift Scale Test and Supporting Laboratory and Field Investigations

Three field thermal tests (Large Block Test, Single Heater Test, and DST) and several laboratory experiments have been performed that help define the role of thermal-hydrologic-chemical processes in the evolution of water and gas chemistry in the near-field, as well as effects on flow and, thus, potentially seepage. By far the most informative and realistic experiment for evaluation of thermal-hydrologic-chemical processes has been the DST. The other tests are documented in *Thermal Testing Measurements Report* (BSC 2002a) and are not discussed further here.

The DST was the second underground thermal test to be carried out in the ESF. The purpose was to investigate the coupled thermal, hydrologic, chemical, and mechanical processes that can take place in unsaturated, fractured tuff over a wide range of temperatures (from 25°C to 200°C) (see Section 2.2.2). Details regarding the DST layout, borehole orientations, operation of the test, and measurements performed (as well as their uncertainties) are published elsewhere (BSC 2002a, Section 6.3; CRWMS M&O 1998).

This section presents chemical data that have been collected from the DST and used for refinement and validation of thermal-hydrologic-chemical process modeling.

DST Aqueous Chemistry—During the 4-year heating phase water samples were periodically collected from multiple locations throughout the DST block and analyzed in the laboratory for metals, anions, and certain isotopes. Boreholes were instrumented to collect both water and gas samples. The sampled intervals were located where different thermal-hydrologic-chemical processes occurred at different times (boiling, dryout, condensation, dissolution, and precipitation). The first water samples were collected 6 months after heating began with subsequent sampling every few months (as indicated). A summary of the water sampling, chemical analyses, and other observations for samples collected throughout much of the heating phase is presented in *Thermal Testing Measurements Report* (BSC 2002a, Section 6.3.4.1). The following discussion is abstracted from that source.

Table 3-1. Input Pore-Water Compositions

Sample ID	HD-PERM ^a (Alcove 5)	ECRB-SYS-CS1000/7.3- 7.7/UC ²	ECRB-SYS-CS2000/16.5- 21.1/UC ^b	SD-9/990.4-991.7/UC ^b	ECRB-SYS-CS500/12.0- 16.7/UC ^b
Lithostratigraphic Unit	Ttptmn	Ttptul (base)	Ttptll	Ttptll	Ttptul
Simulation Water ID	W0	W5	W4	W6	W7
Water Input Type	Fract/Matrix	Fract/Matrix	Fract/Matrix	Fract/Matrix	Fract/Matrix
Temperature (°C)	Boundary	Boundary	Boundary	Boundary	Boundary
Temperature (°C)	25	25	25	25	25
pH (measured)	8.31	7.6	7.4	7.9	8.0
pH (calc) ^c	—	8.062	8.175	8.001	8.073
Na ⁺ (mg/L)	61.5	39	130	84	57
K ⁺ (mg/L)	8	7.6	10.6	7.9	10.3
Ca ²⁺ (mg/L)	101	94	82	56	120
Mg ²⁺ (mg/L)	17	18.1	5.3	0.9	19.3
SiO ₂ (mg/L)	70.5	42.0	48	50	49
Cl ⁻ (mg/L)	117	21	26	23	54
SO ₄ ²⁻ (mg/L)	116	36	39	10	78
HCO ₃ ⁻ (mg/L, measured)	—	333	382	313	286
HCO ₃ ⁻ (mg/L, calc) ^d	200	395	515	335	412
NO ₃ ⁻ (mg/L)	6.5	2.6	4.2	17	6.1
F ⁻ (mg/L)	0.86	3.4	6.01 ⁱ (11)	2.5	4.8
Al ³⁺ (calc) ^e (molal)	6.173 × 10 ⁻¹⁰	1.112 × 10 ⁻⁹	1.082 × 10 ⁻⁹	1.00 × 10 ⁻⁹	8.061 × 10 ⁻¹⁰
Fe ³⁺ (calc) ^f (molal)	1.155 × 10 ⁻¹²	5.000 × 10 ⁻¹³	1.143 × 10 ⁻¹²	1.14 × 10 ⁻¹²	1.138 × 10 ⁻¹²
log(pCO ₂) ^g (bar)	-3.1	-2.5	-2.5	-2.5	-2.5
CO ₂ (ppmv, approx) ^h	900	3100	3100	3100	3100

Source: BSC 2003c, Table 6.2-1.

NOTES: ^a Average of Ttptmn pore-water analyses ESF-HD-PERM-2 (30.1' to 30.5') and ESF HD-PERM-3 (34.8' to 35.1'); DTN: M00005PORWATER.000.^b Pore-water analyses from the ECRB Cross-Drift and borehole SD-9 reported with DTN: GS020408312272.003.^c pH calculated by speciation at the temperature and log(pCO₂) shown (using SOLVEQ/CHILLER V1.0 (LBNL 1999)).^d Total aqueous carbonate as HCO₃⁻, calculated from charge balance computed by speciation at the temperature and pH shown (at measured pH for HD-PERM sample; at calculated pH for other samples) (using SOLVEQ/CHILLER V1.0 (LBNL 1999)). These are slightly different values than values calculated from charge balance reported in DTN: GS020408312272.003, because the latter do not include the effect of speciation.^e Calculated by equilibrating with illite at the temperature and calculated pH shown (using SOLVEQ/CHILLER V1.0 (LBNL 1999)) (BSC 2003c, Section 6.2.2.1).^f Calculated by equilibrating with hematite at the temperature and calculated pH shown (using SOLVEQ/CHILLER V1.0 (LBNL 1999)) (BSC 2003c, Section 6.2.2.1).^g Partial pressure of carbon dioxide (pCO₂) set at values shown except for HD-PERM sample at 25°C (calculated in this case) (BSC 2003c, Section 6.2.2.1).^h Approximate conversion assuming 1 bar total pressure.ⁱ Value shown is calculated at equilibrium with fluorite at 25°C. Value in parentheses is measured.

Compositions shown are those used for initial fracture and matrix water (column labeled "Fract/Matrix") and infiltration water at the model top boundary (column labeled "Boundary").

Although water collection temperatures were recorded in the field, they do not represent in situ borehole temperatures (which are better inferred from nearby temperature sensor measurements). Temperature-dependent field measurements (i.e., pH, alkalinity, total dissolved solids, and electrical conductivity) were determined for the reported temperature. Water samples were analyzed for major ion chemistry and isotope analyses. Metal and anion concentrations were analyzed by inductively coupled plasma-atomic emission spectroscopy and ion chromatography, respectively.

Chemical analyses are available for water samples collected from three borehole arrays spanning the heated region of the test and from boreholes located above and below the heated drift (Figure 2-3). Many water samples were analyzed for which chemistry was consistent with mineral-water interactions, particularly involving fracture-lining minerals such as silica polymorphs and calcium carbonate. Such waters were generally collected from intervals at below boiling and boiling (approximately 96°C) temperatures. These waters were readily discerned from very dilute waters resulting from local condensation (including within the sampling lines) which often originated from intervals at above-boiling temperatures.

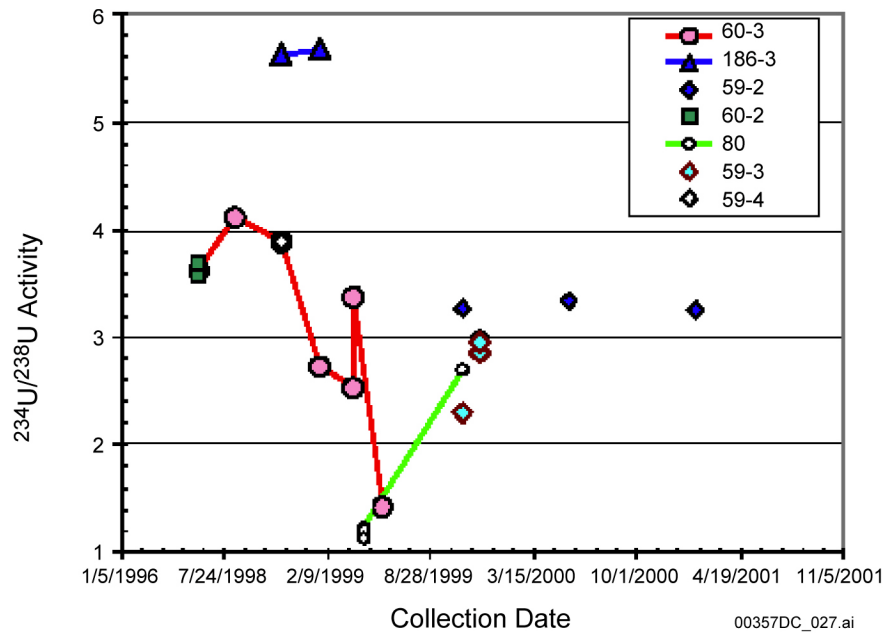
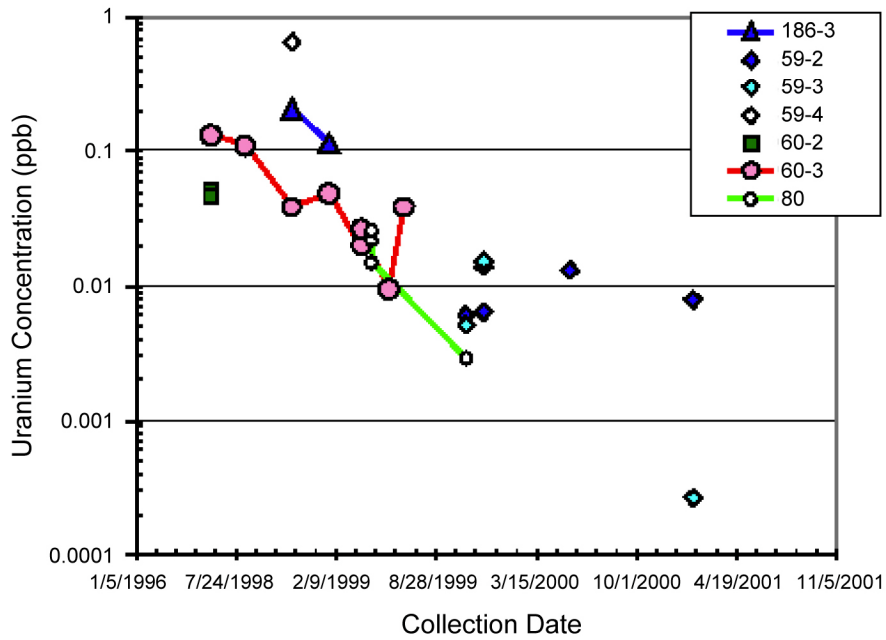
The following trends were observed in formation waters. Measured pH values ranged from about 6.1 to 8.3. Concentrations for specific analytes were variable, but trends were similar. In general, SO_4^{2-} and Cl^- were the dominant anions; $\text{SiO}_2(\text{aq})$ was the principal dissolved species, followed in abundance by Ca^{2+} and Na^+ cations (with similar concentrations). Present, but in lower concentrations, were K^+ , Mg^{2+} , strontium, and NO_3^- .

A small number of samples yielded distinctive, concentrated waters. Borehole 59-4 samples (November 1998 and January 1999) in particular appeared to be evaporatively concentrated, and boreholes 59-2 (August 1999) and 76-3 (October 1999) yielded waters with somewhat elevated concentrations of the principal analytes (BSC 2002a, Section 6.3.4.1).

Strontium and Uranium in DST Water Samples—This section discusses strontium and uranium isotopic data obtained from a subset of water samples collected from the DST during the heating phase (BSC 2002a, Section 6.3.4.1). Measurements of strontium and uranium concentrations and isotopic compositions in water samples may provide information on mineral reactions and water flow paths occurring as the block is heated during the test. In addition, isotopic analyses can provide evidence for interaction of test-produced water with the engineered materials introduced into the test block during construction. Uranium and strontium concentrations were determined by isotope dilution mass spectrometry, and the isotopic ratios were determined by thermal-ionization mass spectrometry (DTNs: GS011108312322.008; GS011108312322.009).

Waters from DST locations sampled at successive times during the heating phase show a systematic decrease in uranium concentration with time (Figure 3-3). Temporal changes in $^{234}\text{U}/^{238}\text{U}$ are not as systematic. The general trends of decreasing uranium concentration with time are consistent with increasing proportions of condensate mixed in with pore water that was mobilized during the DST heating phase. The wide range in uranium concentrations observed in Topopah Spring pore waters makes it difficult to quantify the mixing fraction of condensate; however, all but two samples with uranium concentrations greater than 0.15 $\mu\text{g}/\text{L}$ appear to contain at least some condensate. Samples with uranium concentrations less than 0.01 $\mu\text{g}/\text{L}$

probably consist of more than 90 percent condensate. Even though these samples are particularly susceptible to contamination, most still have $^{234}\text{U}/^{238}\text{U}$ activity ratio within the range of observed pore water.



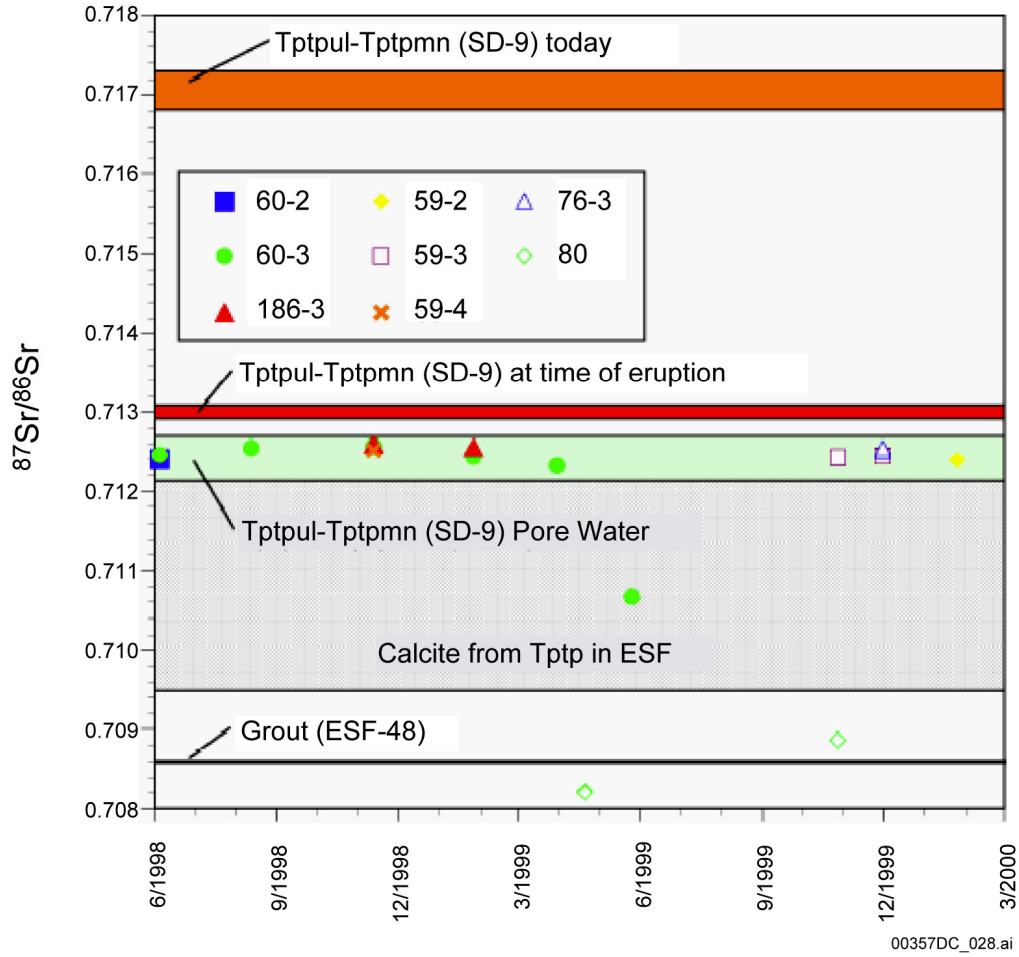
Source: BSC 2002a, Figure 6.3.4.4-2.

Figure 3-3. Uranium Concentration and $^{234}\text{U}/^{238}\text{U}$ Activity Ratios in Drift Scale Test Samples Plotted versus Collection Date

Only four DST samples have $^{234}\text{U}/^{238}\text{U}$ activity ratios outside the expected range. Water from 60-3 collected on May 25, 1999 has a low uranium concentration as well as a $^{234}\text{U}/^{238}\text{U}$ activity ratio of 1.425. Contamination with rock or anthropogenic material is likely to add uranium with a $^{234}\text{U}/^{238}\text{U}$ activity ratio near secular equilibrium value of 1.0. This same sample also shows evidence of contamination of strontium (see below).

Similar to uranium, the strontium concentrations in the test waters approach the values estimated for pore water and decrease with time. For example, borehole 60-3 water samples reached a strontium concentration about 1,000 times less than the zone produced initially. Figure 3-4 shows the variation of strontium isotopic compositions in the test waters compared to various reservoirs of strontium in the DST block. The orange and red bands show the strontium isotopic compositions of the Topopah Spring Tuff (middle nonlithophysal and upper lithophysal zones) today and at the time of their deposition, respectively. The green band is the range of $^{87}\text{Sr}/^{86}\text{Sr}$ in pore water; these data are from borehole USW SD-9, which is the closest vertical borehole to the DST block. Grout introduced into the DST block during emplacement of borehole instrumentation has also been measured and is shown by the black line at an $^{87}\text{Sr}/^{86}\text{Sr}$ value of 0.7086. The grout contains over 800 ppm strontium, providing a potentially important added source.

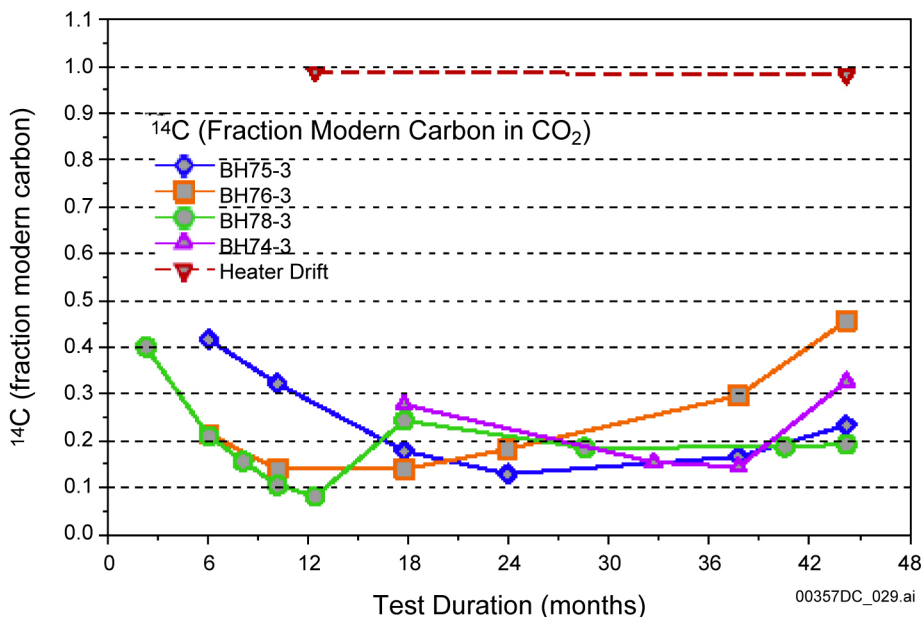
Most of the water obtained during the DST to date has $^{87}\text{Sr}/^{86}\text{Sr}$ values within the range of pore water. A very dilute sample obtained from borehole 60-3 falls outside the range of pore water. The most significant deviations from pore water are exhibited by water from borehole 80. These samples apparently have interacted with the grout used to emplace the liner in this borehole. This is strong evidence of contamination. It is notable that the chemistry of these waters does not show additional evidence of interaction with grout.



Source: BSC 2002a, Figure 6.3.4.4-3.

Figure 3-4. Strontium Isotope Ratio Compositions of Water Samples Collected from Drift Scale Test Boreholes Compared to Compositions of Pore Water, Rock, Calcite, and Grout

DST Gas Chemistry—Gas samples were periodically collected from the hydrology boreholes (Figure 2-3) during the heating phase. These samples were analyzed for CO₂ concentration carbon isotope ratios including ¹⁴C (Figure 3-5), and water vapor fractions were analyzed for stable hydrogen and oxygen isotope ratios. The CO₂ concentration data were an important part of the DST thermal-hydrologic-chemical model validation (Section 3.3.2). ¹⁴C isotope ratios plotted in Figure 3-5 show that while the heater drift air freely exchanged with tunnel ventilation air, the samples collected from boreholes in the rock mass were unaffected by exchange with tunnel ventilation air (BSC 2003c, Section 7.1.14). The CO₂ concentration data were used for model–data comparisons (BSC 2003a, Section 7.1.10.3).



Source: BSC 2003c, Figure 7.1-42.

NOTE: Two samples collected from the heated drift were also analyzed. Measured activities of ¹⁴C are expressed as a fraction of modern carbon.

Figure 3-5. Measured Activities of ¹⁴C in CO₂ from Gas Collected in Several Hydrology Boreholes over Most of the Heating Phase of the Drift Scale Test

DST Pretest Mineralogical and Petrologic Analyses—A pretest mineralogical baseline was acquired from natural fractures sampled in drill core. Mineralogical investigations in the DST were guided by previous examination of posttest overcores from the Single Heater Test (BSC 2002a, Section 6.2.4.2) and by quantitative X-ray diffraction of crushed tuff samples from a laboratory hydrothermal column test (Lowry 2001, p. 29). These studies found no detectable mineralogical alteration of the rock matrix at the conclusion of the hydrothermal tests. Evidence of alteration was limited to fractures and borehole surfaces of the Single Heater Test and to the external surfaces of crushed-tuff particles from the column test.

Mineralogical characterization of pretest ambient natural fracture surfaces was performed on drill core from the DST block using stereoscopic examination supplemented by scanning electron microscope and X-ray diffraction. The DST block contains intervals dominated by vapor-phase features and other intervals where vapor-phase features are not prominent. As seen in the drill core, the dominant vapor-phase features are partings and stringers that dip eastward at

low angles parallel to the rock foliation. Both the partings and stringers are fractures lined with crystalline silica and feldspar fracture coatings, commonly called vapor-phase minerals.

Reconnaissance core suggested that the fracture coatings are different in the vapor-phase and non-vapor-phase intervals, which was confirmed by detailed study. Based on this observation, detailed fracture-mineral studies were performed in two core intervals representing each type. Mineral abundances on the fracture surfaces were determined for stellerite, manganese minerals, crystalline silica and feldspar (combined), clay (probably including minor mordenite), and calcite (BSC 2002a, Section 6.3.4.3; DTN: LA9912SL831151.002). Additional natural minerals observed in small quantities or by scanning electron microscope included mordenite, pyrite, and possible hematite. For the minerals included in the inventory, differences in abundance of crystalline silica plus feldspar and in calcite between the vapor-phase and non-vapor-phase intervals were documented.

DST Mineralogical Analyses of Thermal Test Samples—Thermally driven mineralogical changes were investigated in the walls of boreholes where fracture water collected and evaporated during the test. Investigators learned from the Single Heater Test that mineralogic sampling while a test is in progress is more valuable than collecting samples only after the test is finished. To realize this goal for the DST, a sidewall-sampling tool was used. The tool was deployed in existing boreholes, targeting intervals of fractured rock that were identified from borehole video images. A total of 14 sidewall core samples were collected from three boreholes during the transition from the heating phase to cooling. Analysis of these samples provided information on mineralogic changes in the boiling zone, including elemental abundances and chemical, textural, and mineralogic characteristics (DTN: LA0201SL831225.001).

Sidewall cores collected during the test revealed new mineral deposits on borehole surfaces and on the surfaces of fractures that intersect the boreholes. New mineral deposits were common on the borehole-wall surfaces because the boreholes acted as preferential pathways for fluid flow during the heating phase. Deposits were less common and quantities of new minerals less abundant on the natural fractures from within core samples.

Mineral deposition within the boiling zone is documented by samples from borehole 54 (ESF-HD-CHE-3). The three products observed so far are tentatively identified as amorphous silica, gypsum, and calcite (DTN: LA0201SL831225.001). The tentative identifications of gypsum and calcite are based on identifications of these phases by X-ray diffraction as products of the Single Heater Test (DTN: LA0009SL831151.001). The silica deposits exhibit considerable textural heterogeneity, perhaps because some were deposited when the collection site was in the condensation zone and others were deposited when boiling-zone dryout conditions were reached.

Examples of possible condensation zone silica deposition above the heated drift have been identified. In one example, a fracture surface is completely coated by terrace-like silica deposits up to a few micrometers thick. In another example, several discoid silica deposits (up to about 20 μm across) rest on a surface of earlier-deposited discs cemented and largely obscured by silica particles about 1 or 2 μm across. In both examples, the deposits were built up during multiple episodes of silica deposition, perhaps during the passage of numerous pulses of silica-saturated water.

Very thin (less than 0.5 μm thick), curled silica sheets may be products of final dryout in the boiling zone. There is no textural evidence of successive buildup in the silica sheets. Also lying atop the earlier silica deposits or on preheating fracture surfaces are scattered deposits of prismatic gypsum and rounded mounds of calcite.

Studies of preheating core from the Single Heater Test showed that some of the natural fracture minerals have experienced dissolution caused by ancient or ongoing geochemical processes. This complicates the effort to document mineral dissolution resulting specifically from the DST. To provide documentation of natural alteration, samples of preheating drill core from approximately the same locations as sidewall samples were examined by scanning electron microscope. Images of the typical morphologies of natural fracture-coating minerals and rock-fracture surfaces were recorded. The majority of such documentation was devoted to stellerite because it is the single most abundant fracture-coating mineral.

The natural stellerite fracture coatings in preheating samples did not show clear evidence of dissolution. Stellerite in the sidewall core samples from the DST also showed no evidence of dissolution. The exception occurred on one fracture from the 66.5-ft (20.27-m) depth in borehole ESF-HD-CHE-3. In this location, a highly corroded stellerite crystal, several slightly to moderately corroded stellerite crystals, and a moderately corroded silica crystal were adjacent to or within a lobate deposit of amorphous silica (DTN: LA0201SL831225.001). At the time of sample collection, this sample came from within the boiling zone. However, the sampled rock volume had previously been within the condensation zone before the boiling zone moved to its position farthest away from the heaters. It is possible that the observed mineral dissolution and, perhaps, deposition occurred when the rock volume was in the condensation zone.

3.3 THERMAL-HYDROLOGIC-CHEMICAL PROCESS MODEL DEVELOPMENT AND RESULTS

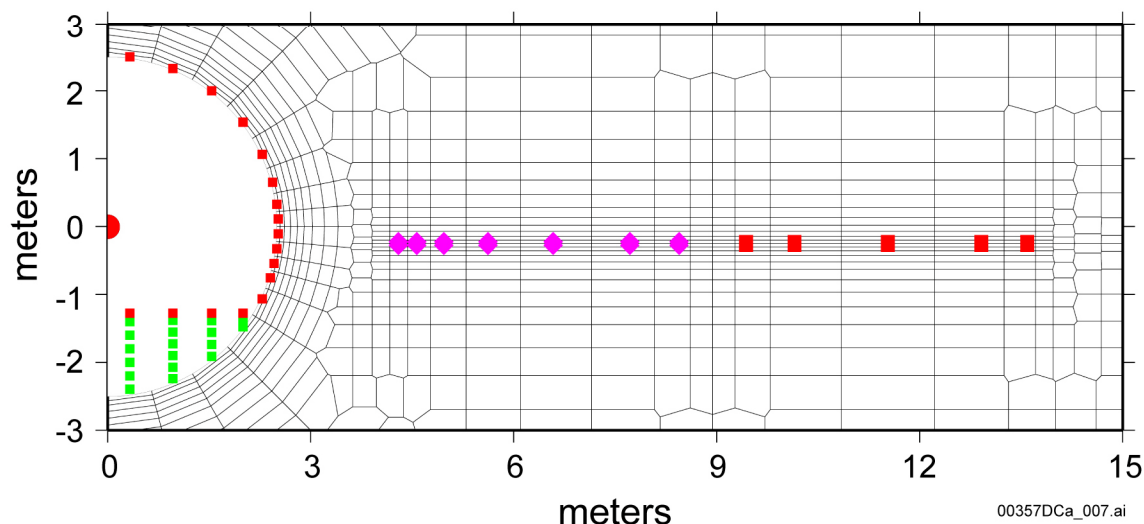
3.3.1 Drift Scale Test Thermal-Hydrologic-Chemical Model

The DST thermal-hydrologic-chemical model is a numerical model used to gain insight into processes taking place during heating of the unsaturated devitrified tuffs. It provides the main basis for extension of the approach to the drift-scale thermal-hydrologic-chemical seepage model (Section 3.3.2). Calibrated drift-scale hydrologic and thermal properties are used as inputs, but were developed separately based on repository data and not data specific to the DST. Modifications were made to the input thermodynamic data to capture aspects of the ambient-system pore-water chemistry. Other model adjustments specific to the DST were limited to adjusting the connectivity of the heated drift to the access drift in order to represent heat and vapor losses through the insulated bulkhead.

The primary objective of the DST is to obtain a more in-depth understanding of the thermal-hydrologic-mechanical-chemical coupled processes anticipated to exist in the local rock mass surrounding the repository. The DST was designed to measure coupled process behavior so that these data can be correlated to respective numerical simulations in comparative analyses. The measured coupled process behavior is considered representative because the coupled processes are thermally driven and the temperature range in the test block varies from ambient (25°C) to a maximum temperature (200°C) along the drift wall. Although some of the physical

features of the DST closely resemble the current design (the 5 m diameter of the heated drift and the 4.6-m-long floor/canister heaters), the DST design was never intended to fully replicate repository conditions. This approach is appropriate given the difficulty in replicating repository conditions, including the ongoing evolution of the design (e.g., the DST ground support system of rock bolts, wire mesh, and a cast-in-place concrete liner are outdated) and the heating duration (more than 1,000 years).

The two-dimensional dual-permeability grid for the DST represents a vertical cross section through the heated drift at a distance approximately 30 m from the insulated bulkhead separating the heated drift from the access drift (Figure 2-3). A typical numerical grid contains 4,485 gridblocks including those representing fracture and matrix continua (DTN: LB0101DSTTHGRD.001) (Figure 3-6). Connections between the interior of the heated drift and the heater test alcove included gridblocks designed to act as a bulkhead and as insulating material. Within the drift, heat is applied directly to the drift wall instead of explicitly representing the electric heaters and calculating heat transfer across the air within the drift. The DST includes a plane of linear wing heaters on each side of the drift that are represented by small gridblocks in the model. Small gridblocks are also used adjacent to the wing heaters and drift wall to capture the strong gradients in temperature and liquid saturation in these regions (Figure 3-6). Other details of the numerical formulation are given in *Drift-Scale Coupled Processes (DST and THC Seepage) Models* (BSC 2003c, Section 6).



Source: BSC 2003c, Figure 7.1-1c.

NOTE: Figure shows locations in the mesh constructed for modeling of central canister heater (red circle), wing heaters (purple diamonds and red squares), concrete inverts (green squares), and drift-wall blocks (small red squares). The full mesh extends symmetrically to the left and in all other directions. The top boundary is approximately 99 m above the drift center; the bottom boundary is approximately 157 m below the center.

Figure 3-6. Two-Dimensional Numerical Mesh for the Drift Scale Test Thermal-Hydrologic-Chemical Model

Simulations of thermal-hydrologic-chemical processes include coupling between heat, water, and vapor flow; aqueous and gaseous species transport; kinetic and equilibrium mineral–water reactions; and feedback of mineral precipitation–dissolution on porosity, permeability, and

capillary pressure (BSC 2003c). Aqueous species included in the model are H^+ , Ca^{2+} , Na^+ , K^+ , $SiO_2(aq)$, Mg^{2+} , Al^{3+} , Fe^{3+} , SO_4^{2-} , HCO_3^- , Cl^- , and F^- , and NO_3^- . Minerals considered include silica phases (cristobalite, quartz, tridymite, amorphous silica, and opal-CT), calcite, feldspars, smectites, illite, kaolinite, sepiolite, zeolites (including stellerite), fluorite, hematite, gypsum, and various salt phases. Treatment of CO_2 includes gas–water equilibration, diffusion, and advection. Simulations were performed using TOUGHREACT V3.0 (LBNL 2002).

Hydrologic and thermal initial and boundary conditions were derived from the unsaturated zone flow model. Models and data for the ambient geochemistry of the unsaturated zone at Yucca Mountain (i.e., chloride, strontium, calcium) support the infiltration rates used as boundary conditions for the unsaturated zone flow model (Sonnenthal and Bodvarsson 1999, p. 107; Liu et al. 2003; Xu et al. 2003). This confidence in the initial and boundary conditions in turn provides confidence in the DST thermal-hydrologic-chemical model.

The top and bottom model boundaries were set to constant temperature, pressure, and liquid saturation based on steady-state values obtained from simulations of a one-dimensional column extending from the ground surface to the water table. The top and bottom boundary of the two-dimensional model extends 150 m above and below the drift center. The percolation flux at the top boundary is approximately 0.5 mm/yr. The bottom boundary is open to gas and liquid flow. The side boundaries of the domain are located 81.5 m away from the drift center on each side (outside the test influence area) and are no-flux for mass and heat. The air pressure and temperature in the observation drift are set to constant values and therefore represent the temporal average response to tunnel pressure fluctuations. The heated drift wall is open to advection and conduction of heat and mass (i.e., air, water vapor, and CO_2).

Initial and boundary geochemical conditions were based on pore-water and mineralogical analyses. All aqueous and gaseous species concentrations in the rock were initially set to uniform values (BSC 2003c, Section 6.2.2.1). The heater alcove and observation drift CO_2 concentrations were fixed to approximately that of the atmosphere. The heated drift CO_2 concentration was initially set to the same value as that in the observation drift but was allowed to exchange CO_2 with the heater test alcove and with the surrounding rock. The initial pore-water chemistry is the HD-PERM water (W0) sample that was ultracentrifuged from rock core obtained adjacent to the DST. Other details regarding the use or modifications to these data are given in *Drift-Scale Coupled Processes (DST and THC Seepage) Models* (BSC 2003c, Sections 7.1.5 and 7.1.6).

Both the top and bottom boundaries are open to gas and aqueous species transport. The boundaries were also set so that no mineral reactions take place (and, therefore, no changes in aqueous species concentrations occur as a result of mineral–water reactions). Their volumes were set to extremely large values, so that they act essentially as constant concentration boundaries. The side boundaries are no-flux for gas and aqueous-species transport.

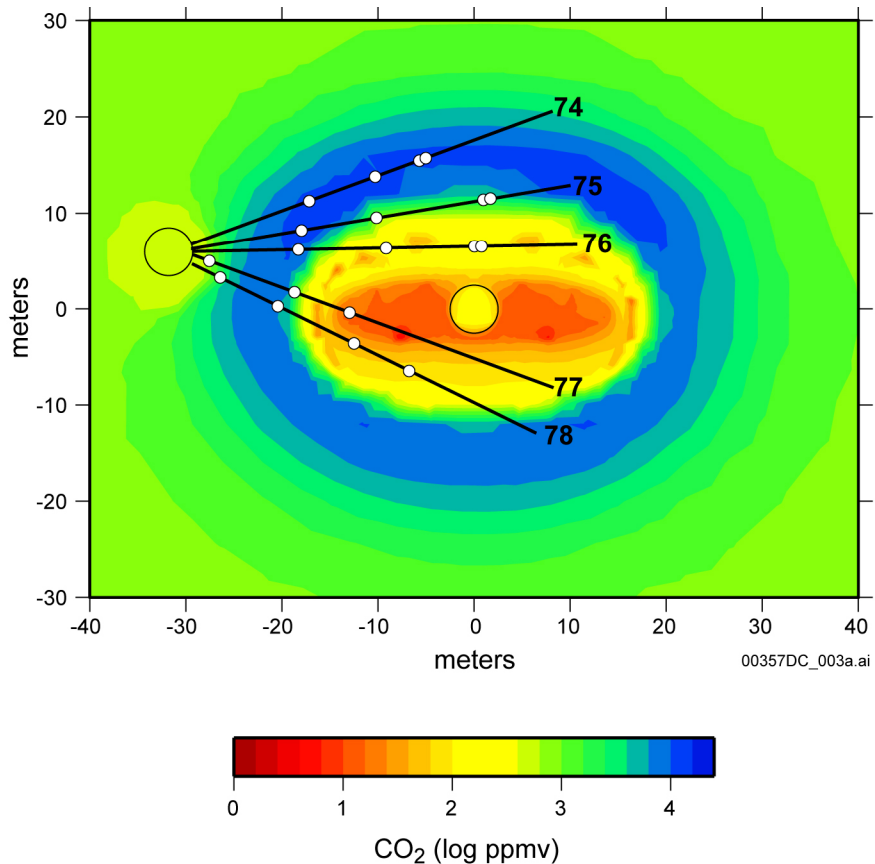
The following discussion provides a partial summary of model–data comparisons using DST results for comparison to the DST thermal-hydrologic-chemical model. Additional information on the sequence of model refinements, simulation of laboratory thermal-hydrologic-chemical experiments, and other validation exercises is given in *Drift-Scale Coupled Processes (DST and THC Seepage) Models* (BSC 2003c, Section 7).

3.3.1.1 Gas-Phase CO₂ Evolution

The concentration of CO₂ in the gas phase is a function of temperature, pressure, aqueous-phase chemistry, mineral–water reactions, and advective and diffusive transport. From a model validation standpoint, the strong effect of CO₂ partial pressure on water pH and the final brine composition formed upon evaporation gives importance to the analysis of CO₂ concentrations. Simulation results are compared to concentrations measured in gas samples taken from boreholes during the heating phase of the DST. CO₂ concentrations in gases collected from the DST also provide a qualitative measure of the influence of atmospheric gas on the system because of the relatively low and constant value in the atmosphere (400 ppmv).

The modeled evolution of CO₂ has been validated by comparison to more than 4 years of measurements from the DST. Simulated CO₂ concentrations in the fracture gas phase are shown after 3 years of heating in Figure 3-7. The results show the general outward migration of elevated CO₂ concentrations as the boiling front moves outward. The peak in CO₂ concentrations takes place at approximately 60°C, above which the concentrations generally decline as a result of degassing and transport with water vapor to cooler regions.

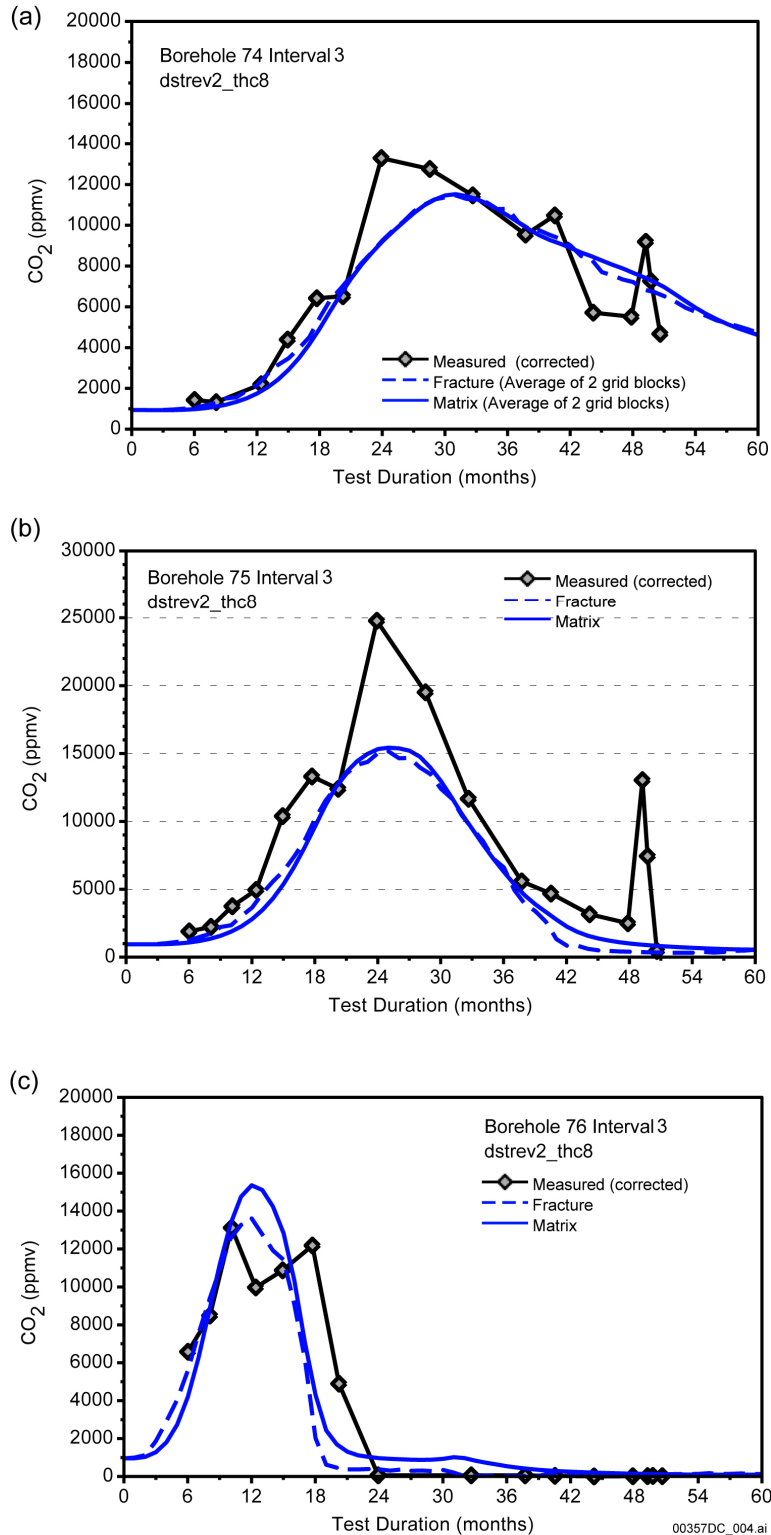
Comparisons of modeled CO₂ to measurements performed on gas samples from boreholes are presented in Figure 3-8. Samples were collected from a zone a few meters (borehole interval 76-3) to about 15 m away from the heated drift (borehole interval 74-3). Measured concentrations were corrected for water vapor condensation that took place as part of the procedure for gas sampling. Zones closest to the heaters (interval 76-3) exhibited narrower and earlier peaks in concentration compared to zones further out in the rock (interval 74-3). Simulated and measured concentrations are close in magnitude and in their trends. Differences between fracture and matrix concentrations are small, because of rapid equilibration by advection and diffusion of gas species and their local equilibration with pore water.



Source: BSC 2003c, Figure 7.1-7c.

NOTE: Locations of boreholes collared in the observation drift (circular region at left).

Figure 3-7. Modeled CO₂ Concentrations in Fractures after Three Years of Heating



Source: BSC 2003c, Figure 7.1-11a, b, and c.

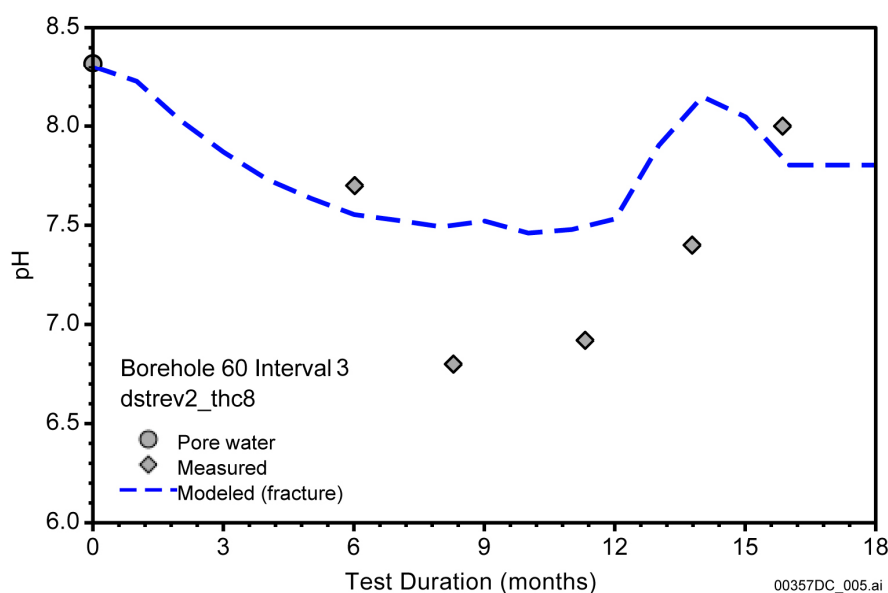
NOTE: (a) Borehole interval 74-3 (average of bounding grid blocks); (b) Borehole interval 75-3; (c) Borehole interval 76-3.

Figure 3-8. Modeled CO₂ Concentrations in Fractures and Matrix Compared to Measured Values from Boreholes (Corrected for Vapor Condensation)

3.3.1.2 Aqueous Species Evolution

The evolution of aqueous species in waters collected in the DST exhibits small reductions in pH (from about pH 8 in the pore water to about pH 6 to 8 in condensate waters). The drop in pH is related to local increases in CO₂ concentrations. Figure 3-9 shows an example of the initial drop in pH during vapor condensation, followed by increasing pH as the zone is further heated and CO₂ is diluted by water vapor.

Modeled and measured concentrations of conservative species, such as Cl⁻, are much lower (more dilute) than in the initial matrix pore water, indicating that fracture–matrix interaction and boiling-induced increases in concentration have been negligible for sampled DST waters. However, reactive species, such as silica and potassium, show significant effects of reaction with fracture-lining silicate minerals.

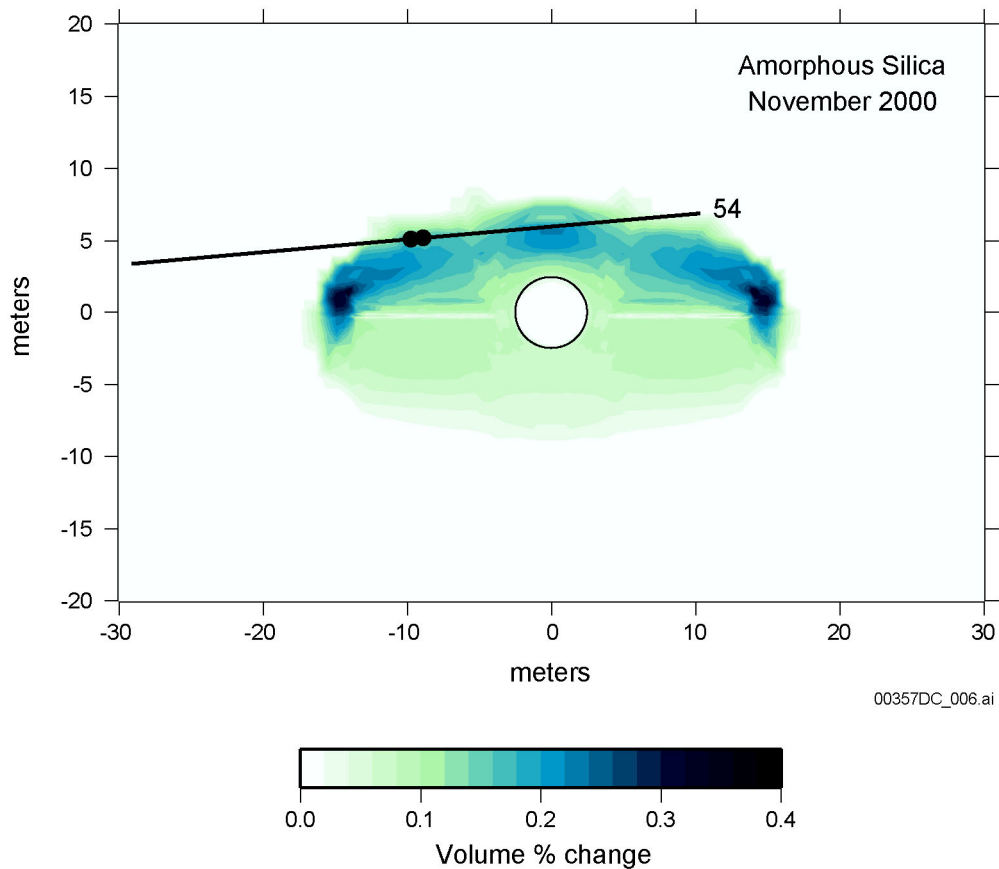


Source: BSC 2003c, Figure 7.1-16a.

Figure 3-9. Measured and Modeled pH (in fractures) for Samples Collected from Borehole Interval 60-3, Located below the Heaters

3.3.1.3 Mineral Precipitation and Dissolution

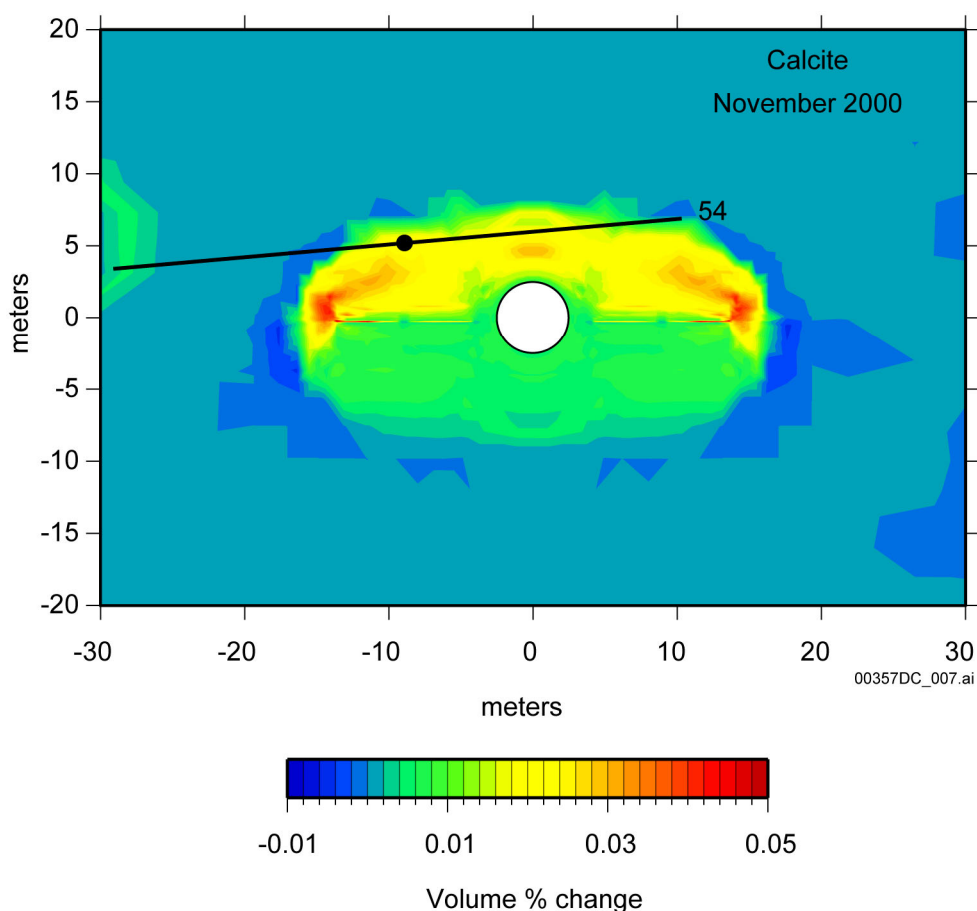
Model predictions suggested that amorphous silica, calcite, and lesser amounts of gypsum will be the dominant phases precipitating in the boiling regions. Later analyses of in situ sidewall core samples showed abundant coatings of glassy amorphous silica and lesser amounts of calcite and gypsum as small crystalline mounds (BSC 2002a). The greatest amount of mineral precipitation was predicted to be above the heaters where reflux of water condensed in fractures dissolves fracture-lining minerals and is boiled. Simulations and measurements of amorphous silica and calcite and locations of observed mineralization are shown in Figures 3-10 and 3-11. Amorphous silica forms only where strong evaporation by boiling takes place. In comparison, calcite that was originally present in fractures dissolves in the lower pH waters that formed in condensation zones around the boiling zone and in the drainage zones below the heaters. Calcite also forms with amorphous silica and gypsum in the boiling zones.



Source: BSC 2003c, Figure 7.1-38.

NOTE: Filled circle indicates sidewall core sample locations where it was observed.

Figure 3-10. Volume Percent Change in Amorphous Silica Abundance in Fractures



Source: BSC 2003c, Figure 7.1-37.

NOTE: Filled circle indicates sidewall core sample locations where it was observed.

Figure 3-11. Volume Percent Change in Calcite Abundance in Fractures

3.3.1.4 Summary of Drift Scale Test Results

The DST provided an unprecedented opportunity to test the thermal-hydrologic-chemical conceptual and numerical models, and parameterization, on a well-constrained system over temporal and spatial scales greater than achievable with simple lab experiments. Model–data comparisons for water chemistry (e.g., pH, $\text{SiO}_2(\text{aq})$, Na^+ , K^+) and gas samples (CO_2) collected over a period of nearly 5 years show that the DST thermal-hydrologic-chemical model captures the trends and the magnitudes of chemical changes. The precipitation zones of secondary mineral phases such as amorphous silica, calcite, and gypsum have also been successfully predicted. Because the chemical changes are so closely tied to thermal-hydrologic processes and fracture–matrix interaction, the modeling of various chemical components provides an independent method for validating and refining thermal-hydrologic models. The methodology developed for the thermal-hydrologic-chemical model of the DST gives added confidence to long-term predictions of nuclear waste repository performance.

3.3.2 Thermal-Hydrologic-Chemical Seepage Model Results

The thermal-hydrologic-chemical seepage model represents the effects of waste package heating over time, changes in heat load caused by preclosure ventilation, effective heat transfer within the drift, and thermal-hydrologic-chemical processes in the unsaturated zone around waste emplacement drifts. Thermal-hydrology is represented in a manner consistent with the models described in Section 2.3, using the same conceptual basis, similar formation properties, initial and boundary conditions, and representations of in-drift processes. Model results predict the chemistry of matrix and fracture water in the host rock next to the drift wall at various locations around the drift, the times of rewetting around the drifts, and the net fluxes of water and gas through the drift wall for a simulation period of 100,000 years. The DST thermal-hydrologic-chemical model develops and evaluates a methodology that is then applied to the thermal-hydrologic-chemical seepage model to represent host-rock controls on the in-drift chemical environment. The thermal-hydrologic-chemical seepage model is, therefore, very similar to the DST thermal-hydrologic-chemical model, differing mainly with respect to the simulation period, thermal loading conditions, and the implementation of climate changes and associated infiltration flux boundary conditions (BSC 2003c). The thermal-hydrologic features of the thermal-hydrologic-chemical seepage model are based on thermal-hydrologic models (BSC 2003c), which are validated using the DST.

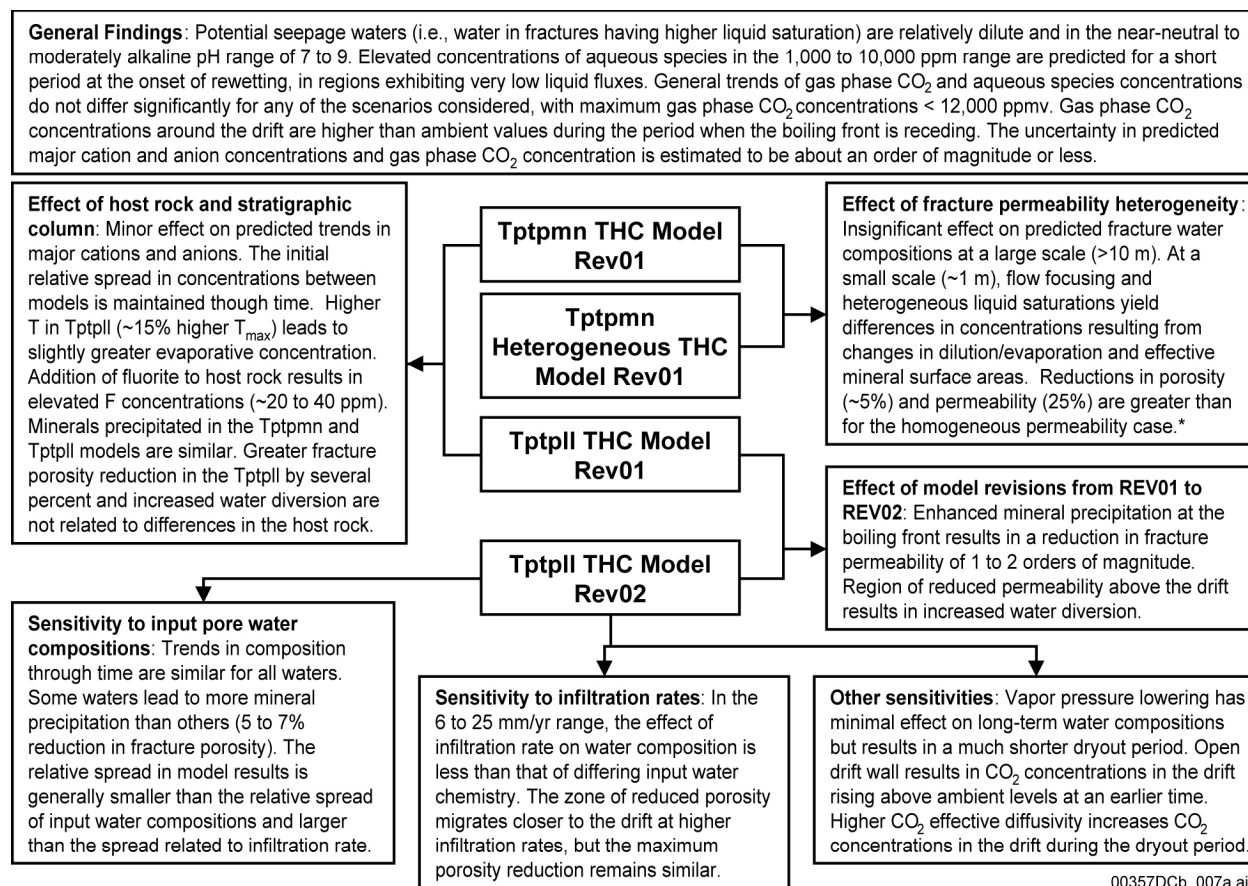
For TSPA, the in-drift temperature and relative humidity are abstracted from the MSTHM. The MSTHM comprises several types of models, including drift-scale thermal-hydrologic models that incorporate the same thermal-hydrologic features as the thermal-hydrologic-chemical seepage model. The common conceptual basis of the MSTHM and thermal-hydrologic-chemical seepage models (as well as the DST thermal-hydrologic-chemical model and other thermal-hydrologic models used to simulate the DST) supports the use of both for repository predictions. The output from the thermal-hydrologic-chemical seepage model consists of multiple realizations for the time-history of the composition of seepage waters and the gas-phase composition. This information is combined with calculated in-drift temperature and relative humidity from the MSTHM in a probabilistic abstraction that captures both variability and uncertainty (Section 4).

Several simulations were performed to characterize the effects of natural variability and uncertainty on the thermal-hydrologic-chemical seepage model predictions. These sensitivity analyses address the following major issues:

- Different repository host-rock geologic units (Ttptmn and Ttptll)
- Alternative geochemical systems (base case and extended case, which adds more mineral species and chemical components)
- Alternative thermodynamic data sets (different equilibrium constants for key minerals)
- Different treatments of mineral–water reactions (different kinetic rate constants and reactive surface areas; equilibrium versus kinetic reactions)
- Spatial heterogeneity in fracture permeability

- Different infiltration rates and effects of climate change
- Alternative water vapor pressure models
- Alternative initial water compositions
- Different effective CO₂ diffusivities
- Alternative drift-wall conceptualizations (open versus closed to liquid flow).

These thermal-hydrologic-chemical seepage model simulations cover a wide range of the most important uncertainties from the standpoint of model validation, bounding analyses, conservatism, impact on model results, and propagation of uncertainty to other models. Based on the natural variability in input water composition and the resulting spread in simulation results, the uncertainties in predicted concentrations of aqueous species and of CO₂ gas are estimated to be up to about one order of magnitude. The key findings of the process model are presented in Figure 3-12.



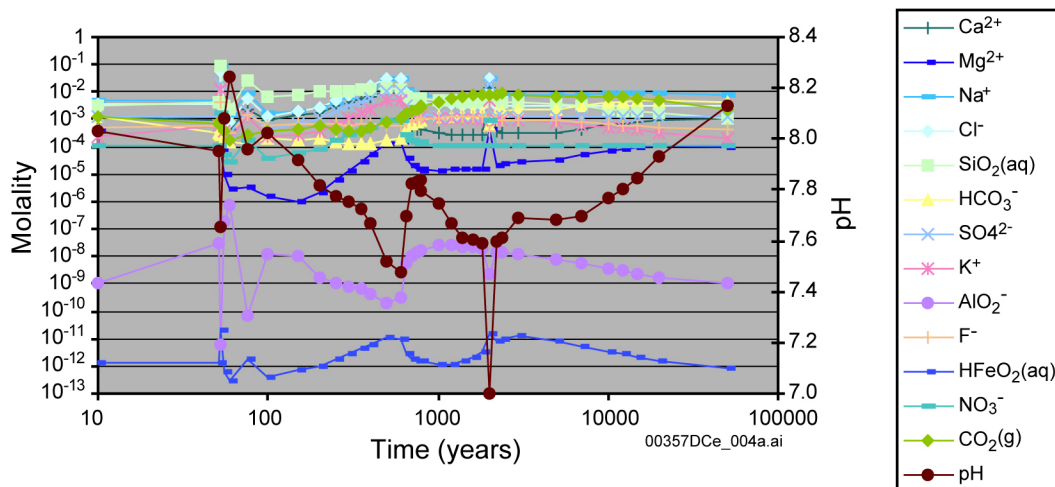
Source: BSC 2003c, Figure 8-1.

NOTE: *The heterogeneous case was run using REV01 (CRWMS M&O 2001) hydrologic properties and with TOUGHREACT V2.3 (LBNL 2001). The use of REV02 (BSC 2003c) properties and TOUGHREACT V3.0 (LBNL 2002) resulted in greater reductions in porosity and permeability for the homogeneous permeability case, which would also be expected for the heterogeneous case.

Figure 3-12. Key Findings of the Thermal-Hydrologic-Chemical Seepage Model

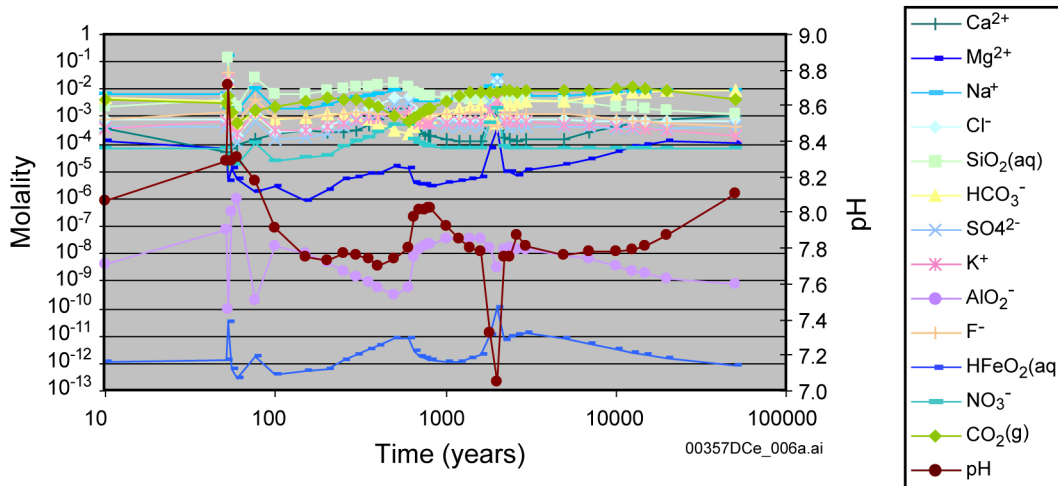
Figures 3-13 through 3-17 show the compositions of the seepage waters through time for locations at the crown of the drift that were selected for use in the seepage abstraction described in Section 4 of this report. The five cases differ only in respect to the initial pore-water composition, and the simulated water compositions are plotted separately for each case (i.e., W0, W4, W5, W6, and W7, as shown on Figure 3-2 and in Table 3-1). The evolution of simulated water compositions has the following common features among the cases evaluated:

- Concentrations of the soluble, noncarbonate species with prograde solubility (e.g., $\text{SiO}_2(\text{aq})$, Na^+ , and Cl^-) increase during the maximum thermal period after closure at 50 years, until approximately 1,000 years.
- Potential seepage waters will be relatively dilute (compared to the matrix pore water used as the initial condition for unsaturated zone water composition) after the boiling period.
- The CO_2 concentration in the gas phase will decrease during the maximum thermal period because of dilution by water vapor and then increase during cooldown as carbonate precipitates are redissolved. Total carbonate concentration and solution alkalinity will track the gas-phase CO_2 , but pH will not be well correlated because of alkalinity changes associated with mineral dissolution-precipitation reactions.
- All the simulations are sensitive to thermal conditions (e.g., closure at 50 years), and percolation flux conditions that increase in response to climate changes imposed at 600 and 2,000 years. The spike in chemical compositions shown at about 2,000 years on Figures 3-13 to 3-17 is a result of the rewetting of the fractures. This occurs at about the same time the infiltration rate changes due to modeled climate change. This rewetting causes the salts that were initially deposited in the fractures to dissolve, thus changing the composition of the waters in the rock.
- Aqueous compositions and gas-phase partial pressure of carbon dioxide ($p\text{CO}_2$) return to ambient (preheating) conditions after approximately 5,000 to 10,000 years.



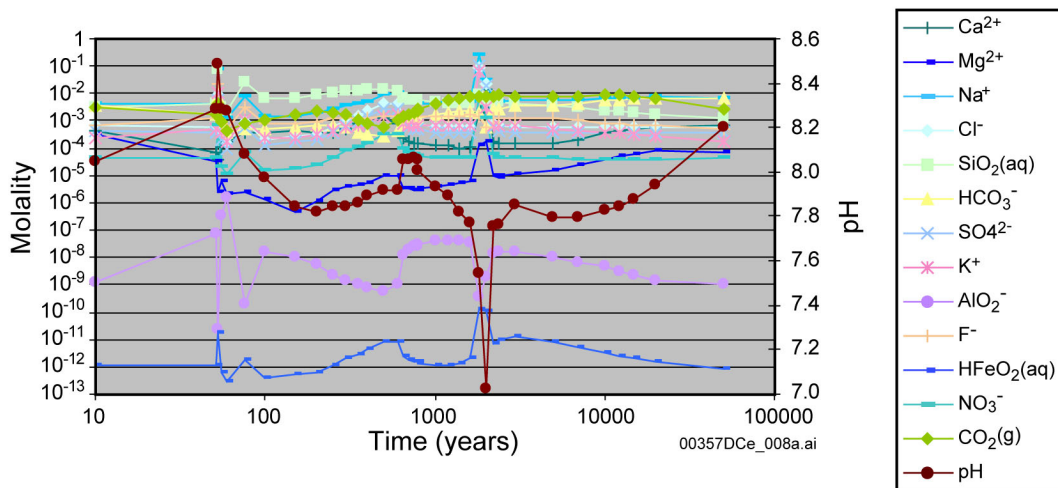
Source: DTN: LB0302DSCPTHCS.002.

Figure 3-13. Incoming Seepage Composition for W0 at the Drift Crown (Fracture Water, Top, Front, Node 4)



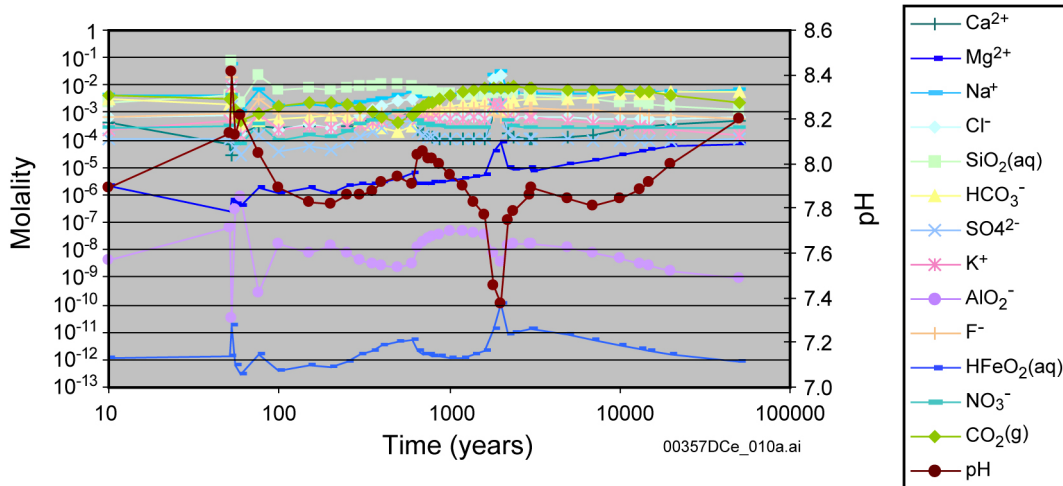
Source: DTN: LB0302DSCPTHCS.002.

Figure 3-14. Incoming Seepage Composition for W4 at the Drift Crown (Fracture Water, Top, Front, Node 4)



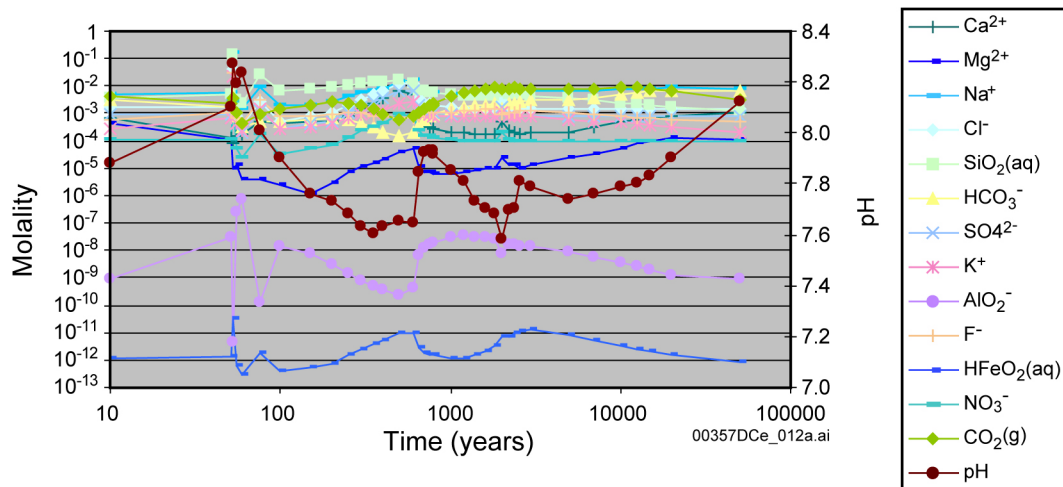
Source: DTN: LB0302DSCPTHCS.002.

Figure 3-15. Incoming Seepage Composition for W5 at the Drift Crown (Fracture Water, Top, Front, Node 4)



Source: DTN: LB0302DSCPTHCS.002.

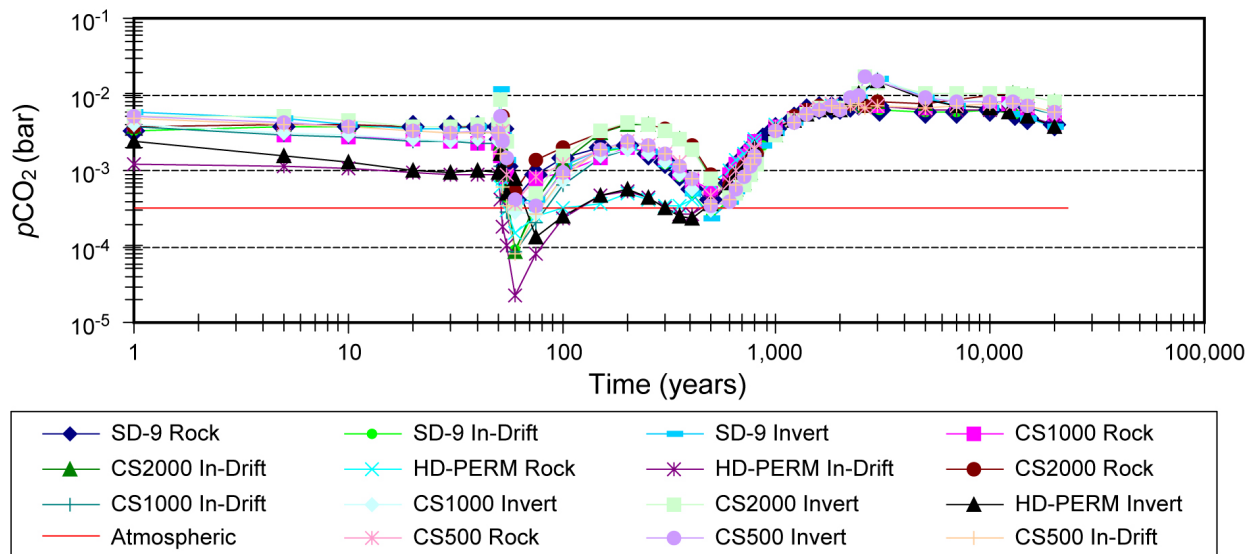
Figure 3-16. Incoming Seepage Composition for W6 at the Drift Crown (Fracture Water, Top, Front, Node 4)



Source: DTN: LB0302DSCPTHCS.002.

Figure 3-17. Incoming Seepage Composition for W7 at the Drift Crown (Fracture Water, Top, Front, Node 4)

Figure 3-18 shows the composition through time of host rock, invert and in-drift pCO_2 selected for use in the in-drift geochemical models. The CO_2 partial pressures were determined with respect to the same water source compositions as are presented in Figures 3-14 to 3-17.



Source: BSC 2003e, Figure 6.7-7.

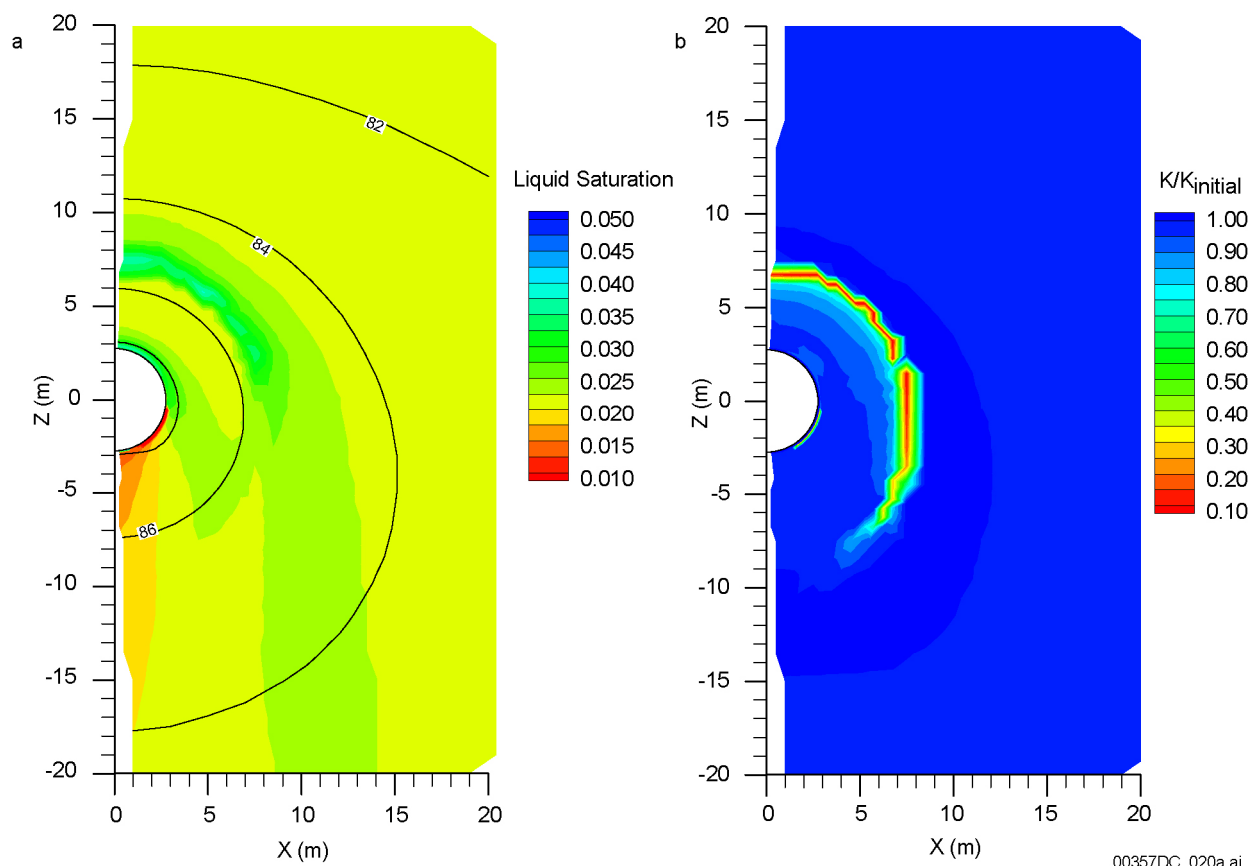
00357DCb_018a.ai

NOTE: HD-PERM is W0; CS2000 is W4; CS1000 is W5; SD-9 is W6; CS500 is W7.

Figure 3-18. pCO₂ Concentration in the Drift, the Near-Drift Environment, and in the Invert through Time

Predicted Changes in Fracture Porosity and Hydrologic Properties—To evaluate the effect of mineral precipitation and dissolution on flow, results of a thermal-hydrologic simulation are evaluated first and compared to results from a similar thermal-hydrologic-chemical simulation. The following discussion follows Section 6.8.5.4 of *Drift-Scale Coupled Processes (DST and THC Seepage) Models* (BSC 2003c). A contour plot of predicted liquid saturations for the simulation (Figure 3-19a) shows that at 2,400 years, after the end of the boiling period, the ambient water percolation is deflected around the drift (this is predicted to occur even at much higher infiltration rates than considered here). As a result, liquid saturations in fractures are somewhat increased above the drift crown, relative to ambient values, and significantly decreased below the drift (shadow zone). This “umbrella” effect results from a thin region of lower permeability (Figure 3-19b) created by mineral deposition at the boiling front during the boiling period. In this case, the permeability has decreased by a factor of about 10, and liquid saturations at the drift crown are less than for the thermal-hydrologic prediction. Similar results were obtained using the other waters as the initial composition but with the permeability decreased by as much as two to three orders of magnitude.

Other thermal-hydrologic-chemical simulations using W0 and the two fixed infiltration rates (6 and 25 mm/yr) and a simulation neglecting vapor-pressure lowering predict the umbrella effect above the drift (BSC 2003c, Figure 6.8-42b). The magnitude of permeability change may also be controlled by the rate of rewetting of the near-field host rock during cooldown (controlled by hydrologic properties and vapor pressure lowering) and the homogeneity of the fracture permeability. However, because the zone of precipitation is thin and located several meters above the drift crown, any focusing of flow in the zone is not anticipated to increase vertical fluxes at the drift crown much beyond what is predicted without considering thermal-hydrologic-chemical processes.

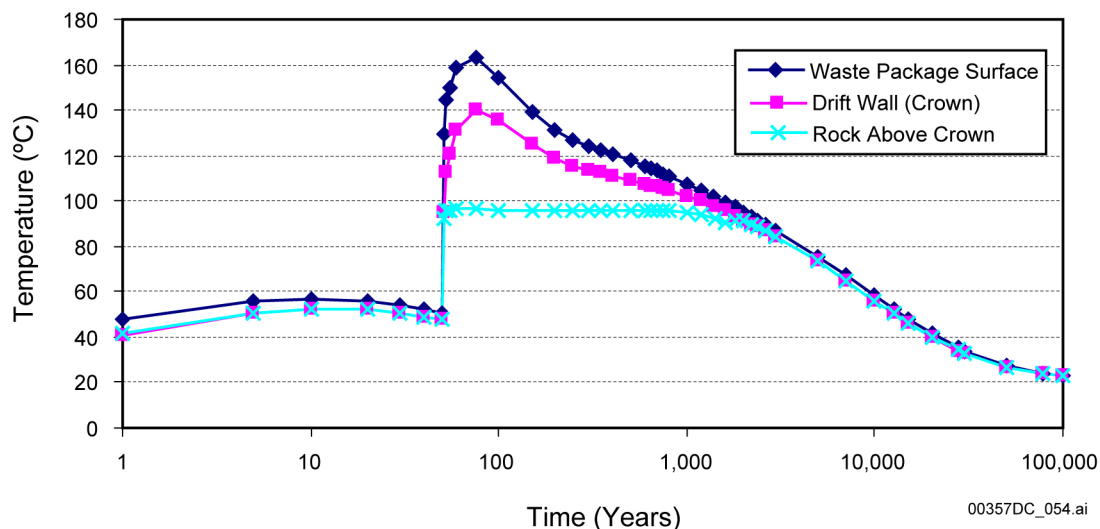


Source: BSC 2003c, Figure 6.8-40.

Figure 3-19. Thermal-Hydrologic-Chemical Simulation (TptplI in Fractures at 2,400 Years—W0): Contour Plot of Modeled Liquid Saturation and Temperature (a) and Permeability Change (b)

In all simulations, the permeability decrease results primarily from the precipitation of amorphous silica and, to a lesser extent, calcite (BSC 2003c, Figures 6.8-43 through 6.8-46). Gypsum precipitation is noticeable only with W0 and W7, as expected, because these waters initially contain a higher proportion of calcium. The fracture porosity is predicted to decrease by approximately 4 to 7 percent depending on the simulation. The maximum porosity decrease occurs in a thin zone during refluxing at the edge of the dryout zone, before the collapse of this zone around the drift.

Predicted Thermal History—The evolution of the drift-wall temperature for the five THC seepage model runs is shown in Figure 3-20. Application of the thermal seepage model (Section 2.3.3) to the drift crown temperature from Figure 3-20, shows that no seepage into the drift will occur from permanent closure until more than 1,000 years have elapsed, because of the vaporization barrier effect. (Similar results with different timing are associated with model results represented in Figure 2-11, where such results produced dryout at the drift crown.) In addition, at every waste package location in the repository the capillary barrier effect is also present at all times regardless of the drift crown temperature (Section 2.3.3).



Source: DTN: LB0302DSCPTHCS.002 (thc6_w4_r.xls and thc6_w4_drift_r.xls).

Figure 3-20 Temperature History for the Drift Crown, the Host Rock above the Crown from Where Water Compositions Were Obtained, and the Waste Package Surface, from the THC Seepage Model

An important point about the THC seepage model water compositions is that they represent fracture water nearest to the drift crown, even if such water is several meters away from the drift opening because of dryout. For the THC seepage model simulation time histories (Figures 3-13 through 3-17), if no liquid water was present in the fractures at the drift wall, then the aqueous composition provided was that of the water farther back into the rock at the edge of the dryout zone (i.e., at the wetting front). It should be noted that these results represent the composition of fracture water in the model that may be available for seepage, but does not mean that seepage will occur, because of the vaporization barrier and capillary barrier effects discussed in Section 2.3.3.

3.4 SUMMARY OF BOUNDARY CONDITIONS IMPORTANT TO IN-DRIFT CHEMICAL MODELS

The discussion above provides process model results and corroborative modeling of tests and experiments that provide primary boundary conditions to the in-drift chemical models (Section 4). The model results presented above provide the composition of seepage and gas near the drift wall through time (see Figures 3-13 through 3-18). This information, when coupled with the results from Section 2 (i.e., drift temperatures, relative humidity, and occurrence of seepage through time), allows for the prediction of the evaporated seepage chemistries (Section 4.1).

INTENTIONALLY LEFT BLANK

4. EVOLUTION OF IN-DRIFT WATER AND GAS CHEMISTRY

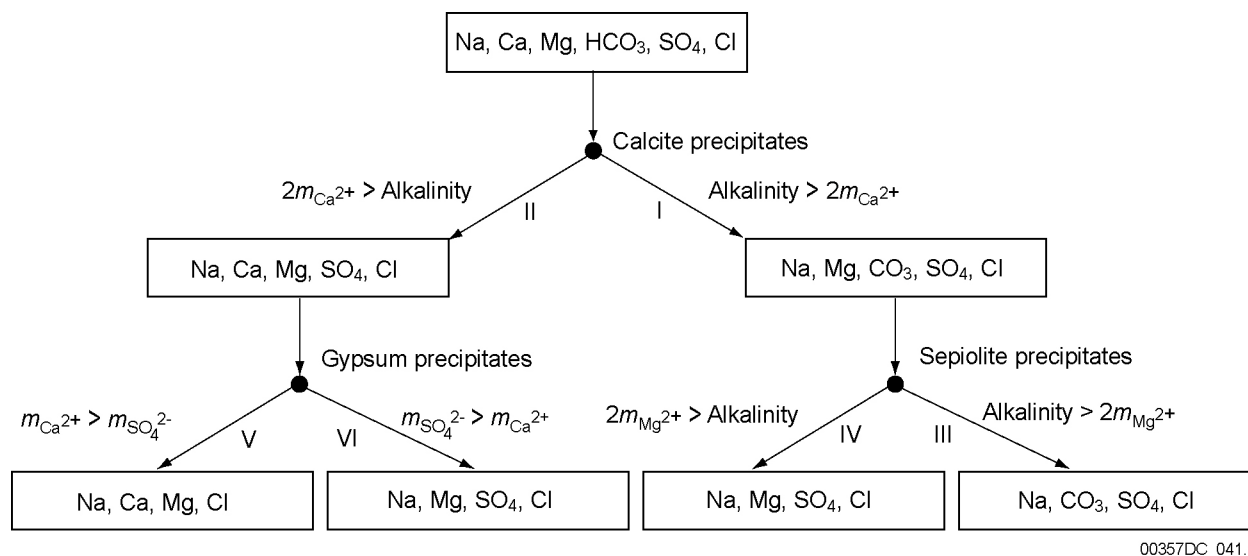
In-drift water and gas chemistry models are needed to characterize the compositions of fluids on waste package and drip shield surfaces that provide the environments for corrosion. The models also provide the composition of fluid that could enter the invert, which provides the pathway for radionuclide transport from breached waste packages to the natural environment and the values of parameters such as $p\text{CO}_2$ to which in-package reactions (e.g., radionuclide solubility) are particularly sensitive.

The period of particular interest to performance of the waste package and drip shield materials is early in the life of the repository (dryout and transition regimes) and ends when the surface temperatures of waste packages fall below the range in which corrosion susceptibility of the waste package (Alloy 22) is significant. During this period of relatively high localized waste package surface temperatures, any seepage water falling on waste package and drip shield surfaces will evaporate and may form highly concentrated brines and deposited salts. In addition, the salts in dust that accumulates on waste package and drip shield surfaces during repository operation may deliquesce, to form brines at temperatures higher than those at which seepage water is expected to enter the drift. In view of the processes leading to the formation of brines on the metal surfaces and the importance of these brines to the corrosion behavior of the waste package and drip shield, the topics of deliquescence, evaporative concentration, dust–condensate interactions, the effects of introduced materials in the drift, and the water and gas chemistries used during corrosion testing are discussed here.

For evolution of solution chemistry within the drift, the two key physical-chemical processes are evaporation and deliquescence, both of which may lead to formation of concentrated brines due to thermally driven changes through time. The changes to those fluid compositions are governed by the mineral dissolution/precipitation that occurs. For evaporative concentration, sequential precipitation leads to changes in the compositional trajectory of the fluids that are referred to as “chemical divide phenomena.”

Chemical Divides—As seepage waters make their way into the drift, their chemical composition can significantly change by evaporation and mineral precipitation. Evaporation causes aqueous species’ concentrations to increase, minerals to precipitate, and the most soluble components to become concentrated in the brine.

When minerals (salts) precipitate, the relative concentrations of dissolved components change. This effect is a result of chemical divides that are encountered whenever a mineral precipitates. The chemical divide is explained by Drever (1988, p. 235): “Whenever a binary salt is precipitated during evaporation, and the effective ratio of the two ions in the salt is different from the ratio of these ions in solution, further evaporation will result in an increase in the concentration of the ion present in greater relative concentration in solution and a decrease in the concentration of the ion present in lower relative concentration.” There are six common geochemical divides for natural lakes (Figure 4-1). These geochemical divides largely control the types of waters that can develop in these lakes.



Source: Drever 1988, p. 236.

Figure 4-1. Simplified Chemical Divide Diagram Based on Evaporative Concentration of Dilute Starting Waters to Form a Suite of Naturally Occurring Lake Waters

In the seepage abstraction, seepage waters were grouped based on the composition of the concentrated brines that form upon each water's evaporation (Section 4.1.3). In accordance with geochemical divide theory, the composition of the water changes due to the sequence of minerals that precipitate from solution. That sequence is a function of the initial water composition, the thermal conditions, and gas composition at the location where the evaporation occurs.

Analogous evaporite minerals are commonly found on desert playa lakes in Nevada as the result of evaporative concentration of relatively dilute and low-solute-content rainwater and snowmelt (Papke 1976, Table 1). For these reasons, model runs simulating the evaporation of Sierra snowmelt were carried out to validate the EQ6 Pitzer brine evaporation modeling (see Section 4.2).

Deliquescence—Some minerals absorb water from the air and incorporate this liquid as waters of hydration within their mineral lattice structure. Common examples of such a process are the sodium-silicate-gel desiccants that are used as packing for transoceanic shipping.

Deliquescent minerals in drift dust are of consequence because of their potential ability to change the microscale liquid environment around dust as they absorb water vapor from the air (Figure 4-2). The presence of liquid water and mineral saturation in solution are both required for the relative humidity (expressed as a unit fraction) of the drift's atmosphere to equal the activity of water for the solution. Campbell and Smith (1951, p. 237) state, "It is clear that if the pressure of the aqueous vapor in the atmosphere is greater than that of the saturated solution of a salt, that salt will, on being placed in the air, form a solution: it will deliquesce." Where deliquescent minerals (salts) are present in the dust, the dust will form a small drop or puddle of liquid water. As shown in Figure 4-2, the evaporative process is the reverse of deliquescence.

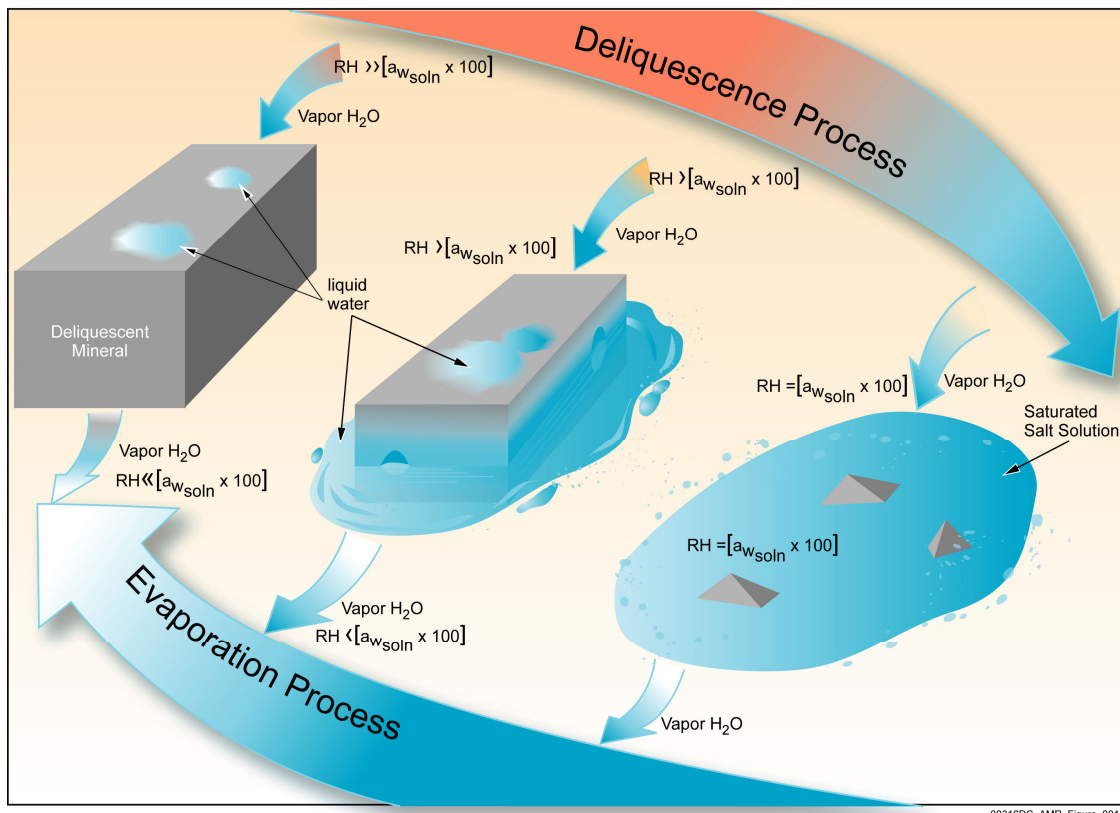
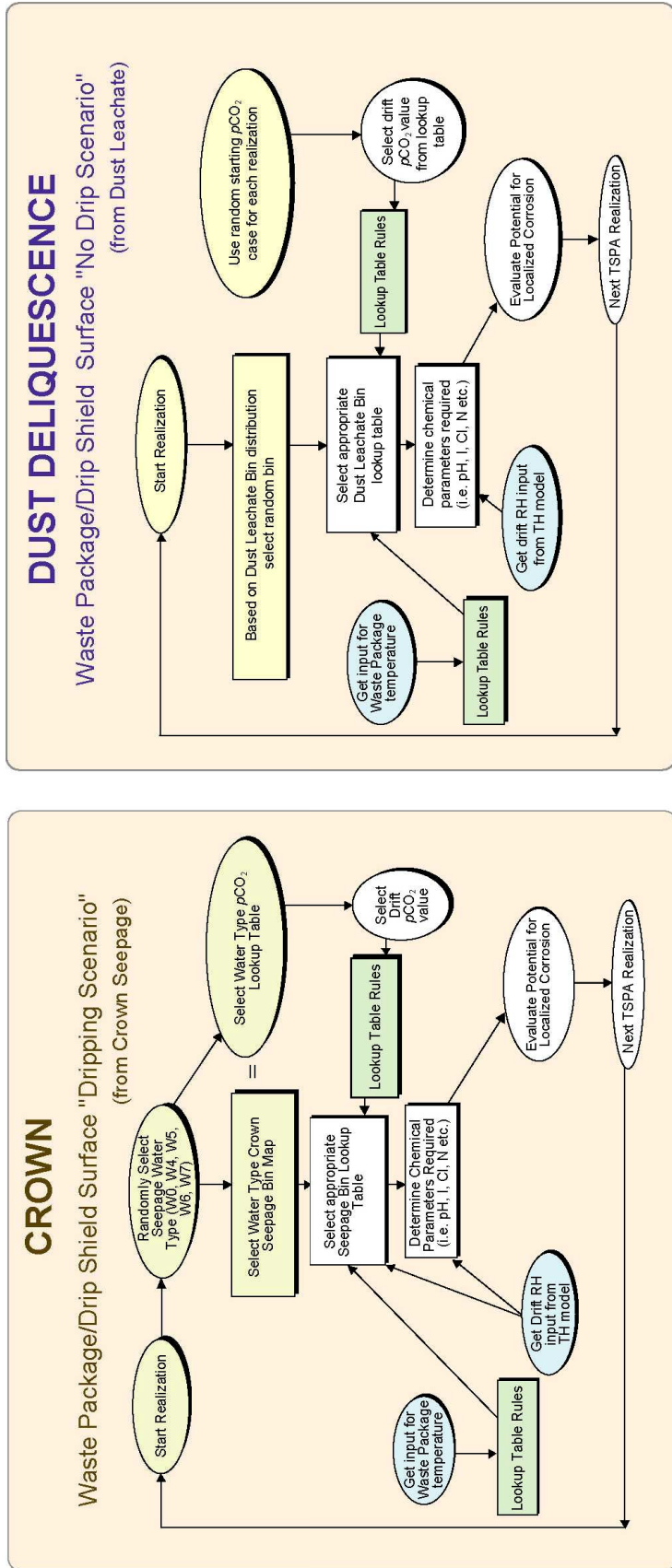


Figure 4-2. Deliquescence and Evaporation Processes

These processes are described by the use of two scenarios of the in-drift chemical environment expected on waste packages and drip shield as shown in Figure 4-3. Figure 4-3 shows the interrelationships between the two scenarios as implemented in the TSPA-LA model. The crown scenario is the seepage scenario.

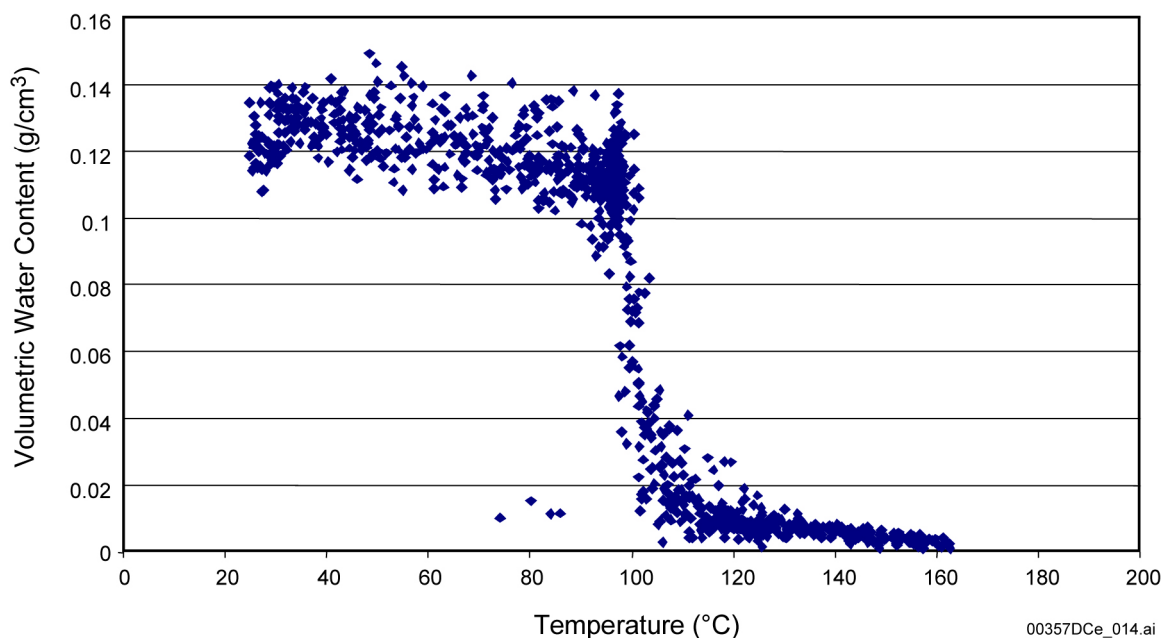
The determination of when these scenarios are operative or dominate the chemistry is important to the type of chemical conditions that could be expected on the waste package or drip shield. As discussed in Section 2.3, the thermal seepage constraints indicate that there can be no seepage at drift temperatures above about 100°C. In addition to this limitation, the results of the DST corroborate the absence of macroscale liquid water available in the host rock at temperatures above about 105°C (Figure 4-4). These constraints indicate that the seepage scenario or environment will not occur above these temperatures. The second scenario (dust deliquescence) can occur even at temperatures too high for seepage to occur if the in-drift relative humidity is higher than the deliquescence relative humidity of the dust salts.



00357DC_042.ai

Source: BSC 2003e, Figure 8.2-1.

Figure 4-3. Engineered Barrier System Environment Water Chemistry Scenarios for Total System Performance Assessment for the License Application for Localized Corrosion on the Waste Package and Drip Shield



Source: BSC 2003e, Figure 6.2-4.

NOTE: This borehole is almost level over an instrumented 40 m section, almost parallel and 9.5 m offset from the center of the drift, and about 3.5 m above the wing heaters that simulate the heat from a waste package. The test was conducted from February 1998 to May 2000.

Figure 4-4. Experimental Relationship between Borehole Temperature and Volumetric Water Content for Borehole 79 during the Drift Scale Test over a 2-Year Period during Heating

4.1 SEEPAGE EVAPORATION

4.1.1 Conceptual Understanding

Evaporative concentration of seepage water leads to the formation of brines and to the deposition of salts on waste package and drip shield surfaces. When relative humidity increases, salts can deliquesce to form aqueous solutions. This section further discusses the types of solutions formed as crown seepage and invert waters evaporate. The types are determined by the same factors that determine the salt assemblages produced by evaporation: the parent groundwater composition, the thermal history, reactions with minerals, and the gas phase in the thermally perturbed host rock and with in-drift construction materials and gases.

4.1.2 Technical Basis

The *In-Drift Precipitates/Salts Model* (BSC 2003d) is the primary process model used by the *Engineered Barrier System: Physical and Chemical Environment Model* (BSC 2003e) and by the analysis of *Environment on the Surfaces of Drip Shield and Waste Package Outer Barrier* (BSC 2003g). This model, which applies the geochemical modeling code EQ3/6 (BSC 2003p), is used to determine the chemical evolution of aqueous solutions in response to evaporation caused by a combination of decreasing relative humidity and (or) increasing temperature (BSC 2003e). The in-drift precipitates and salts model is equally useful in determining the behavior of highly concentrated brines as they are diluted in response to increasing relative

humidity, decreasing temperature, or admixture of dilute waters through seepage (BSC 2003g). In order to predict the behavior of aqueous systems at high salinity conditions, a database including Pitzer parameters extending to elevated temperature (DTN: SN0302T0510102.002) is part of the in-drift precipitates and salts model.

The in-drift precipitates and salts model used to predict the chemistry of seepage at various stages of in-drift physical and chemical evolution was validated against a number of handbook data sets and well-documented natural analogs (BSC 2003d; BSC 2003e). These validation cases also apply to calculations of dust deliquescence and dust leachate evaporation. In the sections that follow, each validation objective is compared to simulation results, which are compared to the estimated model uncertainties listed in Table 4-1. Maximum differences for selected in-drift precipitates and salts model output parameters are summarized in Table 4-2. The values in Table 4-1 are intended to represent reasonable uncertainty ranges bounded by values that would represent approximate 95 percent confidence intervals if the underlying distributions were normally distributed. Uniform probability distributions across these ranges are recommended because supporting data are sparse and uniform distributions are conservative relative to distributions that weigh the middle values more heavily (i.e., uniform distributions tend to err on the side of representing too much uncertainty).

Table 4-1. Model Uncertainty in Selected Output Parameters

IDPS Model Output Parameter	Uncertainty Range	Probability Distribution
pH	± 1 pH unit	Uniform
Ionic Strength	± 30% RPD ^a	Uniform
Cl ⁻	± 30% RPD	Uniform
NO ₃ ⁻	± 30% RPD	Uniform
Cl ⁻ /NO ₃ ⁻ ratio	± 30% RPD	Uniform
RH _d	± 5% RH units	Uniform

Source: DTN: MO0308SPAESMUN.000.

NOTE: ^a relative percent difference. IDPS – in-drift precipitates and salts model.

Table 4-2. Maximum Differences between Predictions and Measurements for pH, Ionic Strength, Cl⁻, NO₃⁻, and the Cl⁻/NO₃⁻ Ratio

Evaporation Simulation	ΔpH (pH units)	ΔIonic Strength (RPD ^a)	ΔCl (RPD)	ΔNO ₃ (RPD)	ΔCl ⁻ /NO ₃ ⁻ Ratio (RPD)
J-13 Evaporation Experiment (BSC 2003d, Section 7.1.1)	0.78	47% ^b	48% ^b	38% ^b	16%
100x J-13 Evaporation Experiment (BSC 2003d, Section 7.1.2)	nm ^c	ne ^d	5%	7%	-3%
Topopah Spring Tuff Pore-Water Evaporation Experiment (BSC 2003d, Section 7.1.3)	0.46	67% ^b	66% ^b	nm	nm
Seawater Evaporation (BSC 2003d, Section 7.1.4)	0.76	15% ^e	10% ^e	nm	nm

Source: DTN: MO0308SPAUCIMV.000.

NOTE: ^a RPD (relative percent difference) = 100% * ([predicted concentration] - [measured concentration]) / [measured concentration].

^b Most of the difference is likely due to overestimation in the concentration factor reported in the data source (see BSC 2003d, Section 7.1.1 or Section 7.1.3 for details).

^c nm – not measured.

^d ne – not estimated, pH needed for estimate.

^e This value disregards the sample with the highest degree of evaporation because it is an outlier (BSC 2003d, Figures 26 and 27). Physically, ionic strength must increase with evaporation or remain constant once at the eutectic point. The last experimental data point is lower than the previous data points and, therefore, is not realistic.

pH—The in-drift precipitates and salts model validation objective for pH is to predict pH within one pH unit (BSC 2003d, Table 18). In each of the simulations, pH is predicted within 0.78 pH unit or less (BSC 2003d, Figures 17, 24, and 27). The maximum pH differences in each of the evaporation data sets are summarized in Table 4-2. The estimated model uncertainty for pH is plus or minus one pH unit (Table 4-1). This estimate is justified and supported by the results.

Ionic Strength—The model validation objective for ionic strength is to predict ionic strength within a factor of 10 (BSC 2003d, Table 18). In each of the simulations, ionic strength is predicted within a factor of 2 or less (see BSC 2003d, Tables 20 and 21, and Figure 27). As shown in Table 4-2, the maximum observed ionic strength difference is 67 percent. However, as discussed below, only a small part of this difference is likely due to uncertainties in the in-drift precipitates and salts model.

The estimated model uncertainty for ionic strength is plus or minus 30 percent (Table 4-1). Most of the error reported in Table 4-2 for ionic strength is not likely due to model uncertainty. Rather, it is likely due to overestimates of the experimental concentration factors reported. This likelihood is assessed and substantiated in *In-Drift Precipitates/Salts Model* (BSC 2003d, Sections 7.1.1 and 7.1.3). Concentration factors were determined and reported more accurately in the seawater evaporation samples. Unlike the J-13 and Topopah Spring Tuff pore-water evaporation experiments, the reported concentration factors for the seawater samples were directly determined from the measured concentration factors of nonreacting dissolved components. The maximum difference between measured and predicted ionic strength in the seawater samples is approximately 15 percent, except for an outlier at the highest degree of

evaporation (BSC 2003d, Figure 27). Considering the accuracy in the predicted seawater ionic strength and the effects of the overestimated concentration factors in the J-13 and Topopah Spring Tuff pore-water evaporation experiments, the estimated plus or minus 30 percent model uncertainty for ionic strength is supported and justified by the model validation analyses.

Deliquescence Relative Humidity—The model validation objective for deliquescence relative humidity (RH_d) is to predict RH_d within 5 percent in relative humidity units (BSC 2003d, Table 18). In each of the deliquescence simulations, the RH_d was predicted within this range, rounding to one significant figure (Table 4-3). The estimated model uncertainty for RH_d is also plus or minus 5 percent in relative humidity units (Table 4-1). This estimate is justified and supported by the results (Table 4-3).

Table 4-3. Model Predictions of Equilibrium Relative Humidity for Saturated Aqueous Solutions in Contact with an Excess of Solid-Phase Salts

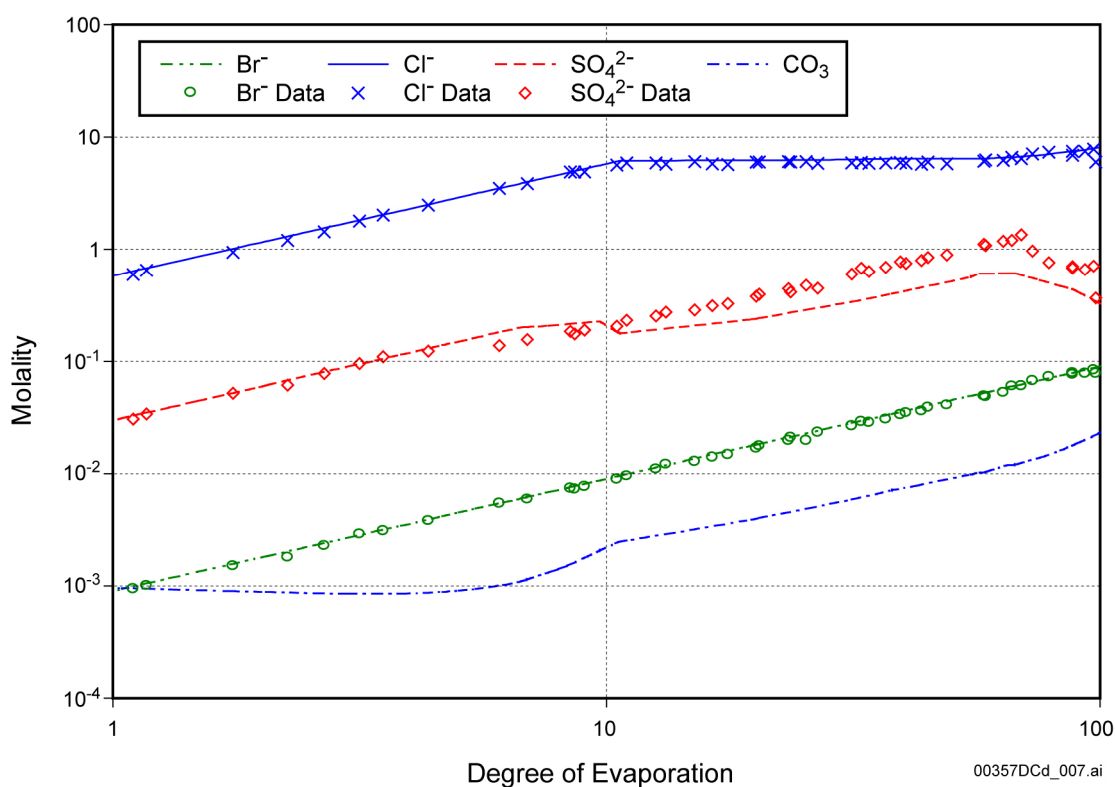
Salt	Predicted Equilibrium Relative Humidity (or Deliquescence Point) (%)	Temperature (°C)	Difference Compared to Handbook Values ^a (%)	Precipitating Mineral
NaCl	74.7	80	-1.7	halite
KCl	77.0	80	-2.5	sylvite
MgCl ₂ ·6H ₂ O	36.9	25	3.9	bischofite
Na ₂ CO ₃ ·10H ₂ O	90.2	24.5	3.2	natron
K ₂ CO ₃ ·2H ₂ O	37.8	40	-4.2	K ₂ CO ₃ ·1.5H ₂ O
NaF	95.9	100	-0.7	villiaumite
KF	28.0	100	5.1	carobbite
Na ₂ SO ₄ ·10H ₂ O	95.6	20	2.6	mirabilite
K ₂ SO ₄	96.4	60	0.4	arcanite
NaNO ₃	62.2	80	-3.3	soda niter
KNO ₃	77.8	60	-4.2	niter

Source: DTN: MO0307MWDUNEVP.000.

NOTE: ^a The handbook values are those listed in Table 12 of *In-Drift Precipitates/Salts Model* (BSC 2003d).

Cl⁻ and NO₃⁻—Model uncertainty in Cl⁻ and NO₃⁻ predictions is estimated to be plus or minus 30 percent (Table 4-1). This estimated model uncertainty is larger than the errors observed for Cl⁻ and NO₃⁻ salts in simple salt solubility model validation simulations (BSC 2003d, Table 23). For the evaporation simulations, the maximum differences in predictions and measurements for Cl⁻ and NO₃⁻ in each of the evaporation data sets are summarized in Table 4-2. Large differences are observed in the J-13 and Topopah Spring Tuff pore-water evaporation experiments; however, they are not likely due to model uncertainty. Rather, these differences likely result from overestimates of the reported concentration factors. These overestimates are evaluated and substantiated in *In-Drift Precipitates/Salts Model* (BSC 2003d, Sections 7.1.1 and 7.1.3). The concentration factor of the Topopah Spring Tuff pore-water evaporation experiment was overestimated by approximately 83 percent based on the concentration factor estimated from the measured Cl⁻ concentrations. For the J-13 evaporation experiment, the reported concentration factors of 157 and 956 should have been closer to 114 and 680, based on median measured concentration of Cl⁻, NO₃⁻, K⁺, and SO₄²⁻. These errors translate into overestimates in

the reported concentration factors of around 40 percent. Concentration factors were determined and reported more accurately in the seawater evaporation samples. Unlike the J-13 and Topopah Spring Tuff pore-water evaporation experiments, the reported concentration factors for the seawater samples (McCaffrey et al. 1987) were directly determined from the measured concentration factors of nonreacting dissolved components. The maximum difference between measured and predicted Cl^- in the seawater samples is approximately 10 percent, except for an outlier at the highest degree of evaporation (Figure 4-5). NO_3^- was not measured in the seawater study. Considering (1) the model accuracy in the predicted solubilities of chloride and sulfate salts, (2) the accuracy of predicted Cl^- concentrations in evaporated seawater samples, and (3) the effects of the overestimated concentration factors in the J-13 and Topopah Spring Tuff pore-water evaporation experiments, the estimated plus or minus 30 percent model uncertainty for predictions of Cl^- and NO_3^- concentrations is supported and justified by the results of the model validation analyses.



Source: McCaffrey et al. 1987; DTN: MO0307MWDSEAEV.000.

Figure 4-5. Predicted versus Measured Br^- , Cl^- , and SO_4^{2-} Concentrations from Evaporation of Inagua Seawater

$\text{Cl}^-/\text{NO}_3^-$ Ratio—Model validation objectives were not established for the $\text{Cl}^-/\text{NO}_3^-$ ratio because objectives were already established for Cl^- and NO_3^- separately (BSC 2003d, Table 18). However, the uncertainty in the $\text{Cl}^-/\text{NO}_3^-$ ratio is an important consideration in corrosion calculations. Consequently, uncertainty in the $\text{Cl}^-/\text{NO}_3^-$ ratio due to in-drift precipitates and salts model uncertainty was directly estimated (independent of the estimated uncertainties in the two anions) for propagation in TSPA-LA (Table 4-1).

The model uncertainty in the $\text{Cl}^-/\text{NO}_3^-$ ratio is estimated to be plus or minus 30 percent (Table 4-1). The maximum differences in this ratio are summarized in Table 4-2 for each of the evaporation data sets that measured both Cl^- and NO_3^- . The largest difference between measurement and prediction is 16 percent. Because only two evaporation data sets provided measurements for the $\text{Cl}^-/\text{NO}_3^-$ ratio, the results justify and support the plus or minus 30 percent estimated model uncertainty in the $\text{Cl}^-/\text{NO}_3^-$ ratio.

Minerals—The in-drift precipitates and salts model predicts aqueous evolution within the specified model validation objectives, which indicates that the in-drift precipitates and salts model reasonably predicts the general compositions of precipitated minerals. Because the thermodynamic databases used in geochemical modeling use idealized mineral phases, model validation for predicting the bulk mineral composition does not imply that the model accurately predicts the exact minerals observed to precipitate in laboratory evaporation experiments, but that the minerals that are included, if not exact matches for the real minerals, provide a reasonable set of proxy phases to capture the behavior in this system. Therefore, the minerals predicted by the model to precipitate are adequate for predicting the evaporative evolution of the aqueous phase as well as the evolution of the solution as those mineral salts redissolve or deliquesce.

4.1.3 Abstraction of Thermal-Hydrologic-Chemical Seepage Model Results for Use in Engineered Barrier System Chemistry Models

The initial boundary water and gas compositions used for in-drift chemistry modeling start with predictions of seepage water chemistry and gas-phase composition in the host rock (near-field environment) adjacent to the drift wall. A discussion of the model used to derive these boundary compositions and their uncertainties is summarized in Section 3.3.

The engineered barrier system physical and chemical environment model (BSC 2003e) uses the output discussed in Section 3.3 (e.g., Figures 3-13 through 3-18) and the *In-Drift Precipitates/Salts Model* (BSC 2003d) to select seepage water and CO_2 gas compositions that would represent the evaporative evolution of in-drift water.

Five complete sets of drift-scale seepage thermal-hydrologic-chemical modeling results were selected to represent the spread of potential pore-water data that serve as starting water compositions for the drift-scale thermal-hydrologic-chemical seepage model (Section 3.2.1). Each of the model runs produces time histories of changing water compositions for many locations around the drift. The thermal-hydrologic-chemical model documents the time history at approximately 50 discrete points distributed in time over the 100,000-year modeling period. An abstraction methodology is used to reduce the number of lookup tables required to represent adequately the effects of evaporation within the drift for any given time period. This methodology involves grouping (or binning) each input water at each point in time by how it evaporatively evolves and then choosing a water within each group (or bin) to represent all waters in the bin.

Abstracting the thermal-hydrologic-chemical model results using the binning methodology requires five steps:

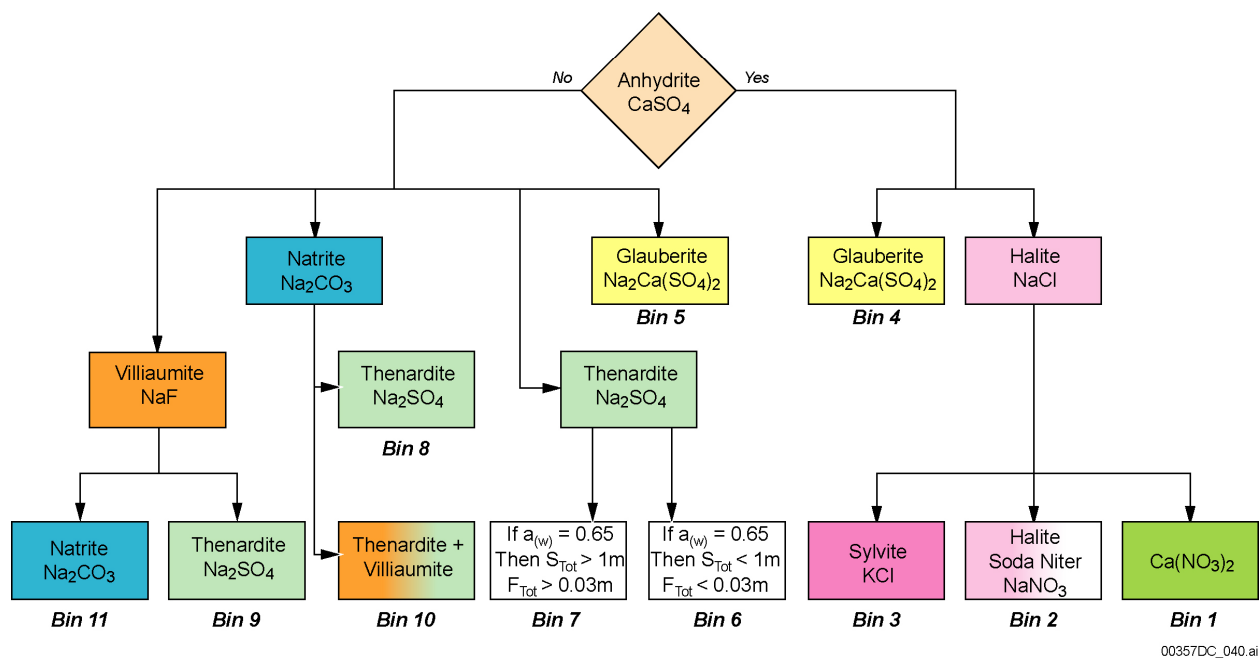
- **Step 1**—Selection of which thermal-hydrologic-chemical model grid nodes and locations are to provide the representative seepage water composition. Before the selection of grid node (1 through 6), saturation zone (Hi-sat or wetting front), matrix or fracture water, and spatial location (crown, side, and base) occurs, there are 18,000 discrete water compositions. The abstraction process selected waters from the crown, fracture, and wetting front at node 4 and from the base, matrix, and wetting front at node 4. Node 4 is the fourth closest calculational node to the drift center that is determined to be “wet”. This reduces the 18,000 chemistries to 500, at which point a data simplification (1 water each selected to represent the 0- to 50-year and 20,000- to 100,000-year periods) allows for the removal of about 14 discrete waters with similar chemistries providing about 36 time dependent water chemistries for use with each location (crown and base) and water (W0, W4, W5, W6, and W7). This abstraction process yields 368 total water compositions. The water at these locations and nodes, over time, represent various stages of evaporation.
- **Step 2**—Evaporate these waters to a common activity of water (0.65) to form a normalized basis of comparison. The in-drift precipitates and salts model (BSC 2003d) using EQ3/6 is implemented with the Pitzer thermodynamic database to evaporate the selected water.
- **Step 3**—The evaporated waters are sorted into groups (or bins) of similar chemistries as described below.
- **Step 4**—A representative water is chosen from the various waters in each bin to represent all of the waters in the bin. This selected water is the one that contains the greatest number of median values for each of the reported chemical parameters.
- **Step 5**—The thermal-hydrologic-chemical results are mapped to the bins so that the time history provided by the thermal-hydrologic-chemical model can be represented by a time series of bin water compositions.

Step 1 reduces the 18,000 input waters down to 368. Steps 2 through 4 reduce the 368 input waters (see Figures 3-13 to 3-17) down to 11 representative waters. These 11 waters are then mapped back to actual thermal-hydrologic-chemical seepage results in step 5. The binning of the evaporated waters called for in Step 3 makes use of the chemical divide phenomenon by applying the following eight criteria:

1. Total aqueous calcium molality greater than 0.1 molal?
2. Total aqueous carbonate molality greater than 0.1 molal?
3. Total aqueous calcium molality less than total aqueous sodium molality?
4. Total aqueous calcium molality greater than total aqueous potassium molality?
5. Total aqueous nitrate molality greater than total aqueous carbonate molality?
6. Total aqueous fluoride molality less than 0.1 molal?
7. Total aqueous fluoride molality less than 0.03 molal?
8. Total aqueous sulfate molality greater than 1 molal?

Table 4-4 shows the frequency of evaporated thermal-hydrologic-chemical waters falling into each bin and the median chemistry of each bin. The frequency is determined from the number of individual waters falling into a given bin divided by the total number of waters selected to enter the drift and multiplying by 100 (Figures 3-13 through 3-17).

Figure 4-6 illustrates the mineral precipitation (chemical divides) that leads to the 11 bins. As is demonstrated, the chemical divide phenomena can be used to explain the formation of the 11 distinct groups of water chemistries. Figure 4-6, unlike Figure 4-1 for surface waters, does not directly include magnesium. This element is understood to be lost from solution by precipitation of a silicate mineral such as sepiolite. This figure represents the chemical divides that occur after calcite (CaCO_3), fluorite (CaF_2), sepiolite ($\text{Mg}_4\text{Si}_6\text{O}_{15}(\text{OH})_2 \cdot 6\text{H}_2\text{O}$), stellerite ($\text{Ca}_2\text{Al}_4\text{Si}_{14}\text{O}_{36} \cdot 14\text{H}_2\text{O}$), erionite ($\text{K}_{1.5}\text{Na}_{0.9}\text{Ca}_{0.9}\text{Al}_{14.2}\text{Si}_{13.8}\text{O}_{36} \cdot 13\text{H}_2\text{O}$) and $\text{SiO}_2(\text{am})$ have precipitated.



Source: BSC 2003e, Figure 6.14-14.

NOTE: Previously precipitating minerals: calcite, fluorite, sepiolite, stellerite, erionite, and $\text{SiO}_2(\text{am})$. The items listed are the binning criteria that differentiate the two bins.

Figure 4-6. Flow Diagram Showing Some of the Precipitated Minerals and Chemical Divides That Are Associated with Each of the 11 Seepage Bins

Table 4-4. Frequency and Compositions of the 11 Binned Input Waters

	Bin 1 Chemistry	Bin 2 Chemistry	Bin 3 Chemistry	Bin 4 Chemistry	Bin 5 Chemistry	Bin 6 Chemistry	Bin 7 Chemistry	Bin 8 Chemistry	Bin 9 Chemistry	Bin 10 Chemistry	Bin 11 Chemistry
Frequency	1.36%	3.53%	3.26%	11.68%	7.34%	2.17%	6.79%	5.98%	15.76%	2.72%	39.40%
T (°C)	111.9	109.1	104.3	104.9	95.62	65.1	56.34	40.18	91.78	56.34	95.61
pH	7.407	7.583	7.615	7.896	7.634	7.70	7.768	7.94	8.139	7.815	7.759
Ca ²⁺	1.75×10^{-2}	6.49×10^{-3}	2.14×10^{-3}	1.08×10^{-3}	1.36×10^{-3}	4.20×10^{-4}	4.46×10^{-4}	5.73×10^{-4}	7.24×10^{-5}	3.52×10^{-4}	3.34×10^{-4}
Mg ²⁺	1.70×10^{-5}	2.95×10^{-6}	4.13×10^{-6}	5.75×10^{-7}	1.13×10^{-5}	4.82×10^{-5}	5.52×10^{-5}	8.51×10^{-5}	2.54×10^{-7}	4.31×10^{-5}	6.34×10^{-6}
Na ⁺	3.89×10^{-3}	2.63×10^{-3}	2.67×10^{-3}	1.26×10^{-3}	5.53×10^{-3}	8.09×10^{-3}	7.65×10^{-3}	7.31×10^{-3}	4.27×10^{-3}	6.82×10^{-3}	4.80×10^{-3}
Cl ⁻	2.01×10^{-2}	5.02×10^{-3}	3.35×10^{-3}	1.03×10^{-3}	3.28×10^{-3}	3.32×10^{-3}	7.44×10^{-4}	5.61×10^{-4}	7.34×10^{-4}	6.00×10^{-4}	1.30×10^{-3}
SiO ₂ (aq)	9.42×10^{-3}	7.42×10^{-3}	6.96×10^{-3}	7.38×10^{-3}	1.22×10^{-2}	2.90×10^{-3}	2.46×10^{-3}	1.79×10^{-3}	4.15×10^{-3}	2.47×10^{-3}	1.19×10^{-2}
HCO ₃ ⁻	5.57×10^{-5}	9.06×10^{-5}	1.95×10^{-4}	1.64×10^{-4}	4.18×10^{-4}	2.93×10^{-3}	6.72×10^{-3}	6.92×10^{-3}	2.04×10^{-3}	5.74×10^{-3}	1.13×10^{-3}
SO ₄ ²⁻	8.87×10^{-3}	4.89×10^{-3}	1.50×10^{-3}	5.88×10^{-4}	1.77×10^{-3}	1.21×10^{-3}	4.12×10^{-4}	3.55×10^{-4}	1.18×10^{-4}	3.80×10^{-4}	7.29×10^{-4}
K ⁺	8.68×10^{-4}	5.40×10^{-4}	5.00×10^{-4}	2.38×10^{-4}	8.68×10^{-4}	6.25×10^{-4}	4.67×10^{-4}	2.76×10^{-4}	5.02×10^{-4}	4.17×10^{-4}	7.50×10^{-4}
AlO ₂ ⁻	3.27×10^{-8}	7.08×10^{-8}	5.02×10^{-8}	9.97×10^{-8}	8.03×10^{-10}	5.36×10^{-9}	3.62×10^{-9}	1.50×10^{-9}	6.09×10^{-8}	4.03×10^{-9}	1.42×10^{-9}
F ⁻	1.93×10^{-4}	2.46×10^{-4}	3.48×10^{-4}	4.28×10^{-4}	1.00×10^{-3}	8.26×10^{-4}	7.81×10^{-4}	6.43×10^{-4}	9.77×10^{-4}	8.61×10^{-4}	1.38×10^{-3}
NO ₃ ⁻	1.30×10^{-3}	5.46×10^{-4}	1.83×10^{-4}	1.33×10^{-4}	2.22×10^{-4}	1.04×10^{-4}	6.87×10^{-5}	3.97×10^{-5}	3.10×10^{-4}	4.25×10^{-5}	1.26×10^{-4}
CO ₂ (g) (bar)	3.89×10^{-4}	4.93×10^{-4}	1.04×10^{-3}	4.88×10^{-4}	1.88×10^{-3}	7.06×10^{-3}	1.19×10^{-2}	6.34×10^{-3}	2.94×10^{-3}	9.19×10^{-3}	4.06×10^{-3}
log CO ₂ (g)	-3.410	-3.307	-2.984	-3.312	-2.726	-2.151	-1.926	-2.198	-2.532	-2.037	-2.392

Source: BSC 2003e, Tables 6.6-4 and 6.6-5.

NOTE: Units for aqueous species are in moles/kg H₂O. The frequencies presented on row 1 represent the percentage of all 368 thermal-hydrologic-chemical seepage model waters used as input. This includes both "crown" waters and "invert" waters. For actual bin probabilities of crown seepage through time see Table 4-5.

4.1.4 Seepage Scenario Process Model Results

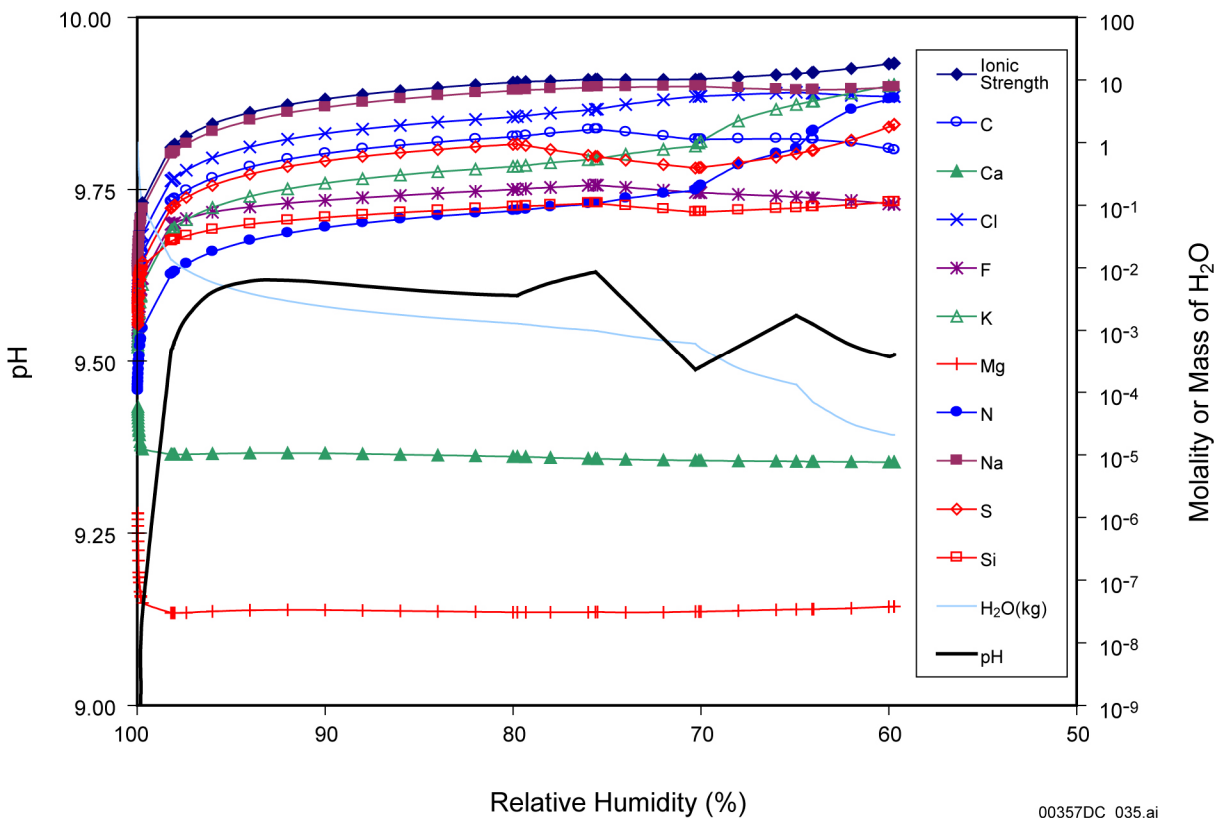
The 11 starting water compositions (or bins) shown on Table 4-4 are used as inputs into the in-drift precipitates and salts model along with a range of temperature (100°C, 70°C, and 40°C) and $p\text{CO}_2$ values (10^{-2} , 10^{-3} , and 10^{-4} bar). These bins are associated with the presence of actual liquid water that could flow into the drift and predicted range of $p\text{CO}_2$ values from the thermal-hydrologic-chemical seepage model through time. These bins and conditions were used to create a set of 99 lookup tables (11 bins \times 3 temperatures \times 3 $p\text{CO}_2$ values) that represent 11 response surfaces of evaporative chemistry. The output for pH, ionic strength, and chemical species in the tables is in terms of relative humidity to account for the evaporative concentration of each of the starting waters. Figures 4-7 and 4-8 are representative results for total elemental aqueous species and precipitating minerals for the most likely bin to occur during the first 20,000 years (bin 7, see Table 4-5) based on the time-integrated bin probability at 70°C and with $p\text{CO}_2$ of 10^{-3} bar.

Table 4-5. Starting Water Composition Scenario Probability (W0 to W7) and Time Integrated Bin Probability (Norm %) of Occurrence for Any Given Crown Seepage Bin for the 20,000-Year Simulation Period

Water	W0 %	W4 %	W5 %	W6 %	W7 %	Sum %	Norm %
Bin 1	0.00	0.00	0.00	0.00	0.00	0.00	0.00
Bin 2	0.00	0.00	0.00	0.00	0.00	0.00	0.00
Bin 3	1.12	0.00	0.00	0.00	0.00	1.12	0.22
Bin 4	2.62	1.00	1.00	1.00	1.50	7.12	1.42
Bin 5	0.56	1.87	1.00	0.00	0.50	3.93	0.79
Bin 6	25.82	0.00	0.00	1.50	0.00	27.32	5.46
Bin 7	31.75	26.48	32.01	0.25	45.25	135.74	27.15
Bin 8	12.50	31.03	12.50	12.50	12.50	81.02	16.20
Bin 9	0.00	12.50	13.00	39.75	12.50	77.75	15.55
Bin 10	0.00	0.25	13.24	45.00	0.00	58.49	11.70
Bin 11	25.63	26.88	27.25	0.00	27.75	107.50	21.50
Sum	100.00	100.00	100.00	100.00	100.00	500.00	100.00

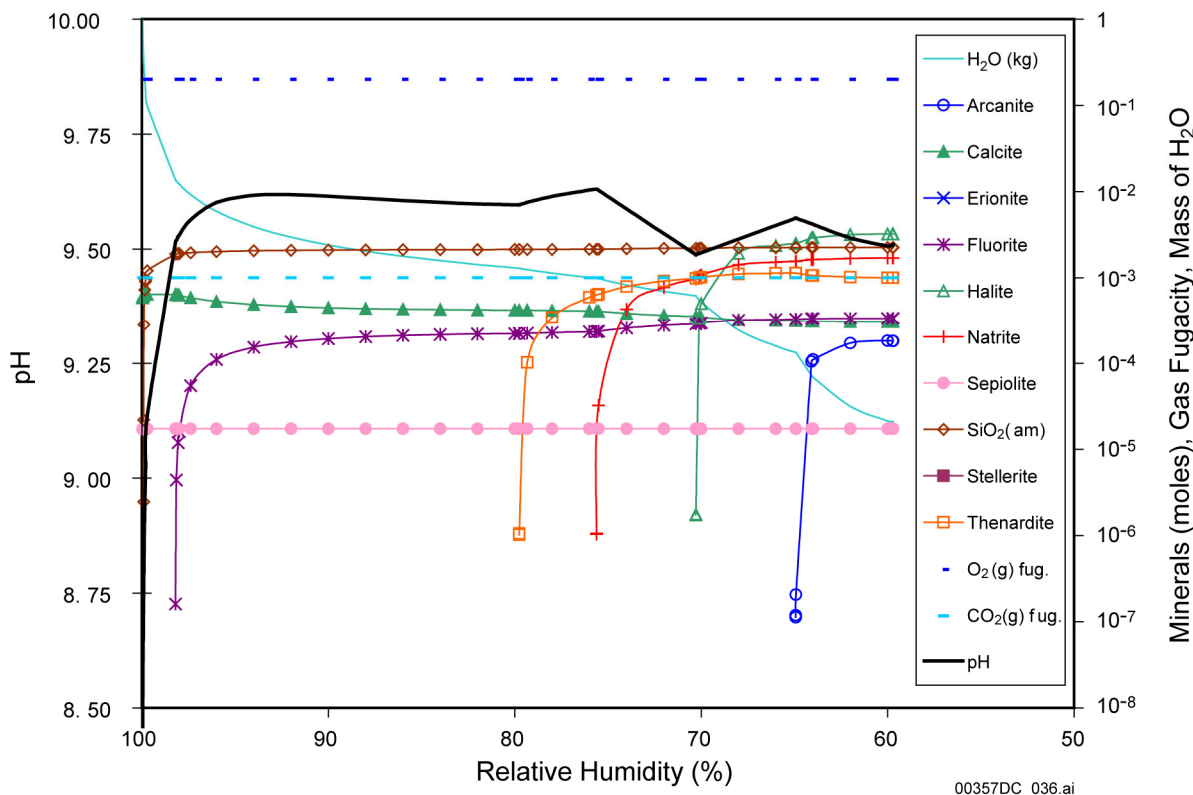
Source: BSC 2003e, Table 6.14-1.

NOTE: W0 through W7 refer to the five thermal-hydrologic-chemical seepage model output starting pore waters as listed in Section 3.2.1. A 1.0 percent time-integrated bin probability implies that a water type exists for 200 years out of the 20,000-year simulation period.



Source: DTN: MO0304SPACSALT.000\07C3T7E.XLS.XLS.

Figure 4-7. Bin 7 Aqueous Composition Evaporation Predictions versus Relative Humidity at 70°C and a $p\text{CO}_2$ of 10^{-3} bar



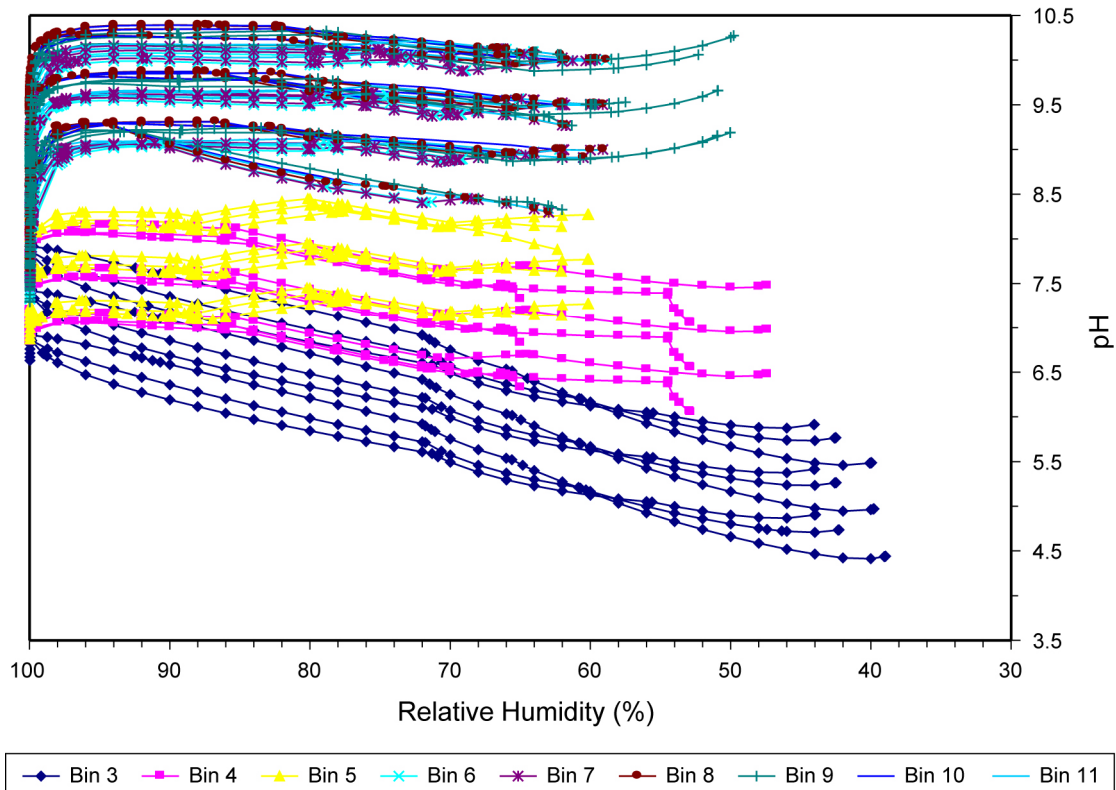
Source: DTN: MO0304SPACSALT.000\07C3T7E.XLS.XLS.

Figure 4-8. Bin 7 Mineral Precipitation Evaporation Predictions versus Relative Humidity at 70°C and a $p\text{CO}_2$ of 10^{-3} bar

The lookup tables represent response surfaces, and, therefore, the potential ranges of outputs for the ranges of inputs simulated. As the critical inputs (temperature and relative humidity) are provided by the *Multiscale Thermohydrologic Model Report* (BSC 2003a, see Section 2), the lookup tables have not been used to determine the actual chemistry at a given point in time outside of the TSPA model. The lookup tables do, however, represent the range of possible chemistries that could be present on the waste package or drip shield given the input parameters. This range of chemistry is discussed in detail in Section 6.14 of the *Engineered Barrier System: Physical and Chemical Environment Model* (BSC 2003e). Given the ranges of expected variation in temperature and relative humidity at any given point in time (see Figure 2-11), only a limited subset of the entire range of chemistry provided by the lookup tables would be expected to be relevant. Thus, the ranges discussed in the paragraph below reasonably bound the expected values.

Figure 4-9 shows the range of pH that is expected (about 10.5 to about 4.5) on the surface of the waste package or drip shield. Note that bin 1 and bin 2 waters are not possible chemistries for the seepage entering the crown of the drift (see Table 4-5). Therefore, these two bins are not expected to drip onto waste package or drip shield surfaces and are not presented in this figure. In addition, the bin 3 waters are only projected to occur in the rock above the drift at times when the drift wall is above 100°C and seepage into the drift is prevented by the vaporization barrier effect. Figures 4-10 through 4-13 show the ranges for aqueous F^- (about 10^{-5} to about 1 molal),

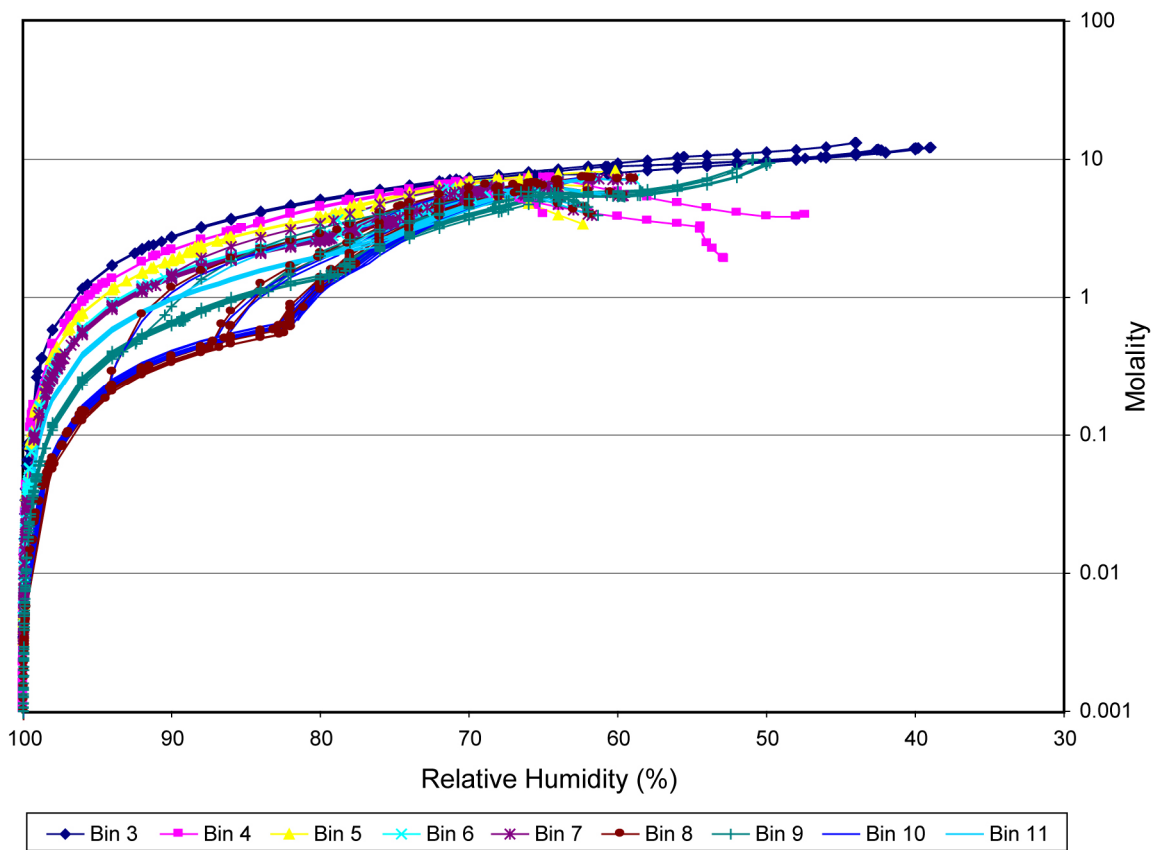
Cl^- (about 0.001 to about 10 molal), ionic strength (about 0.01 to about 30 molal), and $\text{Cl}^-/\text{NO}_3^-$ molal ratio (about 0.1 to about 30). The chemistry for dust leachate or deliquescence conditions falls within these ranges. With the exception of bin 3, the evaporative evolution of the nine possible bins are expected to form K-Cl, K- NO_3 , Na-Cl, or Na- NO_3 solutions. Bin 3 has the potential to form Ca-Cl brines on waste package or drip shield surfaces during its evaporative evolution. However, the time-integrated probability through 20,000 years of this occurring is 0.22 percent (Table 4-5). Closer examination indicates that this would only occur between about 225 to 450 years after waste emplacement (Figure 4-14). This is precisely the time that seepage into the drifts is not expected to occur due to the thermal heat load (Section 2.3.3).



Source: BSC 2003e, Figure 6.14-15.

NOTE: Evaporation of the waters is modeled at each possible combination of three temperatures (40°C, 70°C, and 100°C) and three $p\text{CO}_2$ values (10^{-2} , 10^{-3} , and 10^{-4} bar).

Figure 4-9. Range of pH versus Relative Humidity for the Seepage Evaporation Lookup Tables Representing Bins 3 through 11 (at Three Temperatures and Three $p\text{CO}_2$ Values)

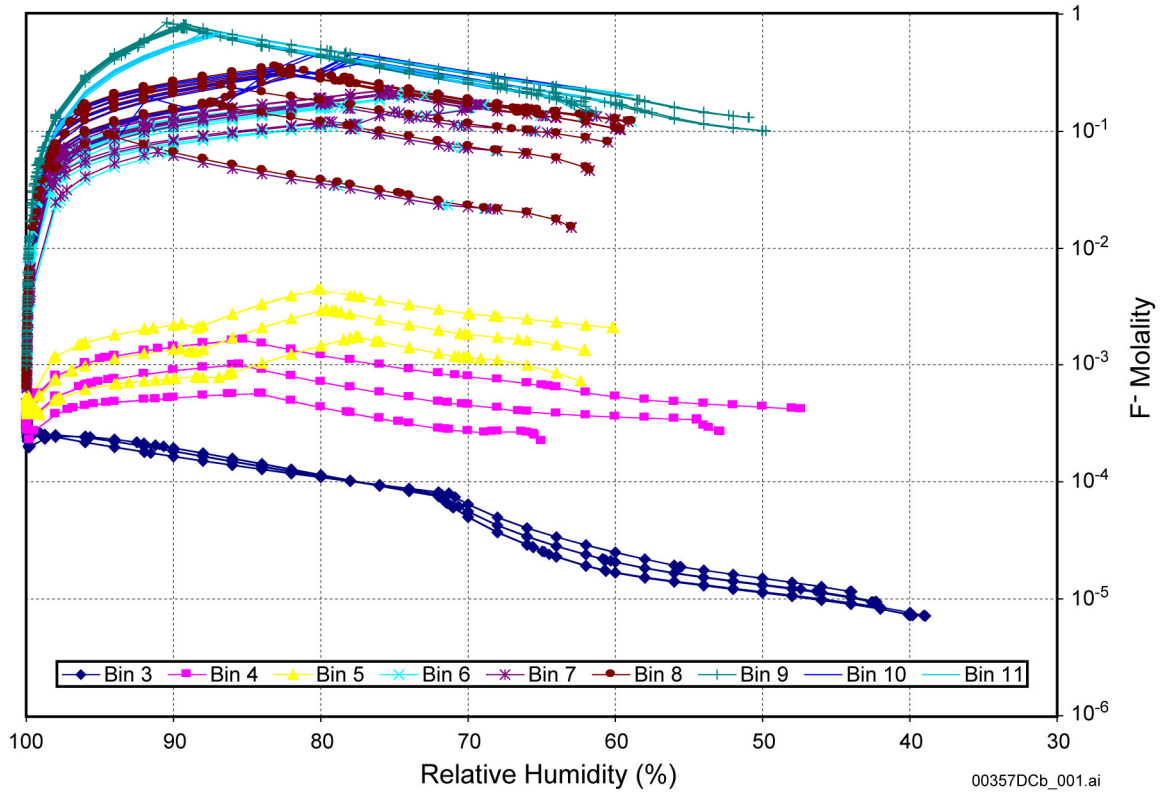


00357DCa_019.ai

Source: BSC 2003e, Figure 6.14-28.

NOTE: Evaporation of the waters is modeled at each possible combination of three temperatures (40°C, 70°C, and 100°C) and three pCO₂ values (10⁻², 10⁻³, and 10⁻⁴ bar).

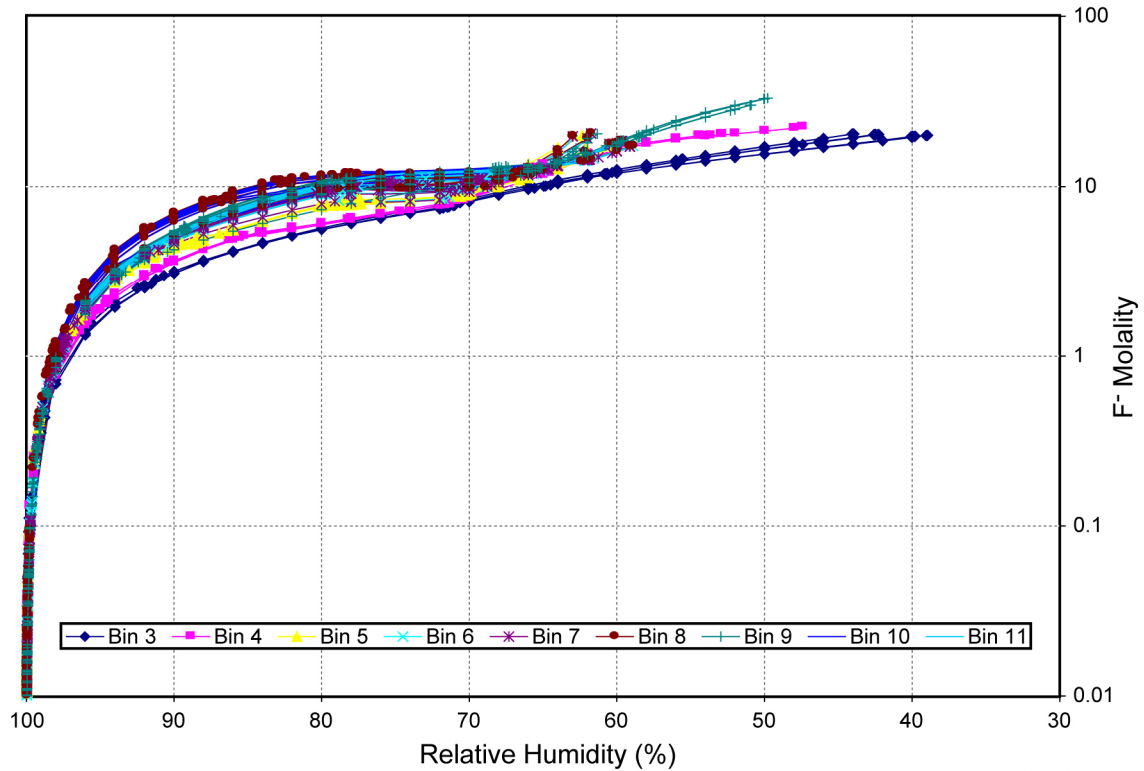
Figure 4-10. Range of Cl⁻ Molality versus Relative Humidity for the Seepage Evaporation Lookup Tables Representing Bins 3 through 11 (at Three Temperatures and Three pCO₂ Values)



Source: BSC 2003e, Figure 6.14-27.

NOTE: Evaporation of the waters is modeled at each possible combination of three temperatures (40°C, 70°C, and 100°C) and three $p\text{CO}_2$ values (10^{-2} , 10^{-3} , and 10^{-4} bar).

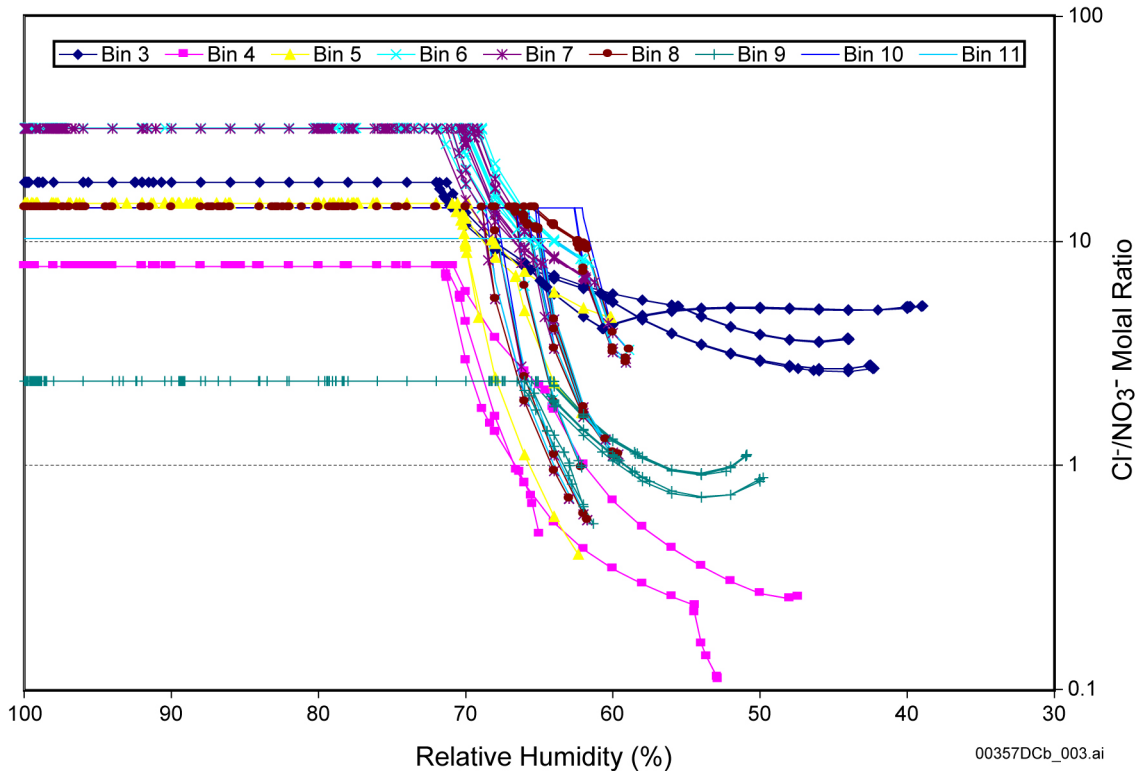
Figure 4-11. Range of F^- Molality versus Relative Humidity for the Seepage Evaporation Lookup Tables Representing Bins 3 through 11 (at Three Temperatures and Three $p\text{CO}_2$ Values)



Source: BSC 2003e, Figure 6.14-33.

NOTE: Evaporation of the waters is modeled at each possible combination of three temperatures (40°C, 70°C, and 100°C) and three $p\text{CO}_2$ values (10^{-2} , 10^{-3} , and 10^{-4} bar).

Figure 4-12. Range of Ionic Strength versus Relative Humidity for the Seepage Evaporation Lookup Tables Representing Bins 3 through 11 (at Three Temperatures and Three $p\text{CO}_2$ Values)



Source: BSC 2003e, Figure 6.14-29.

NOTE: Evaporation of the waters is modeled at each possible combination of three temperatures (40°C, 70°C, and 100°C) and three pCO₂ values (10⁻², 10⁻³, and 10⁻⁴ bar).

Figure 4-13. Range of Cl⁻/NO₃⁻ Molal Ratios for the Seepage Evaporation Lookup Tables Representing Bins 3 through 11 (at Three Temperatures and Three pCO₂ Values)

W0			W4			W5			W6			W7		
Time	Invert	Crown												
10	4	4	10	10	10	10	7	7	10	7	7	10	7	7
51	5	5	51	11	11	51	11	11	51	9	9	51	11	11
53	11	5	53	11	11	53	11	11	53	9	9	53	11	11
55	11	6	55	11	11	55	11	11	55	9	9	55	11	11
60	2	6	60	4	11	60	3	11	60	2	9	60	3	11
75	1	5	75	11	11	75	1	11	75	1	9	75	1	11
100	1	5	100	11	11	100	2	11	100	2	9	100	2	11
150	2	4	150	4	11	150	4	11	150	4	9	150	4	11
200	2	4	200	4	11	200	4	11	200	4	9	200	4	11
250	2	3	250	5	11	250	5	11	250	9	9	250	4	11
300	2	3	300	4	11	300	4	11	300	4	9	300	3	5
350	2	3	350	5	11	350	4	11	350	4	9	350	3	4
400	2	3	400	5	11	400	4	11	400	9	9	400	3	4
500	2	4	500	4	5	500	4	9	500	4	6	500	2	4
600	3	4	600	4	5	600	5	11	600	4	9	600	3	4
650	3	5	650	4	11	650	5	11	650	9	9	650	4	5
700	4	11	700	5	11	700	11	11	700	9	9	700	4	11
751	4	11	751	5	11	751	11	11	751	9	9	751	4	11
790	4	11	801	11	11	785	11	11	801	9	9	784	5	11
801	4	11	804	11	11	801	11	11	865	9	9	801	5	11
1001	5	11	1001	11	11	1001	11	11	1001	9	9	1001	6	11
1201	5	11	1201	11	11	1201	11	11	1201	9	9	1201	11	11
1401	5	11	1401	11	11	1401	11	11	1401	9	9	1401	11	11
1601	5	11	1601	11	11	1601	11	11	1601	9	9	1601	11	11
1801	5	11	1801	11	5	1801	11	5	1801	9	6	1801	11	11
2001	9	4	2001	11	4	2001	11	4	2001	9	4	2001	11	11
2202	11	11	2202	11	11	2202	11	11	2202	9	9	2202	11	11
2402	11	11	2402	11	11	2392	11	11	2402	9	9	2402	11	11
3002	11	11	2597	11	11	2402	11	11	3002	9	9	2592	11	11
5003	11	11	3002	11	11	3002	11	11	3049	9	9	3002	11	11
7005	6	6	5003	11	11	5003	11	11	5003	9	9	5003	11	11
10007	7	6	7005	9	9	7005	9	9	7005	9	9	7005	9	9
12310	7	7	10007	7	7	10007	10	10	10007	10	10	10007	7	7
15010	7	7	12598	7	7	12304	7	7	13054	10	10	12596	7	7
20013	8	8	15010	8	8	15010	7	7	15010	10	10	15010	7	7
50035	8	8	20013	8	8	20013	8	8	20013	8	8	20013	8	8
			50035	8	8	50035	8	8	50035	8	8	50035	8	8

00357DCb_004.ai

Source: BSC 2003e, Figure 6.14-1.

NOTE: Each color uniquely identifies each bin. Time is in units of years.

Figure 4-14. Bin History Maps Showing Bin Occurrence for Crown Seepage and Invert Wicking Locations

4.1.5 Effects of Introduced Materials on Seepage

Evolution of seepage water compositions includes the effects of changes in temperature and relative humidity and considers the potential effects of interactions with natural and introduced materials within the drift. The effects of these interactions are included in the engineered barrier system physical and chemical environment model (BSC 2003e, Sections 6.8 and 6.11). Ground-support elements are expected to corrode as they interact with seepage entering the drift and with seepage waters modified by interactions with other materials such as microbial communities or dust. Corrosion products will also form by interactions with condensate water or humid air.

There are several elements that are or could be present in trace quantities (less than 1 percent of total metal/alloy) in the repository drift. These include nickel, molybdenum, palladium, cobalt, tungsten, boron, and copper. These are present in very low quantities, and as such have very small effects on solution chemistry. These small effects are dwarfed by the uncertainties associated with any bulk geochemical calculation. The more prevalent elements examined in detail are iron and chromium.

The bounding case (or base case) model examined in detail is defined by the following:

- Material (Steel Wire Fabric Stainless Steel Type 316L) and dimensions as defined on IED: 800-IED-WIS0-00302-000-00A (BSC 2003q)
- Bin 11 seepage water
- Predominant Stainless Steel Type 316L corrosion products include iron(III) and chromium(III) compounds
- Primary controlling mineral phases for stainless steel corrosion products: goethite and amorphous chromium hydroxide
- Temperature of 25°C and fugacity of CO₂ at 10⁻³ bar
- Abstracted corrosion rates (see Table 4-6).

Table 4-6. Corrosion Rates for Stainless Steel Type 316L

Hot Dry Period (0 to 2,000 years)	Cooler Period (beyond 2,000 years)	Sensitivity Study Cases
0.113 μm/yr	1.9391 μm/yr	Factor of 10 greater

Source: BSC 2003e, Section 6.8.3 and 6.13.4.

This base case includes a relatively high corrosion rate for the 316L stainless steel ground support wire fabric to maximize the effects of the corrosion products on incoming seepage water for evaluation purposes.

Bin 11 seepage water was chosen because it is prevalent during the relevant time period for the corrosion of Stainless Steel Type 316L (approximately 500 to 5,000 years, see Figure 4-14).

Iron(III) and chromium(III) have been selected as the corrosion end products influencing the seepage water chemistry. Iron(III) was selected rather than iron(II) because it is the oxidation state stable under the relatively oxidizing conditions (atmospheric O₂ concentrations leading to significant dissolved oxygen content) and the mild pH ranges of the seepage waters. Selection of chromium(III) over that of the more soluble chromium(VI) species is based upon the experimental observation of corrosion products, and the kinetics and conditions required to obtain the fully oxidized chromium(VI) state.

Goethite was selected as the iron-controlling mineral phase rather than the more thermodynamically stable hematite for kinetic reasons. The chromium phase that controls the concentrations of chromium(III) was chosen to be the most soluble and kinetically favored amorphous chrome hydroxide (Cr(OH)₃). The bounding case is limited to supporting calculations at 25°C because the solubility of Cr(OH)₃ is known only at this temperature. A CO₂ fugacity of 10⁻³ bar was chosen to be consistent with the median value from the ranges used for in-drift seepage evaporation.

The net effect of considering stainless steel corrosion on the chemistry of Bin 11 waters chosen for evaluation was found to be negligible (Table 4-7). Validation of the application of the model used for these analyses is summarized in Section 4.4.4.

Table 4-7. Absolute (Percent Relative) Differential Effect of Stainless Steel Type 316L Dissolution in Bin 11 Seepage Water at 100 and 98 Percent Relative Humidity

RH	Δ pH	Δ (Ionic Strength)	Δ (Cl moles/ kg H ₂ O)	Δ (Si moles/ kg H ₂ O)	Δ (C moles/ kg H ₂ O)
100	0.0000	2.0×10^{-8} (3×10^{-4})	4.2×10^{-9} (1×10^{-4})	4.6×10^{-10} (2×10^{-5})	1.1×10^{-8} (8×10^{-4})
98	0.0001	-3.8×10^{-4} (-0.05)	-1.1×10^{-4} (-0.05)	-2.4×10^{-5} (0.07)	-5.9×10^{-5} (-0.05)

Source: BSC 2003e, Table 6.8-5.

4.1.6 Seepage Scenario Summary

The following conclusions can be reached from the information presented in Section 4.1:

- The model has been developed to capture the chemical divide phenomenon.
- The model uses the likely range of thermal-hydrologic-chemical seepage model results as direct input into the drift.
- The seepage compositions have been grouped or binned into 11 representative compositions that control the formation of brines in the drift.
- The evaporative evolution of the 11 seepage bin waters predicts that the corrosive calcium- and magnesium-chloride brines are unlikely to form on waste packages and drip shields.
- The upper limit in evaporative F⁻ concentrations is 1 molal.
- Corrosion of ground support materials will not affect the composition of seepage contacting the drip shield or waste package.

4.2. DUST DELIQUESCENCE

4.2.1 Conceptual Understanding

In the absence of solutes, condensation occurs on solid surfaces when the surface temperature is less than the dew point temperature (i.e., when the equivalent relative humidity in the gas phase at this location is 100 percent). (Capillary condensation is relatively unimportant for the temperature and relative humidity conditions discussed here.) Stated differently, liquid water can exist on the surface of the drip shield or waste package when the equivalent relative humidity is 100 percent. At lower values of this relative humidity, water can exist only in thin films, or in concentrated solution conditions that depress the chemical activity of the solvent water. Dissolved solutes (such as salts) therefore lower the relative humidity at which the aqueous (liquid water) conditions can occur on the drip shield or waste packages.

The conceptual basis for the evolution of dust is different from that of seepage waters. Seepage waters are cooler and relatively dilute as they enter the in-drift environment, then become more concentrated when they encounter the warmer surfaces of the drip shield or waste package and evaporate. Dust will tend to accumulate during the preclosure and postclosure periods when temperatures are lower, then deliquesce as relative humidity increases. These dust deliquescence brines will become more dilute as relative humidity continues to rise. Dust deposits on waste packages will form principally from particulate matter and aerosols suspended by preclosure ventilation, although some additional air movement and possible dust deposition may also occur after the drip shields are installed at closure. The dust analyses presented here are based on measured compositions of dust samples acquired from the exploratory tunnels, drifts, and alcoves underground at Yucca Mountain.

Considering locations that are not affected by seepage (e.g., waste packages under intact drip shields) the dust will acquire moisture from humidity in the air. As the relative humidity gradually increases with time after permanent closure (after 50 years in Figure 2-11), the most hygroscopic components of dust will be the first to deliquesce and form aqueous solutions.

4.2.2 Technical Basis

Analysis of the effects of deliquescence is based on *In-Drift Precipitates/Salts Model* (BSC 2003d). The model uses a Pitzer approach and database to represent concentrated solution conditions, as discussed in Section 4.1. This model has been validated by comparison of predictions against measured mineral solubilities and other types of chemical data reported in the technical literature, for solution temperatures up to 125°C. This range is more than adequate for analysis of the in-drift evolution of potential seepage water from the host rock as relative humidity and temperature evolve. Further work is in progress using additional chemical data to extend this validation range to 140°C or greater, specifically to support analysis of dust and salt minerals at higher temperatures. Calculations in this document are reported to 140°C with the expectation that the validation range will be extended, with quantitative uncertainty estimates pertaining to application of the model at the higher temperatures revised accordingly (BSC 2003d).

Additional insight is gained from the known relative solubilities of different salts, particularly the common halide and nitrate salts, at elevated temperatures and associated humidity conditions beyond the validation range for the in-drift precipitates and salts model (BSC 2003e, Section 6.13). Specifically, nitrate salts of sodium and potassium tend to be more soluble than the corresponding chloride salts. Hence, for chemical systems such as dust systems analyzed below, evaporative concentration causes the Cl^-/NO_3^- concentration ratio to be unchanged as both species remain in solution, then on further evaporation the ratio decreases as chloride salts precipitate. This is the expected behavior at temperatures beyond the validation range pursued for the in-drift precipitates and salts model (i.e., greater than 140°C).

4.2.3 Deliquescence Analysis Results

Aqueous chemistry resulting from the response of dust to elevated temperature and decreased relative humidity is evaluated using the in-drift precipitates and salts model as described below (BSC 2003e, Section 6.10). Chemical compositions are reported for six dust systems, for discrete

ranges of temperature, relative humidity, and $p\text{CO}_2$, suitable for use directly in TSPA. The model is also used to determine whether the relative humidity conditions are too dry for liquid water to exist in a particular dust system (i.e., too dry for deliquescence of the salt mineral assemblage in the dust).

The deliquescent response of dust is represented in the physical and chemical environment model using a binning methodology similar to that used for evolution seepage (Section 4.1.3). A total of 52 leaching analyses of the soluble constituents of dust, are arranged into six bins based on similar chemistry. These six bins represent the range of compositions from two series of dust leachate analyses, using dust samples collected in the ESF (DTNs: MO0207EBSDUSTS.020 and MO0209EBSDUST2.030). Table 4-8 represents the median compositions of the six leachate bins at 25°C.

Table 4-8. Total EQ3NR Equilibrated Aqueous Elemental Compositions for the Six Median Waters Selected to Represent the Dust Leachate Bins

Compositions	Bin 1	Bin 2	Bin 3	Bin 4	Bin 5	Bin 6
pH	8.54	8.09	8.23	8.54	8.40	8.05
Ionic Strength	5.43×10^{-3}	2.74×10^{-3}	2.01×10^{-3}	6.29×10^{-3}	3.80×10^{-3}	1.15×10^{-3}
Br^-	5.01×10^{-6}	1.00×10^{-5}	3.75×10^{-6}	1.63×10^{-5}	1.63×10^{-5}	3.75×10^{-6}
CO_3	1.96×10^{-3}	6.50×10^{-4}	8.86×10^{-4}	1.94×10^{-3}	1.36×10^{-3}	5.81×10^{-4}
Ca^{2+}	1.35×10^{-3}	5.41×10^{-4}	3.09×10^{-4}	1.22×10^{-3}	7.17×10^{-4}	1.52×10^{-4}
Cl^-	2.17×10^{-4}	1.44×10^{-4}	1.35×10^{-4}	4.23×10^{-4}	2.82×10^{-4}	1.38×10^{-4}
F^-	3.16×10^{-5}	1.58×10^{-5}	1.58×10^{-5}	2.11×10^{-5}	3.68×10^{-5}	2.11×10^{-5}
K^+	2.63×10^{-4}	1.93×10^{-4}	2.99×10^{-4}	3.32×10^{-4}	2.63×10^{-4}	1.98×10^{-4}
Mg^{2+}	1.65×10^{-4}	5.35×10^{-5}	4.81×10^{-5}	1.63×10^{-4}	7.08×10^{-5}	2.14×10^{-5}
NO_3^-	5.16×10^{-4}	1.77×10^{-4}	1.18×10^{-4}	5.48×10^{-4}	3.23×10^{-4}	5.64×10^{-5}
Na^+	4.24×10^{-4}	4.05×10^{-4}	4.83×10^{-4}	1.34×10^{-3}	9.03×10^{-4}	3.72×10^{-4}
SO_4^{2-}	4.37×10^{-4}	3.96×10^{-4}	1.67×10^{-4}	6.97×10^{-4}	3.44×10^{-4}	6.04×10^{-5}
$\text{SiO}_2(\text{aq})$	1.46×10^{-4}	3.25×10^{-5}	6.27×10^{-5}	4.89×10^{-5}	7.91×10^{-5}	4.78×10^{-5}

Source: BSC 2003e, Table 6.10-9.

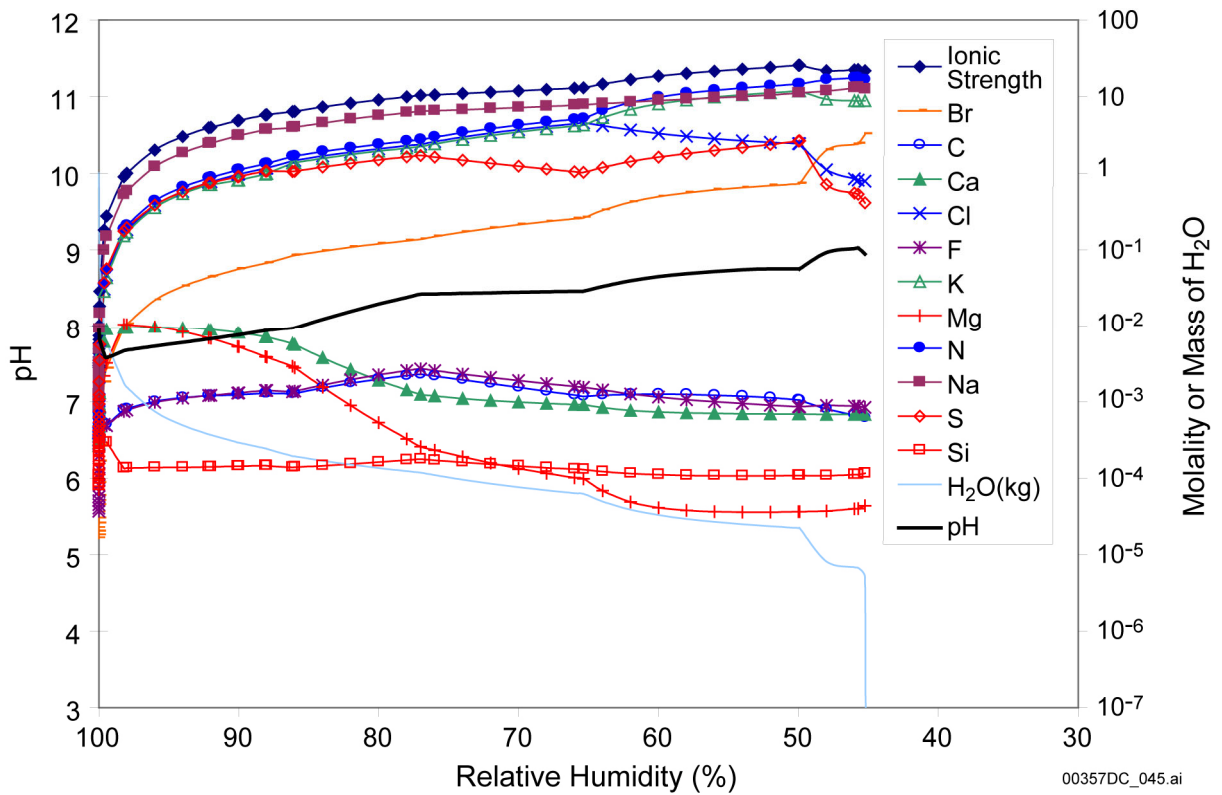
NOTE: Except for pH, all units are in moles/kg H_2O . CO_3 indicates total aqueous carbonate, comprising $\text{CO}_2(\text{aq})$, HCO_3^- , and CO_3^{2-} .

The median compositions of these six bins (Table 4-8) is used as input along with discrete temperature values 140°C, 120°C, 100°C, 70°C, and 40°C and $p\text{CO}_2$ values for equilibrium calculations of 10^{-2} , 10^{-3} , and 10^{-4} bar. The range of $p\text{CO}_2$ values is consistent with the thermal-hydrologic-chemical seepage model (BSC 2003c). A total of 90 calculations were performed (six bins \times five temperatures \times three $p\text{CO}_2$ values). For each set of calculations, a separate lookup table was produced. Within each table the composition was posted for a range of discrete values of relative humidity (water activity). Figures 4-15 and 4-16 are representative results for $T=70^\circ\text{C}$ and $p\text{CO}_2$ 10^{-3} bar, for bin 5 which is the most prevalent (Table 4-9). These lookup tables are used directly in TSPA to represent the expected chemistry of deliquescent dust when no seepage is present in the drift. Figures 4-17 and 4-18 show the $\text{Cl}^-/\text{NO}_3^-$ ratio for all 90 evaporation calculations as a function of relative humidity, and clearly depicts that, below the halite divide (the point at which halite precipitates and the ratio begins to drop), NO_3^- becomes the dominate anionic species. Table 4-10 presents the calculated deliquescence point relative humidities, pH values, and Cl^- and NO_3^- concentrations for each of the dust bin compositions.

Table 4-9. Percentage of Dust Leachate Waters in Each Bin

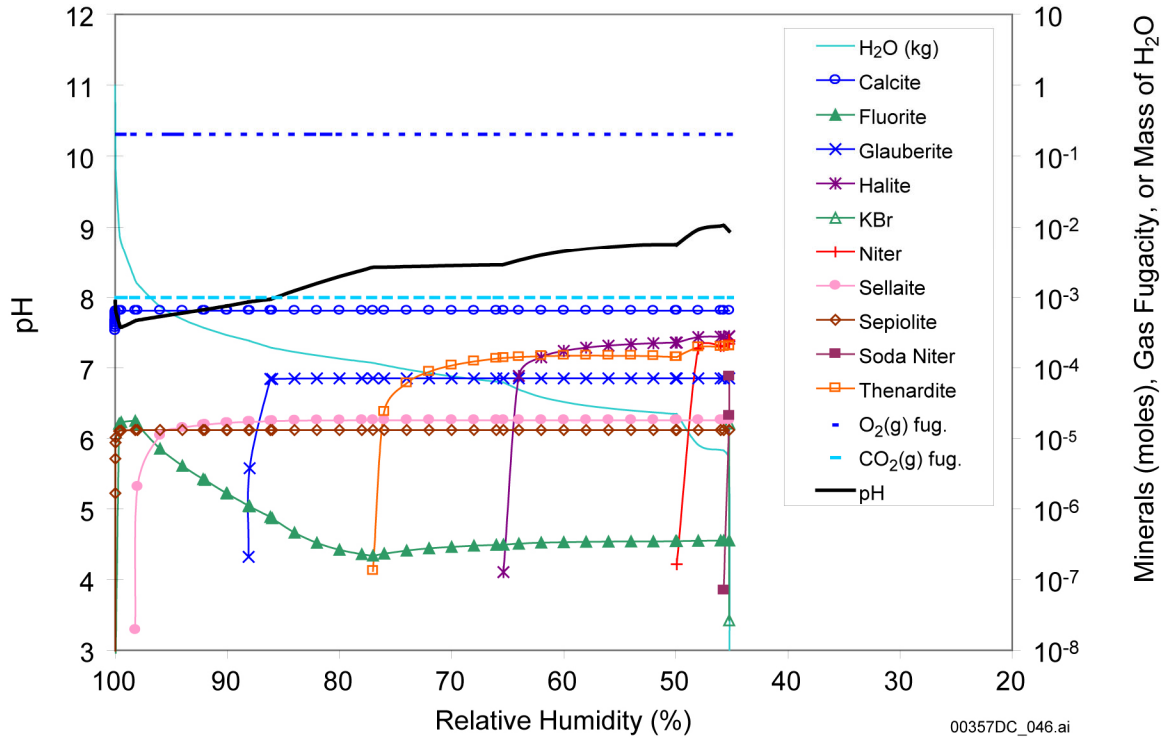
Bin	Number of Waters in the Bin	% of All Evaporated Waters Represented by the Bin
Bin 1	3	5.77
Bin 2	4	7.69
Bin 3	9	17.31
Bin 4	12	23.08
Bin 5	23	44.23
Bin 6	1	1.92
Total	52	100.00

Source: BSC 2003e, Table 6.10-6.



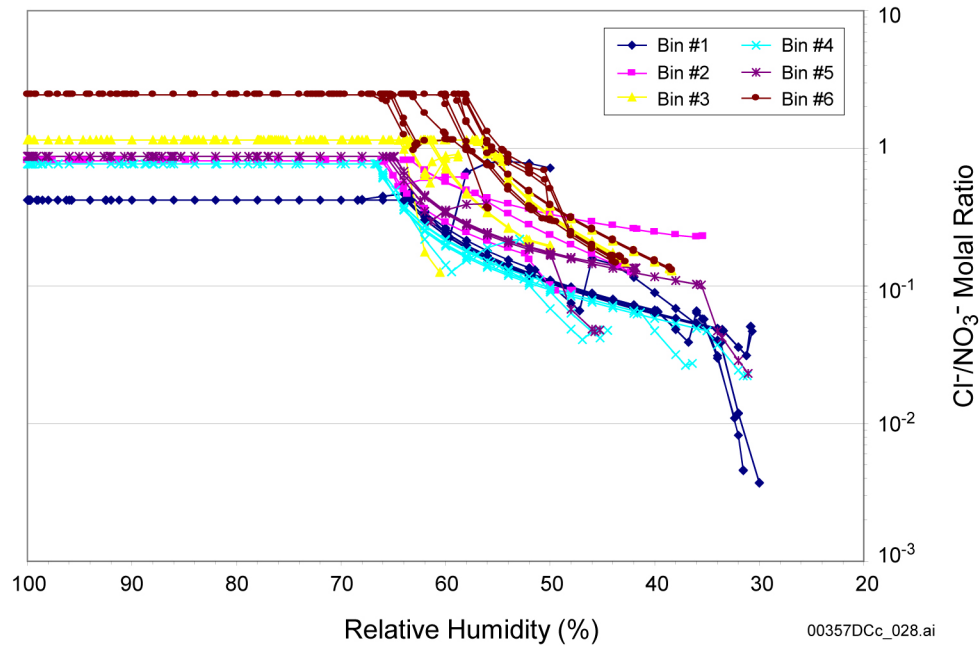
Source: DTN: MO0310SPADLALT.001\D5C3T07.XLS.

Figure 4-15. Bin 5 Aqueous Composition Evaporation Predictions versus Relative Humidity at 70°C and 10⁻³ CO₂ Fugacity



Source: DTN: MO0310SPADLALT.001\D6C3T07.XLS.

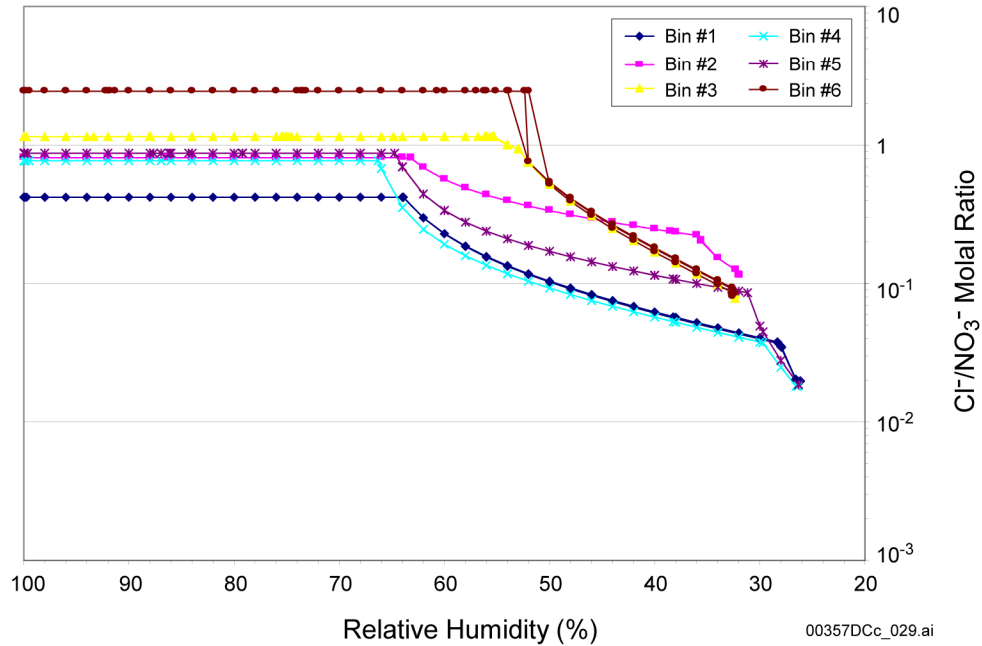
Figure 4-16. Bin 5 Mineral Precipitation Evaporation Predictions versus Relative Humidity at 70°C and 10⁻³ CO₂ Fugacity



Source: BSC 2003e, Figure 6.14-38.

NOTE: Evaporation of the waters is modeled at each possible combination of four temperatures (40°C, 70°C, 100°C, and 120°C) and three $p\text{CO}_2$ values (10^{-2} , 10^{-3} , and 10^{-4} bar).

Figure 4-17. Range of $\text{Cl}^-/\text{NO}_3^-$ Molal Ratios versus Relative Humidity for the Dust Leachate Lookup Tables Representing Bins 1 through 6



Source: BSC 2003e, Figure 6.14-38.

NOTE: Evaporation of the waters is modeled at 140°C and three $p\text{CO}_2$ values (10^{-2} , 10^{-3} , and 10^{-4} bar). Results at this temperature are preliminary pending extension of in-drift precipitates and salts model (BSC 2003d) validation.

Figure 4-18. Preliminary Range of $\text{Cl}^-/\text{NO}_3^-$ Molal Ratios versus Relative Humidity at 140°C for the Dust Leachate Lookup Tables Representing Bins 1 through 6

Table 4-10. Deliquescence Points and Anion Chemistry of Evolved Dust-Associated Waters for the Six Bin Chemistries Shown on Table 4-8

Bin	Temperature (°C)	pCO ₂ (bar)	Deliquescence Point Relative Humidity	pH	Ionic Strength (moles/kg H ₂ O)	Cl ⁻ (moles/kg H ₂ O)	NO ₃ ^{-a} (moles/kg H ₂ O)
1	40	0.0100	50.0% ^b	6.896	1.541 × 10 ¹	4.269	5.921
	70		30.0% ^b	9.106	4.17 × 10 ¹	1.04 × 10 ⁻¹	2.78 × 10 ¹
	100		31.5%	8.780	4.219 × 10 ¹	1.306 × 10 ⁻¹	2.837 × 10 ¹
	120		30.8%	6.486	2.782 × 10 ¹	1.065	2.089 × 10 ¹
	140		26.2%	6.255	2.780 × 10 ¹	5.061 × 10 ⁻¹	2.552 × 10 ¹
	40	0.0010	50.0% ^b	7.402	1.541 × 10 ¹	4.262	5.912
	70		30.0% ^b	9.612	4.178 × 10 ¹	1.027 × 10 ⁻¹	2.782 × 10 ¹
	100		31.5%	9.286	4.227 × 10 ¹	1.294 × 10 ⁻¹	2.842 × 10 ¹
	120		30.7%	6.801	2.732 × 10 ¹	1.031	2.199 × 10 ¹
	140		26.2%	6.752	2.782 × 10 ¹	5.078 × 10 ⁻¹	2.554 × 10 ¹
	40	0.0001	50.0% ^b	7.903	1.541 × 10 ¹	4.261	5.908
	70		30.0% ^b	10.110	4.178 × 10 ¹	1.030 × 10 ⁻¹	2.782 × 10 ¹
	100		32.4%	9.318	3.715 × 10 ¹	2.727 × 10 ⁻¹	2.490 × 10 ¹
	120		30.8%	7.454	2.782 × 10 ¹	1.066	2.106 × 10 ¹
	140		26.2%	7.253	2.783 × 10 ¹	5.038 × 10 ⁻¹	2.557 × 10 ¹
2	40	0.0100	58.1%	7.135	1.181 × 10 ¹	2.404	3.881
	70		47.8%	7.763	1.918 × 10 ¹	1.306	1.423 × 10 ¹
	100		42.2%	7.984	2.108 × 10 ¹	1.893	1.524 × 10 ¹
	120		35.4%	7.929	2.869 × 10 ¹	3.784	1.656 × 10 ¹
	140		32.0%	8.369	2.406 × 10 ¹	2.088	1.827 × 10 ¹
	40	0.0010	58.1%	7.635	1.181 × 10 ¹	2.404	3.881
	70		47.8%	8.263	1.918 × 10 ¹	1.306	1.423 × 10 ¹
	100		42.2%	8.484	2.108 × 10 ¹	1.893	1.524 × 10 ¹
	120		35.4%	8.445	2.840 × 10 ¹	3.752	1.655 × 10 ¹
	140		32.0%	8.869	2.406 × 10 ¹	2.088	1.827 × 10 ¹
	40	0.0001	58.1%	8.135	1.181 × 10 ¹	2.404	3.882
	70		47.8%	8.763	1.918 × 10 ¹	1.306	1.423 × 10 ¹
	100		42.2%	8.984	2.108 × 10 ¹	1.893	1.524 × 10 ¹
	120		35.4%	8.947	2.836 × 10 ¹	3.749	1.654 × 10 ¹
	140		32.0%	9.369	2.406 × 10 ¹	2.088	1.827 × 10 ¹

Table 4-10. Deliquescence Points and Anion Chemistry of Evolved Dust-Associated Waters for the Six Bin Chemistries Shown on Table 4-8 (Continued)

Bin	Temperature (°C)	pCO ₂ (bar)	Deliquescence Point Relative Humidity	pH	Ionic Strength (moles/kg H ₂ O)	Cl ⁻ (moles/kg H ₂ O)	NO ₃ ^{-a} (moles/kg H ₂ O)
3	40	0.0100	60.5%	9.802	1.683 × 10 ¹	1.857	1.469 × 10 ¹
	70		49.9%	10.121	1.866 × 10 ¹	2.207	1.151 × 10 ¹
	100		42.8%	10.768	2.408 × 10 ¹	2.265	1.521 × 10 ¹
	120		38.4%	10.544	2.332 × 10 ¹	2.343	1.821 × 10 ¹
	140		32.4%	10.717	2.810 × 10 ¹	1.554	1.986 × 10 ¹
	40	0.0010	58.8%	10.125	1.351 × 10 ¹	3.128	3.618
	70		50.0%	10.685	1.870 × 10 ¹	2.235	1.146 × 10 ¹
	100		43.2%	11.237	2.376 × 10 ¹	2.425	1.525 × 10 ¹
	120		38.5%	11.027	2.313 × 10 ¹	2.418	1.821 × 10 ¹
	140		32.6%	11.152	2.732 × 10 ¹	1.732	1.995 × 10 ¹
	40	0.0001	58.8%	10.714	1.360 × 10 ¹	3.181	3.508
	70		50.0%	11.180	1.866 × 10 ¹	2.253	1.145 × 10 ¹
	100		43.4%	11.731	2.365 × 10 ¹	2.469	1.525 × 10 ¹
	120		38.6%	11.519	2.307 × 10 ¹	2.451	1.822 × 10 ¹
	140		32.6%	11.644	2.707 × 10 ¹	1.758	1.992 × 10 ¹
4	40	0.0100	52.9%	7.195	1.343 × 10 ¹	1.288	5.884
	70		45.4%	7.850	2.082 × 10 ¹	7.776 × 10 ⁻¹	1.620 × 10 ¹
	100		36.4%	8.286	2.481 × 10 ¹	5.950 × 10 ⁻¹	2.172 × 10 ¹
	120		31.2%	8.518	2.646 × 10 ¹	5.313 × 10 ⁻¹	2.384 × 10 ¹
	140		26.4%	8.680	2.794 × 10 ¹	4.657 × 10 ⁻¹	2.574 × 10 ¹
	40	0.0010	52.9%	7.695	1.343 × 10 ¹	1.288	5.886
	70		44.5%	8.422	2.123 × 10 ¹	8.213 × 10 ⁻¹	1.727 × 10 ¹
	100		36.4%	8.786	2.481 × 10 ¹	5.950 × 10 ⁻¹	2.172 × 10 ¹
	120		31.2%	9.018	2.646 × 10 ¹	5.314 × 10 ⁻¹	2.384 × 10 ¹
	140		26.4%	9.180	2.794 × 10 ¹	4.658 × 10 ⁻¹	2.574 × 10 ¹
	40	0.0001	52.9%	8.195	1.343 × 10 ¹	1.288	5.887
	70		44.5%	8.922	2.123 × 10 ¹	8.213 × 10 ⁻¹	1.727 × 10 ¹
	100		36.4%	9.286	2.481 × 10 ¹	5.950 × 10 ⁻¹	2.172 × 10 ¹
	120		31.2%	9.518	2.646 × 10 ¹	5.314 × 10 ⁻¹	2.384 × 10 ¹
	140		26.4%	9.680	2.794 × 10 ¹	4.658 × 10 ⁻¹	2.574 × 10 ¹

Table 4-10. Deliquescence Points and Anion Chemistry of Evolved Dust-Associated Waters for the Six Bin Chemistries Shown on Table 4-8 (Continued)

Bin	Temperature (°C)	pCO ₂ (bar)	Deliquescence Point Relative Humidity	pH	Ionic Strength (moles/kg H ₂ O)	Cl ⁻ (moles/kg H ₂ O)	NO ₃ ^{-a} (moles/kg H ₂ O)
5	40	0.0100	56.1%	7.787	1.307 × 10 ¹	1.867	4.724
	70		45.2%	8.448	2.171 × 10 ¹	7.877 × 10 ⁻¹	1.646 × 10 ¹
	100		41.8%	8.374	2.728 × 10 ¹	2.307	1.709 × 10 ¹
	120		31.1%	8.904	2.709 × 10 ¹	5.534 × 10 ⁻¹	2.392 × 10 ¹
	140		26.3%	9.031	2.836 × 10 ¹	4.801 × 10 ⁻¹	2.576 × 10 ¹
	40	0.0010	56.1%	8.286	1.307 × 10 ¹	1.868	4.725
	70		45.2%	8.948	2.171 × 10 ¹	7.878 × 10 ⁻¹	1.646 × 10 ¹
	100		41.8%	8.870	2.736 × 10 ¹	2.315	1.709 × 10 ¹
	120		31.1%	9.403	2.709 × 10 ¹	5.536 × 10 ⁻¹	2.392 × 10 ¹
	140		26.3%	9.531	2.836 × 10 ¹	4.803 × 10 ⁻¹	2.576 × 10 ¹
	40	0.0001	56.1%	8.786	1.307 × 10 ¹	1.868	4.725
	70		45.2%	9.448	2.171 × 10 ¹	7.879 × 10 ⁻¹	1.646 × 10 ¹
	100		41.8%	9.374	2.725 × 10 ¹	2.307	1.708 × 10 ¹
	120		31.1%	9.903	2.709 × 10 ¹	5.536 × 10 ⁻¹	2.392 × 10 ¹
	140		26.3%	10.030	2.836 × 10 ¹	4.804 × 10 ⁻¹	2.576 × 10 ¹
6	40	0.0100	59.8%	9.139	1.262 × 10 ¹	3.751	3.274
	70		55.9%	10.203	1.768 × 10 ¹	4.049	1.126 × 10 ¹
	100		42.8%	10.767	2.409 × 10 ¹	2.268	1.521 × 10 ¹
	120		38.4%	10.542	2.333 × 10 ¹	2.351	1.822 × 10 ¹
	140		32.3%	10.654	2.830 × 10 ¹	1.701	2.020 × 10 ¹
	40	0.0010	59.4%	10.124	1.304 × 10 ¹	3.676	3.226
	70		49.7%	10.952	2.074 × 10 ¹	2.687	9.194
	100		43.2%	11.233	2.377 × 10 ¹	2.436	1.525 × 10 ¹
	120		38.5%	11.027	2.313 × 10 ¹	2.418	1.821 × 10 ¹
	140		32.6%	11.215	2.717 × 10 ¹	1.575	1.959 × 10 ¹
	40	0.0001	59.3%	10.714	1.329 × 10 ¹	3.644	3.190
	70		49.4%	11.469	2.102 × 10 ¹	2.693	9.262
	100		43.4%	11.724	2.366 × 10 ¹	2.487	1.525 × 10 ¹
	120		38.6%	11.518	2.307 × 10 ¹	2.456	1.822 × 10 ¹
	140		32.7%	11.683	2.697 × 10 ¹	1.658	1.970 × 10 ¹

Source: BSC 2003e, Table III-2.

NOTE: ^a NO₃⁻ is reported as total aqueous nitrogen.^b Calculations were stopped at relative humidity levels of 50 percent and 30 percent for 40°C and 70°C, respectively, because thermal-hydrologic conditions are never predicted below those levels (see Figure 2-11); this only affected bin 1.

4.2.4 Deliquescence Scenario Summary

The following conclusions can be reached from the information presented in Section 4.2:

- The in-drift precipitates and salts model and the physical and chemical environment models were developed to capture the chemical divide phenomenon.
- The physical and chemical environment model uses analyses of dust samples collected in the ESF to represent the potential dust composition in the repository. These dusts were leached and the reported aqueous compositions of the leachate are used as direct input to the model.
- The dust leachate compositions have been grouped or binned into six representative compositions that control the formation of potentially significantly different types of brines.
- The evaporative evolution of the six dust systems predicts that the corrosive calcium- and magnesium-chloride brines from these fluid compositions are unlikely to form on waste packages and drip shields, and that NO_3^- will become progressively concentrated relative to Cl^- with decreasing relative humidity (see Figures 4-17 and 4-18).

4.3 IMPLEMENTATION IN TOTAL SYSTEM PERFORMANCE ASSESSMENT

The *Engineered Barrier System: Physical and Chemical Environment Model* (BSC 2003e) provides the information that is used by TSPA to determine the composition of aqueous chemical environments on the surfaces of the drip shield and waste package, and in the invert. The following narrative provides a general explanation of the information flow from the seepage and dust models into the TSPA. The information flow is also represented in Figure 4-3.

Physical conditions such as temperature and relative humidity at the drip shield and waste package are extracted from the MSTHM model (BSC 2003a), as described in Section 2.3.2. The $p\text{CO}_2$ is an independent parameter in the look-up tables, so TSPA can represent the chemical environment for a variety of $p\text{CO}_2$ levels (see Figure 3-18 and Section 3.3.2). Within the TSPA, those parameters are used to enter a series of lookup tables developed for seepage and dust compositions (BSC 2003e). The tables are interpolated at appropriate values of temperature, relative humidity, and $p\text{CO}_2$. The tables provide sufficient information to determine whether aqueous conditions exist, and key compositional indicators where such conditions do exist. Chemical environmental indicators interpolated from the lookup tables are then applied as input to other models that represent different modes of corrosion, radionuclide solubility, colloid mobility, and in-package chemistry.

A TSPA realization for the seepage scenario (see Figure 4-3) begins by selecting one of the five starting waters used in the thermal-hydrologic-chemical model runs. This defines the incoming seepage water type and carbon dioxide partial pressure for each time interval in a series of approximately 36 time intervals (Step 1 in Section 4.1.3) covering 100,000 years. Within each time interval (Figure 3-18), temperature and relative humidity change, as predicted in other models (Figure 2-11). Lookup tables for each bin (Figure 4-7) are then consulted for the in-drift

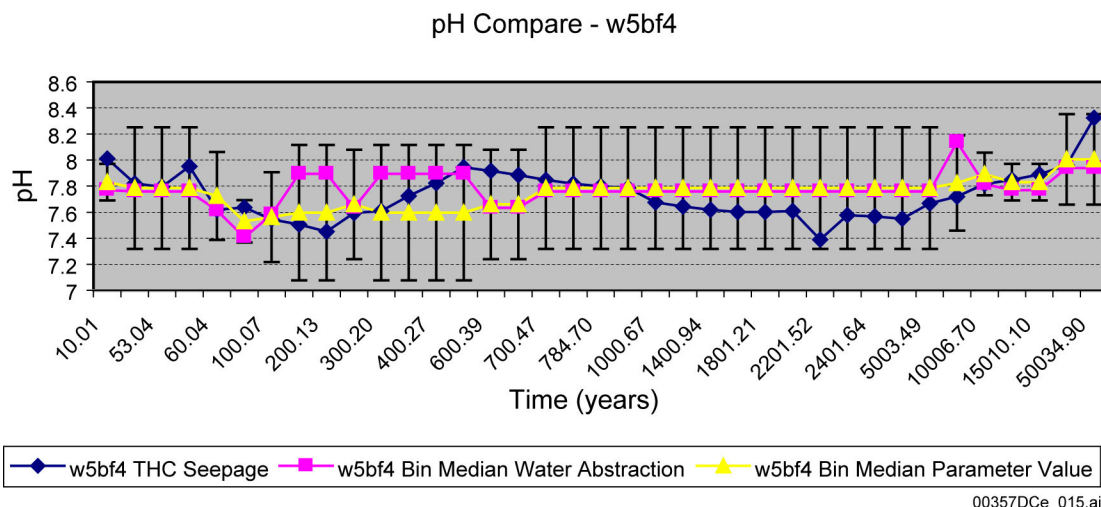
water composition corresponding to the water-type (Figure 4-14), carbon dioxide partial pressure (Figure 3-18), temperature (Figure 2-11), and relative humidity (Figure 2-11). The seepage lookup tables are developed for the following conditions: temperature at 100°C, 70°C, and 40°C; carbon dioxide partial pressure at 10^{-2} , 10^{-3} , and 10^{-4} bar; and relative humidity values from the deliquescence point to nearly 100 percent. Interpolations are made by TSPA for temperature, carbon dioxide partial pressure, and relative humidity. For dust deliquescence scenario chemistry, the dust leachate lookup tables are used in a similar manner (Figure 4-3).

4.4 PHYSICAL AND CHEMICAL ENVIRONMENT MODEL VALIDATION SUMMARY

Several models used directly in the physical and chemical environment model were validated within their corresponding model reports (e.g., in-drift precipitates and salts model discussed in Section 4.1.2, and the thermal-hydrologic-chemical seepage model discussed in Section 3.3.2). The physical and chemical environment model report (BSC 2003e) provides confidence-building discussion on several other topics: abstraction of the thermal-hydrologic-chemical seepage model results, use of the in-drift precipitates and salts model to represent the evolution of dust, and the interaction of seepage with chromium and other metallic components in the drift.

4.4.1 Thermal-Hydrologic-Chemical Seepage Abstraction Compared with Thermal-Hydrologic-Chemical Model Output

Figure 4-19 shows an example comparison of the abstraction vs. the original thermal-hydrologic-chemical input (see also BSC 2003e, Figures 7.2-1 through 7.2-20). The abstraction reduces fluctuations in the thermal-hydrologic-chemical seepage outputs; except for a few cases, all values fall within the 2σ error bars (of the bin median parameter value as shown in Figure 4-19). The abstraction bin information is mapped in Figure 4-14 for water 5, “w5”, in the invert. The thermal-hydrologic-chemical seepage water represents the explicit temporal evolution of water 5 (matrix water at the base of the invert, for the wetting front at node four - w5bf4). The “Bin Median Water” represents the value for the water composition selected to represent an entire bin. The “Bin Median Parameter” represents the statistical median of all of the pH values of a particular bin; note that these median parameters are strictly statistical and taken together do not represent any actual water composition that could exist. Based on comparisons of this type, the abstraction is considered to be a valid representation of the thermal-hydrologic-chemical seepage model results.



Source: BSC 2003e, Figure 7.2-9.

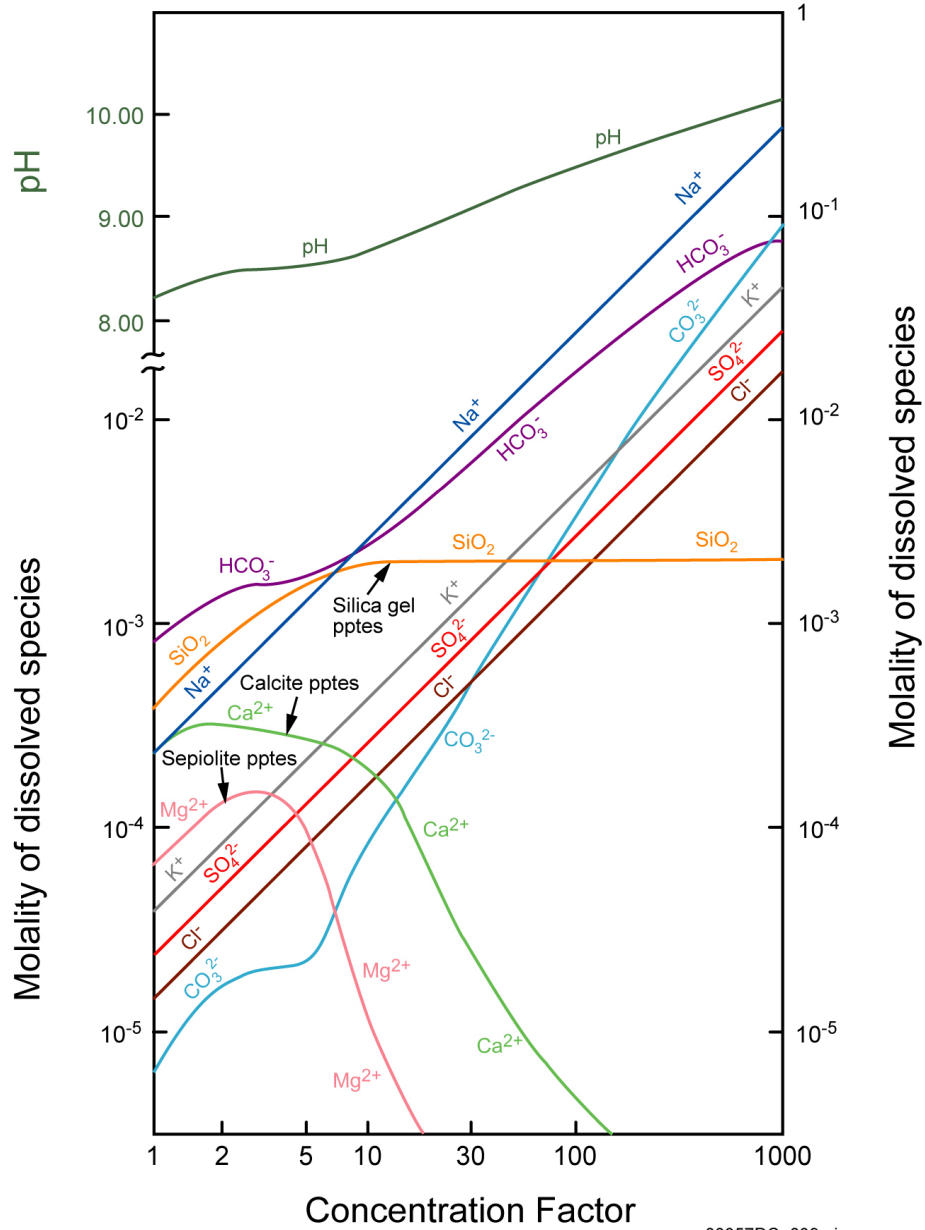
Figure 4-19. Comparison of THC Seepage pH with Abstraction Results for W5 (Base of Invert Front, Node 4 Matrix Water)

4.4.2 Evaporation of Sierra Nevada Spring Water to Brine

The engineered barrier system seepage evaporation model calculations were also evaluated by comparison with a classical model, describing evaporative concentration of dissolved species in solution (including precipitation). Selected for comparison was the well-documented study of the isothermal evaporation, at 25°C and $p\text{CO}_2 = 10^{-3.5}$ atm, of Sierra Nevada spring waters by Garrels and Mackenzie (1967), which has been cited by Drever (1988, pp. 232 to 234) as “a simulation of what might happen if streams from the Sierra Nevada flowed out into one of the arid basins of Nevada” to form saline lake water.

Figures 4-20 and 4-21 compare the evaporation results from Garrels and Mackenzie (1967) with a corresponding EQ3/6 calculation utilizing the Pitzer database as per the in-drift precipitates/salts model. These two figures are similar, despite the differences in how they were derived. The evaporation starts with a near neutral pH, Na-Ca-HCO₃ water and concentrates it to highly alkaline Na-HCO₃-CO₃ water. Calcium and magnesium are removed by early mineral precipitation. Na⁺, K⁺, Cl⁻, and SO₄²⁻ are concentrated without forming solids. HCO₃⁻ and CO₃²⁻ ions deviate from the rates of log-linear concentration by mineral precipitation, in contrast to Na⁺, K⁺, Cl⁻, and SO₄²⁻. Because the Sierra spring waters are originally low in SO₄²⁻, gypsum does not precipitate. Many waters in the repository are expected to concentrate by evaporation in a similar manner.

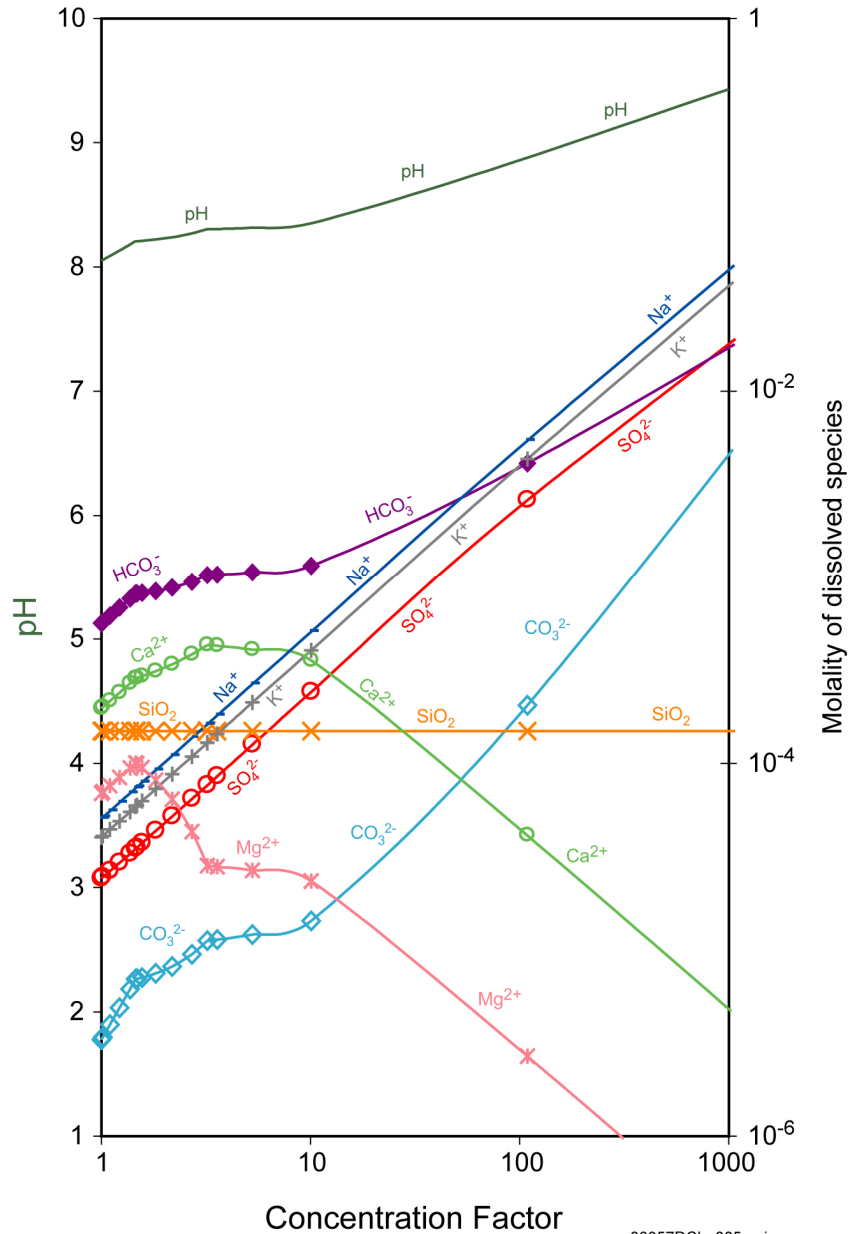
The major difference between the classical model results and the present validation arises from a change in the log *K* (solubility constant) for the solubility of amorphous silica, which was based on more recent experimental and thermodynamic data reviews that were unavailable to Garrels and Mackenzie (1967). In the intervening four decades, the accepted value of the amorphous silica log *K* at 25°C (and above) has decreased as a result of laboratory experiments and field validation tests. In summary, comparison of the evaporative concentration results shown in Figure 4-20 validates the calculated results shown in Figure 4-21.



Source: Garrels and Mackenzie 1967, p. 239.

NOTE: pptes – precipitates.

Figure 4-20. Results of Evaporation of Typical Sierra Nevada Spring Water at 25°C in Equilibrium with Atmospheric $p\text{CO}_2$ at $10^{-3.5}$ atm



Source: BSC 2003e, Figure 7.4-2.

Figure 4-21. Calculated Results of Evaporation of Typical Sierra Nevada Spring Water at 25°C in Equilibrium with Atmospheric $p\text{CO}_2$ at $10^{-3.5}$ atm

4.4.3 Deliquescence Point Comparison

Validation of equilibrium salt deliquescence points was conducted by comparing predictions made using EQ3/6 with the data.ypr Pitzer database and experimental data for simple and mixed electrolytes reported by Greenspan (1977) and Pabalan et al. (2002). Greenspan (1977) presents a compilation of equilibrium relative humidity values for binary salts as a function of temperature. Pabalan et al. (2002) reports salt deliquescence point experiments for selected binary and mixed salts as a function of temperature. A comparison of these results is shown in Table 4-11.

Table 4-11. Comparisons of Relative Humidity Values for Equilibrium Deliquescence Points of Selected Salts between EQ3/6 (Version 8.0–data0.yypf Pitzer Database) and Experimental Data

Salt Composition	Code or Source	Temperature (°C)					^c EQ3NR/EQ6 (Version 8.0) versus Others, Given in % Difference in Relative Humidity (Temperature)
		23.0	38.1	48.0	69.0	85.8	
NaNO ₃	EQ3NR/EQ6 (Version 8.0) (BSC 2003p)	74.3	70.8	68.6	64.3	61.1	—
	Greenspan (1977)	74.7	71.4	69.4	66.2	65.0	-0.5(23), -0.8(38.1), -1.1(48), -2.9(69), -6(86)
	Pabalan et al. (2002)	74.9	—	69.7	62.7	—	-0.8(23), -1.6(48), -2.5(69)
^a MgCl ₂	EQ3NR/EQ6 (Version 8.0) (BSC 2003p)	37.0	35.8	34.8	31.9	28.4	—
	Greenspan (1977)	32.9	31.8	30.8	27.9	25.0	12.5(23), 12.6(38.1), 13(48), 14.3(69), 13.6(86)
	Pabalan et al. (2002)	33.9	31.7	31.0	29.1	—	9.1(23), 12.9(38.1), 12.3(48), 9.6(69)
NaCl + NaNO ₃	EQ3NR/EQ6 (Version 8.0) (BSC 2003p)	68.7	66.9	65.6	62.7	60.1	—
	Pabalan et al. (2002)	74.7	66.4	67.2	59.6	56.0	-8.0(23), -0.7(38.1), -2.4(48), 5.2(69), 7.3(86)
^b NaCl + NaNO ₃ + KNO ₃	EQ3NR/EQ6 (Version 8.0) (BSC 2003p)	66.2	61.4	57.5	48.0	39.0	—
	Pabalan et al. (2002)	67.8	60.7	61.3	51.8	43.4	-2.4(23), 1.1(38.1), -6.2(48), -7.3(69), -10.1(86)

Source: BSC 2003e, Table 7.5-2.

NOTE: ^a MgCl₂ salt solid used in equilibrium calculation is MgCl₂·6H₂O.

^b Pitzer interaction parameters for K⁺ and NO₃⁻ pair are only available at 25°C.

^c Numbers in parenthesis represent temperature.

Overall, differences between predicted and experimental values of less than approximately 15 percent (equivalent to about 5 percent relative humidity units or less) are acceptable for model applications given the combined inherent uncertainties present in both experiments and code calculations using the Pitzer model (BSC 2003e, Table 7.3-1). Therefore, the present comparisons between two different sets of experimental data and the process model predictions validate the application of the computational method to predict salt deliquescence points to an acceptable level of accuracy, also supporting the in-drift precipitates and salts model's uncertainty determination on RH_{dp} of 5 percent relative humidity units.

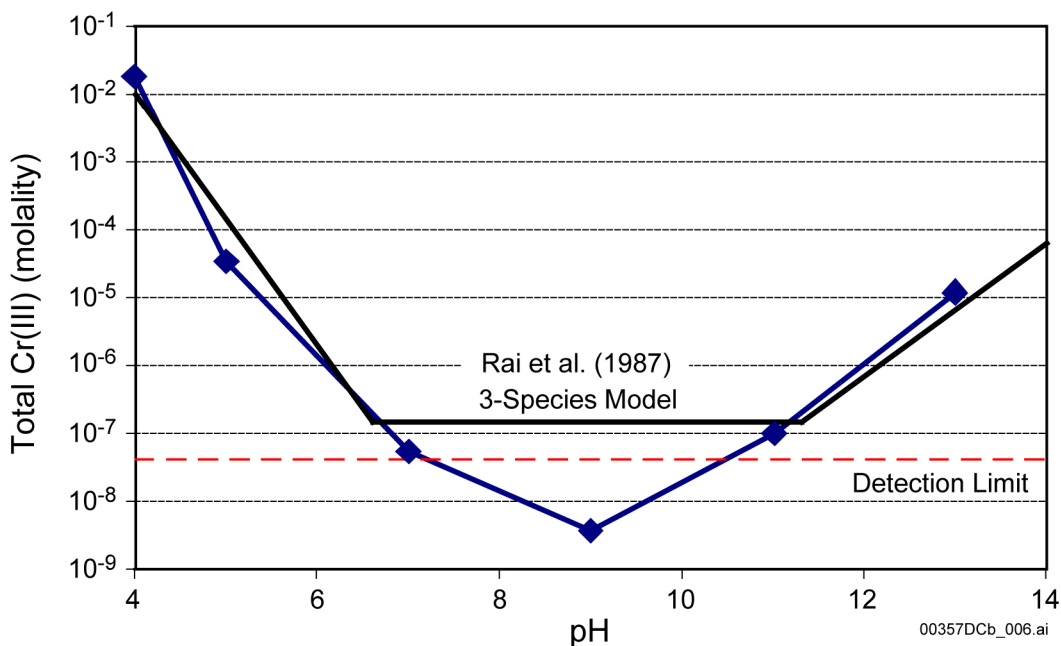
4.4.4 Chromium Speciation

The potential effect on seepage waters by interaction with corroding stainless steel ground support was specifically investigated (BSC 2003e, Section 6.8 and 7.7). It was determined that the most relevant aqueous chromium species would be chromium(III). All chromium(VI) species were suppressed in the EQ3/6 chemical speciation models. This choice of aqueous

chrome redox state is fully discussed in Section 6.8.1.3 of *Engineered Barrier System: Physical and Chemical Environment Model* (BSC 2003e) and is strongly supported by the experimental results of Smith and Purdy (1995). Corrosion of 316 stainless steel and chromium speciation was addressed, and it was concluded that for as long as there is metal alloy to be oxidized there will be a source of iron(II) to reduce any chromium(VI) back to chromium(III). This will always be the case for as long as the ground support is intact to be affecting seepage (about 1,000 years). A sensitivity analysis was performed to examine the effect of using chromium(VI) instead of chromium(III), which indicated only slight (about 1 percent) effect on pH and ionic strength (BSC 2003e, Section 6.13.4.1.2).

Detailed examination of the remaining chromium(III) aqueous species was performed, resulting in suppression of all the chromium(III) polynuclear species. These chromium polynuclear aqueous species were found to be overly stable and, “The polymeric species of chromium(III) are generally absent in solutions at room temperature” (Rai et al. 1987, p. 345 to 346). For example, if included then $\text{Cr}_3(\text{OH})_4^{5+}$ becomes the dominant species (65 percent relative) at pH 5 when the total chromium(III) concentrations are 10^{-4} molal. Discussion of the problems with the polynuclear species was specifically addressed in Ball and Nordstrom (1998).

The solubility of the amorphous chromium(III) hydroxide was then calculated as a function of pH (in the pH range 4 through 13). The results of these calculations were compared to the results of Rai et al. (1987) (Figure 4-22).



Source: BSC 2003e, Figure 7.7-1.

NOTE: EQ3/6 calculated chromium concentrations in equilibrium with $\text{Cr}(\text{OH})_3(\text{am})$ are blue diamonds with lines, nonlinear least-squares regression by Rai et al. (1987, Figure 2) are solid black lines, and detection limit is shown by red dashed line.

Figure 4-22. EQ3/6 Calculated Chromium Concentrations in Equilibrium with $\text{Cr}(\text{OH})_3(\text{am})$ Compared to Nonlinear Least-Squares Regression by Rai et al.

In this comparison, the detection limit reported by Rai et al. probably overestimates solubility in the pH range of 6 through 11. Their raw data show measurements well below their detection limits with values approaching those of the calculations (e.g., about 4×10^{-9} molar aqueous chromium in Figure 1 of Rai et al. (1987), compared to a calculated 3.6×10^{-9} molal at pH of 9 shown in Figure 4-22).

This favorable comparison provided an independent validation of the remaining unsuppressed chromium(III) aqueous species in the data0.ymp.R2 database (DTN: MO0302SPATHDYN.000) as they reproduce chromium(III) solubility based on the log K of hydroxide, $\text{Cr}(\text{OH})_3(\text{am})$, obtained by Ball and Nordstrom (1998) (derived from Rai et al. 1987). The aqueous species themselves were based upon thermodynamic estimates by Shock et al. (1997), who based their estimations upon the enthalpy of Cr^{3+} determined by Dellien et al. (1976).

4.5 RELATION OF PROCESS MODEL RESULTS TO CORROSION TESTING CHEMISTRIES

Initial corrosion testing environments were chosen based on the three types of natural brines: calcium chloride, carbonate, and sulfate. Initial studies focused on the carbonate type brine, based on reasoning that sodium carbonate type waters, as typified by J-13 well water from the saturated zone near Yucca Mountain, were the expected types of waters at the repository (Harrar et al. 1990). A later study (Rosenberg et al. 2001) showed that evaporative concentration of a water based on a reported analysis (Sonenthal et al. 1998) of a pore water from Yucca Mountain resulted in a calcium chloride type brine. The types of aqueous solutions used for corrosion testing will be discussed in the context of the natural brines that follows.

Geochemical literature (e.g., Drever 1997) establishes the three types of brines that result from the evaporative concentration of dilute natural waters at the earth's surface: (1) calcium chloride brine, (2) carbonate brine, and (3) sulfate brine. It is important to note that the compositions of brines are dependent on relative humidity, and the dominant ions in solution can and do change as a function of relative humidity.

The brine type name reflects a characteristic of the brine that distinguishes it from the other brines. When evaporation has gone beyond the classic chemical divides shown in Figure 4-1, this may not necessarily reflect dominant species in the brine. This characterization of surface brine types has in part guided the expected range of brine water chemistry in the repository. However, some differences are expected between brines formed at the earth's surface and brines formed in the repository. These differences are mainly due to differences in the chemistry of seepage waters and surface waters giving rise to brines, and differences between the salt chemistry of dust and the dissolved salt content of the surface waters. Two important general factors specific to the repository brines are the ubiquity of nitrate and more effective mechanisms for the removal of magnesium. It is expected that nitrate will be in these brines because of the multiple potential sources (BSC 2003g, Section 6.7.2.8) and the generally high solubility of nitrate minerals (BSC 2003g, Section 4.1.1.7). It is expected that magnesium will not be significant because of limited sources (for the dust, as well as for at least some ground waters) and multiple removal mechanisms, most of which are enhanced by elevated temperature (BSC 2003g, Sections 6.7.2.10 and 6.7.2.11). Table 4-12 shows the general classification of the

brine types that could be in contact with drip shields and waste packages and the probabilities of contact.

The calcium chloride brines have near neutral pH and no significant bicarbonate-carbonate, fluoride, or sulfate content. These brines may contain other cations such as Na^+ , K^+ , and Mg^{2+} and other anions such as NO_3^- . The endpoint of the evaporative concentration of this type of brine would contain Ca-Cl/ NO_3 or a mixture of Ca/Mg-Cl/ NO_3 . The quantity of Mg^{2+} and Ca^{2+} in this type of brine would be limited due to the precipitation of calcium carbonates and sulfates and magnesium silicates. This is consistent with information on saline lakes where Na^+ is the dominant cation with the percentage of Ca^{2+} varying from insignificant to about 20 percent (Drever 1997). In the repository, the concentration of Mg^{2+} in any type of brine is expected to be insignificant. Thus, a magnesium chloride brine is not expected. NO_3^- is expected to be present, and an end-point brine of this type is likely to be dominated by calcium chloride and calcium nitrate. A brine of the calcium chloride type is expected to have a very limited occurrence in the repository, as indicated in Table 4-12. For brine generated by dust deliquescence, the brine is actually expected to be more of a calcium-nitrate-sodium-chloride brine due to the compositional nature of the dust.

Table 4-12. General Classification of the Brine Types that Could Be in Contact with Drip Shields and Waste Packages and the Probabilities of Contact

Brine Type	Percent Probability		Comments
	Seepage at Drift Crown ^a	Dust Deliquescence ^b	
Calcium chloride	0.22	5.77 ^c	Fluoride, carbonate, sulfate contents are negligible
Sulfate	2.21	75.00	Near neutral pH
Carbonate	97.56	19.23	High pH, no significant calcium or magnesium content

NOTE: ^a The probability of crown seepage represents the 20,000-year time integrated occurrence fraction of the representative water for each bin. Additionally, the mapping from Table 4-13 for the 11 bins are as follows: Bins 1 to 3 are calcium chloride; Bins 4 and 5 are sulfate; and Bins 6 to 11 are carbonate.

^b The probabilities represent the fraction of waste packages subject to dust that may deliquesce into the identified brine type. Additionally, the mapping from Table 4-14 are as follows: Bin 1 is calcium chloride; Bins 2, 4 and 5 are sulfate; and bins 3 and 6 are carbonate.

^c Aqueous solutions are dominated by $\text{Ca}(\text{NO}_3)_2$.

Relative humidity dependence of the calcium chloride brine is as follows. At low relative humidity, the aqueous solutions will be dominated by Ca^{2+} cations (very low sodium and potassium), and Cl^- and NO_3^- anions, since both calcium nitrate and calcium chloride are very soluble. At higher relative humidity, chloride and nitrate salts of sodium and potassium become soluble and could dominate the aqueous solution compositions. This would occur at or above the deliquescence relative humidity for salts composed of these ions.

Corrosion test solutions corresponding to this calcium chloride type of brine include: calcium chloride, calcium chloride plus calcium nitrate, the simulated saturated water (SSW) (see Table 4-15), and sodium chloride aqueous solutions. The SSW and sodium chloride test solutions simulate the moderate relative humidity scenario where calcium is a minor component in the aqueous solution. Numerous electrochemical studies were performed in these test

solutions. Thin film studies were also performed using these types of solutions on coupons of Alloy 22 using an environmental thermogravimetric analyzer.

The carbonate brines are alkaline and do not contain significant calcium or magnesium. In the early stages of the evaporative concentration, calcium precipitates predominately as carbonate minerals (calcite or aragonite). Magnesium precipitates as a minor component in the calcium carbonate species and as magnesium silicate (BSC 2003g, Section 6.7.2.11). In the repository, it is expected that magnesium will be removed efficiently, and potassium may be significant in some of these brines. As shown in Table 4-12, the carbonate brine is expected to be the most common type produced by evaporation of seepage water, and a minor type produced by dust deliquescence.

Relative humidity dependence of carbonate brine is as follows. At low relative humidity, the aqueous solutions will be dominated by Cl^- and NO_3^- anions with NO_3^- ions dominating at the lowest relative humidity. At moderate relative humidity (greater than 70 percent relative humidity) Cl^- could dominate the solution composition. The Cl^- - NO_3^- solutions are expected to have slightly elevated pH due to residual carbonate in solution. Significant amounts of carbonate and SO_4^{2-} are not expected until the relative humidity is greater than 85 percent.

Corrosion test solutions corresponding to the carbonate type of brine include: the simulated dilute water (SDW), simulated concentrated water (SCW), basic saturated water (BSW), and under certain circumstances SSW and simulated acidic water (SAW) aqueous test solutions (see Table 4-15). The BSW test solution is a highly concentrated alkaline solution and could be expected under repository conditions where temperatures could be at its measured boiling point of nominally 112°C to 113°C or where the relative humidity is nominally 70 to 75 percent. The SCW test solution is a moderately concentrated alkaline solution; solutions in this concentration range could be expected to form for relative humidity in the range of 90 to 95 percent. The SDW test solution is a dilute alkaline solution; solutions in this concentration range could be expected to form for high relative humidity (greater than 99 percent). These may have characteristics of solutions at the drift wall, that is, typical of seepage waters.

Under conditions of extreme evaporative concentration (i.e., low relative humidity) the carbonate brine would evolve into a Cl^- - NO_3^- brine with low carbonate content. The SSW test solution has characteristics of this type of brine. Likewise the SAW test solution has characteristics of low carbonate brine and would have characteristics of solutions in equilibrium with relative humidity of nominally 90 percent. The calcium and magnesium content of the SAW test solution tends to make it more able to sustain lower pHs due to the hydrolysis properties of these cations.

The sulfate brines have near-neutral pH and no significant carbonate or calcium content. Calcium precipitates as carbonates and possibly sulfates. In addition, brines typically have only a small amount of magnesium, though some surface brines have been observed to have high magnesium (Drever 1997, Table 15-1, p. 333, brines 1-3). The dominant cation is typically Na^+ . In the repository brines, K^+ may be more significant than Na^+ , and Mg^{2+} is expected to be insignificant. As shown in Table 4-12, the sulfate-brine type is expected to be a minor type produced by evaporation of seepage water, but is expected to be contained in the dust.

Relative humidity dependence of the sulfate brine is as follows. At low relative humidity, the aqueous solutions will be dominated by Cl^- and NO_3^- anions, with NO_3^- ions dominating at the lowest relative humidity. At moderate relative humidity (greater than 70 percent relative humidity) Cl^- ions could dominate the solution composition. However, unlike the carbonate brines these brines are expected to have near neutral to slightly acidic pH because of the lack of a carbonate component. Significant amounts of carbonate and SO_4^{2-} are not expected until the relative humidity is greater than 85 percent because of the increase in solubility of expected sulfate minerals (sodium and potassium sulfates). (Magnesium sulfate is expected to be present in only insignificant quantities in these repository brines.)

The corrosion test solutions corresponding to the sulfate type of brine include the SAW, SSW, and sodium chloride. This type of brine has near neutral to slightly acidic pH and as noted above magnesium is not expected to be present in seepage waters to any significant extent. The SAW test solutions have characteristics of solutions in equilibrium with nominally 90 percent relative humidity. The SSW has characteristics of water that have undergone evaporative concentration to the extent that sulfate precipitates out of solution (this is for the magnesium free situation). Sodium chloride test solutions simulate the scenario where Cl^- is the dominant anion under moderate relative humidity conditions.

The compositions of seepage waters and waters due to deposited salt deliquescence have been discussed in Sections 4.1 and 4.2. The following discussion relates those water brine types to the corrosion test solutions.

Table 4-13 lists the range of environments projected to form within the repository due to water seepage. The classification into bins of water types is discussed in Section 4.1. The conditional probability (if seepage occurs at the drift crown for any particular location) that a water in a particular bin will form is also listed. For each bin, the associated brine and test solution in which corrosion testing was conducted are listed. In terms of brine type the drift crown brines are predominantly the alkaline carbonate brines, although carbonate may not be a dominant component except at higher relative humidities. The composition of each bin water as a function of temperature and relative humidity is given in lookup tables discussed in Section 4.3.

Table 4-13. Drift Crown Seepage Water Limiting Compositions and Probabilities of Their Formation, the Associated Brine Type, and the Corresponding Corrosion Test Solutions

Bin Water	Probability of Crown Seepage ^a	Dominant Constituents in Bin Water at 98% Relative Humidity ^b	Dominant Constituents in Endpoint Brines ^b	Brine Type	Corrosion Test Solution
1	0.00	Ca-Cl	Ca-Cl	Calcium chloride	CaCl ₂ ; CaCl ₂ + Ca(NO ₃) ₂
2	0.00	Na-Cl	Ca-Cl	Calcium chloride	CaCl ₂ ; CaCl ₂ + Ca(NO ₃) ₂
3	0.22	Na-Cl	Ca-Cl; K-Cl	Calcium chloride	CaCl ₂ ; CaCl ₂ + Ca(NO ₃) ₂
4	1.42	Na-Cl	K-NO ₃ ; Na-NO ₃	Sulfate	SSW, SAW, NaCl
5	0.79	Na-Cl	Na-Cl; K-Cl	Sulfate	SSW, SAW, NaCl
6	5.46	Na-Cl	Na-Cl; Na-NO ₃ ; K-Cl	Carbonate	SDW, SCW, BSW, SSW, NaCl
7	27.15	Na-Cl	Na-Cl; Na-NO ₃ ; K-Cl	Carbonate	SDW, SCW, BSW, SSW, NaCl
8	16.2	Na-CO ₃	Na-Cl; Na-NO ₃ ; K-Cl	Carbonate	SDW, SCW, BSW, SSW, NaCl
9	15.55	Na-CO ₃	K-NO ₃ ; K-Cl	Carbonate	SDW, SCW, BSW, SSW, NaCl
10	11.7	Na-CO ₃	Na-Cl; Na-NO ₃ ; K-Cl	Carbonate	SDW, SCW, BSW, SSW, NaCl
11	21.5	Na-Cl	Na-Cl; Na-NO ₃ ; K-Cl	Carbonate	SDW, SCW, BSW, SSW, NaCl

Source: ^a BSC 2003e, Table 6.14-1.

^b BSC 2003e, Table 6.14-8.

NOTE: The probability of crown seepage represents the 20,000-year time-integrated occurrence fraction (in percent) of the representative water for each bin.

Deliquescence of dust deposited on the waste packages and drip shields is another means by which brines can form on these engineered barrier system components. The approaches used to determine the characteristics of such brines were discussed in Section 4.2.3.

Table 4-14 lists the brines that would develop on the waste packages using the representation of dust deliquescence developed for TSPA (Section 4.2). Included in the table are the associated brine type and the corresponding aqueous corrosion test solutions.

Table 4-14. Brines from Dust Deposited on the Waste Packages Including Bromide, the Probabilities of Their Formation, the Associated Brine Type, and the Corresponding Corrosion Test Solutions

Bin Water	Probability of Deliquescence Bin ^a	Dominant Constituents in Bin Water at 98% Relative Humidity ^b	Dominant Constituents in Endpoint Brines ^b	Brine Type	Corrosion Test Solution
1	5.77	Na-NO ₃	Ca-NO ₃	Calcium Chloride	CaCl ₂ ; CaCl ₂ + Ca(NO ₃) ₂
2	7.69	Na-NO ₃	K-NO ₃ ; Na-NO ₃	Sulfate	SSW, SAW, NaCl
3	17.31	Na-SO ₄	K-NO ₃ ; Na-NO ₃	Carbonate	SDW, SCW, BSW, SSW, NaCl
4	23.08	Na-NO ₃	Na-NO ₃	Sulfate	SSW, SAW, NaCl
5	44.23	Na-NO ₃	K-NO ₃ ; Na-NO ₃	Sulfate	SSW, SAW, NaCl
6	1.92	Na-Cl	K-NO ₃	Carbonate	SDW, SCW, BSW, SSW, NaCl

Source: ^a BSC 2003e, Table 6.10-6.

^b BSC 2003e, Table 6.14-9.

NOTE: The probabilities represent the percentage of waste packages subject to dust that may deliquesce into the identified brine type.

Table 4-15 shows the composition of some of the solutions used for corrosion testing. These solutions were developed based on the evaporative concentration of a carbonate-based water with a composition based on J-13 well water, which is a saturated zone water near Yucca Mountain. The solutions represent various stages of evaporative concentration of this type of water. These aqueous solution compositions were concentrated to about 10 times (for SDW) to over 45,000 times (for SSW and BSW) to simulate evaporative concentration of the water upon contacting the waste package or the drip shield. NaCl test solutions were also used where NaCl concentrations varied from 0.5 to 4.0 molar; CaCl₂ and CaCl₂ + Ca(NO₃)₂ test solutions were also used with CaCl₂ concentrations up to 9 molar.

In all cases, the NO₃⁻ component is the most soluble species and would dominate the solution composition at the deliquescent relative humidity or eutectic point of a mineral assemblage at elevated temperatures. It is not until the relative humidity is higher that Cl⁻ could become comparable to NO₃⁻. This is discussed in more detail in *Environment on the Surfaces of Drip Shield and Waste Package Outer Barrier* (BSC 2003g) and the *Engineered Barrier System: Physical and Chemical Environment Model* (BSC 2003e).

Table 4-15. Target Composition of Standard Test Media Based on Evaporative Concentration of a Dilute Carbonate Type Water.

Ion	SDW (mg/L)	SCW (mg/L)	SAW (mg/L)	SSW (mg/L)	BSW-12 (mg/L)
K ⁺	3.4×10^1	3.4×10^3	3.4×10^3	1.42×10^5	6.762×10^4
Na ⁺	4.09×10^2	4.09×10^4	3.769×10^4	4.87×10^4	1.0584×10^5
Mg ²⁺	1	<1	1.00×10^3	0	0
Ca ²⁺	5×10^{-1}	<1	1.00×10^3	0	0
F ⁻	1.4×10^1	1.4×10^3	0	0	1.47×10^3
Cl ⁻	6.7×10^1	6.7×10^3	2.425×10^4	1.28×10^5	1.3083×10^5
NO ₃ ⁻	6.4×10^1	6.4×10^3	2.30×10^4	1.313×10^6	1.3965×10^6
SO ₄ ²⁻	1.67×10^2	1.67×10^4	3.86×10^4	0	1.47×10^4
HCO ₃ ⁻	9.47×10^2	7.0×10^4	0	0	0
Si	27 (60°C), 49 (90°C)	27 (60°C), 49 (90°C)	27 (60°C), 49 (90°C)	0	0
pH	9.8 to 10.2	9.8 to 10.2	2.7	5.5 to 7	12

Source: DTN: LL000320405924.146.

NOTE: The basis for the dilute carbonate water was J-13 well water, a saturated zone water near Yucca Mountain. The SDW, SCW, and BSW test solutions correspond to increasing evaporative concentration of the basis water. The SSW test solution contains only Cl⁻ and NO₃⁻ and corresponds to the scenario where the other anions have precipitated out of solution, that is, a very low relative humidity condition. The SAW test solution is a moderately acidic solution (hence no carbonate because of its volatility) with an ionic strength similar to the SCW test solution. The SAW test solution also does not contain fluoride that was excluded because of its high vapor pressure at the solution pH. pH is measured for actual solutions at room temperature.

INTENTIONALLY LEFT BLANK

5. SUMMARY

The physical and chemical environment within the emplacement drifts is an important factor in the performance of the engineered barriers. Integration of models for thermal, hydrologic, and chemical processes in the drifts and the host rock, supported by data from testing and other technical information, shows that the occurrence of potentially aggressive conditions on the waste package and drip shield will be limited.

The in-drift chemical environment will change with time as the waste decays and as geochemical processes modify the in-drift conditions. Thermal effects from the decaying waste will affect the composition of aqueous solutions entering the drift and the gases within the drifts. The amount of water and its composition, along with the time-dependent evolution of relative humidity and temperature in the drifts and behavior of deliquescent salts that may be present in dust, are used in TSPA to represent the environment for corrosion of the drip shield and waste package.

Evolution of the chemical environment will take place in three general regimes: dryout, transition, and low-temperature. As stated in Section 1, dryout will occur immediately after permanent closure, when the near-field rock temperature increases beyond boiling and the waste package temperature reaches approximately 120°C or higher. For most waste packages, and especially those that contain commercial spent nuclear fuel and are located in the central part of the repository layout, dryout will remove the water in a zone of up to 5 to 10 m around the drift openings. The waste package temperature will peak within a time period of several tens to hundreds of years depending on local heat output and thermal properties. During dryout, no seepage will occur because of the vaporization barrier and capillary barrier effects (Section 2). Also, the matrix in the dryout zone will be dewatered, thus tending to absorb water that enters the dryout zone and hold it until fully evaporated. Although seepage will not occur during the dryout period deliquescence of dust deposits on the waste package and drip shield may produce very small quantities of brines. The analysis in Section 4 shows that because NO_3^- is a relatively abundant soluble component of dust samples such as those acquired from the ESF, the potential compositions of such brines are unlikely to initiate corrosion.

The transition stage will occur as the host-rock drift crown temperature cools through boiling, eliminating the vaporization barrier effect, and the waste package temperature cools through approximately 105°C. At this point, although the vaporization barrier will not be effective, the capillary barrier to seepage will remain active as it is for ambient conditions (Section 2). Although the drip shields will remain in place preventing seepage water from contacting the waste packages, the potential thermal evolution of seepage water chemistry on the waste package surface has been investigated and incorporated into TSPA. As the heat output of the waste decays, the temperature difference between the waste package surface and the host rock at the drift wall will decrease (Section 2). Nevertheless, during the transition stage the waste package temperature will remain a potentially significant factor in corrosion processes, and will be high enough to cause evaporative concentration of seepage waters that may drip onto the waste package surface. Based on analysis of thermal-hydrologic-chemical processes in the host rock, the seepage waters will primarily evolve into carbonate- or sulfate-type brines. Again, the presence of NO_3^- will be an important factor in determining whether seepage waters can initiate localized corrosion. The $\text{Cl}^-/\text{NO}_3^-$ ratio in evaporatively concentrated seepage will be controlled by the starting composition of pore water, which has been investigated extensively in the host

rock at Yucca Mountain (Section 3). Calcium chloride brines are unlikely to form. As the temperature continues to decrease, the relative humidity in the emplacement drifts will increase, so that evaporative concentration of seepage will produce less concentrated chemical conditions (Section 4).

After transition, the low-temperature stage will persist through the end of the regulatory period. The capillary barrier will remain effective, and relative humidity will increase approaching 100 percent. Deliquescence and evaporative concentration under higher humidity and lower temperature will produce more and more dilute conditions on the waste package and drip shield surfaces.

Some primary conclusions can be drawn from in-drift chemical environment modeling presented in this report:

1. Only one of the 11 seepage water compositional bins (bin 3) results in formation of calcium chloride brine that could be deleterious with respect to corrosion (Section 4). This bin only occurs during the dryout stage when temperatures in the host rock are above boiling and seepage into the drift is prevented by the vaporization barrier effect (see Figures 3-20 and 4-14).
2. Other seepage water compositional bins produce a range of brines with varying amounts of the dominant ions Na^+ , K^+ , Cl^- , NO_3^- , SO_4^{2-} , HCO_3^- , and CO_3^{2-} , which are dependent on the in-drift relative humidity. The range of environments in which corrosion tests have been performed is consistent with the range of environments projected to be relevant for waste package and drip shield corrosion under expected repository conditions.
3. Analysis of salt deliquescence, based on dust compositions observed underground at Yucca Mountain, indicates that brines formed from this dust will be relatively abundant in nitrate (see Table 4-14) and will therefore not have significant potential to initiate corrosion.

Detailed models have been developed for the evolution of drift-scale temperature and relative humidity of pore water in the near-field rock, evolution of seepage water, rehydration of soluble salts (deliquescence), and interaction of dusts on the surfaces of the drip shield and waste package. The chemical evolution models address reactions among the major ionic species, with the importance of some minor and trace species also evaluated. The predicted evolution of the in-drift chemical environment is also applied to other process models including in-package chemistry, radionuclide solubility, and colloid formation. These detailed models are linked in the TSPA, which also propagates uncertainties from various sources through the models. The role of F^- has been examined due to its importance to drip shield performance, and chromium has been examined because of its abundance in the environment. Neither of these elements was found to produce effects that require explicit representation in the TSPA.

KTI agreements, as discussed in Appendices A through L, address concerns about various technical aspects of these models.

6. REFERENCES

6.1 DOCUMENTS CITED

- Ball, J.W. and Nordstrom, D.K. 1998. "Critical Evaluation and Selection of Standard State Thermodynamic Properties for Chromium Metal and its Aqueous Ions, Hydrolysis Species, Oxides, and Hydroxides." *Journal of Chemical & Engineering Data*, 43, (6), 895-918. Washington, D.C.: American Chemical Society. TIC: 254015.
- Birkholzer, J.; Li, G.; Tsang, C-F.; and Tsang, Y. 1999. "Modeling Studies and Analysis of Seepage into Drifts at Yucca Mountain." *Journal of Contaminant Hydrology*, 38, (1-3), 349-384. New York, New York: Elsevier. TIC: 244160.
- Birkholzer, J. 2003. "Penetration of Liquid Fingers into Superheated Fractured Rock." *Water Resources Research*, 39, (4), 9-1 through 9-21. Washington, D.C.: American Geophysical Union. TIC: 254362.
- BSC (Bechtel SAIC Company) 2001a. *Thermal Tests Thermal-Hydrological Analyses/Model Report*. ANL-NBS-TH-000001 REV 00 ICN 02. Las Vegas, Nevada: Bechtel SAIC Company. ACC: MOL.20011116.0025.
- BSC 2001b. *In Situ Field Testing of Processes*. ANL-NBS-HS-000005 REV 01. Las Vegas, Nevada: Bechtel SAIC Company. ACC: MOL.20020108.0351.
- BSC 2001c. *Drift Degradation Analysis*. ANL-EBS-MD-000027 REV 01 ICN 01. Las Vegas, Nevada: Bechtel SAIC Company. ACC: MOL.20011029.0311.
- BSC 2002a. *Thermal Testing Measurements Report*. ANL-NBS-HS-000041 REV 00. Las Vegas, Nevada: Bechtel SAIC Company. ACC: MOL.20021004.0314.
- BSC 2002b. *Analysis of Geochemical Data for the Unsaturated Zone*. ANL-NBS-HS-000017 REV 00 ICN 02. Las Vegas, Nevada: Bechtel SAIC Company. ACC: MOL.20020314.0051.
- BSC 2002c. *Geologic Framework Model (GFM2000)*. MDL-NBS-GS-000002 REV 01. Las Vegas, Nevada: Bechtel SAIC Company. ACC: MOL.20020530.0078.
- BSC 2002d. *Mineralogic Model (MM3.0) Analysis Model Report*. MDL-NBS-GS-000003 REV 00 ICN 02. Las Vegas, Nevada: Bechtel SAIC Company. ACC: MOL.20020423.0151
- BSC 2003a. *Multiscale Thermohydrologic Model Report*. ANL-EBS-MD-000049 REV 01C. Las Vegas, Nevada: Bechtel SAIC Company. ACC: MOL.20030910.0158.
- BSC 2003b. *Drift-Scale Coupled Processes (DST and TH Seepage) Models*. MDL-NBS-HS-000015 REV 00C. Las Vegas, Nevada: Bechtel SAIC Company. ACC: MOL.20030910.0160.
- BSC 2003c. *Drift-Scale Coupled Processes (DST and TH Seepage) Models*. MDL-NBS-HS-000001 REV 02. Las Vegas, Nevada: Bechtel SAIC Company. ACC: DOC.20030804.0004.

- BSC 2003d. *In-Drift Precipitates/Salts Model*. ANL-EBS-MD-000045 REV 01. Las Vegas, Nevada: Bechtel SAIC Company. ACC: DOC.20031028.0003.
- BSC 2003e. *Engineered Barrier System: Physical and Chemical Environment Model*. ANL-EBS-MD-000033 REV 02C. Las Vegas, Nevada: Bechtel SAIC Company. ACC: MOL.20031029.0034.
- BSC 2003f. *Ventilation Model and Analysis Report*. ANL-EBS-MD-000030 REV 03 ICN 01. Las Vegas, Nevada: Bechtel SAIC Company. ACC: DOC.20030804.0003.
- BSC 2003g. *Environment on the Surfaces of Drip Shield and Waste Package Outer Barrier*. ANL-EBS-MD-000001 REV 01D. Las Vegas, Nevada: Bechtel SAIC Company. ACC: MOL.20030825.0151.
- BSC 2003h. *Drift Scale THM Model*. MDL-NBS-HS-000017 REV 00. Las Vegas, Nevada: Bechtel SAIC Company. ACC: DOC.20030818.0003.
- BSC 2003i. *UZ Flow Models and Submodels*. MDL-NBS-HS-000006 REV 01. Las Vegas, Nevada: Bechtel SAIC Company. ACC: DOC.20030818.0002.
- BSC 2003j. *Seepage Model for PA Including Drift Collapse*. MDL-NBS-HS-000002 REV 02. Las Vegas, Nevada: Bechtel SAIC Company. ACC: DOC.20030709.0001.
- BSC 2003k. *In-Drift Natural Convection and Condensation Model Report*. MDL-EBS-MD-000001 REV00A. Las Vegas, Nevada: Bechtel SAIC Company. ACC: MOL.20030912.0050.
- BSC 2003l. *Abstraction of Drift Seepage*. MDL-NBS-HS-000019 REV 00. Las Vegas, Nevada: Bechtel SAIC Company. ACC: DOC.20030826.0001.
- BSC 2003m. *Seepage Calibration Model and Seepage Testing Data*. MDL-NBS-HS-000004 REV 02. Las Vegas, Nevada: Bechtel SAIC Company. ACC: DOC.20030408.0004.
- BSC 2003n. *Drift Degradation Analysis*. ANL-EBS-MD-000027 REV 02. Las Vegas, Nevada: Bechtel SAIC Company. ACC: DOC.20030709.0003.
- BSC 2003o. *Calibrated Properties Model*. MDL-NBS-HS-000003 REV 01. Las Vegas, Nevada: Bechtel SAIC Company. ACC: DOC.20030219.0001.
- BSC 2003p. Software Code: EQ3/6. V8.0. PC w/ Windows 95/98/2000/NT 4.0. 10813-8.0-00.
- BSC 2003q. *Repository Design Project, Repository/PA IED Emplacement Drift Committed Materials (2)*. 800-IED-WIS0-00302-000-00A. Las Vegas, Nevada: Bechtel SAIC Company. ACC: ENG.20030627.0004.
- Campbell, A.N. and Smith, N.O. 1951. *The Phase Rule and its Applications*. 9th Edition. New York, New York: Dover Publications. TIC: 254360.

CRWMS M&O (Civilian Radioactive Waste Management System Management and Operating Contractor) 1998. *Drift Scale Test As-Built Report*. BAB000000-01717-5700-00003 REV 01. Las Vegas, Nevada: CRWMS M&O. ACC: MOL.19990107.0223.

CRWMS M&O 2001. *Drift-Scale Coupled Processes (DST and THC Seepage) Models*. MDL-NBS-HS-000001 REV 01. Las Vegas, Nevada: CRWMS M&O. ACC: MOL.20010314.0003

Dellien, I.; Hall, F.M.; and Hepler, L.G. 1976. "Chromium, Molybdenum, and Tungsten: Thermodynamic Properties, Chemical Equilibria, and Standard Potentials." *Chemical Reviews*, 76, (3), 283-310. Washington, D.C.: American Chemical Society. TIC: 248458.

DOE (U.S. Department of Energy) 2002a. *Yucca Mountain Site Suitability Evaluation*. DOE/RW-0549. Washington, D.C.: U.S. Department of Energy, Office of Civilian Radioactive Waste Management. ACC: MOL.20020404.0043.

DOE 2002b. *Yucca Mountain Science and Engineering Report*. DOE/RW-0539, Rev. 1. Washington, D.C.: U.S. Department of Energy, Office of Civilian Radioactive Waste Management. ACC: MOL.20020404.0042.

Drever, J.I. 1988. *The Geochemistry of Natural Waters*. 2nd Edition. Englewood Cliffs, New Jersey: Prentice-Hall. TIC: 242836.

Drever, J.I. 1997. "Evaporation and Saline Waters." Chapter 15 of *The Geochemistry of Natural Waters: Surface and Groundwater Environments*. 3rd Edition. Upper Saddle River, New Jersey: Prentice Hall. TIC: 246732.

Garrels, R.M. and Mackenzie, F.T. 1967. "Origin of the Chemical Compositions of Some Springs and Lakes?" *Equilibrium Concepts in Natural Water Systems*. American Chemical Society Advances in Chemistry Series 67. Pages 222-242. Washington, D.C.: American Chemical Society. TIC: 246519.

Greenspan, L. 1977. "Humidity Fixed Points of Binary Saturated Aqueous Solutions." *Journal of Research of the National Bureau of Standards*, 81A, (1), 89-96. Washington, D.C.: U.S. Department of Commerce. TIC: 241138.

Harrar, J.E.; Carley, J.F.; Isherwood, W.F.; and Raber, E. 1990. *Report of the Committee to Review the Use of J13 Well Water in Nevada Nuclear Waste Storage Investigations*. UCID-21867. Livermore, California: Lawrence Livermore National Laboratory. ACC: NNA.19910131.0274.

Lasaga, A.C. 1998. *Kinetic Theory in the Earth Sciences*. Princeton, New Jersey: Princeton University Press. TIC: 246279.

LBNL (Lawrence Berkeley National Laboratory) 1999. *Software Code: SOLVEQ/CHILLER*. V1.0. PC w/Windows OS. 10057-1.0-00.

LBNL 2001. *Software Code: TOUGHREACT. V2.3. SUN and DEC w/Unix OS.* 10396-2.3-00.

LBNL 2002. *Software Code: TOUGHREACT. V3.0. DEC-Alpha with Unix OSF1 V5.1 and OSF1 V5.0, Sun Solaris 5.5.1, Linux Redhat 7.2.* 10396-3.0-00.

Levy, S.S.; Fabryka-Martin, J.T.; Dixon, P.R.; Liu, B.; Turin, H.J.; and Wolfsberg, A.V. 1997. "Chlorine-36 Investigations of Groundwater Infiltration in the Exploratory Studies Facility at Yucca Mountain, Nevada." *Scientific Basis for Nuclear Waste Management XX, Symposium held December 2-6, 1996, Boston, Massachusetts.* Gray, W.J. and Triay, I.R., eds. 465, 901-908. Pittsburgh, Pennsylvania: Materials Research Society. TIC: 238884.

Liu, H-H.; Haukwa, C.B.; Ahlers, C.F.; Bodvarsson, G.S.; Flint, A.L.; and Guertal, W.B. 2003. "Modeling Flow and Transport in Unsaturated Fractured Rock: An Evaluation of the Continuum Approach." *Journal of Contaminant Hydrology, 62-63,* 173-188. New York, New York: Elsevier. TIC: 254205.

Lowry, W.E. 2001. *Engineered Barrier Systems Thermal-Hydraulic-Chemical Column Test Report.* TDR-EBS-MD-000018 REV 00. Las Vegas, Nevada: Bechtel SAIC Company. ACC: MOL.20020102.0206.

McCaffrey, M.A.; Lazar, B.; and Holland, H.D. 1987. "The Evaporation Path of Seawater and the Coprecipitation of Br⁻ and K⁺ with Halite." *Journal of Sedimentary Petrology, 57,* (5), 928-937. Tulsa, Oklahoma: Society of Economic Paleontologists and Mineralogists. TIC: 254627.

Mukhopadhyay, S. and Tsang, Y.W. 2002. "Understanding the Anomalous Temperature Data from the Large Block Test at Yucca Mountain, Nevada." *Water Resources Research, 38,* (10), 28-1 through 28-12. Washington, D.C.: American Geophysical Union. TIC: 253867.

Or, D. and Ghezzehei, T.A. 2000. "Dripping into Subterranean Cavities from Unsaturated Fractures under Evaporative Conditions." *Water Resources Research, 36,* (2), 381-393. Washington, D.C.: American Geophysical Union. TIC: 246982.

Pabalan, R.T.; Yang, L.; and Browning, L. 2002. *Effects of Salt Formation on the Chemical Environment of Drip Shields and Waste Packages at the Proposed Nuclear Waste Repository at Yucca Mountain, Nevada.* CNWRA 2002-03. San Antonio, Texas: Center for Nuclear Waste Regulatory Analyses. TIC: 254207.

Papke, K.G. 1976. *Evaporites and Brines in Nevada Playas.* Nevada Bureau of Mines and Geology Bulletin 87. Reno, Nevada: University of Nevada, Reno, Mackay School of Mines. TIC: 211869.

Philip, J.R.; Knight, J.H.; and Waechter, R.T. 1989. "Unsaturated Seepage and Subterranean Holes: Conspectus, and Exclusion Problem for Circular Cylindrical Cavities." *Water Resources Research, 25,* (1), 16-28. Washington, D.C.: American Geophysical Union. TIC: 239117.

- Pruess, K.; Wang, J.S.Y.; and Tsang, Y.W. 1990. "On Thermohydrologic Conditions Near High-Level Nuclear Wastes Emplaced in Partially Saturated Fractured Tuff, 1. Simulation Studies with Explicit Consideration of Fracture Effects." *Water Resources Research*, 26, (6), 1235-1248. Washington, D.C.: American Geophysical Union. TIC: 221923.
- Rai, D.; Sass, B.M.; and Moore, D.A. 1987. "Chromium(III) Hydrolysis Constants and Solubility of Chromium(III) Hydroxide." *Inorganic Chemistry*, 26, (3), 345-349. Washington, D.C.: American Chemical Society. TIC: 254060.
- Reamer, C.W. 2001. U.S. Nuclear Regulatory Commission/U.S. Department of Energy Technical Exchange and Management Meeting on Evolution of the Near-Field Environment (January 9–12, 2001). Letter from C.W. Reamer (NRC) to S. Brocoum (DOE/YMSCO), January 26, 2001, with enclosure. ACC: MOL.20010810.0033.
- Reamer, C.W. and Gil, A.V. 2001. Summary Highlights of NRC/DOE Technical Exchange and Management Meeting on Total System Performance Assessment and Integration. Meeting held August 6-10, 2001. Las Vegas, Nevada. Washington, D.C.: U.S. Nuclear Regulatory Commission. ACC: MOL.20010921.0121.
- Reamer, C.W. and Williams, D.R. 2000. Summary Highlights of NRC/DOE Technical Exchange and Management Meeting on Container Life and Source Term. Meeting held September 12-13, 2000, Las Vegas, Nevada. Washington, D.C.: U.S. Nuclear Regulatory Commission. ACC: MOL.20001127.0049.
- Reamer, C.W. and Williams, D.R. 2001. Summary Highlights of NRC/DOE Technical Exchange and Management Meeting on Thermal Effects on Flow. Meeting held January 8-9, 2001, Pleasanton, California. Washington, D.C.: U.S. Nuclear Regulatory Commission. ACC: MOL.20010202.0095 through MOL.20010202.0108.
- Richards, L.A. 1931. "Capillary Conduction of Liquids through Porous Mediums." *Physics*, 1, 318-333. New York, New York: American Physical Society. TIC: 225383.
- Rosenberg, N.D.; Gdowski, G.E.; and Knauss, K.G. 2001. "Evaporative Chemical Evolution of Natural Waters at Yucca Mountain, Nevada." *Applied Geochemistry*, 16, (9-10), 1231-1240. New York, New York: Pergamon. TIC: 249879.
- Shock, E.L.; Sassani, D.C.; Willis, M.; and Sverjensky, D.A. 1997. "Inorganic Species in Geologic Fluids: Correlations Among Standard Molal Thermodynamic Properties of Aqueous Ions and Hydroxide Complexes." *Geochimica et Cosmochimica Acta*, 61, (5), 907-950. New York, New York: Pergamon Press. TIC: 246451.
- Smith, W.H. and Purdy, G.M. 1995. "Chromium in Aqueous Nitrate Plutonium Process Streams: Corrosion of 316 Stainless Steel and Chromium Speciation." *Waste Management*, 15, (7), 477-484. New York, New York: Pergamon. TIC: 254034.

Sonnenthal, E.L. and Bodvarsson, G.S. 1999. "Constraints on the Hydrology of the Unsaturated Zone at Yucca Mountain, NV from Three-Dimensional Models of Chloride and Strontium Geochemistry." *Journal of Contaminant Hydrology*, 38, (1-3), 107-156. New York, New York: Elsevier. TIC: 244160.

Sonnenthal, E.; Spycher, N.; Apps, J.; and Simmons, A. 1998. *Thermo-Hydro-Chemical Predictive Analysis for the Drift-Scale Heater Test*. Milestone SPY289M4. Version 1.0. Berkeley, California: Lawrence Berkeley National Laboratory. ACC: MOL.19980812.0268.

Stuckless, J.S. 2000. *Archaeological Analogues for Assessing the Long-Term Performance of a Mined Geologic Repository for High-Level Radioactive Waste*. Open-File Report 00-181. Denver, Colorado: U.S. Geological Survey. ACC: MOL.20000822.0366.

Tsang, Y.W. and Birkholzer, J.T. 1999. "Predictions and Observations of the Thermal-Hydrologic Conditions in the Single Heater Test." *Journal of Contaminant Hydrology*, 38, (1-3), 385-425. New York, New York: Elsevier. TIC: 244160.

van Genuchten, M.T. 1980. "A Closed-Form Equation for Predicting the Hydraulic Conductivity of Unsaturated Soils." *Soil Science Society of America Journal*, 44, (5), 892-898. Madison, Wisconsin: Soil Science Society of America. TIC: 217327.

Vaniman, D.T.; Chipera, S.J.; Bish, D.L.; Carey, J.W.; and Levy, S.S. 2001. "Quantification of Unsaturated-Zone Alteration and Cation Exchange in Zeolitized Tuffs at Yucca Mountain, Nevada, USA." *Geochimica et Cosmochimica Acta*, 65, (20), 3409-3433. New York, New York: Elsevier. TIC: 251574.

Xu, T.; Sonnenthal, E.; and Bodvarsson, G. 2003. "A Reaction-Transport Model for Calcite Precipitation and Evaluation of Infiltration Fluxes in Unsaturated Fractured Rock." *Journal of Contaminant Hydrology*, 64, (1-2), 113-127. New York, New York: Elsevier. TIC: 254008.

Yang, I.C.; Rattray, G.W.; and Yu, P. 1996. *Interpretation of Chemical and Isotopic Data from Boreholes in the Unsaturated Zone at Yucca Mountain, Nevada*. Water-Resources Investigations Report 96-4058. Denver, Colorado: U.S. Geological Survey. ACC: MOL.19980528.0216 and MOL.20001025.0060.

6.2 DATA, LISTED BY DATA TRACKING NUMBER

GS011108312322.008. Uranium Concentrations and ²³⁴U/²³⁸U Activity Ratios Analyzed between February 1, 1999, and August 1, 2001 for Drift-Scale Heater Test Water Collected between June 1998 and April 2001, and Pore Water Collected between March 1996 and April 1999. Submittal date: 12/19/2001.

GS011108312322.009. Strontium Isotope Ratios and Strontium Concentrations in Water Samples from the Drift Scale Test Analyzed from March 16, 1999 to June 27, 2001. Submittal date: 02/07/2002.

GS020408312272.003. Collection and Analysis of Pore Water Samples for the Period from April 2001 to February 2002. Submittal date: 04/24/2002.

- LA0009SL831151.001. Fracture Mineralogy of the ESF Single Heater Test Block, Alcove 5. Submittal date: 09/28/2000.
- LA0201SL831225.001. Chemical, Textural, and Mineralogical Characteristics of Sidewall Samples from the Drift Scale Test. Submittal date: 01/10/2002.
- LA9912SL831151.002. Percent Coverage by Fracture-Coating Minerals in Core ESF-HD-TEMP-2. Submittal date: 01/05/2001.
- LB0101DSTTHGRD.001. 2D Finite Element Mesh Used for DST Thermal-Hydrologic-Chemical Model Simulations (Input to AMR N0120/U0110 REV. 01). Submittal date: 01/05/2001.
- LB0302DSCPTHCS.002. Drift-Scale Coupled Processes (Thermal-Hydrologic-Chemical Seepage) Model: Data Summary. Submittal date: 02/11/2003.
- LL000320405924.146. Target Compositions of Aqueous Solutions Used for Corrosion Testing. Submittal date: 03/22/2000.
- MO0005PORWATER.000. Perm-Sample Pore Water Data. Submittal date: 05/04/2000.
- MO0207EBSDUSTS.020. Geochemical Composition of Dust Samples. Submittal date: 07/11/2002.
- MO0209EBSDUST2.030. Geochemical Composition of Dust Samples (Phase II). Submittal date: 09/30/2002.
- MO0302SPATHHDYN.000. Thermodynamic Data Input Files - Data0.YMP.R2. Submittal date: 02/05/2003.
- MO0304SPACSAULT.000. EBS Chemistry THC Seepage Model Abstraction Lookup Table for TSPA-LA. Submittal date: 04/14/2003.
- MO0307MWDSEAEV.000. Seawater Evaporation Predictions Using the IDPS Model. Submittal date: 07/31/2003.
- MO0307MWDUNEVP.000. Uncertainties in Evaporation Predictions Using the IDPS Model. Submittal date: 07/31/2003. Imaging in Process Core ESF-HD-TEMP-2. Submittal date: 01/05/2000.
- MO0308SPAESMUN.000. Estimated Model Uncertainties in IDPS Model Outputs. Submittal date: 08/08/2003.
- MO0308SPAUCIMV.000. Uncertainty Comparisons in IDPS Model Validation Cases. Submittal date: 08/08/2003.
- MO0310SPADLALT.001. Dust Leachate Low Temperature Lookup Tables for TSPA-LA. Submittal date: 10/15/2003.
- SN0302T0510102.002. Pitzer Thermodynamic Database (data0.ypf, Revision 1). Submittal date: 02/06/2003.

INTENTIONALLY LEFT BLANK

APPENDIX A

**CREDIBLE RANGE OF BRINE WATER CHEMISTRY AND CONSISTENCY
BETWEEN CORROSION TESTING ENVIRONMENTS AND MODELS
(RESPONSE TO CLST 1.01, TSPAI 3.12, TSPAI 3.13, AND GEN 1.01 (COMMENTS 50,
113, 118, 122, AND 124))**

Note Regarding the Status of Supporting Technical Information

This document was prepared using the most current information available at the time of its development. This Technical Basis Document and its appendices providing Key Technical Issue Agreement responses that were prepared using preliminary or draft information reflect the status of the Yucca Mountain Project's scientific and design bases at the time of submittal. In some cases this involved the use of draft Analysis and Model Reports (AMRs) and other draft references whose contents may change with time. Information that evolves through subsequent revisions of the AMRs and other references will be reflected in the License Application (LA) as the approved analyses of record at the time of LA submittal. Consequently, the Project will not routinely update either this Technical Basis Document or its Key Technical Issue Agreement appendices to reflect changes in the supporting references prior to submittal of the LA.

APPENDIX A

CREDIBLE RANGE OF BRINE WATER CHEMISTRY AND CONSISTENCY BETWEEN CORROSION TESTING ENVIRONMENTS AND MODELS (RESPONSE TO CLST 1.01, TSPAI 3.12, TSPAI 3.13, AND GEN 1.01 (COMMENTS 50, 113, 118, 122, AND 124))

This appendix provides a response for Key Technical Issue (KTI) agreements Container Life and Source Term (CLST) 1.01, Total System Performance Assessment and Integration (TSPAI) 3.12, and TSPAI 3.13, and general agreement (GEN) 1.01, Comments 50, 113, 118, 122, and 124. These KTIs relate to information that will support predictions for the waste package and drip shield lifetimes and show consistency between the total system performance assessment (TSPA) modeling approach and the materials testing program and expected environmental conditions.

A.1 KEY TECHNICAL ISSUE AGREEMENTS

A.1.1 CLST 1.01, TSPAI 3.12, TSPAI 3.13, and GEN 1.01 (Comments 50, 113, 118, 122, and 124)

Agreement CLST 1.01 was reached during the U.S. Nuclear Regulatory Commission (NRC)/U.S. Department of Energy (DOE) Technical Exchange and Management Meeting on Container Life and Source Term held September 12 to 13, 2000, in Las Vegas, Nevada (Schlueter 2000). The main purpose of that meeting was to discuss the current technical basis and path forward for the modeling and testing plans supporting the predictions for the waste package and drip shield lifetimes. The path forward items agreed to at the meeting were to (1) establish credible range of brine water chemistry, (2) evaluate effect of introduced materials on water chemistry, (3) determine likely concentrations and chemical form of minor constituents in Yucca Mountain waters, (4) characterize Yucca Mountain waters with respect to the parameters which define the type of brine which would evolve, and (5) evaluate periodic water drip evaporation.

Agreements TSPAI 3.12 and TSPAI 3.13 were reached during the NRC/DOE Technical Exchange and Management Meeting on Total System Performance Assessment and Integration held August 6 to 10, 2001, in Las Vegas, Nevada (Reamer and Gil 2001a). These two agreements specifically focused on the scenario analysis subissue of having a waste package and drip shield modeling approach to be used for TSPA consistent with the materials testing program and the expected environmental conditions to which these engineered barriers would be subject.

Agreement GEN 1.01 was reached during the NRC/DOE Technical Exchange and Management Meeting on Range of Thermal Operating Temperatures, held September 18 to 19, 2001. At that meeting, the NRC provided additional comments that relate to CLST 1.01. These resulted in GEN 1.01, Comments 21, 50, 64, 113, 118, 122, and 124, and the DOE provided an initial response to those comments (Reamer and Gil 2001b). Comments 21 and 64, however, are related to postclosure criticality and will not be addressed here but will be more appropriately addressed in the response to agreement CLST 5.03.

Specific page number referrals cited below as part of GEN agreement Comments 50, 113, 122, and 124 are from *FY01 Supplemental Science and Performance Analyses, Volume 1: Scientific Bases and Analyses* (BSC 2001).

The wording of these agreements is as follows:

CLST 1.01

Provide the documentation for Alloy 22 and titanium for the path forward items listed on slide 8 [establish credible range of brine water chemistry; evaluate effect of introduced materials on water chemistry; determine likely concentrations and chemical form of minor constituents in YM waters; characterize YM waters with respect to the parameters which define the type of brine which would evolve; evaluate periodic water drip evaporation]. DOE will provide the documentation in a revision to AMR "Environment on the Surfaces of the Drip Shield and Waste Package Outer Barrier" by LA.

TSPAI 3.12¹

DOE should complete testing of corrosion in the chemical environments predicted by the model or provide technical basis why it is not needed (ENG3.1.8). DOE will conduct testing of corrosion in the credible range of chemical environments predicted by the model in accordance with the scope and schedule for existing agreements CLST 1.4 and 1.6 or provide a technical basis why it is not needed.

TSPAI 3.13²

Provide a comparison of the environments for corrosion predicted in the models, to the testing environments used to define empirical corrosion rates in revised documentation (ENG3.2.1). DOE will provide a comparison of the environments for corrosion predicted in the models, to the testing environments utilized to define empirical corrosion rates in revised documentation consistent with the scope and schedule for existing agreement item CLST 1.1.

GEN 1.01 (Comment 50)

- What is the probability of the formation of sufficient conditions leading to localized corrosion?

If none, then

- Which solution compositions hitting the waste package and evaporating could lead to sufficient environmental conditions for the onset of localized corrosion?

¹ (ENG3.1.8) in this agreement refers to item 1.8 of NRC integrated subissue ENG 3 (NRC 2002, Table 1.1-2).

² (ENG3.2.1) in this agreement refer to item 2.1 of NRC integrated subissue ENG 3 (NRC 2002, Table 1.1-2).

- What is the probability that such initial solution compositions could be established?

Basis: The uncertainty in the compositions of the solutions contacting the waste package and drip shield is not acknowledged in the waste package and drip shield analyses reported in Chapter 7 of the SSPA Vol 1. It is stated multiple times in this Chapter that localized corrosion of the waste packages is not feasible as nitrates and sulfates are more abundant than chloride ions.

Based on information in Chapter 6 (pages 6-8, 6-62, and 6-63), it is evident that there is high uncertainty in the solutions that could develop after evaporation.

These solutions are dependent on the initial solution composition. There is a high possibility of formation of solutions highly concentrated in chloride and fluoride.

It is necessary to achieve better integration between the coupled thermal-hydrologic-chemical, evaporation and salt formation models of Chapter 6 and the waste package degradation analyses of Chapter 7.

On page 7-59 of SSPA Vol 1 it is stated that “... the potential for the development of environments leading to localized corrosion of Alloy 22 is unlikely.” Additional technical basis are needed to support this statement.

DOE Initial Response to GEN 1.01 (Comment 50)

Electrochemical studies are being employed to determine the aqueous solution compositions that could lead to conditions necessary for localized corrosion.

The range of water chemistries that could contact the waste packages and drip shields is being determined. This considers a range of sources of soluble ions including seepage waters, particulate matter contained in the ventilation air, drift dust, and other engineered barrier system component interactions contributions to water chemistry.

The determination of the range of water chemistries is covered in the key technical issue (KTI) agreements for Container Life and Source Term (CLST 1.1) and for Evolution of the Near Field Environment (ENFE 2.15 and 2.17).

The studies [of the effect of] environmental conditions on localized corrosion are covered under CLST agreement 1.[01].

GEN 1.01 (Comment 113)

Page 7T-1: Does the pore water compositions shown in Table 7.3.1-2 suggests that the waters in the Yucca Mountain system already exhibit evidence of evolving to a Ca-Mg-Cl type system, thereby making the evolution of the waters due to thermal influences more likely to end up in the Ca-Mg-Cl system (the

concentration factors of Ca, Mg, and Cl from fracture to pore water are much larger than for NO₃)?

DOE Initial Response to GEN 1.01 (Comment 113)

The compositions of the waters shown in Table 7.3.1-2 are examples of waters that have been sampled at Yucca Mountain.

Under CLST KTI agreement 1.1, testing and modeling for a potential TSPA-LA is being performed in order to determine the expected compositions of waters that will be in contact with the waste packages and drip shields. These activities consider seepage water compositions, particulate matter in the ventilation air, and dust that may be deposited on these components.

GEN 1.01 (Comment 118)

DOE's assessment of deliquescence humidity did not consider the mixed salt effect. Mixed salts may lower the [deliquescence] points below that of pure salts.

DOE Initial Response to GEN 1.01 (Comment 118)

The deliquescence of mixed salts will be addressed experimentally in FY02. This work is covered under the CLST KTI agreement 1.1.

GEN 1.01 (Comment 122)

In p. 7-58, fluoride mitigates corrosion. Provide the basis for this mitigation.

DOE Initial Response to GEN 1.01 (Comment 122)

Fluoride ions have an inhibiting effect for some metals under certain situations. A general reference on corrosion inhibitors was cited for this effect (J.G.N. Thomas in *Corrosion: Corrosion Control*, Vol. 2, Chap. 17.3, L.L. Shreir, R.A. Jarman, and G.T. Burstein, eds. Butterworth-Heinemann, Woburn, Massachusetts, 1994.) An inhibiting effect of fluoride ions for Ti and Alloy 22 corrosion has not been established. DOE will provide the basis for this mitigation in accordance with KTI agreements CLST 1.1 and 6.1.

GEN 1.01 (Comment 124)

In p. 7-74, Ferric Chloride generation is very remote spatially. Provide the basis for the hypothesis.

NRC Clarification: Correct page number is 7-64, Section 7.3.7.1:

"...Although useful in ranking a range of alloys, these standard tests utilize aggressive environments (in particular, a ferric chloride solution) that are not

directly relevant to expected waste package surface environments because the potential for ferric chloride generation is very remote. ...”

The NRC expressed a concern that DOE models might neglect the potential accelerating effect of ferric chloride on corrosion/degradation of waste package materials and fuel cladding materials. NRC requested clarification about DOE’s intent to evaluate the potential role of ferric chloride in waste package and fuel cladding degradation.

DOE Initial Response to GEN 1.01 (Comment 124)

Electrochemical corrosion testing is determining the effect that minor constituents will have on the waste package corrosion processes. This will include the effects of ferric ion in the aqueous test solutions. Activities will also determine the extent that minor constituents can concentrate in the aqueous solutions. This work is covered under existing KTI agreement CLST 1.1.

Per existing KTI agreement CLST 3.7, a ferric-chloride local clad corrosion model is being developed that will be documented in a future revision of the *Clad Degradation Summary Abstraction* AMR.

A.1.2 Related Key Technical Issue Agreements

Other KTI agreements related to those addressed in this appendix are ENFE 2.06 (Appendix E), ENFE 2.09 (Appendix F), ENFE 2.10 (Appendix G), ENFE 2.14 (Appendix J), and TSPA 2.02 item 48. The TSPA agreement will be addressed separately in a future response addressing features, events, and processes.

A.2 RELEVANCE TO REPOSITORY PERFORMANCE

The primary consideration for understanding the in-drift environment relates to the impact on waste package and drip shield performance. The environmental conditions that the waste package and drip shield are subjected to and the evolution of the water chemistry play a substantial role in establishing the performance of these engineered barriers. A consistency between the environment for the materials corrosion testing program and the expected environment that will exist on the waste package and drip shield surfaces is essential to adequately demonstrate the understanding and development of the barrier performance models used. Discrepancies can impact engineered barrier lifetime predictions in terms of increasing the uncertainty on barrier performance predictions.

A.3 RESPONSE

A credible range of brine water chemistry on the drip shield and waste package outer barrier due to seepage has been determined by establishing a credible range of dilute water chemistries that may seep through the mountain and modeling the evolution of these waters under repository-relevant conditions (Agreement CLST 1.01).

The range of environments in which the corrosion tests have been performed encompasses the range of environments that have been projected to be relevant for the waste packages under expected repository conditions (Agreement TSPA1 3.12). Table A-1 shows the composition of some of the solutions used for corrosion testing. These aqueous corrosion test solutions include several multi-ionic solutions based on a carbonate-based water, J-13 well water (taken as one of the representative compositions of the incoming waters) and test solutions containing the major species expected to effect corrosion. These solutions include simulated dilute water (SDW), simulated concentrated water (SCW), simulated acidified water (SAW), simulated saturated water (SSW), and basic saturated water (BSW). The SDW and SCW solutions are concentrated solutions of the dilute carbonate water. The SSW formulation is based upon the assumption that evaporation of carbonate water eventually leads to a sodium-potassium-chloride-nitrate solution. The absence of SO_4^{2-} and CO_3 in this test medium is conservative (CO_3 , in the context of this appendix, refers to total aqueous carbonate, comprising $\text{CO}_2(\text{aq})$, HCO_3^- , and CO_3^{2-}). For example, CO_3 would help buffer pH in any occluded geometry such as a crevice, and sulfate can act as a corrosion inhibitor. Small amounts of CO_3 will form in the SSW, SAW, and BSW solutions by interaction with gas-phase carbon dioxide. The amount of carbonate formed was not determined experimentally, since the small amounts were not expected to affect the corrosion processes significantly.

Table A-1. Target Composition of Standard Test Media Based on Carbonate-Based Water

Ion	SDW (mg/L)	SCW (mg/L)	SAW (mg/L)	SSW (mg/L)	BSW-12 (mg/L)
K^+	3.4×10^1	3.4×10^3	3.4×10^3	1.42×10^5	6.762×10^4
Na^+	4.09×10^2	4.09×10^4	3.769×10^4	4.87×10^4	1.0584×10^5
Mg^{2+}	1	<1	1.00×10^3	0	0
Ca^{2+}	5×10^{-1}	<1	1.00×10^3	0	0
F^-	1.4×10^1	1.4×10^3	0	0	1.47×10^3
Cl^-	6.7×10^1	6.7×10^3	2.425×10^4	1.28×10^5	1.3083×10^5
NO_3^-	6.4×10^1	6.4×10^3	2.30×10^4	1.313×10^6	1.3965×10^6
SO_4^{2-}	1.67×10^2	1.67×10^4	3.86×10^4	0	1.47×10^4
HCO_3^-	9.47×10^2	7.0×10^4	0	0	0
Si	27 (60°C), 49 (90°C)	27 (60°C), 49 (90°C)	27 (60°C), 49 (90°C)	0	0
pH	9.8 to 10.2	9.8 to 10.2	2.7	5.5 to 7	12

Source: DTN: LL000320405924.146.

NOTE: pH measured for actual solutions at room temperature.

BSW can have a pH between 11 and 13 and has a boiling point near 110°C (BSW-12 with a pH of 12 is shown in Table A-1). This test medium was established on the basis of results from a distillation experiment. The total concentration of dissolved salts in the starting liquid was more concentrated than that in the standard SCW solution. After evaporation of approximately 90 percent of the water from the starting solution, the residual solution reaches a maximum chloride concentration and has a boiling point of approximately 110°C, with a pH of about 11. The synthetic BSW solution composition can be slightly modified (mainly by adding sodium hydroxide) to cover a range of pH values, yielding BSW-13, BSW-12, and BSW-11.

For the environmental conditions at the drip shields and waste packages that are of low relative humidity, the waters in contact with the engineered barrier system components will be brines which can form either through seepage water evaporative concentration or through salt and (or) dust deliquescence and can be divided into three general types: calcium chloride, sulfate, and carbonate. As defined here, these brine types bear strong affinity to the classical brine types used in classic chemical divide theory for the formation of surface brines by evaporation, as in desert playas (Hardie and Eugster 1970); see also Drever (1997, pp. 327 to 351). There are, however, some key chemical differences between expected seepage waters and dusts on the one hand and surface waters on the other.

All three brine types as relevant to Yucca Mountain will contain relatively significant quantities of chloride and nitrate, whether derived from evaporation of seepage water or deliquescence of salts in dust. Thus, the most concentrated “calcium chloride” brine is in reality likely to be a concentrated solution of both calcium chloride and calcium nitrate. The “sulfate” and “carbonate” brines will also contain significant Cl^- and NO_3^- . At sufficiently high extents of evaporation or at the onset of deliquescence (both corresponding to rather low relative humidity), these brines might more appropriately be described as nitrate brines because the anionic content of the aqueous solutions is dominated by nitrate ions.

Magnesium is not expected to be an abundant constituent in Yucca Mountain brines under anticipated conditions (e.g., due to its incorporation in silicate minerals) (BSC 2003a, Section 6.7.2.11). Thus, the calcium chloride brine type is not expected to include possible magnesium chloride. Also, the sulfate brine, which in playa lake brines is sometimes expressed as magnesium sulfate, is expected in Yucca Mountain to be expressed as a less concentrated alkali metal (Na, K) sulfate brine, with the chloride content being somewhat depressed owing to the relatively high alkali metal concentrations and solubility limits imposed by the associated chloride minerals. It should be noted that evaporation of ambient pore water in the absence of minerals present in the tuff or in dust could lead to the formation of brine with elevated levels of magnesium. However, such a scenario is not expected in the repository because intimate contact between water and dust or tuff (or both) is expected.

The carbonate brine is likely to be of the sodium carbonate type, but it may be better represented as alkali metal (sodium, potassium) carbonate brine.

Typically, sulfate brines are associated with near-neutral pH and carbonate brines with high pH. Since a nitrate-dominated brine can represent the low relative humidity end of the spectrum for either, it should be noted that a nitrate brine might be expected to be associated with either near-neutral or high-pH, depending on genesis. A near-neutral nitrate brine would be expected from the deliquescence of a salt mineral assemblage such as $\text{NaCl-NaNO}_3\text{-KNO}_3$ or from a high extent of evaporation of a sulfate brine. A high pH nitrate brine would be expected at a very high extent of evaporation of a carbonate brine. A nitrate-dominated brine is not considered here as a separate, fourth brine type. This is partly because of the potential pH distinction. However, it is also recognized that NO_3^- , CO_3 , and SO_4^{2-} are all likely inhibitors of localized corrosion. Hence the treatment adopted also makes sense from a corrosion point of view.

The environments for corrosion predicted in the models have been addressed (BSC 2003b, Section 6.14) (Agreement TSPAI 3.13). Environments on the waste package have been modeled

for the scenarios of dust deliquescence and seepage water contact. In both cases high-ionic strength brines are predicted. A thermodynamic database based on the Pitzer formulation is used in conjunction with the EQ3/6 computer code in order to model brine evolution (BSC 2003c), as is discussed in the response for ENFE 2.09 (Appendix F). Note, seepage water brines will not contact the waste package surfaces as long as the drip shields perform their intended function (BSC 2003d, Section 6.3).

Deliquescence of dust deposited on the waste packages and drip shield is another means by which brines can form on these engineered barrier system components. Two different approaches were used to determine the characteristics of the brines from evolution of dust deliquescence with similar results obtained using the alternative methods (see Section A.4). Table A-2 lists the brine type and the percent probabilities of contact with the waste packages and drip shields. Brines of concern for Alloy 22 performance in the predicted repository environment are primarily calcium chloride brines. The integrated fractional occurrence of a calcium chloride type brine from seepage is 0.22 percent. The probability for formation of calcium chloride brine from dust is less than 6 percent and under most scenarios the solutions are nitrate-dominated. The majority of the expected aqueous solutions are dominated by sodium and potassium cations with accompanying chloride and nitrate anions.

Table A-2. General Classification of the Brine Types that Could Be in Contact with Drip Shields and Waste Packages and the Probabilities of Contact

Brine Type	Percent Probability			Comments
	Seepage at Drift Crown	Dust Deliquescence (Method 1)	Dust Deliquescence (Method 2)	
Calcium chloride	0.22	5.77	4	Fluoride, carbonate, sulfate contents are negligible
Sulfate	2.21	75.00	—	Near neutral pH
Carbonate	97.56	19.23	—	High pH, no significant calcium or magnesium content
Sulfate or carbonate	—	—	96	The methodology used in Method 2 does not differentiate between sulfate or carbonate brine types. It determines the mineral assemblages that control deliquescence.

NOTE: The probability of seepage at drift crown represents the 20,000-year time integrated occurrence fraction of the representative water for each bin. Additionally, the mapping from Table A-3 for the 11 bins is as follows: Bins 1 to 3 are calcium chloride; Bins 4 and 5 are sulfate; and Bins 6 to 11 are carbonate. For dust deliquescence the probabilities represent the fraction of waste packages subject to dust that may deliquesce into the identified brine type, and the calcium chloride brines are actually dominated by $\text{Ca}(\text{NO}_3)_2$. For the dust deliquescence Method 1, the mapping comes from Table A-5 as follows: Bin 1 is calcium chloride; Bins 2, 4 and 5 are sulfate; and bins 3 and 6 are carbonate. Dust deliquescence Method 2 originates from Table A-4.

The information in this report is responsive to agreements CLST 1.01, TSPA 3.12, TSPA 3.13, and GEN 1.01 (Comments 50, 113, 118, 122, and 124) made between the DOE and NRC. The report contains the information that DOE considers necessary for NRC review for closure of these agreements.

A.4 BASIS FOR THE RESPONSE

Subsections A.4.1 through A.4.5 provide the basis for each of the path forward items identified as part of Agreement CLST 1.01. These sections collectively encompass the basis for the TSPA 3.12 and TSPA 3.13 in addition to CLST 1.01. Subsections A.4.6 through A.4.10 provide specific responses for the GEN 1.01 comments.

A.4.1 Establish Credible Range of Brine Water Chemistry

Concentrated or high-ionic strength aqueous solutions (brines) are thermodynamically stable under the projected environmental conditions for the drip shields and waste packages. Aqueous solutions in equilibrium with relative humidity less than 90 percent will typically have ionic strengths greater than 1 molal. The projected temperature and relative humidity profiles for the waste packages are discussed in Section 2.3 of this technical basis document.

Geochemical literature establishes the three types of brines that result from the evaporative concentration of dilute natural waters at the earth's surface. These are:

- Calcium chloride brine
- Carbonate brine
- Sulfate brine.

The brine type name reflects a characteristic of the brine that distinguishes it from the other brines. It does not necessarily reflect the dominant species in the brine. This characterization of surface brine types has in part guided the expected range of brine water chemistry in the repository. However, some differences are expected between brines formed at the earth's surface and brines formed in the repository. These differences are mainly due to differences in the chemistry of seepage waters and surface waters giving rise to brines, and differences between the salt chemistry of dust and the dissolved salt content of such surface waters. Two important general factors specific to the repository brines are the ubiquity of nitrate and more effective mechanisms for the removal of magnesium. It is expected that nitrate will always be in the deliquescent brines owing to multiple potential sources (BSC 2003a, Section 6.7.2.8) and generally high solubility of nitrate minerals (e.g., BSC 2003a, Section 4.1.1.7). It is expected that magnesium will never be significant owing to a combination of low source (for the dust, as well as for at least some groundwaters) and multiple removal mechanisms, most of which are enhanced by elevated temperature (BSC 2003a, Sections 6.7.2.10 and 6.7.2.11); these mechanisms are also discussed in Section A.4.4.

The calcium chloride brines have near neutral pH and no significant CO_3 , F^- , and SO_4^{2-} content. These brines may contain other cations such as Na^+ , K^+ , and Mg^{2+} and other anions such as NO_3^- . The endpoint of the evaporative concentration of this type of brine would contain calcium-chloride and -nitrate or a mixture of calcium- and magnesium-chloride and -nitrate. The quantity of magnesium and calcium in this type of brine would be limited due to the precipitation of calcium carbonates and sulfates and magnesium silicates. This is consistent with information on saline lakes where Na^+ is the dominant cation with the percentage of Ca^{2+} varying from insignificant to about 20 percent (Drever 1997). In the repository, the concentration of magnesium in any type of brine is expected to be insignificant, as noted earlier. Thus, a

magnesium chloride brine is not expected. NO_3^- is expected to be present, and a brine of this type will be dominated by calcium chloride and calcium nitrate. A brine of the calcium chloride type is expected to have a very limited occurrence in the repository, as indicated in Table A-2. For brine of this type generated by dust deliquescence, the brine is expected to be more of a calcium nitrate brine.

Relative humidity dependence of the calcium chloride brine is as follows. At low relative humidity, the aqueous solutions will be dominated by Ca^{2+} cations (very low Na^+ and K^+), and Cl^- and NO_3^- anions, since both calcium nitrate and calcium chloride are very soluble. At higher relative humidity, chloride and nitrate salts of sodium and potassium become soluble and could dominate the aqueous solution compositions. This would occur at or above the deliquescence relative humidity for salts composed of these ions.

The carbonate brines are alkaline and do not have significant calcium or magnesium content. In the early stages of the evaporative concentration, calcium precipitates as predominantly carbonate mineral (calcite or aragonite) under equilibrium conditions. Magnesium precipitates as a minor component in the calcium carbonate species and as magnesium silicate (see Section A.4.4 for discussion of magnesium silicate precipitates). As noted above, it is expected that in the repository magnesium will be removed efficiently, and potassium may be significant in some of these brines. As shown in Table A-2, the carbonate brine type is expected to be the most common type produced by evaporation of seepage water, and a minor type produced by dust deliquescence.

Relative humidity dependence of carbonate brine is as follows. At low relative humidity, the aqueous solutions will be dominated by NO_3^- and Cl^- anions with NO_3^- ions dominating at the lowest relative humidity. At moderate relative humidity (above 70 percent) Cl^- ions could dominate the solution composition. The NO_3^- - Cl^- solutions are expected to have slightly elevated pH due to residual CO_3 in solution. Significant amounts of CO_3 and SO_4^{2-} are not expected until the relative humidity is greater than 85 percent.

The sulfate brines have near-neutral pH and no significant bicarbonate-carbonate and calcium content. Calcium precipitates as carbonates and possibly sulfates. In addition, they typically have only a small amount of magnesium, though some surface brines have high magnesium (see Drever 1997, Table 15-1, p. 333, brines 1 to 3). The dominant cation is typically Na^+ . In the repository brines, K^+ may be more significant than Na^+ , and Mg^{2+} is expected to be insignificant. NO_3^- is expected to be relatively high, perhaps more so than sulfate. As shown in Table A-2, the sulfate brine type is expected to be a minor type produced by evaporation of seepage water, but there are nitrate versions of this brine.

Relative humidity dependence of the sulfate brine is as follows. At low relative humidity, the aqueous solutions will be dominated by NO_3^- and Cl^- anions with NO_3^- ions dominating at the lowest relative humidity. At moderate relative humidity (above 70 percent) Cl^- ions could dominate the solution composition. However, unlike the carbonate brines these brines are expected to have near neutral to slightly acidic pH because of the lack of a carbonate component. Significant amounts of CO_3 and SO_4^{2-} are not expected until the relative humidity is greater than 85 percent because of the increase in solubility of expected sulfate minerals (sodium and

potassium sulfates). (Magnesium sulfate is expected to be present in only insignificant quantities in these brines.)

Hence, brines that evolve from natural waters are typically limited to three types: calcium chloride, carbonate, and sulfate. These brines that develop on the waste packages and drip shields will be the result of either (1) evaporative concentration of seepage water or (2) deliquescence of deposited salts. Deposited salts can be due to entrained matter in the ventilation air, dust and debris deposited from within the drifts, or seepage waters that have evaporated to dryness.

Five dilute waters have been chosen as representative of the range of dilute waters that may initially seep through Yucca Mountain. The basis for selection is documented in *Drift-Scale Coupled Processes (DST and THC Seepage) Models* (BSC 2003e). The modeling of the evolution of these waters considers the effects of temperature, relative humidity, and partial pressure of carbon dioxide. The abstraction of evolved seepage waters at the drift crown is discussed in the response for ENFE 2.10 (Appendix G) and documented in *Engineered Barrier System: Physical and Chemical Environment Model* (BSC 2003b). Waters at the drift crown are those that may contact the waste packages and drip shields.

Table A-3 lists the range of environments that are projected to form within the repository due to water seepage. These seepage waters have been categorized into 11 bins, or water types, based on their chemical composition (BSC 2003b). A characteristic water has been determined for each bin. These seepage waters are characterized by their dominant ionic species at relative humidity of 98 percent and under conditions just before dryout. The probability that a particular bin will form at the drift crown is also listed. For each bin, the associated brine type (calcium chloride, carbonate, and sulfate) corresponding to the endpoint composition of the bin is listed, as well as the aqueous corrosion test solution that is associated with the particular brine type. In terms of brine type based on the chemical divide, the drift crown brines are predominately the alkaline carbonate brines, although the CO_3 may not be a dominant constituent in these solutions except at higher relative humidities. The composition of each bin water as a function of repository-relevant conditions, temperature, and relative humidity is given in lookup tables.

Corrosion test solutions corresponding to this calcium chloride type of brine include: calcium chloride, calcium chloride plus calcium nitrate, SSW (see Table A-1), and sodium chloride aqueous solutions. The SSW and sodium chloride test solutions simulate the moderate relative humidity scenario where calcium is a minor component in the aqueous solution. Numerous electrochemical studies were performed in these test solutions. Thin film studies were also performed using these types of solutions on coupons of Alloy 22 using an environmental thermogravimetric analyzer.

Table A-3. Drift Crown Seepage Water Limiting Compositions and Probabilities of Their Formation, the Associated Brine Type, and the Corresponding Corrosion Test Solutions

Bin Water	Probability of Crown Seepage ^a	Dominant Constituents in Bin Water at 98% Relative Humidity ^b	Dominant Constituents in Endpoint Brines ^b	Brine Type	Corrosion Test Solution
1	0.00	Ca-Cl	Ca-Cl	Calcium chloride	CaCl ₂ ; CaCl ₂ + Ca(NO ₃) ₂
2	0.00	Na-Cl	Ca-Cl	Calcium chloride	CaCl ₂ ; CaCl ₂ + Ca(NO ₃) ₂
3	0.22	Na-Cl	Ca-Cl; K-Cl	Calcium chloride	CaCl ₂ ; CaCl ₂ + Ca(NO ₃) ₂
4	1.42	Na-Cl	K-NO ₃ ; Na-NO ₃	Sulfate	SSW, SAW, NaCl
5	0.79	Na-Cl	Na-Cl; K-Cl	Sulfate	SSW, SAW, NaCl
6	5.46	Na-Cl	Na-Cl; Na-NO ₃ ; K-Cl	Carbonate	SDW, SCW, BSW, SSW, NaCl
7	27.15	Na-Cl	Na-Cl; Na-NO ₃ ; K-Cl	Carbonate	SDW, SCW, BSW, SSW, NaCl
8	16.2	Na-CO ₃	Na-Cl; Na-NO ₃ ; K-Cl	Carbonate	SDW, SCW, BSW, SSW, NaCl
9	15.55	Na-CO ₃	K-NO ₃ ; K-Cl	Carbonate	SDW, SCW, BSW, SSW, NaCl
10	11.7	Na-CO ₃	Na-Cl; Na-NO ₃ ; K-Cl	Carbonate	SDW, SCW, BSW, SSW, NaCl
11	21.5	Na-Cl	Na-Cl; Na-NO ₃ ; K-Cl	Carbonate	SDW, SCW, BSW, SSW, NaCl

Sources: ^a BSC 2003e, Table 6.14-1.

^b BSC 2003e, Table 6.14-8.

NOTE: The probability of crown seepage represents the 20,000-year time-integrated occurrence fraction (in percent) of the representative water for each bin.

Corrosion test solutions corresponding to the carbonate type of brine include the SDW, SCW, BSW, and under certain circumstances SSW and simulated acidic water SAW aqueous test solutions (see Table A-1). The BSW test solution is a highly concentrated alkaline solution and could be expected under repository conditions where temperatures could be at its measured boiling point of nominally 112°C to 113°C or where the relative humidity is nominally 70 to 75 percent. The SCW test solution is a moderately concentrated alkaline solution; solutions in this concentration range could be expected to form for relative humidity in the range of 90 to 95 percent. The SDW test solution is a dilute alkaline solution; solutions in this concentration range could be expected to form for high relative humidity (greater than 99 percent). These may have characteristics of solutions at the drift wall, that is, typical of seepage waters.

Under conditions of extreme evaporative concentration (i.e., low relative humidity) the carbonate brine would evolve into a nitrate chloride brine with low carbonate content. The SSW test solution has characteristics of this type of brine. Likewise the SAW test solution has characteristics of low carbonate brine and would have characteristics of solutions in equilibrium with relative humidity of nominally 90 percent. It should be noted that the SAW test solution pH is much lower than would be expected for a carbonate-type brine. The calcium and magnesium

content of the SAW test solution tends to make it more able to sustain lower pHs due to the hydrolysis properties of these cations.

The corrosion test solutions corresponding to the sulfate type of brine include the SAW, SSW, and sodium chloride. This type of brine has near neutral to slightly acidic pH and as noted above magnesium is not expected to be present in seepage waters to any significant extent. The SAW test solutions have characteristics of solutions in equilibrium with nominally 90 percent relative humidity. The SSW has characteristics of water that have undergone evaporative concentration to the extent that sulfate precipitates out of solution (this is for the magnesium-free situation). Sodium chloride test solutions simulate the scenario where Cl^- is the dominant anion under moderate relative humidity conditions.

Deliquescence of dust deposited on the waste packages and drip shields is another means by which brines can form on engineered barrier system components. Two different approaches were used to determine the characteristics of the brines. Brine evolution from dust deliquescence has been developed in *Engineered Barrier System: Physical and Chemical Environment Model* (BSC 2003b) and *Environment on the Surfaces of Drip Shield and Waste Package Outer Barrier* (BSC 2003a). Similar results were obtained using the alternative methods. Both analyses use experimentally determined dilute water compositions that resulted from dissolution of salt from dust samples collected in the Exploratory Studies Facility at Yucca Mountain.

Table A-4 lists the mineral assemblages of dust that are projected to be deposited on the waste packages, the probabilities of their formation, and the associated brine type (BSC 2003a). These deliquescent mineral assemblages were derived from the total mineral assemblages that resulted from evaporating the initial dilute waters to dryness. Bromide minerals were not included in this analysis because it was assumed that the Br^- currently present in waters at Yucca Mountain is principally an artifact of an introduced material (a LiBr tracer used during tunnel construction and during previous hydrologic testing) that will not be used in the emplacement drifts. The water compositions at a given time are determined by the temperature and relative humidity conditions.

Table A-4. Mineral Assemblages of Dust Deposited on the Waste Packages Excluding Bromide, the Probabilities of Their Formation, and the Associated Brine Type

Case	Percent Probability	Mineral Assemblage	Brine Type
A	28	$\text{NaCl-NaNO}_3\text{-KNO}_3$	Carbonate or sulfate
B	68	NaCl-KNO_3	Carbonate or sulfate
C	4	$\text{Ca(NO}_3)_2\text{-NaCl-NaNO}_3\text{-KNO}_3$	Calcium chloride

Sources: BSC 2003a, Table 45; Wolery 2003.

For the greatest percentage of the dust mineral assemblages, Case A and B, the solution compositions at low relative humidity are projected to be mixtures of Na^+ , K^+ , NO_3^- , and Cl^- with the subsequent aqueous solution compositions dependent on temperature and relative humidity conditions.

Case C contains calcium nitrate in addition to Na^+ , K^+ , NO_3^- , and Cl^- . The calcium nitrate dominates the deliquescence behavior. Aqueous solution composition from deliquescence of this

mineral assemblage at low relative humidity and, hence, high temperature under repository conditions would be dominated by nitrate.

Table A-5 lists the brines that would develop on the waste packages using an alternative analysis (BSC 2003b). The dilute waters were categorized into six bins based on their composition at a given relative humidity. Similar results were obtained as compared with the above analysis (Table A-4). The calcium nitrate (Bin 1) is a low probability event and is similar to Case C in Table A-4. The other Bins (2, 3, 4, 5, and 6) are for brines containing Na^+ , K^+ , NO_3^- , and Cl^- and are similar to results above for Cases A and B in Table A-4. The associated brine type and the corresponding aqueous corrosion test solutions are listed in the Table A-5. It should be noted that these aqueous solutions contain Br^- ion. While not a major contributor to the end point brine composition, it is a noteworthy component that was considered in this analysis.

Table A-5. Brines from Dust Deposited on the Waste Packages Including Bromide, the Probabilities of Their Formation, the Associated Brine Type, and the Corresponding Corrosion Test Solutions

Bin Water	Probability of Deliquescence Bin ^a	Dominant Constituents in Bin Water at 98 Percent Relative Humidity ^b	Dominant Constituents in Endpoint Brines ^b	Brine Type	Corrosion Test Solution
1	5.77	Na-NO ₃	Ca-NO ₃	Calcium chloride	CaCl ₂ ; CaCl ₂ + Ca(NO ₃) ₂
2	7.69	Na-NO ₃	K-NO ₃ ;Na-NO ₃	Sulfate	SSW, SAW, NaCl
3	17.31	Na-SO ₄	K-NO ₃ ;Na-NO ₃	Carbonate	SDW, SCW, BSW, SSW, NaCl
4	23.08	Na-NO ₃	Na-NO ₃	Sulfate	SSW, SAW, NaCl
5	44.23	Na-NO ₃	K-NO ₃ ;Na-NO ₃	Sulfate	SSW, SAW, NaCl
6	1.92	Na-Cl	K-NO ₃	Carbonate	SDW, SCW, BSW, SSW, NaCl

Sources: ^a BSC 2003b, Table 6.10-6.

^b BSC 2003b, Table 6.14-9.

NOTE: The probabilities represent the percentage of waste packages subject to dust that may deliquesce into the identified brine type.

The results of the two alternative methods for determining the deliquescence controlling salt minerals are in good agreement. The calcium nitrate brine (Case C and Bin 1) is only expected to occur for a small percentage of the dust. Most of the brines expected to form would contain sodium, potassium, chloride, and nitrate (Cases A and B, and Bins 2, 3, 4, 5, and 6).

In all cases, the nitrate component is the most deliquescent species and would dominate the solution composition at the deliquescent relative humidity. It is not until the relative humidity is much higher that the chloride composition could become comparable to the nitrate composition; this is discussed in more detail in *Environment on the Surfaces of Drip Shield and Waste Package Outer Barrier* (BSC 2003a).

Table A-6 lists the corrosion tests performed to date on the waste package outer barrier material, Alloy 22. The table identifies the type of tests performed, the general number of tests performed, and the aqueous test environments used for the tests.

Table A-6. Aqueous Test Solutions for Electrochemical Tests and Long-Term Immersion Tests for Alloy 22

Test Environment	Temperature (°C)	Open Circuit Potential Short Term (≤24 hr)	Open Circuit Potential Long Term (>1 week)	Polarization Resistance	Cyclic Polarization	Weight Loss	Potentiostatic	Slow Strain Rate Testing	Reversing DC	AC Impedance
SAW	60	G	L	G	G	G	G	L	L	L
SAW	90	G	L	G	G	G	G	G	L	G
SCW	60	G	L	G	G	G	L	L	L	L
SCW	90	G	L	G	G	G	G	G	L	G
BSW	105	—	G	—	L	—	—	G	L	—
SDW	60	—	—	—	—	G	—	—	—	—
SDW	90	—	—	—	—	G	—	—	—	—
1 M NaCl	60	G	L	G	G	L	L	L	L	L
1 M NaCl	90	G	L	G	G	L	L	L	L	L
4 M NaCl	45	G	L	G	G	L	L	L	L	L
4 M NaCl	60	G	L	G	G	L	L	L	L	L
4 M NaCl	75	G	L	G	G	L	L	L	L	L
4 M NaCl	90	G	L	G	G	L	L	L	L	L
4 M NaCl	105	G	L	G	G	L	L	L	L	L
NaCl + Na ₂ SO ₄	45, 60, 75, 90, 105	G	L	G	G	L	L	L	L	L
5 M CaCl ₂	45	G	L	G	G	L	L	L	L	L
5 M CaCl ₂	60	G	L	G	G	L	L	L	L	L
5 M CaCl ₂	75	G	L	G	G	L	L	L	L	L
5 M CaCl ₂	90	G	L	G	G	L	L	L	L	L
5 M CaCl ₂	105	G	L	G	G	L	L	L	L	L
5 M CaCl ₂	120	G	L	G	G	L	L	L	L	L
6 M CaCl ₂	130	L	L	G	G	L	L	L	L	L
7 M CaCl ₂	150	L	L	G	G	L	L	L	L	L
9 M CaCl ₂	170	L	L	G	G	L	L	L	L	L
1:1 CaCl ₂ + Ca(NO ₃) ₂	90	G	L	G	G	L	L	L	L	L
10:1 CaCl ₂ + Ca(NO ₃) ₂	90	G	L	G	G	—	—	—	—	—
100:1 CaCl ₂ + Ca(NO ₃) ₂	90	G	L	G	G	—	—	—	—	—
NaF	60, 90	G	L	G	G	L	L	L	L	L
NaF + NaCl	60, 90	G	L	G	G	L	L	L	L	L
HCl	60, 90	G	L	G	G	L	L	L	L	L
Oxalic Acid	30, 60, 90	G	L	G	G	L	L	L	L	L

NOTE: Test Matrix based on five tests: G indicates more than five tests performed; L indicates less than five tests performed.

Table A-7 lists thermogravimetric studies for brines that develop from deposited salts that have been performed in an environmental thermogravimetric analyzer. Although the compositions of the Table A-7 brines are not known precisely, they are very highly concentrated. The studies to date focused on salts (such as calcium chloride, magnesium chloride, and calcium nitrate) that could form aqueous solutions at very high temperatures. However, magnesium chloride is not expected to be present (BSC 2003a, Section 6.7.2.11).

Table A-7. Test Conditions for Thermogravimetric Analyzer Studies Performed on Alloy 22

Deposited Salt	Temperature (°C)	Relative Humidity (%)
CaCl ₂	150, 125, 100	20 to 22
CaCl ₂ + Ca(NO ₃) ₂	150	20 to 22
MgCl ₂	125, 115	20 to 22

Tables A-8 lists the corrosion tests performed on the drip shield material Titanium Grade 7 except as noted. The table identifies the type of test performed, the general number of tests performed, and the aqueous test environments used.

A.4.2 Evaluate Effect of Introduced Materials on Water Chemistry

Introduced materials are drift ground support materials, and at present, these are stainless and carbon steels; concrete is not in the present design. The effect of dust, which can also be considered an introduced material, on water chemistry is discussed above. The effect of drift ground support materials on the environment is also discussed in detail in the response to ENFE 2.14 (Appendix J) and documented in *Engineered Barrier System: Physical and Chemical Environment Model* (BSC 2003b, Section 6.8).

The potential impact of the corrosion of stainless steel Type 316 wire mesh and rock bolts used as drift ground support on the composition of seepage waters was evaluated. This was done by titration of a solution with dissolved iron and chromium, representative of 316 stainless steel normalized to the amount present over 1 m² of drift wall, into a typical seepage water. The mean corrosion rate used in this study of Stainless Steel Type 316 was 1.9391 μm/yr. The seepage water was a dilute near neutral water that represents about 40 percent of the calculated seepage waters (Bin 11 in Table A-3). The calculations show no impact of the corrosion of stainless steel Type 316 wire mesh and rock bolts on the seepage waters. This is expected because the corrosion products (iron and chromium hydroxides) have very low solubility in the dilute near-neutral waters. Given the solubility of the corrosion products, one might expect to see a decrease in pH, because iron- and chromium-hydroxide precipitation produces H⁺ ions in solution. However, a net change of only 0.0001 pH units was observed in the calculations. Although there was no net change in the major element chemistry represented by Bin 11 seepage water, it is likely that many trace elements in the seepage waters would decrease because they sorb to the iron hydroxide corrosion products. This latter phenomenon has not been evaluated.

Table A-8. Aqueous Test Solutions for Electrochemical and Long-Term Immersion Tests for Titanium Grade 7 Except as Noted

Test Environment	Temp. (°C)	Open Circuit Potential Short Term (≤24 hr.)	Polarization Resistance	Cyclic Polarization	Weight Loss / U-bend / Crevice	Potentiostatic
SAW	90	L	L	L		
SCW	90	L	L	L		
2.5M CaCl ₂	90	L	L	L		
5M CaCl ₂	90	G	G	G		
1M NaF	90	L	L	L		
1M NaF	30	L	L	L		
0.9M NaCl + 0.1 M NaF	90	L	L	L		
0.9M NaCl + 0.1 M NaF	30	L	L	L		
0.99M NaCl + 0.01 M NaF	90	L	L	L		
0.99M NaCl + 0.01 M NaF	30	L	L	L		
1M NaCl + 0.01M NaF	95	G	G	G		L
1M NaCl + 0.01M NaF	60	G	G	G		
1M NaCl + 0.1M NaF	95	G	G	G		L
1M NaCl + 0.1M NaF	60	G	G	G		
4M NaCl + 0.01M NaF	95	G	G	G		L
4M NaCl + 0.01M NaF	60	G	G	G		
4M NaCl + 0.1M NaF	95	G	G	G		L
4M NaCl + 0.1M NaF	60	G	G	G		L
1M NaCl	95	L	L	L		
1M NaCl	60	L	L	L		
4M NaCl	95	L	L	L		L
4M NaCl	60	L	L	L		
SAW	60, 90				G ^a	
SCW	60, 90				G ^a	
SDW	60, 90				G ^a	

NOTES: ^a Titanium Grade 16: 5 years; Titanium Grade 12: 5 years; Titanium Grade 7: 2 years.

Test matrix based on five tests: G indicates more than five tests performed; L indicates fewer than five tests performed.

A.4.3 Determine Likely Concentrations and Chemical Form of Minor Constituents in Yucca Mountain Waters

Minor constituents considered in Yucca Mountain waters include lead, mercury, and arsenic. Minor constituents, which may be present in waters that contact the engineered barrier system components, may enhance the degradation of these components. The likely presence and potential impact of these on the in-drift environmental conditions is also discussed in the response to ENFE 2.04 (Appendix C). The following discussion addresses the issues of lead content in natural waters and those phenomena that may limit the aqueous lead content.

Lead—Lead concentrations measured in groundwater in the vicinity of Yucca Mountain occur at trace levels. The median lead concentrations of 399 groundwater samples (those which had

reported lead concentration) collected within a 100,000-km² area in the southern Great Basin, which includes Yucca Mountain and the Nevada Test Site, is 9 ppb (Perfect et al. 1995). Of the 3,733 entries, only 399 have values for lead. A median of 9 ppb is obtained when only lead concentration entries greater than or equal to zero are considered. This corresponds to 256 entries. Some of the entries had negative values, if these negative values of entries are interpreted as nondetectable and are replaced with zero values, then the median of all 399 entries is 3 ppb. Two samples collected from the Obsidian Butte Brine Pond Site have lead concentrations near 3 ppm. The possible sources of lead at Yucca Mountain include trace concentrations present in the volcanic rock and foreign sources, perhaps wind-blown sediments or aerosols.

Waters with a range of chemical compositions are expected to come in contact with engineered barrier system components at Yucca Mountain. Two types of water have received the most attention based on their chemical composition (BSC 2001, Section 7.3.1.3.1). The first type is water similar in composition to water from well J-13, a water-supply well near Yucca Mountain (Harrar et al. 1990). J-13 well water was used as the basis for estimating the chemistry of drift seepage water in a recent performance assessment (CRWMS M&O 1998). Perfect et al. (1995) reported J-13 well water analyses. In one sample, 3 ppb lead was detected; in the other sample, no lead was detected.

Another assessment of the chemistry of seepage water at Yucca Mountain suggests using a pore water-type composition from rocks in the Paintbrush hydrostratigraphic unit in the unsaturated zone above the repository (Sonnenthal and Bodvarsson 1999). The Paintbrush unit is a nonfractured tuff unit directly above the repository horizon unit, the Topopah Spring Tuff. Although lead analyses of the Paintbrush pore water could not be found, it is likely that dissolved lead concentrations are similar to the trace concentrations reported in the surrounding groundwater.

The trace lead levels measured near Yucca Mountain are similar to lead concentrations measured in other natural groundwater. For example, dissolved lead is less than 1 ppb in the Gorleben aquifer in Germany (Lieser and Ament 1993). Even in groundwaters that contact lead-contaminated sediments, the levels are not high. For example, pore water measured in lead-contaminated estuarine sediments are less than 5 ppb (Carroll et al. 1999).

Dissolved lead concentrations in groundwater are controlled by lead adsorption on mineral surfaces and organic matter, as well as by precipitation of lead minerals (e.g., carbonates, sulfides, and phosphates) (Drever 1997, pp. 189 to 192; Evans et al. 1978, p. 82-I-1).

Current geochemical models (e.g., EQ3/6 V7.2b) may not adequately predict the processes that control lead solubility. Ion exchange and sorption, which may reduce lead concentration, are not included in the models. Also, aqueous complexes that may be important in controlling lead concentration (Rickard and Nriagu 1978; Ferri et al. 1987; Bilinski and Schindler 1982) are not considered in these models.

The lead uptake onto minerals at Yucca Mountain has not been experimentally determined, but based on literature studies of other waters containing minerals found at Yucca Mountain (e.g., smectite, illite, zeolites, glass, cristobalite), it is expected that sorption of lead to mineral

surfaces will be important in limiting lead concentration in groundwater at Yucca Mountain. For example, pure mineral separates suspended in groundwater show that lead is concentrated on quartz, kaolinite, calcite, and smectite (bentonite) surfaces. The greatest sorption coefficient (i.e., the ratio of lead on mineral phase to lead in solution) was measured for smectite (Freedman et al. 1994). The enhanced lead uptake is due to lead exchange for calcium in smectite interlayers (Siantar and Fripiat 1995; Nagy and Kónya, 1998). Roy et al. (1993) also report lead sorption to kaolinite and illite in complex ash–water suspensions at pH 12. In the absence of these minerals, lead remained dissolved in the solution.

Evaporative Evolution of Yucca Mountain Groundwaters and Lead Chemistry—Rosenberg et al. (2000) recently examined the evaporative evolution of both simulated J-13 well water and simulated Paintbrush pore water from the unsaturated zone in a series of subboiling laboratory experiments with and without crushed tuff present. The study did not include lead analysis but is relevant, nonetheless, in terms of expected pH and mineral precipitation.

J-13 Well Water—The J-13 well water experiments indicate loss of Ca^{2+} , Mg^{2+} , and HCO_3^- from solution as carbonates, with Mg^{2+} likely going into a slightly disordered CaCO_3 phase. Evaporation produced an alkaline $\text{Na-HCO}_3\text{-CO}_3$ brine. The pH stabilized at about 10 after an approximately 50-fold concentration. After 1,000-fold concentration, amorphous silica, aragonite, and calcite had precipitated from solution. Some clays also formed after complete evaporation.

Unsaturated Zone Pore Waters—After approximately 1,000-fold concentration, the solution lost Ca^{2+} and SO_4^{2-} , suggesting removal of these species as gypsum. Aqueous concentrations of Mg^{2+} , F^- , HCO_3^- , and $\text{SiO}_2(\text{aq})$ also decreased with evaporation, suggesting some carbonate precipitation as well. The pH stabilized at about 6. Evaporation of this water produced a $\text{Na-K-Ca-Mg-Cl-NO}_3$ brine. The minerals recovered after complete evaporation contain a magnesium-smectite.

These experiments show that minerals that precipitate during evaporation of Yucca Mountain waters produce phases known to sorb lead (Wang and Stumm 1987).

Mercury—Ambient Yucca Mountain groundwater mercury concentrations are expected to be quite low, between 10^{-2} to 10^{-3} ppb. Similar to arsenic, mercury has few solubility controls. However, the ability of mercury to concentrate in brine water will be limited because it is volatile and transfers to the atmosphere, especially at elevated temperatures anticipated in the repository environment. Although mercury does sorb to clay minerals, its role in concentrated brines will be diminished because mercury forms chloride complexes that do not sorb effectively to mineral surfaces.

Arsenic—Because dissolved arsenic has few solubility controls in oxidizing groundwater, it is likely that the trace arsenic levels in ambient Yucca Mountain groundwater (approximately 1 ppb) concentrate in repository brines as the groundwater evaporates and dissolves arsenic present in the volcanic glass. This conclusion is supported by high dissolved arsenic concentrations measured in geothermal waters and in alkaline lakes, which can contain as much as 17,000 times more dissolved arsenic (17 ppm) than the levels in Yucca Mountain groundwater. Sorption processes may limit dissolved arsenic concentrations from pH 4 to 7 in

dilute groundwater. However, arsenic sorption will not be as effective in the more concentrated brines containing high dissolved silica or phosphate that will compete for surface sorption sites. It is possible for some cement minerals to remove arsenic(V) from alkaline water above pH of 10.7. A limitation on the amount of dissolved arsenic will be the dissolution of the volcanic glass that is the source of the arsenic.

A.4.4 Characterize Yucca Mountain Waters with Respect to the Parameters That Define the Type of Brine Which Would Evolve

There are several parameters and processes that control the evolution of the environment on the waste packages and drip shields. These include the geology and geochemistry of Yucca Mountain, the environmental conditions (e.g., temperature and relative humidity) at these engineered barrier system components, the partial pressures of acid gases that influence the chemistry of the aqueous solutions, and physical separation and fractionation that can change the compositions of water. This is also discussed in the response to ENFE 2.06 (Appendix E).

The effects of temperature and relative humidity on the evolution of brine chemistry are discussed above. The effects of the geology and geochemistry are included in the modeling of environment evolution by the choice of mineral precipitates, but because of its importance in determining the solution composition, it is discussed in further detail here. Because the effect of acid gas partial pressure on environment evolution is not fully captured in the modeling of the evolution of the environment discussed above, it is discussed in detail here.

The types of brine that could develop at Yucca Mountain are a function of the geology and geochemistry of Yucca Mountain. The important parameters are those that control the solubility of calcium and magnesium, and to a lesser extent potassium. The controls on solution content of calcium and magnesium include precipitation of carbonate, hydroxide, silicate, fluoride, and sulfate species, and possibly ion exchange. Limitations on potassium solution content are also mineral precipitation and ion exchange reactions.

A major controlling factor on magnesium solubility is precipitation of magnesium silicate species (BSC 2003a). *Environment on the Surfaces of Drip Shield and Waste Package Outer Barrier* (BSC 2003a) includes both laboratory data and observations of natural systems. Very low magnesium content is consistent with the saline lakes in the Great Basin region of which Yucca Mountain is a part. (Saline lakes with high magnesium content are those in the Pacific Northwest region of the United States and British Columbia, Canada.) Magnesium solubility is also limited to some extent by precipitation as a minor component of the calcium carbonate species, calcite and aragonite.

One process theme is the precipitation of magnesium in clays or related silicates such as sepiolite. The parent groundwaters contain elevated silica compared to many other, non-Yucca Mountain groundwaters. However, more silica is readily available at elevated temperatures from the dissolution of volcanic glass and (or) cristobalite and other silicate minerals in the rock at Yucca Mountain. This will also be true of rock dust or dust blown into the repository. Sufficiency of available silica is not the only factor. The precipitation of magnesium from solution effectively adds hydrogen ions to solution that must then be largely neutralized (otherwise a low pH solution develops). Neutralization is possible by several mechanisms,

including acid gas evolution (e.g., of $\text{CO}_2(\text{g})$), ion exchange reactions with minerals (e.g., H^+ for Na^+), and generally slower “weathering” reactions. This process of magnesium removal ensures that a brine of the magnesium sulfate or magnesium chloride type will not form in the repository.

The theme of sequestration of aqueous magnesium in silicate minerals has been observed in a variety of environments. Wolery (1978) pointed this out in the context of the removal of magnesium from seawater in hydrothermal reactions with the basalt of the oceanic crust (basalt is fairly magnesium-rich to begin with, pointing to the strength of the theme). Sequestration of aqueous magnesium is also seen in hydrothermal reaction of seawater with peridotite (e.g., Janecky 1982), an even more magnesium-rich silicate rock. This theme has also been observed in a variety of calculations and experiments in other systems where silicate rock interacts with water at elevated temperature. Of immediate relevance to the repository, magnesium sequestration has been observed in both groundwater evaporation experiments at near-boiling temperatures (Rosenberg et al. 1999a; Rosenberg et al. 1999b; and Rosenberg et al. 2001) and in experimental studies of groundwater-tuff hydrothermal interaction, mostly between 90°C and 150°C (e.g., Knauss and Beiriger 1984; Knauss et al. 1985a; Knauss et al. 1985b; Knauss and Peifer 1986); and Knauss et al. 1987). Most of these studies of evaporation and tuff-groundwater interaction also include examples of modeling that is consistent with the theme of magnesium sequestration in secondary silicates. For a pure modeling study of tuff-groundwater hydrothermal interaction, see Delany (1985).

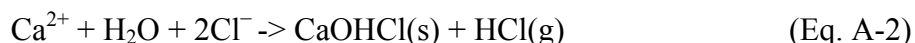
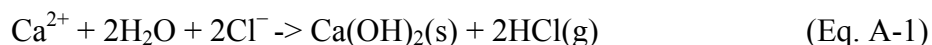
The importance of understanding the potassium content of aqueous solutions is because of its capacity to lower the deliquescence relative humidity for salt mixtures by the mixed ion effect. In term of its effect on corrosion processes, potassium acts much like sodium. Drever (1997) discusses the limitations, ion exchange, and adsorption on potassium solubility in natural systems:

When water flows through a porous medium (sediment or rock), exchange reactions take place between ions in the water and ions adsorbed on the medium. Neutral species, notably H_4SiO_4 , and even the sulfate anion may also be adsorbed on solid surfaces. The cation-exchange capacities of most media are sufficient to have a significant influence on the composition of waters flowing through them.

The major ion most affected by exchange reactions is potassium. Potassium does not form any salts, except at very high concentrations, and calculations such as those of Garrels and Mackenzie (1967) and Hardie and Eugster (1970) predict that potassium should, like sodium, simply build up in solution during evaporation. In practice, however, potassium is almost always found to be depleted relative to sodium in saline waters. Eugster and Jones (1979) showed that the removal took place only when the water was flowing underground (not in a lake, for example) and argued convincingly that the removal process for potassium was sorption on cryptocrystalline surfaces or ion exchange. If a sediment in which the exchange sites are largely divalent calcium is exposed to a relatively saline water, monovalent ions should displace the divalent calcium. In ion-exchange reactions involving clay minerals or zeolites, potassium is greatly favored on the exchange sites over sodium, so potassium is removed from solution. The calcium released in exchange for sodium probably precipitates as a carbonate within the medium.

The exchangeable cation is often initially calcium, because many regions that are now arid were much wetter during the late Pleistocene; waters were generally more dilute then, and ion exchangers in contact with these waters tended to have calcium as the major exchangeable cation. Biological uptake can also remove potassium from waters but appears to be less important than adsorption in regulating potassium concentrations in saline waters.

Acid gas volatility will also exert a control on calcium and magnesium solubility under elevated temperature conditions, although, as noted above, this is not fully implemented in the modeling of the aqueous solution evolution. The loss of the acid component (e.g., HCl) from a solution will cause a rise in the solution pH. This, in turn, will raise the pH, which will cause the precipitation of calcium and magnesium precipitates if the pH increase is sufficient. Hydroxide or carbonate base species would precipitate under these conditions. The overall reactions for loss of HCl from aqueous calcium chloride solution could be one of the following depending on solution pH and the partial pressure of carbon dioxide:



The experimental evidence for these acid gas volatilization processes and the implications for solution evolution are discussed in detail in *Environment on the Surfaces of Drip Shield and Waste Package Outer Barrier* (BSC 2003a, Section 6.7.2.14).

A.4.5 Evaluate Periodic Water Drip Evaporation

The extent of cyclic wetting and drying on aqueous solution chemistry has been evaluated by Drever (1997):

The Hardie-Eugster model is based on the assumption that the dilute water entering an arid basin undergoes continuous evaporation until it becomes a concentrated brine. In nature, however an important process is complete evaporation of a water and deposition of all the solutes in it during a dry period, followed by partial re-solution of these solutes during a wet period. The water undergoing evaporation often occurs in the pores of alluvium or near-surface groundwater rather than as an open lake. If the initial water was already saline, the deposited salts tend to form efflorescent crusts on the ground surface. If it was relatively dilute, the salts may be deposited in the ground just below the surface, or they may form in the capillary fringe above the water table where the water table is near the surface.

During the evaporation stage, all the solutes in the water are deposited as solid phases, presumably in the order predicted by the Hardie-Eugster model. During the re-solution stage very soluble minerals such as sodium salts dissolve rapidly, whereas less soluble compounds such as gypsum, calcite, and especially, silica dissolve only slowly. The end result of an evaporation-solution cycle is a water

that contains all the ions that precipitate only as highly soluble salts, but has lost some of the ions that precipitate as less soluble compounds. The chemistry of the resultant solution is controlled by the kinetics of dissolution of the precipitated phases, and not strictly by their solubility. Waters resulting from such cycles may be strongly undersaturated with respect to gypsum, amorphous silica, and sepiolite, even though the water have clearly lost calcium sulfate, silica, and magnesium relative to the input.

Therefore, the effect of wetting and drying cycles on aqueous solution chemistry is primarily the effect that it has on the less soluble species. Those that are very soluble and control the deliquescence behavior are not expected to be kinetically limited. Hence, water chemistries for the wetting and drying cycles are predictable based on thermodynamics. The range of water compositions that could contact the drip shield and waste package surfaces are also discussed in the response to ENFE 2.10 (Appendix G).

In summary, the range of environments in which the corrosion tests have been performed encompasses the range of environments that have been projected under expected repository conditions.

A.4.6 Specific Response and Basis for GEN 1.01 Comment 50

Aqueous solutions are predicted to form on the waste packages or drip shields from either dust deliquescence or seepage waters. The predicted range of water chemistry from dust deliquescence and seepage water is discussed in Section 4 of this technical basis document with detailed documentation in *Engineered Barrier System: Physical and Chemical Environment Model* (BSC 2003b, Section 6). Table A-2 summarizes the range of water chemistry in terms of brine type. As shown in the table calcium chloride type brines are predicted to occur from both seepage and dust deliquescence. However, the calcium chloride seepage waters occur during the dryout regime when seepage into the drift is not expected. The dust deliquescence calcium chloride brine is dominated by $\text{Ca}(\text{NO}_3)_2$, which is expected to inhibit localized corrosion. The majority of the aqueous solutions on the waste package and drip shield surfaces will be either sulfate or carbonate-type brines with carbonate-type brines dominating the seepage waters and sulfate-type brines dominating the dust deliquescence waters. The expected waters that contact the waste packages will be calculated as part of TSPA.

Aqueous solution formation on the waste package material, Alloy 22, is expected to form from deliquescence of dust and from seepage waters after failure of the drip shields. However, the drip shields are projected to maintain their integrity and keep seepage waters from contacting the waste packages during the regulatory period except after the occurrence of a significant seismic event. Localized corrosion of the waste packages is considered in this context in TSPA.

A model for localized corrosion of Alloy 22 has been developed. Input parameters for the model include temperature, pH, Cl^- concentration, and NO_3^- concentration. The model does predict that localized corrosion will occur for certain combinations of input parameters. This model is documented in *General Corrosion and Localized Corrosion of Waste Package Outer Barrier* (BSC 2003d, Section 6) and discussed in the technical basis document on waste package and drip shield corrosion.

A.4.7 Specific Response and Basis for GEN 1.01 Comment 113

The project has chosen a range of water chemistries as initial aqueous solution compositions for testing. This range spans the range of realistic seepage waters at Yucca Mountain. These waters are then modeled as they evolve in the repository under relevant conditions, that is, as a function of temperature, relative humidity, and partial pressure of carbon dioxide ($p\text{CO}_2$) (BSC 2003b, Section 6.14).

Seepage waters have been modeled at the drift crown. These are the waters that are projected to contact the engineered barrier system components. The calcium chloride type brine is modeled to occur with an integrated fractional occurrence of 0.22 percent. Magnesium is not expected to be a major component of this type of brine due to its precipitation as insoluble minerals (BSC 2003a, Section 6.7.2.11).

A.4.8 Specific Response and Basis for GEN 1.01 Comment 118

The DOE assessment of conditions necessary for aqueous solution formation from salts now incorporates the effects of mixed salts on the deliquescence point (or deliquescence relative humidity) and on aqueous solution composition as a function of temperature and relative humidity. This modeling is performed using the thermodynamic code EQ3/6 with a database that accounts for interactions between ionic species by using the Pitzer formulation for ionic interactions.

The deliquescence behavior of mixed salts is discussed extensively in *Environment on the Surfaces of Drip Shield and Waste Package Outer Barrier* (BSC 2003a, Section 6.7.2). The behavior is modeled using the thermodynamic code EQ3/6. The lowering of the deliquescence point of mixed salts relative to the pure salts is documented for repository-relevant salts.

Compositions of the aqueous solutions from dust deliquescence are contained in *Engineered Barrier System: Physical and Chemical Environment Model* (BSC 2003b, Section 6.14). These analyses also use the thermodynamic code EQ3/6.

A.4.9 Specific Response and Basis for GEN 1.01 Comment 122

In bulk aqueous solutions, literature and project data show that fluoride has an accelerating effect on the degradation of titanium-based alloys. However, the effect of fluoride on the drip shield has been evaluated and it has been determined that the presence of fluoride will not significantly enhance the general corrosion of drip shield material and will not limit the lifetime of titanium alloys in repository environments (BSC 2003f). Alloy 22 does not suffer localized corrosion in fluoride-only solutions, although there appears to be a synergistic effect in chloride plus fluoride aqueous solutions. For multi-ionic solutions containing fluoride, however, no localized corrosion has been observed (BSC 2003d, Section 6).

A.4.10 Specific Response and Basis for GEN 1.01 Comment 124

The effect of ferric chloride on engineered barrier system component corrosion is to raise the corrosion potential (ferric ions are oxidizing) in acidic chloride aqueous solutions. The project has evaluated the effect of oxidizing aqueous chloride solution using electrochemical techniques.

Aqueous ferric chloride solutions are not expected to be stable under relevant repository conditions, even though ferric ions could be formed by corrosion of ground support materials. Ferric ions are stable in aqueous solutions lower than pH 3 and oxidizing conditions. The low pH necessary to stabilize the ferric ions is not expected under repository conditions (BSC 2003b, Section 6.14).

A.5 REFERENCES

A.5.1 Documents Cited

Bilinski, H. and Schindler, P. 1982. "Solubility and Equilibrium Constants of Lead in Carbonate Solutions (25°C, I = 0.3 mol dm⁻³)." *Geochimica et Cosmochimica Acta*, 46, 921-928.

New York, New York: Pergamon Press. TIC: 247074.

BSC (Bechtel SAIC Company) 2001. *FY01 Supplemental Science and Performance Analyses, Volume 1: Scientific Bases and Analyses*. TDR-MGR-MD-000007 REV 00 ICN 01.

Las Vegas, Nevada: Bechtel SAIC Company. ACC: MOL.20010801.0404; MOL.20010712.0062; MOL.20010815.0001.

BSC 2003a. *Environment on the Surfaces of Drip Shield and Waste Package Outer Barrier*.

ANL-EBS-MD-000001 REV 01D. Las Vegas, Nevada: Bechtel SAIC Company.

ACC: MOL.20030825.0151.

BSC 2003b. *Engineered Barrier System: Physical and Chemical Environment Model*.

ANL-EBS-MD-000033 REV 02C. Las Vegas, Nevada: Bechtel SAIC Company.

ACC: MOL.20031029.0034.

BSC 2003c. *In-Drift Precipitates/Salts Model*. ANL-EBS-MD-000045 REV 01. Las Vegas,

Nevada: Bechtel SAIC Company. ACC: DOC.20031028.0003.

BSC 2003d. *General Corrosion and Localized Corrosion of Waste Package Outer Barrier*.

ANL-EBS-MD-000003 REV 01. Las Vegas, Nevada: Bechtel SAIC Company.

ACC: DOC.20030916.0010.

BSC 2003e. *Drift-Scale Coupled Processes (DST and THC Seepage) Models*. MDL-NBS-HS-

000001 REV 02. Las Vegas, Nevada: Bechtel SAIC Company. ACC: DOC.20030804.0004.

BSC 2003f. *General Corrosion and Localized Corrosion of the Drip Shield*. ANL-EBS-MD-

000004 REV 01. Las Vegas, Nevada: Bechtel SAIC Company. ACC: DOC.20030626.0001.

Carroll, S.; Esser, B.; Randall, S.; O'Day, P.; Bono, A.; and Luther, G.W., III 1999.

Geochemical Characterization of Seaplane Lagoon Sediments, Alameda Naval Air Station.

UCRL-ID-135193. Livermore, California: Lawrence Livermore National Laboratory.

TIC: 249746.

CRWMS M&O (Civilian Radioactive Waste Management System Management and Operating

Contractor) 1998. *Total System Performance Assessment - Viability Assessment Base Case*.

B00000000-01717-0210-00011 REV 01. Las Vegas, Nevada: CRWMS M&O.

ACC: MOL.19981202.0279.

- Delany, J.M. 1985. *Reaction of Topopah Spring Tuff with J-13 Water: A Geochemical Modeling Approach Using the EQ3/6 Reaction Path Code*. UCRL-53631. Livermore, California: Lawrence Livermore National Laboratory. ACC: HQS.19880517.2419.
- Drever, J.I. 1997. "Evaporation and Saline Waters." Chapter 15 of *The Geochemistry of Natural Waters: Surface and Groundwater Environments*. 3rd Edition. Upper Saddle River, New Jersey: Prentice Hall. TIC: 246732.
- Evans, H.T.; Manheim, F.T., Jr.; and Landergren, S. 1978. "Molybdenum." Section 42 of *Handbook of Geochemistry: Elements Kr(36) to Ba(56)*. Wedepohl, K.H., ed. Volume II/4. New York, New York: Springer-Verlag. TIC: 243504.
- Ferri, D.; Grenthe, I.; Hietanen, S.; and Salvatore, F. 1987. "Studies on Metal Carbonate Equilibria.18. Lead(II) Carbonate Complexes in Alkaline Solutions." *Acta Chemica Scandinavica. Series A: Physical and Inorganic Chemistry, A41*, 349-354. Copenhagen, Denmark: Munksgaard. TIC: 249841.
- Freedman, Y.E.; Magaritz, M.; Long, G.L.; and Ronen, D. 1994. "Interaction of Metals with Mineral Surfaces in a Natural Groundwater Environment." *Chemical Geology, 116*, (1-2), 111-121. Amsterdam, The Netherlands: Elsevier. TIC: 249834.
- Hardie, L.A. and Eugster, H.P. 1970. *The Evolution of Closed-Basin Brines*. Mineralogical Society of America Special Paper 3. Pages 273-290. Washington, D.C.: Mineralogical Society of America. TIC: 254408.
- Harrar, J.E.; Carley, J.F.; Isherwood, W.F.; and Raber, E. 1990. *Report of the Committee to Review the Use of J-13 Well Water in Nevada Nuclear Waste Storage Investigations*. UCID-21867. Livermore, California: Lawrence Livermore National Laboratory. ACC: NNA.19910131.0274.
- Janecky, D.R. 1982. *Serpentinization of Peridotite within the Oceanic Crust: Experimental and Theoretical Investigations of Seawater-Peridotite Interaction at 200°C and 300°C, 500 Bars*. Ph.D. dissertation. Minneapolis, Minnesota: University of Minnesota. TIC: 246544.
- Knauss, K.G. and Beiriger, W.B. 1984. *Report on Static Hydrothermal Alteration Studies of Topopah Spring Tuff Wafers in J-13 Water at 150°C*. UCRL-53576. Livermore, California: Lawrence Livermore National Laboratory. ACC: HQS.19880517.2007.
- Knauss, K.G.; Beiriger, W.J.; and Peifer, D.W. 1987. *Hydrothermal Interaction of Solid Wafers of Topopah Spring Tuff with J-13 Water at 90 and 150°C Using Dickson-Type, Gold-Bag Rocking Autoclaves: Long-Term Experiments*. UCRL-53722. Livermore, California: Lawrence Livermore National Laboratory. ACC: NNA.19870713.0081.
- Knauss, K.G.; Beiriger, W.J.; and Peifer, D.W. 1985a. *Hydrothermal Interaction of Crushed Topopah Spring Tuff and J-13 Water at 90, 150, and 250°C Using Dickson-Type, Gold-Bag Rocking Autoclaves*. UCRL-53630. Livermore, California: Lawrence Livermore National Laboratory. ACC: NNA.19931005.0010.

Knauss, K.G.; Delany, J.M.; Beiriger, W.J.; and Peifer, D.W. 1985b. "Hydrothermal Interaction of Topopah Spring Tuff with J-13 Water as a Function of Temperature." *Scientific Basis for Nuclear Waste Management VIII, Symposium held November 26-29, 1984, Boston, Massachusetts*. Jantzen, C.M.; Stone, J.A.; and Ewing, R.C., eds. 44, 539-546. Pittsburgh, Pennsylvania: Materials Research Society. TIC: 203665.

Knauss, K.G. and Peifer, D.W. 1986. *Reaction of Vitric Topopah Spring Tuff and J-13 Ground Water Under Hydrothermal Conditions Using Dickson-Type, Gold-Bag Rocking Autoclaves*. UCRL-53795. Livermore, California: Lawrence Livermore National Laboratory. ACC: NNA.19891102.0117.

Lieser, K.H. and Ament, A. 1993. "Radiochemical Investigation of the Partition and Sorption of Lead in Groundwater/Sediment Systems." *Radiochimica Acta*, 60, (2/3), 153-158. München, Germany: R. Oldenbourg Verlag. TIC: 249835.

Nagy, N.M. and Kónya, J. 1998. "Ion-Exchange Processes of Lead and Cobalt Ions on the Surface of Calcium-Montmorillonite in the Presence of Complex-Forming Agents, I. The Effect of EDTA on the Sorption of Lead and Cobalt Ions on Calcium-Montmorillonite." *Colloids and Surfaces A: Physicochemical and Engineering Aspects*, 137, (1-3), 231-242. New York, New York: Elsevier. TIC: 249837.

NRC (U.S. Nuclear Regulatory Commission) 2002. *Integrated Issue Resolution Status Report*. NUREG-1762. Washington, D.C.: U.S. Nuclear Regulatory Commission, Office of Nuclear Material Safety and Safeguards. TIC: 253064.

Perfect, D.L.; Faunt, C.C.; Steinkampf, W.C.; and Turner, A.K. 1995. *Hydrochemical Data Base for the Death Valley Region, California and Nevada*. Open-File Report 94-305. Denver, Colorado: U.S. Geological Survey. ACC: MOL.19940718.0001.

Reamer, C.W. and Gil, A.V. 2001a. Summary Highlights of NRC/DOE Technical Exchange and Management Meeting on Total System Performance Assessment and Integration. Meeting held August 6-10, 2001. Las Vegas, Nevada. Washington, D.C.: U.S. Nuclear Regulatory Commission. ACC: MOL.20010921.0121.

Reamer, C.W. and Gil, A.V. 2001b. Summary Highlights of NRC/DOE Technical Exchange and Management Meeting of Range on Thermal Operating Temperatures, September 18-19, 2001. Washington, D.C.: U.S. Nuclear Regulatory Commission. ACC: MOL.20020107.0162.

Rickard, D.T. and Nriagu, J.O. 1978. "Aqueous Environmental Chemistry of Lead." Chapter 8 of *The Biogeochemistry of Lead in the Environment*. Nriagu, J.O., ed. New York, New York: Elsevier. TIC: 248543.

Rosenberg, N.D.; Knauss, K.G.; and Dibley, M.J. 1999a. *Evaporation of J13 Water: Laboratory Experiments and Geochemical Modeling*. UCRL-ID-134852. Livermore, California: Lawrence Livermore National Laboratory. TIC: 246322.

Rosenberg, N.D.; Knauss, K.G.; and Dibley, M.J. 1999b. *Evaporation of Topopah Spring Tuff Pore Water*. UCRL-ID-135765. Livermore, California: Lawrence Livermore National Laboratory. TIC: 246231.

Rosenberg, N.D.; Gdowski, G.E.; and Knauss, K.G. 2000. *Evaporative Chemical Evolution of Natural Waters at Yucca Mountain, Nevada*. UCRL-JC-137818. Livermore, California: Lawrence Livermore National Laboratory. ACC: MOL.20000427.0039.

Rosenberg, N.D.; Gdowski, G.E.; and Knauss, K.G. 2001. "Evaporative Chemical Evolution of Natural Waters at Yucca Mountain, Nevada." *Applied Geochemistry*, 16, (9-10), 1231-1240. New York, New York: Pergamon. TIC: 249879.

Roy, W.R.; Krapac, I.G.; and Steele, J.D. 1993. "Soil Processes and Chemical Transport, Sorption of Cadmium and Lead by Clays from Municipal Incinerator Ash-Water Suspensions." *Journal of Environmental Quality*, 22, 537-543. Madison, Wisconsin: American Society of Agronomy. TIC: 249842.

Schlueter, J. 2000. "U.S. Nuclear Regulatory Commission/U.S. Department of Energy Technical Exchange and Management Meeting on Container Life and Source Term (September 12-13, 2000)." Letter from J. Schlueter (NRC) to S. Brocoum (DOE/YMSCO), October 4, 2000, with enclosure. ACC: MOL.20010731.0161.

Siantar, D.P. and Fripiat, J.J. 1995. "Lead Retention and Complexation in a Magnesium Smectite (Hectorite)." *Journal of Colloid and Interface Science*, 169, (2), 400-407. Orlando, Florida: Academic Press. TIC: 249847.

Sonnenthal, E.L. and Bodvarsson, G.S. 1999. "Constraints on the Hydrology of the Unsaturated Zone at Yucca Mountain, NV from Three-Dimensional Models of Chloride and Strontium Geochemistry." *Journal of Contaminant Hydrology*, 38, (1-3), 107-156. New York, New York: Elsevier. TIC: 244160.

Wang, Z-J. and Stumm, W. 1987. "Heavy Metal Complexation by Surfaces and Humic Acids: A Brief Discourse on Assessment by Acidimetric Titration." *Netherlands Journal of Agricultural Science*, 35, 231-240. Wageningen, The Netherlands: Koninklijk Genootschap voor Landbouwwetenschap. TIC: 249855.

Wolery, T.J. 1978. Some Chemical Aspects of Hydrothermal Processes at Mid-Oceanic Ridges - A Theoretical Study. I. Basalt-Sea Water Reaction and Chemical Cycling Between the Oceanic Crust and the Oceans. II. Calculation of Chemical Equilibrium Between Aqueous Solutions and Minerals. Ph.D. dissertation. Evanston, Illinois: Northwestern University. TIC: 219640.

Wolery, T.J. 2003. "Modification of Dust Salt Analysis." Letter from T. Wolery to D. Salmon, October 28, 2003. ACC: MOL.20031029.0001.

A.5.2 Data, Listed by Data Tracking Number

LL000320405924.146. Target Compositions of Aqueous Solutions Used for Corrosion Testing. Submittal date: 03/22/2000.

APPENDIX B

**UNCERTAINTY AND VARIABILITY
IN THE NEAR-FIELD GEOCHEMICAL ENVIRONMENT
(RESPONSE TO ENFE 1.05, TSPA 3.09,
AND GEN 1.01 (COMMENTS 81, 93, 98, 104, AND 110))**

Note Regarding the Status of Supporting Technical Information

This document was prepared using the most current information available at the time of its development. This Technical Basis Document and its appendices providing Key Technical Issue Agreement responses that were prepared using preliminary or draft information reflect the status of the Yucca Mountain Project's scientific and design bases at the time of submittal. In some cases this involved the use of draft Analysis and Model Reports (AMRs) and other draft references whose contents may change with time. Information that evolves through subsequent revisions of the AMRs and other references will be reflected in the License Application (LA) as the approved analyses of record at the time of LA submittal. Consequently, the Project will not routinely update either this Technical Basis Document or its Key Technical Issue Agreement appendices to reflect changes in the supporting references prior to submittal of the LA.

APPENDIX B

UNCERTAINTY AND VARIABILITY IN THE NEAR-FIELD GEOCHEMICAL ENVIRONMENT (RESPONSE TO ENFE 1.05, TSPAI 3.09, AND GEN 1.01 (COMMENTS 81, 93, 98, 104, AND 110))

This appendix provides a response for Key Technical Issue (KTI) agreements Evolution of the Near-Field Environment (ENFE) 1.05 and Total System Performance Assessment and Integration (TSPAI) 3.09 and general agreement (GEN) 1.01, Comments 81, 93, 98, 104, and 110. These KTI agreements relate to the representation of uncertainty and variability in water and gas chemistry in the near-field environment and the treatment of the uncertainty in the thermal-hydrologic-chemical (THC) model.

B.1 DESCRIPTION OF KEY TECHNICAL ISSUE AGREEMENTS

B.1.1 ENFE 1.05, TSPAI 3.09, and GEN 101 (Comments 81, 93, 98, 104, and 110)

Agreement ENFE 1.05 was reached during the U.S. Nuclear Regulatory Commission (NRC)/U.S. Department of Energy (DOE) Technical Exchange and Management Meeting on Evolution of the Near-Field Environment held on January 9 to 11, 2001, in Pleasanton, California (Reamer 2001a), in the area of ENFE Subissue 1, Effects of Coupled Thermal-Hydrologic-Chemical Processes on Seepage and Flow. ENFE 1.05 stems from the NRC concern about uncertainties in geochemical submodels and data used to predict quantity and chemistry of water contacting waste packages and waste forms have not been adequately evaluated and documented (NRC 2002, p. 3.3.3-18).

Agreement TSPAI 3.09 was reached during the NRC/DOE Technical Exchange and Management Meeting on Total System Performance Assessment and Integration (TSPAI) held August 6 to 10, 2001, in Las Vegas, Nevada (Reamer 2001b), in the area of TSPAI Subissue 3, Model Abstraction within the total system performance assessment (TSPA) methodology. TSPAI 3.09 relates to DOE providing more information about the representation of uncertainty and variability in water and gas chemistry entering the drift in the near-field environment abstractions in the total system performance assessment (TSPA). During the August 2001 meeting, which included a discussion of the 14 specific integrated subissues (Reamer 2001b, pp. 6 to 10), integrated subissue ENG3 was related to the Quantity and Chemistry of Water Contacting Waste Packages and Waste Forms. The NRC concern was that near-field geochemical variables in TSPA for the site recommendation (CRWMS M&O 2000a, pp. 183 to 184) were abstracted to represent constant variables (see BSC 2001, p. MA-26). The NRC indicated that more information and a technical basis would be needed for the simplifications used in the near-field environment abstraction process. The DOE initially responded that the abstraction, documented in *Abstraction of Drift-Scale Coupled Processes* (CRWMS M&O 2000b), would be updated with appropriate values selected in the process model in a yet-to-be-determined document.

Agreement GEN 1.01 Comments 81, 93, 98, 104, and 110 were reached during NRC/DOE Technical Exchange and Management Meeting on Range of Thermal Operating Temperatures,

held September 18 to 19, 2001. At that meeting, the NRC provided additional comments (GEN 1.01, Comments 81, 93, 98, 104, and 110) relating to ENFE 1.05, and the DOE provided an initial response to those comments (Reamer and Gil 2001).

There has been no correspondence with the NRC pertaining to these KTI agreements. The only correspondence has been relating to the submittal of Revision 1 of *Drift-Scale Coupled Processes (DST and THC Seepage) Models* (CRWMS M&O 2001) and the expectation for the delivery of Revision 2 of that report (BSC 2003a; Schlueter 2002).

Wording of these agreements is as follows:

ENFE 1.05

Address the various sources of uncertainty (e.g., model implementation, conceptual model, and data uncertainty (hydrologic, thermal, and geochemical)) in the THC model. The DOE will evaluate the various sources of uncertainty in the THC process model, including details as to how the propagation of various sources of uncertainty are calculated in a systematic uncertainty analysis. The DOE will document that uncertainty evaluation in the Drift-Scale Coupled Processes (DST and THC Seepage) Models AMR (MDL-NBS-HS-000001) Rev 02 (or in another future document), expected to be available in FY 02.

TSPAI 3.09

Provide the documentation that presents the representation of uncertainty and variability in the near-field environment abstractions in the TSPA (ENG3.1.4). DOE will present the representation of uncertainty and variability in water and gas chemistry entering the drift in the near-field environment abstractions for the TSPA. This will be documented in the Abstraction of Drift-Scale Coupled Processes (ANL-NBS-HS-000029) or other document expected to be available in FY 2003.

GEN 1.01 (Comment 81)¹

More comments on the abstraction of uncertainty:

Page 3-57: It is unclear how the mountain-scale THC model can address uncertainties in the drift-scale THC seepage models. If the mountain-scale models predict bulk changes to some things, like large-scale gas convection or lateral flow, this would change the boundary conditions to the THC seepage models. If the THC seepage models are not run with the altered boundary conditions, it is unclear how they would evaluate the impact.

¹ The specific page number and section number references in the GEN 1.01 comments are from *FY 01 Supplemental Science and Performance Analyses, Volume 1: Scientific Bases and Analyses* (BSC 2001).

Page 3-66. The ranges in water and gas compositions are wider than those predicted by the drift-scale THC models at a given time as a direct result of edge effects.

Page 3-70: The argument that thermal-hydrologic-mechanical processes result in a change to permeability fields that are within the original uncertainty distribution, and are therefore unimportant needs quantification. The process would likely result in a shifting of the mean or median of the distribution and changes to its shape. Having a broad uncertainty distribution may not encompass this effect.

DOE Initial Response to GEN 1.01 (Comment 81)

KTI agreement ENFE 1.05 will address these issues.

GEN 1.01 (Comment 93)

Page 3F-43: Chloride reaches 100,000 mg/L for an extent of 200 m. Wouldn't sorption be potentially a lot different here, compared to ambient chemistry? What about carrier plume effects?

DOE Initial Response to GEN 1.01 (Comment 93)

DOE will address this issue consistent with KTI agreement ENFE 1.05.

GEN 1.01 (Comment 98)

Page 4F-34: It is not obvious that the results shown on this page demonstrate good predictability.

DOE Initial Response to GEN 1.01 (Comment 98)

DOE understands that this NRC concern is related to the seemingly discrepancy between the modeled and measured concentrations for borehole 60-3. This may be a visual artifact resulting from the lack of water samples during the rapid dry-out period as discussed in the response to Comment 49. This issue is addressed in KTI agreement ENFE 1.5.

GEN 1.01 (Comment 104)

The DOE has not adequately addressed the possibility that edge effects predicted by the 3-D mountain scale thermal-hydrologic model (Section 3.3.6) could influence results from the coupled THC models (Section 4.3.6).

DOE Initial Response to GEN 1.01 (Comment 104)

Duplicate with 81, refer to Comment 81 response.

GEN 1.01 (Comment 110)

Page 6T-1

2: Capillary pressure effect on chemical potentials of reacting species. It is unclear how this is taken into account because calibration of thermodynamic data result in reproduction of ambient water compositions. The ambient pore waters are at high saturations which result in relatively low capillary forces. When the rock dries out, the capillary forces may become extremely large. Therefore, it would appear that a calibrated model for a given state of the system is being argued to address an uncertainty for which the calibrated model is likely not valid.

DOE Initial Response to GEN 1.01 (Comment 110)

The effect of capillary pressure would be larger in the rock matrix upon near complete dryout than under ambient conditions. However, most of the fluid transport takes place in fractures where the capillarity is minimal. In addition, the potential for water-rock interactions and fluid movement is larger in zones of large liquid saturations (reflux zone) than in nearly dried-out areas (thus, under liquid saturation/capillary pressure conditions closer to those in the ambient system than in the nearly-dry system).

This uncertainty is not addressed for the case of high capillary pressures under nearly dry conditions in the rock matrix. In this case, this uncertainty may not have a significant impact on predicted seepage water compositions given the low mobility of waters at small residual saturation in the rock matrix. Reasonable model validation against field and experimental data (Section 6.3.1.4.5) would seem to indicate that this capillary effect does not need to be taken into account.

This aspect of model uncertainty will be addressed as part of KTI agreement ENFE 1.05.

B.1.2 Related Key Technical Issue Agreements

Other KTI agreements that are related to those addressed in this appendix are ENFE 2.05 (addressed in Appendix D) and ENFE 2.17 (addressed in Appendix K). ENFE 2.05 pertains to data and model uncertainties primarily related to downstream models, which use the Drift Scale Test (DST) and THC seepage model results as input. ENFE 2.17 pertains to the description of the data used to calibrate models and data to support model predictions, and the assessment of data uncertainty used in the DST and THC seepage model as well as the models using the DST and THC seepage model results as inputs.

Agreement TSPA 2.02 J-21 is also related to those addressed in this appendix. TSPA 2.02 J-21 questions the basis for excluding gas pressure effects on the basis of low probability and low consequence. The NRC noted that the buildup of water vapor pressure within rock matrix blocks due to the heat from the waste packages was not considered. The DOE agreed to improve the technical basis for the screening argument in response to KTI agreements ENFE 1.05, ENFE 1.07, and ENFE 2.16. Agreement ENFE 2.16 is complete, and completion of ENFE 1.07 will complete the response to TSPA 2.02 J-21.

B.2 RELEVANCE TO REPOSITORY PERFORMANCE

For ENFE 1.05, the adequate quantification of uncertainty relative to the development of the seepage water chemistries and constituents that can be present in the in-drift environment is important so that the engineered barrier performance can be adequately represented at the process model level. The agreement TSPA 3.09 is relevant to repository performance since the abstraction of drift-scale coupled processes (i.e., seepage quantity and chemistry) is directly used in the TSPA, and therefore the uncertainty and variability in the abstraction of the seepage chemistry entering the drift must be represented.

B.3 RESPONSE

The information in this report is responsive to agreements ENFE 1.05, TSPA 3.09, and to GEN 1.01 (Comments 81, 93, 98, 104, and 110) made between the DOE and NRC. The report contains the information that the DOE considers necessary for NRC review for closure of these agreements.

B.3.1 Response to ENFE 1.05 and TSPA 3.09

Drift-Scale Coupled Processes (DST and THC Seepage) Models (BSC 2003a) addresses both qualitatively and quantitatively uncertainties in conceptual models, model implementation, and various input data related to geochemical, hydrologic, and thermal properties. For license application, the abstraction of near-field geochemical variables is also included in *Drift-Scale Coupled Processes (DST and THC Seepage) Models* (BSC 2003a). This document discusses the representation of uncertainty and variability in water and gas chemistry entering the drift in the near-field environment. The uncertainty analyses performed cover uncertainty owing to natural variability in input water and gas compositions, as well as ranges in key parameter values. The approach to evaluating uncertainty was to perform a number of simulations to characterize the propagation of natural variability and uncertainty on the THC seepage model predictions. This approach was chosen because it captures the range in potential seepage water and gas chemistry by systematically covering the ranges in the most important parameters. Results of modeling and analyses obtained in *Drift-Scale Coupled Processes (DST and THC Seepage) Models* (BSC 2003a) therefore provide the basis for addressing ENFE 1.05 and TSPA 3.09.

Specifically, uncertainty and variability in the near-field geochemical environment were addressed by evaluating results of THC simulations over an expected range of input conditions. The resulting spread of predicted concentrations of aqueous species and CO₂ gas is related to the natural variability of input water compositions, the model conceptualizations (vapor pressure model, drift location, stratigraphic columns, open versus closed drift wall), and the ranges of input parameters other than water composition (infiltration rates and CO₂ diffusion coefficients). Simulation of coupled THC processes is computation-intensive, which renders it impractical to apply Monte-Carlo-type uncertainty analyses. As a result, selected sensitivity analyses were performed to evaluate the impact of the following factors on the near-field geochemical environment:

- Uncertainty and variability resulting from initial input water chemistry
- CO₂-soil boundary conditions determined from ambient geochemical measurements

- Vapor-pressure lowering
- Spatial variability of model output
- Uncertainty and variability of the model with respect to percolation flux, as affected by climate change and variability in surface infiltration rates
- The methods by which this identified uncertainty and variability are captured in the model.

The following paragraphs provide the response addressing each of these issues, with detailed technical basis described in sections parenthesized.

Uncertainty and Variability of Initial Water Chemistry (Section B.4.1.1)—Five alternate water compositions are used in *Drift-Scale Coupled Processes (DST and THC Seepage) Models* (BSC 2003a, Section 6.2.2.1) simulations, approximately covering the compositional variability of pore waters in repository host units. Uncertainty is assessed by comparing predictions of ambient water compositions with measured ambient pore-water compositions and pore-gas CO₂ concentrations. Input water compositions affect predicted water compositions around the drift, likely more so through infiltration/transport than through reaction. Simulations in *Drift-Scale Coupled Processes (DST and THC Seepage) Models* (BSC 2003a) indicate that the spread in predicted concentrations introduced by using these water compositions is in the range of one order of magnitude, and is generally larger than the spread introduced by other considered ranges of input parameters (infiltration rates, CO₂ diffusivity) or model conceptualization (with or without vapor-pressure lowering).

CO₂ Soil Boundary Conditions Determined from Ambient Geochemical Measurements (Section B.4.1.2)—The CO₂ concentration at the top model boundary was set to a constant 3,100 ppmv ($p\text{CO}_2 = 10^{-2.5}$) (with the pH and bicarbonate in all infiltration water adjusted to reflect this partial pressure) to reflect a value consistent with the range of higher concentrations measured in shallow geologic units in borehole UZ-1 (Yang et al. 1996, Table 8; BSC 2003a, Section 6.2.2.1). These higher CO₂ concentrations are most likely the result of biological activity near the ground surface.

Vapor-Pressure Lowering (Section B.4.1.3)—The effect of vapor-pressure lowering resulting from capillary pressure is evaluated by running simulations with and without vapor-pressure lowering (BSC 2003a, Section 6.8.5.2). No large effect on computed gas and water chemistries was observed; however, a large effect on the predicted time of rewetting of fractures and matrix at the drift wall was observed with a much shorter dryout period occurring with vapor-pressure lowering.

Spatial Variability of Model Output (Section B.4.1.4)—Spatial variability of model output was evaluated by comparing simulations for two stratigraphic units (Ttptmn and Ttptll) and comparing the water chemistry at grid blocks meeting certain criteria (e.g., highest saturation above the drift within 25 m of the drift centerline) from a single stratigraphic unit. Similar trends in water and gas compositions were predicted for modeled cases with heat loading in the Ttptmn and in the Ttptll geologic units. Fluorite dissolution enhanced fluoride concentrations in the

Tptpll unit (BSC 2003a, Section 6.7.5.2). However, the spread in predicted water compositions around the modeled drift (for a given stratigraphic unit) is generally much larger than differences related to the drift location (i.e., Tptpmn versus Tptpll).

The predicted composition of fracture waters in the six most saturated model elements within an arc of 45° from the drift crown and within 25 meters of the drift centerline over time are presented in *Drift-Scale Coupled Processes (DST and THC Seepage) Models* (BSC 2003a, Section 6.8.5.3.2). These simulation results illustrate the variability in the computed geochemical response, indicating that the predicted overall trend is robust. The calculated variability is generally much less than an order of magnitude and is usually smaller than that caused by the natural variability in the input water composition.

Uncertainty and Variability of the Model with Respect to Percolation Flux, as Affected by Climate Change and Variability in Surface Infiltration Rates (Section B.4.1.5)—Alternative infiltration rate scenarios were used to bracket potential infiltration fluxes (BSC 2003a, Section 6.8-2). The mean infiltration case consists of a stepwise increase of 6 mm/yr for 0 to 600 years (present day), 16 mm/yr from 600 to 2,000 years (monsoon), and 25 mm/yr for 2,000 to 100,000 years (glacial transition). Two other constant infiltration rates are used; the mean low (6 mm/yr) and the mean high (25 mm/yr). Between infiltration rates of 6 and 25 mm/y, there is a small effect on predicted concentrations at the drift wall. However, this effect is less than that of differing water chemistry. The effect would be greater under lower rates of infiltration (when reaction effects start to dominate transport), but such conditions would be less likely to cause in-drift seepage. At high-infiltration rates, which are most conducive to in-drift seepage, water compositions are more a function of transport than of reaction with host rock minerals, such that the uncertainty regarding the composition of the infiltration water, rather than the rate of mineral dissolution/precipitation, becomes more important.

Documentation of the Method Uncertainty is Captured in the Model (Section B.4.1.6)—The methods by which the identified uncertainty and variability are captured in the model are described in *Drift-Scale Coupled Processes (DST and THC Seepage) Models* (BSC 2003a, Section 6.9). The model sensitivity to key input parameters was evaluated by performing a variety of simulations with the model with a reasonably expected range of input conditions (infiltration rates, initial water chemistry, CO₂ diffusion rates) and model conceptualizations (with and without vapor-pressure lowering, drift location, stratigraphic columns, open versus closed drift wall). Furthermore, confidence in model results was obtained by comparing model results against data from the DST and laboratory experiments and improving the model conceptualization and mathematical formulation as necessary to yield a reasonably good agreement between calculated and measured data. Additional treatment of uncertainty and variability in the THC modeling can be found in *Drift-Scale Coupled Processes (DST and THC Seepage) Models* (BSC 2003a, Section 6.9).

B.3.2 Response to GEN 1.01 Comments 81, 93, 98, 104, and 110

Responses to these GEN 1.01 NRC comments are specifically addressed in Sections B.4.2 through B.4.5.

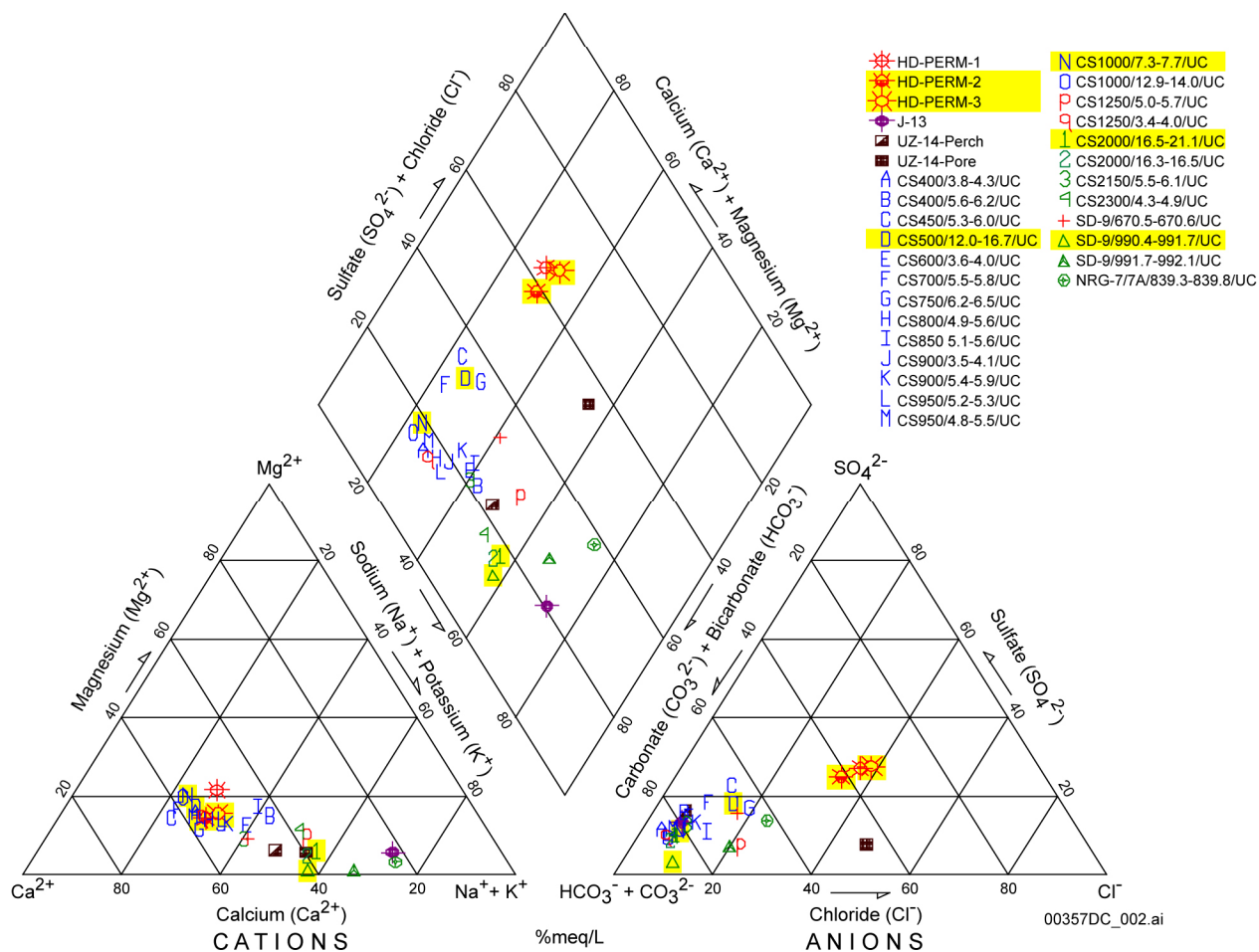
B.4 BASIS FOR THE RESPONSE

B.4.1 Basis for the Response to ENFE 1.05 and TSPA I 3.09

B.4.1.1 Uncertainty and Variability Resulting from Initial Water Chemistry

The initial water and pore gas chemistry in *Drift-Scale Coupled Processes (DST and THC Seepage) Models* (BSC 2003a, Section 6.2.2.1) is determined from the composition of actual pore waters from unsaturated regions within or above the repository units. The initial water composition input into the model could be chosen from either the pore-water chemistry in the unsaturated zone at or above the repository horizon or from the perched water or saturated zone. The perched waters are generally much more dilute than unsaturated zone pore waters. Chlorine, oxygen, deuterium, hydrogen, and carbon isotopic compositions ($^{36}\text{Cl}/\text{Cl}$, $^{18}\text{O}/^{16}\text{O}$, D/H, ^{14}C) and Cl^- concentrations suggest that the perched waters have a large proportion of late Pleistocene/early Holocene water (Levy et al. 1997, p. 906; Sonnenthal and Bodvarsson 1999, pp. 107 to 108). The saturated zone water is also more dilute than pore waters, and neither saturated nor perched water reflect calculated CO_2 partial pressures consistent with CO_2 concentrations in gas measured in the unsaturated zone in repository units. The saturated zone and perched-water compositions are therefore deemed poor candidates as initial input water compositions for the THC seepage model.

Analyses of three water samples that were ultracentrifuged from core samples collected from the Tptpmn geologic unit in Alcove 5 near the DST (HD-PERM-1, HD-PERM-2, and HD-PERM-3) from the same suite of core and yielded very similar compositions. A series of pore-water samples from repository host units have also been analyzed. These samples were ultracentrifuged from core collected in the Enhanced Characterization of the Repository Block (ECRB) Cross-Drift and in boreholes SD-9 and NRG-7/7A. The compositions of these waters are shown on a Piper diagram in Figure B-1 (BSC 2003a, Figure 6.2-4), together with the composition of HD-PERM samples, of perched water and pore water at similar depths (base of Tptpln) in borehole UZ-14, and of groundwater from well J-13. This figure also shows the hydrogeologic units from which the water samples were extracted. It is evident from Figure B-1 that the span of potential initial water compositions to use in the THC seepage model is wide, with HD-PERM samples at one end (calcium-sulfate-chloride type) and groundwater from well J-13 at the other end (sodium-bicarbonate type). This figure also shows a tendency for samples from deeper hydrogeologic units to exhibit higher Na^+ (plus K^+) concentrations relative to Ca^{2+} (plus Mg^{2+}) concentrations, and a higher proportion of total aqueous carbonate (relative to Cl^- and SO_4^{2-}) compared to shallower waters.



Source: BSC 2003a, Figure 6.2-4.

NOTE: Samples labeled HD-PERM are pore waters from the Tptpmn unit in Alcove 5 of the Exploratory Studies Facility. Sample IDs starting with CS represent pore waters from the ECRB Cross-Drift and are listed in order of increasing distance (ft) into the drift (down stratigraphy), with labels reflecting lithostratigraphic units as follows: Ttpul (capitals A-O), Tptpmn (lower case p-q), and Ttppl (numbers 1 to 4). Sample IDs starting with SD-9 and NRG-7 represent pore waters from boreholes with the same names and show the sampling interval in feet from ground surface. The first SD-9 sample at 670 ft is from the base of the Ttpul, and the others are from the Ttppl. The NRG-7 sample is from the Tptpmn. Highlighted samples were chosen for this study (see text).

Figure B-1. Piper Plot of Water Compositions (meq/L) from Repository Units

The differences in the proportions (not absolute values) of cations and anions in analyzed waters have an important bearing on the types of residual brines that could develop upon evaporation and boiling due to thermal loading (BSC 2003b). Should these waters seep onto the surface of a hot waste package, knowledge of their end-brine composition is important to assess the likelihood and intensity of waste package corrosion (BSC 2003c). Therefore, the span of selected input water compositions should take into account factors that influence the end-brine composition of these waters. One important factor is whether calcium- and magnesium-chloride brines could develop instead of sodium-chloride brines. Calcium-chloride brines are stable at higher temperatures (i.e., exist at a lower relative humidity, more hygroscopic) than sodium-chloride brines. Such brines are more likely to form if the total calcium concentration

(in meq/L) exceeds the total aqueous carbonate concentration (in meq/L) in the initial water (calcite precipitation chemical divide; e.g., Drever 1997). Waters with such compositions would have a tendency to plot in the upper half of the diamond-shaped area in Figure B-1, although other waters may also plot in this area if their magnesium concentrations were high relative to calcium. Other chemical divides after calcite precipitation (e.g., Drever 1997, p. 331; see also Rosenberg et al. 2001, p. 1,238) could result in the development of brines that are less hygroscopic than calcium or magnesium chloride, even though the calcium content of the original waters (in equivalents) exceeds their total carbonate content. Less hygroscopic brines are more likely to develop if the NO_3^- and SO_4^{2-} concentration in the original solution were elevated relative to Cl^- (BSC 2003b). No simple *a priori* criteria have been developed to determine with certainty the end-brine composition of a given water. However, factors such as composition plotting in the upper half of the diamond-shape area of Figure B-1, together with low NO_3^- and SO_4^{2-} concentrations relative to Cl^- , could be used to infer a higher likelihood of potentially deleterious brines developing.

The choice of input water composition must also consider the natural variability of pore-water compositions in the repository units. This natural variability is illustrated in Figure B-1. The spatial scale of pore-water variability is small (i.e., samples extracted from the same borehole but a few feet apart show absolute concentration variations in major constituents by a factor up to around 3) (DTN: GS020408312272.003). However, initial conditions in the THC seepage model assume that the composition of pore waters around the drift is homogenous. In the real system, waters mobilized around the drift in fractures (mostly through drainage of condensed water vapor) over meter scales would tend to develop compositions averaging, or integrating, the effects introduced by such small-scale heterogeneity in initial pore water compositions. Such averaging is expected to result in evolution of water compositions that would tend to be intermediate to the range of model results from the analyses of THC processes using the five representative compositions. This provides additional confidence that the range of variability captured by these five scenarios encompasses the anticipated range of evolution of the thermally perturbed system. From the considerations discussed above, one could expect deeper waters to exhibit lower calcium and higher total carbonate concentrations and therefore be less conducive to the formation of calcium-chloride brines. However, other factors could affect the spatial distribution of pore-water compositions in the repository units. These factors include variations of infiltration rates in various parts of the repository footprint (Sonnenthal and Bodvarsson 1999, pp. 122 to 123) and possibly the presence or absence of ion-exchanging zeolites in areas above the repository. Furthermore, as noted above, the evolution of brine composition upon evaporation and boiling follows many other chemical divides besides the first calcite divide mentioned earlier.

Given these considerations, initial water compositions were selected for simulations based on the following criteria (BSC 2003a):

1. Capture the spread of pore-water compositions shown on Figure B-1 and include, to the extent practicable, waters that may yield different end-brine compositions
2. Include at least one pore water from the most important repository host unit (Ttptll)

3. Use analyses that best balance charge if more than one sample meets the other criteria
4. Limit the number of waters to limit overall computational effort.

On these bases, the following water compositions were selected, listed here with an arbitrary identification (W0, W5, etc.):

- W0: HD-PERM water, from the Tptpmn unit in Alcove 5. This is an average composition (from Samples HD-PERM-2 and HD-PERM-3) used for all *Drift-Scale Coupled Processes (DST and THC Seepage) Models* (CRWMS M&O 2001) work. The HD-PERM samples plot higher than other pore waters on the diamond-shaped area in Figure B-1, bounding the range of compositions in the calcium-sulfate-chloride field.
- W5: Sample CS-1000/7.3-7.7/UC, from the base of the Tptpul lithostratigraphic unit in the ECRB Cross-Drift. This sample was selected because it exhibits one of the highest $(Ca+Mg)/(Na+K)$ ratios of the ECRB Cross-Drift samples, and exhibits better charge balance than other samples with high $(Ca+Mg)/(Na+K)$ ratios.
- W4: Sample CS-2000/16.5-21.1/UC, from the Tptpll lithostratigraphic unit in the ECRB Cross-Drift. This sample exhibits the lowest $(Ca+Mg)/(Na+K)$ ratio of the ECRB Cross-Drift samples and exhibits better charge balance than other samples of similar composition. Also, this sample is from the main repository host unit. It also contains a higher fluoride concentration than the other samples.

Two additional samples were also considered:

- W6: Sample SD-9/990.4-991.7, from the Tptpll lithostratigraphic unit in borehole SD-9. This sample exhibits a low $(Ca+Mg)/(Na+K)$ ratio nearly identical to that of W4, but exhibits a better charge balance than W4 and a higher NO_3^- concentration compared to most other samples. This water is very similar in composition to Water W4.
- W7: Sample CS500/12.0-16.7, from the Tptpul lithostratigraphic unit in ECRB Cross-Drift. This sample plots between the HD-PERM waters and Water W5 on Figure B-1, further capturing the variability of water compositions in the upper part of Figure B-1.

As shown in Figure B-1, the water compositions chosen for input into the THC seepage model capture fairly well the spread of currently available pore-water compositions in repository units. Water compositions W4, W5, and W6 plot in the lower half of the diamond-shaped area on Figure B-1. The HD-PERM waters and W7 plot in the upper half of this area, and for this reason may be more likely to evolve toward a calcium-chloride brine than the other waters upon evaporation. Simulations in *Drift-Scale Coupled Processes (DST and THC Seepage) Models* (BSC 2003a, Section 6) indicate that the spread in model results for predicted concentrations introduced by using these water compositions (thus from natural variability) is in the range of one order of magnitude and is generally larger than the spread introduced by other considered

ranges of input parameters (infiltration rates, CO₂ diffusivity) or model conceptualization (with or without vapor-pressure lowering).

In summary, five alternate water analyses were used in *Drift-Scale Coupled Processes (DST and THC Seepage) Models* REV02 simulations (BSC 2003a), approximately covering the compositional variability of pore waters in repository host units. As stated above, simulations in *Drift-Scale Coupled Processes (DST and THC Seepage) Models* (BSC 2003a) indicate that the spread in predicted concentrations introduced by using these water compositions is in the range of one order of magnitude and is generally larger than the spread introduced by other considered ranges of input parameters (infiltration rates, CO₂ diffusivity) or model conceptualization (with or without vapor-pressure lowering). Uncertainty was assessed by comparing predictions of ambient water compositions with measured ambient pore-water compositions and pore-gas CO₂ concentrations. Input water compositions affect predicted water compositions around the drift, and likely more so through infiltration/transport than through reaction (BSC 2003a, Section 6).

B.4.1.2 CO₂ Soil Boundary Conditions Available from Geochemical Measurements

The CO₂ concentration at the top model boundary was set to a constant 3,100 ppmv ($p\text{CO}_2 = 10^{-2.5}$ atm) (with the pH and bicarbonate in all infiltration water adjusted to reflect this partial pressure) to reflect a value consistent with the range of higher concentrations measured in shallow geologic units in borehole UZ-1 (Yang et al. 1996, Table 8; BSC 2003a, Section 6.2.2.1). These higher CO₂ concentrations are most likely the result of biological activity near the ground surface. The initial equilibrium CO₂ partial pressure was set by the initial water composition input into the model (Section B.4.1.1) and ranges between 10^{-3} atm (for W0) and $10^{-2.5}$ atm (W4 through W7). For the Tptpmn THC seepage model, the initial CO₂ partial pressure in the drift was set to be consistent with a CO₂ concentration of 400 ppm by volume (ppmv) in the drift, which is within the range of measured ambient concentrations in the Exploratory Studies Facility (DTN: LB990630123142.003). For the Tptpll seepage model, the initial CO₂ partial pressure in the drift was assumed to be at equilibrium with the initial composition of pore water around the drift.

Drift-Scale Coupled Processes (DST and THC Seepage) Models (BSC 2003a, Section 6.2.2.1) shows that the composition of the simulated infiltration water essentially dictates the boundary CO₂ pressure. Therefore, the uncertainty in infiltrating water composition is significantly larger and overwhelms the uncertainty in boundary CO₂ pressure. Various infiltrating waters were assumed to equilibrate at the same boundary CO₂ pressure (3,100 ppmv), estimated from observed CO₂ pressures. A large effect is not expected within the possible range of observed natural concentrations because the range of thermally induced CO₂ partial pressures is much larger than (and thus overwhelms) background values.

B.4.1.3 Vapor-Pressure Lowering

Simulations documented in *Drift-Scale Coupled Processes (DST and THC Seepage) Models* (BSC 2003a, Section 6.8.5.2) account for vapor-pressure lowering due to capillary pressure (using the EOS4 option of TOUGHREACT V3.0) (LBNL 2002), whereas earlier simulations, referred to as REV01 simulations (CRWMS M&O 2001), did not (with the EOS3 option of TOUGHREACT V3.0) (LBNL 2002). The differences between the results of the sets of

simulations are presented below. Differences in the thermal-hydrologic prediction results between REV01 (CRWMS M&O 2001) and REV02 (BSC 2003a) simulations were caused by vapor-pressure lowering and other factors, such as changes in the rock properties and heat removal due to ventilation.

The main impact of vapor-pressure lowering is the smaller extent of dryout around the drift in the rock matrix than in fractures, even though temperatures are essentially the same in both media. Consequently, the rock matrix at the drift wall is predicted to rewet earlier (at around 200 to 300 years) than in previous models (1,200 to 1,400 years). In fractures, however, the time of rewetting around the drift wall is similar for both model revisions.

Temperature profiles from THC simulations (BSC 2003a, Figure 6.8-11) are similar for model runs with and without vapor-pressure lowering, but with slightly higher peak temperatures predicted without vapor-pressure lowering.

Other than these differences in peak temperature and the extent of dryout, predicted aqueous-species and CO₂ gas concentrations (BSC 2003a, Figures 6.8-12 through 6.8-20) generally show similar trends in fracture gas and water chemistry through time with and without vapor-pressure lowering except for CO₂, which has about 10 percent lower concentration for the vapor-pressure lowering case after 20,000 years.

In summary, sensitivity analyses performed with models that include and exclude vapor-pressure-lowering effects were performed to examine its impact on the near-field geochemical environment. No large effect on computed gas and water chemistries was observed. However, a large effect on the predicted time of rewetting of the matrix at the drift wall was observed with a much shorter dryout period occurring with vapor-pressure lowering.

B.4.1.4 Spatial Variability of Model Output

Spatial variability of model output was evaluated in two ways: (a) comparing simulations for two stratigraphic units (Tptpmn and Tptpll) (BSC 2003a, Sections 6.5.5 and 6.7.5), and (b) comparing the water chemistry at grid blocks meeting certain criteria (e.g., highest saturation above the drift within 25 m of the drift centerline) (BSC 2003a, Section 6.8.5.3.2). These analyses show that the spread in predicted water compositions around the modeled drift (for a given simulation) is generally much larger than differences related to the drift location (i.e., Tptpmn versus Tptpll).

The effects of temperature differences at specific locations within the repository also contribute to spatial variability. These effects can be inferred from simulation results presented in *FY 01 Supplemental Science and Performance Analyses, Volume 1: Scientific Bases and Analyses* (BSC 2001, Section 6.3.1.5.1), which compare THC effects for higher- and lower-temperature repository operating modes. Above-average temperatures may be expected near the center of the repository, and below-average temperatures towards the edges. In this discussion, the lower-temperature case does not result in boiling and dryout does not occur, whereas the higher-temperature case results in temperatures above boiling in rock around the drift and dryout, with the extent depending on the infiltration rate and rock thermal properties. The higher temperature case may be viewed as providing an upper bound on the effects of evaporative

concentration, whereas in the lower temperature case, the effects of evaporative concentration at the drift wall are significantly reduced.

Predicted water compositions are more affected at high temperatures than at low temperatures, with temperature primarily affecting THC processes in three ways: extent and duration of the dryout zone; mineral stability and solubility; and CO₂ solubility. In the higher-temperature case, the drift wall is predicted to dry out for approximately 1,600 years, after which time the drift crown starts to rewet. No dryout is predicted for the lower-temperature case.

Mineral reaction and stability are temperature-dependent, and this will affect the composition of fluids that may enter drifts. Most rock-forming minerals are less stable and dissolve faster at high temperatures. One exception is calcite, which has decreasing solubility with temperature. For most major cations and anions, except aqueous carbonate species, initial concentrations predicted in fractures at the drift crown at the time of rewetting (high temperature case) are considerably larger (one or more orders of magnitude) than concentrations predicted in the low temperature case. This is primarily because of the larger evaporative concentration. Accordingly, the higher concentrations correspond to significantly smaller water saturations in fractures, which results in lower percolation fluxes. In this case, the predicted water saturation in fractures at the time of rewetting is too small for any significant water movement to occur. These effects of evaporative concentration, together with the depletion of aqueous carbonate species, appear to be more significant than the effect of mineral reactions (at least with respect to the compositions of fluids at the drift wall).

The pore water contains a large number of naturally dissolved carbonate species, and a significant effect of increasing temperature on water chemistry is the exsolution of carbon dioxide from the pore water. The bulk of the water (moisture) present in the rock is contained in the matrix, not the fractures. When heated, carbon dioxide exsolved from the matrix water is transported into fractures. This can cause the carbon dioxide partial pressure to rise above ambient values in fractures, and also cause pH to decrease in fracture water when steam condenses. However, during the dryout period in the higher temperature case, carbon dioxide concentrations at the drift wall fall largely below ambient values (i.e., decrease up to four orders of magnitude) as the result of boiling and displacement by steam. During the early rewetting of fractures at the drift crown, the carbon dioxide partial pressure in the higher temperature case is still depressed relative to the lower temperature case, causing predicted pH values approximately 0.4 units higher than in the lower-temperature case. The exsolution of carbon dioxide causes total aqueous carbonate concentrations at the drift wall to decrease below ambient values in fractures (by a factor of approximately 2 in the lower-temperature case and approximately 4 in the higher-temperature case).

B.4.1.4.1 Tptpmn and Tptpll

With respect to water and gas chemistry for ambient conditions, trends simulated for both stratigraphic units are fairly similar, with some fluctuations resulting mostly from changes in infiltration rates (BSC 2003a, Section 6.7.5.2). The minor differences in input mineralogic data and mineral surface areas between the Tptpmn model and this Tptpll model have only a small effect on predicted ambient water compositions, at least within the 100,000-year time period

investigated. The same can be said for the effect of differences in hydrologic properties between both units.

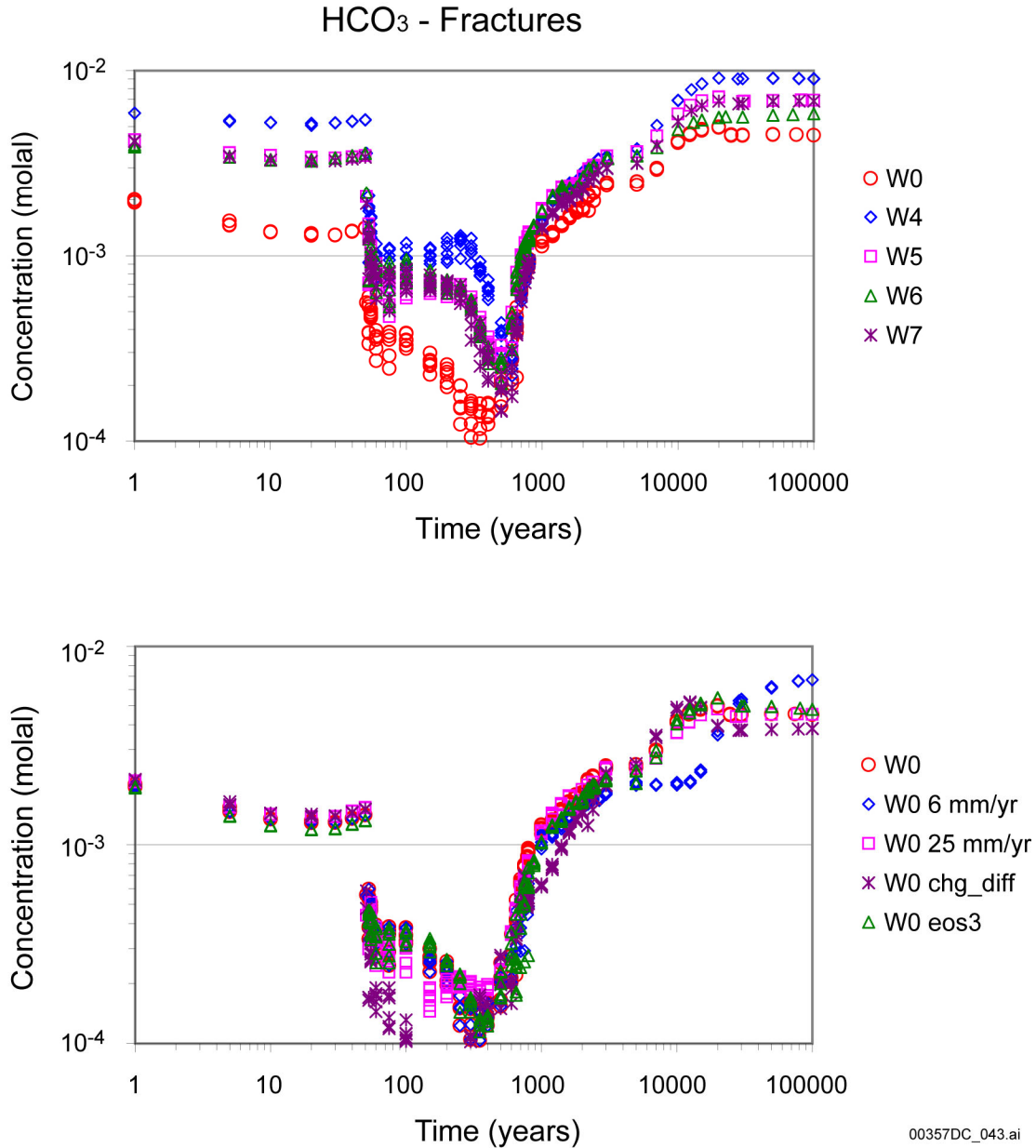
Under thermal loading, modeled concentration trends in fractures for the chemical species in the Tptpll model are similar to those modeled in the Tptpmn. The base of the drift does not dry out during the entire time span of the preclosure period shown on the time profiles (in contrast to the Tptpmn model results). Evaporation at the base of the drift, combined with the “shadow” effect of the drift, generally results in increased concentrations at this location in both the Tptpmn and Tptpll models. However, because of the higher fracture capillarity in the Tptpll model, evaporative concentration below the drift occurs to a larger degree than in the Tptpmn model. Also, noteworthy differences exist in pH and CO₂, total carbonate (as HCO₃⁻), and calcium concentrations at the side of the drift when modeled with the extended system. These concentrations do not return to ambient values after rewetting because of significant calcite precipitation at this location.

Before and after dryout, the greater evaporation caused by higher temperatures in the Tptpll model results in somewhat higher predicted concentrations of most aqueous species, compared to the Tptpmn model. Elevated concentrations are predicted only for small liquid saturations that are not subject to significant fluid movement.

Predicted fluoride concentrations in the Tptpll model under ambient and thermal loading conditions are higher than in the Tptpmn model because of fluorite (CaF₂) dissolution. This mineral is included as one of the mineral constituents of the Tptpll (and of other units to a lesser extent), while it was not included as a primary mineral in the Tptpmn model. Ambient fluoride concentrations tend toward equilibrium with fluorite (5 to 6 mg/L for the modeled ambient geochemical conditions) because of the fast reaction rate of this mineral.

B.4.1.4.2 Grid Blocks with Highest Saturation

Predicted concentration profiles at fixed model grid blocks at the crown, side, and base of the drift provide only limited information on the chemistry of waters that could seep into drifts (BSC 2003a, Section 6.8.5.3.2). Such profiles do not fully capture the spatial variability of model results around the drift and, more importantly, cannot show water compositions as long as the selected model grid blocks remain dry. To better capture spatial variability, as well as predicted water compositions during the dryout period, concentration time-profiles were generated for dynamic zones following the expanding, then receding, boiling and condensation fronts around the drift. An example of these results is presented for grid blocks with highest liquid saturation above the drift in fractures in Figure B-2. More specifically, data were extracted for model grid blocks located within a 45° arc from the drift crown down, and for the first six of such grid blocks having the highest liquid saturation in fractures, within 25 m from drift centerline.



Source: BSC 2003a, Figure 6.8-27.

NOTE: Grid blocks are those with highest liquid saturation in fractures within a 25-m radius from drift center and a 45° arc from the drift crown. Data are shown for simulations using different initial water compositions (W0 - W7). Except as noted below, all simulations were run using a stepwise-increasing infiltration rate (6, 16, and 25 mm/y) and with vapor-pressure lowering. Alternatives using Water W0 include simulations without vapor-pressure lowering (W0 - eos3), and with fixed 25 and 6 mm/y infiltration rates (W0 - 6 mm/y and W0 - 25 mm/y, respectively).

Figure B-2. Thermal-Hydrologic-Chemical Simulations (TptII Model REV02): Time Profiles of Modeled Total Aqueous Carbonate Concentrations (as HCO₃⁻) in Fracture Water, in Areas of Highest Liquid Saturation above the Drift Crown

Various time profiles for data have been extracted in this manner (thus, data for six grid blocks are plotted per point in time for each run) and are presented in *Drift-Scale Coupled Processes (DST and THC Seepage) Models* (BSC 2003a). To assess the model sensitivity to initial water compositions and other alternative conceptualizations, time profiles were generated for simulations considering:

- The five different input initial water compositions
- Three different infiltration scenarios (using the HD-PERM (W0) input water composition): stepwise increase from 6 to 25 mm/yr, fixed 6 mm/yr, and fixed 25 mm/yr
- The two different water vapor-pressure models implemented in TOUGHREACT V3.0 (LBNL 2002) modules EOS4 and EOS3 (using the HD-PERM input water composition), with and without vapor-pressure lowering due to capillary pressure.

Therefore, time profiles generated in this way capture a spread of concentrations related to (1) the natural variability of input water compositions, (2) alternative model conceptualizations, and (3) for each model run at any given time, the spatial variability of model results for grid blocks of highest liquid saturation above the drift crown. In addition to this spread, fluctuations of computed concentrations with time arising from THC effects (as discussed below) are also captured.

Three observations from the predicted profiles of concentration versus time for CO₂ gas and 12 aqueous species or species ratios of interest are particularly significant:

1. In general, the different input water compositions (i.e., natural variability) produce a larger relative spread in predicted water and gas compositions than the range of infiltration rates considered or the selected water-vapor pressure module.
2. At those grid blocks with highest liquid saturation above the drift crown, the relative spread of predicted concentrations for the various modeled alternatives generally does not exceed an order of magnitude and is often much less (see Section B.4.1.1).
3. For all simulations shown, the predicted general concentration trends are quite similar.

In summary, selected simulation results illustrate the variability in the computed geochemical response, indicating that the predicted overall trend is robust. The calculated variability is generally much less than an order of magnitude and is usually smaller than that caused by the natural variability in the input water composition.

B.4.1.5 Uncertainty and Variability Due to Percolation Flux Changes Stemming from Climate Change and Infiltration Rates

To investigate percolation fluxes caused by changes in climate conditions, several infiltration rate scenarios were considered in *Drift-Scale Coupled Processes (DST and THC Seepage) Models* (BSC 2003a, Section 6.8.2), as summarized in Table B-1. The results are shown in *Drift-Scale Coupled Processes (DST and THC Seepage) Models* (BSC 2003a, Figures 6.8-22

through 6.8-38). In summary, general trends of predicted concentrations with time remained similar for all modeled infiltration scenarios. The evaporative concentration stage ends earlier at the higher infiltration rate (constant 25 mm/yr), as would be expected (BSC 2003a, Section 6.8.5.3.2, p. 209). The relative spread of predicted concentrations resulting from the natural variability of pore water compositions (around an order of magnitude) is typically larger than the spread resulting from the range of considered infiltration rates (BSC 2003a, Section 6.9.2, p. 241).

Table B-1. Tptpl Thermal-Hydrologic-Chemical Model Infiltration Rates

Case	Infiltration Rate (mm/yr)	Time Period (years)	Reference
Mean Infiltration (increasing stepwise)	6 16 25	0 to 600 (present day) 600 to 2,000 (monsoon) 2,000 to 100,000 (glacial transition)	BSC 2003a Table 4.1-1
Mean low (fixed)	6	0 to 100,000	NA (sensitivity only)
Mean high (fixed)	25	0 to 100,000	NA (sensitivity only)

Source: BSC 2003a, Table 6.8-2.

NOTE: All simulations were carried out with the present day mean calibrated rock properties set.

B.4.1.6 Documentation of the Method Uncertainty Is Captured in the Model

The simulations of THC processes include coupling between heat, water, and vapor flow, aqueous and gaseous species transport, kinetic and equilibrium mineral-water reactions, and feedback of mineral precipitation/dissolution on porosity, permeability, and capillary pressure (hydrologic properties) for a dual-permeability (fracture-matrix) system. As such, the THC seepage model takes into account the effects of mineral dissolution and precipitation, the effects of carbon dioxide exsolution and transport in the region surrounding emplacement drifts, and the resulting changes to porosity, permeability, seepage, and chemical composition of percolating waters. The large number of input parameters, the numerical methods implemented in simulating coupled processes, and the simplification and approximations pertaining to the physical setup of the THC seepage model, all contribute to uncertainties in the predictions. Discussion of the uncertainties and results of sensitivity analyses are given in *Drift-Scale Coupled Processes (DST and THC Seepage) Models* (BSC 2003a, Section 6.9). Uncertainties in model input data that affect calculated water and gas compositions include (Table B-2):

- Thermodynamic data (equilibrium constants for mineral–water reactions and aqueous species dissociation, for some minerals adjusted within their uncertainty—see below)
- Kinetic data (rate constants, reactive surface areas, and activation energies)
- Initial compositions of pore water and pore gas
- Initial composition of infiltrating water and gas
- Infiltration rates

- Transport parameters (diffusion coefficients of aqueous species and gases, tortuosity)
- Initial rock mineralogy (model location and stratigraphy)
- Number of geochemical constituents included in the simulations
- Number and types of potential secondary mineral phases
- Rock thermal, physical, and hydrologic properties (including input data for both water-saturated and unsaturated rock).

The THC seepage model takes into account the effects of mineral dissolution and precipitation; carbon dioxide exsolution and transport in the region surrounding emplacement drifts; changes to porosity, permeability, seepage, and chemical composition of percolating waters. Simulations of THC processes using the TOUGHREACT V3.0 numerical code (LBNL 2002) include coupling between heat, water, and vapor flow, aqueous and gaseous species transport, kinetic and equilibrium mineral–water reactions, and feedback of mineral precipitation/dissolution on porosity, permeability, and capillary pressure (hydrologic properties) for a dual-permeability (fracture-matrix) system. Process model uncertainties may also affect the calculated water and gas compositions. These include:

- Formulation of models to simulate fluid flow in dual permeability media (e.g., fracture-matrix interactions; relative permeability and saturation-capillary pressure models)
- Activity coefficient models
- Kinetic mineral precipitation and dissolution models
- Inclusion or exclusion of certain specific thermal, hydrologic, or chemical processes (e.g., active fracture model, vapor-pressure lowering, mineral solid solutions, redox reactions)
- Physical model representation (stratigraphic/geologic extrapolations)
- Representation of the fracture and matrix continua in the model mesh
- Model discretization (in space and time)
- Boundary conditions (e.g., drift open versus closed to fluid flow).

Table B-2. Summary of Uncertainties Affecting Chemical Processes in the Thermal-Hydrologic-Chemical Seepage Model

Category	Issue	Treatment	Consequences
Conceptual uncertainties	Geochemical system considered (minerals, gases, and aqueous species)	<p>Treated by including major rock-forming minerals, major aqueous species, and major gases of interest (CO₂, air, water vapor) in the system and also minor minerals such as clays. Effects of secondary mineral phase precipitation is most uncertain at higher temperatures and may require further evaluation. Uncertainty is limited under ambient conditions if ambient water concentrations can be reproduced.</p> <p>Trace minerals and aqueous species are not considered (not within the current scope for the THC seepage model). However, results of model validation (BSC 2003a, Section 7) against the DST and other experiments suggest the geochemical system, as modeled, is constrained enough to reproduce the experimental data within validation criteria. Also, the range of incoming waters considered in the model capture, at least in some part, the range of uncertainties related to the geochemical system.</p>	<p>Precipitation of secondary phases not currently included in simulations could affect the predicted composition of waters around the drift at high temperature. Reactions involving trace minerals (e.g., other clay minerals or Mg, Fe, Mn minerals) could affect pH which, in turn, could affect the precipitation/dissolution of other mineral phases and indirectly affect the concentrations of major species.</p> <p>The type of mineral precipitating could also affect the calculated porosity change (i.e., effect of different molar volume), although this effect would be minimal because the bulk of the precipitation consists of amorphous silica.</p> <p>Uncertainties affecting the precipitation of secondary phases would increase at near dryout conditions, however, such conditions (i.e., small liquid saturations) are not conducive to seepage.</p>
	Drift wall conceptualization: closed versus open to advective fluid flow; also, hydrologic effect of ventilation is neglected	<p>Both cases of open and closed drift wall were addressed.</p> <p>Infiltration rates (even at high rates indicative of future wet climates) are below seepage thresholds, so there is little effect of closing the drift wall on water percolation fluxes around the drift.</p> <p>Evaporative concentration effects (due to ventilation) are indirectly taken into account by "downstream" in-drift evaporation models, which are expected to bound those from ventilation.</p>	<p>Boundary conditions of pressure and relative humidity in the drift could affect evaporative concentration effects at the drift wall, mostly during the preclosure ventilation period.</p> <p>In-drift interactions are not considered (this was not a goal of the THC seepage model).</p>
	Precipitation/nucleation kinetics	<p>Not treated mechanistically.</p> <p>This affects minerals such as silica and calcite, which have fast reaction rates. The reaction of calcite at equilibrium with a supersaturation gap (as done here) may approximate nucleation processes.</p> <p>Silica precipitation is modeled with a very fast reaction rate.</p>	<p>In areas where rapid boiling occurs, predicted silica concentrations are overestimated and silica precipitation is underestimated. However, the water saturation in these areas is very small and therefore the actual amounts of silica are minute.</p>

Table B-2. Summary of Uncertainties Affecting Chemical Processes in the Thermal-Hydrologic-Chemical Seepage Model (Continued)

Category	Issue	Treatment	Consequences
Conceptual uncertainties (cont.)	Water chemistry is not computed below a set water saturation limit (10^{-5}) or above a set ionic strength limit (4) (Activity coefficient model limitations)	In REV02 (BSC 2003a, Section 6.4.5) models, salt precipitation in the last remaining water when boiling or evaporating is taken into account using a simple model. These salts are then available for dissolution upon rewetting, providing a conceptually correct (although simplified) representation of actual processes accompanying dryout and rewetting. In REV01 (CRWMS M&O 2001) models, the composition of the last aqueous phase for which geochemical speciation is computed (prior to dryout) is saved. Water with this composition is assumed to mix instantly with percolating water during rewetting.	In REV02 (BSC 2003a) models, the type and sequence of salts assumed to precipitate upon dryout affects computed water compositions at the very early stages of rewetting only. In REV01 (CRWMS M&O 2001) models, assuming instant dissolution may overpredict dissolved salt concentrations when rewetting occurs.
	Vapor-pressure lowering due to capillary pressure	Treated by running simulations with and without vapor-pressure lowering.	No large effect on computed gas and water chemistries. However, a large effect on the predicted time of rewetting of fractures and matrix at the drift wall was observed. Neglecting vapor-pressure lowering could increase the effect of evaporative concentration around the drift, resulting in higher water salinities, although this was not noticeable.
	Oxidation-reduction processes are neglected	Not treated (considers only oxidized conditions). Oxidizing conditions prevail in the unsaturated zone at Yucca Mountain such that the redox species considered in the THC seepage model (iron and sulfate) occur only in their oxidized state.	Limited anticipated effect because of the prevailing oxidized conditions. Likely no effect for iron and sulfate in the current models. Redox reactions involving microbial processes and species not presently modeled (nitrates, phosphates) could have a limited effect on pH.
	Mineral solid-solutions	Ideal solid-solution treatment for clays; no treatment for other minerals. Taken indirectly into account through adjustments of thermodynamic data necessary to reproduce ambient water compositions. ^a Compositions of primary solid solution phases, when known, are directly taken into account by the relative amounts of individual end-members input into the model. Individual mineral phases with fixed solid-solution compositions (determined by analysis) are included in the simulations (e.g., zeolites).	Limited anticipated effect because solid solutions are partially treated as described in the adjacent table column. In the current THC seepage model, this would primarily affect the composition of precipitating alkali feldspars (thus affecting predicted Na and K concentrations). However, these minerals form nearly pure secondary phases in nature (i.e., as modeled). Zeolites in the repository host units (mostly stellerite) are not abundant and not particularly variable in composition.

Table B-2. Summary of Uncertainties Affecting Chemical Processes in the Thermal-Hydrologic-Chemical Seepage Model (Continued)

Category	Issue	Treatment	Consequences
Conceptual uncertainties (cont.)	Ion-exchange and surface complexation	Not treated. Dominant primary rock minerals in the repository host units are not strong ion exchangers (for major ions). THC seepage simulations do not include trace elements that could be strongly affected by surface complexation.	Limited effect for the current application range of the THC Seepage Model. The results cover a wide range of variation in Na, K, Ca, and Mg, providing sufficient variation to capture in the downstream models.
	Capillary pressure effect on chemical potentials of reacting species	Not treated. It is taken indirectly into account through adjustments of thermodynamic data such that ambient water compositions can be reproduced.	Could potentially shift predicted concentrations of some species.
Data uncertainties	Infiltration water and initial pore-water composition	Five alternate water analyses are used in REV02 (BSC 2003a) simulations, covering fairly well the compositional variability of pore waters in repository host units. Uncertainty can be assessed by comparing predictions of ambient water compositions with measured ambient pore-water compositions and pore-gas CO ₂ concentrations.	Input water compositions affect predicted water compositions around the drift, and likely more so through infiltration/transport than through reaction.
	Carbon dioxide partial pressures	Composition of infiltrating water input into the model essentially dictates the boundary CO ₂ pressure; therefore, the uncertainty in infiltrating water composition overcomes this uncertainty. However, here, various infiltrating waters were assumed to equilibrate at the same boundary CO ₂ pressure (around 3200 ppmv).	A large effect is not expected within the possible range of observed natural concentrations, because the range of thermally induced CO ₂ partial pressures is much larger than (and thus overwhelms) background concentrations.
	Thermodynamic and kinetic data	Treated partly through sensitivity studies on long-term behavior of ambient system chemistry, assuming a fixed infiltration rate and different thermodynamic data for clays and zeolites (the model is very sensitive to the thermodynamic data for these minerals). When possible within the uncertainty of the original data, treated by revising the data to reproduce observed water compositions and mineralogical data. Other uncertainties evaluated through model validation (DST and laboratory experiments).	Currently one of the main uncertainties affecting predicted water compositions around the drift. However, it can be constrained by adjustments and model validation against observed data, such that ambient simulations predict concentrations consistent with observed values.

Table B-2. Summary of Uncertainties Affecting Chemical Processes in the Thermal-Hydrologic-Chemical Seepage Model (Continued)

Category	Issue	Treatment	Consequences
Data uncertainties (cont.)	Host rock mineralogy	Treated by considering alternative drift locations (Ttpmn versus Ttpll host rock unit). Bulk chemical composition of the repository host units do not differ significantly.	No significant effect on the predicted compositions of major aqueous species. Small amounts of fast-reacting minerals containing elements present in minor quantities in pore water (e.g., fluorite) can have a large effect on the predicted concentrations of these minor species (e.g., F ⁻), but not affect the major ion chemistry.
	Infiltration rates	Alternative infiltration rate scenarios are used.	Between 6 and 25 mm/y, there is a small effect on predicted concentrations at the drift wall. The effect would be greater under lower rates of infiltration (when reaction effects start to dominate transport), but such conditions would be less likely to cause in-drift seepage. At high-infiltration rates, most conducive to in-drift seepage, water compositions are more function of transport than of reaction with host rock minerals, such that the uncertainty regarding the composition of the infiltration water, rather than the rate of mineral dissolution/ precipitation, becomes more important.
Parameter uncertainties	Heterogeneity	Heterogeneous fracture permeability treated in REV01 (CRWMS M&O 2001). Heterogeneity in matrix properties not treated. Local heterogeneity in mineralogy not treated; however, the bulk composition of host rocks is fairly uniform. Heterogeneity in initial water geochemistry not treated directly; treated indirectly through testing with alternate water compositions.	Possible local changes in predicted water compositions around the drift. However, the bulk composition of waters around the drift is not expected to be significantly affected, because the rock chemical composition and mineralogy in the repository units is fairly homogeneous.

Table B-2. Summary of Uncertainties Affecting Chemical Processes in the Thermal-Hydrologic-Chemical Seepage Model (Continued)

Category	Issue	Treatment	Consequences
Parameter uncertainties (cont.)	Transport parameters (effective diffusivity)	The CO ₂ diffusion coefficient was increased by a factor of 6 between REV01 (CRWMS M&O 2001) and REV02 (BSC 2003a) analyses (and a factor of 30 since pre-REV01 (CRWMS M&O 2001) simulations). Sensitivity to diffusion coefficient for aqueous species was not investigated. However, tortuosity was changed from 0.2 to 0.7 between earlier report revisions (REV00 CRWMS M&O 2000c and REV01 CRWMS M&O 2001) without noticeable effect.	CO ₂ diffusion coefficient mainly affects in-drift predicted CO ₂ concentrations during dryout. At other times, predicted CO ₂ concentrations are mainly dictated by water compositions.

Source: BSC 2003a, Table 6.9.1.

NOTE: ^a Thermodynamic data for some minerals were adjusted within their uncertainty such that predicted ambient pore water compositions over thousands of years were more consistent with measured data. These adjustments were performed independently of, and prior to, model validation using the DST THC model (BSC 2003a, Section 7.1), and do not involve calibration to the DST data.

Although many of the above uncertainties cannot be assigned a quantitative value, which makes a systematic analysis of the overall model uncertainty difficult, a number of numerical simulations were performed to characterize the effects of natural variability and uncertainty on the THC seepage model predictions. These sensitivity analyses address the following major issues, most of which are described in the previous sections:

1. Different repository host-rock lithostratigraphic units (Tptpmn and Tptpll)
2. Alternative geochemical systems (base case and extended case, additional minerals and chemical components)
3. Alternative thermodynamic data sets (different equilibrium constants for key minerals)
4. Different treatments of mineral-water reactions (different kinetic rate constants and reactive surface areas; equilibrium versus kinetic reactions)
5. Spatial heterogeneity in fracture permeability
6. Different infiltration rates and effects of climate change
7. Alternative water vapor pressure models
8. Alternative initial water compositions
9. Different effective CO₂ diffusivities
10. Alternative drift-wall conceptualizations (open versus closed to liquid flow).

These THC seepage model simulations covered a wide range of the most important uncertainties from the standpoint of model validation, bounding analyses, conservatism, their impact on model results, and their propagation to other models. Such uncertainties, their treatment in the model, and their effect on model results are summarized in Table B-2. The THC seepage model was validated using the DST THC model and data collected during the DST. It is noted that prior to validation using the DST THC model (BSC 2003a, Section 7.1), thermodynamic data (equilibrium constants) for some minerals were adjusted within their uncertainty such that predicted ambient pore water compositions over thousands of years were more consistent with observed ambient water compositions. These adjustments were performed independently of, and prior to, model validation and did not involve any calibration to the DST data.

Temperature is also a critical parameter affecting modeling results, but it can generally be predicted to within a few degrees; therefore, it is not included in Table B-2. Temperature directly affects equilibrium constants and reaction rates, the degree of water evaporation and boiling, and the amount of carbon dioxide volatilization from pore water, with direct implications for computed water and gas chemistries. Uncertainties affecting predicted temperatures could significantly affect computed aqueous and gas species concentrations. However, important changes in design heat load are likely to affect model results more than uncertainties associated with input parameters used to calculate temperatures (e.g., rock thermal conductivity and heat capacity). In the model report, only the heat load from the current repository design was considered. This heat load results in temperatures in the vicinity of emplacement drifts that exceed the boiling point of water for several hundred years if ventilation is not maintained after the 50-year preclosure period. The increased water-rock-gas interactions resulting from higher temperatures are expected to affect water chemistry and flow.

The spread in predicted concentrations of aqueous species and CO₂ gas is related to:

- The natural variability of input water compositions (BSC 2003a, Section 6.2.2.1)
- The various investigated model conceptualizations (vapor-pressure model, drift location, stratigraphic columns, open versus closed drift wall) (BSC 2003a, Table 6-1)
- Ranges of input parameters other than water composition (in this case, infiltration rates and CO₂ diffusion coefficients) (BSC 2003a, Section 6.8.5.3).

The relative spread caused by the variability of input water compositions (computed as standard deviation) is shown as a function of time in Table B-3. This spread is up to around one order of magnitude and in most cases is larger than the spread introduced by the various model conceptualizations and ranges of other input data considered in the model.

Uncertainties in kinetic and thermodynamic data could affect the standard deviations shown in Table B-3, although the results of model validation against the DST and other laboratory experiments, as well as the results of simulations of ambient conditions, suggest these data are constrained to the extent that the model results are generally consistent with measured data. The model validation results (BSC 2003a, Section 7) also provide confidence that some of the other uncertainties listed in Table B-2 do not significantly affect the spread in model results. A summary of the key findings and their uncertainties is given in Figure B-3.

In summary, the model sensitivity to key input parameters was evaluated by performing a variety of simulations with the model with a reasonably expected range of input conditions (infiltration rates, initial water chemistry, CO₂ diffusion rates) and model conceptualizations (with and without vapor-pressure lowering, drift location, stratigraphic columns, open versus closed drift wall). Furthermore, confidence in model results was obtained by comparing model results against data from the DST and laboratory experiments, and improving the model conceptualization and mathematical formulation as necessary to yield a reasonably good agreement between calculated and measured data.

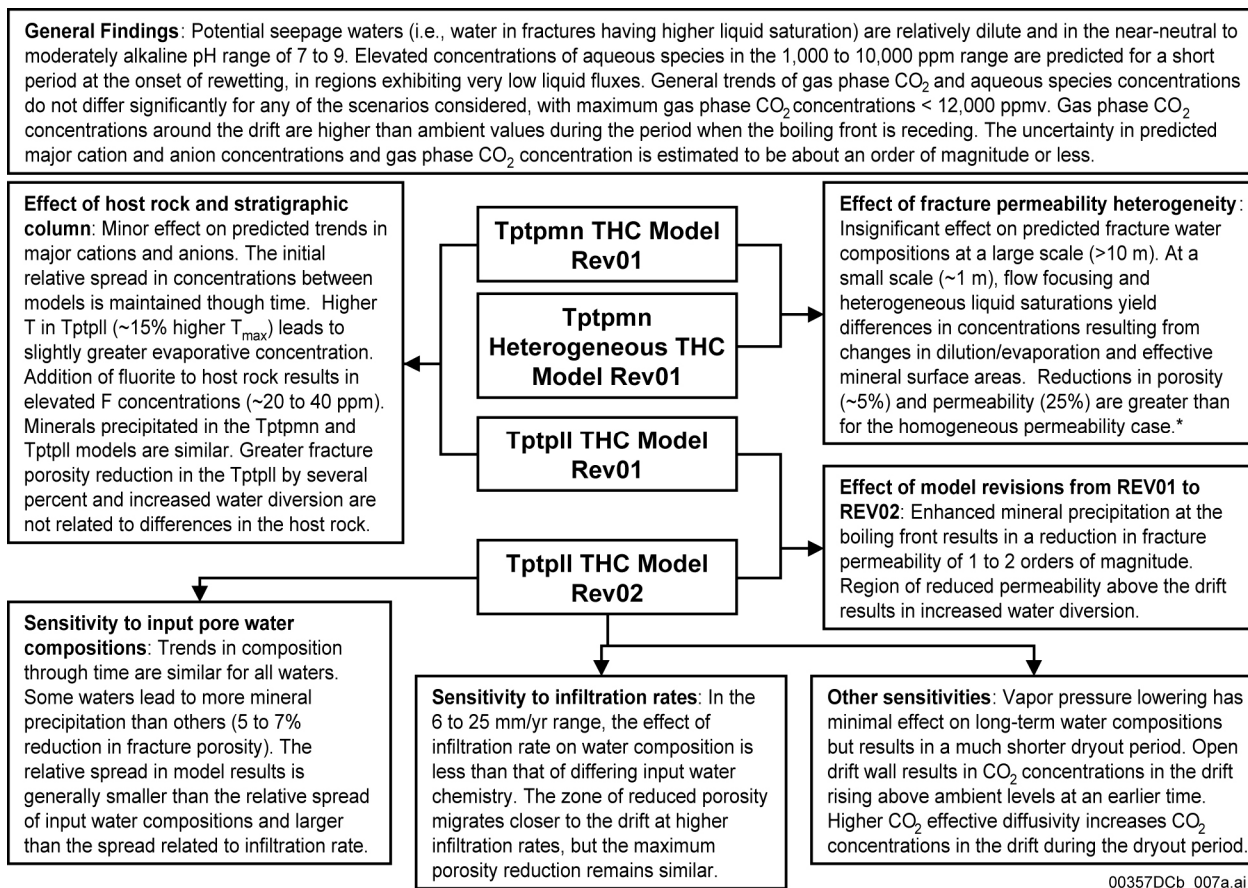
Table B-3. Standard Deviations in Water and Gas Compositions Predicted Using Five Different Input Water Compositions (W0, W4, W5, W6, and W7)

Time (years)	pH	Ca	Mg	Na	Cl	SiO ₂ (aq)	HCO ₃	SO ₄	K	F	NO ₃	CO ₂ (gas)	Ca/HCO ₃	NO ₃ /Cl	Na/Cl	Ca/Cl
0	0.11	0.11	0.52	0.18	0.29	0.08	0.14	0.37	0.06	0.30	0.27	0.23	0.19	0.38	0.36	0.24
1	0.10	0.17	0.90	0.13	0.29	0.05	0.16	0.37	0.12	0.06	0.27	0.21	0.30	0.38	0.34	0.17
53	0.14	0.15	0.82	0.25	0.37	0.20	0.22	0.44	0.24	0.25	0.35	0.32	0.33	0.38	0.27	0.31
100	0.13	0.04	0.23	0.11	0.31	0.06	0.16	0.39	0.11	0.08	0.30	0.29	0.19	0.38	0.29	0.27
200	0.09	0.23	0.38	0.16	0.40	0.14	0.23	0.46	0.16	0.12	0.33	0.32	0.45	0.38	0.32	0.21
300	0.10	0.40	0.35	0.26	0.46	0.19	0.30	0.51	0.27	0.18	0.42	0.34	0.68	0.37	0.28	0.19
400	0.11	0.35	0.38	0.24	0.40	0.16	0.22	0.44	0.24	0.13	0.40	0.25	0.53	0.37	0.19	0.12
500	0.15	0.41	0.49	0.29	0.44	0.17	0.13	0.51	0.29	0.12	0.39	0.13	0.51	0.37	0.17	0.11
600	0.17	0.42	0.47	0.26	0.40	0.16	0.13	0.45	0.27	0.13	0.41	0.08	0.54	0.38	0.16	0.17
700	0.10	0.24	0.34	0.15	0.31	0.06	0.10	0.38	0.16	0.08	0.29	0.07	0.33	0.38	0.17	0.16
801	0.10	0.20	0.28	0.12	0.30	0.04	0.07	0.37	0.12	0.07	0.28	0.07	0.27	0.38	0.18	0.14
1,000	0.09	0.16	0.23	0.10	0.29	0.02	0.06	0.37	0.10	0.05	0.27	0.03	0.22	0.38	0.20	0.15
1,200	0.09	0.15	0.22	0.09	0.29	0.02	0.08	0.37	0.09	0.04	0.27	0.01	0.23	0.38	0.21	0.15
2,000	0.08	0.18	0.19	0.08	0.32	0.01	0.07	0.38	0.08	0.07	0.28	0.01	0.25	0.38	0.23	0.15
2,200	0.06	0.18	0.17	0.06	0.29	0.02	0.08	0.37	0.07	0.07	0.27	0.03	0.26	0.38	0.23	0.12
2,400	0.06	0.18	0.17	0.06	0.29	0.02	0.07	0.37	0.07	0.07	0.27	0.02	0.25	0.38	0.23	0.12
5,000	0.05	0.14	0.14	0.06	0.29	0.01	0.07	0.37	0.07	0.06	0.27	0.04	0.21	0.38	0.23	0.15
10,000	0.03	0.14	0.10	0.06	0.29	0.01	0.08	0.37	0.06	0.05	0.27	0.08	0.17	0.38	0.25	0.20
20,000	0.04	0.14	0.11	0.06	0.29	0.01	0.09	0.37	0.06	0.06	0.27	0.12	0.15	0.38	0.26	0.22
100,000	0.03	0.13	0.08	0.05	0.29	0.02	0.10	0.37	0.05	0.05	0.27	0.11	0.15	0.38	0.26	0.24

Source: BSC 2003a, Table 6.9-2.

NOTE: Standard deviations computed (BSC 2003a) for zones of highest liquid saturation above the drift, representing:

- For pH, standard deviation of pH values in (\pm) pH units
- For other data, standard deviation of logarithmic values: i.e., (\pm) change in log₁₀ values of concentrations and concentration ratios around the mean of log₁₀ values (thus, a value of 0.5 corresponds to a total spread of one order of magnitude)



Source: BSC 2003a, Figure 8-1.

NOTE: The heterogeneous case was run using REV01 (CRWMS M&O 2001) hydrologic properties and with TOUGHREACT V2.3 (LBNL 2001). The use of REV02 (BSC 2003a) properties and TOUGHREACT V3.0 (LBNL 2002) resulted in greater reductions in porosity and permeability for the homogeneous permeability case, which would also be expected for the heterogeneous case.

Figure B-3. Key Findings of the Thermal-Hydrologic-Chemical Seepage Model

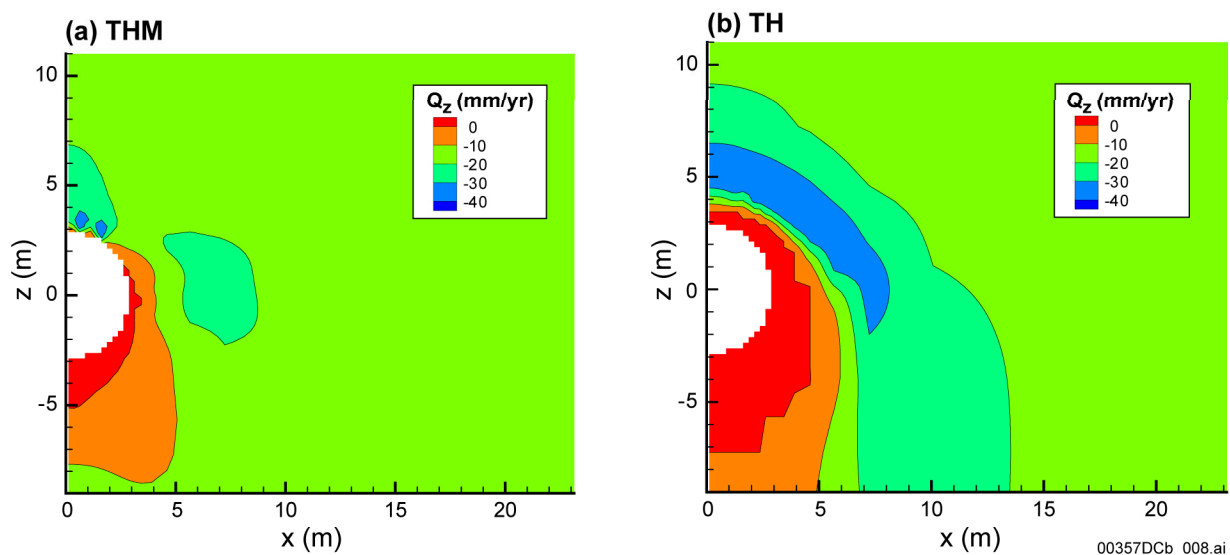
B.4.2 Specific Response and Basis for GEN 1.01 Comments 81 and 104

Uncertainties in the drift-scale THC seepage models have been addressed in *Drift-Scale Coupled Processes (DST and THC Seepage) Models* (BSC 2003a). To investigate the potential variability of the natural system, among other varied inputs, five waters of different initial chemistry were used to bracket expected potential initial water chemistry, and a range of infiltration rates was investigated, including stepped to reflect different climates, constant high, and ambient. Large-scale gas convection could alter the partial pressure of carbon dioxide, affecting pH to some extent. Additionally, large-scale convection and lateral diversion could locally increase or decrease percolation flux. The range of inputs used in *Drift-Scale Coupled Processes (DST and THC Seepage) Models* (BSC 2003a) was established in Sections 4 and 6 of that document.

Thermal-hydrologic-mechanical processes and effects on flow are addressed in *Drift-Scale Coupled Processes (DST and THC Seepage) Models* (BSC 2003a). This study evaluated the thermal-hydrologic-mechanical effects on flow in the Tptpmn and Tptpll units. This study

concluded that the impact of stress-induced changes in hydrologic properties on the flow field is small to moderate, with the strongest impact occurring for a repository located in the Tptpmn model domain. While the liquid vertical flux distribution in the fracture continuum is slightly affected, the main impact appears to be on the dryout zone near the repository drift. When stress-induced changes in hydrologic properties are considered, the extent of the dryout zone is slightly smaller, and consequently liquid water is predicted to reach the drift wall in a shorter time (Figure B-4). In the longer term, at around 10,000 years, vertical permeability is still significantly decreased, especially just above the repository drift. The impact of this reduction in permeability is small, but tends to prevent vertical flux from reaching the drift wall at the drift crown (Figure B-5).

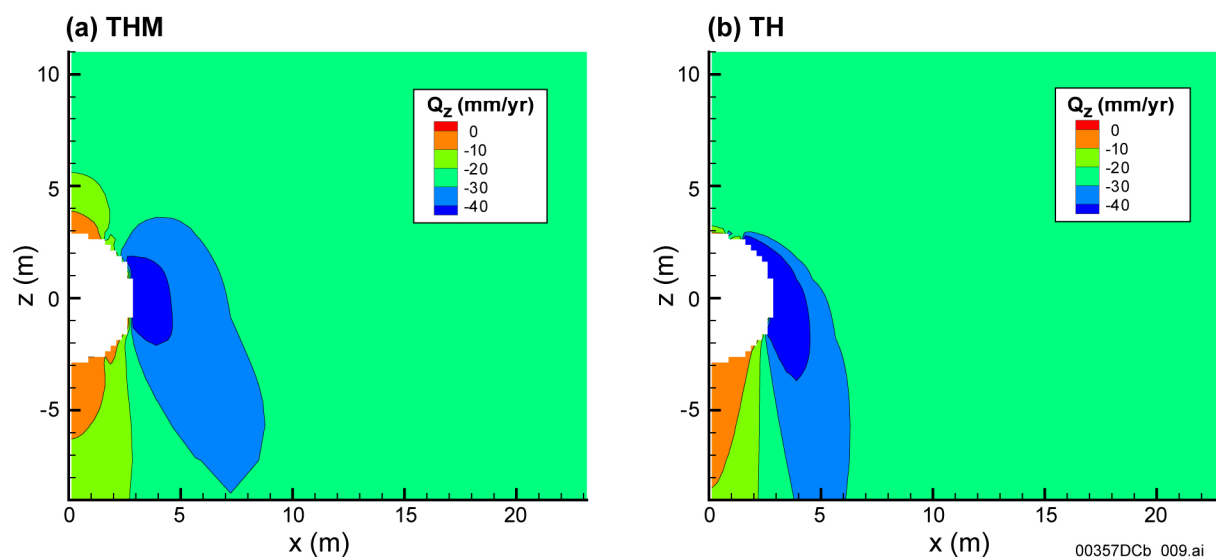
The impact of stress-induced changes in hydraulic properties on the flow field around a repository in the Tptpll unit is similar to those for a repository in the Tptpmn unit, but the magnitude of impact is much smaller. The reason for a smaller impact in the Tptpll unit is that both the initial stresses and initial fracture permeability are higher in the Tptpll unit than in the Tptpmn unit. Higher initial stresses imply that fractures are initially already compressed to a higher stiffness and closer to their residual aperture value, which prevents further closure during the thermal period. Higher initial fracture permeability results in a larger residual fracture aperture, and therefore the possible relative reduction in permeability is smaller.



Source: BSC 2003e, Figure 6.5.5-4.

NOTE: THM = thermal-hydrologic-mechanical; TH = thermal-hydrologic.

Figure B-4. Comparison of the Vertical Percolation Flux (Q_z) in Fractures at 1,000 Years for a Fully Coupled Thermal-Hydrologic-Mechanical Simulation and Thermal-Hydrologic Simulation (Tptpmn Model Domain)



Source: BSC 2003e, Figure 6.5.5-5.

NOTE: THM = thermal-hydrologic-mechanical; TH = thermal-hydrologic.

Figure B-5. Comparison of the Distribution of Vertical Percolation Flux (Q_z) in Fractures at 10,000 Years for a Fully Coupled Thermal-Hydrologic-Mechanical Simulation and Thermal-Hydrologic Simulation (Tptpmn Model Domain)

B.4.3 Specific Response and Basis for GEN 1.01 Comment 93

The question on carrier plume effects is interpreted to mean characteristics of the transporting fluid that are different from the characteristics of the ambient fluids (e.g., temperature, density, ionic strength, and pH) particularly those affecting sorption. Sorption has been shown to be dependent on many factors, including temperature, ionic strength, and competition between ions for sorption sites. Sorption coefficients used in *Radionuclide Transport Models Under Ambient Conditions* (BSC 2003d, Attachment I) were determined from laboratory experiments using the UE p#1 water chemistry (with a higher ionic strength than J-13 water and a Cl^- concentration of up to 130 mg/L) as an end-member composition to bracket the impact of water composition on sorption coefficients.

Simulated high Cl^- concentrations in *FY 01 Supplemental Science and Performance Analyses, Volume 1: Scientific Bases and Analyses* (BSC 2001, Figure 3.3.6-5) are the result of evaporation, leaving the surroundings quite dry. For practical purposes, at such locations where Cl^- concentrates as a result of evaporation, any radionuclide initially dissolved in fracture water would become effectively immobilized, sorption would be largely irrelevant, and its transport would be significantly limited in that region.

B.4.4 Specific Response and Basis for GEN 1.01 Comment 98

The DST THC model adequately predicts the trends in the data discussed in NRC Comment 98 (BSC 2003a, Section 7.1.7.1). Data from the DST used for comparison with model results consist of (1) analyses of water and gas samples from borehole intervals between packers

(hydrology boreholes) and (2) observations of mineral precipitation in boreholes (rock samples obtained from rock side-coring). Borehole intervals were selected based upon the availability of a long, continuous sample record and the absence of confounding factors, such as the sampling interval being too long to compare with a particular model grid block or pair of grid blocks, or boreholes being near either end of the DST and affected by three-dimensional transport. The locations of the hydrology boreholes, sampling intervals, and temperature sensors are shown in *Drift-Scale Coupled Processes (DST and THC Seepage) Models* (BSC 2003a, Figure 7.1-2).

Differences between the DST THC model predictions and the DST measurements are important to this validation. There are several reasons (listed below) why observations may disagree with predictions, and yet be consistent with validation of the DST THC model. Individual data points may not agree closely with model predictions, but model validation requirements can be met. It is important that these considerations are kept in mind when reviewing the model comparisons to measured data.

1. The DST THC model is a continuum model, using average hydrologic, thermal, and mineralogical properties for individual hydrostratigraphic units at Yucca Mountain, rather than specifically for the DST.
2. The continuum model does not simulate individual fractures, which may intersect boreholes near sampling points, their aperture and frequency resulting in different local flow rates and temperatures, thus affecting the chemistry of the gas and water samples in that interval.
3. All samples were taken from long borehole intervals (approximately 8 to 10 m long), which cross regions of large gradients in gas species concentrations (up to a few orders of magnitude) and exhibit temperature variations of tens of degrees. Furthermore, the samples are only known to have been derived from the borehole itself and may not have the same composition as the gas and liquid flowing in fractures. In addition, waters collected from boreholes have resided in the boreholes for different lengths of time, interacting with the surface of the borehole, interchanging components with the matrix, affected by gas flow and condensation in the borehole, and interacting with engineered materials. In contrast, the model results represent compositions in fractures or matrix at an instant in time.
4. The model represents a two-dimensional slice taken approximately at midlength of the DST; it does not simulate transport in the third dimension. Because the initial permeabilities and geochemical properties are unknown at every point inside the rock, a three-dimensional model would not be expected to significantly improve matches to geochemical data, because the model would still rely on average properties. Although a three-dimensional model would reduce some of the uncertainty because of slight improvements in capturing the distribution of heat, fluid, and chemical species transport, it would not yield any significant improvement in the conceptual understanding or validation of the model approach and input data. In addition, a three-dimensional model at the minimum resolution required for a reactive-transport simulation would have in excess of 100,000 grid blocks, which would be computationally infeasible (several months or more of computation time).

5. The model does not consider all deviations from planned operation. These deviations include the exact time periods of power losses, variations or uncertainty in heat losses through the bulkhead, changes in pressure owing to forced ventilation, the effect of the many boreholes on the behavior of the system, and barometric pressure changes. Because of this, and reasons 1, 2, and 4 above, the changes occurring at a particular time in the model may be shifted from that occurring in the DST by several months or more, depending on the time when the temperatures are similar or the point at which water completely evaporates.
6. Gas and water samples are affected by condensation of water vapor as the sample cools in the collection tubes from the borehole interval to the sample containers. This results in a variety of changes to the gas and water compositions. CO₂ concentrations in the gas can increase dramatically as the water vapor is preferentially removed from the gas. Many aqueous species concentrations will become lower as the sample is diluted by pure water condensed in the tubes and mixed with the water being sampled. The pH of the water may drop as the pure condensate formed under elevated partial pressures of CO₂ is mixed with the water from the borehole.

Given these considerations, and the model requirements in mind, model results cannot be expected to exactly replicate measured data, and the model predictions are considered reasonable. The criterion for model validation was that any two of the three following criteria be satisfied for a majority of the samples collected (but not all samples if conditions as given above are expected to be important):

- Observed concentrations of gas and aqueous species match predicted concentrations within an order of magnitude (e.g., one pH unit). This range is reasonable because chemical potential is proportional to the logarithm of concentration.
- The simulated trend of CO₂ over time in the sampling interval is clearly followed. “Clearly followed” is understood to mean that model and observations show the same initial trend of increase or decrease, and any observed reversal is predicted. Simulated CO₂ concentrations will be within one order of magnitude of measured data.
- Observations of mineral precipitation shall agree qualitatively with predictions of locations where mineral precipitation is most likely to occur.

B.4.5 Specific Response and Basis for GEN 1.01 Comment 110

Uncertainties affecting chemical processes in the THC Seepage Model were evaluated in *Drift-Scale Coupled Processes (DST and THC Seepage) Models* (BSC 2003a, Section 6.9). The effect of capillary pressure on chemical potentials of reacting species was not treated directly in this study, however, it is taken indirectly into account through adjustments of thermodynamic data such that ambient water compositions can be reproduced. Not accounting for this effect could potentially shift predicted concentrations of some species. The effect of capillary pressure would be larger in the rock matrix upon near-complete dryout than under ambient conditions. However, most of the fluid transport takes place in fractures where the capillarity is minimal. In addition, the potential for water–rock interactions and fluid movement is larger in zones of large

liquid saturations (reflux zone) than in nearly dried-out areas (thus, under liquid saturation/capillary pressure conditions closer to those in the ambient system than in the nearly dry system).

This uncertainty should not have a significant impact on predicted seepage water compositions given the low mobility of waters at small residual saturation in the rock matrix. Reasonable model validation against field and experimental data, as described in *Drift-Scale Coupled Processes (DST and THC Seepage) Models* (BSC 2003a, Section 7.1), indicates that this capillary effect does not need to be taken into account.

B.5 REFERENCES

B.5.1 Documents Cited

BSC (Bechtel SAIC Company) 2001. *FY 01 Supplemental Science and Performance Analyses, Volume 1: Scientific Bases and Analyses*. TDR-MGR-MD-000007 REV 00 ICN 01. Las Vegas, Nevada: Bechtel SAIC Company. ACC: MOL.20010801.0404; MOL.20010712.0062; MOL.20010815.0001.

BSC 2003a. *Drift-Scale Coupled Processes (DST and THC Seepage) Models*. MDL-NBS-HS-000001 REV 02. Las Vegas, Nevada: Bechtel SAIC Company. ACC: DOC.20030804.0004.

BSC 2003b. *In-Drift Precipitates/Salts Model*. ANL-EBS-MD-000045 REV 01. Las Vegas, Nevada: Bechtel SAIC Company. ACC: DOC.20031028.00003.

BSC 2003c. *Engineered Barrier System: Physical and Chemical Environment Model*. ANL-EBS-MD-000033 REV 02C. Las Vegas, Nevada: Bechtel SAIC Company. ACC: MOL.20031029.0034.

BSC 2003d. *Radionuclide Transport Models Under Ambient Conditions*. MDL-NBS-HS-000008 REV 01A. Las Vegas, Nevada: Bechtel SAIC Company. ACC: MOL.20030828.0326.

BSC 2003e. *Drift Scale THM Model*. MDL-NBS-HS-000017 REV00. Las Vegas, Nevada: Bechtel SAIC Company. ACC: DOC.20030818.0003.

CRWMS M&O (Civilian Radioactive Waste Management System Management and Operating Contractor) 2000a. *Total System Performance Assessment (TSPA) Model for Site Recommendation*. MDL-WIS-PA-000002 REV 00. Las Vegas, Nevada: CRWMS M&O. ACC: MOL.20001226.0003.

CRWMS M&O 2000b. *Abstraction of Drift-Scale Coupled Processes*. ANL-NBS-HS-000029 REV 00. Las Vegas, Nevada: CRWMS M&O. ACC: MOL.20000525.0371.

CRWMS M&O 2000c. *Drift-Scale Coupled Processes (DST and THC Seepage) Models*. MDL-NBS-HS-000001 REV 00. Las Vegas, Nevada: CRWMS M&O. ACC: MOL.19990721.0523.

CRWMS M&O 2001. *Drift-Scale Coupled Processes (DST and THC Seepage) Models*. MDL-NBS-HS-000001 REV 01. Las Vegas, Nevada: CRWMS M&O. ACC: MOL.20010314.0003

Drever, J.I. 1997. *The Geochemistry of Natural Waters, Surface and Groundwater Environments*. 3rd Edition. Upper Saddle River, New Jersey: Prentice Hall. TIC: 246732.

LBNL 2002. *Software Code: TOUGHREACT*. V3.0. DEC-Alpha with Unix OSF1 V5.1 and OSF1 V5.0, Sun Solaris 5.5.1, Linux Redhat 7.2. 10396-3.0-00.

Levy, S.S.; Fabryka-Martin, J.T.; Dixon, P.R.; Liu, B.; Turin, H.J.; and Wolfsberg, A.V. 1997. "Chlorine-36 Investigations of Groundwater Infiltration in the Exploratory Studies Facility at Yucca Mountain, Nevada." *Scientific Basis for Nuclear Waste Management XX, Symposium held December 2-6, 1996, Boston, Massachusetts*. Gray, W.J. and Triay, I.R., eds. 465, 901-908. Pittsburgh, Pennsylvania: Materials Research Society. TIC: 238884.

NRC (U.S. Nuclear Regulatory Commission) 2002. *Integrated Issue Resolution Status Report*. NUREG-1762. Washington, D.C.: U.S. Nuclear Regulatory Commission, Office of Nuclear Material Safety and Safeguards. TIC: 253064.

Reamer, C.W. 2001a. "U.S. Nuclear Regulatory Commission/U.S. Department of Energy Technical Exchange and Management Meeting on Evolution of the Near-Field Environment (January 9-12, 2001)." Letter from C.W. Reamer (NRC) to S. Brocoum (DOE/YMSCO), January 26, 2001, with enclosure. ACC: MOL.20010810.0033.

Reamer, C.W. 2001b. "U.S. Nuclear Regulatory Commission/U.S. Department of Energy Technical Exchange and Management Meeting on Total System Performance Assessment and Integration (August 6 through 10, 2001)." Letter from C.W. Reamer (NRC) to S. Brocoum (DOE/YMSCO), August 23, 2001, with enclosure. ACC: MOL.20011029.0281.

Reamer, C.W. and Gil, A.V. 2001. Summary Highlights of NRC/DOE Technical Exchange and Management Meeting of Range on Thermal Operating Temperatures, September 18-19, 2001. Washington, D.C.: U.S. Nuclear Regulatory Commission. ACC: MOL.20020107.0162.

Rosenberg, N.D.; Gdowski, G.E.; and Knauss, K.G. 2001. "Evaporative Chemical Evolution of Natural Waters at Yucca Mountain, Nevada." *Applied Geochemistry*, 16, (9-10), 1,231-1,240. New York, New York: Pergamon. TIC: 249879.

Schlueter, J. 2002. "Evolution of the Near-Field Environment Key Technical Agreements." Letter from J. Schlueter (NRC) to S. Brocoum (DOE/YMSCO), February 14, 2002, with enclosure. ACC: MOL.20020607.0086.

Sonnenthal, E.L. and Bodvarsson, G.S. 1999. "Constraints on the Hydrology of the Unsaturated Zone at Yucca Mountain, NV from Three-Dimensional Models of Chloride and Strontium Geochemistry." *Journal of Contaminant Hydrology*, 38, (1-3), 107-156. New York, New York: Elsevier. TIC: 244160

Yang, I.C.; Rattray, G.W.; and Yu, P. 1996. *Interpretation of Chemical and Isotopic Data from Boreholes in the Unsaturated Zone at Yucca Mountain, Nevada*. Water-Resources Investigations Report 96-4058. Denver, Colorado: U.S. Geological Survey. ACC: MOL.19980528.0216.

B.5.2 Source Data, Listed by Data Tracking Number

GS020408312272.003. Collection and Analysis of Pore Water Samples for the Period from April 2001 to February 2002. Submittal date: 04/24/2002.

LB990630123142.003. Fourth, Fifth, and Sixth Quarters TDIF Submission for the DST, September 1998 to May 1999. Submittal date: 06/30/1999.

APPENDIX C
EVALUATION OF TRACE ELEMENTS AND FLUORIDE
(RESPONSE TO ENFE 2.04)

Note Regarding the Status of Supporting Technical Information

This document was prepared using the most current information available at the time of its development. This Technical Basis Document and its appendices providing Key Technical Issue Agreement responses that were prepared using preliminary or draft information reflect the status of the Yucca Mountain Project's scientific and design bases at the time of submittal. In some cases this involved the use of draft Analysis and Model Reports (AMRs) and other draft references whose contents may change with time. Information that evolves through subsequent revisions of the AMRs and other references will be reflected in the License Application (LA) as the approved analyses of record at the time of LA submittal. Consequently, the Project will not routinely update either this Technical Basis Document or its Key Technical Issue Agreement appendices to reflect changes in the supporting references prior to submittal of the LA.

APPENDIX C

EVALUATION OF TRACE ELEMENTS AND FLUORIDE (RESPONSE TO ENFE 2.04)

This appendix provides a response for Key Technical Issue (KTI) agreement Evolution of the Near-Field Environment (ENFE) 2.04. This KTI relates to providing the technical basis for bounding the trace elements and fluoride for the geochemical environment affecting the drip shield and waste package.

C.1 KEY TECHNICAL ISSUE AGREEMENT

C.1.1 ENFE 2.04

Agreement ENFE 2.04 was reached during the U.S. Nuclear Regulatory Commission (NRC)/U.S. Department of Energy (DOE) Technical Exchange and Management Meeting on Evolution of the Near-Field Environment held January 9 to 11, 2001, in Pleasanton, California (Reamer 2001). ENFE KTI subissues 1, 2, 3, and 4 were discussed at that meeting. There have been no specific submittals to the NRC or meetings subsequent to the original technical exchange on this subject.

Wording of the agreement is as follows:

ENFE 2.04

Provide the technical basis for bounding the trace elements and fluoride for the geochemical environment affecting the drip shield and waste package, including the impact of engineered materials. The DOE will document the concentrations of trace elements and fluoride in waters that could contact the drip shield and waste package in a revision to the Environment on the Surfaces of the Drip Shield and Waste Package Outer Barrier AMR (ANL-EBS-MD-000001), which will be available in FY02. In addition, trace elements and fluoride concentrations in introduced materials in the EBS (including cement grout, structural steels, and other materials as appropriate) will be addressed in a revision to the Engineered Barrier System: Physical and Chemical Environment Model AMR (ANL-EBS-MD-000033), expected to be available in FY 02.

C.1.2 Related Key Technical Issue Agreements

Other KTI agreements related to the trace elements and fluoride considerations in the in-drift environment are CLST 1.01 (Appendix A), ENFE 2.06 (Appendix E), ENFE 2.11 (Appendix H), and ENFE 2.14 (Appendix J).

C.2 RELEVANCE TO REPOSITORY PERFORMANCE

The range of the bulk chemistry possible in the in-drift environment is important to many repository models: drip shield and waste package degradation, the chemistry within degraded packages, waste-form degradation, and radionuclide and colloid transport properties. Within the

framework of this KTI, the understanding of the in-drift environment is important because of its impact on the analyses of waste package and drip shield performance (i.e., lifetimes). Certain trace elements and fluoride (F^-) as well as other elements potentially deleterious to waste package and drip shield performance are believed to be considered adequately through the evolution of the environment on the drip shield and waste package surface sufficient to warrant their specific exclusion from the total system performance assessment (TSPA) modeling consideration.

C.3 RESPONSE

Trace elements are present in such low abundance that they are considered unlikely to significantly affect major constituent geochemistry, and therefore are not generally included in the models that determine the geochemistry of the system. However, some trace or minor elements such as fluoride may be more important to corrosion of engineered materials. The minor and trace elements that have been explicitly evaluated are those that have the potential to directly affect an engineered barrier in the engineered barrier system. The following have been evaluated in some detail and are discussed further here: F^- , bromide (Br^-), lead, and chromium.

Fluoride has been included adequately in the development of the model predicting the constituents for the in-drift geochemical environment (BSC 2003a, Sections 6.6 and 6.14). The amount of fluoride is controlled through concentrations in evaporated seepage or deliquescence water and is limited primarily by precipitation of fluorite (CaF_2) at low stages of evaporation and villiaumite (NaF) at more extreme stages of evaporation. Relative to corrosion processes on the titanium drip shield, “it is also concluded that the presence of a high concentration of $CaCl_2$ and fluoride ions will not significantly enhance the general corrosion of drip shield material under the repository conditions” (BSC 2003b, p. 96, Section 8.3).

Trace quantities of Br^- , a halide that behaves like chloride (Cl^-) on metal alloys, tend to concentrate during evaporation and have been included in models predicting the constituents for the in-drift geochemical environment (BSC 2003a, Section 6.13.4.2). These trace quantities of Br^- as they accumulate during evaporation have been determined not to affect the bulk water chemistry or the evolution of seepage brines during evaporation (see Section C.4.3).

Relative to corrosion processes on the waste package, lead has been considered in certain waste package corrosion testing environments with no impact on general or localized corrosion being seen. Lead was considered as a possibly aggressive trace element, and adequate to also represent trace elements such as arsenic and mercury relative to waste package corrosion processes (BSC 2003c, Section 6.3.4; BSC 2003d).

Other trace elements, as well as minor and major constituent elements resulting from introduced materials are considered to the extent they impact the system pH and ionic strength as a result of degradation of the stainless steels. Chromium and iron, considered major constituents of the introduced materials in the drift, and also trace elements in the seepage waters entering the drift, are specifically considered. Chromium is the most abundant of the metal additives in the steels, and it is believed that its chemical effects are similar to those from other transition metals, such as manganese, cobalt, molybdenum, and tungsten, so it is considered as a surrogate for other minor metals contained in the steels in the disposal drifts. The pH impacts of any introduced

materials normally considered trace elements in natural systems are adequately accounted for by the chromium evaluation and are considered negligible (BSC 2003a, Sections 6.8 and 7.7).

Cement grout has been removed from emplacement drift ground support in current repository design and is no longer of concern (BSC 2003e).

The information in this report is responsive to agreement ENFE 2.04 made between the DOE and NRC. The report contains the information that the DOE considers necessary for NRC review for closure of this agreement.

C.4 BASIS FOR THE RESPONSE

C.4.1 Introduction

The terms “minor” and “trace” used in reference to solutes in natural water cannot be precisely defined. Commonly, the terms are used for substances that always or nearly always occur in concentrations less than 1.0 mg/L (Hem 1985, pp. 129 to 130). Trace elements from the natural system that are potentially present in the in-drift seepage waters that have been identified and considered to be potentially problematic for the waste package and drip shield degradation are lead, arsenic, and mercury. The chemical composition of the rhyolite tuff that makes up the repository horizon is well characterized and essentially uniform in composition (Peterman and Cloke 2002). Compositions of pore waters extracted from the tuff at the repository horizon have been characterized for trace element composition. Table C-1 shows the composition of selected minor and trace elements in the pore waters extracted from cores collected in the Enhanced Characterization of the Repository Block Cross-Drift. As can be seen from Table C-1, lead and mercury concentrations and more than one-third of the arsenic concentrations are below the detection limit.

Fluoride, trace elements in seepage, and elements in introduced materials that are normally considered as trace species in natural waters may be important to certain in-drift processes yet not be significant contributors to the major ion geochemistry. In-drift processes such as corrosion and radionuclide mobility may be particularly affected because of the possible local accumulation of these elements as chemical conditions evolve in response to changes in physical conditions such as temperature and relative humidity. Most analyses presented to date have focused on the chemical reactions among major constituents because these are considered to be the primary system drivers controlling the in-drift environmental conditions. Bruno et al. (1998) also conclude in their studies of trace metals in natural systems that good characterization of the site mineralogy and a sound understanding of the main geochemical driving forces (i.e., bulk chemistry) are needed to further investigate the reactions of trace species. A summary of the work done with respect to trace elements is included below.

Table C-1. Compositions of F⁻ and Trace Elements in Enhanced Characterization of the Repository Block Pore Water Samples

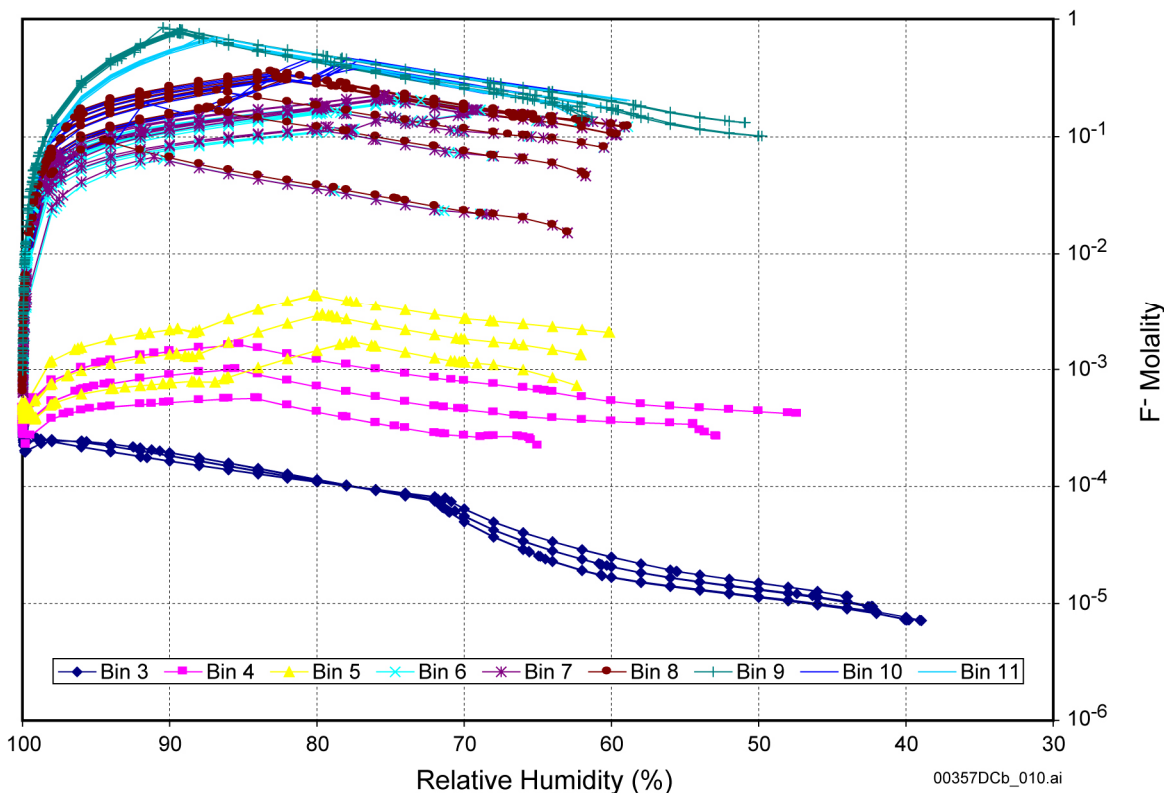
SAMPLE DESIGNATION	F	Br	Mn	Co	Zn	Rb	Sr	As	Mo	Ba	Hg	Pb	U
ECRB-SYS-CS400/3.8-4.3/UC	3.7	<1	410	<2.5	<100	41	3580	8	13	420	< 1.0	< 2.0	6.9
ECRB-SYS-CS400/5.6-6.2/UC	1.7	<1	43	<2.5	<100	30	1480	<6.0	4.8	<30	< 1.0	< 2.0	<0.3
ECRB-SYS-CS600/3.6-4.0/UC	2	<	39	<2.5	<100	16	1750	<6.0	5.3	<30	< 1.0	< 2.0	0.5
ECRB-SYS-CS1000/7.3-7.7/UC	3.4	<1	23	<2.5	<100	21	1040	<6.0	5.3	<30	< 1.0	< 2.0	0.8
ECRB-SYS-CS750/6.2-6.5/UC	1.2	<1	54	<2.5	<100	22	1160	<6.0	6.2	<30	< 1.0	< 2.0	10.3
ECRB-SYS-CS2150/5.5-6.1/UC	5.3	<0.2	38	<1.3	<100	16	1110	5.7	8.9	<15	< 1.0	< 1.0	4.1
ECRB-SYS-CS900/5.4-5.9/UC	1.7	<0.2	77	<1.3	<100	12	1980	5.4	7.4	<15	< 1.0	< 1.0	0.3
ECRB-SYS-CS850/5.1-5.6/UC	2.9	<0.2	14	<1.3	<100	9.3	1150	8.3	13	<15	< 1.0	< 1.0	2.7
ECRB-SYS-CS900/3.5-4.1/UC	2	0.3	470	1.1	<50	20	4090	3.4	9.5	<15	< 1.0	< 1.0	1.2
ECRB-SYS-CS1000/12.9-14.0/UC	2	<0.1	47	<1.0	<40	24	1110	5.4	11	61	< 1.0	< 1.0	6.9
ECRB-SYS-CS450/5.3-6.0/UC	1.1	0.4	100	<1.0	40	32	1240	5.7	5.1	46	< 1.0	< 1.0	0.1
ECRB-SYS-CS2300/4.3-4.9/UC	1.7	<0.1	260	<2.5	<100	22	590	<6.0	14	29	< 1.0	< 2.0	7.6
ECRB-SYS-CS500/12.0-16.7/UC	4.8	0.4	26	<2.5	<100	20	1100	7.6	14	<30	< 1.0	< 2.0	2.5
ECRB-SYS-CS2000/16.5-21.1/UC	11	<0.2	58	<1.3	<100	33	1390	5.9	22	<20	< 1.0	< 1.0	22.7
ECRB-SYS-CS2000/16.3-16.5/UC	6	<0.2	130	<1.3	<100	22	1260	<3.0	22	<15	1.2 ^a	< 1.0	11.3
ECRB-SYS-CS950/5.2-5.3/UC	1.9	<0.2	62	<1.8	<100	10	1240	4	3.4	<25	< 1.0	< 1.6	<0.2
ECRB-SYS-CS950/4.8-5.5/UC	4.9	<0.2	130	<1.3	<100	11	2070	3.9	4.8	<15	< 1.0	< 1.0	0.2
ECRB-SYS-CS1250/5.0-5.7/UC	3	0.2	18	<1.3	<50	22	480	11	22	42	< 1.0	< 1.0	15
ECRB-SYS-CS1250/3.4-4.0/UC	2.1	M	200	<1.0	50	29	1390	<8.0	8	150	< 1.0	< 1.0	3.6
ECRB-SYS-CS800/4.9-5.6/UC	1.6	M	34	<1.0	<25	12	1140	6.7	6.3	36	< 1.0	< 1.0	0.9
ECRB-SYS-CS700/5.5-5.8/UC	6.2	<0.1	330	<7.5	<300	22	2970	<18	18	72	< 2.5	< 6.0	6.1

Source: DTN: GS020408312272.003.

NOTE: ^a >200 ppb tungsten in sample- possible interference for mercury.
F⁻ and Br⁻ are in mg/L, all others are µg/L; M indicates not measured.

C.4.2 Fluoride

Engineered Barrier System: Physical and Chemical Environment Model (BSC 2003a, Sections 6.6 and 6.14) includes F⁻ in the chemistry of seepage waters as they evolve within the drift by applying the *In-Drift Precipitates/Salts Model* (BSC 2003f). F⁻ concentrations in evaporated seepage or deliquescence water are limited by precipitation of fluorite (CaF₂) in early stages of evaporation and by villiaumite (NaF) in more concentrated waters (BSC 2003a, Section 6.14, Table 6.14-6). The limitation in F⁻ concentration that may develop during seepage evolution also limits the role F⁻ may play in drip shield corrosion. Figure C-1 shows the range to which F⁻ can be concentrated from the evaporation of the seepage that may contact the drip shield or waste package. This range runs from about 10⁻⁵ to about 1.0 molal, and depends on the in-drift temperature, partial pressure of carbon dioxide (pCO₂), and relative humidity. The range of concentrations of F⁻ available from dust deliquescence is similar to that of the seepage (see BSC 2003a, Section 6.14.4.2). The potential impacts of F⁻ on corrosion processes have also been evaluated and found to not significantly enhance the general corrosion of the drip shield under repository conditions (BSC 2003b, Section 8.3).

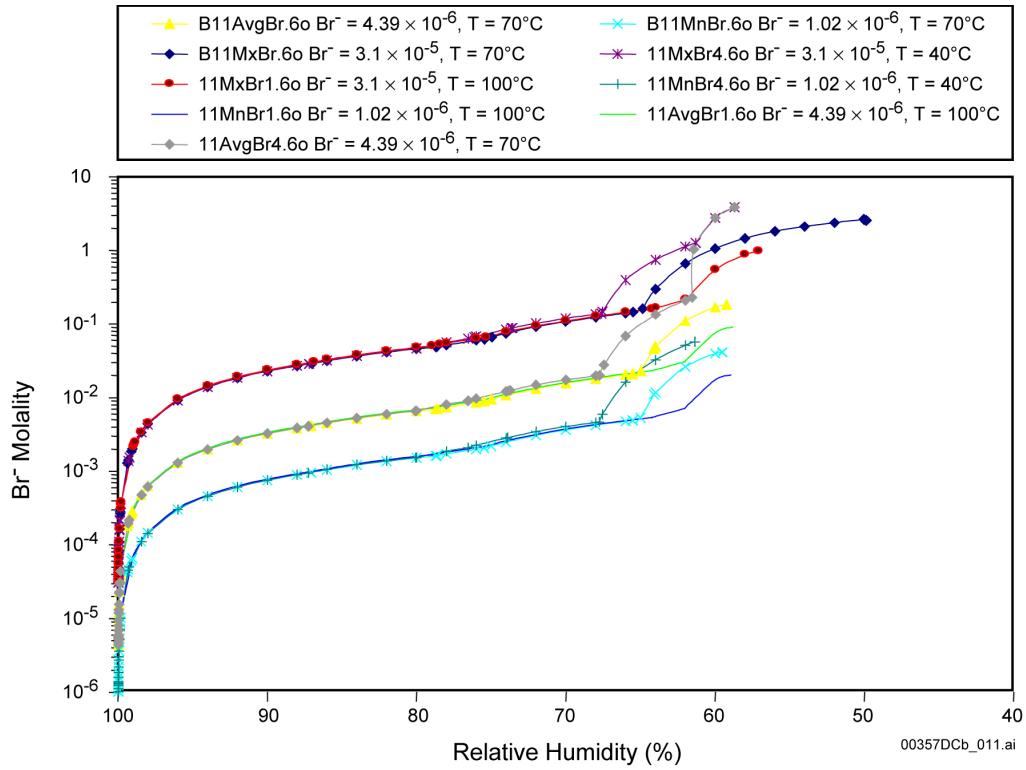


Source: BSC 2003a, Figure 6.14-27.

Figure C-1. Range of F^- Molality versus Relative Humidity for the Seepage Evaporation Lookup Tables Representing Bins 3 through 11 at Three Temperatures and Three pCO_2 Values

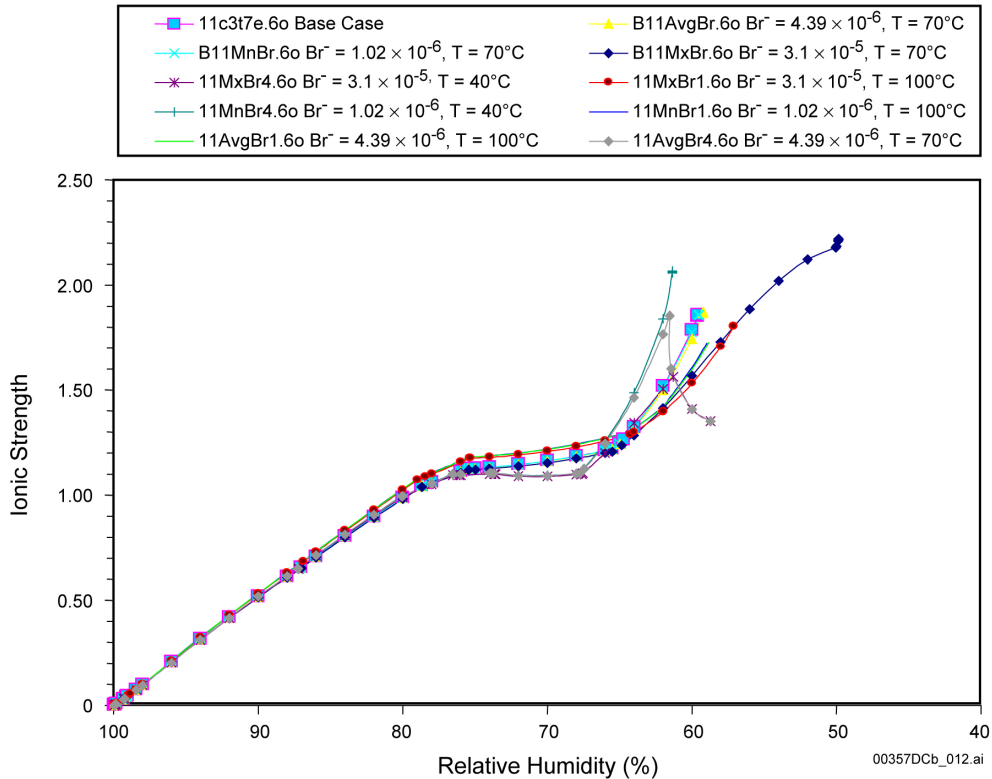
C.4.3 Bromide

In the initial seepage abstraction and lookup table generation for TSPA, the *Engineered Barrier System: Physical and Chemical Environment Model* (BSC 2003a) did not consider Br^- . As Br^- can concentrate in evaporated waters and is a halide that is known to cause corrosion in metals, an uncertainty analysis was conducted on one of the most likely seepage waters (bin 11, BSC 2003a, Section 6.13) to determine the impact on the lookup table results. Figure C-2 depicts the Br^- concentration added to the starting water covering the range in concentrations found in pore water analyses (from Table C-1), as the bin 11 seepage water is evaporated. Concentrations of Br^- can become large as evaporation progresses and brines become more and more concentrated. Below a relative humidity of about 70 percent, the results start to show the temperature dependency of the precipitation of KBr ; higher Br^- concentrations tend to be possible at lower temperatures. At very low relative humidity, the Br^- concentrations in solution can become rather high, on the order of 1 to 3 molal. The impact of Br^- on the lookup table results showed no significant change in pH or ionic strength (see Figures C-3 and C-4). Additionally, Cl^- is always dominant (most results have a Cl^-/Br^- ratio of 25 or greater; see DTN: MO0310SPAPCEUA.002); therefore, the addition of Br^- has little relative impact.



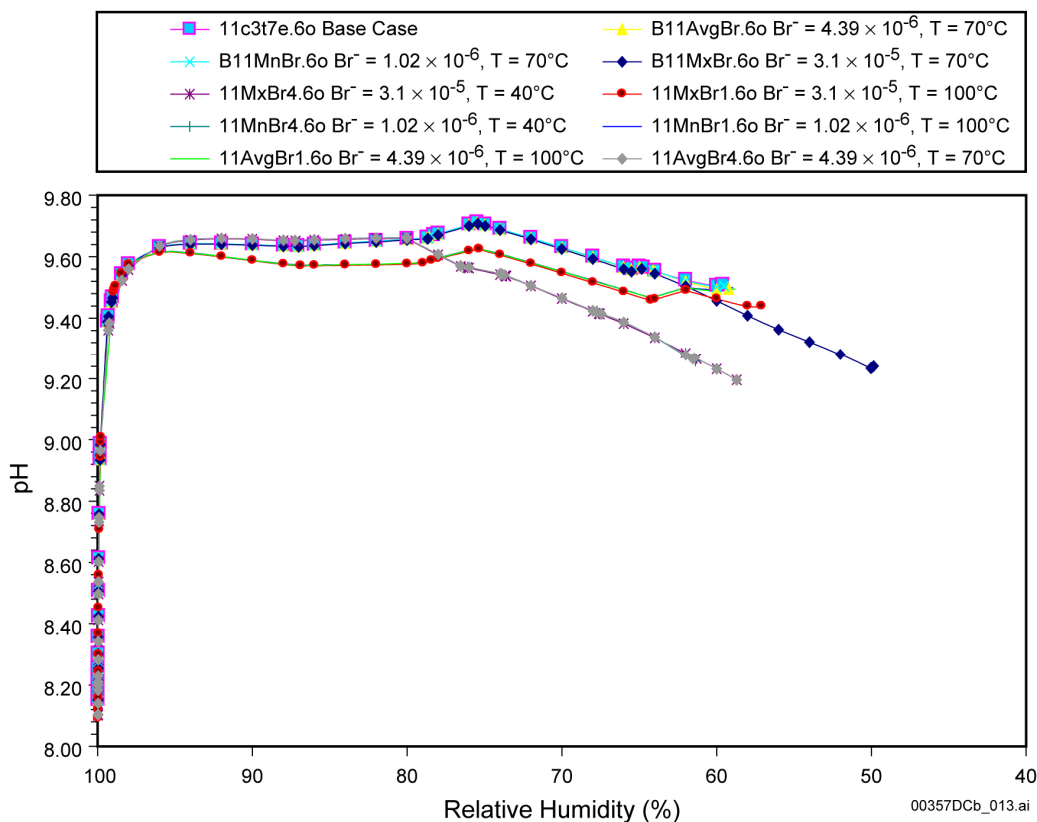
Source: BSC 2003a, Figure 6.13-1.

Figure C-2. Uncertainty in Bin 11 Seepage Compositions from the Addition of Br⁻



Source: BSC 2003a, Figure 6.13-2.

Figure C-3. Uncertainty in Bin 11 Ionic Strength Due to Adding Br⁻



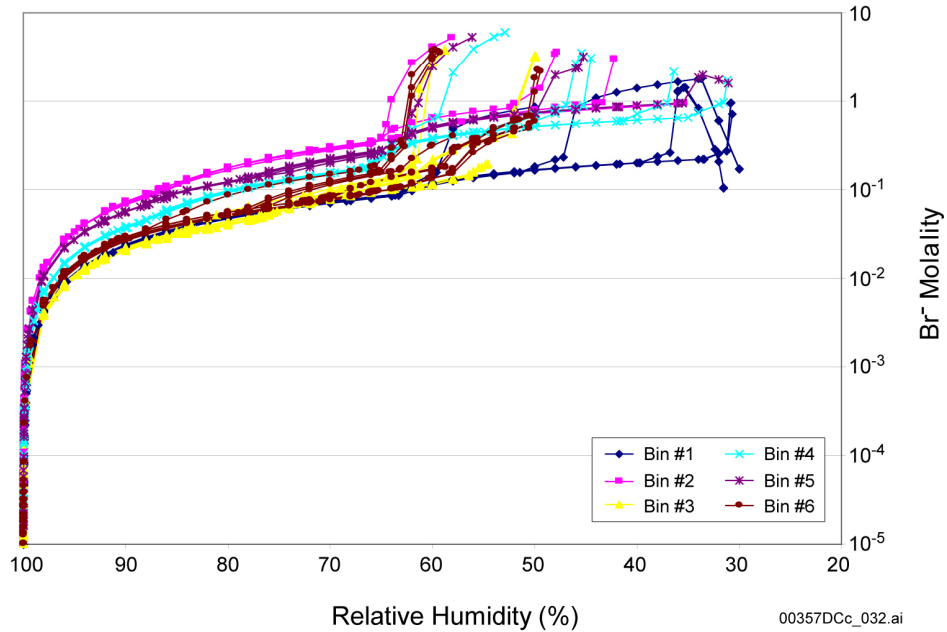
Source: BSC 2003a, Figure 6.13-3.

Figure C-4. Uncertainty in Bin 11 pH Due to Adding Br^-

For the dust deliquescence analyses in *Engineered Barrier System: Physical and Chemical Environment Model* (BSC 2003a, Section 6.13.4.2), Br^- was directly included. Figures C-5 and C-6 show the range in Br^- concentration with respect to activity of water (a_w , which is analogous to relative humidity). The range in concentration is about 1×10^{-5} to about 8 molal depending on the in-drift temperature, $p\text{CO}_2$, and relative humidity. Br^- concentration rises significantly only in the last stages of evaporative concentration, when Cl^- also increases precipitously. Either Cl^- or NO_3^- predominates throughout.

C.4.4 Chromium

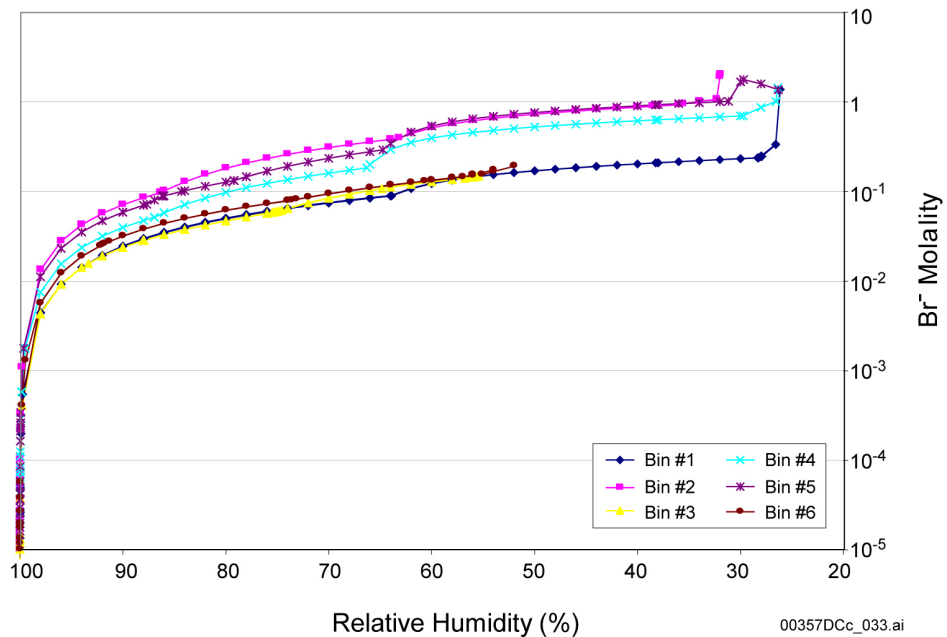
The only metallic elements specifically considered at this time are iron and chromium. It is recognized that other stainless steel components, such as nickel, may have similar effects (BSC 2003a, Section 6.8). Iron and chromium were selected for specific evaluation because of the importance of those elements in the stainless steel included in the current design and because the impact of chromium oxidation on solution chemistry is expected to be at least as severe as the effects of the other steel admixture elements. In addition, the other elements have oxidation and solution chemistry similar to the reactions exhibited by either iron or chromium in the anticipated repository conditions. Arsenic impacts (e.g., on pH) are generally considered through mass balance, and iron and chromium are present in such large proportion, neglecting other trace and minor constituents is deemed adequate.



Source: BSC 2003a, Figure 6.13-5.

NOTE: Evaporation of the waters is modeled at each possible combination of four temperatures (40°C, 70°C, 100°C, and 120°C) and three pCO_2 values (10^{-2} , 10^{-3} , and 10^{-4} bar).

Figure C-5. Comparative Evaporative Concentration of Br^- Molality in Dust Leachate Water Lookup Tables (Curves Represent Six Bins, Four Temperatures, and Three pCO_2 Values)



Source: BSC 2003a, Figure 6.13-5.

NOTE: Evaporation of the waters is modeled at 140°C and three pCO_2 values (10^{-2} , 10^{-3} , and 10^{-4} bar). Results at this temperature are preliminary pending extension of in-drift precipitates and salts model (BSC 2003f) validation.

Figure C-6. Preliminary Range of Br^- Molality versus Relative Humidity at 140°C for the Dust Leachate Lookup Tables Representing Bins 1 through 6

The effects of chromium contained in stainless steel designated for use in the repository have been evaluated in detail (BSC 2003a, Section 6.8). Geochemical modeling studies were performed using the thermodynamic database Data0.ymp.R2 (DTN: MO0302SPATHDYN.000) to determine the extent and nature of impact to seepage chemistry from the corrosion of stainless steel. The modeling study was carried out only for relative humidity values of 100 percent (no evaporation) and 98 percent. Lower relative humidity values result in solutions with ionic strength in excess of 1 molal, which is beyond the useful range of the available geochemical modeling database. Pitzer correction parameters, allowing one to model at higher ionic strengths, are not available for chromium aqueous species at this time. Results concerning the effect of chromium on solution chemistry (BSC 2003a, Section 6.8.4) demonstrate that the corrosion rate of stainless steel in expected repository conditions has only minor impact on the major chemical parameters of the solutions. These results are shown on Table C-2.

Table C-2. Absolute (Percent Relative) Differences Due to Stainless Steel Type 316L Dissolution in Bin 11 Seepage Water at 100 and 98 Percent Relative Humidity

Relative Humidity	ΔpH	$\Delta(\text{Ionic Strength})$	$\Delta(\text{Cl moles/ kg H}_2\text{O})$	$\Delta(\text{Si moles/ kg H}_2\text{O})$	$\Delta(\text{C moles/ kg H}_2\text{O})$
100	0.0000	2.0×10^{-8} (3×10^{-4})	4.2×10^{-9} (1×10^{-4})	4.6×10^{-10} (2×10^{-5})	1.1×10^{-8} (8×10^{-4})
98	0.0001	-3.8×10^{-4} (-0.05)	-1.1×10^{-4} (-0.05)	-2.4×10^{-5} (0.07)	-5.9×10^{-5} (-0.05)

Sources: BSC 2003a, Table 6.8-5; DTN: MO0306SPAPCESS.000 (in 316SS-base.xls within BaseCase.zip).

C.4.5 Lead

Certain waste package testing environments have considered the addition of lead to the system under various pH conditions (BSC 2003c, Section 6.3.7). High concentrations of lead (1,000 ppm) were evaluated in the basic saturated water conditions and showed no impact relative to stress corrosion cracking initiated crack growth rates. Additionally, lead was considered in acidic conditions (pH of about 3, with 0.005 percent lead nitrate added) in saturated acidic water brine solution, and again no effect of lead is seen on stress corrosion cracking susceptibility. Lead, as a potentially aggressive trace element, is considered to represent adequately the other trace elements of concern (mercury and arsenic) for waste package performance. With this consideration and the tests taking lead into consideration, the basis for not specifically including this set of trace elements in the abstraction to be used for TSPA for the license application is adequate (see also Appendix A).

C.4.6 Cement

Cement grout implications are no longer of concern as no cement grout is included in the emplacement drift ground support in the current repository design (BSC 2003e).

C.5 REFERENCES

C.5.1 Documents Cited

Bruno, J.; Duro, L.; de Pablo, J.; Casas, I.; Ayora, C.; Delgado, J.; Gimeno, M.J.; Peña, J.; Linklater, C.; Pérez del Villar, L.; and Gómez, P. 1998. "Estimation of the Concentrations of Trace Metals in Natural Systems. The Application of Codissolution and Coprecipitation Approaches to El Berrocal (Spain) and Poços de Caldas (Brazil)." *Chemical Geology*, 151, 277-291. Amsterdam, The Netherlands: Elsevier. TIC: 246492.

BSC (Bechtel SAIC Company) 2003a. *Engineered Barrier System: Physical and Chemical Environment Model*. ANL-EBS-MD-000033 REV 02C. Las Vegas, Nevada: Bechtel SAIC Company. ACC: MOL.20031029.0034.

BSC 2003b. *General Corrosion and Localized Corrosion of the Drip Shield*. ANL-EBS-MD-000004 REV 01. Las Vegas, Nevada: Bechtel SAIC Company. ACC: DOC.20030626.0001.

BSC 2003c. *Stress Corrosion Cracking of the Drip Shield, the Waste Package Outer Barrier, and the Stainless Steel Structural Material*. ANL-EBS-MD-000005 REV 01 ICN 00. Las Vegas, Nevada: Bechtel SAIC Company. ACC: DOC.20030717.0001.

BSC 2003d. *General Corrosion and Localized Corrosion of Waste Package Outer Barrier*. ANL-EBS-MD-000003 REV 01. Las Vegas, Nevada: Bechtel SAIC Company. ACC: DOC.20030916.0010.

BSC 2003e. *Repository Design Project, Repository/PA IED Emplacement Drift Committed Materials*. 800-IED-EBS0-00300-000-00A. Las Vegas, Nevada: Bechtel SAIC Company. ACC: ENG.20030311.0021.

BSC 2003f. *In-Drift Precipitates/Salts Model*. ANL-EBS-MD-000045 REV 01. Las Vegas, Nevada: Bechtel SAIC Company. ACC: DOC.20031028.00003.

Hem, J.D. 1985. *Study and Interpretation of the Chemical Characteristics of Natural Water*. 3rd Edition. Geological Survey Water-Supply Paper 2254. Washington, D.C.: U.S. Government Printing Office. ACC: NNA.19940427.0181.

Peterman, Z.E. and Cloke, P.L. 2002. "Geochemistry of Rock Units at the Potential Repository Level, Yucca Mountain, Nevada (includes Erratum)." *Applied Geochemistry*, 17, (6, 7), 683-698, 955-958. New York, New York: Pergamon. TIC: 252516; 252517.

Reamer, C.W. 2001. U.S. Nuclear Regulatory Commission/U.S. Department of Energy Technical Exchange and Management Meeting on Evolution of the Near-Field Environment (January 9–12, 2001). Letter from C.W. Reamer (NRC) to S. Brocoum (DOE/YMSCO), January 26, 2001, with enclosure. ACC: MOL.20010810.0033.

C.5.2 Data, Listed by Data Tracking Number

GS020408312272.003. Collection and Analysis of Pore Water Samples for the Period from April 2001 to February 2002. Submittal date: 04/24/2002.

MO0302SPATHDYN.000. Thermodynamic Data Input Files - Data0.YMP.R2. Submittal date: 02/05/2003.

MO0306SPAPCESS.000. EBS P&CE Model Stainless Steel Abstraction. Submittal date: 06/04/2003.

MO0310SPAPCEUA.002. EBS P&CE Uncertainty Analyses for $p\text{CO}_2$, Br, and MineralSuppressions. Submittal date: 10/15/2003.

INTENTIONALLY LEFT BLANK

APPENDIX D
IN-DRIFT GEOCHEMICAL DATA AND MODEL UNCERTAINTIES
(RESPONSE TO ENFE 2.05)

Note Regarding the Status of Supporting Technical Information

This document was prepared using the most current information available at the time of its development. This Technical Basis Document and its appendices providing Key Technical Issue Agreement responses that were prepared using preliminary or draft information reflect the status of the Yucca Mountain Project's scientific and design bases at the time of submittal. In some cases this involved the use of draft Analysis and Model Reports (AMRs) and other draft references whose contents may change with time. Information that evolves through subsequent revisions of the AMRs and other references will be reflected in the License Application (LA) as the approved analyses of record at the time of LA submittal. Consequently, the Project will not routinely update either this Technical Basis Document or its Key Technical Issue Agreement appendices to reflect changes in the supporting references prior to submittal of the LA.

APPENDIX D

IN-DRIFT GEOCHEMICAL DATA AND MODEL UNCERTAINTIES (RESPONSE TO ENFE 2.05)

This appendix provides a response for Key Technical Issue (KTI) agreement Evolution of the Near-Field Environment (ENFE) 2.05. This KTI relates to providing an evaluation of data and model uncertainties for in-drift geochemical environment submodels.

D.1 KEY TECHNICAL ISSUE AGREEMENT

D.1.1 ENFE 2.05

Agreement ENFE 2.05 was reached during the U.S. Nuclear Regulatory Commission (NRC)/U.S. Department of Energy (DOE) Technical Exchange and Management Meeting on Evolution of the Near-Field Environment held January 9 to 11, 2001, in Pleasanton, California (Reamer 2001). ENFE KTI subissues 1, 2, 3, and 4 were discussed at that meeting.

Wording of the agreement is as follows:

ENFE 2.05

Evaluate data and model uncertainties for specific in-drift geochemical environment submodels used in total system performance assessment (TSPA) calculations and propagate those uncertainties following the approach described in Agreement #5, Subissue 1. The DOE will evaluate data and model uncertainties for specific in-drift geochemical environment submodels used in TSPA calculations and propagate those uncertainties following the approach described in Subissue 1, Agreement #5. The DOE will document the evaluation in an update to the Engineered Barrier System: Physical and Chemical Environment Model AMR (ANL-EBS-MD-000033) (or in another future document), expected to be available in FY 02.

D.1.2 Related Key Technical Issue Agreements

Other KTI agreements related to ENFE 2.05 are ENFE 1.05 and Total System Performance Assessment and Integration (TSPAI) 3.09 (Appendix B), ENFE 2.06 (Appendix E), ENFE 2.17 (Appendix K), and TSPAI 2.02 Item 55. Agreements ENFE 1.05, TSPAI 3.09, and ENFE 2.17, like ENFE 2.05, are concerned with model and data uncertainty, the propagation of the model and data uncertainties, and the description of how these uncertainties are being accounted for in the TSPA. Agreement ENFE 2.06 describes the modeling results to which the propagated uncertainties from ENFE 2.05 are applied. The TSPAI agreement will be addressed separately in a future response addressing features, events, and processes.

D.2 RELEVANCE TO REPOSITORY PERFORMANCE

The primary consideration for understanding the in-drift environment relates to its impact on the waste package and drip shield performance (lifetimes). The environmental conditions that the

waste package and drip shield are subjected to and the chemical evolution of waters potentially contacting them play a substantial role in establishing the performance of these engineered barriers. Model and data uncertainty are key to defining the range of possible repository environments, which in turn can impact predictions of the continued effectiveness of these engineered barriers.

D.3 RESPONSE

Data and model uncertainty pertaining to the in-drift physical and chemical environment have been evaluated and propagated into model output that will be used for the TSPA. An approach parallel to that used to address ENFE 1.05 (see Appendix B) is used here to address uncertainty in the model input data and the process model. The detailed evaluation of these uncertainties is documented in *Engineered Barrier System: Physical and Chemical Environment Model* (BSC 2003a, Section 6.13), referred to as the physical and chemical environment model. The in-drift physical and chemical environment model provides water chemistry lookup tables for abstraction into TSPA. Uncertainties in output parameters are also provided to TSPA and account for both uncertainties in model input, propagated through the model from upstream process models, and sources of uncertainty internal to the physical and chemical environment model. Process models feeding the physical and chemical environment model are the *Drift-Scale Coupled Processes (DST and THC Seepage) Models* (BSC 2003b), and the *In-Drift Precipitates/Salts Model* (BSC 2003c). The first provides the compositions of seepage waters and gasses entering the drift, and the second describes the geochemical model used to model dust deliquescence and the compositional changes in the seepage waters due to in-drift processes and provides estimates of model uncertainties. Data uncertainties are addressed within these two submodels as discussed in the response to ENFE 2.17 (see Appendix K). Sources of uncertainty within the physical and chemical environment model are primarily due to discretization error arising from the binning abstraction process used to group waters with similar compositions and to determine a representative water for each group.

Additionally, sensitivity analyses were done to demonstrate that the uncertainties associated with some in-drift processes and modeling assumptions were not significant relative to the input and data uncertainties propagated into the TSPA abstraction. These analyses specifically addressed the effects of water interactions with long-lived ground support materials, the impacts of the exclusion of bromide and the use of alternate mineral suppressions in the thermodynamic modeling, and uncertainty arising when the partial pressure of carbon dioxide ($p\text{CO}_2$) is extrapolated beyond the ranges provided in the lookup tables provided to TSPA.

The information in this report is responsive to agreement ENFE 2.05 made between the DOE and NRC. The report contains the information that the DOE considers necessary for NRC review for closure of this agreement.

D.4 BASIS FOR THE RESPONSE

The primary sources of uncertainty in the physical and chemical environment model are from the input *In-Drift Precipitates/Salts Model* (BSC 2003c), to be referred to as the in-drift precipitates and salts model, and from the variability of the results introduced by the water chemistry binning

and abstraction process. A brief discussion of these uncertainties and their propagation into the TSPA is considered as applied to seepage water and dust leachate water composition.

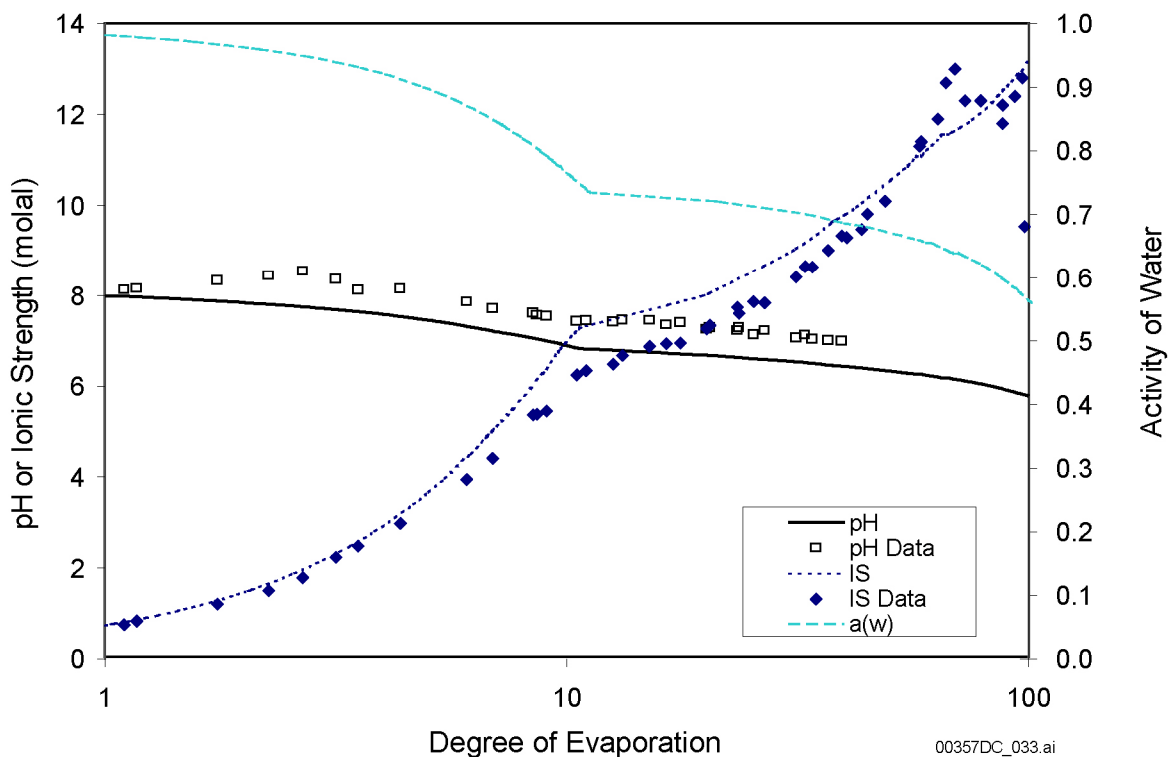
The input model uncertainties were quantified in the in-drift precipitates and salts model (BSC 2003c, Section 7), with the uncertainty of the data used for its validation fully discussed in Appendix K (Section K.4.2) and propagated throughout the physical and chemical environment model. The resulting in-drift precipitates and salts model uncertainties are presented in Table D-1, where the values represent two standard deviations (2σ), and encompass approximately 95 percent of the estimated uncertainty in these values. The values for ionic strength, Cl^- and $\text{Cl}^-/\text{NO}_3^-$ ratio are in units of relative percent difference and also determined as their log-base uncertainties. The units for pH and RH_{dp} (the relative humidity at the deliquescent point) are standard pH units and standard percent relative humidity units, respectively.

Table D-1. Input Model Uncertainty Ranges from In-Drift Precipitates and Salts Model

Output Parameter	Uncertainty (2σ)	log Uncertainty (2σ)
pH	± 1 pH unit	–
ionic strength (molal)	$\pm 30\%$	± 0.11
Cl^- (molal)	$\pm 30\%$	± 0.11
$\text{Cl}^-/\text{NO}_3^-$ (mole ratio)	$\pm 30\%$	± 0.11
RH_{dp}	$\pm 5\%$ relative humidity	–

Sources: BSC 2003c, Table 19; BSC 2003a, Table 6.13-29.

These uncertainty estimates for the in-drift precipitates and salts model are based on comparisons with the results of multicomponent evaporation experiments, sample data for evaporated seawater, handbook aqueous solubilities and deliquescence relative humidity values of simple salts, and predictions using an independent database (BSC 2003c, Section 7). An example of the validation is shown in Figure D-1, where good agreement between measurements by McCaffrey et al. (1987) and EQ6 predictions were obtained for pH and ionic strength (BSC 2003c, Section 7). The largest difference observed for pH was approximately 0.76 pH units. For ionic strength, the largest difference was approximately 15 percent, excepting the experimental sample at the highest degree of evaporation, which cannot be valid. Ionic strength must increase with evaporation or remain constant once the eutectic point is reached; the large drop in the last experimental data point is not realistic. The predicted activity of water is also plotted in this figure to show how it changes as a function of the degree of evaporation.



Source: BSC 2003c, Figure 27.

Figure D-1. EQ6 Predicted versus Measured pH and Ionic Strength from Evaporation of Inagua Seawater

Incoming seepage water and gas compositions to be used for TSPA were abstracted from the thermal-hydrologic-chemical (THC) model (BSC 2003b) using methods described in the physical and chemical environment model (BSC 2003a, Sections 6.5 and 6.6). Data uncertainty from the drift-scale test, used for validating the THC model, is discussed in Appendix K (Section K.4.1). Because all five THC model input water compositions are included in the physical and chemical environment abstraction, the range of compositions used in the physical and chemical environment model implicitly includes the effects of uncertainty and variability in the THC model (see Appendix B, ENFE 1.05 and total system performance assessment and integration TSPA 3.09, for those details). The choice of input water compositions therefore considers natural variability of pore-water compositions in the repository units, and relative spread in predicted seepage concentrations of aqueous species. The spread in CO_2 concentrations from the set of input water compositions is, in most cases, larger than the spread introduced by the THC model and model input uncertainties. See Appendix B (addressing ENFE 1.05 and TSPA 3.09) for the full description of the various uncertainties considered in the THC model and Table D-2 for the standard deviation in the predicted water compositions based upon the five input waters.

Dust leachate water compositions used for TSPA were abstracted from U.S. Geological Survey data (DTNs: MO0207EBSDUSTS.020; MO0209EBSDUST2.030) using methods very similar to that for seepage water abstraction (BSC 2003a, Sections 6.5 and 6.10).

The abstraction process model uses a binning methodology that groups chemically similar waters together. For the incoming seepage waters, there are 11 groups, or bins, and there are 6 bins for the dust leachate waters. A median representative is then selected from each group. These median waters are used to generate TSPA lookup tables. The discretization uncertainty introduced by using a median composition to represent all of the waters in the bin is quantified by the chemical distribution within each bin. The uncertainty is determined by measuring the standard deviation for each chemical parameter in each bin and is quantified as two standard deviations. These uncertainties due to the abstraction binning process model are compiled in Tables D-2 and D-3 for seepage and dust leachate waters, respectively.

Table D-2. Abstraction Uncertainty Determined for the Log of Seepage Water Lookup Tables Values

Parameter	Bin 1	Bin 2	Bin 3	Bin 4	Bin 5	Bin 6	Bin 7	Bin 8	Bin 9	Bin 10	Bin 11
±pH	0.15	0.25	0.49	0.68	0.58	0.73	0.32	0.33	0.46	0.20	1.05
±log Ionic strength	0.04	0.06	0.03	0.08	0.07	0.11	0.04	0.04	0.07	0.03	0.05
±log Cl ⁻	0.13	0.10	0.04	0.31	0.13	0.28	0.48	0.50	0.38	0.11	0.43
±log Cl ⁻ /NO ₃ ⁻	0.92	0.67	0.43	1.10	0.57	1.11	0.56	0.73	0.53	0.75	0.33

Source: BSC 2003a, Table 6.13-4.

Table D-3. Abstraction Uncertainty Determined for Log of Dust Leachate Lookup Tables Values

Parameter	Bin 1	Bin 2	Bin 3	Bin 4	Bin 5
±pH	0.44	0.10	0.38	0.27	0.25
±log Ionic strength	0.03	0.07	0.06	0.04	0.05
±log Cl ⁻	0.16	0.19	0.27	0.19	0.21
±log Cl ⁻ /NO ₃ ⁻	0.23	0.28	0.33	0.35	0.44

Source: BSC 2003a, Table 6.13-8.

NOTE: Bin 6 consists of a single water and therefore has no abstraction uncertainty.

Convolution of the uncertainty in the in-drift precipitates and salts model output that is passed to the physical and chemical environment model (Table D-1) and the uncertainty of the process model (i.e., the physical and chemical environment abstractions, Tables D-2 and D-3 from BSC 2003c, Sections 6.6 and 6.10), both of which are described as having uniform probability distributions, is calculated by taking the square root of the sum of the variances. This convolution is approximated to yield another uniform distribution for pH, log ionic strength, log Cl⁻, and log(Cl⁻/NO₃⁻). The final uncertainty values are shown in Tables D-4 and D-5 for seepage and dust leachate waters, respectively.

Table D-4. Total Uncertainty on the Total System Performance Assessment Seepage Water Lookup Tables

Parameter	Bin 1	Bin 2	Bin 3	Bin 4	Bin 5	Bin 6	Bin 7	Bin 8	Bin 9	Bin 10	Bin 11
±pH	1.01	1.03	1.11	1.21	1.16	1.26	1.05	1.05	1.10	1.02	1.45
±log ionic strength	0.12	0.13	0.12	0.14	0.13	0.16	0.12	0.12	0.13	0.12	0.12
±log Cl ⁻	0.17	0.15	0.12	0.33	0.17	0.30	0.49	0.51	0.40	0.16	0.44
±log (Cl ⁻ /NO ₃ ⁻)	0.93	0.68	0.44	1.11	0.58	1.12	0.57	0.74	0.54	0.76	0.35

Source: BSC 2003a, Table 6.13-31.

Table D-5. Total Uncertainty in the Total System Performance Assessment Dust Leachate Lookup Tables

Parameter	Bin 1	Bin 2	Bin 3	Bin 4	Bin 5	Bin 6
±pH	1.09	1.00	1.07	1.04	1.03	1.00
± log ionic strength	0.12	0.13	0.13	0.12	0.12	0.11
±log Cl ⁻	0.20	0.22	0.29	0.22	0.24	0.11
±log (Cl ⁻ /NO ₃ ⁻)	0.26	0.30	0.35	0.37	0.45	0.11

Source: BSC 2003a, Table 6.13-30.

In addition to the uncertainties applied directly to the TSPA lookup tables, a suite of specific perturbations to the seepage water process model was examined for potential impact to those results supplied to TSPA. Process model uncertainties that were specifically analyzed (BSC 2003a, Section 6.13.4) and their effects upon the TSPA lookup table outputs are summarized in Table D-6. These are described here briefly as dealing with:

- Interactions between 316L Stainless Steel and its corrosion products and the in-drift seepage waters
- The effect of bromide on model output water compositions when added to the THC seepage water compositions in amounts observed in the starting input waters
- Extrapolation of $p\text{CO}_2$ beyond the inclusive range of the lookup tables
- Mineral suppressions, where alternate suppression or inclusion of three mineral species was specifically investigated for their effect upon seepage water composition.

The uncertainties resulting from these process model perturbations are well below the overall convoluted uncertainties (Tables D-4 and D-5) and were therefore deemed nonimpacting.

Table D-6. Other Sources of Process Model Uncertainty, Evaluated as Nonimpacting and Not Propagated into TSPA

Source of Uncertainty	Maximum Calculated Deviations			
	pH	Ionic Strength	Chloride	Nitrate
316L Stainless Steel ^a	0.04	0.01 molal	Neg.	Neg.
Bromide ^b	Neg.	8%	Neg.	Neg.
pCO ₂ ^c	0.15	Neg.	Neg.	Neg.
MineralSuppressions ^d	<0.2	Neg.	Neg.	Neg.

Source: BSC 2003a, Section 6.13.4.

NOTE: "Neg." is for a qualitatively negligible uncertainty determined.

^aAnalysis limited to 98 percent relative humidity.

^bFrom BSC 2003a, Section 6.13.4.2.3.

^cUncertainty from extrapolation of pCO₂ from 1 x 10⁻² to 2 x 10⁻² bar (BSC 2003a, Section 6.13.4.3.2).

^dMaximum deviations as seen at 65 percent relative humidity from four alternate suppressions examined (BSC 2003a, Section 6.13.4.4).

D.5 REFERENCES

D.5.1 Documents Cited

BSC (Bechtel SAIC Company) 2003a. *Engineered Barrier System: Physical and Chemical Environment Model*. ANL-EBS-MD-000033 REV 02C. Las Vegas, Nevada: Bechtel SAIC Company. ACC: MOL.20031029.0034.

BSC 2003b. *Drift-Scale Coupled Processes (DST and THC Seepage) Models*. MDL-NBS-HS-000001 REV 02. Las Vegas, Nevada: Bechtel SAIC Company. ACC: DOC.20030804.0004.

BSC 2003c. *In-Drift Precipitates/Salts Model*. ANL-EBS-MD-000045 REV 01. Las Vegas, Nevada: Bechtel SAIC Company. ACC: DOC.20031028.0003.

McCaffrey, M.A.; Lazar, B.; and Holland, H.D. 1987. "The Evaporation Path of Seawater and the Coprecipitation of Br⁻ and K⁺ with Halite." *Journal of Sedimentary Petrology*, 57, (5), 928-937. Tulsa, Oklahoma: Society of Economic Paleontologists and Mineralogists. TIC: 254627.

Reamer, C.W. 2001. U.S. Nuclear Regulatory Commission/U.S. Department of Energy Technical Exchange and Management Meeting on Evolution of the Near-Field Environment (January 9–12, 2001). Letter from C.W. Reamer (NRC) to S. Brocoum (DOE/YMSCO), January 26, 2001, with enclosure. ACC: MOL.20010810.0033.

D.5.2 Data, Listed by Data Tracking Number

MO0207EBSDUSTS.020. Geochemical Composition of Dust Samples. Submittal date: 07/11/2002.

MO0209EBSDUST2.030. Geochemical Composition of Dust Samples (Phase II). Submittal date: 09/30/2002.

INTENTIONALLY LEFT BLANK

APPENDIX E

**THE RANGE OF LOCAL CHEMISTRY CONDITIONS
AT THE DRIP SHIELD AND WASTE PACKAGE SURFACES
(RESPONSE TO ENFE 2.06)**

Note Regarding the Status of Supporting Technical Information

This document was prepared using the most current information available at the time of its development. This Technical Basis Document and its appendices providing Key Technical Issue Agreement responses that were prepared using preliminary or draft information reflect the status of the Yucca Mountain Project's scientific and design bases at the time of submittal. In some cases this involved the use of draft Analysis and Model Reports (AMRs) and other draft references whose contents may change with time. Information that evolves through subsequent revisions of the AMRs and other references will be reflected in the License Application (LA) as the approved analyses of record at the time of LA submittal. Consequently, the Project will not routinely update either this Technical Basis Document or its Key Technical Issue Agreement appendices to reflect changes in the supporting references prior to submittal of the LA.

APPENDIX E

THE RANGE OF LOCAL CHEMISTRY CONDITIONS AT THE DRIP SHIELD AND WASTE PACKAGE SURFACES (RESPONSE TO ENFE 2.06)

This appendix provides a response for Key Technical Issue (KTI) agreement Evolution of the Near-Field Environment (ENFE) 2.06. This KTI relates to providing an evaluation of the impact of the range of local chemistry conditions at the drip shield and waste package.

E.1 KEY TECHNICAL ISSUE AGREEMENT

E.1.1 ENFE 2.06

Agreement ENFE 2.06 was reached during the U.S. Nuclear Regulatory Commission (NRC)/U.S. Department of Energy (DOE) Technical Exchange and Management Meeting on Evolution of the Near-Field Environment held January 9 to 12, 2001, in Pleasanton, California (Reamer 2001). ENFE KTI subissues 1, 2, 3, and 4 were discussed at that meeting. There has been no submittal related to this KTI agreement to the NRC.

Wording of the agreement is as follows:

ENFE 2.06

Evaluate the impact of the range of local chemistry (e.g., dripping of equilibrated evaporated cement leachate and corrosion products) conditions at the drip shield and waste package considering the chemical divide phenomena that may propagate small uncertainties into large effects. The DOE will evaluate the range of local chemical conditions at the drip shield and waste package (e.g., local variations in water composition associated with cement leaching or the presence of corrosion products), considering potential evaporative concentration and the chemical divide effect whereby small differences in initial composition could cause large differences in brine characteristics. This evaluation will be documented in a revision to the Engineered Barrier System: Physical and Chemical Environment Model AMR (ANL-EBS-MD-000033), expected to be available in FY02.

E.1.2 Related Key Technical Issue Agreements

Other KTI agreements related to ENFE 2.06 are CLST 1.01 (Appendix A), ENFE 2.04 (Appendix C), ENFE 2.05 (Appendix D), ENFE 2.09 and ENFE 2.15 (Appendix F), ENFE 2.10 (Appendix G), ENFE 2.14 (Appendix J), and TSPA 2.02 items 42, 54, 60, J-3, and J-9. The TSPA agreement will be addressed separately in a future response addressing features, events, and processes.

E.2 RELEVANCE TO REPOSITORY PERFORMANCE

In the broad sense, understanding of the range of local chemistry possible in the in-drift environment is important to drip shield and waste package degradation, to the chemistry within degraded packages, to waste-form degradation, and to radionuclide and colloid transport properties. Within the framework of this KTI, understanding the in-drift environment is important because of its impact on the waste package and drip shield performance (lifetimes). The range of water chemistries that may contact the waste package and drip shield have the potential to substantially impact the performance of these engineered barriers, which in turn could increase the risk significance for total system performance assessment (TSPA).

E.3 RESPONSE

Chemical conditions on the drip shield and waste package surfaces are established by the chemistry of water leaving the host rock as modified by reactions with drift support materials and in-drift gases, by evaporation from warmer drip shield and waste package surfaces, and by microbial activity. Aqueous solutions will also form by deliquescence of dust on drip shields and waste packages. To develop an understanding of changes in water chemistry due to these processes, to establish a basis for geochemical modeling of water chemical evolution, and to provide data tables for TSPA purposes, the relationship between water chemistry and relative humidity has been established in *Engineered Barrier System: Physical and Chemical Environment Model* (BSC 2003a) and *Environment on the Surfaces of Drip Shield and Waste Package Outer Barrier* (BSC 2003b). The primary modeling tool used to investigate the evolution of in-drift chemical environments is the *In-Drift Precipitates/Salts Model* (BSC 2003c). Both the in-drift precipitates and salts model and the engineered barrier system physical and chemical environment model use the conceptual model of chemical divides to explain the chemical evolution of evaporating seepage waters and the composition of brines forming by dust deliquescence. Additional information about the range of composition of waters that could contact the drip shield or waste package is provided in the response to ENFE 2.10 (see Appendix G). The effects of dust are summarized in the response to KTI agreement ENFE 2.13 (see Appendix I).

The effects of cementitious grout were not included in this response because grouted rock bolts are not part of the emplacement drift ground support in the current repository design.

The information in this report is responsive to agreement ENFE 2.06 made between the DOE and NRC. The report contains the information that DOE considers necessary for NRC review for closure of this agreement.

E.4 BASIS FOR THE RESPONSE

E.4.1 Introduction

Evaporation processes are particularly important in establishing the chemistry of fluids present at a given time. The extent to which these processes occur depends on the relative humidity in the drift because of the equivalence of the thermodynamic activity of water in a solution and the relative humidity of the gas phase with which it is in equilibrium (BSC 2003b, Section 6.3). The activity of water in a solution is controlled by its composition and solute concentration, so that

the relative humidity corresponding to a solution decreases as its total solute content increases. The chemistry of water modified by evaporation has been abstracted in terms of the relative humidity.

During evaporation, not only does the salinity of a water increase, lowering the thermodynamic activity of water and the corresponding relative humidity, but the ratio of major dissolved ions also changes as different mineral species become saturated and precipitate out.

E.4.2 Chemical Divides

As seepage waters make their way into the drift, their chemical composition can significantly change by evaporation and mineral precipitation. If the relative proportion of the cationic and anionic species in a precipitated mineral varies from the proportion of those ions in solution, the ratio of those ions in the solution will change as evaporation and precipitation continues. The concentrations of the two ions diverge, and a “chemical divide” develops. The basis of a chemical divide is according to Drever (1988, p. 235): “whenever a binary salt is precipitated during evaporation, and the effective ratio of the two ions in the salt is different from the ratio of these ions in solution, further evaporation will result in an increase in the concentration of the ion present in greater relative concentration in solution and a decrease in the concentration of the ion present in lower relative concentration.”

The chemical divide phenomenon provides a formalism for establishing the types of brines and precipitating solids that will result when waters of various initial compositions evaporate on the surface of the drip shield or waste package. The principles underlying this phenomenon are straightforward, but their manifestation in waters with a number of dissolved constituents, such as will be found in the drifts, is more complex. A chemically simple water will be used to illustrate the principles of chemical divides.

Consider a solution containing only Na^+ , Ca^{2+} , Cl^- , SO_4^{2-} , and CO_3 (in the context of this appendix, “ CO_3 ” indicates total aqueous carbonate, comprising $\text{CO}_2(\text{aq})$, HCO_3^- , and CO_3^{2-}). As it evaporates, concentrations of all solutes will increase equally until the solution becomes saturated with the least soluble solid that can be formed from the dissolved constituents. For most waters, this solid will be CaCO_3 . As evaporation continues, this solid will continue to precipitate, depleting the solution in both Ca^{2+} and CO_3 until the concentration of one of them has been reduced essentially to zero. If the amount of Ca^{2+} (in equivalents) is greater than the CO_3 -alkalinity in the starting solution, virtually all the CO_3 -alkalinity will be lost into the solid, leaving a Na-Ca-Cl- SO_4 solution. If the CO_3 -alkalinity is greater than the amount of Ca^{2+} in the starting solution, virtually all the Ca^{2+} will be lost into the solid, leaving a Na-Cl- SO_4 - CO_3 solution.

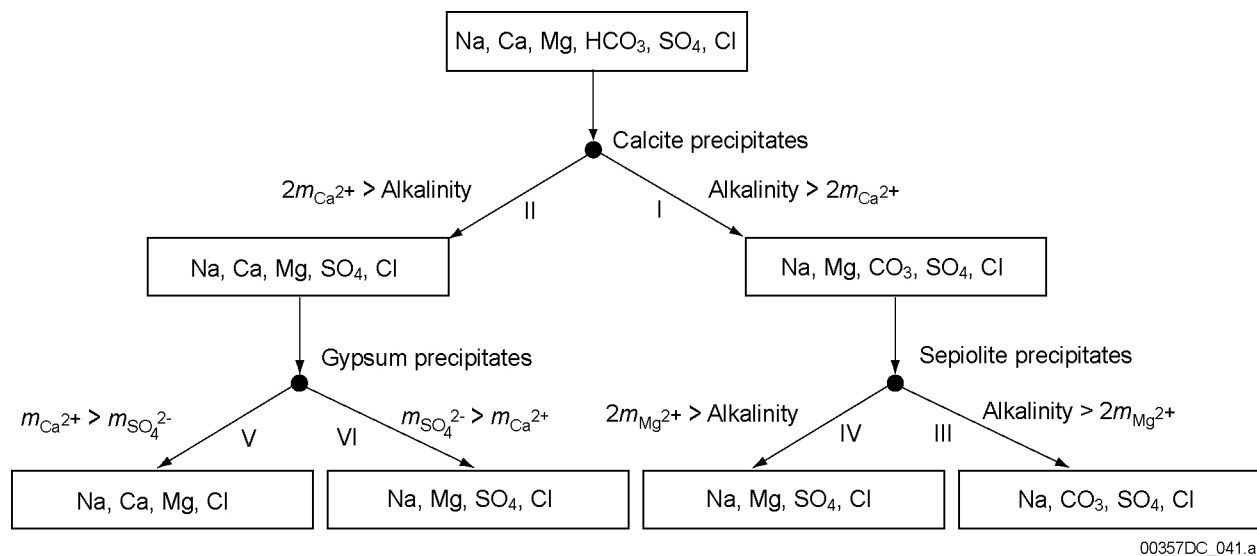
When two ions are removed from an evaporating solution by precipitation, the concentration of one will build up in the solution while that of the other will decrease to virtually zero. The criterion for this illustrative divide is whether Ca^{2+} is greater than or less than CO_3 -alkalinity. (Should Ca^{2+} be equal to CO_3 -alkalinity, the concentrations of both will approach zero together.)

The illustration can be continued with the case where Ca^{2+} is greater than CO_3 -alkalinity, leading to a Na-Ca-Cl- SO_4 solution. The next solid to reach saturation with continuing evaporation is

likely to be a calcium sulfate phase (gypsum, $\text{CaSO}_4 \cdot 2\text{H}_2\text{O}$, or anhydrite, CaSO_4). Precipitation of this solid will lead to depletion of either Ca^{2+} or SO_4^{2-} depending on their ratio at the stage where precipitation begins. If the amount of Ca^{2+} is greater than the amount of SO_4^{2-} in the initial solution, virtually all the SO_4^{2-} will be lost into the solid, leaving a Na-Ca-Cl solution. If the amount of SO_4^{2-} is greater than the amount of Ca^{2+} in the initial solution, virtually all the Ca^{2+} will be lost into the solid, leaving a Na-Cl- SO_4 solution.

The description of chemical divides, represents a simplified system. The concept of chemical divides was developed to describe natural stream and spring waters evaporating to form saline lakes, which occur with a variety of water chemical types. Figure E-1 shows the minerals that precipitate and the resulting divides, leading to a suite of natural saline lake waters. The in-drift waters that may evaporate to form brines on drip shield and waste package surfaces will have components in addition to those needed to model lake evolution. Furthermore, they may have compositions that will lead to divides that are unimportant for natural surface waters. The additional components include F^- , which may lead to CaF_2 solids, and NO_3^- , which may lead to high NO_3^- concentrations in residual brines. High Na^+ or Cl^- relative concentrations, which were specifically excluded in the water used the simplified for illustration above, can lead to early precipitation of NaCl.

Chemical divides are a function of chemical equilibrium and are implicitly included in all geochemical modeling done in *Engineered Barrier System: Physical and Chemical Environment Model* (BSC 2003a) and *In-Drift Precipitates/Salts Model* (BSC 2003c).



Source: Drever 1988, p. 236.

Figure E-1. Simplified Chemical Divides Diagram Based on Evaporative Concentration to Form Natural Lake Waters

E.4.3 Evaluation Methodology

The primary boundary condition for engineered barrier system chemical models are the composition of seepage waters entering the drift through time and the predicted fluxes of O₂ and CO₂ gas into the drift. These compositions are modeled in *Drift-Scale Coupled Processes (DST and THC Seepage) Models* (BSC 2003d). The output of the thermal-hydrologic-chemical (THC) seepage model is based on the design basis thermal load and thermal decay rate using five input pore waters that broadly cover the range of pore water variability and uncertainty within the repository horizon. A set of five THC seepage model outputs are used as input to *Engineered Barrier System: Physical and Chemical Environment Model* (BSC 2003a) to represent the temporal and spatial range of seepage water and gas phase compositions likely to enter the drift. The remaining engineered barrier system chemistry model boundary conditions, in-drift temperature and relative humidity, are calculated by the multiscale thermohydrologic model (BSC 2003e). These temperature and relative humidity values are the same in-drift environmental conditions used in the TSPA model.

The five complete sets of drift-scale seepage THC modeling results were based on five waters selected to represent the spread of potential pore water compositions that serve as starting waters for the drift-scale THC seepage modeling. These waters are designated W0, W4, W5, W6, and W7. Outputs of five THC seepage model runs using each of these waters as input cover the expected range of spatial and temporal variability and uncertainty in the THC seepage model. Each of the five sets of results includes about 3,600 water chemistries distributed over locations around the drift at 50 distributed points in time over a 100,000-year modeling period. This very large number of possible input water chemistries was abstracted by selecting representative waters from each run, normalizing their chemistries so they could be compared, and grouping them into similar water types (bins) to derive the water chemistry lookup tables used by the TSPA model.

The abstraction methodology has five steps:

- **Step 1**—Selection of which THC model grid nodes and locations are to provide the representative seepage water composition (BSC 2003a, Section 6.6.2). Before the selection of grid nodes (1 through 6), saturation zones (high saturation or wetting front), matrix or fracture waters, and spatial locations (crown, side, and base) occur, there are 18,000 discrete water compositions. The abstraction process selected waters from the crown, fracture, and wetting front at node 4 and from the base, matrix, and wetting front at node 4. Node 4 is the fourth closest calculational node to the drift center that is determined to be “wet.” This reduces the 18,000 chemistries to 500. At this point, a data simplification (one water each selected to represent the 0- to 50-year and 20,000- to 100,000-year periods) allows for the removal of about 14 discrete waters with similar chemistries, providing about 36 time-dependent water chemistries for use with each location (crown and base) and water (W0, W4, W5, W6, and W7). This abstraction process yields 368 water compositions. Because the water at these locations and nodes, over time, represents various stages of evaporation, Step 2 calls for evaporating these waters to a common activity of water to form a normalized basis of comparison.

- **Step 2**—Use *In-Drift Precipitates/Salts Model* (BSC 2003c) to calculate compositions that result from evaporating the seepage waters identified in Step 1 to a common water activity equal to 0.65 (BSC 2003a, Section 6.6.3). This step characterizes the seepage compositions by chemical properties of the waters they yield when concentrated by evaporation, the in-drift process of concern. In other words, at a common water activity of 0.65, many (if not all) of the chemical divides of interest will have been encountered during the evaporation process. As the EQ6 software simulates evaporation and mineral precipitation, the composition of the aqueous phase changes. The evolutionary pathway that the brine follows, and the final brine composition, is a function of the initial composition of the water, of the minerals that precipitate out, and of the resulting chemical divides. It is these chemical divides that determine the compositional path followed by the water during evaporation, as discussed in Section E.4.2, above.
- **Step 3**—Sort the evaporated seepage water compositions from Step 2 into groups that exhibit similar chemical characteristics and use these to bin the original seepage water compositions from Step 1 (BSC 2003a, Section 6.6.4). The result is a set of seepage water composition bins, each populated with compositions that yield chemically similar solutions after they are concentrated by evaporation. This step is where chemical divides are used explicitly as rationale for the choice of binning criteria.
- **Step 4**—Identify the median water composition in each bin and use it as an approximation for all the seepage water compositions in the bin (BSC 2003a, Section 6.6.5). This approach uses the statistical median of the group or bin established in Step 3. For each aqueous parameter of interest (i.e., pH, Cl^- , F^- , NO_3^- , etc.), the statistical median is used as a target whereby the water compositions are evaluated to determine which water is nearest the median value. Those waters with the nearest value are flagged and the number of flags counted so that the median water selected is the water with the most flags. This is done so that an actual THC seepage model water composition is used and not a statistically calculated composition. This approach maintains consistency with the EQ6 evaporation modeling results. In addition, it maintains charge balance and avoids the need to add ions such as Na^+ or Cl^- to re-establish charge balance during speciation calculations. Adding Na^+ or Cl^- could change the ultimate compositional character of the brines on the waste package.
- **Step 5**—Approximate each THC output seepage water composition time history with a time-sequence of median bin compositions from Step 4 (BSC 2003a, Section 6.6.6). These time sequences are shown on Figure E-2. This figure was used to create a time-integrated probability of occurrence of waters of each bin and initial water type for a 20,000-year time interval. The results for crown seepage waters are shown in Table E-1.

Step 1 reduces the 18,000 input waters to 368. Steps 2 through 4 reduce the 368 input waters to 11 representative waters. These 11 waters are then mapped back to the actual THC seepage results in Step 5. The binning of the evaporated waters called for in Step 3 makes use of the chemical divide phenomenon by applying the following eight criteria:

1. Total aqueous calcium molality greater than 0.1 molal?
2. Total aqueous carbonate molality greater than 0.1 molal?
3. Total aqueous calcium molality less than total aqueous sodium molality?
4. Total aqueous calcium molality greater than total aqueous potassium molality?
5. Total aqueous nitrate molality greater than total aqueous carbonate molality?
6. Total aqueous fluoride molality less than 0.1 molal?
7. Total aqueous fluoride molality less than 0.03 molal?
8. Total aqueous sulfate molality greater than 1 molal?

These 11 waters (see Table E-2) are used to cover the entire span of seepage waters entering the drift and are further discussed in Section E.4.5.

Dust leachate waters extracted from dust samples collected in the Exploratory Studies Facility were binned using a similar process to produce six likely compositions for brines formed by deliquescence (BSC 2003a, Section 6.10).

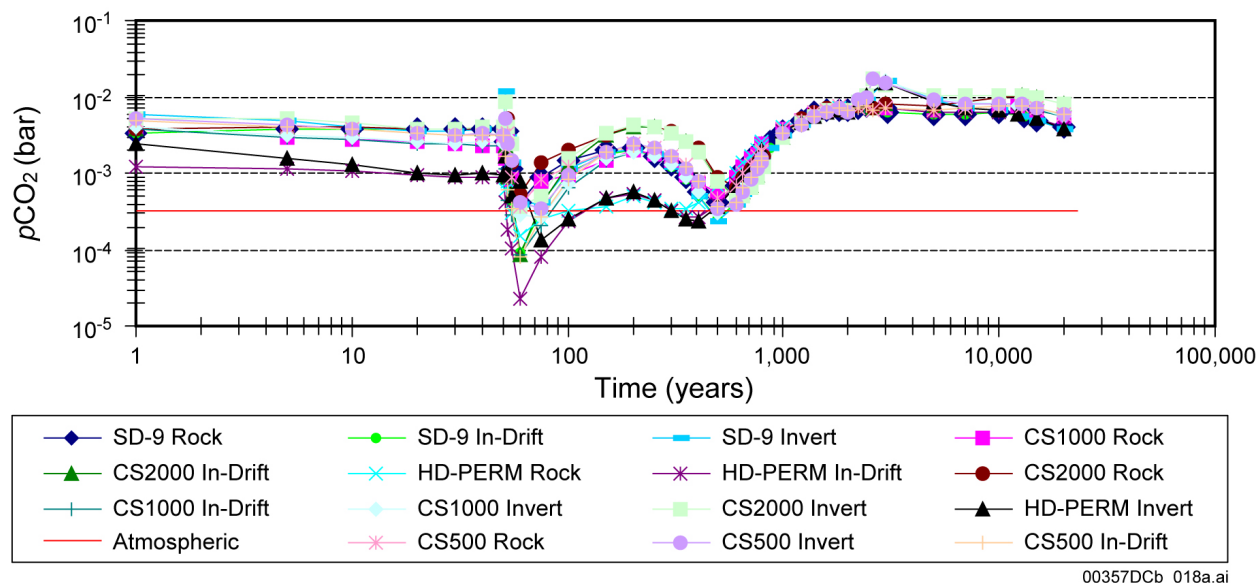
The evolution of the in-drift gas composition and temperature was also examined to produce tables of partial pressure of carbon dioxide ($p\text{CO}_2$) values as functions of time. The $p\text{CO}_2$ values within the drift vary with time and differ for each of the five starting water compositions. Values were abstracted from the THC seepage model outputs from which the water chemistry abstractions were taken and are plotted as a function of time (see Figure E-3). Note that only the in-drift values are used for modeling water chemistries on waste packages or drip shields.

Table E-2. Compositions of the Binned Input Waters

Species	Bin 1	Bin 2	Bin 3	Bin 4	Bin 5	Bin 6	Bin 7	Bin 8	Bin 9	Bin 10	Bin 11
Water/ File Name	w7bf4/ 75.60	w0bf4/ 250.60	w0bf4/ 650.60	w4bf4/ 600.60	w7tf4/ 300.60	w0tf4/ 7004.60	w4bf4/ 10006.60	w5tf4/ 20013.60	w6tf4/ 51.60	w5bf4/ 10006.60	w4tf4/ 300.60
T (°C)	111.9	109.1	104.3	104.9	95.62	65.10	56.34	40.18	91.78	56.34	95.61
pH	7.407	7.583	7.615	7.896	7.634	7.70	7.768	7.94	8.139	7.815	7.759
Ca ²⁺	1.75×10^{-2}	6.49×10^{-3}	2.14×10^{-3}	1.08×10^{-3}	1.36×10^{-3}	4.20×10^{-4}	4.46×10^{-4}	5.73×10^{-4}	7.24×10^{-5}	3.52×10^{-4}	3.34×10^{-4}
Mg ²⁺	1.70×10^{-5}	2.95×10^{-6}	4.13×10^{-6}	5.75×10^{-7}	1.13×10^{-5}	4.82×10^{-5}	5.52×10^{-5}	8.51×10^{-5}	2.54×10^{-7}	4.31×10^{-5}	6.34×10^{-6}
Na ⁺	3.89×10^{-3}	2.63×10^{-3}	2.67×10^{-3}	1.26×10^{-3}	5.53×10^{-3}	8.09×10^{-3}	7.65×10^{-3}	7.31×10^{-3}	4.27×10^{-3}	6.82×10^{-3}	4.80×10^{-3}
Cl ⁻	2.01×10^{-2}	5.02×10^{-3}	3.35×10^{-3}	1.03×10^{-3}	3.28×10^{-3}	3.32×10^{-3}	7.44×10^{-4}	5.61×10^{-4}	7.34×10^{-4}	6.00×10^{-4}	1.30×10^{-3}
SiO ₂ (aq)	9.42×10^{-3}	7.42×10^{-3}	6.96×10^{-3}	7.38×10^{-3}	1.22×10^{-2}	2.90×10^{-3}	2.46×10^{-3}	1.79×10^{-3}	4.15×10^{-3}	2.47×10^{-3}	1.19×10^{-2}
CO ₃	5.57×10^{-5}	9.06×10^{-5}	1.95×10^{-4}	1.64×10^{-4}	4.18×10^{-4}	2.93×10^{-3}	6.72×10^{-3}	6.92×10^{-3}	2.04×10^{-3}	5.74×10^{-3}	1.13×10^{-3}
SO ₄ ²⁻	8.87×10^{-3}	4.89×10^{-3}	1.50×10^{-3}	5.88×10^{-4}	1.77×10^{-3}	1.21×10^{-3}	4.12×10^{-4}	3.55×10^{-4}	1.18×10^{-4}	3.80×10^{-4}	7.29×10^{-4}
K ⁺	8.68×10^{-4}	5.40×10^{-4}	5.00×10^{-4}	2.38×10^{-4}	8.68×10^{-4}	6.25×10^{-4}	4.67×10^{-4}	2.76×10^{-4}	5.02×10^{-4}	4.17×10^{-4}	7.50×10^{-4}
AlO ₂ ⁻	3.27×10^{-8}	7.08×10^{-8}	5.02×10^{-8}	9.97×10^{-8}	8.03×10^{-10}	5.36×10^{-9}	3.62×10^{-9}	1.50×10^{-9}	6.09×10^{-8}	4.03×10^{-9}	1.42×10^{-9}
F ⁻	1.93×10^{-4}	2.46×10^{-4}	3.48×10^{-4}	4.28×10^{-4}	1.00×10^{-3}	8.26×10^{-4}	7.81×10^{-4}	6.43×10^{-4}	9.77×10^{-4}	8.61×10^{-4}	1.38×10^{-3}
NO ₃ ⁻	1.30×10^{-3}	5.46×10^{-4}	1.83×10^{-4}	1.33×10^{-4}	2.22×10^{-4}	1.04×10^{-4}	6.87×10^{-5}	3.97×10^{-5}	3.10×10^{-4}	4.25×10^{-5}	1.26×10^{-4}
CO ₂ (g)(bar)	3.89×10^{-4}	4.93×10^{-4}	1.04×10^{-3}	4.88×10^{-4}	1.88×10^{-3}	7.06×10^{-3}	1.19×10^{-2}	6.34×10^{-3}	2.94×10^{-3}	9.19×10^{-3}	4.06×10^{-3}
log CO ₂ (g)	-3.410	-3.307	-2.984	-3.312	-2.726	-2.151	-1.926	-2.198	-2.532	-2.037	-2.392

Source: BSC 2003a, Table 6.6-5.

NOTE: Unless otherwise marked, units are in moles per kilogram of water. CO₃ represents total aqueous carbonate, comprising CO₂(aq), HCO₃⁻, and CO₃²⁻.



Source: BSC 2003a, Figure 6.7-7.

NOTE: HD-PERM is W0; CS2000 is W4; CS1000 is W5; SD-9 is W6; CS500 is W7.

Figure E-3. $p\text{CO}_2$ Concentration in the Drift, the Invert, and Near-Drift Environment through Time

The effects of in-drift materials on the water chemistry and gas composition in the drift were also examined, as called for by the KTI agreement. The KTI agreement called for analyses of the effects of cement and corrosion products on seepage water composition. The cement analysis was not performed because the repository design no longer includes grouted rock bolts (BSC 2003f). The possible effects of corrosion products on the in-drift water and gas compositions were determined.

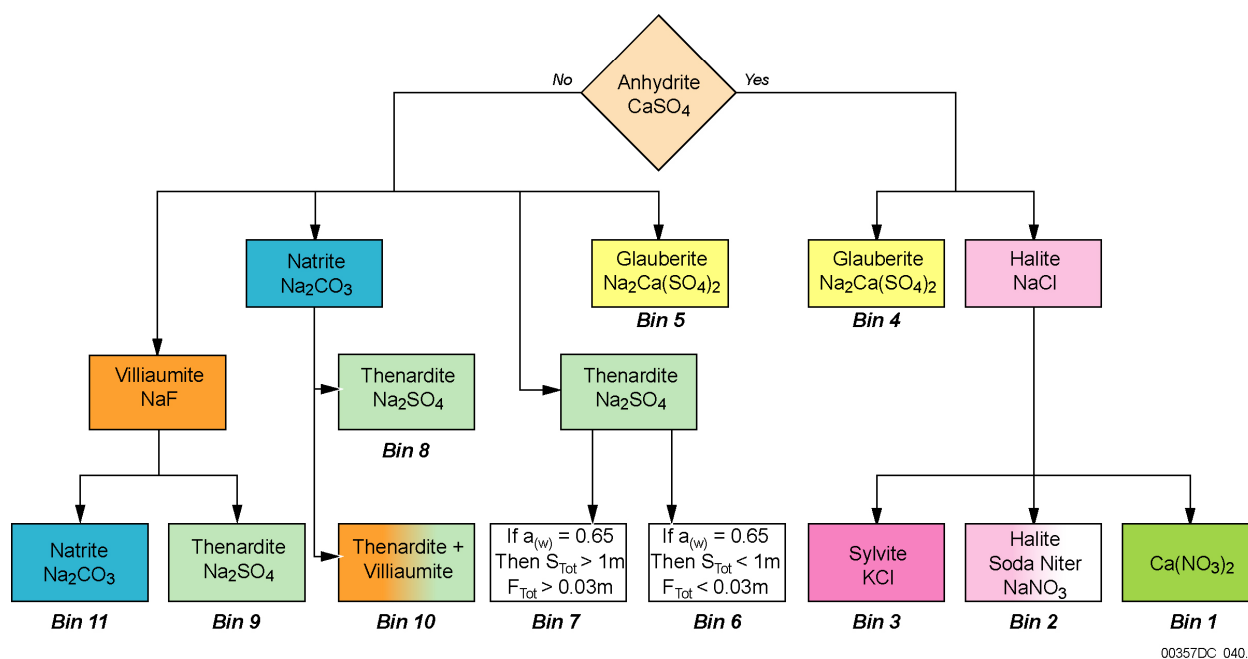
Estimated corrosion rates and longevities for the in-drift committed materials are provided in *Engineered Barrier System: Physical and Chemical Environment Model* (BSC 2003a). The committed materials fall into three broad categories: those materials with relatively short lifetimes, which could not affect seepage compositions in the drift for more than a few hundred years (i.e., carbon steel); those with such long lifetimes that potential interactions with seepage water are minimal, and the material can be considered inert (i.e., Alloy 22 or titanium); and those materials with intermediate lifetimes that could have a potential impact on water chemistry by active corrosion (i.e., 316L stainless steel). Introduced materials are also discussed in the response to ENFE 2.04 (Appendix C) and the response to ENFE 2.14 (Appendix J). Modeling corrosion and dissolution of 316L stainless steel material shows that the solubilities of iron and chromium, the major constituents of 316L stainless steel, are low enough that the maximum differences in drift water chemistry (i.e., pH, ionic strength, Cl^- , $\text{SiO}_2(\text{aq})$, and total aqueous carbonate) due to its corrosion would be less than 0.1 percent (BSC 2003a, Section 6.8).

The rate of corrosion of introduced materials and the level of microbial activity in the drift were evaluated to determine whether these processes could consume enough O_2 to produce anoxic conditions within the drifts (BSC 2003a, Section 6.7). The results indicate that, except possibly during the first few hundred years after closure (when the mild carbon steel ground support components are corroding), oxic conditions would be maintained in the drift. The analysis also

concluded that CO₂ production from in-drift microbial communities could not significantly affect the partial pressure of CO₂ in the drift. The variability of $p\text{CO}_2$ in the THC seepage model output, as used in the engineered barrier system chemistry models, is great enough to capture any fluctuations that might occur due to microbial respiration.

E.4.4 Chemical Divides and Binning Results

As discussed above, the five abstraction steps resulted in 11 starting seepage water compositions. These 11 starting waters (see Table E-2) are used to cover the entire span of seepage waters entering the drift. Evaporation of these waters to dryness was modeled and the precipitating minerals giving rise to the chemical divides were noted. Figure E-4 shows the minerals that account for each divide leading to the various bins. As is demonstrated, the chemical divide phenomena explain the formation of the 11 distinct groups of water chemistry. Note that this figure, unlike the preceding figure for surface waters, does not directly include magnesium. This element is understood to be lost from solution by precipitation of a silicate mineral such as sepiolite. This figure represents the chemical divides that occur after calcite (CaCO₃), fluorite (CaF₂), sepiolite (Mg₄Si₆O₁₅(OH)₂·6H₂O), stellerite (Ca₂A₁₄Si₁₄O₃₆·14H₂O), erionite (K_{1.5}Na_{0.9}Ca_{0.9}A_{14.2}Si_{13.8}O₃₆·13H₂O), and SiO₂(am) have precipitated.



Source: BSC 2003a, Figure 6.14-14.

NOTE: Previously precipitating minerals: calcite, fluorite, sepiolite, stellerite, erionite, SiO₂(am). Bin 6 and Bin 7 do not tie directly to a precipitating mineral that defines the bin. The items listed are the binning criteria that differentiate the two bins; see BSC 2003a, Table 6.6-3.

Figure E-4. Flow Diagram Showing Some of the Precipitated Minerals and Chemical Divides Associated with Each of the 11 Seepage Bins

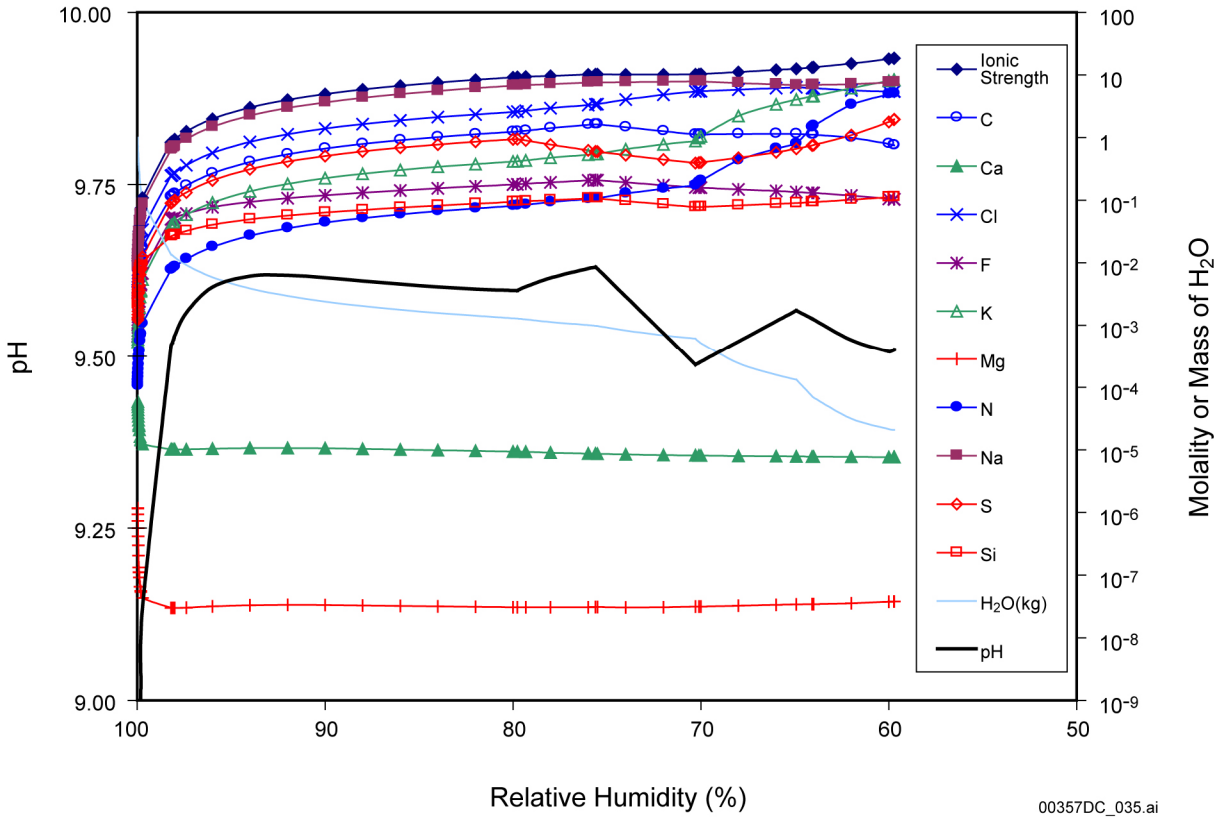
E.4.5 In-Drift Chemical Environments on the Drip Shield and Waste Package

Local in-drift conditions at any given time depend on the in-drift temperature and relative humidity, which, for TSPA purposes, are taken from *Multiscale Thermohydrologic Model Report* (BSC 2003e); the $p\text{CO}_2$, abstracted as described above; and the appropriate incoming water chemistry bin for that time (see Figure E-2). Water chemistries for specific temperature and relative humidity conditions were generated by modeling the evaporation of the binned waters (11 for seepage and 6 for dust leachate) at temperatures of 40°C, 70°C, and 100°C and $p\text{CO}_2$ values of 10^{-2} , 10^{-3} , and 10^{-4} bar. Each temperature was run for each CO_2 fugacity, resulting in nine combinations (or lookup tables) for each bin water (BSC 2003a, Section 6.14.1.2).

As an example of the modeling results, Figure E-5 represents the most likely seepage bin (Bin 7) at 70°C and a $p\text{CO}_2$ of 10^{-3} bar (Attachment II for seepage and Attachment III for dust leachate of BSC 2003a include complete sets of figures).

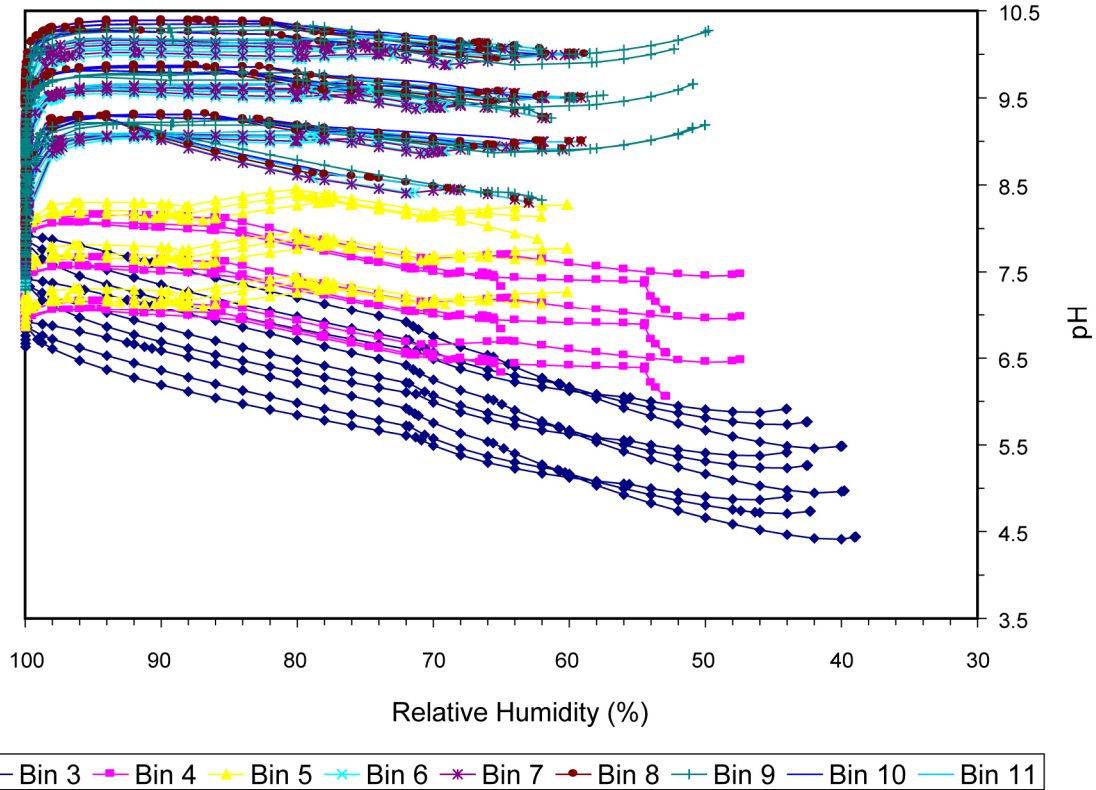
The lookup tables represent response surfaces, giving the potential ranges of outputs for the ranges of inputs simulated. The lookup tables have not been used to determine the actual chemistry at a given point in time outside of the total system performance assessment (TSPA) model because the critical inputs (temperature and relative humidity) are provided directly to TSPA by the *Multiscale Thermohydrologic Model Report* (BSC 2003e). However, the lookup tables can be used independently of TSPA to examine the range of possible chemistries that could be present on the waste package or drip shield surface (BSC 2003a, Section 6.14).

Figure E-6 shows the range of possible pH values (about 10.5 to about 4.5) on the surface of the waste package or drip shield. Note that Bin 1 and Bin 2 waters are not possible chemistries for the seepage entering the crown of the drift (see Table E-1). These two bins are not expected to drip onto waste package or drip shield surfaces and are not presented in this figure. Figures E-7 through E-10 show the ranges for aqueous F^- (about 10^{-5} to about 1 molal), Cl^- (about 10^{-3} to about 10 molal), ionic strength (about 0.01 to about 30 molal), and $\text{Cl}^-/\text{NO}_3^-$ molal ratio (about 0.1 to about 30). The chemistry for brines formed by deliquescence also fall within these ranges. With the exception of Bin 3, the evaporation of the nine possible bins results in formation of K-Cl, K- NO_3 , Na-Cl, or Na- NO_3 solutions, which are generally benign with respect to waste package corrosion. Bin 3 has the potential to form Ca- Cl_2 brines on waste package or drip shield surfaces during its evaporative evolution. However, the time-integrated probability of Bin 3 waters entering the repository over the 20,000-year simulation period is only 0.22 percent (see Table E-1). In other words, Bin 3 waters will, on the average, be present in the crown for only 44 years out of the first 20,000 years. This would only occur between about 225 to 450 years after waste emplacement (see Figure E-2). This is the time that seepage into the drifts is most limited due to the thermal heat load.



Source: DTN: MO0304SPACSAULT.000\07C3T7E.XLS.XLS.

Figure E-5. Predicted Compositional Evolution of Bin 7 Water, Evaporated at 70°C and $p\text{CO}_2$ of 10^{-3} bar

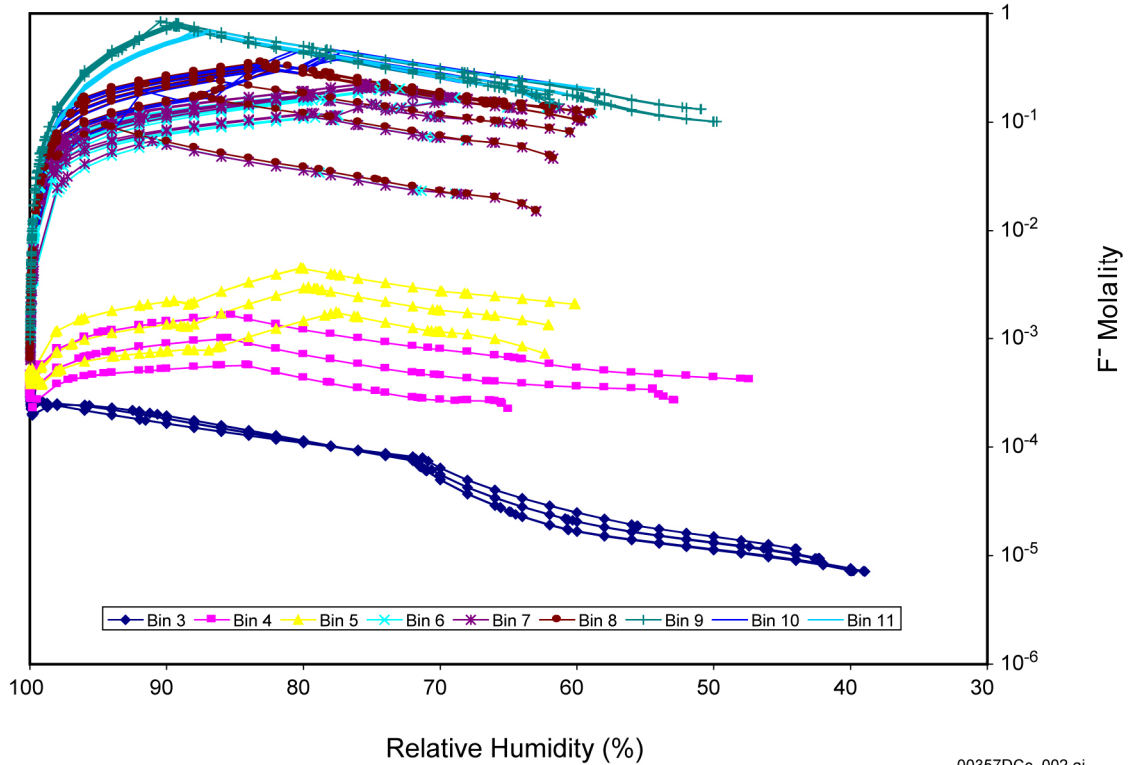


00357DCc_001.ai

Source: BSC 2003a, Figure 6.14-15.

NOTE: Evaporation of the waters is modeled at each possible combination of three temperatures (40°C, 70°C, and 100°C) and three $p\text{CO}_2$ values (10^{-2} , 10^{-3} , and 10^{-4} bar).

Figure E-6. Range of pH versus Relative Humidity for the Seepage Evaporation Lookup Tables Representing Bins 3 through 11 (at Three Temperatures and Three $p\text{CO}_2$ Values)

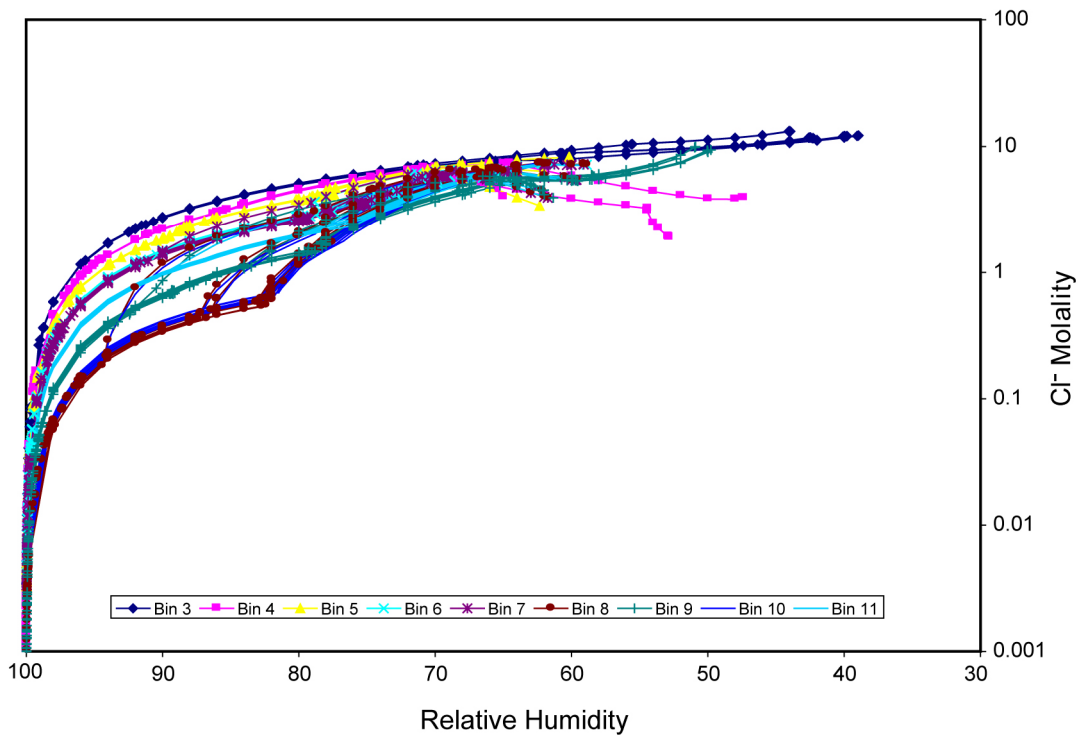


Source: BSC 2003a, Figure 6.14-27.

00357DCc_002.ai

NOTE: Evaporation of the waters is modeled at each possible combination of three temperatures (40°C, 70°C, and 100°C) and three $p\text{CO}_2$ values (10^{-2} , 10^{-3} , and 10^{-4} bar).

Figure E-7. Range of F⁻ Molality versus Relative Humidity for the Seepage Evaporation Lookup Tables Representing Bins 3 through 11 (at Three Temperatures and Three $p\text{CO}_2$ Values)

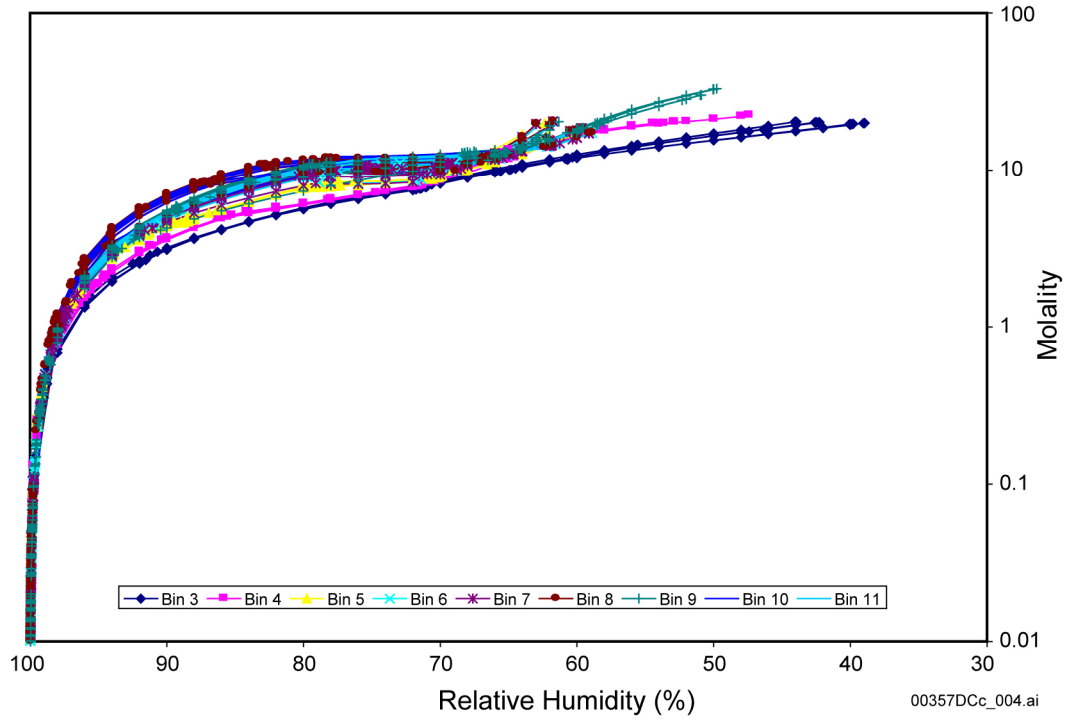


00357DCc_003.ai

Source: BSC 2003a, Figure 6.14-28.

NOTE: Evaporation of the waters is modeled at each possible combination of three temperatures (40°C, 70°C, and 100°C) and three $p\text{CO}_2$ values (10^{-2} , 10^{-3} , and 10^{-4} bar).

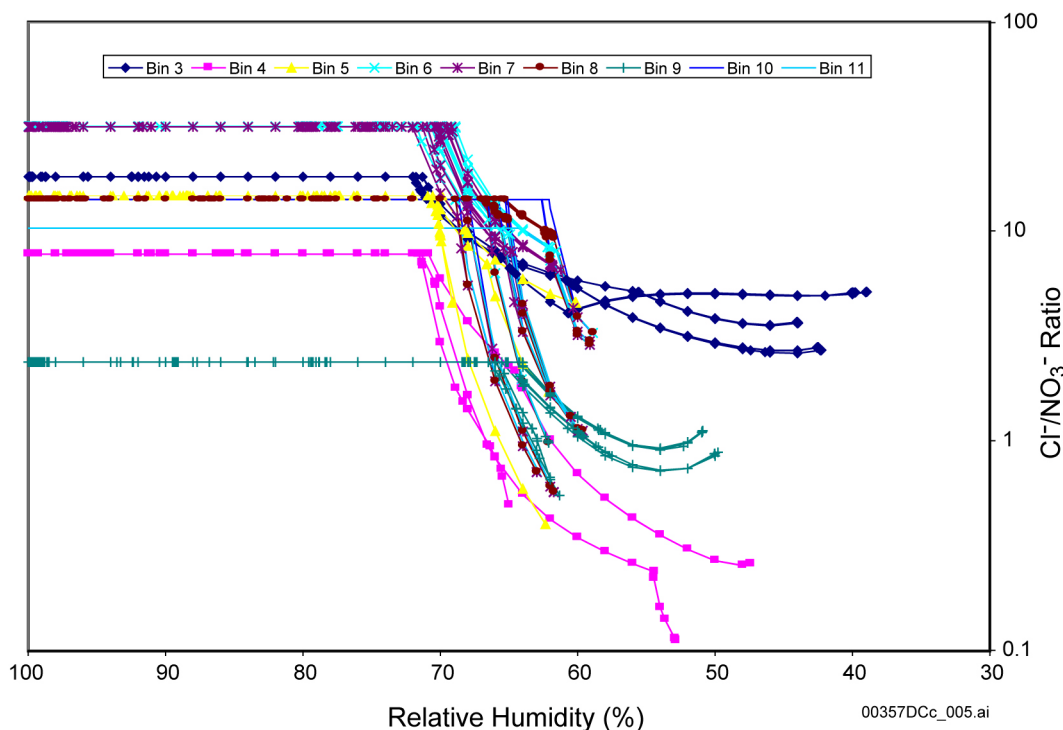
Figure E-8. Range of Cl⁻ Molality versus Relative Humidity for the Seepage Evaporation Lookup Tables Representing Bins 3 through 11 (at Three Temperatures and Three $p\text{CO}_2$ Values)



Source: BSC 2003a, Figure 6.14-33.

NOTE: Evaporation of the waters is modeled at each possible combination of three temperatures (40°C, 70°C, and 100°C) and three $p\text{CO}_2$ values (10^{-2} , 10^{-3} , and 10^{-4} bar).

Figure E-9. Range of Ionic Strength versus Relative Humidity for the Seepage Evaporation Lookup Tables Representing Bins 3 through 11 (at Three Temperatures and Three $p\text{CO}_2$ Values)



Source: BSC 2003a, Figure 6.14-29.

NOTE: Evaporation of the waters is modeled at each possible combination of three temperatures (40°C, 70°C, and 100°C) and three $p\text{CO}_2$ values (10^{-2} , 10^{-3} , and 10^{-4} bar).

Figure E-10. Range of $\text{Cl}^-/\text{NO}_3^-$ Molal Ratios for the Seepage Evaporation Lookup Tables Representing Bins 3 through 11 (at Three Temperatures and Three $p\text{CO}_2$ Values)

E.5 REFERENCES

E.5.1 Documents Cited

BSC (Bechtel SAIC Company) 2003a. *Engineered Barrier System: Physical and Chemical Environment Model*. ANL-EBS-MD-000033 REV 02C. Las Vegas, Nevada: Bechtel SAIC Company. ACC: MOL.20031029.0034.

BSC 2003b. *Environment on the Surfaces of Drip Shield and Waste Package Outer Barrier*. ANL-EBS-MD-000001 REV 01D. Las Vegas, Nevada: Bechtel SAIC Company. ACC: MOL.20030825.0151.

BSC 2003c. *In-Drift Precipitates/Salts Model*. ANL-EBS-MD-000045 REV 01. Las Vegas, Nevada: Bechtel SAIC Company. ACC: DOC.20031028.0003.

BSC 2003d. *Drift-Scale Coupled Processes (DST and THC Seepage) Models*. MDL-NBS-HS-000001 REV 02. Las Vegas, Nevada: Bechtel SAIC Company. ACC: DOC.20030804.0004.

BSC 2003e. *Multiscale Thermohydrologic Model Report*. ANL-EBS-MD-000049 REV 01C. Las Vegas, Nevada: Bechtel SAIC Company. ACC: MOL.20030910.0158.

BSC 2003f. *Repository Design Project, Repository/PA IED Emplacement Drift Committed Materials*. 800-IED-EBS0-00300-000-00A. Las Vegas, Nevada: Bechtel SAIC Company. ACC: ENG.20030311.0021.

Drever, J.I. 1988. *The Geochemistry of Natural Waters*. 2nd Edition. Englewood Cliffs, New Jersey: Prentice-Hall. TIC: 242836.

Reamer, C.W. 2001. U.S. Nuclear Regulatory Commission/U.S. Department of Energy Technical Exchange and Management Meeting on Evolution of the Near-Field Environment (January 9–12, 2001). Letter from C.W. Reamer (NRC) to S. Brocoum (DOE/YMSCO), January 26, 2001, with enclosure. ACC: MOL.20010810.0033.

E.5.2 Data, Listed by Data Tracking Number

MO0304SPACSALT.000. EBS Chemistry THC Seepage Model Abstraction Lookup Table for TSPA-LA. Submittal date: 04/14/2003.

INTENTIONALLY LEFT BLANK

APPENDIX F
MODELING OF SALT INTERACTIONS AT LOW RELATIVE HUMIDITY
(RESPONSE TO ENFE 2.09 AND ENFE 2.15)

Note Regarding the Status of Supporting Technical Information

This document was prepared using the most current information available at the time of its development. This Technical Basis Document and its appendices providing Key Technical Issue Agreement responses that were prepared using preliminary or draft information reflect the status of the Yucca Mountain Project's scientific and design bases at the time of submittal. In some cases this involved the use of draft Analysis and Model Reports (AMRs) and other draft references whose contents may change with time. Information that evolves through subsequent revisions of the AMRs and other references will be reflected in the License Application (LA) as the approved analyses of record at the time of LA submittal. Consequently, the Project will not routinely update either this Technical Basis Document or its Key Technical Issue Agreement appendices to reflect changes in the supporting references prior to submittal of the LA.

APPENDIX F

MODELING OF SALT INTERACTIONS AT LOW RELATIVE HUMIDITY (RESPONSE TO ENFE 2.09 AND ENFE 2.15)

This appendix provides a response for Key Technical Issue (KTI) agreements Evolution of the Near-Field Environment (ENFE) 2.09 and ENFE 2.15. These KTIs relate to providing information and analyses relating to low relative humidity model suppression.

F.1 KEY TECHNICAL ISSUE AGREEMENTS

F.1.1 ENFE 2.09 and ENFE 2.15

Agreements ENFE 2.09 and ENFE 2.15 were reached during the U.S. Nuclear Regulatory Commission (NRC)/U.S. Department of Energy (DOE) Technical Exchange and Management Meeting on Evolution of the Near-Field Environment held January 9 to 12, 2001, in Pleasanton, California (Reamer 2001). ENFE KTI subissues 1, 2, 3, and 4 were discussed at that meeting. There has been no submittal related to these KTI agreements to the NRC.

The wording of these agreements is as follows:

ENFE 2.09

Provide the In-Drift Precipitates/Salts Analysis AMR, Rev. 00, ICN 02, including (1) the major anionic (e.g., fluoride or chloride) and cationic species, and (2) additional technical basis for the low relative humidity model. The DOE will provide the In-Drift Precipitates/Salts Analysis AMR (ANL-EBS-MD-000045), Rev. 00, ICN 02, including the major anionic (e.g., fluoride or chloride) and cationic species, in January 2001. The DOE will provide to the NRC an update to the In-Drift Precipitates/Salts Analysis AMR (ANL-EBS-MD-000045) that will provide additional technical bases for the low relative humidity model, expected to be available in FY 02.

ENFE 2.15

Provide the additional data to constrain the interpolative low relative humidity salts model. The data should provide the technical basis as to why the assumption of the presence of sodium nitrate is conservative, when modeling and experimental results indicate the presence of other mineral phases for which the deliquescence point is unknown. The DOE will provide additional information to constrain the low-relative humidity salts model. The information will include the deliquescence behavior of mineral assemblages derived from alternative starting water compositions (including bulk water compositions, and local variations associated with cement leaching or the presence of corrosion products) representing the range of potential water compositions in the emplacement drifts. This information will be documented in a revision to the In-Drift Precipitates/Salts Analysis AMR (ANL-EBS-MD-000045), expected to be available in FY02.

F.1.2 Related Key Technical Issue Agreements

Other KTI agreements related to those addressed in this appendix are CLST 1.01 (Appendix A), ENFE 2.06 (Appendix E), ENFE 2.10 (Appendix G), and GEN 1.01 comments 50 and 109. GEN 1.01 comment 50 deals with the probability of the formation of sufficient conditions leading to localized corrosion and, therefore, is addressed in Appendix A. GEN 1.01 comment 109 pertains to uncertainty propagation and is addressed in response to ENFE 2.17 (Appendix K).

F.2 RELEVANCE TO REPOSITORY PERFORMANCE

The in-drift precipitates/salts model is developed to predict the effects of evaporation on water composition, mineral precipitation, and deliquescence in the repository for the total system performance assessment for the license application (TSPA-LA). Evaporation can have a profound effect on the chemical composition of water that could potentially seep into the repository. It could turn dilute groundwater into corrosive brine, and complete evaporation can result in the precipitation of hygroscopic salts. Deliquescence of dusts and salts could additionally form corrosive brines. These processes affecting the water chemistry, mineral precipitation, and deliquescence in the environment have the potential to impact the performance of the drip shield and the waste package.

F.3 RESPONSE

The low relative humidity model as referred to in this KTI agreement is no longer being used. The rigorous approach that was used for the high relative humidity salts model, which was applied down to 85 percent relative humidity for the analysis performed supporting the site recommendation (DOE 2002), has been extended to encompass the entire range of relative humidity relevant for system analyses. This revised model uses a Pitzer approach to represent the solute interactions in the solution. The revised *In-Drift Precipitates/Salts Model* (BSC 2003a) incorporates experimental and laboratory data derived from the ongoing waste package evaporative concentration and deliquescence tests that validate the revised Pitzer model for the full range of relative humidity.

The revised model covers the system Na-K-H-Mg-Ca-Al-Cl-F-NO₃-SO₄-Br-CO₃-SiO₂-CO₂-O₂-H₂O and is limited to a temperature range of 0°C to 125°C (BSC 2003a, Section 1). The included binary and ternary Pitzer parameters for ion interactions in this system are listed in Tables F-1 and F-2. The compositional system treated by this model encompasses the major ion chemistry output parameters potentially important to downstream models used to estimate corrosion of metals, colloid stability, degradation of engineered barrier system materials, dust deliquescence, and radionuclide transport. These parameters include pH, ionic strength, the total aqueous concentrations of chemical components, the aqueous concentrations of species that potentially contribute to acid-neutralizing capacity, and mineral precipitation. Validation of this revised model to high temperatures (greater than 100°C) and high dissolved concentrations (greater than 20 molal) has been accomplished using independent measures of solubility, equilibrium relative humidity, and observed concentrations in evaporation and deliquescence tests.

Table F-1. Binary Pitzer Database Input Parameters

Ions	Parameter Name	Parameter Type	Parameter Units	Ions	Parameter Name	Parameter Type	Parameter Units
Na ⁺ – Cl ⁻	$\beta^{(0)}$, $\beta^{(1)}$, and $C^{(\phi)}$	Binary	kg/mol, kg/mol, and (kg/mol) ² respectively	K ⁺ – SO ₄ ²⁻	$\beta^{(0)}$, $\beta^{(1)}$, and $C^{(\phi)}$	Binary	kg/mol, kg/mol, and (kg/mol) ² respectively
Na ⁺ – SO ₄ ²⁻	$\beta^{(0)}$, $\beta^{(1)}$, and $C^{(\phi)}$	Binary	kg/mol, kg/mol, and (kg/mol) ² respectively	K ⁺ – Br ⁻	$\beta^{(0)}$, $\beta^{(1)}$, and $C^{(\phi)}$	Binary	kg/mol, kg/mol, and (kg/mol) ² respectively
Na ⁺ – HSO ₄ ⁻	$\beta^{(0)}$, $\beta^{(1)}$, and $C^{(\phi)}$	Binary	kg/mol, kg/mol, and (kg/mol) ² respectively	Ca ²⁺ – Cl ⁻	$\beta^{(0)}$, $\beta^{(1)}$, and $C^{(\phi)}$	Binary	kg/mol, kg/mol, and (kg/mol) ² respectively
Na ⁺ – OH ⁻	$\beta^{(0)}$, $\beta^{(1)}$, and $C^{(\phi)}$	Binary	kg/mol, kg/mol, and (kg/mol) ² respectively	Ca ²⁺ – SO ₄ ²⁻	$\beta^{(0)}$, $\beta^{(1)}$, and $C^{(\phi)}$	Binary	kg/mol, kg/mol, and (kg/mol) ² respectively
Na ⁺ – NO ₃ ⁻	$\beta^{(0)}$, $\beta^{(1)}$, and $C^{(\phi)}$	Binary	kg/mol, kg/mol, and (kg/mol) ² respectively	Ca ²⁺ – NO ₃ ⁻	$\beta^{(0)}$, $\beta^{(1)}$, and $C^{(\phi)}$	Binary	kg/mol, kg/mol, and (kg/mol) ² respectively
Na ⁺ – CO ₃ ⁻	$\beta^{(0)}$, $\beta^{(1)}$, and $C^{(\phi)}$	Binary	kg/mol, kg/mol, and (kg/mol) ² respectively	Li ⁺ – Cl ⁻	$\beta^{(0)}$, $\beta^{(1)}$, and $C^{(\phi)}$	Binary	kg/mol, kg/mol, and (kg/mol) ² respectively
Na ⁺ – HCO ₃ ⁻	$\beta^{(0)}$, $\beta^{(1)}$, and $C^{(\phi)}$	Binary	kg/mol, kg/mol, and (kg/mol) ² respectively	Li ⁺ – Br ⁻	$\beta^{(0)}$, $\beta^{(1)}$, and $C^{(\phi)}$	Binary	kg/mol, kg/mol, and (kg/mol) ² respectively
Na ⁺ – Br ⁻	$\beta^{(0)}$, $\beta^{(1)}$, and $C^{(\phi)}$	Binary	kg/mol, kg/mol, and (kg/mol) ² respectively	Mg ²⁺ – SO ₄ ²⁻	$\beta^{(0)}$, $\beta^{(1)}$, and $C^{(\phi)}$	Binary	kg/mol, kg/mol, and (kg/mol) ² respectively
Na ⁺ – AlO ₂ ⁻	$\beta^{(0)}$, $\beta^{(1)}$, and $C^{(\phi)}$	Binary	kg/mol, kg/mol, and (kg/mol) ² respectively	Mg ²⁺ – Cl ⁻	$\beta^{(0)}$, $\beta^{(1)}$, and $C^{(\phi)}$	Binary	kg/mol, kg/mol, and (kg/mol) ² respectively
H ⁺ – Cl ⁻	$\beta^{(0)}$, $\beta^{(1)}$, and $C^{(\phi)}$	Binary	kg/mol, kg/mol, and (kg/mol) ² respectively	Cs ⁺ – Br ⁻	$\beta^{(0)}$, $\beta^{(1)}$, and $C^{(\phi)}$	Binary	kg/mol, kg/mol, and (kg/mol) ² respectively
H ⁺ – NO ₃ ⁻	$\beta^{(0)}$, $\beta^{(1)}$, and $C^{(\phi)}$	Binary	kg/mol, kg/mol, and (kg/mol) ² respectively	Cs ⁺ – Cl ⁻	$\beta^{(0)}$, $\beta^{(1)}$, and $C^{(\phi)}$	Binary	kg/mol, kg/mol, and (kg/mol) ² respectively
H ⁺ – SO ₄ ²⁻	$\beta^{(0)}$, $\beta^{(1)}$, and $C^{(\phi)}$	Binary	kg/mol, kg/mol, and (kg/mol) ² respectively	NH ₄ ⁺ – SO ₄ ²⁻	$\beta^{(0)}$, $\beta^{(1)}$, and $C^{(\phi)}$	Binary	kg/mol, kg/mol, and (kg/mol) ² respectively
H ⁺ – HSO ₄ ⁻	$\beta^{(0)}$, $\beta^{(1)}$, and $C^{(\phi)}$	Binary	kg/mol, kg/mol, and (kg/mol) ² respectively	NH ₄ ⁺ – Cl ⁻	$\beta^{(0)}$, $\beta^{(1)}$, and $C^{(\phi)}$	Binary	kg/mol, kg/mol, and (kg/mol) ² respectively
K ⁺ – Cl ⁻	$\beta^{(0)}$, $\beta^{(1)}$, and $C^{(\phi)}$	Binary	kg/mol, kg/mol, and (kg/mol) ² respectively				

Source: BSC 2003a, Table 2.

Table F-2. Ternary Pitzer Database Input Parameters

Ions	Parameter Name	Parameter Type	Parameter Units	Ions	Parameter Name	Parameter Type	Parameter Units
$\text{Na}^+ - \text{K}^+$	θ	Ternary	kg/mol	$\text{CO}_2(\text{aq}) - \text{SO}_4^{2-}$	λ	Ternary	kg/mol
$\text{Na}^+ - \text{Ca}^{2+}$	θ	Ternary	kg/mol	$\text{CO}_2(\text{aq}) - \text{H}^+ - \text{Cl}^-$	ζ	Ternary	kg/mol
$\text{K}^+ - \text{Ca}^{2+}$	θ	Ternary	kg/mol	$\text{CO}_2(\text{aq}) - \text{Na}^+ - \text{Cl}^-$	ζ	Ternary	kg/mol
$\text{Na}^+ - \text{Mg}^{2+}$	θ	Ternary	kg/mol	$\text{CO}_2(\text{aq}) - \text{K}^+ - \text{Cl}^-$	ζ	Ternary	kg/mol
$\text{K}^+ - \text{Mg}^{2+}$	θ	Ternary	kg/mol	$\text{CO}_2(\text{aq}) - \text{Ca}^{2+} - \text{Cl}^-$	ζ	Ternary	kg/mol
$\text{NO}_3^- - \text{AlO}_2^-$	θ	Ternary	kg/mol	$\text{CO}_2(\text{aq}) - \text{Mg}^{2+} - \text{Cl}^-$	ζ	Ternary	kg/mol
$\text{OH}^- - \text{AlO}_2^-$	θ	Ternary	kg/mol	$\text{CO}_2(\text{aq}) - \text{H}^+ - \text{SO}_4^{2-}$	ζ	Ternary	kg/mol
$\text{Cl}^- - \text{OH}^-$	θ	Ternary	kg/mol	$\text{CO}_2(\text{aq}) - \text{Na}^+ - \text{SO}_4^{2-}$	ζ	Ternary	kg/mol
$\text{Cl}^- - \text{SO}_4^{2-}$	θ	Ternary	kg/mol	$\text{CO}_2(\text{aq}) - \text{K}^+ - \text{SO}_4^{2-}$	ζ	Ternary	kg/mol
$\text{HSO}_4^- - \text{SO}_4^{2-}$	θ	Ternary	kg/mol	$\text{CO}_2(\text{aq}) - \text{Mg}^{2+} - \text{SO}_4^{2-}$	ζ	Ternary	kg/mol
$\text{SO}_4^{2-} - \text{OH}^-$	θ	Ternary	kg/mol	$\text{SiO}_2 - \text{H}^+ - \text{NO}_3^-$	ζ	Ternary	kg/mol
$\text{Ca}^{2+} - \text{Mg}^{2+}$	θ	Ternary	kg/mol	$\text{SiO}_2 - \text{Na}^+ - \text{Cl}^-$	ζ	Ternary	kg/mol
$\text{Cs}^+ - \text{H}^+$	θ	Ternary	kg/mol	$\text{SiO}_2 - \text{Mg}^{2+} - \text{Cl}^-$	ζ	Ternary	kg/mol
$\text{Cs}^+ - \text{K}^+$	θ	Ternary	kg/mol	$\text{O}_2(\text{aq}) - \text{Na}^+ - \text{Cl}^-$	ζ	Ternary	kg/mol
$\text{Cs}^+ - \text{Li}^+$	θ	Ternary	kg/mol	$\text{O}_2(\text{aq}) - \text{Na}^+ - \text{Br}^-$	ζ	Ternary	kg/mol
$\text{Cs}^+ - \text{Na}^+$	θ	Ternary	kg/mol	$\text{O}_2(\text{aq}) - \text{Na}^+ - \text{OH}^-$	ζ	Ternary	kg/mol
$\text{H}^+ - \text{K}^+$	θ	Ternary	kg/mol	$\text{O}_2(\text{aq}) - \text{Na}^+ - \text{NO}_3^-$	ζ	Ternary	kg/mol
$\text{H}^+ - \text{Li}^+$	θ	Ternary	kg/mol	$\text{O}_2(\text{aq}) - \text{Na}^+ - \text{SO}_4^{2-}$	ζ	Ternary	kg/mol
$\text{H}^+ - \text{Mg}^{2+}$	θ	Ternary	kg/mol	$\text{O}_2(\text{aq}) - \text{K}^+ - \text{Cl}^-$	ζ	Ternary	kg/mol
$\text{H}^+ - \text{Na}^+$	θ	Ternary	kg/mol	$\text{O}_2(\text{aq}) - \text{K}^+ - \text{Br}^-$	ζ	Ternary	kg/mol
$\text{H}^+ - \text{NH}_4^+$	θ	Ternary	kg/mol	$\text{O}_2(\text{aq}) - \text{K}^+ - \text{OH}^-$	ζ	Ternary	kg/mol
$\text{H}^+ - \text{Sr}^{2+}$	θ	Ternary	kg/mol	$\text{O}_2(\text{aq}) - \text{K}^+ - \text{NO}_3^-$	ζ	Ternary	kg/mol
$\text{K}^+ - \text{Li}^+$	θ	Ternary	kg/mol	$\text{O}_2(\text{aq}) - \text{K}^+ - \text{SO}_4^{2-}$	ζ	Ternary	kg/mol
$\text{K}^+ - \text{Mg}^{2+}$	θ	Ternary	kg/mol	$\text{O}_2(\text{aq}) - \text{H}^+ - \text{Cl}^-$	ζ	Ternary	kg/mol
$\text{K}^+ - \text{Li}^+$	θ	Ternary	kg/mol	$\text{O}_2(\text{aq}) - \text{Li}^+ - \text{Cl}^-$	ζ	Ternary	kg/mol
$\text{Li}^+ - \text{Na}^+$	θ	Ternary	kg/mol	$\text{O}_2(\text{aq}) - \text{Ca}^{2+} - \text{Cl}^-$	ζ	Ternary	kg/mol
$\text{SiO}_2 - \text{NO}_3^-$	λ	Ternary	kg/mol	$\text{O}_2(\text{aq}) - \text{Ca}^{2+} - \text{NO}_3^-$	ζ	Ternary	kg/mol
$\text{SiO}_2 - \text{Na}^+$	λ	Ternary	kg/mol	$\text{O}_2(\text{aq}) - \text{Na}^+ - \text{HCO}_3^-$	ζ	Ternary	kg/mol

Table F-2. Ternary Pitzer Database Input Parameters (Continued)

Ions	Parameter Name	Parameter Type	Parameter Units	Ions	Parameter Name	Parameter Type	Parameter Units
SiO ₂ – Cl ⁻	λ	Ternary	kg/mol	O ₂ (aq) – Na ⁺ – CO ₃ ²⁻	ζ	Ternary	kg/mol
SiO ₂ – SO ₄ ²⁻	λ	Ternary	kg/mol	Na ⁺ – K ⁺ – Cl ⁻	ψ	Ternary	kg/mol
SiO ₂ – Mg ²⁺	λ	Ternary	kg/mol	Na ⁺ – K ⁺ – SO ₄ ²⁻	ψ	Ternary	kg/mol
O ₂ (aq) – Na ⁺	λ	Ternary	kg/mol	Na ⁺ – Ca ²⁺ – Cl ⁻	ψ	Ternary	kg/mol
O ₂ (aq) – K ⁺	λ	Ternary	kg/mol	Na ⁺ – Ca ²⁺ – SO ₄ ²⁻	ψ	Ternary	kg/mol
O ₂ (aq) – Mg ²⁺	λ	Ternary	kg/mol	Na ⁺ – Mg ²⁺ – Cl ⁻	ψ	Ternary	kg/mol
O ₂ (aq) – Ca ²⁺	λ	Ternary	kg/mol	Na ⁺ – Cl ⁻ – OH ⁻	ψ	Ternary	kg/mol
O ₂ (aq) – Al ³⁺	λ	Ternary	kg/mol	Na ⁺ – Cl ⁻ – SO ₄ ²⁻	ψ	Ternary	kg/mol
O ₂ (aq) – Cl ⁻	λ	Ternary	kg/mol	Na ⁺ – NO ₃ ⁻ – AlO ₂ ⁻	ψ	Ternary	kg/mol
O ₂ (aq) – Br ⁻	λ	Ternary	kg/mol	Na ⁺ – OH ⁻ – SO ₄ ²⁻	ψ	Ternary	kg/mol
O ₂ (aq) – OH ⁻	λ	Ternary	kg/mol	Na ⁺ – OH ⁻ – AlO ₂ ⁻	ψ	Ternary	kg/mol
O ₂ (aq) – SO ₄ ²⁻	λ	Ternary	kg/mol	K ⁺ – Ca ²⁺ – Cl ⁻	ψ	Ternary	kg/mol
O ₂ (aq) – H ⁺	λ	Ternary	kg/mol	K ⁺ – Mg ²⁺ – Cl ⁻	ψ	Ternary	kg/mol
O ₂ (aq) – Li ⁺	λ	Ternary	kg/mol	K ⁺ – Cl ⁻ – SO ₄ ²⁻	ψ	Ternary	kg/mol
O ₂ (aq) – NH ₄ ⁺	λ	Ternary	kg/mol	Ca ²⁺ – Cl ⁻ – SO ₄ ²⁻	ψ	Ternary	kg/mol
O ₂ (aq) – Ba ²⁺	λ	Ternary	kg/mol	Mg ²⁺ – Cl ⁻ – SO ₄ ²⁻	ψ	Ternary	kg/mol
O ₂ (aq) – I ⁻	λ	Ternary	kg/mol				
O ₂ (aq) – HCO ₃ ⁻	λ	Ternary	kg/mol				
O ₂ (aq) – CO ₃ ²⁻	λ	Ternary	kg/mol				
CO ₂ (aq) – Ca ²⁺	λ	Ternary	kg/mol				
CO ₂ (aq) – K ⁺	λ	Ternary	kg/mol				
CO ₂ (aq) – Mg ²⁺	λ	Ternary	kg/mol				
CO ₂ (aq) – Na ⁺	λ	Ternary	kg/mol				
CO ₂ (aq) – H ⁺	λ	Ternary	kg/mol				
CO ₂ (aq) – Cl ⁻	λ	Ternary	kg/mol				
CO ₂ (aq) – HSO ₄ ⁻	λ	Ternary	kg/mol				

Source: BSC 2003a, Table 3.

The previous assumption (used in the analysis supporting the site recommendation (DOE 2002), that sodium nitrate would be present and would control the critical relative humidity point at which deliquescence could begin, is no longer used, nor is it still applied to the analyses of chemical environment on the surfaces of the drip shield and waste package outer barrier. The revised model considers sodium nitrate as only one of a number of salts evaluated simultaneously for saturation/precipitation in evaporating solutions (BSC 2003a) and as only one of many possible salt phases within dust deposits (BSC 2003b). Table F-3 lists some of the important salts considered in the current thermodynamic model. Several model salt assemblages are now defined as representative of the dust salt assemblage (BSC 2003c, Sections 6.7.2.8 and 6.7.2.10) and are used to evaluate possible mixed-salt deliquescence curves (i.e., critical relative humidity versus temperature) that could create water at higher temperature conditions. The pure CaCl_2 deliquescence curve is evaluated also as a possible bounding constraint on critical relative humidity for the dripping case only (refer to Appendix G, the response to ENFE 2.10, which describes the dripping versus no dripping scenario).

Table F-3. Aqueous Solubilities of Na, K, Ca, and Mg Salts

Salt	Aqueous Solubility at 25°C (mass percent of solute)	Aqueous Solubility at 100°C (mass percent of solute)
NaCl	26.45	28.05
KCl	26.22	36.05
CaCl_2	44.83	59.94
MgCl_2	35.90	42.15
NaHCO_3	9.32	19.10
KHCO_3	26.6	40.45 at 70°C
Na_2CO_3	23.5	30.09
K_2CO_3	52.7	61.0
NaF	3.97	4.82
KF	50.4	60.0 at 80°C
CaF_2	0.0016	not reported above 25°C
MgF_2	0.013	not reported above 25°C
Na_2SO_4	21.94	29.67
K_2SO_4	10.7	19.3
CaSO_4	0.205	0.163
MgSO_4	26.3	33.3
NaBr	48.6	54.9
KBr	40.4	50.8
CaBr_2	61.0	73.0 at 60°C
MgBr_2	50.6	55.7
NaNO_3	47.7	63.8
KNO_3	27.7	70.8
$\text{Ca}(\text{NO}_3)_2$	59.0	78.5
$\text{Mg}(\text{NO}_3)_2$	41.6	72.0

Source: Lide 2000, pp. 8-102 to 8-110.

The sequence of salt precipitation by evaporation depends on the chemistry of the solution and the environment (e.g., temperature, relative humidity, gas fugacities). The relative and total concentrations of the dissolved salt species and the solubilities of the solid salt phases determine when a dissolved species becomes supersaturated, when it begins to precipitate, which other species precipitate with it, and which species continue to concentrate in the remaining solution. The process model allows evaluation of the sequences of mineral precipitation–dissolution and solution composition evolution for either evaporative conditions or deliquescence behavior. These processes are observed commonly in natural systems.

For example, in naturally occurring brines, high sulfate concentrations are attributed to the dissolution of gypsum in geologic strata or the oxidation of sulfides such as pyrite, which is widespread in the western United States (Eugster and Hardie 1978, p. 243). In a carbonate-poor (calcium-rich) brine, such as a brine derived from the evaporation of seawater, sulfate precipitates as gypsum or anhydrite before halite precipitates (Kinsman 1976, p. 275). In carbonate-rich alkaline brines, sulfate precipitates as a sodium salt (Eugster and Hardie 1978, p. 246).

Literature values of the equilibrium relative humidity of aqueous solutions saturated with a given salt (see Table F-4) were used to validate the process model. Lower values in this table indicate lower water activity and, therefore, higher salt solubility. This relation is apparent when comparing the values in Table F-4 with corresponding solubility values in Table F-3. For evaporating seawater, when the water activity equilibrates to 0.93 (i.e., at relative humidity of 93 percent), calcium sulfate precipitates (Kinsman 1976, p. 273). In this same water, when the water activity is equilibrated 0.77 due to net evaporation of water into air having a relative humidity less than 77 percent, halite precipitates (Kinsman 1976, pp. 274 to 275). Thus, as water evaporates, the water activity in the brine decreases, forcing less hygroscopic, less soluble salts to precipitate before more hygroscopic, more soluble salts. A rough estimate can be made based on the values in Tables F-3 and F-4. For example, the sequence of precipitation in a calcium-poor (carbonate-rich) brine is likely sodium sulfate followed by halite. The process model developed in *In-Drift Precipitates/Salts Model* (BSC 2003a) allows explicit, rigorous analysis of such solutions as they undergo evaporative concentration or deliquescent formation and dilution.

Cementitious materials and their effects on the in-drift chemical environment are no longer of concern as the current repository emplacement drift (ground support) design does not include cement grout within the emplacement drifts (BSC 2003b, Table 6.4.3-1).

The information in this report is responsive to agreements ENFE 2.09 and ENFE 2.15 made between the DOE and the NRC. The report contains the information that the DOE considers necessary for NRC review for closure of these agreements.

Table F-4. Equilibrium Relative Humidity for Saturated Aqueous Solutions in Contact with an Excess of Solid-Phase Salts

Salt	Equilibrium Relative Humidity (%)	Temperature of Measurement (°C)
NaCl	76.4	80
KCl	79.5	80
MgCl ₂ ·6H ₂ O	33.0	25
Na ₂ CO ₃ ·10H ₂ O	87 ^a	24.5
K ₂ CO ₃ ·2H ₂ O	42	40
NaF	96.6 ^a	100
KF	22.9 ^a	100
Na ₂ SO ₄ ·10H ₂ O	93 ^a	20
K ₂ SO ₄	96	60
NaNO ₃	65.5	80
KNO ₃	82	60
KNO ₃ , NaNO ₃ , and NaCl	30.49 ^a	16.39

Source: Dean 1992, p. 11.6.

NOTE: ^a Weast and Astle 1981, p. E-44.

F.4 BASIS FOR THE RESPONSE

The *In-Drift Precipitates/Salts Model* (BSC 2003a) provides both an integrated process model for explicit, rigorous analysis of solutions evaporating to precipitate minerals or solid salt phases deliquescing to brines and subsequently more dilute solutions and a conceptual abstraction approach for generating water compositional lookup tables to be used by the TSPA-LA. The second part, the abstraction form and approach, is essentially unchanged from the high relative humidity analysis performed supporting the site recommendation. *In-Drift Precipitates/Salts Model* (BSC 2003a) provides technical details and explanations of the chemical reactions of the in-drift salts and the essential factors that influence the dissolution and precipitation mechanisms. The conceptual abstraction model is used as input to the analysis performed in the physical and chemical environment model (BSC 2003b).

The *In-Drift Precipitates/Salts Model* (BSC 2003a) is limited by two assumptions. First, water in the drift is assumed to be represented by bulk aqueous solution, meaning that its properties are not affected by factors associated with interfacial energies, such as capillary or surface tension. Second, chemical equilibrium is assumed as the controlling factor for all reactions, except for precipitation of “suppressed” minerals. An exception to this assumption is that the aqueous solution does not have to be at equilibrium with respect to a specific value of relative humidity when the inputs to a problem are such that the relative humidity is calculated as an output. Despite these assumptions and limitations, however, the model is validated for the general intended use of predicting the effects of evaporative processes on salt and brine formation so that the potential implications of these processes on total system performance can be assessed.

The model and analysis uses as the primary input binary and ternary Pitzer parameters shown in Tables F-1 and F-2, as previously discussed. The model output as abstracted provides lookup tables that can be used for the entire possible range of relative humidity in the drift. To cover

this range, the bin waters were both evaporated to dryness and diluted by a factor of 100. The starting bin waters were sufficiently dilute that they represented solutions in equilibrium with relative humidity between 99.9 and 99.99 percent. For potential relative humidity values higher than the starting bin water, condensation of pure water was simulated. Thus, for each temperature and CO₂ fugacity combination, two model runs were required, one for evaporation and one for condensation.

Using this process, the in-drift precipitates/salts model was used to generate lookup tables, primarily designed for the incoming water compositions predicted by the thermal-hydrologic-chemical model (BSC 2003d), for both downstream modeling and uncertainty analyses. The downstream model to generate these lookup tables is the physical and chemical environment model (BSC 2003b).

In-drift precipitates/salts model lookup tables, as generated in the physical and chemical environment model (BSC 2003b), provide model parameter outputs for a full range of equilibrium relative humidity values and steady-state relative evaporation rate values. Specifically, three types of model output are tabulated in the lookup tables: boundary values, abstraction output, and supplemental calculations. The first two types of output are directly provided in the EQ6 output files. The third type, supplemental calculations, consists of simple algebraic manipulations of the EQ6 output.

“Boundary values” include temperature, the fugacities of carbon dioxide and oxygen, and the reaction progress. These values are, for all practical purposes, input values. The reaction progress is a measure of the extent of evaporation or condensation that has occurred for a set of equilibrium output values.

“Abstraction output” includes all EQ6 calculations for the aqueous output variables of interest in the TSPA-LA. It includes the pH, activity of water, ionic strength, mass of solvent water remaining, total concentrations of each element, concentrations of select aqueous species that potentially contribute to acid-neutralizing capacity, and amounts of solids precipitating in a given EQ6 run. This information is useful in understanding how a starting water chemically evolves for a given set of boundary conditions. It is also used to support downstream calculations that evaluate interaction of this water with potential cementitious materials (were such to be included in the repository design, which presently they are not), steel, and microbes.

“Supplemental calculations” include lookup table calculations for relative humidity, concentration factor, relative evaporation rate, and dilution factor.

These tables are designed to define a response surface from which in-drift-precipitates/salts-based model outputs can be obtained or interpolated for given incoming water compositions. The lookup tables provide the major anionic and cationic species considered for the in-drift precipitates and salts analysis.

F.5 REFERENCES

- BSC (Bechtel SAIC Company) 2003a. *In-Drift Precipitates/Salts Model*. ANL-EBS-MD-000045 REV 01. Las Vegas, Nevada: Bechtel SAIC Company. ACC: DOC.20031028.0003.
- BSC 2003b. *Engineered Barrier System: Physical and Chemical Environment Model*. ANL-EBS-MD-000033 REV 02C. Las Vegas, Nevada: Bechtel SAIC Company. ACC: MOL.20031029.0034.
- BSC 2003c. *Environment on the Surfaces of Drip Shield and Waste Package Outer Barrier*. ANL-EBS-MD-000001 REV 01D. Las Vegas, Nevada: Bechtel SAIC Company. ACC: MOL.20030825.0151.
- BSC 2003d. *Drift-Scale Coupled Processes (DST and THC Seepage) Models*. MDL-NBS-HS-000001 REV 02. Las Vegas, Nevada: Bechtel SAIC Company. ACC: DOC.20030804.0004.
- Dean, J.A. 1992. *Lange's Handbook of Chemistry*. 14th Edition. New York, New York: McGraw-Hill. TIC: 240690.
- DOE (U.S. Department of Energy) 2002. *Yucca Mountain Science and Engineering Report*. DOE/RW-0539, Rev. 1. Washington, D.C.: U.S. Department of Energy, Office of Civilian Radioactive Waste Management. ACC: MOL.20020404.0042.
- Eugster, H.P. and Hardie, L.A. 1978. "Saline Lakes." *Lakes, Chemistry, Geology, Physics*. Lerman, A., ed. Pages 237-293. New York, New York: Springer-Verlag. TIC: 240782.
- Kinsman, D.J.J. 1976. "Evaporites: Relative Humidity Control of Primary Mineral Facies." *Journal of Sedimentary Petrology*, 46, 273-279. Tulsa, Oklahoma: Society of Economic Paleontologists and Mineralogists. TIC: 238672.
- Lide, D.R., ed. 2000. *CRC Handbook of Chemistry and Physics*. 81st Edition. Boca Raton, Florida: CRC Press. TIC: 253056.
- Reamer, C.W. 2001. U.S. Nuclear Regulatory Commission/U.S. Department of Energy Technical Exchange and Management Meeting on Evolution of the Near-Field Environment (January 9–12, 2001). Letter from C.W. Reamer (NRC) to S. Brocoum (DOE/YMSCO), January 26, 2001, with enclosure. ACC: MOL.20010810.0033.
- Weast, R.C. and Astle, M.J., eds. 1981. *CRC Handbook of Chemistry and Physics*. 62nd Edition. Boca Raton, Florida: CRC Press. TIC: 240722.

APPENDIX G
RANGE OF WATER COMPOSITIONS THAT COULD CONTACT THE DRIP SHIELD
OR WASTE PACKAGE SURFACES
(RESPONSE TO ENFE 2.10)

Note Regarding the Status of Supporting Technical Information

This document was prepared using the most current information available at the time of its development. This Technical Basis Document and its appendices providing Key Technical Issue Agreement responses that were prepared using preliminary or draft information reflect the status of the Yucca Mountain Project's scientific and design bases at the time of submittal. In some cases this involved the use of draft Analysis and Model Reports (AMRs) and other draft references whose contents may change with time. Information that evolves through subsequent revisions of the AMRs and other references will be reflected in the License Application (LA) as the approved analyses of record at the time of LA submittal. Consequently, the Project will not routinely update either this Technical Basis Document or its Key Technical Issue Agreement appendices to reflect changes in the supporting references prior to submittal of the LA.

APPENDIX G

RANGE OF WATER COMPOSITIONS THAT COULD CONTACT THE DRIP SHIELD OR WASTE PACKAGE SURFACES (RESPONSE TO ENFE 2.10)

This appendix provides a response for Key Technical Issue (KTI) agreement Evolution of the Near-Field Environment (ENFE) 2.10. This KTI relates to providing additional information about the range of composition of waters that could contact the drip shield or waste package.

G.1 DESCRIPTION OF THE KEY TECHNICAL ISSUE AGREEMENT

G.1.1 ENFE 2.10

Agreement ENFE 2.10 was reached during the U.S. Nuclear Regulatory Commission (NRC)/U.S. Department of Energy (DOE) Technical Exchange and Management Meeting on Evolution of the Near-Field Environment held January 9 to 12, 2001, in Pleasanton, California (Reamer 2001). ENFE KTI subissues 1, 2, 3, and 4 were discussed at that meeting. There has been no submittal related to this KTI agreement to the NRC.

Wording of the agreement is as follows:

ENFE 2.10

Provide additional information about the range of composition of waters that could contact the drip shield or waste package, including whether such waters are of the bicarbonate or chloride-sulfate type. The DOE will describe the range of bulk composition for waters that could affect corrosion of the drip shield or waste package outer barrier, in a revision to the Environment on the Surfaces of the Drip Shield and Waste Package Outer Barrier AMR (ANL-EBS-MD-000001), expected to be available in FY02.

G.1.2 Related Key Technical Issue Agreements

Other KTI agreements related to ENFE 2.10 are CLST 1.01 (Appendix A), ENFE 1.05 (Appendix B), ENFE 2.06 (Appendix E), ENFE 2.09 and ENFE 2.15 (Appendix F), ENFE 2.13 (Appendix I) and TSPAI 2.02 items 42, 54, and J-3. The TSPAI agreement will be addressed separately in a future response addressing features, events, and processes.

G.2 RELEVANCE TO REPOSITORY PERFORMANCE

In the broad sense, understanding the range of local chemistry possible in the in-drift environment is important to drip shield and waste package degradation, chemistry within degraded packages, waste-form degradation, and radionuclide and colloid transport properties. Within the framework of this KTI the understanding of the in-drift environment is important because of its impact on the waste package and drip shield performance (lifetimes). The range of water chemistries that may contact the waste package and drip shield have the potential to substantially impact the performance of these engineering barriers.

G.3 RESPONSE

Aqueous solutions on drip shield and waste package surfaces will result from water absorption by deliquescent salts deposited on these surfaces or from evaporative concentration of seepage waters that come into contact with them. Deliquescent salts may be deposited on the surfaces from dust and aerosols entrained in ventilation air, by waters that completely evaporate upon contact with the surfaces, and even by deposition of aerosols formed in the repository by the dripping (splashing) of seepage water.

The formation of brines and salt minerals by evaporation in natural systems is limited to certain types that are dependent on the chemistry of the dilute source waters. Depending on the relative ratios of the cations and anions in the source waters, various mineral phases will precipitate out during evaporation of the solutions and, hence, change the ionic composition of the waters. Chemically distinct brines have different characteristics, such as the deliquescence point of the salt mixtures that precipitate from them, their boiling point, and solution pHs. Similar themes pertain to the evaporation and (in reverse) deliquescence processes that are expected to occur in the repository. The path along which a water will evolve chemically during evaporation is determined by the chemical divide phenomenon, which is described in the response to KTI 2.06 (see Appendix E).

Both *Engineered Barrier System: Physical and Chemical Environment Model* (BSC 2003a) and *Environment on the Surfaces of Drip Shield and Waste Package Outer Barrier* (BSC 2003b) discuss solutions on drip shield and waste package surfaces. *Engineered Barrier System: Physical and Chemical Environment Model* (BSC 2003a) provides tables of compositions of solutions formed both by evaporation of seepage and deliquescence of dust at temperatures of 40°C, 70°C, and 100°C (and additional higher dust temperatures of 120°C and 140°C), partial pressure of carbon dioxide ($p\text{CO}_2$) of 10^{-2} , 10^{-3} , and 10^{-4} bar, at relative humidity value intervals of about 2 percent from a relative humidity of about 100 percent down to the relative humidity of the end point of the evaporation. This results in lookup tables for the total system performance assessment for the license application (TSPA-LA) model. These lookup tables are used in conjunction with the temperature and relative humidity data provided to TSPA-LA to derive discrete chemical values through time. The lookup tables contain the full range of process model chemistry (i.e., pH, ionic strength, Ca^{2+} , Na^+ , K^+ , SO_4^{2-} , F^- , Mg^{2+} , $\text{SiO}_2(\text{aq})$, etc.); however, TSPA-LA uses only the data for pH, ionic strength, total Cl^- , and $\text{Cl}^-/\text{NO}_3^-$ ratio. This information is used for TSPA corrosion module in the integrated waste package model (BSC 2003c).

Environment on the Surfaces of Drip Shield and Waste Package Outer Barrier (BSC 2003b) provides a corroborative analysis of the presence or absence of liquid water as a function of temperature and relative humidity along with an analysis of solution composition when such a solution is predicted to occur. However, *Environment on the Surfaces of Drip Shield and Waste Package Outer Barrier* (BSC 2003b) does not present process model results that discuss the range of chemistry that could be present on the waste package or drip shield.

Both reports include a dripping case (seepage evaporation) and a no dripping case (deliquescence of dust). The dripping and no-dripping cases in abstracted form are direct feeds to TSPA and the integrated waste package degradation model (BSC 2003c) for TSPA.

A comparison of results presented below from the two chemical scenarios, dripping (seepage chemistry) with no dripping (deliquescence chemistry), indicate that the deliquescent conditions have less of a potential to affect localized corrosion. The brines generated by the deliquescence conditions tend to be carbonate, nitrate, and sulfate brines, whereas the brines generated by seepage conditions are generally chloride type brines.

The information in this report is responsive to agreement ENFE 2.10 made between the DOE and NRC. The report contains the information that DOE considers necessary for NRC review for closure of this agreement.

G.4 BASIS FOR THE RESPONSE

G.4.1 Chemistry of Water on the Drip Shield and Waste Package

The main parameter of interest for drip shield performance is the concentration of F^- in the solution, in addition to pH and ionic strength, which are important factors in most geochemical modeling. For the waste package environment, the primary chemical parameters of concern include Cl^- , NO_3^- , and SO_4^{2-} concentrations. Also important are the deliquescence points of salt mixtures on the drip shield and waste package surfaces, brine compositions, and brine evolution pathways (BSC 2003a, Section 6.14.4). Each of these is discussed in terms of the two major sources of water to the surfaces: seepage (dripping case) and dust deliquescence (no dripping case). In general, the values presented below represent total aqueous elemental compositions.

G.4.2 Seepage Conditions

The seepage water chemistries are based on a number of starting water compositions and were chosen to be representative of seepage waters entering the drift through time. The seepage water chemistries are derived from five realizations (designated W0, W4, W5, W6, and W7) of *Drift-Scale Coupled Processes (DST and THC Seepage) Models* (BSC 2003d), abstracted into 11 groups (bins) of like water types (BSC 2003a, Section 6.6). Lookup tables of solution compositions were constructed by simulating evaporation of the eleven seepage bin chemistries (see Table G-1) at temperatures of 40°C, 70°C, and 100°C with pCO_2 values of 10^{-2} , 10^{-3} , and 10^{-4} bar, using the geochemical modeling code EQ3/6 (BSC 2003e), with model output being produced at relative humidity value intervals of about 2 percent (in many instances less than this) from a relative humidity of about 100 percent down to the relative humidity of the end point of the evaporation.

The lookup tables represent response surfaces, so they suggest the potential ranges of outputs for the given inputs. Based on temperature and relative humidity values provided by the *Multiscale Thermohydrologic Model Report* (BSC 2003f), the lookup tables yield the chemistry used at given times within the TSPA-LA model. Overall, the lookup tables represent the full range of possible chemistries that could be present on the waste package or drip shield given the range of input parameters (BSC 2003a, Section 6.14). As the actual ranges of temperature and relative humidity are limited at any given point in time, the entire range of water chemistries provided by the lookup tables would not be possible. Thus, the ranges discussed in the paragraphs below, which reflect the full ranges given in the tables, bound the values expected at any given time.

Table G-1. Compositions of the 11 Binned Waters

Species	Bin 1	Bin 2	Bin 3	Bin 4	Bin 5	Bin 6	Bin 7	Bin 8	Bin 9	Bin 10	Bin 11
T (°C)	111.9	109.1	104.3	104.9	95.62	65.10	56.34	40.18	91.78	56.34	95.61
pH	7.407	7.583	7.615	7.896	7.634	7.70	7.768	7.94	8.139	7.815	7.759
Ca ²⁺	1.75 × 10 ⁻²	6.49 × 10 ⁻³	2.14 × 10 ⁻³	1.08 × 10 ⁻³	1.36 × 10 ⁻³	4.20 × 10 ⁻⁴	4.46 × 10 ⁻⁴	5.73 × 10 ⁻⁴	7.24 × 10 ⁻⁵	3.52 × 10 ⁻⁴	3.34 × 10 ⁻⁴
Mg ²⁺	1.70 × 10 ⁻⁵	2.95 × 10 ⁻⁶	4.13 × 10 ⁻⁶	5.75 × 10 ⁻⁷	1.13 × 10 ⁻⁵	4.82 × 10 ⁻⁵	5.52 × 10 ⁻⁵	8.51 × 10 ⁻⁵	2.54 × 10 ⁻⁷	4.31 × 10 ⁻⁵	6.34 × 10 ⁻⁶
Na ⁺	3.89 × 10 ⁻³	2.63 × 10 ⁻³	2.67 × 10 ⁻³	1.26 × 10 ⁻³	5.53 × 10 ⁻³	8.09 × 10 ⁻³	7.65 × 10 ⁻³	7.31 × 10 ⁻³	4.27 × 10 ⁻³	6.82 × 10 ⁻³	4.80 × 10 ⁻³
Cl ⁻	2.01 × 10 ⁻²	5.02 × 10 ⁻³	3.35 × 10 ⁻³	1.03 × 10 ⁻³	3.28 × 10 ⁻³	3.32 × 10 ⁻³	7.44 × 10 ⁻⁴	5.61 × 10 ⁻⁴	7.34 × 10 ⁻⁴	6.00 × 10 ⁻⁴	1.30 × 10 ⁻³
SiO ₂ (aq)	9.42 × 10 ⁻³	7.42 × 10 ⁻³	6.96 × 10 ⁻³	7.38 × 10 ⁻³	1.22 × 10 ⁻²	2.90 × 10 ⁻³	2.46 × 10 ⁻³	1.79 × 10 ⁻³	4.15 × 10 ⁻³	2.47 × 10 ⁻³	1.19 × 10 ⁻²
CO ₃	5.57 × 10 ⁻⁵	9.06 × 10 ⁻⁵	1.95 × 10 ⁻⁴	1.64 × 10 ⁻⁴	4.18 × 10 ⁻⁴	2.93 × 10 ⁻³	6.72 × 10 ⁻³	6.92 × 10 ⁻³	2.04 × 10 ⁻³	5.74 × 10 ⁻³	1.13 × 10 ⁻³
SO ₄ ²⁻	8.87 × 10 ⁻³	4.89 × 10 ⁻³	1.50 × 10 ⁻³	5.88 × 10 ⁻⁴	1.77 × 10 ⁻³	1.21 × 10 ⁻³	4.12 × 10 ⁻⁴	3.55 × 10 ⁻⁴	1.18 × 10 ⁻⁴	3.80 × 10 ⁻⁴	7.29 × 10 ⁻⁴
K ⁺	8.68 × 10 ⁻⁴	5.40 × 10 ⁻⁴	5.00 × 10 ⁻⁴	2.38 × 10 ⁻⁴	8.68 × 10 ⁻⁴	6.25 × 10 ⁻⁴	4.67 × 10 ⁻⁴	2.76 × 10 ⁻⁴	5.02 × 10 ⁻⁴	4.17 × 10 ⁻⁴	7.50 × 10 ⁻⁴
AlO ₂ ⁻	3.27 × 10 ⁻⁸	7.08 × 10 ⁻⁸	5.02 × 10 ⁻⁸	9.97 × 10 ⁻⁸	8.03 × 10 ⁻¹⁰	5.36 × 10 ⁻⁹	3.62 × 10 ⁻⁹	1.50 × 10 ⁻⁹	6.09 × 10 ⁻⁸	4.03 × 10 ⁻⁹	1.42 × 10 ⁻⁹
F ⁻	1.93 × 10 ⁻⁴	2.46 × 10 ⁻⁴	3.48 × 10 ⁻⁴	4.28 × 10 ⁻⁴	1.00 × 10 ⁻³	8.26 × 10 ⁻⁴	7.81 × 10 ⁻⁴	6.43 × 10 ⁻⁴	9.77 × 10 ⁻⁴	8.61 × 10 ⁻⁴	1.38 × 10 ⁻³
NO ₃ ⁻	1.30 × 10 ⁻³	5.46 × 10 ⁻⁴	1.83 × 10 ⁻⁴	1.33 × 10 ⁻⁴	2.22 × 10 ⁻⁴	1.04 × 10 ⁻⁴	6.87 × 10 ⁻⁵	3.97 × 10 ⁻⁵	3.10 × 10 ⁻⁴	4.25 × 10 ⁻⁵	1.26 × 10 ⁻⁴
CO ₂ (g)(bar)	3.89 × 10 ⁻⁴	4.93 × 10 ⁻⁴	1.04 × 10 ⁻³	4.88 × 10 ⁻⁴	1.88 × 10 ⁻³	7.06 × 10 ⁻³	1.19 × 10 ⁻²	6.34 × 10 ⁻³	2.94 × 10 ⁻³	9.19 × 10 ⁻³	4.06 × 10 ⁻³
log CO ₂ (g)	-3.410	-3.307	-2.984	-3.312	-2.726	-2.151	-1.926	-2.198	-2.532	-2.037	-2.392

Source: BSC 2003a, Table 6.6-5.

NOTE: Unless otherwise marked, units are in moles/kg H₂O. CO₃ represents total aqueous carbonate, comprising CO₂(aq), HCO₃⁻, and CO₃²⁻.

The time-integrated probability of the occurrence of these 11 bins or water types as seepage from the crown of the drift is given in Table G-2 (right-hand column). Note that bin 1 and 2 waters do not occur among the types of crown seepage waters that could affect the drip shield or waste package. Table G-3 shows the prevalence of the nine possible bins during five general periods of repository time associated with general thermal or operational constraints. They include the preclosure period (0 to 50 years), boiling period (51 to 700 years), hot period (701 to 2,000 years), cool down period (2,001 to 7,000 years), and return to ambient period (7,001 to 20,000 years). In Section 1, three thermal regimes are listed: the dryout regime, the transition regime, and the low-temperature regime. The dryout regime corresponds to the first half of the boiling period; the transition regime corresponds to the latter half of the boiling period and the first portions of the hot period; the low-temperature regime corresponds to the last half of the hot period, the cool-down period, and the first part of the return to ambient period.

Table G-2. Starting Water Composition Scenario Probability (W0 Percent to W7 Percent) and Time-Integrated Probability (Norm Percent) of Occurrence for Any Given Crown Seepage Bin for the 20,000-Year Simulation Period

Water	W0 %	W4 %	W5 %	W6 %	W7 %	Sum %	Norm %
Bin 1	0.00	0.00	0.00	0.00	0.00	0.00	0.00
Bin 2	0.00	0.00	0.00	0.00	0.00	0.00	0.00
Bin 3	1.12	0.00	0.00	0.00	0.00	1.12	0.22
Bin 4	2.62	1.00	1.00	1.00	1.50	7.12	1.42
Bin 5	0.56	1.87	1.00	0.00	0.50	3.93	0.79
Bin 6	25.82	0.00	0.00	1.50	0.00	27.32	5.46
Bin 7	31.75	26.48	32.01	0.25	45.25	135.74	27.15
Bin 8	12.50	31.03	12.50	12.50	12.50	81.02	16.20
Bin 9	0.00	12.50	13.00	39.75	12.50	77.75	15.55
Bin 10	0.00	0.25	13.24	45.00	0.00	58.49	11.70
Bin 11	25.63	26.88	27.25	0.00	27.75	107.50	21.50
Sum	100.00	100.00	100.00	100.00	100.00	500.00	100.00

Source: BSC 2003a, Table 6.14-1.

Table G-3. Dominant Seepage Water Types (Bins) Associated with Each Different Period in the Thermal History of the Repository that Could Contact Drip Shields and Waste Packages

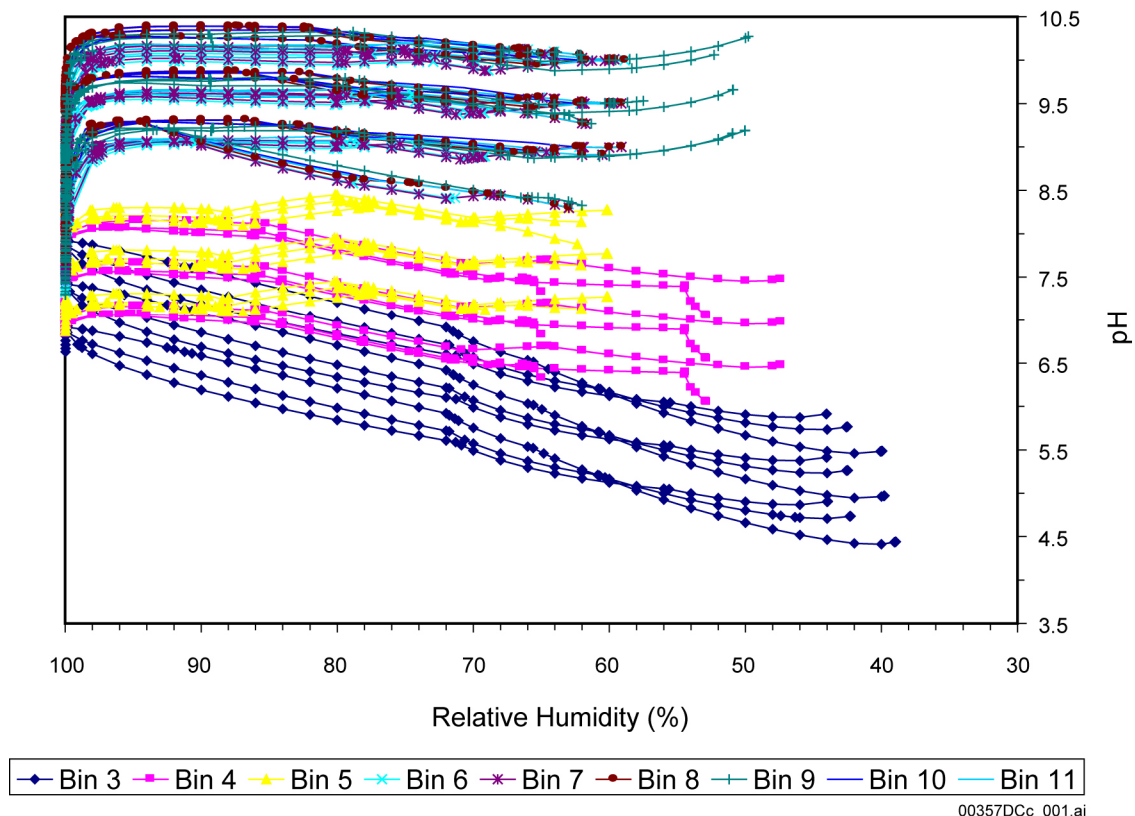
Water Location	0 to 50 Years (Preclosure)	51 to 700 Years (Boiling)	701 to 2,000 Years (Hot)	2,001 to 5,000 Years (Cool Down)	5,001 to 20,000 Years (Return to Ambient)
Crown	4,7,10	3,4,5,6,9,11	4,5,6, 9,11	6, 9,11	6, 7,8,9,10
Invert	4,7,10	1,2,3,4,5,9,11	4,5,6,9,11	6, 9,11	6, 7,8,9,10

Source: BSC 2003a, Table 6.14-3.

NOTE: Bins marked in bold are the most likely for the period based on BSC 2003a, Figure 6.14-1.

Figures G-1 through G-5 show selected chemical properties of the solutions formed by the evaporation of waters of Bins 3 through 11 for a range of relative humidity values. Bin 1 and Bin 2 waters are not possible chemistries for the seepage entering the crown of the drift (see

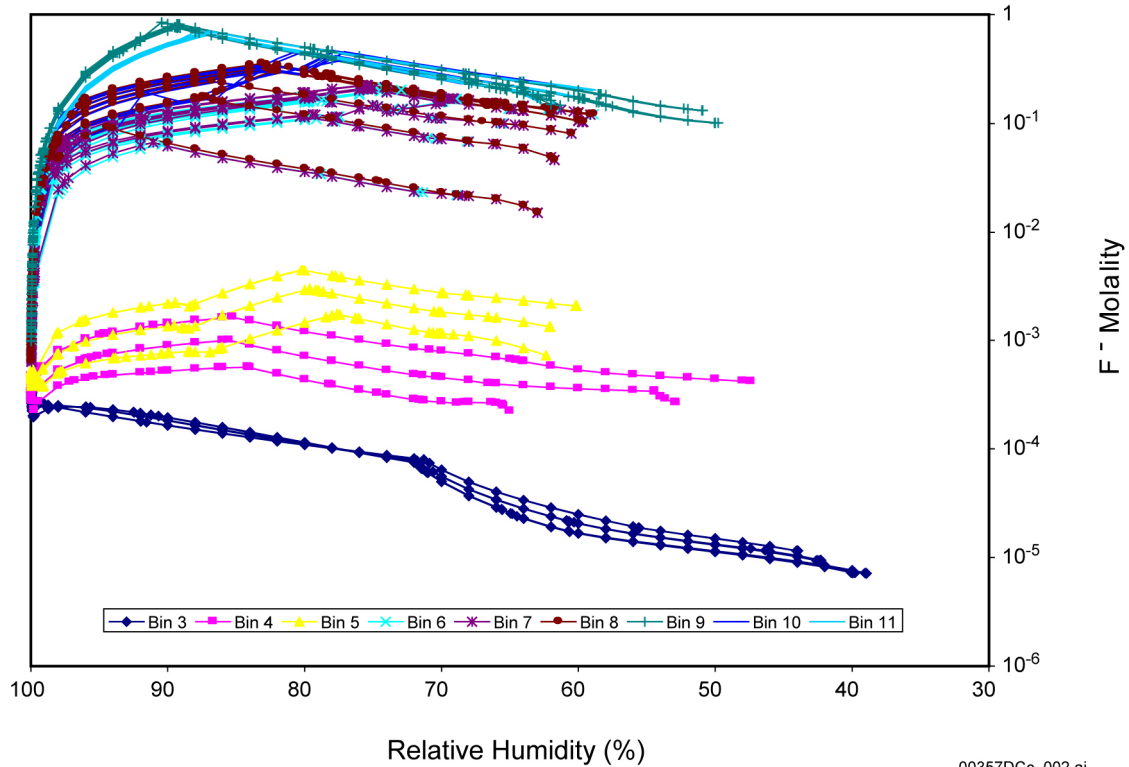
Table G-2). These two bins are not expected to drip onto waste package or drip shield surfaces and are not presented in these figures. Evaporation of the waters is modeled at each possible combination of three temperatures (40°C, 70°C, and 100°C) and three $p\text{CO}_2$ values (10^{-2} , 10^{-3} , and 10^{-4} bar). Figure G-1 shows the range of pH that is possible (about 10.5 to about 4.5) on the surface of the waste package or drip shield for seepage and evaporatively modified seepage waters. Figures G-2 through G-5 show the ranges for aqueous F^- (about 10^{-5} to about 1 molal), Cl^- (about 10^{-3} to about 10 molal), ionic strength (about 0.01 to about 30 molal), and $\text{Cl}^-/\text{NO}_3^-$ molal ratio (about 0.1 to about 30). The chemistry for dust leachate or deliquescence conditions fall within these ranges (see Section G.4.3).



Source: BSC 2003a, Figure 6.14-15.

NOTE: Evaporation of the waters is modeled at each possible combination of three temperatures (40°C, 70°C, and 100°C) and three $p\text{CO}_2$ values (10^{-2} , 10^{-3} , and 10^{-4} bar).

Figure G-1. Range of pH versus Relative Humidity for the Seepage Evaporation Lookup Tables Representing Bins 3 through 11 (at Three Temperatures and Three $p\text{CO}_2$ Values)

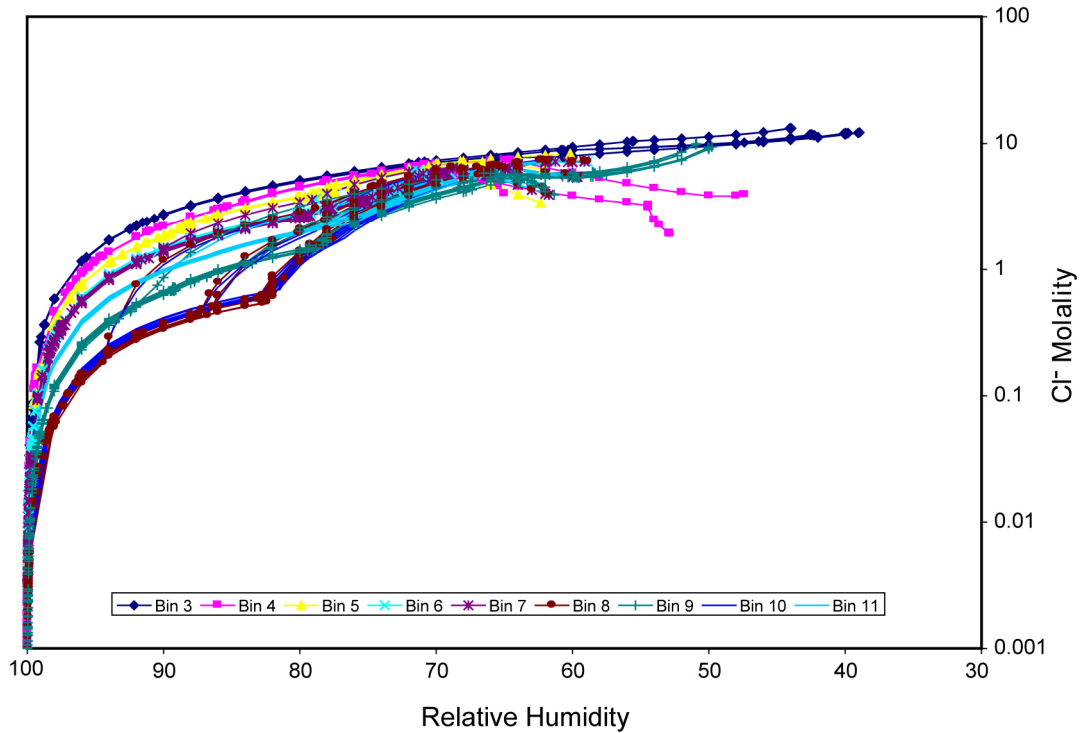


00357DCc_002.ai

Source: BSC 2003a, Figure 6.14-27.

NOTE: Evaporation of the waters is modeled at each possible combination of three temperatures (40°C, 70°C, and 100°C) and three $p\text{CO}_2$ values (10^{-2} , 10^{-3} , and 10^{-4} bar).

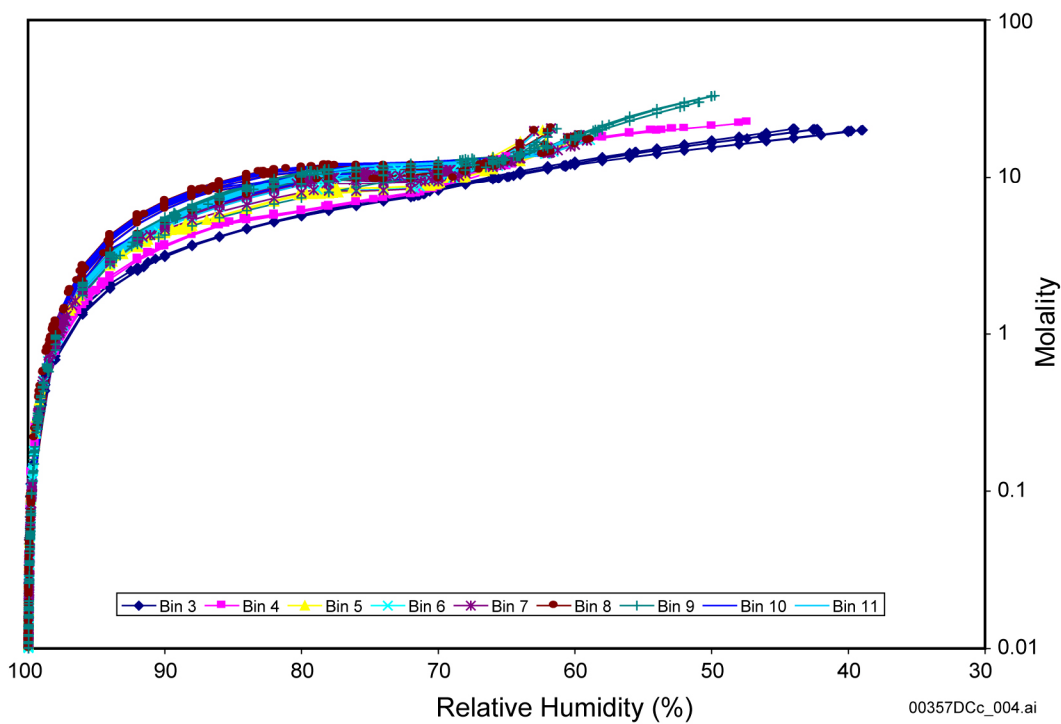
Figure G-2. Range of F⁻ Molality versus Relative Humidity for the Seepage Evaporation Lookup Tables Representing Bins 3 through 11 (at Three Temperatures and Three $p\text{CO}_2$ Values)



Source: BSC 2003a, Figure 6.14-28.

NOTE: Evaporation of the waters is modeled at each possible combination of three temperatures (40°C, 70°C, and 100°C) and three $p\text{CO}_2$ values (10^{-2} , 10^{-3} , and 10^{-4} bar).

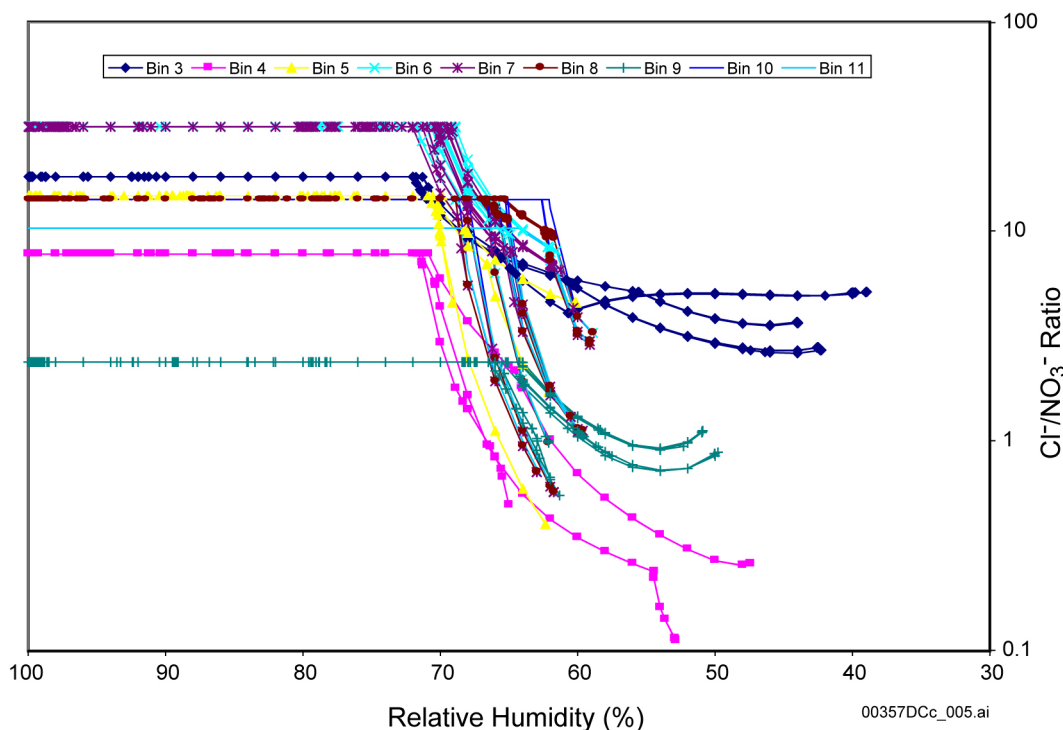
Figure G-3. Range of Cl⁻ Molality versus Relative Humidity for the Seepage Evaporation Lookup Tables Representing Bins 3 through 11 (at Three Temperatures and Three $p\text{CO}_2$ Values)



Source: BSC 2003a, Figure 6.14-33.

NOTE: Evaporation of the waters is modeled at each possible combination of three temperatures (40°C, 70°C, and 100°C) and three $p\text{CO}_2$ values (10^{-2} , 10^{-3} , and 10^{-4} bar).

Figure G-4. Range of Ionic Strength versus Relative Humidity for the Seepage Evaporation Lookup Tables Representing Bins 3 through 11 (at Three Temperatures and Three $p\text{CO}_2$ Values)



Source: BSC 2003a, Figure 6.14-29.

NOTE: Evaporation of the waters is modeled at each possible combination of three temperatures (40°C, 70°C, and 100°C) and three $p\text{CO}_2$ values (10^{-2} , 10^{-3} , and 10^{-4} bar).

Figure G-5. Range of $\text{Cl}^-/\text{NO}_3^-$ Molal Ratios versus Relative Humidity for the Seepage Evaporation Lookup Tables Representing Bins 3 through 11 (at Three Temperatures and Three $p\text{CO}_2$ Values)

Table G-4 shows the brine compositions that develop during evaporative concentration of the seepage waters as presented in the TSPA lookup tables. Also shown is the end-point relative humidity of the brines represented by the 11 bins. Under most conditions, the seepage waters can be classified as one of three brine types: calcium chloride, carbonate, or sulfate. These are chemical divide-based characterizations (see Appendix E). The sulfate brine is actually dominated by sodium chloride. Brines dominated by sodium nitrate, potassium nitrate, and potassium chloride are also possible. In Bins 1 through 3, the accumulation of Ca^{2+} and Cl^- is sufficient to make them the dominant cation and anion, respectively, as relative humidity decreases. Under these conditions, the potential for aggressive localized corrosion exists. However, bins 1 and 2 are not possible as crown seepage and the time integrated bin probability for Bin 3 over the 20,000-year timeframe is 0.22 percent (Table G-2). In fact, Bin 3 only occurs during the first several hundred years (Table G-3) when drift temperatures are high and liquid water is least likely to enter the drift (the water compositions discussed here represent the compositions present at locations of high saturation nearest the drift—not necessarily at the drift face—and, hence, most likely to represent seepage, if it can occur; however, when drift-wall temperatures are above boiling, these waters cannot enter the drift). In Bins 4, 5, 6, 9, and 11 (72 percent of the total) the dominant anion is Cl^- , which could provide the potential for localized corrosion. However, Bins 4 through 7 and 11 are not expected to be as aggressive as Bin 3 because of the low Ca^{2+} concentrations. Also evident from Figure G-5 is the potential for

six of the bins to have a $\text{Cl}^-/\text{NO}_3^-$ ratio above 10 at relative humidity conditions above 70 percent. In Bins 6 and 7, $\text{Cl}^-/\text{NO}_3^-$ ratios above 30 are possible. $\text{Cl}^-/\text{NO}_3^-$ ratios above 10 are more conducive for initiating localized corrosion of waste packages. Bin 7 is associated with the cool down and preclosure periods and has a relatively high probability of occurrence in the 10,000- to 20,000-year interval (Table G-3). Bin 6 is associated with the hotter waste package temperatures that occur early in the repository history, and waters in this bin are much less likely to occur.

Table G-4. The End-Point Relative Humidity and Brine Composition Evolution for Each Bin Water

Bin	Number of Waters in Bin	Percentage of All Waters (368 total)	Temp. °C	pCO_2 (bar)	Endpoint RH	98% RH Brine	85% RH Brine	65% RH Brine	Endpoint Brine
1	5	1.4%	100	10^{-2}	20.0%	Ca-Cl	Ca-Cl	Ca-Cl	Ca-Cl
			40	10^{-2}	18.1%	Ca-Cl	Ca-Cl	Ca-Cl	Ca-Cl
			70	10^{-2}	18.7%	Ca-Cl	Ca-Cl	Ca-Cl	Ca-Cl
			100	10^{-3}	20.0%	Ca-Cl	Ca-Cl	Ca-Cl	Ca-Cl
			40	10^{-3}	18.1%	Ca-Cl	Ca-Cl	Ca-Cl	Ca-Cl
			70	10^{-3}	18.7%	Ca-Cl	Ca-Cl	Ca-Cl	Ca-Cl
			100	10^{-4}	20.0%	Ca-Cl	Ca-Cl	Ca-Cl	Ca-Cl
			40	10^{-4}	18.2%	Ca-Cl	Ca-Cl	Ca-Cl	Ca-Cl
			70	10^{-4}	18.7%	Ca-Cl	Ca-Cl	Ca-Cl	Ca-Cl
2	13	3.5%	100	10^{-2}	24.0%	Na-Cl	Na-Cl	Na-Cl	Ca-Cl
			40	10^{-2}	23.1%	Na-Cl	Na-Cl	Na-Cl	Ca-Cl
			70	10^{-2}	23.4%	Na-Cl	Na-Cl	Na-Cl	Ca-Cl
			100	10^{-3}	24.0%	Na-Cl	Na-Cl	Na-Cl	Ca-Cl
			40	10^{-3}	23.1%	Na-Cl	Na-Cl	Na-Cl	Ca-Cl
			70	10^{-3}	24.0%	Na-Cl	Na-Cl	Na-Cl	Ca-Cl
			100	10^{-4}	24.0%	Na-Cl	Na-Cl	Na-Cl	Ca-Cl
			40	10^{-4}	23.1%	Na-Cl	Na-Cl	Na-Cl	Ca-Cl
			70	10^{-4}	24.0%	Na-Cl	Na-Cl	Na-Cl	Ca-Cl
3	12	3.3%	100	10^{-2}	43.9%	Na-Cl	Na-Cl	Na-Cl	K-Cl
			40	10^{-2}	38.9%	Na-Cl	Na-Cl	Na-Cl	Ca-Cl
			70	10^{-2}	42.3%	Na-Cl	Na-Cl	Na-Cl	K-Cl
			100	10^{-3}	44.0%	Na-Cl	Na-Cl	Na-Cl	K-Cl
			40	10^{-3}	39.8%	Na-Cl	Na-Cl	Na-Cl	Ca-Cl
			70	10^{-3}	42.5%	Na-Cl	Na-Cl	Na-Cl	K-Cl
			100	10^{-4}	44.0%	Na-Cl	Na-Cl	Na-Cl	K-Cl
			40	10^{-4}	40.0%	Na-Cl	Na-Cl	Na-Cl	Ca-Cl
			70	10^{-4}	42.5%	Na-Cl	Na-Cl	Na-Cl	K-Cl
4	43	11.7%	100	10^{-2}	47.4%	Na-Cl	Na-Cl	K-Cl	K-N
			40	10^{-2}	65.0%	Na-Cl	Na-Cl	Na-N	Na-N
			70	10^{-2}	52.9%	Na-Cl	Na-Cl	Na-N	Na-N
			100	10^{-3}	47.4%	Na-Cl	Na-Cl	K-Cl	K-N
			40	10^{-3}	65.0%	Na-Cl	Na-Cl	Na-N	Na-N
			70	10^{-3}	52.9%	Na-Cl	Na-Cl	Na-N	Na-N
			100	10^{-4}	47.4%	Na-Cl	Na-Cl	K-Cl	K-N
			40	10^{-4}	65.0%	Na-Cl	Na-Cl	Na-N	Na-N
			70	10^{-4}	52.9%	Na-Cl	Na-Cl	Na-N	Na-N
5	27	7.3%	100	10^{-2}	60.1%	Na-Cl	Na-Cl	Na-Cl	Na-Cl
			40	10^{-2}	69.1%	Na-Cl	Na-Cl	No Brine	Na-Cl
			70	10^{-2}	62.1%	Na-Cl	Na-Cl	Na-Cl	K-Cl
			100	10^{-3}	60.1%	Na-Cl	Na-Cl	Na-Cl	Na-Cl
			40	10^{-3}	69.9%	Na-Cl	Na-Cl	No Brine	Na-Cl
			70	10^{-3}	62.1%	Na-Cl	Na-Cl	Na-Cl	K-Cl
			100	10^{-4}	60.1%	Na-Cl	Na-Cl	Na-Cl	Na-Cl
			40	10^{-4}	62.4%	Na-Cl	Na-Cl	Na-N	Na-N
			70	10^{-4}	62.1%	Na-Cl	Na-Cl	Na-Cl	K-Cl
6	8	2.2%	100	10^{-2}	59.1%	Na-Cl	Na-Cl	Na-Cl	K-Cl
			40	10^{-2}	63.0%	Na-Cl	Na-Cl	Na-Cl	Na-N
			70	10^{-2}	60.5%	Na-Cl	Na-Cl	Na-Cl	K-Cl
			100	10^{-3}	59.1%	Na-Cl	Na-Cl	Na-Cl	Na-Cl
			40	10^{-3}	61.7%	Na-Cl	Na-Cl	Na-Cl	Na-N
			70	10^{-3}	59.7%	Na-Cl	Na-Cl	Na-Cl	K-Cl
			100	10^{-4}	58.9%	Na-Cl	Na-Cl	Na-Cl	Na-Cl
			40	10^{-4}	64.1%	Na-Cl	Na-Cl	Na-Cl	Na-Cl
			70	10^{-4}	59.6%	Na-Cl	Na-Cl	Na-Cl	K-Cl

00357DC_032pt1b.ai

Table G-4. The End-Point Relative Humidity and Brine Composition Evolution for each Bin Water (Continued)

Bin	Number of Waters in Bin	Percentage of All Waters (368 total)	Temp. °C	pCO ₂ (bar)	Endpoint RH	98% RH Brine	85% RH Brine	65% RH Brine	Endpoint Brine
7	25	6.8%	100	10 ⁻²	59.1%	Na-Cl	Na-Cl	Na-Cl	K-Cl
			40	10 ⁻²	63.0%	Na-Cl	Na-Cl	Na-Cl	Na-N
			70	10 ⁻²	60.5%	Na-Cl	Na-Cl	Na-Cl	K-Cl
			100	10 ⁻³	59.1%	Na-Cl	Na-Cl	Na-Cl	Na-Cl
			40	10 ⁻³	61.7%	Na-Cl	Na-Cl	Na-Cl	Na-N
			70	10 ⁻³	59.7%	Na-Cl	Na-Cl	Na-Cl	K-Cl
			100	10 ⁻⁴	60.0%	Na-Cl	Na-Cl	Na-Cl	Na-Cl
			40	10 ⁻⁴	66.2%	Na-Cl	Na-Cl	No Brine	Na-Cl
			70	10 ⁻⁴	59.6%	Na-Cl	Na-Cl	Na-Cl	K-Cl
8	22	6.0%	100	10 ⁻²	59.1%	Na-C	Na-C	Na-Cl	K-Cl
			40	10 ⁻²	63.0%	Na-C	Na-Cl	Na-N	Na-N
			70	10 ⁻²	60.5%	Na-C	Na-C	Na-Cl	K-Cl
			100	10 ⁻³	59.1%	Na-C	Na-C	Na-Cl	Na-Cl
			40	10 ⁻³	61.7%	Na-C	Na-C	Na-Cl	Na-N
			70	10 ⁻³	59.7%	Na-C	Na-C	Na-Cl	K-Cl
			100	10 ⁻⁴	58.9%	Na-C	Na-C	Na-Cl	Na-Cl
			40	10 ⁻⁴	62.2%	Na-C	Na-C	Na-Cl	Na-Cl
			70	10 ⁻⁴	59.6%	Na-C	Na-C	Na-Cl	K-Cl
9	58	15.8%	100	10 ⁻²	50.9%	Na-C	Na-C	Na-Cl	K-Cl
			40	10 ⁻²	62.0%	Na-C	Na-Cl	Na-Cl	K-N
			70	10 ⁻²	50.0%	Na-C	Na-C	Na-Cl	K-N
			100	10 ⁻³	50.9%	Na-C	Na-C	Na-Cl	K-Cl
			40	10 ⁻³	61.3%	Na-C	Na-C	Na-Cl	K-N
			70	10 ⁻³	57.5%	Na-C	Na-C	Na-Cl	K-N
			100	10 ⁻⁴	52.3%	Na-Si	Na-C	Na-Cl	K-N
			40	10 ⁻⁴	62.1%	Na-C	Na-C	Na-Cl	K-N
			70	10 ⁻⁴	49.8%	Na-C	Na-C	Na-Cl	K-N
10	10	2.7%	100	10 ⁻²	59.0%	Na-C	Na-C	Na-Cl	Na-Cl
			40	10 ⁻²	66.1%	Na-C	Na-Cl	No Brine	Na-Cl
			70	10 ⁻²	60.3%	Na-C	Na-C	Na-Cl	K-Cl
			100	10 ⁻³	59.0%	Na-C	Na-C	Na-Cl	Na-Cl
			40	10 ⁻³	61.5%	Na-C	Na-C	Na-Cl	Na-N
			70	10 ⁻³	59.6%	Na-C	Na-C	Na-Cl	K-Cl
			100	10 ⁻⁴	58.8%	Na-Si	Na-C	Na-Cl	Na-Cl
			40	10 ⁻⁴	62.1%	Na-C	Na-C	Na-Cl	Na-N
			70	10 ⁻⁴	59.5%	Na-C	Na-C	Na-Cl	K-Cl
11	145	39.4%	100	10 ⁻²	59.0%	Na-Cl	Na-Cl	Na-Cl	Na-Cl
			40	10 ⁻²	62.7%	Na-Cl	Na-Cl	Na-Cl	Na-N
			70	10 ⁻²	60.4%	Na-Cl	Na-Cl	Na-Cl	K-Cl
			100	10 ⁻³	59.0%	Na-Cl	Na-Cl	Na-Cl	Na-Cl
			40	10 ⁻³	61.5%	Na-Cl	Na-Cl	Na-Cl	Na-N
			70	10 ⁻³	59.6%	Na-Cl	Na-Cl	Na-Cl	K-Cl
			100	10 ⁻⁴	58.8%	Na-Cl	Na-Cl	Na-Cl	Na-Cl
			40	10 ⁻⁴	62.1%	Na-Cl	Na-Cl	Na-Cl	Na-N
			70	10 ⁻⁴	59.5%	Na-Cl	Na-Cl	Na-Cl	K-Cl

00357DC_032pt2b.ai

Source: BSC 2003a, Table 6.14-8.

G.4.3 Solutions Formed by Dust Deliquescence

Water compositions that could form by deliquescence of dust were modeled by simulating evaporation of dust leachate solutions, formed by leaching soluble components from dust samples from the Exploratory Studies Facility (ESF). This is also discussed in the response for ENFE 2.13 (Appendix I). Data used in the dust leachate analysis were collected in the ESF several years after initial construction of the tunnel. The following activities known to occur in the ESF could influence or alter the initial composition of dusts generated by the construction of emplacement drifts:

- Diesel emission from trains
- Welding activities
- Conveyor belt operations

- Dust suppression activities
- Operation of construction equipment
- Drilling and blasting activities
- Accumulation of human and animal waste.

Each of these activities could impact both local and repository-wide dust compositions. In all cases, trace elements and organics are possible airborne particulates.

Nitrate is of special interest because of its role as a corrosion inhibitor. The nitrate in the tunnel dusts likely has multiple sources. Dissolved nitrate is present in Yucca Mountain pore waters. Nitrate minerals (e.g., niter, KNO_3 ; soda niter, NaNO_3 ; and nitrocalcite, $\text{Ca}(\text{NO}_3)_2 \cdot 4\text{H}_2\text{O}$) have not been reported from Yucca Mountain. In general, nitrate tends to be a common component of desert terrain and subterranean environments. *Environment on the Surfaces of Drip Shield and Waste Package Outer Barrier* (BSC 2003b, Section 6.7.2.8) summarizes the sources of nitrate in the environment (e.g., electrical production in the upper atmosphere, oxidation of organic matter in the lower soil zone) and occurrence of nitrate minerals in the subsurface environment, as noted in the scientific literature on caves. Hence, the presence of nitrate in the mountain (at the least in dissolved form) is expected. Anthropogenic sources are also possible. These could be local in the tunnels (e.g., by fuel burning to run machinery) or, to the extent that outside dust is present, regional (e.g., fuel burning, agricultural operations). Calcium nitrate is added to certain types of fuel as a desiccant. On the other hand, relatively little blasting (a potential source of nitrate) appears to have been employed in the construction of the tunnels.

During construction and waste emplacement at the repository, dust generated inside the repository will greatly overwhelm any externally derived atmospheric component. However, atmospheric dust may become important during the ventilation period, following repository closure. Atmospheric dust has not been characterized directly as part of this project, but information in the literature on the general properties of this dust, on relevant atmospheric processes, and on material from desert playas in Nevada has been summarized in *Environment on the Surfaces of Drip Shield and Waste Package Outer Barrier* (BSC 2003b, Section 6.7.2.8). In general, nitrate is an important component of atmospheric dusts, primarily due to its production in the upper atmosphere by electrical phenomena. Nitrate salts are recognized as an important component of atmospheric dusts and aerosols, and their properties (including deliquescence) are considered important to the understanding of certain weather and climatic phenomena. Anthropogenic sources add to the nitrate burden of atmospheric dust. The extent to which playa dusts add to this burden is not well known. Nitrate minerals are not commonly described as components of surficial playa salts, so playas are probably not a significant source of nitrate in atmospheric dust.

The dust leachates were abstracted into six groups (bins) of like water types using a similar method as that described for seepage waters (BSC 2003a, Section 6.10). Six representative bin water chemistries (see Table G-5) were then used to derive lookup tables for compositions of solutions formed by deliquescence. As with the seepage waters, this was done by simulating evaporation to dryness with EQ3/6 at temperatures of 40°C, 70°C, 100°C, 120°C, and 140°C and $p\text{CO}_2$ values of 10^{-2} , 10^{-3} , and 10^{-4} bar. Note that the results at 140°C are considered preliminary pending completion of the extension of the *In-Drift Precipitates/Salts Model* (BSC 2003g) validation range up to 140°C. The model output was produced at relative humidity

value intervals of about 2 percent (in many instances less than this) from a relative humidity of about 100 percent down to the relative humidity of the end point of the evaporation. As with the seepage lookup tables above, the lookup tables represent response surfaces, so they suggest the potential ranges of outputs for the given inputs. The number of waters in each bin is given in Table G-6. The bin percentages given in Table G-6 represent probability of occurrence of each of the dust leachate bins on waste package and drip shield surfaces.

Table G-5. Total EQ3NR-Equilibrated Aqueous Elemental Compositions for the 6 Bins

	Bin 1	Bin 2	Bin 3	Bin 4	Bin 5	Bin 6
Temp (°C)	25	25	25	25	25	25
pH	8.54	8.09	8.23	8.54	8.40	8.05
(I)	5.43×10^{-3}	2.74×10^{-3}	2.01×10^{-3}	6.29×10^{-3}	3.80×10^{-3}	1.15×10^{-3}
Br	5.01×10^{-6}	1.00×10^{-5}	3.75×10^{-6}	1.63×10^{-5}	1.63×10^{-5}	3.75×10^{-6}
C	1.96×10^{-3}	6.50×10^{-4}	8.86×10^{-4}	1.94×10^{-3}	1.36×10^{-3}	5.81×10^{-4}
Ca	1.35×10^{-3}	5.41×10^{-4}	3.09×10^{-4}	1.22×10^{-3}	7.17×10^{-4}	1.52×10^{-4}
Cl	2.17×10^{-4}	1.44×10^{-4}	1.35×10^{-4}	4.23×10^{-4}	2.82×10^{-4}	1.38×10^{-4}
F	3.16×10^{-5}	1.58×10^{-5}	1.58×10^{-5}	2.11×10^{-5}	3.68×10^{-5}	2.11×10^{-5}
K	2.63×10^{-4}	1.93×10^{-4}	2.99×10^{-4}	3.32×10^{-4}	2.63×10^{-4}	1.98×10^{-4}
Mg	1.65×10^{-4}	5.35×10^{-5}	4.81×10^{-5}	1.63×10^{-4}	7.08×10^{-5}	2.14×10^{-5}
N	5.16×10^{-4}	1.77×10^{-4}	1.18×10^{-4}	5.48×10^{-4}	3.23×10^{-4}	5.64×10^{-5}
Na	4.24×10^{-4}	4.05×10^{-4}	4.83×10^{-4}	1.34×10^{-3}	9.03×10^{-4}	3.72×10^{-4}
S	4.37×10^{-4}	3.96×10^{-4}	1.67×10^{-4}	6.97×10^{-4}	3.44×10^{-4}	6.04×10^{-5}
Si	1.46×10^{-4}	3.25×10^{-5}	6.27×10^{-5}	4.89×10^{-5}	7.91×10^{-5}	4.78×10^{-5}

Source: BSC 2003a, Table 6.10.6-9.

NOTE: Except for temperature and pH, all units are in moles/kg H₂O; total C includes carbonate species, total N comprises nitrate species, and total S comprises sulfate species.

Table G-6. Percentage of Dust Leachate Waters in Each Bin

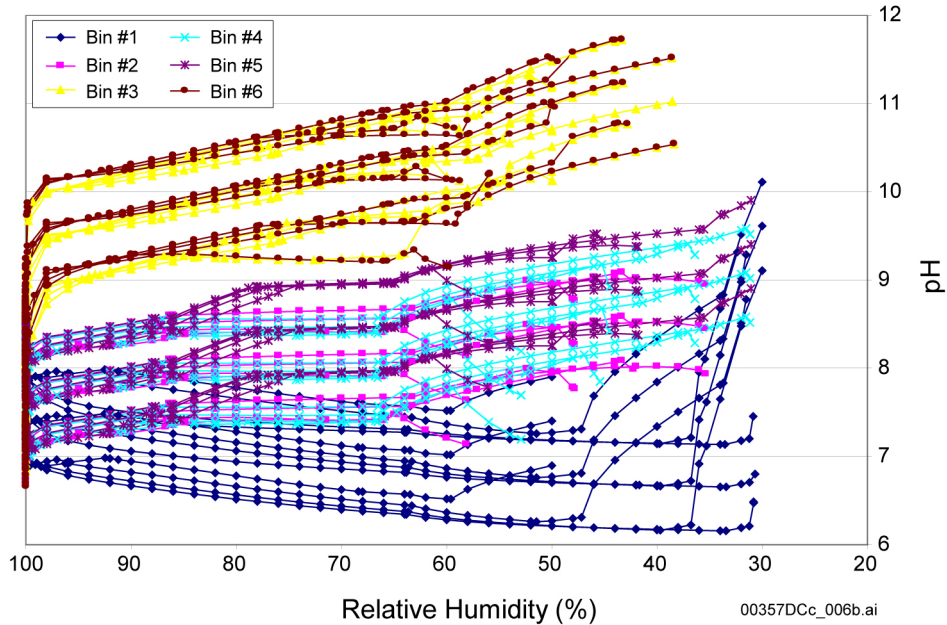
Bin	Number of Waters in the Bin	% of All Evaporated Waters Represented by the Bin
Bin 1	3	5.77
Bin 2	4	7.69
Bin 3	9	17.31
Bin 4	12	23.08
Bin 5	23	44.23
Bin 6	1	1.92
Total	52	100.00

Source: BSC 2003a, Table 6.10-6.

The lookup table calculations for dusts show that the brine pH is more sensitive to the in-drift temperature and $p\text{CO}_2$ changes than to the other parameters. Figure G-6 shows three groupings of curves for each bin. These three groupings reflect the $p\text{CO}_2$ concentrations trending downward from lowest to highest. As a result of the decrease of $p\text{CO}_2$, the concentrations of calcium and magnesium are decreased due to the precipitation of carbonate minerals. However, the effect of temperature on brine pH is more complicated, and it varies with humidity. Temperature effects are shown on Figure G-6 by looking at each bundle of four lines (one line for each temperature: 40°C, 70°C, 100°C, and 120°C) that is associated with a given $p\text{CO}_2$ group. The change of temperature from 40°C to 120°C generally results in pH variations of less than one-half a pH unit except for bin 1 waters at low relative humidities. As Table G-6 indicates, bin 1 waters occur less than 6 percent of the time. The pH variation for the preliminary 140°C runs is shown on Figure G-7.

The variations of brine chemistry among six representative dusts are shown in Figures G-6 through G-17. Figures G-6 and G-7 indicate that the maximum pH of water that can be had from deliquescing water on waste packages is 11.7 and ranges down to a value slightly greater than 6. Figures G-8 and G-9 show that F^- concentrations are less than one molal for all samples during the evaporation because of the precipitation of CaF_2 . Figures G-10 and G-11 indicate that the ionic strength ranges from 10^{-3} molal to values as great as about 50 molal at low humidities. Figures G-12 and G-13 show at a low humidity, the brine condensed on dust could have a Cl^- concentration as high as 9 molal. The NO_3^- concentrations can be as high as about 20 molal (Figures G-14 and G-15). Figures G-16 and G-17 show that high ratios of $\text{Cl}^-/\text{NO}_3^-$ occur only for dust leachate Bin 6. At least 81 percent of waste packages should never attain ratios higher than one.

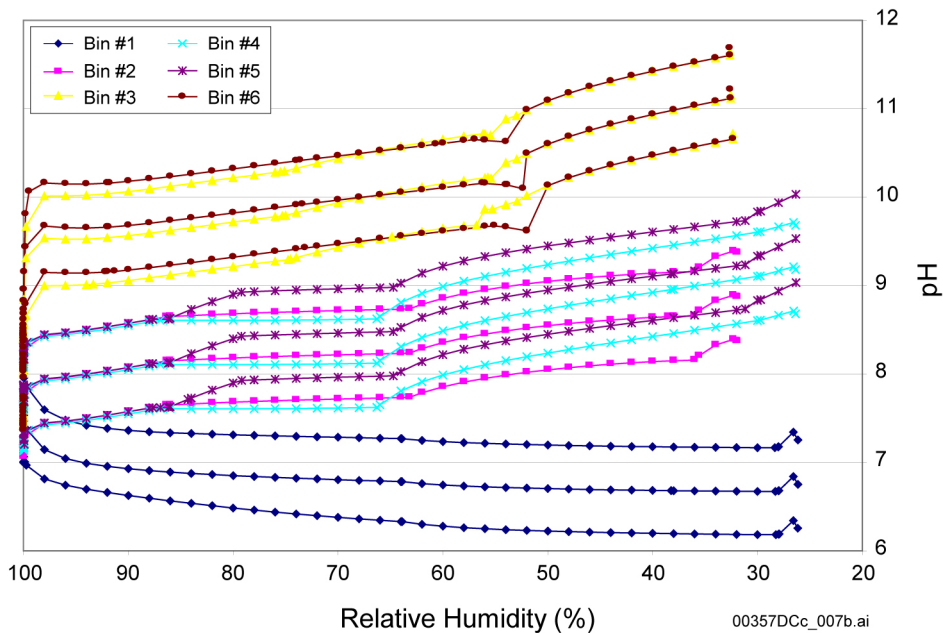
Table G-7 shows the brine compositions that develop during evaporative concentration of the dust leachate, as presented in the TSPA lookup tables. Also shown in this figure is the end-point relative humidity of the brines represented by the six bins. For most of the evaporative process, the brines formed from dust leachate waters tend to be dominated by sodium nitrate, sodium sulfate, calcium nitrate, potassium nitrate, or potassium carbonate. Only Bin 1 shows an accumulation of Ca^{2+} sufficient to make it the dominant cation, yet the dominant anion in this bin through all relative humidity values is NO_3^- . Bin 3 is the only bin that shows any generation of a chloride-type brine. Based on the given distribution, this could occur about 16.4 percent of the time (see Table G-6). In the most likely case (Bin 5), the brine is a sodium nitrate type water.



Source: BSC 2003a, Figure 6.14-26.

NOTE: Evaporation of the waters is modeled at each possible combination of four temperatures (40°C, 70°C, 100°C, and 120°C) and three $p\text{CO}_2$ values (10^{-2} , 10^{-3} , and 10^{-4} bar).

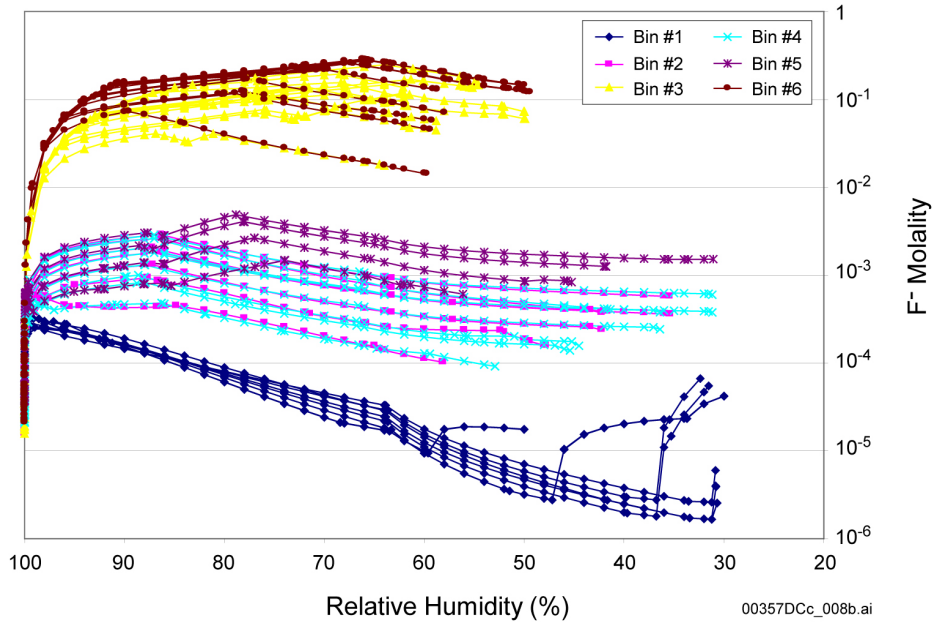
Figure G-6. Range of pH versus Relative Humidity for the Dust Leachate Lookup Tables Representing Bins 1 through 6



Source: BSC 2003a, Figure 6.14-26.

NOTE: Evaporation of the waters is modeled at 140°C and three $p\text{CO}_2$ values (10^{-2} , 10^{-3} , and 10^{-4} bar). Results at this temperature are preliminary pending extension of in-drift precipitates and salts model (BSC 2003g) validation.

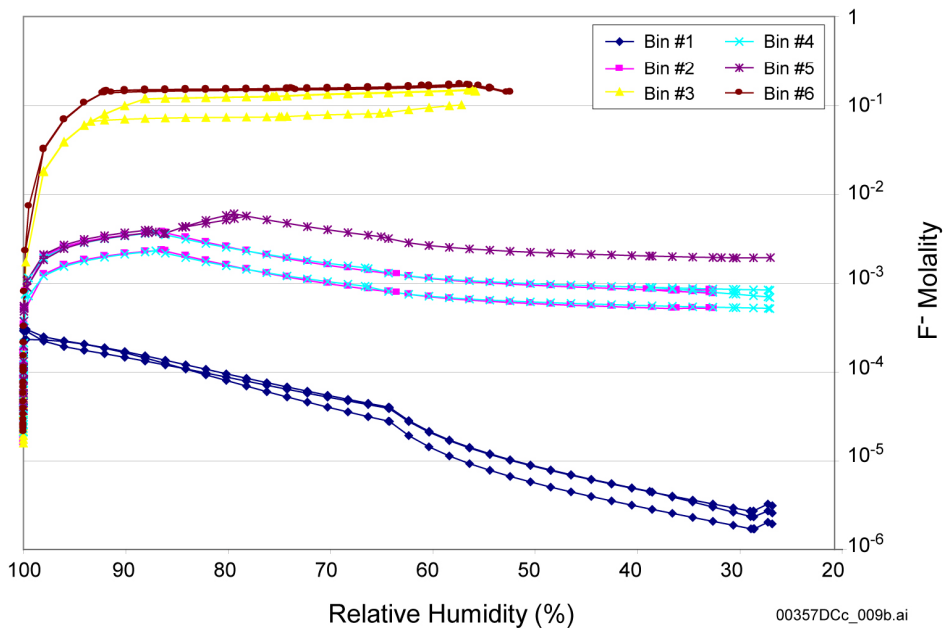
Figure G-7. Preliminary Range of pH versus Relative Humidity at 140°C the Dust Leachate Lookup Tables Representing Bins 1 through 6



Source: BSC 2003a, Figure 6.14-35.

NOTE: Evaporation of the waters is modeled at each possible combination of four temperatures (40°C, 70°C, 100°C, and 120°C) and three $p\text{CO}_2$ values (10^{-2} , 10^{-3} , and 10^{-4} bar).

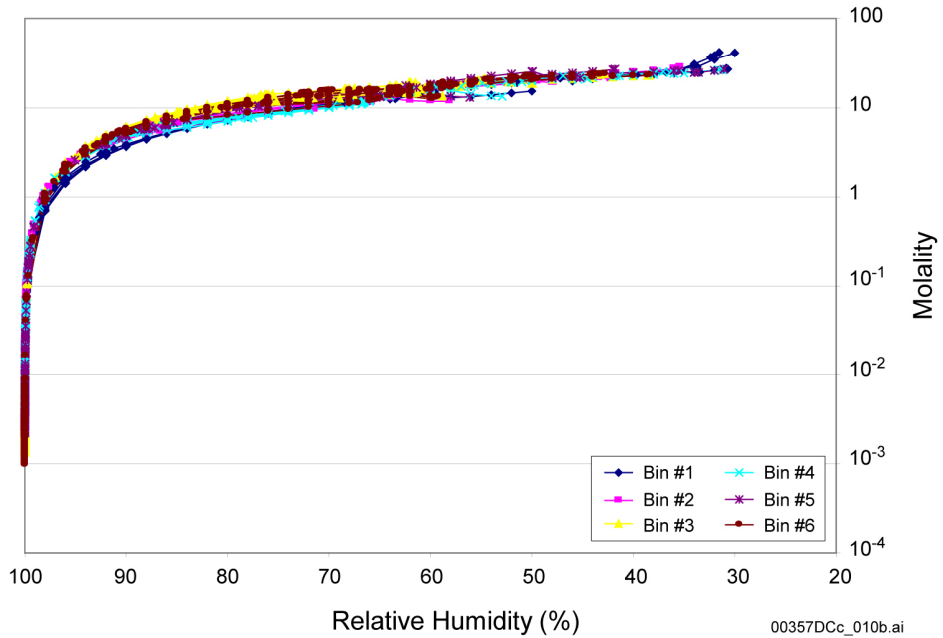
Figure G-8. Range of F^- Molality versus Relative Humidity for the Dust Leachate Lookup Tables Representing Bins 1 through 6



Source: BSC 2003a, Figure 6.14-35.

NOTE: Evaporation of the waters is modeled at 140°C and three $p\text{CO}_2$ values (10^{-2} , 10^{-3} , and 10^{-4} bar). Results at this temperature are preliminary pending extension of in-drift precipitates and salts model (BSC 2003g) validation.

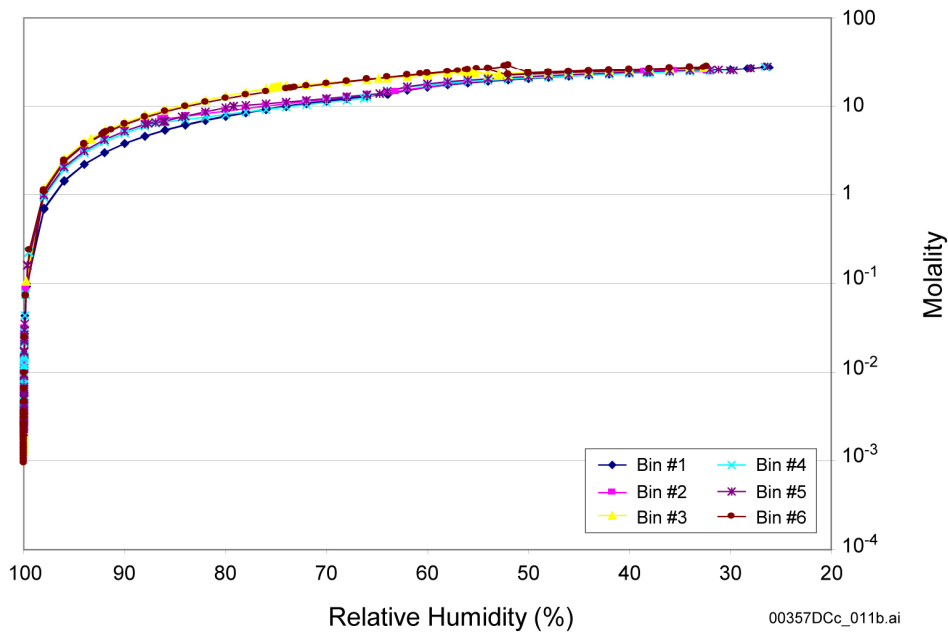
Figure G-9. Preliminary Range of F^- Molality versus Relative Humidity at 140°C for the Dust Leachate Lookup Tables Representing Bins 1 through 6



Source: BSC 2003a, Figure 6.14-36.

NOTE: Evaporation of the waters is modeled at each possible combination of four temperatures (40°C, 70°C, 100°C, and 120°C) and three $p\text{CO}_2$ values (10^{-2} , 10^{-3} , and 10^{-4} bar).

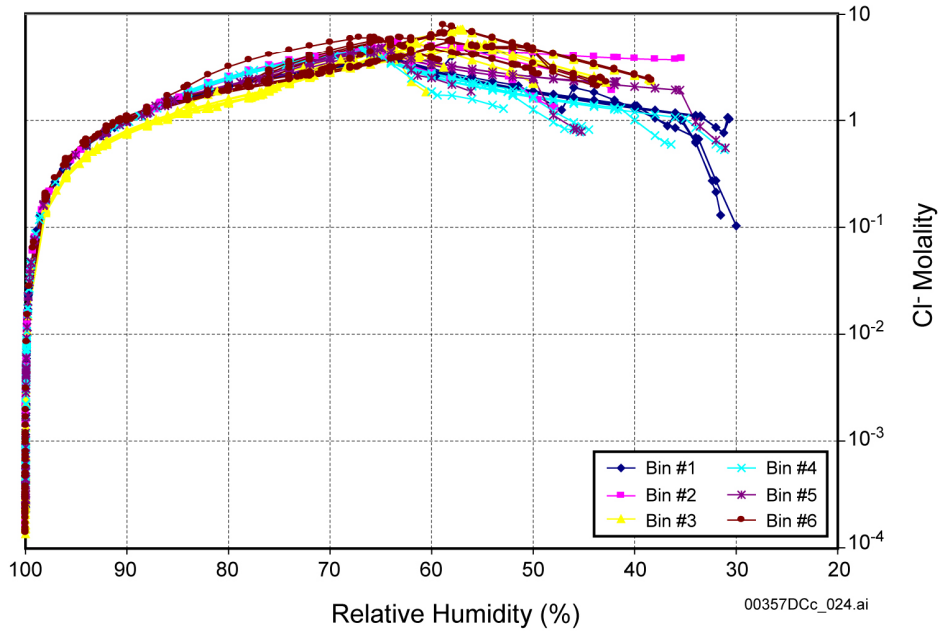
Figure G-10. Range of Ionic Strength versus Relative Humidity for the Dust Leachate Lookup Tables Representing Bins 1 through 6



Source: BSC 2003a, Figure 6.14-36.

NOTE: Evaporation of the waters is modeled at 140°C and three $p\text{CO}_2$ values (10^{-2} , 10^{-3} , and 10^{-4} bar). Results at this temperature are preliminary pending extension of in-drift precipitates and salts model (BSC 2003g) validation.

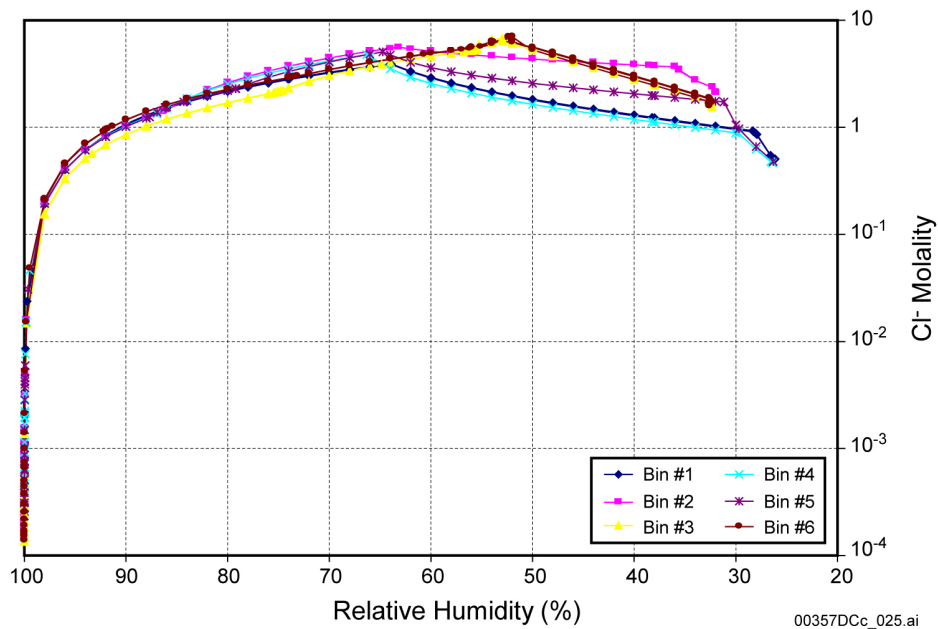
Figure G-11. Preliminary Range of Ionic Strength versus Relative Humidity at 140°C for the Dust Leachate Lookup Tables Representing Bins 1 through 6



Source: BSC 2003a, Figure-6.14-37.

NOTE: Evaporation of the waters is modeled at each possible combination of four temperatures (40°C, 70°C, 100°C, and 120°C) and three pCO₂ values (10⁻², 10⁻³, and 10⁻⁴ bar).

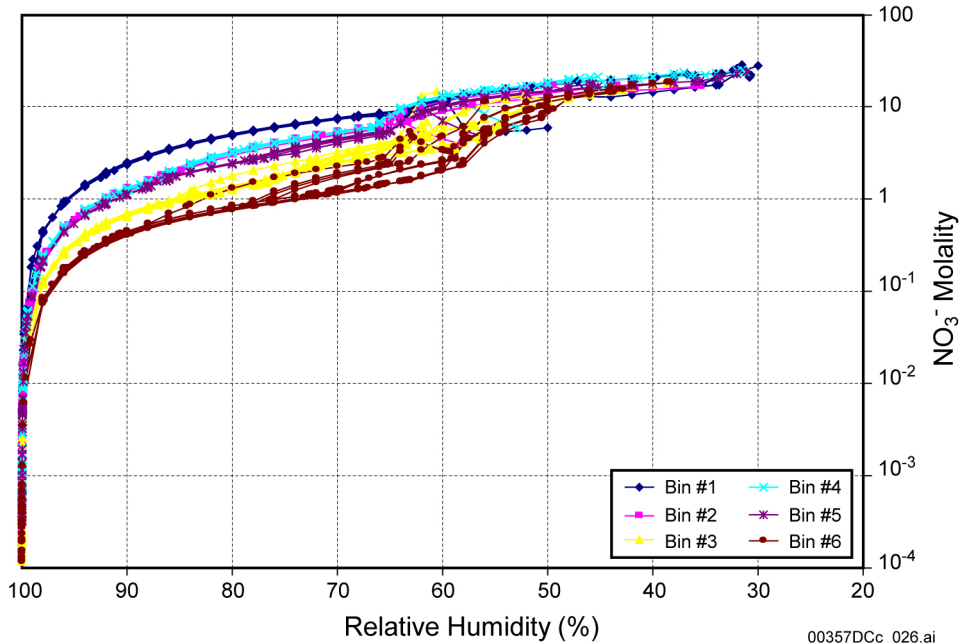
Figure G-12. Range of Cl⁻ Molality versus Relative Humidity for the Dust Leachate Lookup Tables Representing Bins 1 through 6



Source: BSC 2003a, Figure 6.14-37.

NOTE: Evaporation of the waters is modeled at 140°C and three pCO₂ values (10⁻², 10⁻³, and 10⁻⁴ bar). Results at this temperature are preliminary pending extension of in-drift precipitates and salts model (BSC 2003g) validation.

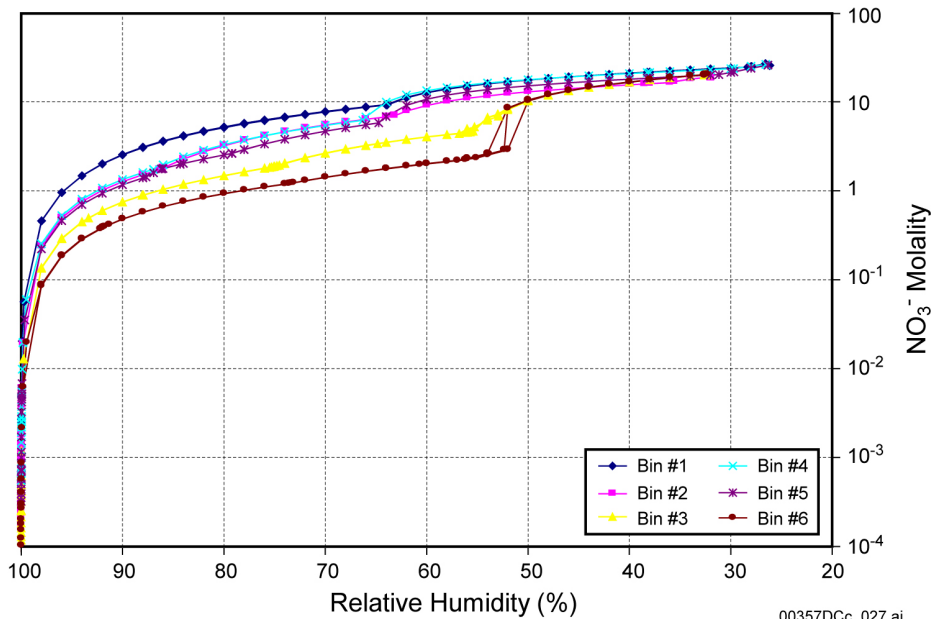
Figure G-13. Preliminary Range of Cl⁻ Molality versus Relative Humidity at 140°C for the Dust Leachate Lookup Tables Representing Bins 1 through 6



Source: BSC 2003a, Figure 6.14-39.

NOTE: Evaporation of the waters is modeled at each possible combination of four temperatures (40°C, 70°C, 100°C, and 120°C) and three pCO₂ values (10⁻², 10⁻³, and 10⁻⁴ bar).

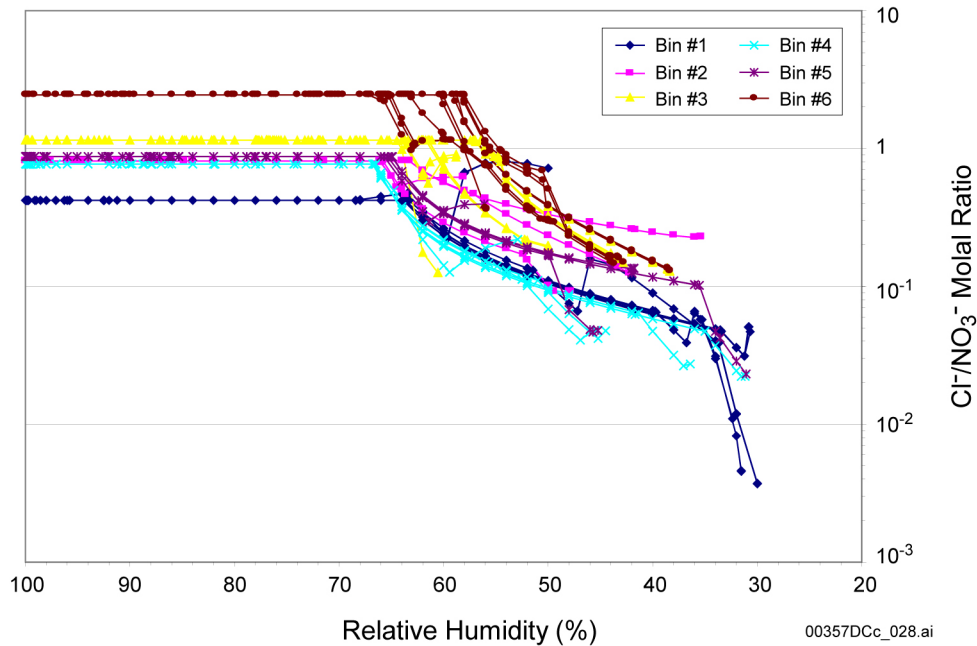
Figure G-14. Range of NO₃⁻ Molality versus Relative Humidity for the Dust Leachate Lookup Tables Representing Bins 1 through 6



Source: BSC 2003a, Figure 6.14-39.

NOTE: Evaporation of the waters is modeled at 140°C and three pCO₂ values (10⁻², 10⁻³, and 10⁻⁴ bar). Results at this temperature are preliminary pending extension of in-drift precipitates and salts model (BSC 2003g) validation.

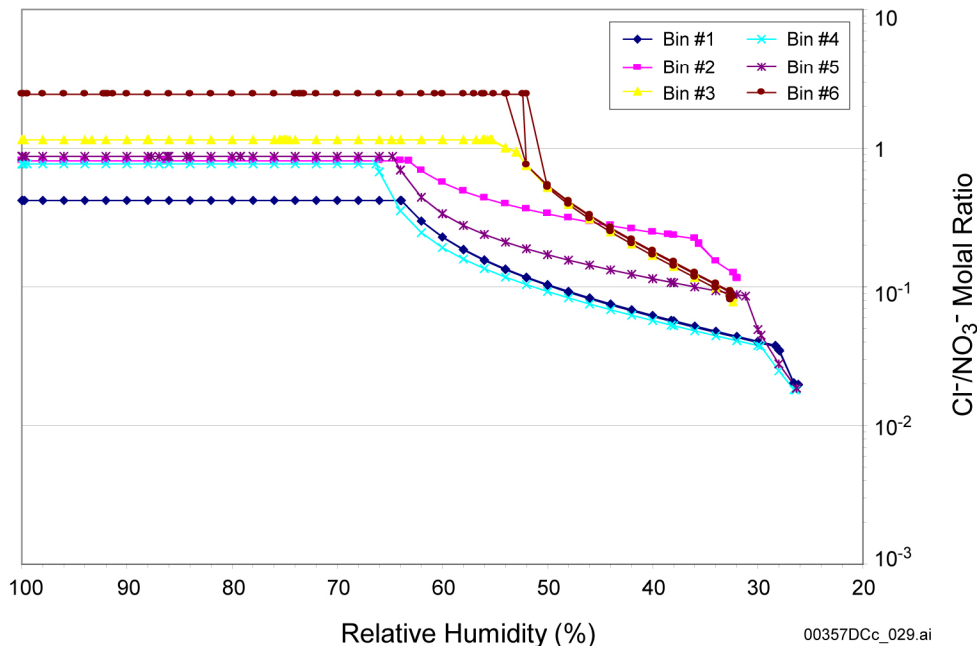
Figure G-15. Preliminary Range of NO₃⁻ Molality versus Relative Humidity at 140°C for the Dust Leachate Lookup Tables Representing Bins 1 through 6



Source: BSC 2003a, Figure 6.14-38.

NOTE: Evaporation of the waters is modeled at each possible combination of four temperatures (40°C, 70°C, 100°C, and 120°C) and three pCO₂ values (10⁻², 10⁻³, and 10⁻⁴ bar).

Figure G-16. Range of Cl⁻/NO₃⁻ Molal Ratios versus Relative Humidity for the Dust Leachate Lookup Tables Representing Bins 1 through 6



Source: BSC 2003a, Figure 6.14-38.

NOTE: Evaporation of the waters is modeled at 140°C and three pCO₂ values (10⁻², 10⁻³, and 10⁻⁴ bar). Results at this temperature are preliminary pending extension of in-drift precipitates and salts model (BSC 2003g) validation.

Figure G-17. Preliminary Range of Cl⁻/NO₃⁻ Molal Ratios versus Relative Humidity at 140°C for the Dust Leachate Lookup Tables Representing Bins 1 through 6

Table G-7. The End-Point Relative Humidity and Brine Evolution Composition for Each Dust Leachate Bin Water

Bin	% of All 52 Waters	Temp. (°C)	pCO ₂ (bar)	Endpoint Relative Humidity	98% Relative Humidity Brine	85% Relative Humidity Brine	65% Relative Humidity Brine	Endpoint Brine
1	5.8	40	1 × 10 ⁻²	50.0%	Na-N	Na-N	Na-N	Ca-N
		70		30.0%	Na-N	Na-N	Na-N	Ca-N
		100		31.5%	Na-N	Na-N	Na-N	Ca-N
		120		30.8%	Na-N	Na-N	Na-N	K-N
		140		26.2%	Na-N	Na-N	Na-N	Na-N
		40	1 × 10 ⁻³	50.0%	Na-N	Na-N	Na-N	Ca-N
		70		30.0%	Na-N	Na-N	Na-N	Ca-N
		100		31.5%	Na-N	Na-N	Na-N	Ca-N
		120		30.7%	Na-N	Na-N	Na-N	K-N
		140		26.2%	Na-N	Na-N	Na-N	Na-N
		40	1 × 10 ⁻⁴	50.0%	Na-N	Na-N	Na-N	Ca-N
		70		30.0%	Na-N	Na-N	Na-N	Ca-N
		100		32.4%	Na-N	Na-N	Na-N	Ca-N
		120		30.8%	Na-N	Na-N	Na-N	K-N
		140		26.2%	Na-N	Na-N	Na-N	Na-N
2	7.7	40	1 × 10 ⁻²	58.1%	Na-N	Na-N	Na-N	Na-Br
		70		47.8%	Na-N	Na-N	Na-N	Na-N
		100		42.2%	Na-N	Na-N	K-N	K-N
		120		35.4%	Na-N	Na-N	K-N	K-N
		140		32.0%	Na-N	Na-N	K-N	K-N
		40	1 × 10 ⁻³	58.1%	Na-N	Na-N	Na-N	Na-Br
		70		47.8%	Na-N	Na-N	Na-N	Na-N
		100		42.2%	Na-N	Na-N	K-N	K-N
		120		35.4%	Na-N	Na-N	K-N	K-N
		140		32.0%	Na-N	Na-N	K-N	K-N
		40	1 × 10 ⁻⁴	58.1%	Na-N	Na-N	Na-N	Na-Br
		70		47.8%	Na-N	Na-N	Na-N	K-N
		100		42.2%	Na-N	Na-N	K-N	K-N
		120		35.4%	Na-N	Na-N	K-N	K-N
		140		32.0%	Na-N	Na-N	K-N	K-N
3	17.3	40	1 × 10 ⁻²	60.5%	Na-S	Na-Cl	Na-Cl	Na-N
		70		49.9%	Na-S	Na-S	Na-Cl	K-N
		100		42.8%	Na-S	Na-S	Na-Cl	K-N
		120		38.4%	Na-S	Na-S	Na-Cl	K-N
		140		32.4%	Na-S	Na-S	Na-Cl	K-N
		40	1 × 10 ⁻³	58.8%	Na-S	Na-S	Na-Cl	Na-Br
		70		50.0%	Na-S	Na-S	Na-Cl	Na-N
		100		43.2%	Na-S	Na-S	Na-Cl	K-N
		120		38.5%	Na-S	Na-S	Na-Cl	K-N
		140		32.6%	Na-S	Na-S	Na-Cl	K-N
		40	1 × 10 ⁻⁴	58.8%	Na-S	Na-S	Na-Cl	Na-Br
		70		50.0%	Na-S	Na-S	Na-Cl	Na-N
		100		43.4%	Na-S	Na-S	Na-Cl	K-N
		120		38.6%	Na-S	Na-S	Na-Cl	K-N
		140		32.6%	Na-S	Na-S	Na-Cl	K-N

00357DCc_030.ai

Table G-7. The End-Point Relative Humidity and Brine Evolution Composition for Each Dust Leachate Bin Water (Continued)

Bin	% of All 52 Waters	Temp. (°C)	pCO ₂ (bar)	Endpoint Relative Humidity	98% Relative Humidity Brine	85% Relative Humidity Brine	65% Relative Humidity Brine	Endpoint Brine
4	23.1	40	1 × 10 ⁻²	52.9%	Na-N	Na-N	Na-N	Na-Br
		70		45.4%	Na-N	Na-N	Na-N	Na-N
		100		36.4%	Na-N	Na-N	Na-N	Na-N
		120		31.2%	Na-N	Na-N	Na-N	Na-N
		140		26.4%	Na-N	Na-N	Na-N	Na-N
		40	1 × 10 ⁻³	52.9%	Na-N	Na-N	Na-N	Na-Br
		70		44.5%	Na-N	Na-N	Na-N	Na-N
		100		36.4%	Na-N	Na-N	Na-N	Na-N
		120		31.2%	Na-N	Na-N	Na-N	Na-N
		140		26.4%	Na-N	Na-N	Na-N	Na-N
		40	1 × 10 ⁻⁴	52.9%	Na-N	Na-N	Na-N	Na-Br
		70		44.5%	Na-N	Na-N	Na-N	Na-N
		100		36.4%	Na-N	Na-N	Na-N	Na-N
		120		31.2%	Na-N	Na-N	Na-N	Na-N
		140		26.4%	Na-N	Na-N	Na-N	Na-N
5	44.2	40	1 × 10 ⁻²	56.1%	Na-N	Na-N	Na-N	Na-Br
		70		45.2%	Na-N	Na-N	Na-N	Na-N
		100		41.8%	Na-N	Na-N	Na-N	K-N
		120		31.1%	Na-N	Na-N	Na-N	Na-N
		140		26.3%	Na-N	Na-N	Na-N	Na-N
		40	1 × 10 ⁻³	56.1%	Na-N	Na-N	Na-N	Na-Br
		70		45.2%	Na-N	Na-N	Na-N	Na-N
		100		41.8%	Na-N	Na-N	Na-N	K-N
		120		31.1%	Na-N	Na-N	Na-N	Na-N
		140		26.3%	Na-N	Na-N	Na-N	Na-N
		40	1 × 10 ⁻⁴	56.1%	Na-N	Na-N	Na-N	Na-Br
		70		45.2%	Na-N	Na-N	Na-N	Na-N
		100		41.8%	Na-N	Na-N	Na-N	K-N
		120		31.1%	Na-N	Na-N	Na-N	Na-N
		140		26.3%	Na-N	Na-N	Na-N	Na-N
6	1.9	40	1 × 10 ⁻²	59.8%	Na-C	Na-Cl	Na-Cl	Na-Br
		70		55.9%	Na-C	Na-C	Na-Cl	K-N
		100		42.8%	Na-C	Na-Cl	Na-Cl	K-N
		120		38.4%	Na-C	Na-Cl	Na-Cl	K-N
		140		32.3%	Na-Cl	Na-Cl	Na-Cl	K-N
		40	1 × 10 ⁻³	59.4%	Na-C	Na-Cl	Na-Cl	Na-Cl
		70		49.7%	Na-Cl	Na-Cl	Na-Cl	K-N
		100		43.2%	Na-Cl	Na-Cl	Na-Cl	K-N
		120		38.5%	Na-Cl	Na-Cl	Na-Cl	K-N
		140		32.6%	Na-Cl	Na-Cl	Na-Cl	K-N
		40	1 × 10 ⁻⁴	59.3%	Na-Cl	Na-Cl	Na-Cl	Na-Cl
		70		49.4%	Na-Cl	Na-Cl	Na-Cl	K-N
		100		43.4%	Na-Cl	Na-Cl	Na-Cl	K-N
		120		38.6%	Na-Cl	Na-Cl	Na-Cl	K-N
		140		32.7%	Na-Cl	Na-Cl	Na-Cl	K-N

00357DCc_031.ai

Source: BSC 2003a, Table 6.14-9.

G.5 REFERENCES

- BSC (Bechtel SAIC Company) 2003a. *Engineered Barrier System: Physical and Chemical Environment Model*. ANL-EBS-MD-000033 REV 02C. Las Vegas, Nevada: Bechtel SAIC Company. ACC: MOL.20031029.0034.
- BSC 2003b. *Environment on the Surfaces of Drip Shield and Waste Package Outer Barrier*. ANL-EBS-MD-000001 REV 01D. Las Vegas, Nevada: Bechtel SAIC Company. ACC: MOL.20030825.0151.
- BSC 2003c. *WAPDEG Analysis of Waste Package and Drip Shield Degradation*. ANL-EBS-PA-000001 REV 01A. Las Vegas, Nevada: Bechtel SAIC Company. ACC: MOL.20030910.0142.
- BSC 2003d. *Drift-Scale Coupled Processes (DST and THC Seepage) Models*. MDL-NBS-HS-000001 REV 02. Las Vegas, Nevada: Bechtel SAIC Company. ACC: DOC.20030804.0004.
- BSC 2003e. Software Code: EQ3/6. V8.0. PC w/ Windows 95/98/2000/NT 4.0. 10813-8.0-00.
- BSC 2003f. *Multiscale Thermohydrologic Model Report*. ANL-EBS-MD-000049 REV 01C. Las Vegas, Nevada: Bechtel SAIC Company. ACC: MOL.20030910.0158.
- BSC 2003g. *In-Drift Precipitates/Salts Model*. ANL-EBS-MD-000045 REV 01. Las Vegas, Nevada: Bechtel SAIC Company. ACC: MOL.20031028.0003.
- Reamer, C.W. 2001. U.S. Nuclear Regulatory Commission/U.S. Department of Energy Technical Exchange and Management Meeting on Evolution of the Near-Field Environment (January 9–12, 2001). Letter from C.W. Reamer (NRC) to S. Brocoum (DOE/YMSCO), January 26, 2001, with enclosure. ACC: MOL.20010810.0033.

APPENDIX H
KINETICS OF CHEMICAL PROCESSES
(RESPONSE TO ENFE 2.11)

Note Regarding the Status of Supporting Technical Information

This document was prepared using the most current information available at the time of its development. This Technical Basis Document and its appendices providing Key Technical Issue Agreement responses that were prepared using preliminary or draft information reflect the status of the Yucca Mountain Project's scientific and design bases at the time of submittal. In some cases this involved the use of draft Analysis and Model Reports (AMRs) and other draft references whose contents may change with time. Information that evolves through subsequent revisions of the AMRs and other references will be reflected in the License Application (LA) as the approved analyses of record at the time of LA submittal. Consequently, the Project will not routinely update either this Technical Basis Document or its Key Technical Issue Agreement appendices to reflect changes in the supporting references prior to submittal of the LA.

APPENDIX H

KINETICS OF CHEMICAL PROCESSES (RESPONSE TO ENFE 2.11)

This appendix provides a response for Key Technical Issue (KTI) agreement Evolution of the Near-Field Environment (ENFE) 2.11. This KTI relates to providing the technical basis for the treatment of the kinetics of chemical processes in the in-drift geochemical models.

H.1 KEY TECHNICAL ISSUE AGREEMENT

H.1.1 ENFE 2.11

Agreement ENFE 2.11 was reached during the U.S. Nuclear Regulatory Commission (NRC)/U.S. Department of Energy (DOE) Technical Exchange and Management Meeting on Evolution of the Near-Field Environment held January 9 to 11, 2001, in Pleasanton, California (Reamer 2001). ENFE KTI subissues 1, 2, 3, and 4 were discussed at that meeting. There have been no specific submittals to the NRC on this subject.

The wording of the agreement is as follows:

ENFE 2.11

Provide the technical basis for the current treatment of the kinetics of chemical processes in the in-drift geochemical models. This basis should address data in the figure on page 16 of the G. Gdowski Subissue 2 presentation with appropriate treatment of time as related to abstractions used in TSPA. The DOE will provide additional technical basis for the treatment of precipitation-dissolution kinetics by the in-drift geochemical models, in a revision to the Engineered Barrier System: Physical and Chemical Environment Model AMR (ANL-EBS-MD-000033), expected to be available in FY02. The technical basis will include reaction progress simulation for laboratory evaporative concentration tests, and will include appropriate treatment of time as related to the residence times associated with the abstractions used to represent in-drift processes in TSPA.

H.1.2 Related Key Technical Issue Agreements

Agreement ENFE 2.04 (Appendix C) is related to ENFE 2.11 which deals with the technical basis for bounding the trace elements and fluoride.

H.2 RELEVANCE TO REPOSITORY PERFORMANCE

It is necessary to demonstrate an understanding of the environment that the drip shield and waste package are subjected to during the regulatory period because a significant portion of the postclosure repository performance is attributed to these engineered components. Precipitation-dissolution, evaporative concentration, and deliquescence of salts all have the potential to reduce waste package and drip shield lifetimes due to their impacts on general and localized corrosion. Since these processes may be kinetically controlled, it is important to

consider what impact an equilibrium as opposed to a kinetic formulation for chemical reactions might have on the prediction of in-drift chemical processes.

H.3 RESPONSE

Explicit treatment of chemical kinetics is not included in the analysis of in-drift processes. An example of these in-drift processes is the evaporation and resulting concentration of seepage water, which was studied experimentally and served partly as the motivation for this KTI agreement (Gdowski 2001, p. 16). The effect of chemical kinetics, however, is indirectly incorporated into in-drift chemical models in several ways. One way is through the suppression of mineral phases that are not expected to precipitate within the time scale defined by the regulatory period. A second way is through the inclusion of kinetically controlled corrosion reactions that provide a time-dependent source of metals that affect the otherwise equilibrium reaction path resulting from evaporation of in-drift seepage water (BSC 2003a, Section 6.8). Since these metal corrosion rates are not compared explicitly with other time-dependent physical and chemical processes in the drift, they serve the purpose primarily of providing an upper bound on possible metal concentrations (specifically Fe and Cr) in seepage water. The effect of metal corrosion rates on microbial growth is also examined in the In-Drift Microbial Communities section of the *Engineered Barrier System: Physical and Chemical Environment Model* (BSC 2003a, Section 6.11), although these effects are not considered in modeling of the evaporative concentration of seepage water (Gdowski 2001, p. 16).

The information in this report is responsive to agreement ENFE 2.11 made between the DOE and NRC. The report contains the information that the DOE considers necessary for NRC review for closure of this agreement.

H.4 BASIS FOR THE RESPONSE

As stated above, the explicit treatment of chemical kinetics is not included in the analysis of in-drift processes. This was done in part because of the need to provide model abstractions that are independent of time, since a kinetically controlled reaction path will produce output that is time-dependent except in the case of steady-state conditions. In general, steady-state kinetically controlled reaction paths, as would develop in the case of explicit consideration of flow and transport, were not considered in the analysis of in-drift chemistry.

The effect of chemical kinetics, however, is indirectly incorporated into in-drift chemical models by considering suppression of mineral phases that are not expected to precipitate within the time scale defined by the regulatory period (BSC 2003a). This leads to a quasi-equilibrium model in which both stable and metastable equilibrium states may exist. Mineral phases that are suppressed are those that are not observed as reaction products in natural (field) settings where the time scales extend to on the order of hundreds of thousands to millions of years, in contrast to the more limited time scale defined by the regulatory period. On the other hand, all other reactions are assumed to proceed to equilibrium over time scales shorter than the time scale for significant corrosion to occur.

This apparent paradox, in which some reaction times greatly exceed while others are far less than the relevant in-drift time scales (primarily the time scale for significant waste package or drip

shield corrosion to occur), can in fact be justified on the basis of the kind of reactions involved. Suppression of mineral phases is justified where they are extremely slow to nucleate below a critical supersaturation and (or) temperature threshold (Steeffel and Van Cappellen 1990; Stumm 1992). Even where seed crystals are present, some minerals like quartz apparently grow by a nucleation-controlled mechanism that requires a high degree of supersaturation at low temperature. The highly nonlinear character of mineral nucleation and (or) nucleation-controlled crystal growth rates means that below the critical supersaturation, rates are effectively zero. Within the temperature range where the thermodynamically stable phase (for example, quartz) is not observed as a reaction product because of the difficulty in nucleating it, supersaturation with respect to another more easily nucleated or precipitated (but more soluble) phase may occur (e.g., amorphous silica). In other words, if the solubility of a metastable phase is less than the critical supersaturation for nucleation of the thermodynamically more stable phase, then the system will tend to form the metastable phase and remain in metastable equilibrium, possibly for a substantial interval of time. The empirical observation that metastable minerals may form first and persist is explained by the Gay-Lussac-Ostwald (GLO) or Ostwald step rule (Sposito 1989, 1994; Steeffel and Van Cappellen 1990; Langmuir 1997).

Except for the mineral phases whose nucleation or precipitation is suppressed, the assumption is made that all other reactions occur sufficiently rapidly that they come to equilibrium within the time scale of interest in the drift. Based on the arguments above, this might occur where nucleation of the mineral phase is not difficult (as in the case of salts), or where dissolution of a preexisting precursor phase occurs relatively rapidly. In general, phases that can precipitate in laboratory experiments (typically on time scales of days to weeks) are not subject to large kinetic barriers. Still, no reaction proceeds instantaneously, so reaction times should ideally be compared with the other relevant time scales in the drift environment. Reaction rates may be determined explicitly through experimentation, or inferred approximately from the fact that reaction products appear in experiments or based on the ability to match the time evolution of solution chemistry with an equilibrium calculation.

In considering the potential effects of corrosion of metal-bearing introduced materials on the in-drift chemical environment, some indirect use of chemical kinetics is made. The analysis presented in *Engineered Barrier System: Physical and Chemical Environment Model* (BSC 2003a) makes use of published corrosion rates to provide an estimate of metal concentrations that might develop in seepage water. However, since no explicit time scale is considered other than the total duration of a particular “period” in the evolution of conditions in the drift (e.g., the “wet” period lasting 2,000 years), the metal concentrations developing in the seepage water are really upper bounds limited primarily by the solubility of various secondary mineral phases (BSC 2003a). No direct comparison, for example, is made with contact times likely between seepage water and metal-bearing introduced materials. Further discussion of this is provided in ENFE 2.14 (Appendix J).

No specific time scales for in-drift chemical processes are made use of in the total system performance assessment (TSPA) model, other than taking as input the number of waste packages likely to fail within a given amount of time. In this respect, the TSPA does not consider time-dependent source terms that could be compared, for example, to rates of transport and (or) temperature change. These failure rates currently make use of general corrosion rates determined for Alloy 22. Process-level models based on waste package corrosion in specific

concentrated electrolyte solutions (e.g., CaCl_2) use water compositions calculated assuming chemical equilibrium. There is no fundamental reason why transient seepage water chemistries and their effect on waste package and drip shield corrosion could not be considered, if such transient chemistries were identified. Consideration of water compositions formed by kinetically controlled reaction paths, however, could in theory expand the range of compositions that need to be included in corrosion tests. As an example, consider the case of seepage water interacting with cementitious grout, although it should be noted that there are currently no plans to use grout in the drift environment (in part for the reasons that follow). Leaching of the cementitious grout produces a high pH, calcium-rich solution that, if evaporated very quickly before significant gas exchange and carbonate precipitation can occur, forms an aggressive CaCl_2 brine. Based on laboratory experiments conducted at 25°C , exchange of this high pH solution with CO_2 in the drift atmosphere will cause the pH and the calcium concentration to decrease significantly on the time scale of hours if fluid volumes are small (DTN: LL020805523125.002). In this case, the assumption of equilibrium with respect to atmospheric CO_2 would greatly underestimate how aggressive the seepage water is over short times, but given enough time (hours to days), the attainment of chemical equilibrium should result in the development of a more benign solution.

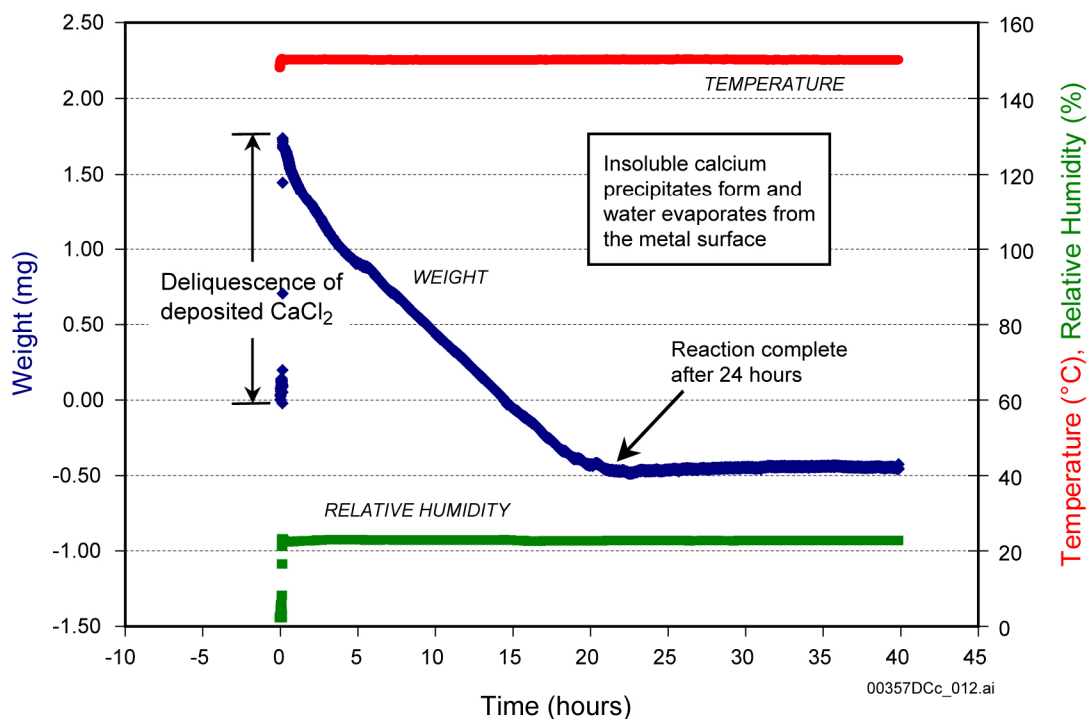
Another time scale potentially of interest is the rate of heating and cooling in the drift. If heating and cooling is rapid, reaction overstepping could, in theory, occur as rates cannot keep up with temperature changes. However, both the heating and cooling in the drift environment are predicted to occur relatively slowly. For example, the time for the drift environment to decrease from its peak temperature close to 160°C down to about 120°C is predicted to be on the order of hundreds of years. Therefore, rates of heating and cooling are very unlikely to have a significant impact on the applicability of the assumption of chemical equilibrium.

In evaluating the appropriate time scales to compare to the rates of reaction, the results depend on how aqueous solutions contact the waste package and drip shield. In the case of dust containing deliquescent salts, moisture will collect locally on these dust accumulations. These water accumulations will act as small “batch” systems open to the atmosphere in and around the drifts—given enough time, they will achieve local equilibrium with their environment. Similar results would occur for seepage water that accumulates intermittently in places on the waste package or drip shield. These cases are discussed further below. In contrast, a “flow through” system, where continuous dripping or seepage provides a steady stream of water along the waste package or drip shield, may give very different results. Here the relevant time scale is the residence time of the fluid along any particular section of the engineered barrier system. At steady state, time-invariant but kinetically controlled solution compositions may occur where the solutions first contact the waste package or drip shield. If the stream of water is large enough and continuous enough that dryout in this location does not occur, then the kinetics of the reactions should be considered relative to the flow rate of the seepage water along the waste package or drip shield. No kinetic reaction paths have been identified to date that result in significantly more aggressive solutions than is obtained in the equilibrium case, with the exception of the hyperalkaline case, which is no longer relevant since cementitious grout is not included in the repository emplacement drift ground support design. Other possible problematic reaction paths might include those where a phase containing a corrosive agent (e.g., fluoride) does not form as rapidly as predicted by the equilibrium modeling.

In the case of moisture accumulating on dust containing deliquescent salts or as a result of intermittent seepage, the most important time scale that is relevant for comparison of reaction times is the time for significant waste package or drip shield corrosion to occur. If slow reactions were to produce a more benign water than in the equilibrium case, then the equilibrium assumption is conservative. Where kinetic effects could result in a more aggressive solution contacting the waste package or drip shield, the question becomes whether it is transformed to the more benign equilibrium solution before causing significant local corrosion. Some calculations have shown that evaporation of seepage water could occur within seconds where temperatures are high in the drift. This could lead to either complete evaporation of all water, in which case a completely dry assemblage of minerals is formed, or it could lead to the formation of a brine through mineral deliquescence. In the completely dry case, no effect on waste package or drip shield corrosion is foreseen. In the case where mineral deliquescence leads to wet conditions on the waste package or drip shield, the aqueous solution will continue to interact with minerals in contact with the brine and with the gases in the local drift atmosphere. The time scale for reaction, therefore, is considerably longer than the actual time required to evaporate a given mass of seepage water. Based on these arguments, the equilibrium assumption is valid for the deliquescent dust and intermittent seepage case if equilibrium conditions are attained before significant corrosion of the waste package or drip shield has occurred.

Evidence for the time scale for waste package corrosion is provided by experiments in which a CaCl_2 salt was allowed to deliquesce on coupons of Alloy 22 at 150°C and a relative humidity of 22.5 percent, thus forming a thin film of CaCl_2 solution. These experiments indicate that HCl devolatilization accompanied by precipitation of a calcium-bearing phase (most likely CaOHCl) occurred within 24 hours (Figure H-1). During this same period, no localized corrosion of the Alloy 22 coupons was observed as indicated by the lack of metal ion incorporation in the precipitates (BSC 2003b). The transformation resulted in a mineral assemblage that was not deliquescent under the experimental relative humidity conditions, so complete dryout occurred. At 125°C , slow degassing occurred for 600 hours while the specimen visibly dried. The slower rate of devolatilization may reflect the lower HCl fugacity at this temperature compared to 150°C , rather than anything to do with the intrinsic reaction kinetics. No evidence for corrosion of the Alloy 22 coupon was observed at the end of this time. The HCl devolatilization, which is predicted with equilibrium simulations (BSC 2003b), suggests that time scales are quite rapid relative to corrosion rates. It is not completely clear, however, whether the rapid gas flushing rates in the thermogravimetric analysis experiments reflect conditions likely to occur in the drift environment. These experimental rates may be the result of transport control under fast flow conditions, so rates in the in-drift environment could be substantially different.

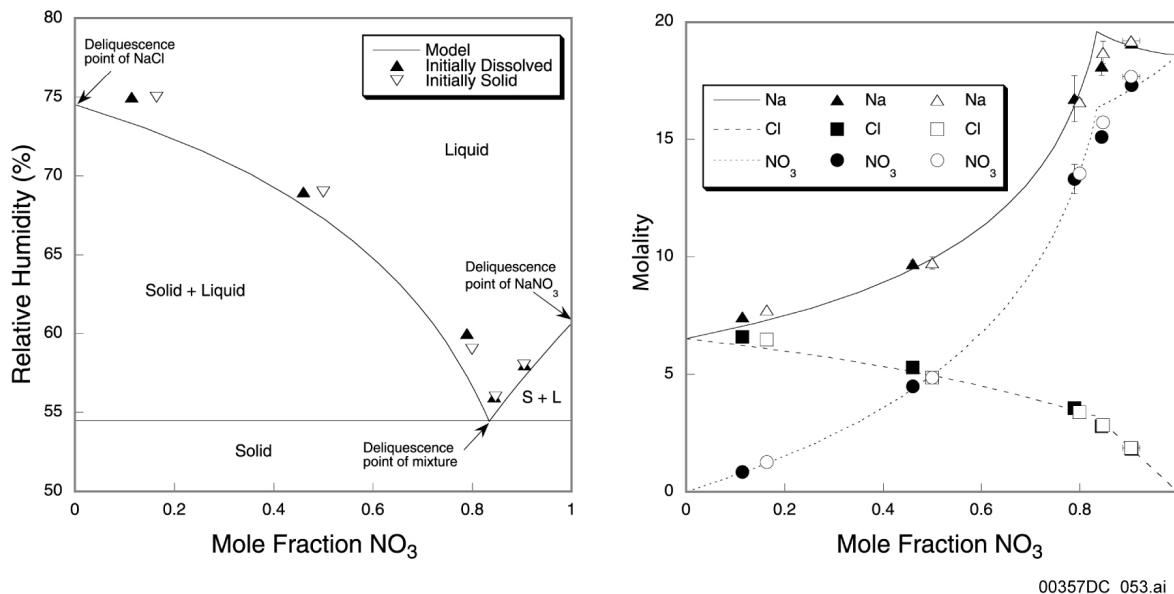
In the case of deliquescent salts, recently collected data (DTNs: LL030405223121.025; LL030506823121.029) indicate that these reactions are reversible on laboratory time scales. These studies carried out on the NaCl-NaNO_3 system show that virtually identical results are obtained whether beginning initially with a solution or with a solid, indicating that near chemical equilibrium conditions must apply (Figure H-2). These laboratory time scales for reaction are considerably shorter than the time required for significant waste package or drip shield corrosion to occur. If equilibrium conditions are attained within this relatively short time scale, then the assumption of equilibrium at the longer time scales for waste package corrosion to occur under in situ conditions is justified.



Source: BSC 2003b, Figure 35.

Figure H-1. Weight Change Curve for Deliquescent CaCl_2 150°C and 22.5 Percent Relative Humidity

While the reversibility of the deliquescence experiments mentioned above and shown in Figure H-2 suggest that the equilibrium approximation is justified, the atmospheric chemistry literature discriminates deliquescence relative humidity from efflorescence relative humidity, where efflorescence is equivalent to complete dryout. It has been observed at low temperature and under “pristine” conditions, in the sense of lacking suitable surfaces for mineral nucleation, that salt mineral supersaturation may occur during dryout (BSC 2003b). Such a system might consist of an aerosol composed only of an aqueous solution surrounded by “clean” atmosphere. Even minor scratches in laboratory glassware can provide nucleation sites, suggesting that in a heterogeneous “dirty” system like that expected in the drift environment, kinetic effects associated with efflorescence are not expected. Higher temperature also limits salt mineral supersaturation by enhancing reaction rates.



Source: DTNs: LL030405223121.025; LL030506823121.029.

NOTE: The ability to reverse the reactions experimentally indicates near chemical equilibrium conditions.

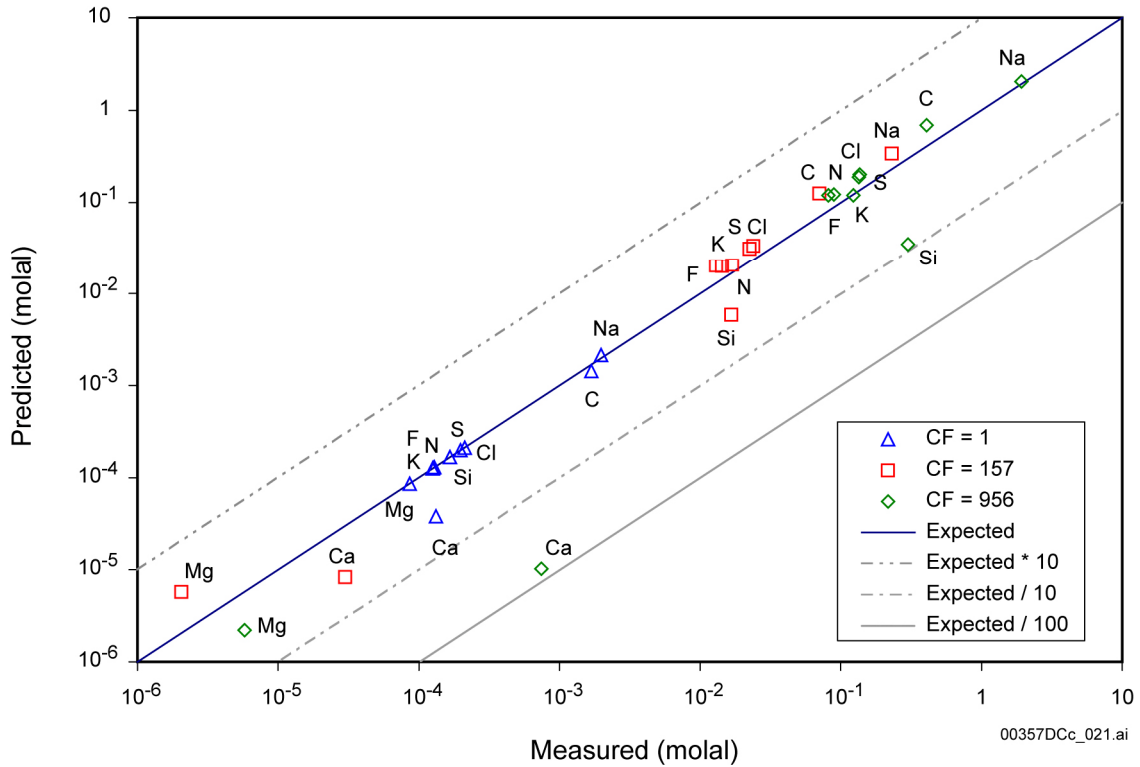
Figure H-2. Deliquescence in the NaCl-NaNO₃ System Showing Reversal of Precipitation and Dissolution Reactions for the Salts

No consideration of mineral dissolution kinetics has been included in the in-drift chemical models, except where waste package corrosion is allowed to affect the chemistry of aqueous solutions collected on the waste package. In many models of water-rock interaction, dissolution kinetics is assumed to be the slowest and therefore rate-limiting step. However, these environments generally involve the dissolution of silicate minerals, as in the near field environment at Yucca Mountain. The thermal-hydrologic-chemical reactive transport models of processes in the near field environment, for example, do include an explicit treatment of mineral dissolution kinetics. In the in-drift environment, very little rock material is available for dissolution even during the heating stage where dissolution could occur due to the prograde solubility of most minerals. The major justification for the neglect of dissolution kinetics, however, is that the minerals that might dissolve in the in-drift environment consist of phases precipitated during evaporation of seepage water, rather than rock-forming minerals expected to dissolve slowly. As evaporation drives the chemical composition of the aqueous solution through a “reaction path,” early formed minerals may dissolve at the expense of mineral phases that are more stable for a given evolving chemical composition. In the case of dust on the waste packages, it consists largely of finely comminuted silicate phases that could be expected to react fairly rapidly (for silicates) with any liquids present. Since some types of brines formed by dust deliquescence may persist for very long times, one expects to see significant dissolution of silicates and precipitation of new silicate phases (e.g., dissolution of feldspars to form clays), so the time scale is sufficiently long that dissolution kinetics are not a major issue.

Evaporation experiments described by Rosenberg et al. (2001) may show some effects of chemical kinetics that have not been captured in equilibrium-based modeling, although the discrepancies between experiment and model fit may also be the result of either uncertainties in

the thermodynamic database or analytical errors, particularly those associated with the analysis of inorganic carbon. Similar evaporation experiments were mentioned in the development of ENFE 2.11 (Gdowski 2001, p. 16). Recent modeling of the experiments described in Rosenberg et al. (2001) using EQ3/6 version 8.0 software (BSC 2003c) and the Pitzer database data0.ypf.R0 (SN0302T0510102.002) reported in *In-Drift Precipitates/Salts Model* (BSC 2003d) shows a good match with most elements over the course of the experiment with the exception of Mg^{2+} and Ca^{2+} (Figure H-3). A slight underprediction of the pH is shown in Figure H-4. The match with the equilibrium modeling, to the extent that it occurs, suggests that the equilibrium approach is adequate, although it does not prove it. The modeling tends to underpredict the concentrations of Mg^{2+} and Ca^{2+} , suggesting that either: (1) precipitation rates of silicates incorporating Mg^{2+} and calcite incorporating Ca^{2+} are not sufficiently rapid that equilibrium is maintained over the time scale of the experiment, (2) that the solubility of magnesium-silicates is higher than predicted by the available thermodynamic database, (3) the thermodynamic values for the important calcium- and magnesium-bearing silicate phases are slightly incorrect, or (4) that analytical errors in the determination of some species, most likely inorganic carbon, could result in poor prediction for Ca^{2+} and Mg^{2+} . It was possible to obtain a good match with the Mg^{2+} data by increasing the log K (equilibrium constant) for sepiolite ($Mg_4Si_6O_{15}(OH)_2 \cdot 6H_2O$) by 6 log K units (BSC 2003d). While this may seem like a very large change, it is within the range of uncertainties for sheet-like silicates (which also tend to have large molecular formulas, a factor that creates relatively high uncertainties in associated log K values), since stoichiometrically equivalent but more soluble analogs may form at the expense of the stable phase (Steeffel and Van Cappellen 1990; Langmuir 1997). For example, halloysite often forms as stoichiometrically equivalent analog of kaolinite, but has an equilibrium constant about four log K units larger (Steeffel and Van Cappellen 1990). No direct use of these experiments is made in the case for the license application. Rather, these experiments can be viewed as test cases specifically referred to in response to this agreement where the applicability of the equilibrium assumption (which is used extensively elsewhere in developing the case for the license application) can be evaluated.

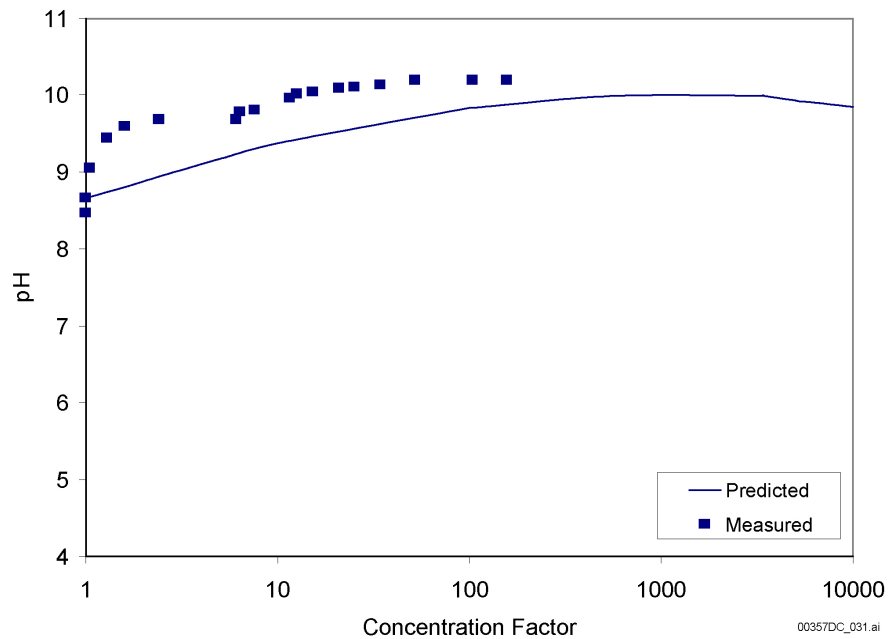
With regard to the Ca^{2+} in the above-cited experiments, it is very unlikely that the equilibrium constant for calcite is incorrect. Calcite is typically supersaturated in seawater due to the poisoning of the mineral surface by Mg^{2+} (Drever 1997, pp. 223 to 224), so the same kinetic mechanism may apply here. It should be noted, however, that the overprediction of the inorganic carbon concentration in Figure H-3 may be responsible for the underprediction of Ca^{2+} . The error in carbon, for example, is nearly 0.1 molal, which would translate to a large error in the Ca^{2+} prediction if equilibrium or near-equilibrium with respect to calcite is maintained. Overprediction of inorganic carbon would also tend to produce an underprediction in pH (Figure H-4). Similar effects, through the pH, could affect the calculation of Mg^{2+} concentrations in equilibrium with sepiolite.



Source: BSC 2003d, Figure 16; Rosenberg et al. 1999.

NOTE: CF = concentration factor.

Figure H-3. Predicted versus Measured Concentrations for Synthetic J-13 Water Evaporation Experiments



Sources: BSC 2003d, Figure 17; Rosenberg et al. 1999.

Figure H-4. Predicted versus Measured pH Values for Synthetic J-13 Water Evaporation Experiments

Given the uncertainties in the thermodynamic values used and the possibility that relatively small errors in the analyses of some components (especially inorganic carbon) could translate to correspondingly larger errors in such cations as Mg^{2+} and Ca^{2+} , it is not clear that kinetic effects are responsible for the mismatch between equilibrium reaction path modeling and the results of evaporation experiments. In any case, the longer time scales expected to apply in the drift environment compared to the laboratory evaporation experiments suggest that the equilibrium approximation is reasonable.

H.5 REFERENCES

H.5.1 Documents Cited

BSC (Bechtel SAIC Company) 2003a. *Engineered Barrier System: Physical and Chemical Environment Model*. ANL-EBS-MD-000033 REV 02C. Las Vegas, Nevada: Bechtel SAIC Company. ACC: MOL.20031029.0034.

BSC 2003b. *Environment on the Surfaces of Drip Shield and Waste Package Outer Barrier*. ANL-EBS-MD-000001 REV 01D. Las Vegas, Nevada: Bechtel SAIC Company. ACC: MOL.20030825.0151.

BSC 2003c. *Software Code: EQ3/6*. V8.0. PC w/ Windows 95/98/2000/NT 4.0. 10813-8.0-00.

BSC 2003d. *In-Drift Precipitates/Salts Model*. ANL-EBS-MD-000045 REV 01. Las Vegas, Nevada: Bechtel SAIC Company. ACC: DOC.20031028.0003.

Drever, J.I. 1997. "Evaporation and Saline Waters." Chapter 15 of *The Geochemistry of Natural Waters: Surface and Groundwater Environments*. 3rd Edition. Upper Saddle River, New Jersey: Prentice Hall. TIC: 246732.

Gdowski, G. 2001. "Subissue 2: Range of Water Chemistry and Trace Elements in the Waste Package Chemical Environment." Presentation to the DOE/NRC Technical Exchange on Key Technical Issue and Subissues Related to Evolution of the Near-Field Environment, January 9-12, 2001, Pleasanton, California. Las Vegas, Nevada: Yucca Mountain Site Characterization Office. ACC: MOL.20011017.0391.

Langmuir, D. 1997. *Aqueous Environmental Geochemistry*. Upper Saddle River, New Jersey: Prentice Hall. TIC: 237107.

Reamer, C.W. 2001. U.S. Nuclear Regulatory Commission/U.S. Department of Energy Technical Exchange and Management Meeting on Evolution of the Near-Field Environment (January 9-12, 2001). Letter from C.W. Reamer (NRC) to S. Brocoum (DOE/YMSCO), January 26, 2001, with enclosure. ACC: MOL.20010810.0033.

Rosenberg, N.D.; Gdowski, G.E.; and Knauss, K.G. 2001. "Evaporative Chemical Evolution of Natural Waters at Yucca Mountain, Nevada." *Applied Geochemistry*, 16, (9-10), 1231-1240. New York, New York: Pergamon. TIC: 249879.

Rosenberg, N.D.; Knauss, K.G.; and Dibley, M.J. 1999. *Evaporation of J13 Water: Laboratory Experiments and Geochemical Modeling*. UCRL-ID-134852. Livermore, California: Lawrence Livermore National Laboratory. TIC: 246322.

Sposito, G. 1989. *The Chemistry of Soils*. New York, New York: Oxford University Press. TIC: 237211.

Sposito, G. 1994. *Chemical Equilibria and Kinetics in Soils*. New York, New York: Oxford University Press. TIC: 254883.

Steeffel, C.I. and Van Cappellen, P. 1990. "New Kinetic Approach to Modeling Water-Rock Interaction: The Role of Nucleation, Precursors, and Ostwald Ripening." *Geochimica et Cosmochimica*, 54, 2657-2677. New York, New York: Pergamon Press. TIC: 240813.

Stumm, W. 1992. *Chemistry of the Solid-Water Interface, Processes at the Mineral-Water and Particle-Water Interface in Natural Systems*. New York, New York: John Wiley & Sons. TIC: 237213.

H.5.2 Data, Listed by Data Tracking Number

LL020805523125.002. Experimental Studies of Cement Grout-Water Chemical Interaction. Submittal date: 08/28/2002.

LL030405223121.025. Mixed Salts Experiment #S 9, 10, 11 and 12 (MS-9, MS-10, MS-11, AND MS-12) Solution Composition. Submittal date: 07/23/2003.

LL030506823121.029. Mixed Salts Experiments #13 (MS-13) Solution Composition. Submittal date: 07/18/2003.

SN0302T0510102.002. Pitzer Thermodynamic Database (data0.ypf, Revision 1). Submittal date: 02/06/2003.

INTENTIONALLY LEFT BLANK

APPENDIX I
THE IMPACTS OF DUST DEPOSITION ON THE SALT ANALYSIS
(RESPONSE TO ENFE 2.13)

Note Regarding the Status of Supporting Technical Information

This document was prepared using the most current information available at the time of its development. This Technical Basis Document and its appendices providing Key Technical Issue Agreement responses that were prepared using preliminary or draft information reflect the status of the Yucca Mountain Project's scientific and design bases at the time of submittal. In some cases this involved the use of draft Analysis and Model Reports (AMRs) and other draft references whose contents may change with time. Information that evolves through subsequent revisions of the AMRs and other references will be reflected in the License Application (LA) as the approved analyses of record at the time of LA submittal. Consequently, the Project will not routinely update either this Technical Basis Document or its Key Technical Issue Agreement appendices to reflect changes in the supporting references prior to submittal of the LA.

APPENDIX I

THE IMPACTS OF DUST DEPOSITION ON THE SALT ANALYSIS (RESPONSE TO ENFE 2.13)

This appendix provides a response for Key Technical Issue (KTI) agreement Evolution of the Near-Field Environment (ENFE) 2.13. This KTI relates to providing documentation regarding the deposition of dust and its impact on the salt analysis.

I.1 KEY TECHNICAL ISSUE AGREEMENT

I.1.1 ENFE 2.13

Agreement ENFE 2.13 was reached during the U.S. Nuclear Regulatory Commission (NRC)/U.S. Department of Energy (DOE) Technical Exchange and Management Meeting on Evolution of the Near-Field Environment held January 9 to 11, 2001, in Pleasanton, California (Reamer 2001). ENFE KTI subissues 1, 2, 3, and 4 were discussed at that meeting. There have been no specific submittals to the NRC subsequent to the original technical exchange on this subject.

The wording of the agreement is as follows:

ENFE 2.13

Provide documentation regarding the deposition of dust and its impact on the salt analysis. The DOE will provide documentation of dust sampling in the Exploratory Studies Facility, and analysis of the dust and evaluation of its impact on the chemical environment on the surface of the drip shield and waste package, in a revision to the Engineered Barrier System: Physical and Chemical Environment Model AMR (ANL-EBS-MD-000033), expected to be available in FY02.

I.1.2 Related Key Technical Issue Agreements

Other KTI agreements related to ENFE 2.13 are ENFE 2.06 (Appendix E), and ENFE 2.14 (Appendix J).

I.2 RELEVANCE TO REPOSITORY PERFORMANCE

The primary consideration in the in-drift environment is the impact of processes and materials on the waste package and drip shield performance (lifetimes). The deposition of dust on the surface of these engineered barriers has the potential to impact the evolution of water chemistry, potentially affecting the performance of the waste package and drip shield.

I.3 RESPONSE

Dust deposition and its impact on the salt analysis is discussed and addressed in *Engineered Barrier System: Physical and Chemical Environment Model* (BSC 2003a) with additional

corroborative analyses in *Environment on the Surfaces of Drip Shield and Waste Package Outer Barrier* (BSC 2003b). The description provided in the section below extracts the relevant information from these reports in addressing this agreement.

Samples of dust were collected in the Exploratory Studies Facility (ESF) and both bulk chemical analyses and analyses of aqueous leachates were made by the U.S. Geological Survey. The bulk analyses show that the dust comprises crushed and comminuted (ground) tuff host rock generated during construction, mixed with dust from a variety of anthropogenic sources. Systematic trends in the water-soluble Ca^{2+} , Mg^{2+} , K^+ , Na^+ , Cl^- , F^- , SO_4^{2-} , and NO_3^- contents with particle size indicate that salts of evaporated construction and native pore water are important components. During construction and waste emplacement at the repository, dust generated inside the repository will greatly overwhelm any externally derived atmospheric component. However, atmospheric dust may become important during the ventilation period, following repository closure. Atmospheric dust has not been characterized directly as part of this project, but information in the literature on the general properties of this dust, on relevant atmospheric processes, and on material from desert playas in Nevada has been evaluated. From this it is concluded that nitrate (and other soluble salt components) are likely more abundant in “outside” dust than in the current tunnel dusts.

The measured, water-soluble leachate compositions were used to evaluate the mineralogy of deliquescent salt minerals that might be present in the dust, and the composition and probability of occurrence of brines that might form through deliquescence. Results of modeling the evaporation of the leachate solutions to dryness or to their eutectic point were used for (1) binning and abstraction of the leach water compositions, to evaluate the composition and probability of occurrence of deliquescent brines, and (2) evaluation of the minerals that precipitated during evaporation to dryout and that are present at the eutectic point. Six groups of water types or bins were developed in the abstraction. The final brine compositions are functions of both the initial leachate composition and of the modeled minerals that precipitate during evaporation, according to the chemical divide principal. The information required for potential total system performance assessment (TSPA) use is the deliquescence relative humidity at a range of temperatures and partial pressures of carbon dioxide ($p\text{CO}_2$), and the water chemistry that would be produced by deliquescence. This was developed by modeling evaporation of the waters of the median composition of each bin at temperatures of 40°C, 70°C, 100°C, and 120°C and $p\text{CO}_2$ values of 10^{-2} , 10^{-3} , and 10^{-4} bar. Values at 140°C are also developed, but they must be considered preliminary pending the completion of the ongoing validation of the model (BSC 2003c) to this temperature for the relevant salts.

The information in this report is responsive to agreement ENFE 2.13 made between the DOE and NRC. The report contains the information that DOE considers necessary for NRC review for closure of this agreement.

I.4 BASIS FOR THE RESPONSE

Dust accumulation on waste packages or drip shields may contain soluble salts, which could cause water condensation if the in-drift humidity became higher than the minimum deliquescence point of the salts. The resulting solution could potentially affect the degradation of the engineered barriers.

The thermodynamic activity of water in a solution corresponds to the relative humidity of the gas phase with which it is in equilibrium (BSC 2003b, Section 6.3). The water activity of a solution in turn depends on its solute concentration such that the relative humidity corresponding to a solution decreases as its total solute content increases. This allows evaporation modeling by computer codes such as EQ3/6 to be interpreted in terms of the relative humidity of the environment.

This response begins with a description of the sampling of dust for determination of its chemical properties and amounts deposited at the time of sampling (Section I.4.1). The bulk chemical analysis procedures applied to the dust and the chemical analyses of the water-soluble fractions of the dust are discussed next with an interpretation of the results in terms of the possible origins of the dust (Section I.4.2). The modeling results of the evaporation of these solutions to dryness are summarized (Section I.4.3), and provide the assemblages of salts precipitated during the evaporation to dryness. The resulting assemblages of salts precipitated during evaporation and their deliquescent properties are discussed last (Section I.4.4) and used to construct tables showing the temperature and relative humidity values at which the several assemblages would begin to deliquesce. This information is used by the TSPA corrosion module, to determine whether deliquescence can begin for a given temperature–relative humidity state. If so, an aqueous phase could be present on the drip shield or waste package surface.

I.4.1 Dust Sampling

Samples of dust were collected in the ESF and analyzed by the U.S. Geological Survey. Peterman et al. (2003) describe the sampling procedures, summarize the results of the chemical analyses, and discuss the origins of the dust. This section is based on that report.

Two sets of dust samples were collected. In 2001, 26 small (multigram) samples were collected from the tunnel walls, service pipes, and various flat surfaces such as the tops of transformers. The dust was brushed onto glassine paper sheets or a plastic dustpan using small paintbrushes and transferred to plastic bottles. These samples were screened and the 60 mesh (250 μm) fractions were analyzed for major and trace elements (total dissolution) and water-soluble anions and cations. In early 2002, 12 dust samples were collected using a commercial battery-operated vacuum cleaner attached to a small stainless-steel cyclone dust collector designed for the U.S. Environmental Protection Agency. Dust particles greater than about 5 μm were trapped by the cyclone directly into 250-mL glass sample bottles. This method allowed much larger samples to be collected by vacuuming larger areas of tunnel wall (typically 2 to 4 m^2) than could be sampled by brushing. At 9 of the 12 sampling sites, the area vacuumed was measured to determine the amount of dust accumulation. The amount of dust accumulation varied from 0.012 to 0.023 grams/cm^2 , except for the site nearest the North Portal, which had 0.080 g/cm^2 . The remaining eight sites have an average areal accumulation of $0.017 \pm 0.004 \text{ g}/\text{cm}^2$ (1σ).

Fractions of the samples collected in 2002 larger than 60 mesh were screened out prior to analyses to remove small rock particles dislodged from the tunnel walls during vacuuming. The 60 to 200 mesh fraction is the most abundant in the sample collected just outside the North Portal and in the two samples closest to the North Portal in the ESF. The fractions less than 200 mesh comprise 50 percent or more of the total material for the remaining nine samples.

Given the number of dust samples collected and analyzed, it has been assumed that the U.S. Geological Survey data capture the variability of dust composition across the whole ESF (BSC 2003a, Section 5.2.3).

I.4.2 Analyses and Origins of Dust

Bulk chemical analyses of the dust samples (total fusion and bulk dissolution) were done by wavelength dispersive X-ray fluorescence, inductively coupled plasma mass spectrometry, ion chromatography, and other element-specific methods. In addition, water-soluble anions and cations were analyzed on leachate aliquots of the dust samples. The second set of dust samples was large enough to permit chemical analyses of size-classified aliquots. Three size distributions were prepared for chemical analysis: 60 to 200 mesh, 200 to 325 mesh, and less than 325 mesh.

No mineralogical analyses of the dust samples were performed, so it was necessary to infer the identity of the solids from the chemical data. Major, minor, and trace element analyses of bulk and size-classified dust samples and of water-soluble fractions show systematic trends in chemical composition and interelement correlations that are related to the various sources of the dust. The dust in the ESF consists primarily of crushed and comminuted (ground) tuff host rock generated during construction, mixed with dust from a variety of anthropogenic sources. The effect of the introduced components on dust composition can be estimated by comparing the dust composition with the mean composition of the Topopah Spring Tuff, the ESF host rock that is the source of most of the dust. Relative to the mean composition of the rock, the dust is enriched in FeO, MgO, CaO, TiO₂, MnO, Cl, F, and CO₂. Organic carbon was also measured in the dust, but this must have been introduced by anthropogenic activities, because the host rock is devoid of organic carbon. Systematic trends in the water-soluble Ca²⁺, Mg²⁺, K⁺, Na⁺, Cl⁻, F⁻, SO₄²⁻, and NO₃⁻ contents with particle size indicate that salts of evaporated construction and native pore water are important components of the dust. The enrichment of trace quantities of transition metals and other metals in the dust, compared with Topopah Spring Tuff values, identifies a component of ferrous metals, likely introduced during construction activities (Peterman et al. 2003).

In addition to the bulk analyses, the water-soluble anions and cations (Ca²⁺, Mg²⁺, K⁺, Na⁺, SiO₂(aq), Cl⁻, Br⁻, F⁻, NO₃⁻, SO₄⁻, Pb, and As) in the dust were analyzed by the U.S. Geological Survey. In these experiments, aliquots of the dust were leached and filtered. The leachate was then analyzed by inductively coupled plasma mass spectrometry and ion chromatography. The results are given in full in DTNs: MO0207EBSDUSTS.020 and MO0209EBSDUST2.030 and utilized for evaporation modeling (Section I.4.3).

Nitrate in the tunnel dusts likely has multiple sources. Dissolved NO₃⁻ is present in Yucca Mountain pore waters. Nitrate minerals (e.g., niter, KNO₃; soda niter, NaNO₃; and nitrocalcite, Ca(NO₃)₂·4H₂O) have not been reported from Yucca Mountain. In general, nitrate tends to be a common component of desert terrains and subterranean environments. *Environment on the Surfaces of Drip Shield and Waste Package Outer Barrier* (BSC 2003b, Section 6.7.2.8) summarizes data from the literature on the sources of nitrate in the environment (e.g., electrical production in the upper atmosphere, oxidation of organic matter in the lower soil zone) and on the occurrence of nitrate minerals in the subsurface environment as noted in the scientific literature on caves. Hence, the presence of NO₃⁻ in the mountain (at the least in dissolved form)

is expected. Anthropogenic sources are also possible. These could be local, in the tunnels themselves (e.g., by fuel burning to run machinery) or to the extent that outside dust is present, regional (e.g., fuel burning, agricultural operations). One usage of calcium nitrate is adding it to certain types of fuel to keep the fuel dry. On the other hand, relatively little blasting (a potential source of nitrate) appears to have been employed in the construction of the tunnels.

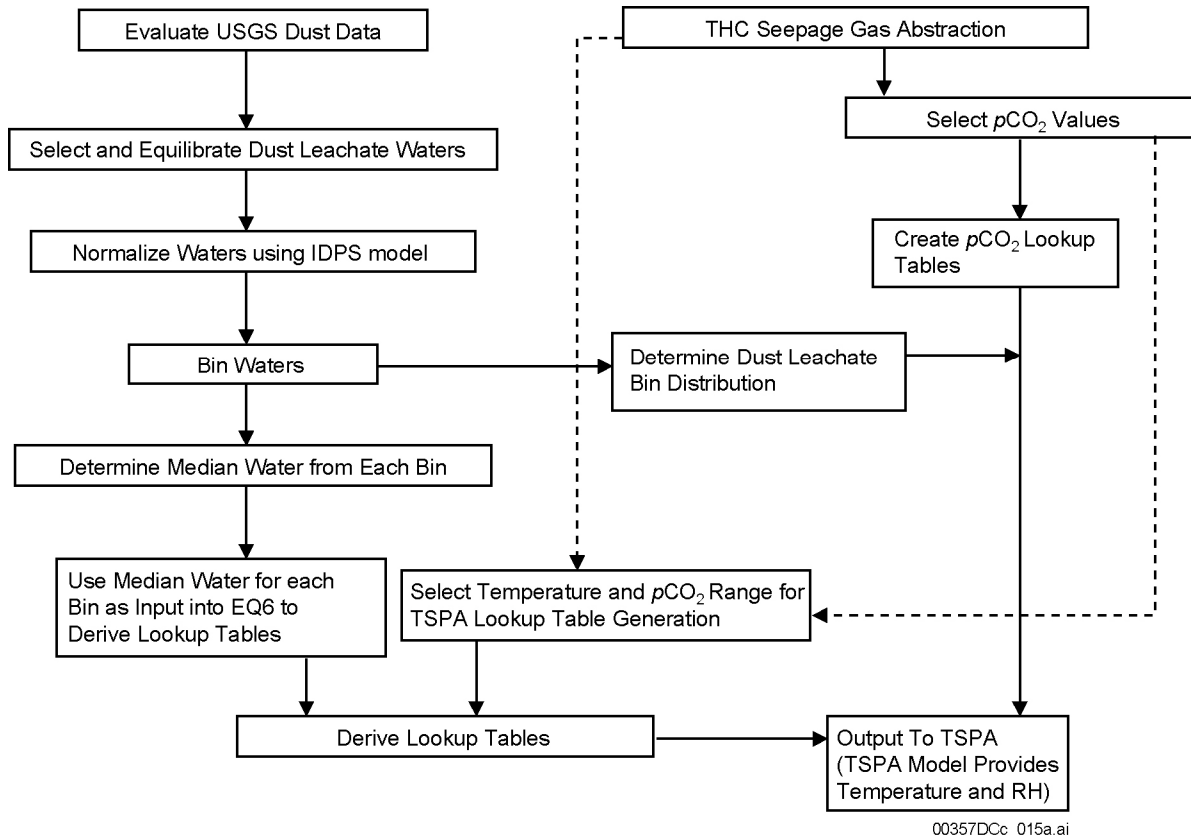
During construction and waste emplacement at the repository, dust generated inside the repository will greatly overwhelm any externally derived atmospheric component. However, atmospheric dust may become important during the ventilation period, following repository closure. Atmospheric dust has not been characterized directly as part of this project, but information in the literature on the general properties of this dust, on relevant atmospheric processes, and on material from desert playas in Nevada, has been summarized in *Environment on the Surfaces of Drip Shield and Waste Package Outer Barrier* (BSC 2003b, Section 6.7.2.8). In general, nitrate is an important component of atmospheric dusts, primarily due to its production in the upper atmosphere by electrical phenomena as noted above. Nitrate salts are recognized an important component of atmospheric dusts and aerosols and their properties (including deliquescence) are considered important to the understanding of certain weather and climatic phenomena. Anthropogenic sources add to the nitrate burden of atmospheric dust. The extent to which playa dusts add to this burden is not well known. Nitrate minerals are not commonly described as components of surficial playa salts, so playas are probably not a significant source of nitrate in atmospheric dust.

I.4.3 Evaporation Modeling of Dust Leachates

The measured water-soluble leachate compositions were used to evaluate the mineralogy of deliquescent salt minerals that might be present in the dust, and the composition and probability of occurrence of brines that might form through deliquescence. Evaporation of the leachate solutions was simulated using EQ3/6 version 8.0 software (BSC 2003d); see also the *Software User's Manual, EQ3/6, Version 8.0* (SNL 2003) with its supporting Pitzer-based thermodynamic database data0.ypf.R1 (DTN: SN0302T0510102.002). This modeling is described with specific detail in *Engineered Barrier System: Physical and Chemical Environment Model* (BSC 2003a, Section 6.10), and in general, in the *In-Drift Precipitates/Salts Model* (BSC 2003c; note that this model is also discussed in the response to KTI agreement ENFE 2.09). The solutions were evaporated to dryness or to the eutectic point, which in this context corresponds to the lowest water activity (lowest relative humidity) at which a separate water phase is still present. The modeling results were used for (1) binning and abstraction of the leach water compositions to determine the composition and probability of occurrence of deliquescent brines as discussed in the remainder of this section and (2) determination of the minerals that precipitated during evaporation to dryout and that are present at the eutectic point, as discussed in the following section.

Abstraction of the dust leachate water chemistries is described in the *Engineered Barrier System: Physical and Chemical Environment Model* (BSC 2003a, Section 6.10). A flowchart of the process is shown in Figure I-1. It is similar to that used for the abstraction of the seepage water chemistries summarized in the response to KTI ENFE 2.06. As with the seepage waters, the dust leachates were binned based upon the composition of the brines that would form upon evaporation of each leachate to a given activity of water (0.65). The final brine compositions are

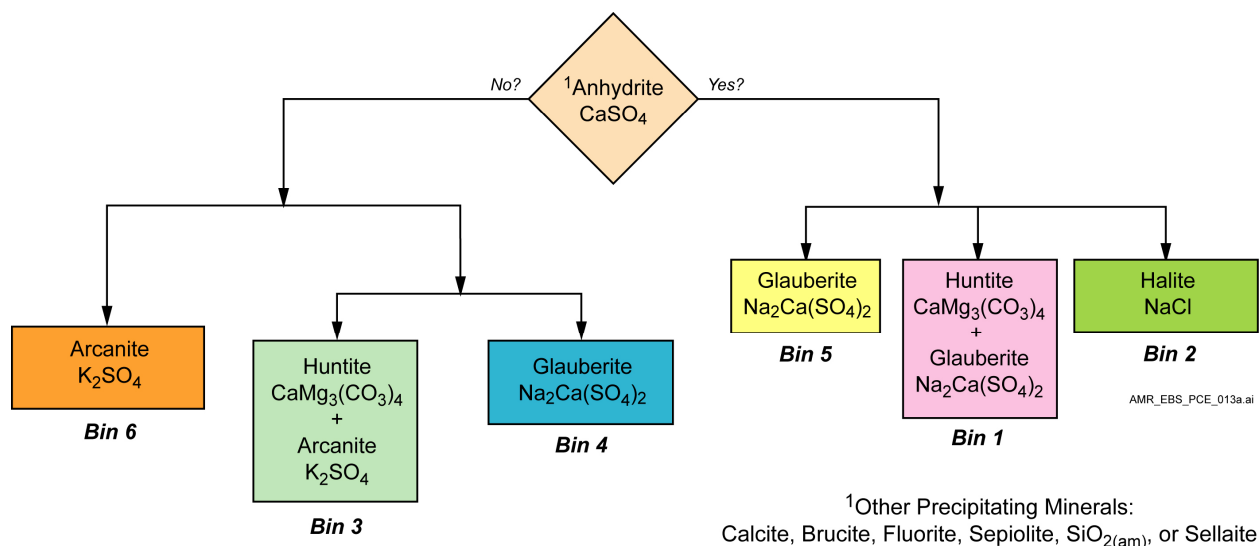
functions of both the initial leachate composition and of the modeled minerals that precipitate during evaporation (a full discussion on chemical divides is provided in the response to ENFE 2.06). The waters were grouped into six bins. Figure I-2 is a simplified schematic of the mineral precipitation observed during continued evaporation at 25°C. Additional minerals were observed, such as some complex nitrate salts, in a few cases, although they are not of significance to the overall results.



Source: BSC 2003a, Figure 6.10-1.

NOTE: USGS = U.S. Geological Survey; RH = relative humidity.

Figure I-1. Flowchart Representing the Dust Leachate Analysis Abstraction Process



Source: BSC 2003a, Figure 6.14-25.

Figure I-2 Flow Diagram Showing Some of the Precipitating Minerals That Are Associated with Each of the Six Dust Leachate Brine Evaporation Bins

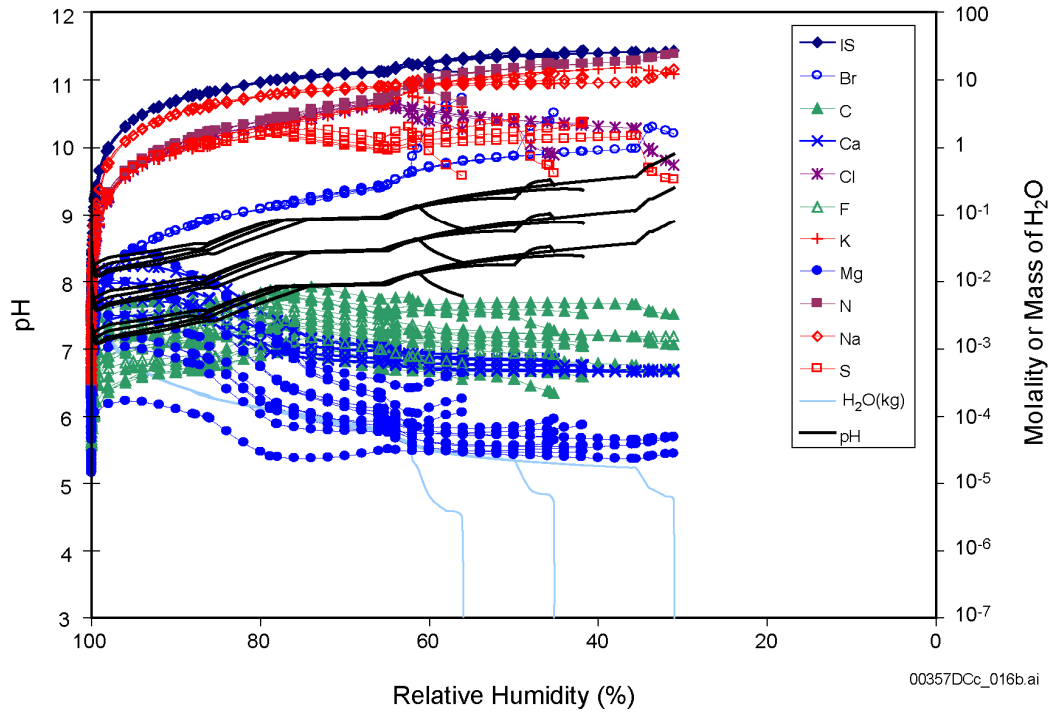
Six groups of water types (bins) were developed in this abstraction with the chemistries shown in Table I-1. The precipitates associated with the chemical divides leading to each bin are shown in Figure I-2. The information required for potential TSPA use is the water chemistry that would be produced by deliquescence at a range of temperatures and $p\text{CO}_2$ values. This was developed by modeling evaporation of the waters of the median composition of each bin at temperatures of 40°C, 70°C, 100°C, and 120°C and $p\text{CO}_2$ values of 10^{-2} , 10^{-3} , and 10^{-4} bar. Values at 140°C are also developed but these must be considered preliminary pending completion of the ongoing validation of the model (BSC 2003c) to this temperature for the relevant salts. Figure I-3 shows the aqueous compositions predicted for the most likely bin at each of the four temperatures and $p\text{CO}_2$ values (Figure I-4 shows the chemistry from the most likely bin at 140°C). The evaporation chemistry of water in each bin is shown in Figures 6.14-18 through 6.14-23 of *Engineered Barrier System: Physical and Chemical Environment Model* (BSC 2003a).

Table I-1. Total EQ3NR Equilibrated Aqueous Elemental Compositions for the 6 Bins, as Represented by Their Median Water

	Bin 1	Bin 2	Bin 3	Bin 4	Bin 5	Bin 6
Temp (°C)	25	25	25	25	25	25
pH	8.54	8.09	8.23	8.54	8.40	8.05
(I)	5.43×10^{-3}	2.74×10^{-3}	2.01×10^{-3}	6.29×10^{-3}	3.80×10^{-3}	1.15×10^{-3}
Br	5.01×10^{-6}	1.00×10^{-5}	3.75×10^{-6}	1.63×10^{-5}	1.63×10^{-5}	3.75×10^{-6}
C	1.96×10^{-3}	6.50×10^{-4}	8.86×10^{-4}	1.94×10^{-3}	1.36×10^{-3}	5.81×10^{-4}
Ca	1.35×10^{-3}	5.41×10^{-4}	3.09×10^{-4}	1.22×10^{-3}	7.17×10^{-4}	1.52×10^{-4}
Cl	2.17×10^{-4}	1.44×10^{-4}	1.35×10^{-4}	4.23×10^{-4}	2.82×10^{-4}	1.38×10^{-4}
F	3.16×10^{-5}	1.58×10^{-5}	1.58×10^{-5}	2.11×10^{-5}	3.68×10^{-5}	2.11×10^{-5}
K	2.63×10^{-4}	1.93×10^{-4}	2.99×10^{-4}	3.32×10^{-4}	2.63×10^{-4}	1.98×10^{-4}
Mg	1.65×10^{-4}	5.35×10^{-5}	4.81×10^{-5}	1.63×10^{-4}	7.08×10^{-5}	2.14×10^{-5}
N	5.16×10^{-4}	1.77×10^{-4}	1.18×10^{-4}	5.48×10^{-4}	3.23×10^{-4}	5.64×10^{-5}
Na	4.24×10^{-4}	4.05×10^{-4}	4.83×10^{-4}	1.34×10^{-3}	9.03×10^{-4}	3.72×10^{-4}
S	4.37×10^{-4}	3.96×10^{-4}	1.67×10^{-4}	6.97×10^{-4}	3.44×10^{-4}	6.04×10^{-5}
Si	1.46×10^{-4}	3.25×10^{-5}	6.27×10^{-5}	4.89×10^{-5}	7.91×10^{-5}	4.78×10^{-5}

Source: BSC 2003a, Table 6.10-9.

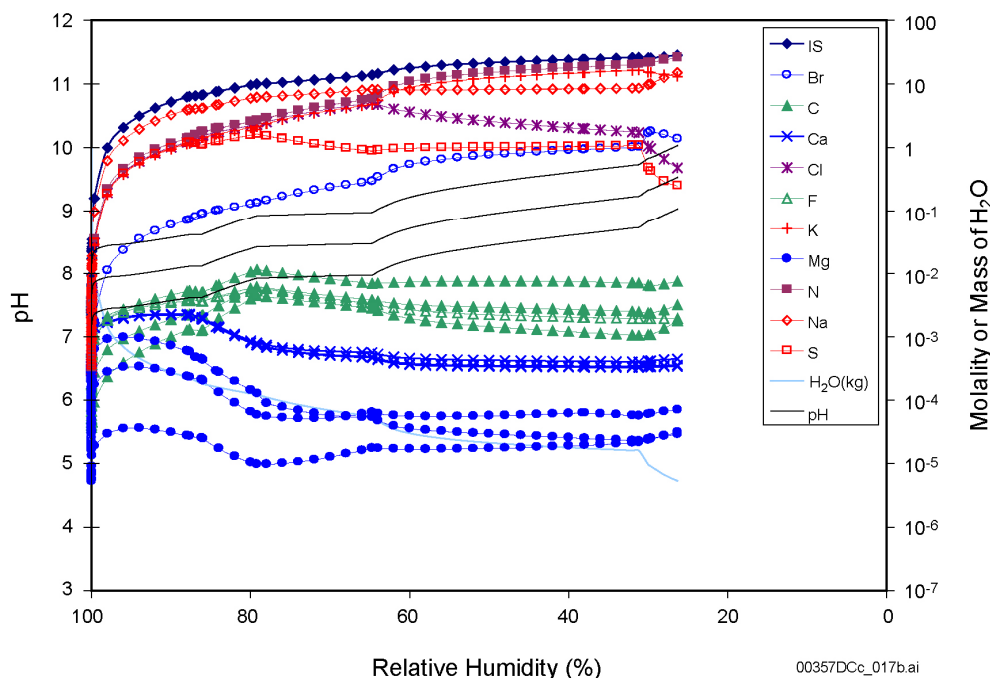
NOTE: Except for temperature and pH, all units are in Moles/kg H₂O; C includes carbonate species, N comprises nitrate species, and S comprises sulfate species.



Source: BSC 2003a, Figure 6.14-22.

NOTE: Each data set, or set of lookup tables, represents the compositional evolution of the representative bin water under a given set of $p\text{CO}_2$ (10^{-2} , 10^{-3} , and 10^{-4} bar) and temperature conditions (40°C , 70°C , 100°C , and 120°C).

Figure I-3. Range of Chemistry for Bin 5 Dust Leachate Water at Four Temperatures and Three $p\text{CO}_2$ Values



Source: BSC 2003a, Figure 6.14-22.

NOTE: Evaporation of the waters is modeled at 140°C and three $p\text{CO}_2$ values (10^{-2} , 10^{-3} , and 10^{-4} bar). Results at this temperature are preliminary pending extension of in-drift precipitates and salts model (BSC 2003c) validation.

Figure I-4. Preliminary Range of Chemistry for Bin 5 Dust Leachate Water at 140°C

I.4.4 Salts Present at Dryout and Their Deliquescence Behavior

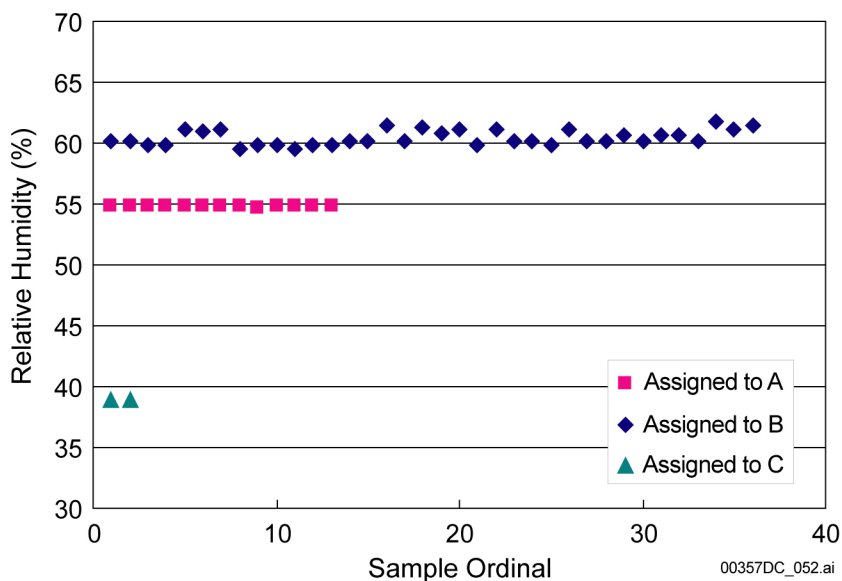
The relative amount and composition of solids present at dryout for each of the aqueous leachate compositions were also evaluated by the evaporation modeling at 25°C. These solids are taken to represent the soluble minerals present in the original dust. After screening all available data, analysis of the starting waters produced 16 distinct mineral assemblages at dryout. These modeled mineral assemblages were used as input to the corroborative evaluation of deliquescence on waste package and drift shield surfaces described in *Environment on the Surfaces of Drip Shield and Waste Package Outer Barrier* (BSC 2003b). A small group of specific solids that dominate the relative humidity–temperature behavior of all the assemblages were abstracted from the 16 mineral assemblages. Consideration of these controlling solids permits prediction of the $\text{NO}_3^-/\text{Cl}^-$ ratios of the waters first formed during deliquescence.

Examination of the water activities (relative humidities) corresponding to each of the starting waters at its eutectic point showed three groups of like samples (Figure I-5). This indicates that, while there may be 16 distinct groups of minerals that precipitate from the waters, only three groups of minerals actively control the relative humidity at which each of the starting waters will deliquesce. The key relative humidity controlling salt assemblages in each of these three groups are shown in Table I-2. This table also compares the average relative humidity for each group calculated by the in-drift precipitates salts modeling with the relative humidity calculated from the properties of the key salt assemblages alone.

Table I-2. Calculated Deliquescence Relative Humidity Values for Key Assemblages at 25°C and for $10^{-3.5}$ bar CO₂ Pressure

Case	Key Salts	Deliquescence Relative Humidity Percent for Pure Key System	Deliquescence Relative Humidity Percent for Actual Associated Sample Cases	Deliquescence Relative Humidity Percent Excluding KBr
A	NaCl-NaNO ₃ -KNO ₃ -KBr	54.91	54.80 ± 0.02	65.7
B	NaCl-KNO ₃ -KBr	62.97	60.44 ± 0.61	69.5
C	Ca(NO ₃) ₂ -NaCl-NaNO ₃ -KNO ₃ -KBr	38.98	38.93 ± 0.00	49.5

Sources: BSC 2003b, Tables 39 and 40; Wolery 2003.



Source: BSC 2003b, Figure 27.

NOTE: The "Sample Ordinal" is an arbitrary serial number assigned to the samples in each group listed in Table I-2. Note that there are essentially three distinct values of water activity represented in the samples shown.

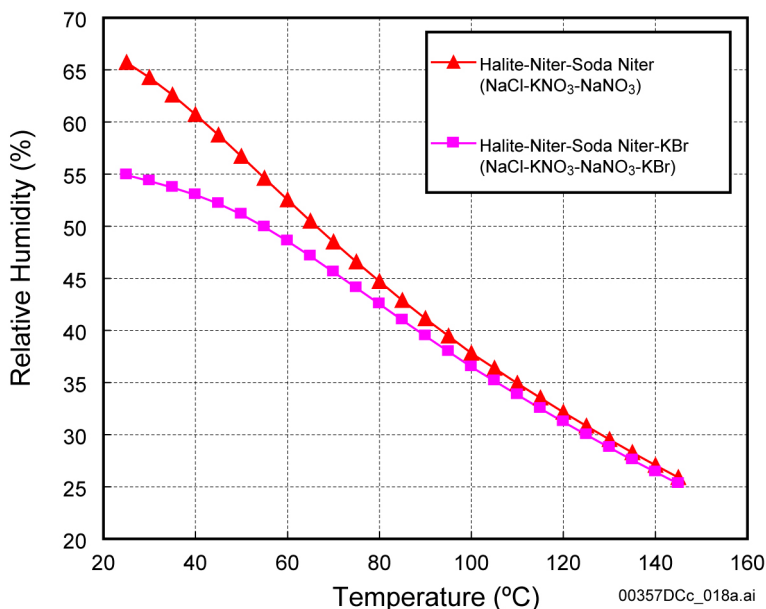
Figure I-5. Eutectic Relative Humidity Percent Values (25°C) from EQ3/6 Calculations of Reconstituted Salt Minerals in Dust Samples

In *Environment on the Surfaces of Drip Shield and Waste Package Outer Barrier* (BSC 2003b, Section 6.7.2.10), it is noted that the deliquescent salt KBr appears in all the dust leachate evaporation calculations and thence in the three abstracted key salt mineral assemblages. Its presence in the evaporation calculations traces back to the bromide concentrations in the dust leachate solutions. These levels of bromide seem high in comparison to chloride (e.g., for the Phase I samples in DTN: MO0207EBSDUSTS.020, mean Br⁻ is 28.7 ppm, mean Cl⁻ is 181 ppm). This high level of bromide is considered an artifact due to the use of bromide as a tracer in water used in tunnel construction and hydrologic testing. Thus, it is of interest to examine the deliquescence relative humidity of the key salt groups without including KBr. This was done in

the *Environment on the Surfaces of Drip Shield and Waste Package Outer Barrier* (BSC 2003b). The removal of KBr from the key salt mineral assemblages has two principal effects. First, it has a slight effect on the potassium content but no effect on the resulting chemical divides. Second, it results in mineral assemblages that are less deliquescent. This is illustrated in the last column of Table I-2, which compares the results of EQ3/6 calculations for cases in which KBr was excluded from the deliquescing salt assemblage. The effect on deliquescence relative humidity at 25°C is marked (note that these results have no practical dependence on the $p\text{CO}_2$). The effect of eliminating the KBr is much diminished with increasing temperature. This is illustrated for case A in Figure I-6.

Water chemistry lookup tables provided in *Engineered Barrier System: Physical and Chemical Environment Model* (BSC 2003a) are based on the full chemistries of the dust leachates and hence correspond to what one would generate with the complete mineral assemblages. The key salt assemblage concept applied (BSC 2003b, Sections 6.7.2.9 and 6.7.2.10) and provided in Table I-2 shows that the effect on deliquescence relative humidity of using key instead of full assemblages is small (close to experimental reproducibility of deliquescence relative humidity for salt minerals).

As pointed out above (Section I.4.2), dust from the tunnels is apparently a mixture of rock dust generated during tunneling and dust brought in from the outside air during ventilation. This mixture is dominated by rock dust; its bulk chemistry is very similar to that of the tuff host rock (BSC 2003a, Section 6.10). The abundance of bromine, which was used as a tracer (as LiBr) in the construction waters sprayed to control dust, also suggests that most of the dust originated from construction and tunneling. However, it is not known whether LiBr will be added to water used during construction of the repository drifts themselves. Regardless, the deliquescence tables provided by the *Engineered Barrier System: Physical and Chemical Environment Model* (BSC 2003a) provide appropriate values for use by the corrosion modules of the TSPA models for license application. If LiBr is not used during repository construction, deliquescence relative humidities at higher temperatures will not be significantly different (see Figure I-6) and will be higher at lower temperatures (see Table I-2).



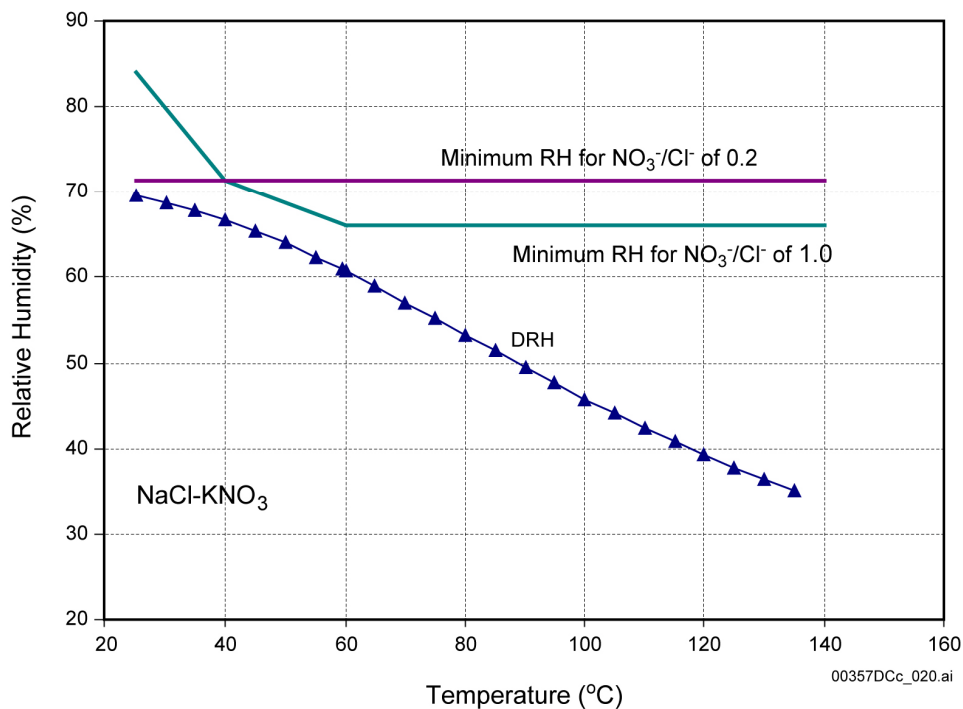
Source: BSC 2003b, Figure 29.

NOTE: Validated range only extends up to 125°C.

Figure I-6. Deliquescence Relative Humidity as a Function of Temperature for the Assemblages Halite-Niter-Soda Niter ($\text{NaCl-KNO}_3\text{-NaNO}_3$) and Halite-Niter-Soda Niter-KBr ($\text{NaCl-KNO}_3\text{-NaNO}_3\text{-KBr}$)

The composition of the first-formed solutions at the initiation of deliquescence will be at the eutectic composition of the multicomponent system. The eutectic composition is also a function of the temperature at which the deliquescence occurs. Further deliquescence will continue to form solutions of that composition until one (or more) of the salts in the salt mixture is completely dissolved. Further deliquescence will result in compositions that move away from that eutectic composition as dictated by the relative amounts of the various salts present in the mixture. As a result, the $\text{NO}_3^-/\text{Cl}^-$ ratio will vary as deliquescence continues.

The analysis of the key salt mineral assemblages in *Environment on the Surfaces of Drip Shield and Waste Package Outer Barrier* (BSC 2003b) shows that while they are generally highly deliquescent, at least at elevated temperature, they also tend to have high $\text{NO}_3^-/\text{Cl}^-$ ratios at the relatively low relative humidity values at which deliquescence first occurs. Lower $\text{NO}_3^-/\text{Cl}^-$ ratios (of say 0.2 to 1.0) are only achievable at significantly higher relative humidity values (much closer to the deliquescence relative humidity for pure halite). This is illustrated in Figure I-7 for the NaCl-KNO_3 system. In addition to the usual deliquescence relative humidity curve, this figure depicts as a function of temperature the minimum relative humidity required to obtain $\text{NO}_3^-/\text{Cl}^-$ ratios of 1.0 and 0.2. Note that the minimum relative humidity curves correspond to essentially constant values above 60°C. Below this temperature, the “1.0” curve rises and crosses the “0.2” curve (which remains nearly flat) near 40°C. This crossover is due to a reversal in the relative solubilities of the two salts. At 25°C, NaCl is more soluble than KNO_3 . The solubility of KNO_3 increases rapidly with temperature, while that of NaCl increases more slowly. At 100°C, for example, KNO_3 is substantially more soluble than NaCl. Similar relations are shown for the $\text{NaCl-KNO}_3\text{-NaNO}_3$ system in *Environment on the Surfaces of Drip Shield and Waste Package Outer Barrier* (BSC 2003b, Figure 32).



Source: BSC 2003b, Figure 31.

NOTE: The crossover of the two minimum relative humidity curves is caused by an inversion in the relative solubilities of NaCl and KNO₃. Validated range only extends up to 125°C. RH = relative humidity; DRH = deliquescence relative humidity.

Figure I-7. Deliquescence Relative Humidity and Minimum Relative Humidity Values to Achieve NO₃⁻/Cl⁻ Ratios of 1.0 and 0.2 as a Function of Temperature for the Assemblage Halite-Niter (NaCl-KNO₃)

I.5 REFERENCES

I.5.1 Documents Cited

BSC (Bechtel SAIC Company) 2003a. *Engineered Barrier System: Physical and Chemical Environment Model*. ANL-EBS-MD-000033 REV 02C. Las Vegas, Nevada: Bechtel SAIC Company. ACC: MOL.20031029.0034.

BSC 2003b. *Environment on the Surfaces of Drip Shield and Waste Package Outer Barrier*. ANL-EBS-MD-000001 REV 01D. Las Vegas, Nevada: Bechtel SAIC Company. ACC: MOL.20030825.0151.

BSC 2003c. *In-Drift Precipitates/Salts Model*. ANL-EBS-MD-000045 REV 01. Las Vegas, Nevada: Bechtel SAIC Company. ACC: DOC.20031028.0003.

BSC 2003d. Software Code: EQ3/6. V8.0. PC w/ Windows 95/98/2000/NT 4.0. 10813-8.0-00.

Peterman, Z.E., Paces, J.B., Neymark, L.A., and Hudson, D., 2003. "Geochemistry of Dust in the Exploratory Studies Facility, Yucca Mountain, Nevada." *Proceedings of the 10th International High-Level Radioactive Waste Management Conference (IHLRWM), March 30-April 2, 2003, Las Vegas, Nevada.* Pages 637-645. La Grange Park, Illinois: American Nuclear Society. TIC: 254559. ACC: MOL.20030624.0313.

Reamer, C.W. 2001. U.S. Nuclear Regulatory Commission/U.S. Department of Energy Technical Exchange and Management Meeting on Evolution of the Near-Field Environment (January 9–12, 2001). Letter from C.W. Reamer (NRC) to S. Brocoum (DOE/YMSCO), January 26, 2001, with enclosure. ACC: MOL.20010810.0033.

SNL (Sandia National Laboratories) 2003. *Software User's Manual, EQ3/6, Version 8.0.* SDN: 10813-UM-8.0-00. Albuquerque, New Mexico: Sandia National Laboratories. ACC: MOL.20030312.0084.

Wolery, T.J. 2003. Modification of Dust Salt Analysis. Letter from T. Wolery to D. Salmon, October 28, 2003. ACC: MOL.20031029.0001.

I.5.2 Source Data, Listed by Data Tracking Number

MO0207EBSDUSTS.020. Geochemical Composition of Dust Samples. Submittal date: 07/11/2002.

MO0209EBSDUST2.030. Geochemical Composition of Dust Samples (Phase II). Submittal date: 09/30/2002.

SN0302T0510102.002. Pitzer Thermodynamic Database (data0.ypf, Revision 1). Submittal date: 02/06/2003.

INTENTIONALLY LEFT BLANK

APPENDIX J
ANALYSIS OF LABORATORY SOLUTION OF INTRODUCED MATERIALS
(RESPONSE TO ENFE 2.14)

Note Regarding the Status of Supporting Technical Information

This document was prepared using the most current information available at the time of its development. This Technical Basis Document and its appendices providing Key Technical Issue Agreement responses that were prepared using preliminary or draft information reflect the status of the Yucca Mountain Project's scientific and design bases at the time of submittal. In some cases this involved the use of draft Analysis and Model Reports (AMRs) and other draft references whose contents may change with time. Information that evolves through subsequent revisions of the AMRs and other references will be reflected in the License Application (LA) as the approved analyses of record at the time of LA submittal. Consequently, the Project will not routinely update either this Technical Basis Document or its Key Technical Issue Agreement appendices to reflect changes in the supporting references prior to submittal of the LA.

APPENDIX J

ANALYSIS OF LABORATORY SOLUTION OF INTRODUCED MATERIALS (RESPONSE TO ENFE 2.14)

This appendix provides a response for Key Technical Issue (KTI) agreement Evolution of the Near-Field Environment (ENFE) 2.14. This KTI relates to providing an analysis of laboratory solutions of introduced materials that might impact waste package and drip shield performance (lifetimes).

J.1 KEY TECHNICAL ISSUE AGREEMENT

J.1.1 ENFE 2.14

KTI Agreement ENFE 2.14 was reached during the U.S. Nuclear Regulatory Commission (NRC)/U.S. Department of Energy (DOE) Technical Exchange and Management Meeting on Evolution of the Near-Field Environment held January 9 to 11, 2001, in Pleasanton, California (Reamer 2001). ENFE KTI subissues 1, 2, 3, and 4 were discussed at that meeting. There has been no submittal related to this KTI agreement to the NRC.

Wording of the agreement is as follows:

ENFE 2.14

Provide the analysis of laboratory solutions that have interacted with introduced materials. The DOE will provide additional information about laboratory solutions that have interacted with introduced materials, in a revision to the Environment on the Surfaces of the Drip Shield and Waste Package Outer Barrier AMR (ANL-EBS-MD-000001), expected to be available in FY02.

J.1.2 Related Key Technical Issue Agreements

Other KTI agreements related to those addressed in this appendix are CLST 1.01 (Appendix A), ENFE 2.04 (Appendix C), 2.06 (Appendix E), and 2.13 (Appendix I). These all deal with issues pertaining to how the environment on the waste package and drip shield surfaces may be impacted, including interactions from introduced materials.

J.2 RELEVANCE TO REPOSITORY PERFORMANCE

The primary consideration in the in-drift environment is the impact of processes and materials on the waste package and drip shield performance (lifetimes). Introduced materials in the repository can impact the evolution of water chemistry within the drift, potentially affecting the performance of the waste package and drip shield. For the purposes of establishing waste package and drip shield degradation rates and performance, it is critical to carry out testing and analyses that are consistent with anticipated conditions in the drift environment.

J.3 RESPONSE

The consideration of the effects of introduced materials and their impacts on the water chemistry and in-drift environmental conditions are addressed primarily through computer simulation as opposed to laboratory testing (as called for in the text of ENFE 2.14). Laboratory tests have been carried out on seepage water interaction with cementitious grout, but since grout is no longer part of the ground support design, these analyses are not relevant. Other laboratory analyses of introduced materials were not done. Therefore, this appendix primarily provides additional information regarding computer simulations of the effects of solutions with introduced materials.

The current design for the drifts includes ground support materials comprised of only carbon steels and 316L stainless steel materials. The analysis presented in *Engineered Barrier System: Physical and Chemical Environment Model* (BSC 2003a) evaluated introduced materials likely to affect the composition of water in the drift environment (see also responses addressing ENFE 2.04 and 2.06). Without cementitious materials, the analysis focused on the stainless steel components and their corrosion and utilizes published rates of corrosion and the materials composition used in the engineered barrier system. The analysis provides a conservative first order estimate of the effects of stainless steel corrosion in the drift environment. The analysis, however, does not consider the corrosion of rock bolts, which are likely to change considerably in terms of their quantity and perhaps type in the repository design. Once higher humidity conditions develop after a period of dryout following closure, carbon-low alloy steels are expected to have a very short lifetime on the order of 100 years per inch thickness and, therefore, to have minimal effect on seepage water chemistry over the long term. The results presented in *Engineered Barrier System: Physical and Chemical Environment Model* (BSC 2003a, Section 6.8) indicate that stainless steel corrosion is likely to have only a very minor effect on seepage water chemistry.

The consideration and impacts of the effects of introduced dust is addressed in the response for ENFE 2.13.

The information in this report is responsive to agreement ENFE 2.14 made between the DOE and NRC. The report contains the information that DOE considers necessary for NRC review for closure of this agreement.

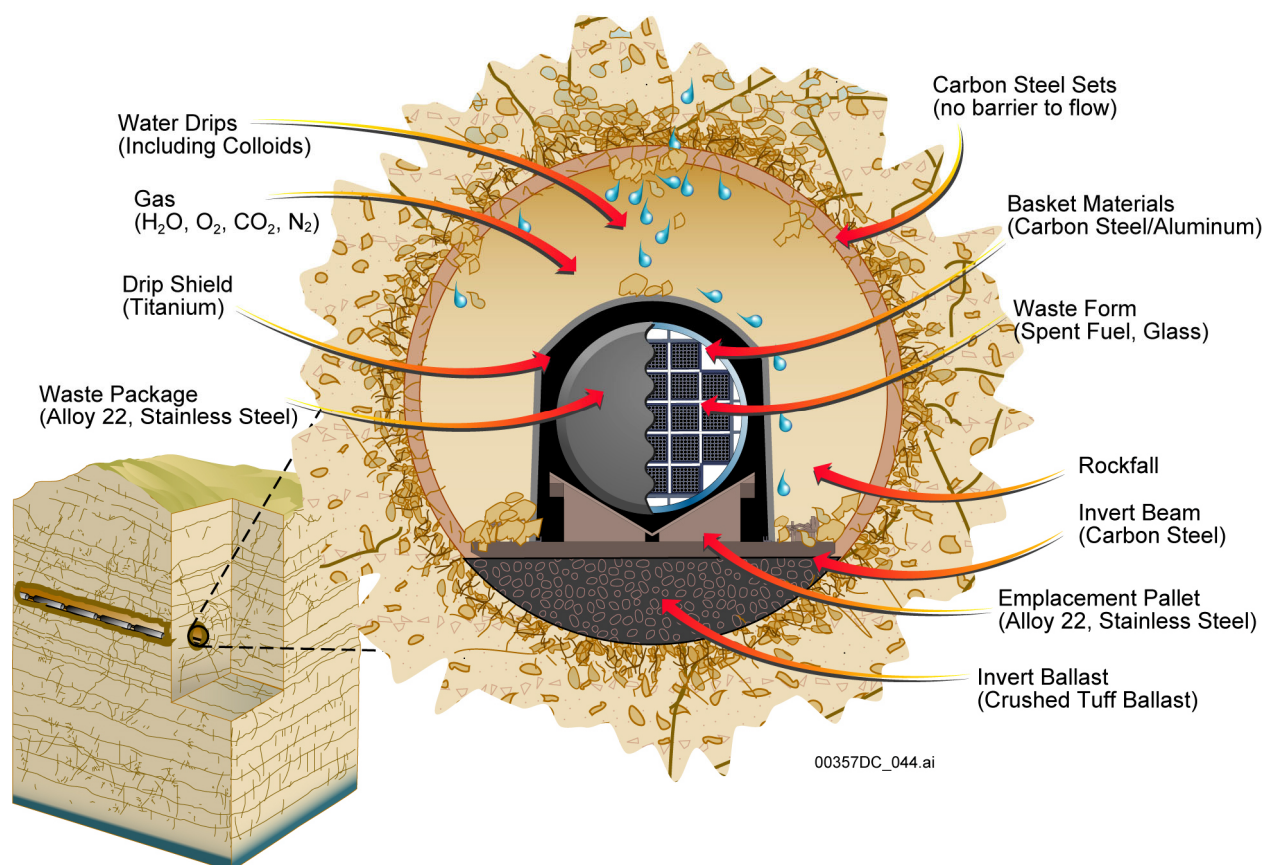
J.4 BASIS FOR THE RESPONSE

A discussion of the detailed analysis of the chemical composition of solutions that have interacted with introduced materials in the drift environment, especially steel bolts, wire mesh, and rails, is contained in *Engineered Barrier System: Physical and Chemical Environment Model* (BSC 2003a). The analysis in that report is based primarily on published rates of corrosion and the composition of materials to be used in the Engineered Barrier System.

J.4.1 Introduced Materials

Figure J-1 shows the general configuration of the introduced materials in a repository drift. These materials are not expected to remain pristine after the introduction into the repository environment. Their longevity and evolution affects the geochemical evolution of seepage

infiltrating into the drift and waters from condensation or salt deliquescence in the drift. The focus in this section is on the designated introduced materials in the repository drifts, exclusive of the drip shield and waste package, as listed in the introduced materials input tables in *Engineered Barrier System: Physical and Chemical Environment Model* (BSC 2003a, Section 4.1). It should be noted that the list of introduced materials provided in *Repository Design Project, Repository/PA IED Emplacement Drift Committed Materials 1 of 2* (BSC 2003b) and *Repository Design Project, Repository/PA IED Emplacement Drift Committed Materials (2)* (BSC 2003c) are based on a preliminary design.



Source: BSC 2003a, Figure 6.4-1.

NOTE: Not shown are the welded wire fabric and rock bolts. These items are part of the ground support design and are located in or adjacent to the drift wall.

Figure J-1. General Location of Engineered Barrier System Components and Materials

The compositions of introduced materials presently designated for use in the Engineered Barrier System are given in Table J-1.

Table J-1. Compositions of Materials Designated for Use in the Engineered Barrier System

Component	Material Conformance ASTM Manual	Type of Material	Chemical Composition	Residual ^a (%)
Ground Support				
Steel Sets W6x20	A572/A 572M-01 (Page 2, Table 2)	Grade 65 [450]	Fe _{97.9} C _{0.26} Mn _{1.35} P _{0.04} S _{0.05} Si _{0.4}	
Pipe Spacers 1-1/4"	A53/A 53M-02 (Page 2, Table 1)	Type S, Grade B	Fe _{96.78} C _{0.3} Mn _{1.2} P _{0.05} S _{0.045} V _{0.08} Cu _{0.4} Ni _{0.4} Cr _{0.4} Mo _{0.15}	
Tie Rods 5/8"	A307-00 (Page 5, Section S1.5.1)	Bolts Suitable for Welding	Fe _{98.11} C _{0.3} Mn _{1.0} P _{0.04} S _{0.05} Si _{0.5}	
Steel Wire Fabric 3"x3" grid	A276-02 (Page 3, Table 1)	316L SS [S31603]	Fe _{61.895} C _{0.03} Mn _{2.0} P _{0.045} S _{0.03} Si _{1.0} Ni _{14.0} Cr _{18.0} Mo _{3.0}	
Bearing Plates	F432-95 (Page 2, Table 1)	Bearing and Header Plates	Fe _{98.84} C _{1.04} P _{0.058} S _{0.06}	
Rock Bolts 1-1/8"	F432-95 (Page 2, Table 1)		Fe _{99.094} C _{0.79} P _{0.058} S _{0.058}	
Invert				
Transverse Beams w/ Stiffeners	A588/A 588M-00a (Page 2, Table 1)	Grade B	Fe _{96.16} C _{0.2} Mn _{1.35} V _{0.1} Cu _{0.4} P _{0.04} S _{0.05} Si _{0.5} Ni _{0.5} Cr _{0.7}	
Longitudinal Support Beams	A588/A 588M-00a (Page 2, Table 1)	Grade B	Fe _{96.16} C _{0.2} Mn _{1.35} V _{0.1} Cu _{0.4} P _{0.04} S _{0.05} Si _{0.5} Ni _{0.5} Cr _{0.7}	
Stiffener Brackets	A588/A 588M-00a (Page 2, Table 1)	Grade B	Fe _{96.16} C _{0.2} Mn _{1.35} V _{0.1} Cu _{0.4} P _{0.04} S _{0.05} Si _{0.5} Ni _{0.5} Cr _{0.7}	
Base Plates	A588/A 588M-00a (Page 2, Table 1)	Grade B	Fe _{96.16} C _{0.2} Mn _{1.35} V _{0.1} Cu _{0.4} P _{0.04} S _{0.05} Si _{0.5} Ni _{0.5} Cr _{0.7}	
Anchor Bolts	A307-00 (Page 5, Section S1.5.1)	Bolts Suitable for Welding	Fe _{98.11} C _{0.3} Mn _{1.0} P _{0.04} S _{0.05} Si _{0.5}	
Structural Bolts	A490-02 (Page 3, Table 2)	Type 3	Fe _{97.635} C _{0.55} Mn _{0.37} Cu _{0.63} P _{0.04} S _{0.045} Ni _{0.17} Cr _{0.42} Mo _{0.14}	
Miscellaneous Plates	A588/A 588M-00a (Page 2, Table 1)	Grade B	Fe _{96.16} C _{0.2} Mn _{1.35} V _{0.1} Cu _{0.4} P _{0.04} S _{0.05} Si _{0.5} Ni _{0.5} Cr _{0.7}	
Gantry Rail Assembly				
Rail Runway Beams	A588/A 588M-00a (Page 2, Table 1)	Grade B	Fe _{96.16} C _{0.2} Mn _{1.35} V _{0.1} Cu _{0.4} P _{0.04} S _{0.05} Si _{0.5} Ni _{0.5} Cr _{0.7}	
Cap Plate	A588/A 588M-00a (Page 2, Table 1)	Grade B	Fe _{96.16} C _{0.2} Mn _{1.35} V _{0.1} Cu _{0.4} P _{0.04} S _{0.05} Si _{0.5} Ni _{0.5} Cr _{0.7}	
Guide Beams	A588/A 588M-00a (Page 2, Table 1)	Grade B	Fe _{96.16} C _{0.2} Mn _{1.35} V _{0.1} Cu _{0.4} P _{0.04} S _{0.05} Si _{0.5} Ni _{0.5} Cr _{0.7}	
Gantry Rails	A759-00 (Page 2, Table 1)		Fe _{97.47} C _{0.84} Mn _{1.1} P _{0.04} S _{0.05} Si _{0.5}	
Conductor Bar (Copper)	MO0003SPAARD38.026	Solid Copper	Cu _{94.0} C _{3.158} H _{0.347} O _{0.493} Cl _{2.002}	
Conductor Bar Fittings	MO0001SPARSD38.014	Steel	Fe _{97.48} C _{0.23} Mn _{1.65} V _{0.15}	
Emplacement Pallet				
Emplacement Pallet (316L SS)	A240/A 240M-01 (Page 4, Table 1)	316L SS [S31603]	Fe _{61.775} C _{0.03} Mn _{2.0} P _{0.045} S _{0.03} Si _{0.75} Ni _{14.0} Cr _{18.0} Mo _{3.0} N _{0.1}	
Emplacement Pallet (Alloy C-22)	B575-99a (Page 2, Table 1)	C-22 Alloy [N06022]	Fe _{6.0} C _{0.015} Mn _{0.5} P _{0.02} S _{0.02} Si _{0.08} V _{0.35} Ni _{50.02} Co _{2.5} W _{3.5} Cr _{22.5} Mo _{14.5}	
Emplacement Pallet Weld Metal	B575-99a (Page 2, Table 1)	SFA-5.14 N06022	Fe _{6.0} C _{0.015} Mn _{0.5} P _{0.02} S _{0.02} Si _{0.08} V _{0.35} Ni _{50.02} Co _{2.5} W _{3.5} Cr _{22.5} Mo _{14.5}	

Table J-1. Compositions of Materials Designated for Use in the Engineered Barrier System (Continued)

Component	Material Conformance ASTM Manual	Type of Material	Chemical Composition	Residual ^a (%)
Drip Shield				
Drip Shield	B265-99 (Page 3, Table 2)	Titanium Grade 7	Ti _{98.675} Fe _{0.3} C _{0.08} H _{0.015} O _{0.25} Pd _{0.25} N _{0.03}	0.4
Drip Shield (Bulkheads Posts, and	B265-99 (Page 3, Table 2)	Titanium Grade 24	Ti _{87.525} Fe _{0.4} C _{0.08} H _{0.015} O _{0.2} Pd _{0.08} N _{0.05} V _{4.5} Al _{6.75}	0.4
Drip Shield (Base Alloy C-22)	B575-99a (Page 2, Table 1)	C-22 Alloy [N06022]	Ni _{50.02} Fe _{6.0} C _{0.015} Mn _{0.5} P _{0.02} S _{0.02} Si _{0.08} V _{0.35} Co _{2.5} W _{3.5} Cr _{22.5} Mo _{14.5}	
Drip Shield Weld Metal	B265-99 (Page 3, Table 2)	SFA-5 16 R52401	Ti _{90.342} Fe _{0.2} C _{0.03} V _{4.5} H _{0.008} O _{0.15} Pd _{0.25} N _{0.02} Al _{4.5}	
Miscellaneous Materials				
Communications Cable			Cu _{50.0} C _{42.82} H _{7.18}	
Waste Package Materials				
Inner Barrier	A240/A 240M-01 (Page 4, Table 1)	SA-240 S31600	Fe _{61.995} Mn _{2.0} P _{0.045} S _{0.03} Si _{0.75} Ni _{14.0} Cr _{18.0} Mo _{3.0} N _{0.08}	
Alloy 22 Welds	B575-99a (Page 2, Table 1)	SFA-5.14 N06022	Fe _{6.0} C _{0.015} Mn _{0.5} P _{0.02} S _{0.02} Si _{0.08} V _{0.35} Ni _{50.02} Co _{2.5} W _{3.5} Cr _{22.5} Mo _{14.5}	
316 Welds	A240/A 240M-01 (Page 4, Table 1)	SFA-5.9 S31680	Fe _{61.775} C _{0.03} Mn _{2.0} P _{0.045} S _{0.03} Si _{0.75} Ni _{14.0} Cr _{18.0} Mo _{3.0} N _{0.1}	
Fuel Basket Plate	MO0001SPANEU38.018	Neutronit A 978	Fe _{66.66} C _{0.04} Cr _{18.5} Co _{0.20} Ni _{13.00} B _{1.6}	
Outer Barrier	B575-99a (Page 2, Table 1)	SB-575 N06022	Fe _{6.0} C _{0.015} Mn _{0.5} P _{0.02} S _{0.02} Si _{0.08} V _{0.35} Ni _{50.02} Co _{2.5} W _{3.5} Cr _{22.5} Mo _{14.5}	
Fuel Basket Plate	B209M-02e1 (Table 1, Page 2)	SB-209 A96061 T 4	Al _{95.85} Fe _{0.7} Mn _{0.15} Mg _{1.2} Cu _{0.4} Si _{0.8} Ti _{0.15} Cr _{0.35} Zn _{0.3}	
Basket Stiffener	A516/A516M-01 (Table 1, Page 2)	SA-516 K02700	Fe _{97.87} C _{0.31} Mn _{1.3} P _{0.035} S _{0.035} Si _{0.45}	

Source: BSC 2003a, Table 6.4-20.

NOTE: ^aA residual is an element present in a metal or an alloy in small quantities and is inherent to the manufacturing process but not added intentionally. In titanium, these elements include aluminum, vanadium, tin, chromium, molybdenum, niobium, zirconium, hafnium, bismuth, ruthenium, palladium, yttrium, copper, silicon, cobalt, tantalum, nickel, boron, manganese, and tungsten.

The corrosion rates of these materials have been summarized in *Engineered Barrier System: Physical and Chemical Environment Model* (BSC 2003a, Table 6.4.2-1) and are provided in Table J-2.

Although expressed as corrosion rates here, these can be converted into rates of release into solution of the components of the various materials by making use of the chemical composition formulas in Table J-1 and the molar volumes of the material. The information in Table J-2 also provides an idea of which introduced materials are likely to affect the composition of water in the drift environment. Alloy 22, for example, is very unlikely to have any impact given its very slow rate of corrosion.

Table J-2. Selected Corrosion Rates of Metallic and Alloy Materials for Use in Engineered Barrier System Chemical Environment Calculations

Material	Environmental Conditions	Maximum Corrosion ($\mu\text{m}/\text{yr}$)	Mean Corrosion ($\mu\text{m}/\text{yr}$)	Minimum Corrosion ($\mu\text{m}/\text{yr}$)	Reference in P&CE AMR (BSC 2003a)	Comments
Titanium	Steam and Atmospheric	0.07	0.012065	0.00254	Tables 6.4-2 and 6.4-3	SAW steam at 90°C and 100% relative humidity for maximum and Ti in hostile atm at lower temp for mean and minimum
Alloy 22	Steam	0.47	0.07	0.02	Table 6.4-5	SCW 90°C for maximum, mean, and SCW 60°C for minimum
Alloy 22	Simulated Water	0.25	0.08	0.03	Table 6.4-5	SCW 90°C for maximum, mean, and SCW 60°C for minimum
Inconel Alloy X-750 and 600 SS	Simulated Water	0.24	0.08	0.05	Table 6.4-7	Inconel Alloy 625 was used as surrogate. SCW 90°C for maximum, mean, and SCW 60°C for minimum
Copper Alloy	Steam and Atmospheric	6.6	4.79	3.15	Table 6.4-8	J-13 steam, 95 to 100°C, near 100 relative humidity
Aluminum Alloy	Fresh/Salt Water	124.46	12.95	0.4	Table 6.4-9	Saltwater for maximum, fresh water for mean, and minimum
316L SS	Steam and Atmospheric	0.517	0.115	0.099	Table 6.4-11	Marine atm for maximum and mean and 100°C J13 steam for minimum
316L SS	Fresh/Salt Water	14.79	1.9391	0.2286	Table 6.4.11	26.7°C saltwater for maximum and mean and 70°C fresh water for minimum
304L SS	Fresh/Salt Water	36.902	9.934	1.588	Table 6.4-13	26.7°C saltwater for maximum, mean and minimum
Borated SS (Neutronit)	Fresh/Salt Water	29.22	11.0595	1.81	Table 6.4-14	26.7°C saltwater for maximum, mean and minimum
Borated SS (0.3%B in 304L)	Fresh/Salt Water	147	94.67	38.22	Table 6.4-14	26.7°C saltwater for maximum, mean and minimum
Borated SS (1.5%B in 304L)	Fresh/Salt Water	1893.36	1225.98	937.86	Table 6.4-14	Maximum boiling saline, mean ambient saline solution, and minimum 50°C saline solution
Carbon-Low Alloy Steels	Steam and Atmospheric	851.09	195.39	85.5	Table 6.4-15	Maximum marine atm, mean marine atm with 80% relative humidity, and minimum industrial atm
Carbon-Low Alloy Steels	Simulated Water	180.42	88.79	41.31	Table 6.4-15	SCW 90°C for maximum, and SDW 60°C for mean and minimum

Source: BSC 2003a, Table 6.4-18.

NOTE: SCW = simulated concentrated water; SDW = simulated dilute water; SAW = simulated acidic concentrated water.

Environment on the Surfaces of Drip Shield and Waste Package Outer Barrier (BSC 2003d) includes a substantial discussion of the effects of introduced dust, and this is summarized in the Appendix I (ENFE 2.13). The compositions of the leachate from dust samples collected in the Exploratory Studies Facility at Yucca Mountain were the basis of the analyses. No other analyses of laboratory solutions derived from interaction with introduced materials are included in that report.

J.4.2 Impact of Corrosion Products

This section is intended to examine the chemical impact of seepage water entering the repository drift and coming into contact with the ground support system and the corrosion products that result. The subsurface design calls for using 316L stainless steel wire mesh and rock bolts (BSC 2003c) as the drift ground support system. Therefore, the metallic elements contained within this steel are discussed, and their primary components are examined in detail with respect to their corrosion and subsequent effect upon seepage water chemistry.

This base case discussion that follows represents a reasonable corrosion rate for the 316L stainless steel ground support wire fabric and rock bolts and the corrosion product effect on incoming seepage water, within the limitations of the available model. The base case model to be examined in detail is defined by the following:

- Material (Steel Wire Fabric 316L stainless steel) and dimensions as defined in 800-IED-WIS0-00302-000-00A (BSC 2003c).
- “Bin 11” seepage water (abstracted in *Engineered Barrier System: Physical and Chemical Environment Model* (BSC 2003a, Section 6.6.6, results in DTN: MO0304MWDSAB11.001) as it is the most likely water chemistry.
- Predominant 316L stainless steel oxidation corrosion products include iron(III) and chromium(III).
- Primary controlling mineral phases for stainless steel corrosion products: goethite and amorphous chromium hydroxide.
- Temperature of 25°C and fugacity of CO₂ at 10⁻³ bar.
- Abstracted 316L stainless steel corrosion rates given below (BSC 2003a, Section 6.4).

Interaction with the abstracted “Bin 11” seepage water was chosen, as this is the most likely water, occurring in almost 40 percent of the abstracted periods (BSC 2003a). In addition, Bin 11 water is seen to occur during the relevant period for the corrosion of 316L stainless steel, in the range of about 500 to 5,000 years for three of the four seepage water compositions considered.

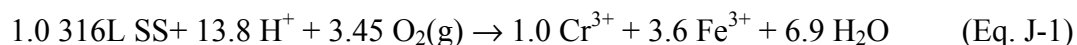
Iron(III) and chromium(III) have been selected as the corrosion end products influencing the seepage water chemistry. Selection of iron(III) as opposed to chromium(II) is proper given the relatively oxidizing conditions (atmospheric O₂ concentrations leading to significant dissolved oxygen content) and the mild pH ranges of the seepage waters.

Selection of chromium(III) over that of the more soluble chromium(VI) species is based on the experimental observation of corrosion products and the kinetics and conditions required to obtain the fully oxidized chromium(VI) state (Smith and Purdy 1995), although this is contrary to the prediction of equilibrium thermodynamics under oxidizing conditions. Smith and Purdy's examination of the actual chromium speciation as a result of corrosion of 316 stainless steel demonstrated a predominance of the less soluble chromium(III) species, except under the conditions of hot concentrated nitric acid (111°C and greater than 7 molar HNO₃) (Smith and Purdy 1995, Figure 6).

Goethite was selected as the iron controlling mineral phase and not the more thermodynamically stable hematite. Selection of the proper chromium phase that controls concentrations of chromium(III) in these seepage-stainless steel interacted waters is very important. The amorphous chrome hydroxide (Cr(OH)₃) was selected based on Ball and Nordstrom (1998), who provided a review of the original work by Rai et al. (1987).

J.4.3 Abstraction of 316L Stainless Steel and Its Corrosion Rate

The examinations of the effects of 316L stainless steel (316L SS) corrosion products on seepage water consider only iron (Fe) and chromium (Cr) in the abstracted model. The reaction proceeds according to:



which shows the basic irreversible corrosion reaction, though without including the formation of expected secondary solid products of chromium(III) and iron(III).

The corrosion rate of 316L stainless steel controls the quantity of the corrosion product and the extent to which it then affects the crown seepage water chemistry. Analyses (BSC 2003a, Section 6.8) produce a final base case value for the corrosion rate in moles per kg water at a given year. Briefly, the calculation takes the 316L wire fabric dimensions (76.2-mm × 76.2-mm grid spacing, 5.7-mm diameter wires from 800-IED-WIS0-00302-000-00A (BSC 2003c) and determines the total quantity of this wire over a 1-m² section of drift wall. A step-function for the corrosion rate is used to approximate the transition from dry to wet drift-wall conditions, which is estimated to occur around 2,000 years after emplacement as shown by the thermal-hydrologic-chemical data (DTN: LB0302DSCPTHCS.002). Seepage amounts are also taken as those from the thermal-hydrologic-chemical analyses (DTN: LB0302DSCPTHCS.002, from "distance" sheet for fractures).

The "mean" corrosion rate selected for the wet period comes from those shown in Table J-2 and listed under Material "316L SS," and the Environmental Conditions of "fresh/salt water" as 1.9391 μm/yr (BSC 2003a, Section 6.4). The rate of corrosion during a hot and dry period after closure was similarly taken from the Environmental Condition listed as "steam and atmospheric" "mean" rate, contained in Table J-2 as 0.115 μm/yr (BSC 2003a, Section 6.4). The analysis then applies a simple, constant corrosion rate for the dry period (up to 2,000 years) to the wire fabric diameter. At more than 2,000 years, the larger "fresh/salt water" corrosion rate is applied to continue decreasing the wire diameter through time. To obtain the corrosion quantity (moles) of steel, the calculation combines the remaining diameter of wire with the corrosion rate and factors

in the density of 316L stainless steel (ASTM G 1-90) and its compositional makeup (ASTM A 240/A 240M-02a). This mole quantity of iron and chrome, as corrosion amount per year, is then combined with the infiltration water amount used by the thermal-hydrologic-chemical analyses (DTN: LB0302DSCPTHCS.002, in “notes” sheet), and this generates a final molal quantity for input into EQ3/6 speciation calculations.

The abstracted model for stainless steel ground support interaction with seepage water consists of the following sequential EQ3/6 runs:

1. Initial EQ3NR speciation of Bin 11 seepage water (DTN: MO0304MWDSAB11.001) with trace quantities of Fe^{2+} (1×10^{-30} molal) and Cr^{3+} (1×10^{-20} molal) added and chromium(VI) oxide phases suppressed; output pickup file from this feeds into runs 2 and 3
2. EQ6 evaporation to 98 percent relative humidity of the Bin 11 water for basis of comparison
3. EQ6 “titration” run dissolving abstracted Stainless Steel Type 316L mineral by corrosion quantity; output second half of pickup file from this feeds into run 4
4. EQ6 evaporation to 98 percent relative humidity of the steel corrosion product containing Bin 11 water.

The effect of the abstracted 316L stainless steel dissolution into the Bin 11 crown seepage water is summarized in Table J-3. Values in this table represent the values calculated with the Stainless Steel Type 316L dissolution minus the values of pure Bin 11 seepage waters, as determined at 100 and 98 percent relative humidity. The largest differences seen are all below 0.1 percent.

Table J-3. Absolute (Relative) Differential Effect of the Stainless Steel Type 316L Dissolution in Bin 11 Seepage Water at 100 and 98 Percent Relative Humidity

Relative Humidity	ΔpH	$\Delta(\text{Ionic Strength})$	$\Delta(\text{Cl moles/ kg H}_2\text{O})$	$\Delta(\text{Si moles/ kg H}_2\text{O})$	$\Delta(\text{C moles/ kg H}_2\text{O})$
100	0.0000	2.0×10^{-8} (3×10^{-4})	4.2×10^{-9} (3×10^{-4})	4.6×10^{-10} (2×10^{-5})	1.1×10^{-8} (8×10^{-4})
98	-0.0001	-3.8×10^{-4} (-0.05)	-1.1×10^{-4} (-0.05)	-2.4×10^{-5} (0.07)	-5.9×10^{-5} (-0.05)

Source: BSC 2003a, Table 6.8-5.

There are no significant differences in the amounts of the mineral phases that exist in both Stainless Steel Type 316L interacted and pure Bin 11 water at either 100 or 98 percent relative humidity; those minerals are fluorite, sepiolite and $\text{SiO}_2(\text{am})$. Goethite and $\text{Cr}(\text{OH})_3(\text{am})$ are found only in the Stainless Steel Type 316L interacted water. Several trace (less than 1×10^{-8} moles) solid species are found only in one or the other of the waters; these consist of natronite (Ca and K derivatives), erionite, and stellerite.

J.5 REFERENCES

J.5.1 Documents Cited

Ball, J.W. and Nordstrom, D.K. 1998. "Critical Evaluation and Selection of Standard State Thermodynamic Properties for Chromium Metal and its Aqueous Ions, Hydrolysis Species, Oxides, and Hydroxides." *Journal of Chemical & Engineering Data*, 43, (6), 895-918. Washington, D.C.: American Chemical Society. TIC: 254015.

BSC (Bechtel SAIC Company) 2003a. *Engineered Barrier System: Physical and Chemical Environment Model*. ANL-EBS-MD-000033 REV 02C. Las Vegas, Nevada: Bechtel SAIC Company. ACC: MOL.20031029.0034.

BSC 2003b. *Repository Design Project, Repository/PA IED Emplacement Drift Committed Materials 1 of 2*. 800-IED-WIS0-00301-000-00A. Las Vegas, Nevada: Bechtel SAIC Company. ACC: ENG.20030627.0003.

BSC 2003c. *Repository Design Project, Repository/PA IED Emplacement Drift Committed Materials (2)*. 800-IED-WIS0-00302-000-00A. Las Vegas, Nevada: Bechtel SAIC Company. ACC: ENG.20030627.0004.

BSC 2003d. *Environment on the Surfaces of Drip Shield and Waste Package Outer Barrier*. ANL-EBS-MD-000001 REV 01D. Las Vegas, Nevada: Bechtel SAIC Company. ACC: MOL.20030825.0151.

Rai, D.; Sass, B.M.; and Moore, D.A. 1987. "Chromium(III) Hydrolysis Constants and Solubility of Chromium(III) Hydroxide." *Inorganic Chemistry*, 26, (3), 345-349. Washington, D.C.: American Chemical Society. TIC: 254060.

Reamer, C.W. 2001. U.S. Nuclear Regulatory Commission/U.S. Department of Energy Technical Exchange and Management Meeting on Evolution of the Near-Field Environment (January 9–12, 2001). Letter from C.W. Reamer (NRC) to S. Brocoum (DOE/YMSCO), January 26, 2001, with enclosure. ACC: MOL.20010810.0033.

Smith, W.H. and Purdy, G.M. 1995. "Chromium in Aqueous Nitrate Plutonium Process Streams: Corrosion of 316 Stainless Steel and Chromium Speciation." *Waste Management*, 15, (7), 477-484. New York, New York: Pergamon. TIC: 254034.

J.5.2 Codes, Standards, and Regulations

ASTM A 240/A 240M-02a. 2002. Standard Specification for Chromium and Chromium-Nickel Stainless Steel Plate, Sheet, and Strip for Pressure Vessels and for General Applications. West Conshohocken, Pennsylvania: American Society for Testing and Materials. TIC: 253994.

ASTM G 1-90 (Reapproved 1999) 1999. *Standard Practice for Preparing, Cleaning, and Evaluating Corrosion Test Specimens*. West Conshohocken, Pennsylvania: American Society for Testing and Materials. TIC: 238771.

J.5.3 Data, Listed by Data Tracking Number

LB0302DSCPTHCS.002. Drift-Scale Coupled Processes (THC Seepage) Model: Data Summary. Submittal date: 02/11/2003.

MO0304MWDSAB11.001. EBS THC Seepage Abstraction 11 BIN EQ3 3I, 3P, and 3O Files. Submittal date: 04/08/2003.

INTENTIONALLY LEFT BLANK

APPENDIX K

**ASSESSMENT OF DATA UNCERTAINTY AND DOCUMENTATION OF DATA USED
TO CALIBRATE MODELS AND SUPPORT MODEL PREDICTIONS
(RESPONSE TO ENFE 2.17 AND GEN 1.01 (COMMENTS 47 AND 109))**

Note Regarding the Status of Supporting Technical Information

This document was prepared using the most current information available at the time of its development. This Technical Basis Document and its appendices providing Key Technical Issue Agreement responses that were prepared using preliminary or draft information reflect the status of the Yucca Mountain Project's scientific and design bases at the time of submittal. In some cases this involved the use of draft Analysis and Model Reports (AMRs) and other draft references whose contents may change with time. Information that evolves through subsequent revisions of the AMRs and other references will be reflected in the License Application (LA) as the approved analyses of record at the time of LA submittal. Consequently, the Project will not routinely update either this Technical Basis Document or its Key Technical Issue Agreement appendices to reflect changes in the supporting references prior to submittal of the LA.

APPENDIX K

ASSESSMENT OF DATA UNCERTAINTY AND DOCUMENTATION OF DATA USED TO CALIBRATE MODELS AND SUPPORT MODEL PREDICTIONS (RESPONSE TO ENFE 2.17 AND GEN 1.01 (COMMENTS 47 AND 109))

This appendix provides a response for Key Technical Issue (KTI) agreement Evolution of the Near-Field Environment (ENFE) 2.17 and general agreement (GEN) 1.01, Comments 47 and 109. This KTI relates to providing an assessment of data uncertainty and the documentation of data used to calibrate models and support model predictions.

K.1 KEY TECHNICAL ISSUE AGREEMENTS

K.1.1 ENFE 2.17 and GEN 1.01 (Comments 47 and 109)

Agreement ENFE 2.17 was reached during the U.S. Nuclear Regulatory Commission (NRC)/U.S. Department of Energy (DOE) Technical Exchange and Management Meeting on Evolution of the Near-Field Environment held January 9 to 12, 2001, in Pleasanton, California. ENFE KTI subissues 1, 2, 3, and 4 were discussed at that meeting (Reamer 2001). There has been no submittal to the NRC related to this KTI agreement.

There are three items from agreement GEN 1.01 (Comments 47, 50, and 109) related to this KTI. Agreement GEN 1.01 was reached during the NRC/DOE Technical Exchange and Management Meeting on Range of Thermal Operating Temperatures, held September 18 through 19, 2001. At that meeting, the NRC provided additional comments (Comments 47, 50, and 109) relating to ENFE 2.17, and the DOE provided an initial response to those comments (Reamer and Gil 2001). Comment 50, however, will not be addressed in this appendix. That comment relates to the probability of the formation of sufficient conditions leading to localized corrosion, so it is discussed, more appropriately, in Appendix A.

Wording of the agreements is as follows:

ENFE 2.17

Provide documentation of data used to calibrate models and data to support model predictions, and an assessment of data uncertainty (e.g., sampling and analytical), that includes critical analyses of variables that affect the data measurements and their interpretations (e.g., drift-scale thermal test and evaporation tests). The DOE will provide documentation of data used to calibrate models and data to support model predictions, and an assessment of data uncertainty (e.g., sampling and analytical) in the area of water and gas chemistry from the drift-scale thermal tests and evaporation tests. This documentation will be provided in revisions to the following AMRs: Environment on the Surfaces of the Drip Shield and Waste Package Outer Barrier (ANL-EBS-MD-000001), Engineered Barrier System: Physical and Chemical Environment Model (ANL-EBS-MD-000033), and Drift-Scale Coupled Processes (DST and THC Seepage) Models (MDL-NBS-HS-000001), or other documents as appropriate. All documents or revisions are expected to be available in FY 02.

This agreement stems from the NRC concerns that the data used to calibrate and validate several process-level models are not adequate and that the technical reliability and representativeness of these data have not been adequately addressed (NRC 2002). In *Integrated Issue Resolution Status Report* (NRC 2002), the NRC states that a significant amount of experimental data was collected for use in *Drift-Scale Coupled Processes (DST and THC Seepage) Models* (CRWMS M&O 2000a), but insufficient analyses were performed to interpret the data and to establish that the parameter values are bounded. The NRC also concluded in the *Integrated Issue Resolution Status Report* that the criterion used to include and exclude individual water and gas measurements for use in these models had not been clearly documented, and the NRC expressed similar concerns about the reliability of data used to validate and calibrate the in-drift precipitates and salts model (CRWMS M&O 2001). The NRC was also concerned that the DOE did not make a transparent distinction between calibration and validation efforts in either of these reports and pointed out that data should be used to either calibrate or validate, but not to simultaneously calibrate and validate (NRC 2002).

Specific page number referrals cited below in GEN agreement Comments 47 and 109 are from *FY 01 Supplemental Science and Performance Analyses, Volume 1: Scientific Bases and Analyses* (BSC 2001).

GEN 1.01 (Comment 47)

The DOE should fully document all observational and experimental data used to validate models, and provide an analysis on the reliability of these data.

Basis: Evaporation studies performed at LLNL and water and gas data from the Drift Scale Heater Test, for example, are used to support model validation of the DOE's Coupled THC models and Salts/Precipitates Analyses, but analytical uncertainties and data interpretation efforts were not adequately described in Chapter 6.

DOE Initial Response to GEN 1.01 (Comment 47)

Should the observational and experimental data be carried forward to the base case analyses, additional uncertainty information and data analyses will be documented to support further validation of future EBS precipitates/salts models prior to any potential LA, as documented in KTI agreement ENFE 2.17.

GEN 1.01 (Comment 109)

Page 6T-15 provides an example of using average values in a model and not propagating uncertainty/variability through the coupled models.

DOE Initial Response to GEN 1.01 (Comment 109)

Uncertainty is propagated to SSPA Volume 2 by providing several such tables that span salts/precipitates model calculations based on abstractions of several THC calculations. The THC calculations span a range of inputs that represent the major source of uncertainty. See the source document, Jolley 2001 [DIRS

154762] under Table 6.3.3-1 (page 6T-15) for the other tables of results from the salts/precipitates model calculations. See also response to Item 50 above and KTI agreements ENFE 2.15 and ENFE 2.17.

K.1.2 Related Key Technical Issue Agreements

KTI agreements ENFE 1.05 (Appendix B) and ENFE 2.05 (Appendix D) are related to ENFE 2.17 in that these are also concerned with model and data uncertainty, primarily involving unsaturated zone seepage into the drifts. Agreement ENFE 2.09 (Appendix F) is related in that it discusses the developed model for describing and predicting the postclosure effects of evaporation and deliquescence on the chemical composition of water in the in-drift environment and its attendant uncertainties.

K.2 RELEVANCE TO REPOSITORY PERFORMANCE

The primary consideration for understanding the in-drift environment relates to the impact on the waste package and drip shield performance (lifetimes). The environmental conditions to which the waste package and drip shield are subjected through time play a substantial role in establishing the performance of these engineered barriers. Model and data uncertainty are key to defining the range of possible repository environments that, in turn, can impact these engineered barrier lifetime predictions.

K.3 RESPONSE

This response provides documentation of data from the Drift Scale Test (DST) and evaporation tests and an assessment of data uncertainty (e.g., sampling and analytical) in the area of water and gas chemistry from these tests. Sections K.3.1 and K.3.2 provide the summary response concerning the DST and evaporation tests (also the subject of GEN 1.01, Comment 47), with the detailed technical basis provided in Sections K.4.1 and K.4.2, respectively. Section K.3.3 addresses GEN 1.01, Comment 109.

K.3.1 Response Concerning Data Supporting the Drift Scale Test Coupled Processes Models

Data used in validation of the DST thermal-hydrologic-chemical (THC) model have been collected from the DST under appropriate project quality assurance procedures and have been documented in *Thermal Testing Measurements Report* (BSC 2002, Section 6.3.4) and interpreted in *Drift-Scale Coupled Processes (DST and THC Seepage) Models* (BSC 2003a, Section 7). Additional analyses have also been conducted to assess the impact of materials introduced during field tests (YMP 2002; Williams 2003). For the evaluation of the near-field chemical environment, in general, and of the chemistry of seepage into emplacement drifts, in particular, these data were used primarily for validation of the DST THC model and the THC seepage model, supporting model predictions using the THC seepage model as documented in *Drift-Scale Coupled Processes (DST and THC Seepage) Models* (BSC 2003a). This report documents the model for the seepage water chemistry into emplacement drifts. The DST THC model was developed to validate the THC seepage model against measured water and gas chemistry data from the DST and includes documentation of uncertainty in computed water and gas chemistry data from the THC seepage models (BSC 2003a, Section 6.9 and 7). Water and gas chemistry

data from the DST were used for model validation efforts independently of calibration of the model.

The DST THC model used calibrated hydrological properties as determined through inversions to data collected elsewhere in Yucca Mountain (surface-based boreholes, and Exploratory Studies Facility and Enhanced Characterization of the Repository Block niches). Pore water collected from boreholes near the DST unaffected by heating, were used to calibrate thermodynamic and kinetic data for a few minerals in order to create initial conditions consistent with the ambient chemical conditions (approximation to an initial steady-state condition; BSC 2003a, Section 4.1). These calibrated input data were then used in subsequent DST THC model simulations for validation against the DST heating phase data and in THC seepage model simulations.

For the purpose of this response, assessment of DST data uncertainty is addressed primarily in the context of measurement and analytical uncertainties with details provided in Section K.4.1. The interpretation and application of the DST data in the validation of the THC seepage model, including the treatment of data uncertainties, are described in Appendix B, which provides a response to related KTI agreements ENFE 1.05 and TSPA I 3.09.

K.3.2 Response Concerning the Evaporation Tests

In-Drift Precipitates/Salts Model (BSC 2003b) documents the model for describing and predicting the postclosure effects of evaporation and deliquescence on the chemical composition of water within the engineered barrier system. Evaporation tests were utilized primarily for model validation efforts and not for calibration.

As provided within the model report and summarized below, various potential sources of data sampling and analytical uncertainty are discussed. The specific assessment of data uncertainty is also compared to the model uncertainty. When specific sampling and analytic uncertainty related to data obtained in support of one of the identified tests supporting model validation was not directly quantitative, these uncertainties have been estimated and the model uncertainty has been expanded to account for these estimates.

Data used to validate the in-drift precipitates and salts model came from four sources:

- Rosenberg et al. 1999a, evaporation of average J-13 well water at 85°C
- *Environment on the Surfaces of the Drip Shield and Waste Package Outer Barrier* (CRWMS M&O 2000b), evaporation of 100× average J-13 well water at 90°C and 85 percent relative humidity
- Rosenberg et al. 1999b, evaporation of Topopah Spring Tuff pore water at 75°C
- McCaffrey et al. 1987, evaporation path of seawater.

K.3.3 GEN 1.01 Comment 109

A discussion of the treatment of propagation of uncertainty and variability through the physical and chemical environment model is presented in Appendix D. In brief, uncertainty is propagated by providing lookup tables that span precipitates and salts model calculations based on abstractions of THC calculations and dust deliquescence. Abstraction of THC calculations resulted in 11 bins. For the dust deliquescence calculations, six bins were found to be necessary. The lookup tables span a range of inputs that represent the major source of uncertainty.

The information in this report is responsive to agreements ENFE 2.17 and GEN 1.01 comments 47 and 109 made between the DOE and NRC. The report contains the information that DOE considers necessary for NRC review for closure of these agreements.

K.4 BASIS FOR THE RESPONSE

Uncertainties in data used in model calibration, validation, and to support model predictions for the drift-scale coupled processes models and the in-drift precipitates and salts model are presented and evaluated here and in other reports (e.g., BSC 2002, 2003a, 2003b). Data uncertainties vary due to collection method, storage, sample contamination, and analytic uncertainties. Therefore, data to be used to support models are screened using the available reports and information to provide an understanding of the overall data uncertainty and interpreted as necessary to span the differences between the model and data.

K.4.1 Uncertainties in Data Used to Support the Drift Scale Test Coupled Processes Models

Data used to validate the drift-scale THC process model and input for the drift-scale THC seepage model are described here and discussed in *Drift-Scale Coupled Processes (DST and THC Seepage) Models* (BSC 2003a, Section 7). The primary means of validation of the drift-scale THC seepage model is the DST THC model and the data collected from the DST. The data used for DST THC model validation are summarized below.

It is important to recognize that thermal-hydrologic processes (e.g., boiling and condensation) can lead to differences in the water and gas chemistry of several orders of magnitude (BSC 2003a, Section 7.1.10.2) over very small increments in temperature. Mineral-water reactions can also accentuate those differences. In contrast, temperature exhibits much less variation in space, because it is governed mainly by conduction in the rock matrix. Uncertainties due to analytical methods are typically much less than these chemical differences. However, some sampling uncertainties (e.g., the temperature of a sample prior to sampling from a packed-off region having a significant temperature gradient, particularly near the boiling point) may have a large impact on data interpretation.

Sources of data used for drift-scale THC process model validation are shown in Table K-1.

Table K-1. Sources of Data Used for Model Validation or Corroboration

DTNs	Description
Analytical Water and Gas Chemistry Data	
LB0102CO2DST98.001	CO ₂ gas analyses (1st, 2nd, 3 rd , and 7th quarter)
LB990630123142.003	4th, 5th, and 6th quarter DST CO ₂ data
LB000121123142.003	DST CO ₂ data (August to November 1999)
LB0011CO2DST08.001	DST CO ₂ data (November 1999 to August 2000)
LB0208ISODSTHP.001	DST CO ₂ and isotopic data (combined)
MO0005PORWATER.000	Analyses of pore waters from Alcove 5 core samples in the ESF (HD-PERM-2 and HD-PERM-3 samples)
LL990702804244.100	Aqueous chemistry of water sampled from the DST (6/4/98 to 3/30/99)
LL001100931031.008	Aqueous chemistry of water sampled from the DST (collected 10/27/99 to 1/25/00)
MO0207AL5WATER.001	Water sampling in Alcove 5 (Results from 2/4/1997 through 4/20/1999). Submittal date: 07/11/2002
SN0203F3903102.001	Drift Scale Test water sampling (with results from 4/17/2001 through 1/14/2002). Submittal date: 03/29/2002
LL020405123142.019	Aqueous geochemistry of condensed fluids collected during studies of introduced materials. Submittal date: 05/22/2002
LL020302223142.015	Aqueous geochemistry of DST samples collected from HYD boreholes. Submittal date: 03/07/2002
LL001200231031.009	Aqueous chemistry of water sampled from the DST (8/9/99 and 8/10/99)
MO0101SEPFDDST.000	Field pH of water sampled from DST on 5/23/00 and 6/29/00

Procedures followed in gathering water and gas chemistry field samples and in analyzing the samples from the DST are described in this section. Documentation of data used to calibrate models and data to support model predictions for DST models are contained in *Thermal Testing Measurements Report* (BSC 2002), along with an assessment of data uncertainty (e.g., sampling and analytical), including critical analyses of variables that affect the data measurements and their interpretations. Further data interpretation and screening are found in *Drift-Scale Coupled Processes (DST and THC Seepage) Models* (BSC 2003a), where selected data are used in model validation. Sampling procedures are documented in *Thermal Testing Measurements Report* (BSC 2002, Section 6.3.4), and subsequent analyses of the effects of introduced materials during the field tests are presented in *Effects of Introduced Materials in the Drift Scale Test* (YMP 2002) and by Williams (2003).

K.4.1.1 Water and Gas Sampling and Analytical Techniques

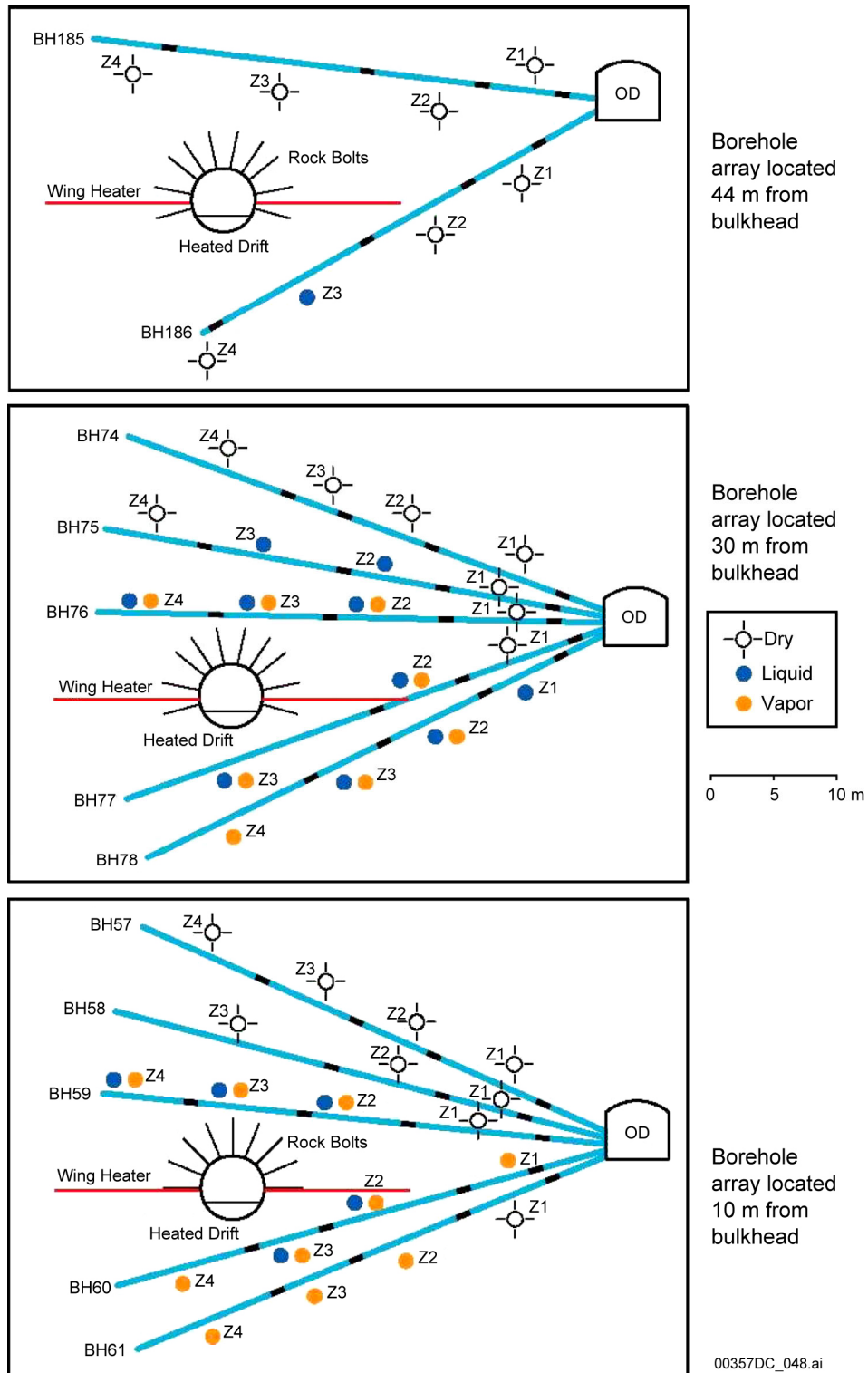
Water samples have been collected from multiple locations in the DST block throughout the heating and cooling phases of the DST and analyzed in the laboratory for concentrations of metals, anions, and certain isotopes. Aqueous sampling is conducted from boreholes, instrumented to include water and gas sampling capabilities. The field measurement

data are identified in DTNs: MO0207AL5WATER.001, MO0101SEPFDDST.000, and SN0203F3903102.001.

Aqueous samples collected for chemical analyses were acquired from several hydrology boreholes during the 4 years of heating. The first samples were collected 6 months after heating began, with subsequent sampling activities about every 2 to 3 months (more or less frequently, as indicated) (BSC 2002, Table 6.3.4.1-1). The test zones, formed by inflatable packers in 12 hydrology boreholes located in three arrays and instrumented to measure temperature, pressure, and relative humidity, produced water samples during water collection activities in the DST heating stage (Figure K-1). The DST aqueous sampling and field characterization activities are controlled through field procedure TIP-NF-33, *Collection and Field Analysis of Water Samples from Boreholes In the Exploratory Studies Facility*.

Water samples collected from the hydrology boreholes were prioritized for several analytical tests including major ion chemistry and certain isotope analyses. Metal (cation) and anion concentrations were measured by inductively coupled plasma and atomic emission spectroscopy and ion chromatography, respectively. The major ion data compiled for the samples analyzed are presented in *Thermal Testing Measurements Report* (BSC 2002, Table 6.3.4.1-2), including values for major cations and major anions as well as field pH and field HCO_3^- . Data selected for use in model validation are also presented in Table K-2 (BSC 2003a).

For some properties that may change rapidly after sampling (e.g., pH, electrical conductivity, total dissolved solids, and alkalinity), field measurements were obtained using calibrated instruments. Samples for laboratory analysis were appropriately treated and preserved (e.g., filtering, acidifying, and storing in appropriate bottles) for later analysis in the laboratory. Every effort was made during each sampling trip to make field measurements and collect samples for laboratory analysis. However, occasionally, the protocol could not be followed (e.g., a meter battery was out, replacement bottles and supplies had not arrived before the sampling trip). In those cases, samples were collected and deviations were described in field notes. These deviations from protocol were not considered to have significant impact on the data because of the small number of occurrences. Although attempts were made to minimize the time between collection and analysis, some delays did occur. These delays were not considered detrimental because of precautions taken to properly collect and preserve the samples.



Source: BSC 2002, Figure 6.3.4.1-1.

Figure K-1. Three Arrays of Drift Scale Test Hydrology Boreholes Showing Relative Packer Positions and Fluid Sampling Zones

The use of peristaltic pumping to acquire water from the hydrology boreholes is generally considered a suitable method for obtaining a representative, in situ DST water sample. However, certain conditions inherent to the thermal test environment may introduce uncertainty into some geochemical parameters. First, because of the relatively dry host rock, most water accumulations have been insufficient to achieve and maintain water-filled lines during the sample collection process. Water passing through the tubing may potentially equilibrate with air in the line and, thereby, affect the concentrations of dissolved gases (CO₂, for example). Another issue arises when water is pumped to sequentially fill multiple bottles. Water samples clearly marked with the order in which they were filled (BSC 2002, see time notations in Tables 6.3.4.1-1 and corresponding analyses in Table 6.3.4.1-2) may exhibit increasingly dilute concentrations with time. This suggests that as the standing water in the borehole is depleted, the heated vapors present condense and dilute water in the line. This is a problem if the initial sample is designated and preserved for metals testing, the second sample is designated for anions, and the final sample is used for field measurements (pH, electrical conductivity, and HCO₃⁻) because a charge balance calculation and a check of the electrical neutrality would indicate inconsistency.

Gas samples were periodically collected from the hydrology boreholes during the heating phase from December 3, 1997, through January 14, 2002. The purpose of these samples was to measure the concentration and carbon isotope ratio of CO₂ and the hydrogen and oxygen isotope ratios of water vapor. The CO₂ concentrations and isotope compositions for both the gas samples and the condensate samples collected in 16 sampling trips through the heating phase are provided in the following DTNs: LB980420123142.005, LB980715123142.003, LB981016123142.004, LB990630123142.003, LB000121123142.003, LB000718123142.003, LB0102CO2DST98.001, LB0108CO2DST05.001, LB0203CO2DSTEH.001, and LB0206C14DSTEH.001.

The CO₂ and isotopic compositions, as well as details of the CO₂ concentration analyses, are given in *Thermal Testing Measurements Report* (BSC 2002, Table 6.3.4.2-1). After measuring the CO₂ concentration in the gas samples, the CO₂ was cryogenically separated from the samples for isotopic analyses. For large enough yields of CO₂ (greater than 30 μmoles), two aliquots of CO₂ were collected. The stable carbon (δ¹³C value) and oxygen (δ¹⁸O value) isotope ratios were analyzed according to the YMP Technical Implementing Procedure YMP-LBNL-TIP/TT-7.0, *Extraction and Analysis of the Stable Isotopic Compositions of CO₂ in Gas Samples*. If there were problems with the first analysis, the split was used for a second stable isotope analysis. If there were no problems, the splits were catalogued and stored for possible radiocarbon (¹⁴C) analysis.

The hydrogen and oxygen isotope compositions of the vapor-condensate samples were measured to gain an estimate of the isotopic composition of the pore water in the rock (BSC 2002, Table 6.3.4.2-3). The hydrogen isotope ratios (δD values) were measured following YMP Technical Implementing Procedure YMP-LBNL-TIP/TT-9.0, *Hydrogen Isotope Analyses of Waters*. The oxygen isotope ratios (δ¹⁸O values) were measured following YMP Technical Implementing Procedure YMP-LBNL-TIP/TT-10.0, *Analysis of the Oxygen Isotopic Composition of Water Samples using the ISOPREP 18*. The isotopic composition of the pore water is calculated from the isotopic composition of the vapor according to the method of Horita and Wesolowski (1994), assuming the pore water is in isotopic equilibrium with the vapor in the

gas samples at the temperature of the rock. This information provides valuable insights into the degree of dryout in the rock and the extent of vapor transport.

K.4.1.2 Sampling and Measurement Uncertainties

The various measurement uncertainties, including uncertainties in sampling techniques and analytical procedures, are documented in *Thermal Testing Measurements Report* (BSC 2002, Sections 6.3.4.1 and 6.3.4.2) and are summarized below.

K.4.1.2.1 Uncertainty in Drift Scale Test Water Chemistry Data

The DST THC model is compared with but not calibrated to geochemical data collected from the DST from borehole intervals between packers. The calibrated drift-scale hydrologic properties and thermal properties used as inputs to the DST THC model are based on Yucca Mountain site data and not data specific to the DST. Some modifications were made to the thermodynamic data to capture aspects of the ambient-system pore-water chemistry (BSC 2003a, Section 4.1.4).

Borehole intervals selected for water chemistry data comparison were based upon the availability of a long, continuous sample record and the absence of confounding factors, such as the sampling interval being too long to compare with a particular gridblock or pair of gridblocks, or boreholes being near either end of the DST and affected by three-dimensional transport. The gridblocks selected for comparison to data were on the order of 2 to 4 m² in size typically located on the cooler side (slightly more distant from the heated drift) near the water collection points. Although the water collected from these sampling locations may have originated from another location (e.g., a fracture intersecting the borehole), the water obtained had been allowed to collect at the sampling location for some time (up to approximately three months) equilibrating with the CO₂ concentration and temperature there. Gridblocks on the cooler side should compare more closely to the measured data because the two-dimensional model has no heat loss in the rock perpendicular to the drift and produces temperatures that are somewhat higher than the measured temperatures after approximately the first year of heating.

Causes for differences between the DST THC model predictions and the DST measurements are important to DST THC model validation. These are discussed in Appendix B (Section B.4.4) and in *Drift-Scale Coupled Processes (DST and THC Seepage) Models* (BSC 2003a, Section 7.7.1). Sources of data uncertainty are discussed below.

Field Measurements—Field measurements of pH are reported for the temperature at the time of the measurement. The temperatures at which the pH was measured were typically much lower than that in the rock where the sample originated (BSC 2002, p. 6.3-42). This could result in greater differences between modeled and measured pH values, but the effect is uncertain because several competing processes could be taking place as the water is sampled. These processes include (1) degassing of CO₂ from the water leading to an increase in pH, (2) condensation of water vapor under higher partial pressures of CO₂ and mixing with the water leading to a decrease in pH, and (3) equilibration of water with observation drift air having a lower CO₂ partial pressure leading to an increase in pH. Certainly, vapor condensation is likely to have affected some samples more than others, as evidenced by the many water samples that formed

solely from condensation in the sampling tubes. The estimated uncertainty in the pH data is 0.5 pH units, and the estimated uncertainty in temperature measurement is 2.2°C.

Effects of Introduced Materials—Although relatively low concentrations of dissolved solids were measured in many of the samples collected from the DST, some water samples showed relatively high concentrations of dissolved solids and low pH values relative to background values. The samples were limited to regions where the rock was well above the boiling temperature, and generally above 140°C. To reduce overall data uncertainty, a series of field and laboratory tests were conducted to determine whether the high concentrations of dissolved solids were due to degradation of the packer materials or water-rock interactions under thermal load (YMP 2002; Williams 2003). The results of the field and laboratory tests confirmed that the source of elevated F^- was due to the packer materials (Viton[®]) and not the host rock. The laboratory tests also demonstrated that the volcanic tuff is not a source of hydrofluoric acid. In addition, laboratory tests also demonstrated that neoprene can release significant quantities of Cl^- , especially when exposed to a higher temperature vapor system. Because of this potential problem, precautions will be taken to ensure introduction of these types of packer materials to an operating repository will be avoided, especially in regions of elevated temperatures.

Laboratory Analyses—For both inductively coupled plasma and atomic emission spectroscopy and ion chromatography, method detection limits are determined for each analyte. The method detection limit represents the minimum concentration that can be identified, measured, and reported with 99 percent confidence that the analyte concentration is greater than zero. Generally, reportable concentrations (as established by laboratory chemists) are required to be greater than 3 to 5 times the method detection limit. For the concentrations reported in *Thermal Testing Measurements Report* (BSC 2002, Table 6.3.4.1-2), values determined to be less than the “practical reporting limit” are indicated as nondetected. Therefore, no distinction is made for analytes that are present at some very low level and those with no measurable concentration.

Additional uncertainty is introduced into analytical results for samples that require dilution. Samples may need to be diluted by the addition of reagent grade water when concentrations exceed the measurement range for analytes of interest, or, if the total sample volume is very small. In such cases, the concentration measured, as well as the limits of detection, are multiplied by the dilution ratio. Consequently, very small errors are increased.

Holding times present another source of uncertainty. Ideally, all sample analyses should be performed as soon after sample collection as possible to ensure that the analyses are representative of the in situ water chemistry. The U.S. Environmental Protection Agency (EPA) has established maximum hold times for analyses of water samples. The EPA hold times, which typically ranged from 2 to 25 days, were suggested in TIP-AC-03, *Determination of Inorganic Anions by Ion Chromatography (EPA Method 300.00)*. The guidelines have generally been met, with the exception of the holding time recommendations for nitrate, nitrite, and phosphate (48 hours). The measured concentrations for these less stable anions may be impacted as a result.

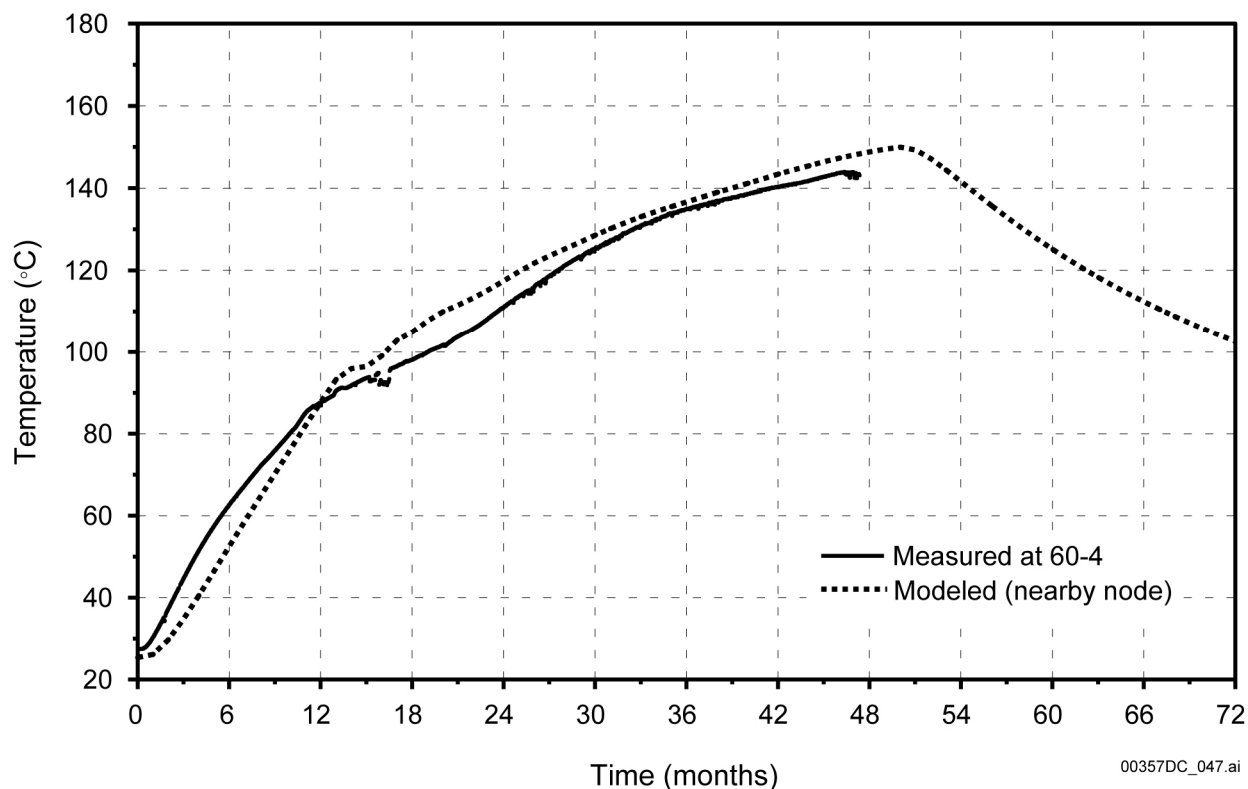
Quality control in the analytical laboratories is maintained using reagent blanks, laboratory control samples, and matrix-spiked samples submitted in duplicate with sample batches (approximately 10 samples or less). Analytical precision is assessed using the duplicate analyses

of both the laboratory control and matrix-spiked samples (typically prepared with analyte concentrations approximately midpoint of that expected for the samples). Acceptance limits for measured concentrations in the control samples are plus or minus 10 percent of the known true value. The accuracy of the results is based upon the percent recoveries for each analyte in the control and matrix-spiked samples. The total recoveries of method analytes in the control sample and matrix-spiked sample must be within 80 to 120 percent to be acceptable.

In general, the uncertainties associated with laboratory analysis are approximately 5 percent or less (see column 3 of Table K-8). It is good practice to consider uncertainties due to factors such as water condensing in lines (discussed below), exceeding holding times, and the effect of introduced materials, by reviewing data submittals and notes associated with sample collection and analysis when the data are used. Exceeding the holding time for nitrate, nitrite, and phosphate may compromise the analysis for these analytes to the extent that the results for these anions only are unusable. The results of the analyses for other anions are independent of changes in these ions for the collection and preservation techniques specified.

Temperature—Temperature in the DST is measured with resistance temperature detectors and thermocouples. The estimated uncertainty on resistance temperature detectors measurements is 2°C and on thermocouples is 3.5°C (BSC 2002, p 6.3-6). Figure K-2 shows a comparison between measured temperature (from resistance temperature detectors) and modeled temperature for the sensor located at borehole 60 location 4 (60-4).

Data Used in Model Validation—Chemical compositions of water samples indicating that they were wholly or mostly derived from water that had resided in a borehole (rather than formed during condensation of water vapor in the collection tube) are given in Table K-2. The water samples collected during the test were obtained from zones that were hotter than the temperatures given for the samples because the samples cooled substantially as they were pumped out of the rock through the sample collection tubing and into the sample containers. Also listed in Table K-2 are the compositions of pore waters that had been ultracentrifuged out of the rock matrix from a dry-drilled borehole near the DST (“HD-PERM” designations).



Source: BSC 2003a, Figure 7.1-4; Output-DTN: LB0307DSTTHCR2.001 (modeled), Table 7.1-1 (DTNs for measured temperatures).

NOTE: Modeled temperatures are for a nearby grid node.

Figure K-2. Comparison of Modeled and Measured Temperatures over Time for the Sensor Located at Hydrology Borehole Packer 60-4

In *Drift-Scale Coupled Processes (DST and THC Seepage) Models* (BSC 2003a, Section 7), model results are compared to a data set from borehole intervals 60-3, 59-2, and 76-3, which is above the heaters in an array closer to the area where the maximum drift crown temperature was reached (30 m from the bulkhead). Waters were collected from other borehole intervals but on only one or two occasions. Compositional trends from so few samples cannot be discerned, nor is validation of the model by comparison to these samples very useful. However, these data do provide additional information on the range of potential water compositions.

These water samples (Table K-2) are considered to be representative of fracture waters produced by THC processes in the region around the DST. However, the borehole intervals from which the waters were collected are approximately 8 to 10 m in length and, at times, have temperatures several tens of degrees different at each end. Therefore, vapor flow from the hot end to the cool end of an interval, accompanied by condensation and reaction with the rock lining the borehole, could account for some of the water found in the boreholes. Because the borehole surface mineralogy is not identical to the fracture surface mineralogy, the water chemistry in the borehole may have some differences to the chemistry of water in the fractures. Yet, because the rock surface in the borehole was freshly drilled, it may be more reactive with respect to silicate mineral reactions and, hence, potentially produce higher concentrations of species making up the

silicate mineral phases. The fresh mineral surfaces in the borehole could, therefore, result in dissolution rates greater than that in the fractures, even though the surface area of the smooth borehole is likely to be less than that of the irregular fracture surface.

Many water samples were collected from borehole intervals above boiling temperatures that were clearly derived from water vapor that condensed in the tubing leading out of the interval. In most cases, such samples are clearly recognizable from the water samples pumped directly out of boreholes (and in contact with rock), based on (1) their significantly lower pH (most below pH 5) relative to “true” water samples (nearly all above pH 6), (2) their extremely low anion and cation content (total dissolved solids around 10 ppm or less), and (3) very low total silicon concentrations (most much less than 10 mg/L) compared to water samples having total silicon concentrations mostly greater than 40 mg/L.

Specific exceptions to these criteria are those samples collected from intervals at high temperatures (greater than 140°C) that have relatively low pH values (less than pH 4), elevated F^- concentrations (greater than 10 mg/L) and relatively high total silicon values but contain few other measurable constituents. These samples were affected by introduced materials. Samples of water from boreholes may be affected in subtle ways by the above processes.

Some of the processes that could explain the water chemistry of samples collected in the hydrology boreholes include mixing of pure condensate water with fracture pore waters, equilibration of condensate waters with matrix pore waters via molecular diffusion, reaction of condensate waters with fracture-lining minerals, and mineral precipitation. Waters that were collected from the hydrology boreholes at elevated temperatures are generally more dilute (lower Cl^- and SO_4^{2-}) and lower in pH than the initial pore water. Aqueous silica concentrations are similar to or much higher than in the pore water, indicating that these waters are not simple mixtures of pore water and pure condensate water. Some clear trends in water chemistry of the condensate waters over time are increases in pH and $SiO_2(aq)$ concentration and a drop in Ca^{2+} . The higher silica concentration in the waters collected at later times in several boreholes (and at higher temperatures), relative to Cl^- and the initial pore-water silica concentration is consistent with dissolution of a silicate phase rather than with increased concentration via boiling. Concentrations of K^+ , Mg^{2+} , and Na^+ are also higher than what would be expected by dilution of original pore water (as evidenced by the low Cl^- concentrations). Therefore, the silicate phases that dissolved must have been some combination of silica polymorphs (i.e., opal, cristobalite, tridymite, and quartz) and feldspar, clays, or zeolites, rather than just a pure silica phase. Many of the waters show a drop in Ca^{2+} over time, consistent with calcite precipitation as the water was heated further and underwent CO_2 degassing.

Table K-2. Measured Concentrations in Tptpmn Pore Water from Alcove 5 and Chemistry of Water Samples from Hydrology Boreholes

SMF No. (SPC0...) Collection Date Collection Time Sample ID	1002488 Pre-Htng. PERM-1 ⁴	1002586 Pre-Htng. PERM-2 ⁴	1002525 Pre-Htng. PERM-3 ⁴	05279699 06/04/98 BH 60-2	05279689 06/04/98 BH 60-2	0527915 ⁸ 08/12/98 BH 60-2	0527977 ⁸ 06/04/98 BH 60-3	0527916 ⁸ 8/12/98 BH 60-3	0541804 ⁸ 11/12/98 BH 60-3	05041804 11/12/98 BH 60-3	05043968 01/26/99 BH 60-3	0529637-#1 ⁸ 03/30/99 9:50 AM BH 60-3	0529637-#2 ⁸ 03/30/99 9:55 AM BH 60-3
Field pH ²	7.79	8.32	8.31	7.5	na	6.9	7.7	6.8	6.92	6.92	7.4	8.0	na
Metals / Cations													
Na (mg/L)	60.5	61.0	61.5	20.0	na	20.4	24.0	17.2	10.1	20.3	19.1	11.2	11.0
Si (mg/L)	37	31	35	56	na	51.8	41	43.5	60.0	53.8	65.0	62.8	59.8
Ca (mg/L)	98.17	106.17	96.67	20	na	19.9	25	18.7	15.3	13.9	5.93	2.06	2.27
K (mg/L)	6.0	7.0	9.0	6.0	na	5.4	4.5	4.5	8.7	7.8	4.1	2.4	2.4
Mg (mg/L)	25.65	16.55	17.35	2.9	na	1.21	5.7	4.0	3.35	3.00	1.17	0.27	0.26
Al (mg/L)	<0.06	<0.06	<0.06	0.12	na	<0.06	0.017 ⁵	0.033 ⁵	0.033 ⁵	0.033 ⁵	<0.06	0.36, 0.27 ⁵	0.36, 0.27 ⁵
B (mg/L)	3.05	2.75	2.75	1.2	na	1.84	0.92	1.14	1.58	1.41	1.75	2.10	2.11
S (mg/L)	42.25	38.6	38.65	5.5	na	4.5	9.2	5.2	11.6	10.5	6.4	1.83	1.82
Fe (mg/L)	<0.02	<0.02	<0.02	0.04	na	0.02	<0.02	0.12	<0.02	<0.02	<0.02	<0.02	<0.02
Li (mg/L)	0.1	0.45	0.05	0.07	na	0.03	0.07	0.040	0.040	0.040	0.02	0.02	<0.01
Sr (mg/L)	1.4	1	1.05	0.18	na	0.11	0.34	2.21	0.22	0.20	0.02	0.09	0.02
Anions													
HCO ₃ (mg/L) ³				na	na	na	na	na	na	na	41	25.0	na
F (mg/L)	0.36	0.96	0.76	na	1.00	0.71	0.82	0.43	0.49	0.50	1.27	1.02	0.97
Cl (mg/L)	122.73	109.93	123.13	na	10	6.14	16	5.52	19.5	19.6	10.3	4.15	3.92
Br (mg/L)	0.6	0.76	1.2	na	0.84	0.05	0.73	0.21	0.6	0.51	0.15	<0.04	<0.04
SO ₄ (mg/L)	124.18	111.38	119.78	na	17	4.88	30	8.81	30.6	30.8	13.5	3.83	3.75
PO ₄ (mg/L)	<0.07	<0.07	<0.07	na	<0.07	0.25	<0.07	0.16	<0.02	<0.2	<0.05	<0.05	<0.05
NO ₂ (mg/L)	<0.04	<0.04	<0.04	na	<0.01	<0.04	<0.01	<0.04	<0.10	<0.10	<0.03	<0.03	<0.03
NO ₃ (mg/L)	21.72	2.52	10.40	na	3.00	0.46	3.6	0.60	3.38	3.17	2.56	0.92	0.84

Table K-2. Measured Concentrations in Tptpmn Pore Water from Alcove 5 and Chemistry of Water Samples from Hydrology Boreholes (Continued)

SMF No. (SPC0...) Collection Date Collection Time Sample ID	0551159 ⁵ 08/09/99 BH 59-2 (AC)	0551160 ⁸ 08/09/99 BH 59-2 (BC)	0557029 ⁵ 10/27/99 BH-59-2	0557032 10/27/99 BH-59-2	0557033 ⁵ 10/27/99 BH-59-2	0557080 11/30/99 BH-59-2	0557081 11/30/99 BH-59-2	0557083 11/30/99 BH-59-2	0557022 01/25/00 BH-59-2	0550671 01/25/00 BH-59-2	0550673 01/25/00 BH-59-2	0550681 05/23/00 BH 59-2	0550682 05/23/00 BH 59-2
Field pH ²	na	na	na	5.93	6.08	6.86	7.24	na	7.07	6.68	na	6.96	6.96
Metals / Cations													
Na (mg/L)	30	24	na	9.2	9.2	6.6	7.7	na	8.1	6.6	na	17	18
Si (mg/L)	78	81	na	44.5	44.9	38.0	39.9	na	42.8	41.7	na	59.4	59.2
Ca (mg/L)	47	39	na	7.53	7.47	4.33	5.63	na	7.54	2.89	na	4.7	4.4
K (mg/L)	8	6	na	3.4	3.6	2.6	3.0	na	3.6	2.8	na	4.3	4.4
Mg (mg/L)	13	11	na	1.81	1.72	1.02	1.38	na	1.78	0.72	na	1.1	1.1
Al (mg/L)	<0.2	<0.2	na	0.033 ⁷	0.033 ⁷	0.030	0.030	na	<0.05	0.043	na	<0.053	<0.053
B (mg/L)	0.8	0.6	na	0.27	0.21	0.14	0.17	na	0.29	0.21	na	na	na
S (mg/L)	22	17	na	2.52	2.50	0.76	1.33	na	6.44	.65	na	na	na
Fe (mg/L)	0.41	0.32	na	0.20	0.19	0.09	0.14	na	0.07	<0.02	na	<0.038	<0.038
Li (mg/L)	<4	<4	na	.16	0.01	0.01	0.01	na	<0.01	<0.01	na	0.021	0.022
Sr (mg/L)	0.54	0.45	na	0.11	0.08	0.06	0.08	na	0.091	0.036	na	<0.013	<0.013
Anions													
HCO ₃ (mg/L) ³	na	na	23.5	na	23.5	na	na	22.3	na	na	22.8	31.4	31.4
F (mg/L)	0.725	0.575	0.27	na	0.27	na	na	0.35	na	na	0.73	0.58	0.55
Cl (mg/L)	88.3	71.0	9.5	na	9.1	na	na	5.0	na	na	3.8	10.15	10.6
Br (mg/L)	0.515	0.46	0.61	na	0.58	na	na	<0.03	na	na	<0.1	<0.1	0.38
SO ₄ (mg/L)	64.2	53.5	6.2	na	6.3	na	na	2.8	na	na	1.8	2.9	3.18
PO ₄ (mg/L)	<0.02	<0.02	<0.02	na	<0.02	na	na	<0.02	na	na	0.62	<0.2	<0.2
NO ₂ (mg/L)	<0.007	<0.007	<0.007	na	<0.007	na	na	<0.007	na	na	<0.05	<0.06	<0.06
NO ₃ (mg/L)	3.79	2.83	1.32	na	1.40	na	na	<0.02	na	na	0.77	0.56	0.54

Table K-2. Measured Concentrations in Tptpmn Pore Water from Alcove 5 and Chemistry of Water Samples from Hydrology Boreholes (Continued)

SMF No. (SPC0...) Collection Date Collection Time Sample ID	0550684 05/23/00 BH 59-2	0550693 06/29/00 BH 59-2	0550694 06/29/00 BH 59-2	0550689 06/29/00 BH 59-2	0550690 06/29/00 BH 59-2	0530398 01/23/01 BH 59-2	0557036 ^b 10/27/99 BH 59-3	0557038 ^b 10/27/99 BH 59-3	0552575 11/30/99 BH 59-3	0557043 11/30/99 BH 59-3	0541803 ^b 11/12/98 BH 59-4	0541803 ^b 11/12/98 BH 59-4
Field pH ²	6.95	6.99-7.08	6.99-7.08	na	na	na	na	6.64	7.47	na	6.63	6.63
Metals / Cations												
Na (mg/L)	17	16	15	na	na	29	na	19.3	15.6	na	22.6	135
Si (mg/L)	59.3	62.7	57.5	na	na	84.5	na	84.2	92.5	na	33.5	44.2
Ca (mg/L)	4.5	4.3	3.8	na	na	7.8	na	13.2	2.86	na	476	450
K (mg/L)	4.4	4.7	4.2	na	na	5.8	na	5.6	3.9	na	29.5	37.8
Mg (mg/L)	1.1	1.1	1.0	na	na	1.8	na	1.49	0.29	na	64.1	83.9
Al (mg/L)	<0.053	<0.053	<0.053	na	na	<0.053	na	0.040	0.071	na	0.01 ⁵	<0.06
B (mg/L)	na	0.86	1.06	na	4.47	4.13						
S (mg/L)	na	14.48	3.25	na	50.7	64.8						
Fe (mg/L)	<0.038	<0.038	<0.038	na	na	<0.038	na	<0.02	<0.02	na	<0.02	<0.02
Li (mg/L)	0.021	0.019	0.018	na	na	0.033	na	0.02	0.02	na	0.21	0.20
Sr (mg/L)	<0.013	<0.013	<0.013	na	na	<0.013	na	<0.13	0.03	na	4.02	3.71
Anions												
HCO ₃ (mg/L) ³	31.4	na	na	29.4	29.4	na	12.4	12.4	na	20.7	na	na
F (mg/L)	0.49	na	na	0.15	0.15	0.78	0.64	0.73	na	1.3	0.8	4.3
Cl (mg/L)	10.15	na	na	.32	.32	25.20	12.9	12.9	na	8.8	1,130	1,250
Br (mg/L)	<0.1	na	na	.48	.48	<0.1	0.89	0.51	na	<0.03	1.13	<0.07
SO ₄ (mg/L)	3.1	na	na	.42	.42	9.5	40.7	40.3	na	8.2	226	213
PO ₄ (mg/L)	<0.2	na	na	<0.2	<0.2	<0.2	<0.04	<0.04	na	<0.02	<5	<0.2
NO ₂ (mg/L)	<0.06	na	na	<0.06	<0.06	<0.06	<0.01	<0.01	na	<0.007	<3	<10
NO ₃ (mg/L)	0.71	na	na	0.65	0.48	0.99	3.06	3.05	na	2.4	3.12	7.81

Table K-2. Measured Concentrations in Tptpmn Pore Water from Alcove 5 and Chemistry of Water Samples from Hydrology Boreholes (Continued)

SMF No. (SPC0...) Collection Date Collection Time Sample ID	0504397 ⁸ 01/26/99 BH 59-4	0551169 ⁸ 08/10/99 BH 61-3	0559464 04/17/01 BH 76-2	0559458 04/17/01 BH 76-2	0559456 04/17/01 BH 76-2	1016082 01/07/02 BH 76-2	0557040 ⁸ 10/27/99 BH-76-3	0552578 11/30/99 BH-76-3	0552579 11/30/99 BH-76-3	0550697 05/23/00 BH-76-3	0541805 ⁸ 11/12/98 BH-186-3	0541805 ^{6,8} 11/12/98 BH-186-3	0527961 ⁸ 01/26/99 BH-186-3
Field pH ²	na	na	7.68	8.22	8.29	7.8	6.14-6.46	6.94	na	6.92-6.96	6.83	6.83	7.2
Metals / Cations													
Na (mg/L)	219	19	9	9	9	na	64.5	28.2	na	29	105	17.0	25.9
Si (mg/L)	12.0	67	42.6	44.1	45.6	na	133.4	92.8	na	96.0	16.0	27.2	49.3
Ca (mg/L)	429	14	1.3	1.1	1.3	na	59.5	22.3	na	7.1	11.5	20.2	2.92
K (mg/L)	29.7	5	1.6	1.6	1.9	na	13.4	7.4	na	6.5	3.5	3.9	5.9
Mg (mg/L)	164	3.2	0.27	0.22	0.23	na	13.8	4.71	na	1.4	5.1	5.68	6.32
Al (mg/L)	0.086 ⁵	<0.2	0.42	0.43	0.45	na	0.010	0.031	na	<0.053	<0.003 ⁵	<0.003 ⁵	<0.06
B (mg/L)	6.68	1.5	na	na	na	na	2.38	0.81	na	na	0.51	0.58	0.84
S (mg/L)	109	3.1	na	na	na	na	34.55	9.46	na	na	8.47	9.42	7.9
Fe (mg/L)	<0.02	1.2	0.40	0.40	0.39	na	<0.02	0.10	na	<0.038	0.02	<0.02	<0.09
Li (mg/L)	0.33	<4	0.0098	0.010	0.0076	na	0.13	0.04	na	0.045	0.05	0.05	0.05
Sr (mg/L)	5.84	0.14	<0.013	<0.013	<0.013	na	0.78	0.26	na	<0.013	0.30	0.34	0.37
Anions													
HCO ₃ (mg/L) ³	na	na	na	na	na	<5	na	na	82.3	na	na	na	116
F (mg/L)	0.51	0.835	na	0.38	0.47	0.4	1.11	na	1.3	0.76	0.56	0.62	1.20
Cl (mg/L)	1,160	24.1	na	1.9	1.71	275	81.9	na	19	14.5	18.7	18.6	23.3
Br (mg/L)	1.51	0.35	na	<0.1	<0.1	<0.2	0.97	na	<0.03	<0.1	0.67	0.60	0.32
SO ₄ (mg/L)	240	9.13	na	0.89	0.85	1.02	94.6	na	26.0	4.98	26.3	26.2	21
PO ₄ (mg/L)	<0.5	<0.02	na	<0.2	<0.2	<0.3	<0.02	na	<0.02	<0.2	<0.2	<0.2	<0.1
NO ₂ (mg/L)	<.3	<0.007	na	<0.06	<0.06	<0.2	<0.007	na	<0.007	<0.06	<.1	<.1	<0.05
NO ₃ (mg/L)	11.6	0.825	na	<0.09	<0.09	<0.2	6.42	na	2.5	1.47	7.47	7.27	6.73

NOTES: ¹ na = not available; < = not detected (less than "practical reporting limit"); Field chemistry of samples for high fluoride study (11/8/01 to 12/5/01) are reported in BSC 2002, Table 6.3.4.5-1.

² See BSC 2002, Table 6.3.4.1-1, of for temperature of pH measurements.

³ HCO₃⁻ - field measurement.

⁴ Pore water samples (baseline): sample ultracentrifuged from borehole core.

⁵ Low detection limit analysis - sample filtered to 0.10 mm and acidified.

⁶ Sample filtered in the field and laboratory (Lawrence Livermore National Laboratory) prior to analyses.

⁷ Sample ID SPC0057028 submitted for low detection for Al analysis.

⁸ Analytical results are corroborating data (as defined in Section 3.6 of AP-SIII.3Q) and non-qualified.

See Table 7-1 for Source DTNs.

K.4.1.2.2 Uncertainty in Concentration and Isotopic Ratios of Drift Scale Test Gas Chemistry Data

CO₂ Concentration—Gas-phase CO₂ concentrations and stable isotopic ratios ($\delta^{13}\text{C}$, $\delta^{18}\text{O}$, δD , and ^{14}C) were measured from gases pumped from hydrology boreholes (BSC 2002, Table 6.3.4.2-1). For the gas-phase compositions, direct comparisons of model results for model validation have been made only to CO₂ concentrations. Isotopic ratios have not been used in the validation of the DST coupled processes models because predictive capabilities for isotopic compositions had not yet been included in the simulator.

The concentration of CO₂ in the gas phase is a function of temperature, pressure, aqueous-phase chemistry, mineral-water reactions, and advective and diffusive transport. Numerous measurements of CO₂ concentrations in gas collected from the DST have been made as a function of space and time, and, therefore, a more complete comparison of the model results to CO₂ data can be made than to the relatively fewer number of water-chemistry measurements. CO₂ concentrations in gases collected from the DST also provide a qualitative measure of the influence of atmospheric gas on the system, because of the relatively low and constant value in the atmosphere (approximately 400 ppmv). Isotopic compositions of CO₂ (BSC 2003a, Section 7.1.14) yield insight into the sources of CO₂.

In addition to the uncertainties associated with the measurements, there were a number of other factors that affected the measured CO₂ concentrations. These are listed below, together with an assessment of the potential impact on the measured CO₂ concentrations:

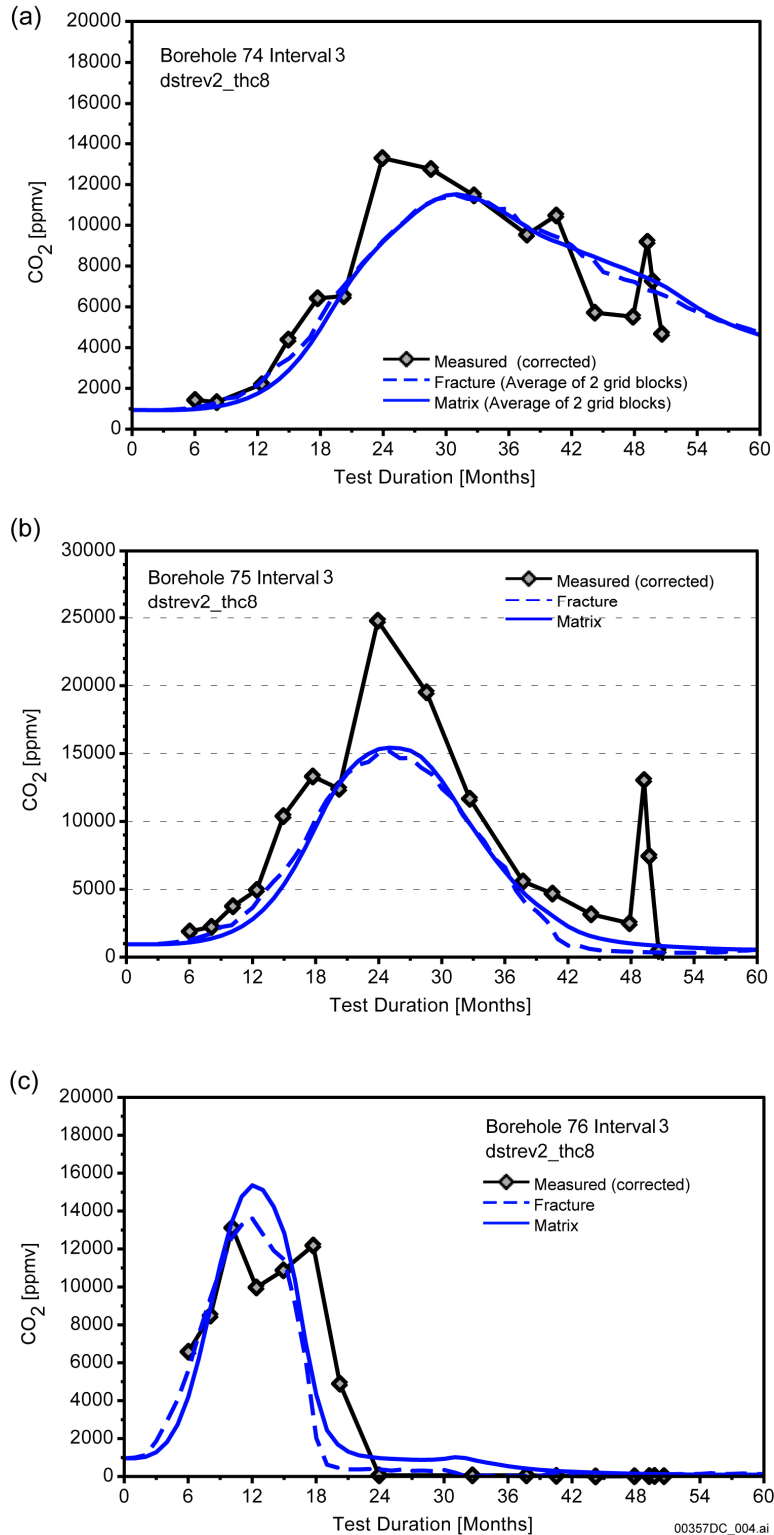
1. **Removal of Water Vapor from the Samples**—Gas samples were taken from several meter-long borehole intervals that spanned a range of temperatures as a result of their orientation relative to the heaters. As part of the sampling procedure, the gas samples had much of their water vapor removed before analyses were performed, and, therefore, measured CO₂ concentrations are for the noncondensable gas fraction. The noncondensable gas fraction is very high (greater than 95 percent) at the ambient temperature of about 25°C but may drop to extremely low values (less than 1 percent) under boiling conditions. Hence, reported CO₂ concentrations at temperatures close to boiling are much higher than if the measurements were made on a complete gas composition (air + CO₂ + H₂O). This effect must be considered when comparing model results to measured values.

To assess the effect of water extraction from the gas during collection, CO₂ concentrations were corrected for the approximate amount of water removed during chilling of the gas sample from the temperature of the sampling interval to 25°C (BSC 2003a). The method assumes that the gas is vapor-saturated, removes the appropriate amount of water vapor to the amount at saturation at 25°C, and adds some of the CO₂ into solution (the condensate) as HCO₃⁻, based on the equilibrium partitioning of CO₂ into H₂O. The actual temperature of the chiller was 4°C; however, the efficiency of the unit was such that not all water was taken out when the gas was at boiling temperatures (BSC 2003a). Therefore, for consistency, the chill temperature was set to 25°C for all samples. Because the difference in water vapor content between 25°C and 4°C is small, this approximation is valid. For samples with temperatures below

approximately 60°C, the correction is very small; however, at temperatures near boiling, the correction may be close to an order of magnitude. The corrections are documented by Wang (2003, pp. 60 to 63). Figure K-3 shows measured CO₂ concentrations that have been corrected for the effect of water-vapor condensation during sample collection.

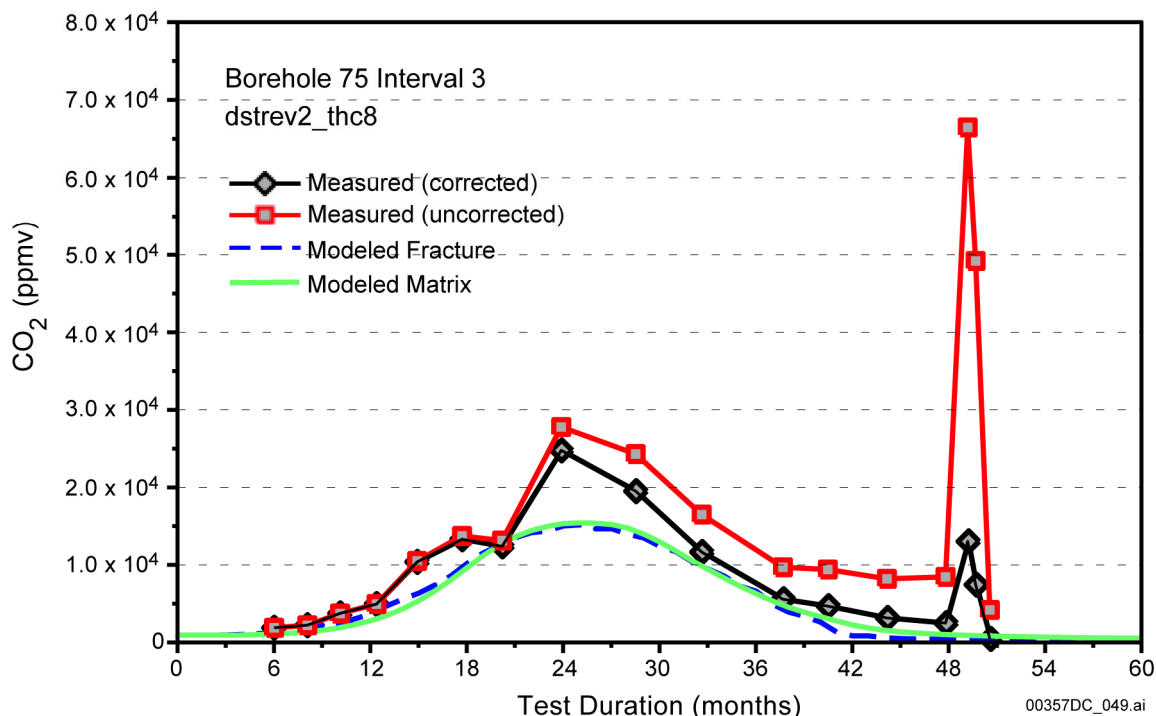
The effect of the correction on the measured CO₂ concentrations is a gradual (but increasing) reduction up to the boiling temperature, where the sharp second spike in the uncorrected data largely disappears. It is clear that the correction to the measured concentrations substantially improves the comparison to the modeled data at higher temperatures. Figure K-4 shows an example of the effect of the correction on the CO₂ concentrations for borehole interval 75-3.

2. **Small Leaks in the Sampling Apparatus**—Leaks could lead to contamination of the samples with air from the observation drift. This was probably not significant except in samples where the noncondensable gas flow rates were very low (e.g., those intervals with high vapor contents in the gas due to zone temperatures being near boiling). In those instances, the measured concentrations could be diluted by as much as 50 percent relative to the actual concentrations, which is not so large compared to the concentration fluctuations induced by heating, which were up to two orders of magnitude. It is possible to calculate the effect of small leaks diluting the collected samples using both concentration and isotopic data.
3. **Other Tests Using the Hydrology Boreholes**—The hydrology boreholes were used for a variety of other measurements, including air-permeability tests and sampling of water. The impact of these other measurements on water sampling was probably minimal, but the air-permeability measurements (which consisted of injecting N₂ gas into the intervals) could significantly dilute the CO₂. Therefore, gas sampling was scheduled just before any air-permeability tests were performed to minimize the effects of the air-permeability measurements on the CO₂ measurements.
4. **Deflated Packers**—Over time, several packers in the hydrology boreholes developed leaks and deflated. This was especially prevalent in the higher-temperature intervals. Even when deflated, the packers still formed a barrier between the intervals (their deflated diameter is only slightly less than the diameter of the borehole). However, it is likely that samples taken from intervals with deflated packers contained some gas from the intervals on the other side of the deflated packers. After April 2000 (when the problem became more prevalent), investigators began noting which samples were collected from intervals with deflated packers by including the adjacent intervals in the sample name. For instance, when the packer between interval 3 and 4 in borehole 57 was deflated and a sample was collected from interval 3, the sampling interval was noted as 57-3/4 indicating that the sample was taken from borehole 57, interval 3, but may contain input from interval 4. Several of the packers began leaking before April 2000 and were deflated (most notably in borehole 77), but this was not indicated by the sampling interval. Sample intervals and data are indicated in *Thermal Testing Measurements Report* (BSC 2002, Table 6.3.4.1-1).



Source: BSC 2003a, Figure 7.1-11; DTNs: LB0208ISODSTHP.001 (measured CO₂ uncorrected), LB0307DSTTHCR2.001 (modeled).

Figure K-3. Comparison of Modeled CO₂ Concentrations (Extended Case) in Fractures to Measured (Corrected) Concentrations in (a) Borehole Interval 74-3 (Average of Bounding Gridblocks), (b) Borehole Interval 75-3, (c) Borehole Interval 76-3



Source: BSC 2003a, Figure 7.1-12; DTNs: LB0208ISODSTHP.001 (measured CO₂ uncorrected), LB0307DSTTHCR2.001 (modeled).

Figure K-4. Comparison of Measured and Corrected Concentrations for Borehole Interval 75-3 and the Model Simulation Results

5. **Precision and Accuracy**—A discussion of precision and accuracy of these measured data can be found in Section 6.3.4.2.2 of *Thermal Testing Measurements Report* (BSC 2002). In general, precision was about plus or minus 1 percent or less. For samples having CO₂ concentrations in excess of 0.2 percent measured with the Li-Cor infrared analyzer, measurements are low by approximately 16 percent; however, precision below 0.2 percent CO₂ with this instrument was approximately plus or minus 1 percent. CO₂ concentrations above 0.2 percent measured with the Columbus Instruments gas analyzer were accurate to within plus or minus 0.3 percent.

Isotopic Composition of Pore Water Estimated from That of Condensate—As stated earlier, no isotopic compositions have been used to validate the DST THC models. There are a number of uncertainties that limit the reliability of these estimates:

1. **Temperature Uncertainties**—The temperature can vary within a sampled interval, making it difficult to determine the temperature to use for calculating the isotopic composition of the water.
2. **Condensation in Sample Tubing**—During sampling, the water vapor moves from the hot temperatures in the rock to the cooler temperatures in the observation drift. This can lead to condensation of water vapor in the tubing prior to the chiller unit. This effect is believed to have been minimal because of the large volume of air flushed

through the tubing and the increase in the temperature of the tubing during sampling. However, this still may account for some loss of vapor prior to the chiller unit. Since the δD and $\delta^{18}O$ values of the vapor are lower than those of the liquid (i.e., lighter isotopes are preferentially fractionated into the vapor), this will cause the δD and $\delta^{18}O$ values of the water vapor that reaches the condensate trap to be lower than in the water vapor in the rock. The amount of condensation in the tubing was less than 10 percent (and probably less than 2 percent) of the total water vapor collected in the traps. Assuming the maximum isotopic fractionation, which would occur for condensation at 25°C (approximately the ambient temperature in the tunnel), this would lead to a maximum shift of less than -0.8 per mil for the oxygen isotope ratio of the condensate and less than -6 per mil for the hydrogen isotope ratio of the condensate. The actual shift was probably much less (about 20 percent of these values) and would be offset by any error due to inefficient trapping by the chiller unit. The net effect of these two sources of error on the isotopic composition of the condensed water vapor is estimated to be within the uncertainty of the measurements (plus or minus 0.2 per mil for the oxygen isotope measurements and plus or minus 3 per mil for the hydrogen isotope measurements).

3. **Inefficient trapping by the chiller unit**—The chiller unit used for this sampling was not capable of completely cooling high-temperature water vapor (greater than 80°C) to 4°C. As a result, a fraction of the water vapor in the higher-temperature samples passed through the chiller unit. The water vapor that does not condense in the trap will have lower δD and $\delta^{18}O$ values than the water in the trap, which will lead to high values for the condensate. To minimize this effect, any water in the pump trap (generally less than 10 ml) after the chiller unit was mixed back into the water in the chiller trap. Altogether, the amount of water vapor loss is believed to be less than 5 percent. For this amount of loss, the net effect on the δD values will be less than 3 per mil; on the $\delta^{18}O$ values it will be less than 0.5 per mil. As noted above, this shift and any shift caused by condensation in the sample tubing would partially offset each other.

K.4.1.2.3 Summary of Sampling and Analytical Uncertainties in Data Collected from the Drift Scale Test

In summary, uncertainties in sampling techniques and analytical procedures for water and gas chemistry are documented in *Thermal Testing Measurements Report* (BSC 2002, Sections 6.3.4.1 and 6.3.4.2). Compositions of water collected from hydrology boreholes during the test have uncertainties primarily related to the effects of condensation and dilution in the boreholes, the residence times in the boreholes, and for a few species the time spent in sample containers prior to performing the chemical analyses.

Most of the aqueous samples collected and analyzed appear to fall into two main groups: (1) water samples for which chemistries have been consistent with mineral/water interactions, particularly fracture-lining minerals such as silica polymorphs and calcium carbonate and (2) very dilute water samples obtained from intervals near or above boiling that were consistent with derivation from condensed moisture in the sampling line (although it was recognized from the beginning, these samples were not considered to add value to the aqueous geochemistry

study). During field collection, samples were collected from nearly all zones, regardless of temperature, and regardless of the potential origin of the sample (i.e., from vapor condensing in the tube or from actual water pumped out of the borehole). These distinctions were made after sample collection by examination of the field measurements (pH and conductivity) and finally by inspection of the full analytical results on cation and anion concentrations (see *Thermal Testing Measurements Report* (BSC 2002) and *Drift-Scale Coupled Processes (DST and THC Seepage) Models* (BSC 2003a)).

Analytical uncertainties in the water analyses are less than those introduced by sampling or the interpretation based on location and temperature. Effects of variable amounts of dilution affect the range in the chemical compositions and particularly the pH values but do not change the overall compositional trends of the water. Therefore, such uncertainties result in some limitation in the interpretations derived from individual measurements, but do not invalidate their use in model validation. Water samples derived from vapor condensation in the sampling tubes were not used for model validation (BSC 2003a, Section 7). However, some water samples were used for model validation that appear to have been affected by dilution through mixing of condensed water vapor, but noted as such.

Uncertainties in CO₂ concentrations and in isotopic compositions of vapor samples are greatest for the samples collected at near-boiling temperatures when water and water vapor are present. As for the water samples, condensation of vapor in the sampling tubes derived from zones at near-boiling temperatures can be the major source of uncertainty for the vapor compositions. However, because most gas samples were collected at temperatures below or above boiling, the uncertainties in a few samples do not limit their use in model validation. Many CO₂ concentrations are affected by less than 20 percent and most less than 50 percent for a range of over two orders of magnitude in concentration (BSC 2003a, Figure 7.1-12).

K.4.2 Evaporative Concentration Tests, Data, and Uncertainties

The in-drift precipitates and salts model assessed four primary sources of evaporation data for use in validating the model (BSC 2003b, Section 7). Note that a discussion of the in-drift precipitates and salts model is presented in the response to agreements ENFE 2.09 and 2.15 (Appendix F). The evaporation tests include the evaporation of average J-13 well water at 85°C (Rosenberg et al. 1999a); the evaporation of 100× average J-13 well water at 90°C and 85 percent relative humidity (CRWMS M&O 2000b); evaporation of Topopah Spring Tuff pore water at 75°C (Rosenberg et al. 1999b); and the evaporation path of seawater (McCaffrey et al. 1987). The primary data used from these sources are provided in Tables K-3 through K-7.

Table K-3. Water Chemistry Data from Experimental J-13 Well Water Evaporation at 85°C

Constituent	Units	Synthetic J-13 Well Water for evap1	Evaporated Synthetic J-13 Well Water for evap1 (Concentration Factor: 956)	Synthetic J-13 Well Water for evap4	Evaporated Synthetic J-13 Well Water for evap4 (Concentration Factor: 157)
Ca ²⁺	mg/kg	6.4	29.86	5.3	1.2
Mg ²⁺	mg/kg	2.2	0.14	2.1	0.05
Na ⁺	mg/kg	46	44082	45.4	5298
K ⁺	mg/kg	5.3	4792	4.9	560
SiO ₂	mg/kg	11.3	18008	10	999
NO ₃ ⁻	mg/kg	8.0	5532	8.0	1050
HCO ₃ ⁻	mg/kg	108	24878	103	4295
Cl ⁻	mg/kg	6.9	4835	7.5	849
F ⁻	mg/kg	2.2	1550	2.4	247
SO ₄ ²⁻	mg/kg	18.1	12926	19	2162
pH	pH	7.84	NR	8.33	10.18

Source: DTN LL991008104241.042 (Tables S00004_001 and S00004_004); Rosenberg et al. 1999a.

NOTE: NR = not reported.

Table K-4. pH Data from Experimental J-13 Well Water Evaporation at 85°C

Concentration Factor	pH
1	8.46
1	8.65
1.05	9.04
1.29	9.43
1.6	9.58
2.41	9.67
6.08	9.67
6.37	9.77
7.59	9.79
11.6	9.95
12.6	10
15.3	10.03
20.9	10.08
25.2	10.09
34.4	10.12
52.1	10.18
104	10.18
157	10.18

Source: DTN LL991008104241.042 (Table S00004_003); Rosenberg et al. 1999a.

Table K-5. Water Chemistry Data from Experimental 100x J-13 Well Water

Constituent	Units	Synthetic 100x J-13 Well Water	Evaporated Synthetic 100x J-13 Well Water
Ca ²⁺	mg/L	5	36
Mg ²⁺	mg/L	2	0
Na ⁺	mg/L	4032	7,6314
K ⁺	mg/L	513	10,832
NO ₃ ⁻	mg/L	732	14,085
HCO ₃ ⁻	mg/L	4142	5,4614
Cl ⁻	mg/L	730	14,419
F ⁻	mg/L	208	3,630
SO ₄ ²⁻	mg/L	1,632	29,783
pH	pH	NR	NR

Source: CRWMS M&O 2000b; DTN LL000202905924.117
(Table S00134_002).

NOTE: NR = not reported.

Table K-6. Water Chemistry Data from Topopah Spring Tuff Pore Water Evaporation Experiment

Constituent	Units	Synthetic Pore Water	Evaporated Synthetic Pore Water (Concentration Factor: 1243x)
Ca ²⁺	mg/kg	57.2	15,629
Mg ²⁺	mg/kg	11.7	5,478
Na ⁺	mg/kg	8.2	5,961
K ⁺	mg/kg	4.2	2,779
SiO ₂	mg/kg	9.8	513
NO ₃ ⁻	mg/kg	11.0	nm ^a
HCO ₃ ⁻	mg/kg	16.2	< 35
Cl ⁻	mg/kg	78.0	53,084
F ⁻	mg/kg	2.3	< 577
SO ₄ ²⁻	mg/kg	81.7	2,077
pH	pH	7.68	6-6.5 ^b

Source: DTN LL991008004241.041 (Table S00002_002); Rosenberg et al. 1999b.

NOTE: ^a not reported.
^b estimation from pH paper.

Table K-7. Sample Data for Evaporated Seawater

Brine	T (°C)	Den. ^a (mg/cm ³)	pH	Ionic Strength (Molal)	Deg. of Ev. ^b	Total Concentration (molal)						
						Cl ⁻	Br ⁻	SO ₄ ²⁻	Mg ²⁺	Ca ²⁺	K ⁺	Na ⁺
w63	28.4	1024	8.19	0.72	0.95	0.579	0.000883	0.0294	0.0520	0.00987	0.0107	0.497
w64	—	1024	—	0.73	0.98	0.585	0.000917	0.0303	0.0541	0.00985	0.0111	0.497
w49	28.6	1028	8.12	0.75	1.10	0.594	0.000931	0.0305	0.0604	0.0108	0.0120	0.506
w53	29.9	1028	8.15	0.83	1.17	0.649	0.00099	0.0339	0.0642	0.0118	0.0132	0.582
w57	30.0	1040	8.33	1.21	1.75	0.947	0.00149	0.0518	0.0965	0.0192	0.0179	0.839
w54	32.6	1050	8.43	1.5	2.26	1.21	0.00177	0.0615	0.124	0.0210	0.0219	1.01
w55	29.6	1060	8.53	1.79	2.68	1.44	0.00224	0.0781	0.147	0.0247	0.0266	1.22
w52	30.4	1075	8.35	2.23	3.16	1.79	0.00285	0.0956	0.174	0.0316	0.0348	1.60
w56	31.4	1088	8.11	2.48	3.53	2.03	0.00305	0.110	0.194	0.0401	0.0392	1.71
w51	30.2	1103	8.14	2.98	4.36	2.49	0.00375	0.123	0.240	0.0325	0.0468	2.16
w50	29.8	1141	7.85	3.95	6.07	3.50	0.00536	0.138	0.334	0.0171	0.0623	2.93
w58	32.3	1151	7.70	4.41	6.91	3.87	0.00584	0.156	0.381	0.0185	0.0723	3.36
w48	28.8	1181	7.60	5.37	8.45	4.90	0.00733	0.184	0.466	0.0123	0.0905	4.17
w59	32.6	1181	7.56	5.39	8.62	4.90	0.00722	0.175	0.475	0.0121	0.0877	4.21
w61	32.1	1187	7.53	5.46	9.03	4.90	0.00757	0.190	0.498	0.0107	0.0914	4.22
w46	33.2	1215	7.42	6.25	10.5	5.67	0.00880	0.205	0.579	0.00610	0.112	5.00
w62	34.1	1215	7.43	6.34	11.0	5.88	0.00938	0.232	0.604	0.00581	0.109	4.83
w37	29.5	1220	7.41	6.49	12.6	5.91	0.0108	0.254	0.691	0.00433	0.115	4.70
w43	32.5	1220	7.45	6.68	13.2	5.75	0.0119	0.274	0.728	0.00352	0.152	5.02
w35	28.9	1224	7.44	6.88	15.1	6.04	0.0127	0.287	0.830		0.157	4.74
w42	32.8	1224	7.34	6.94	16.4	5.82	0.0138	0.314	0.904		0.180	4.67
w44	31.9	1225	7.40	6.96	17.6	5.72	0.0146	0.328	0.968		0.190	4.48
w34	31.8	1231	7.25	7.27	20.1	5.98	0.0167	0.381	1.11		0.208	4.14
w32	32.0	1231	7.28	7.34	20.4	6.01	0.0174	0.399	1.13		0.212	4.13
w33	30.7	1236	7.22	7.75	23.4	6.08	0.0195	0.446	1.29		0.249	4.11
w30	31.4	1239	7.28	7.61	23.6	5.98	0.0208	0.417	1.30		0.242	3.96
w28	32.4	1239	7.13	7.87	25.4	6.08	0.0195	0.478	1.40		0.253	3.81
w41	32.7	1242	7.22	7.84	26.8	5.85	0.0230	0.450	1.48		0.278	3.72
w45	35.1	1249	7.06	8.42	31.4	5.92	0.0264	0.600	1.73		0.33	3.32
w38	29.6	1254	7.12	8.65	32.8	5.96	0.0287	0.678	1.81		0.339	3.17
w36	29.9	1254	7.03	8.64	34.0	5.83	0.0282	0.632	1.87		0.342	3.19
w40	32.1	1260	7.00	9.01	36.8	5.89	0.0299	0.694	2.03		0.379	3.06
w39	32.6	1260	6.99	9.33	39.4	5.93	0.0331	0.776	2.17		0.402	2.83
36#1				9.29	40.4	5.86	0.0343	0.753	2.23		0.417	2.63
40#1				9.47	43.5	5.74	0.0356	0.796	2.39		0.443	2.31
36#2				9.81	44.8	6.03	0.0384	0.849	2.47		0.449	2.27
40#2				10.1	48.9	5.80	0.0401	0.895	2.70		0.495	1.96
36#3				11.3	58.1	6.10	0.0482	1.11	3.20		0.591	1.37
40#3				11.4	58.6	6.26	0.0481	1.09	3.23		0.588	1.50
40#4				11.9	63.6	6.23	0.0518	1.19	3.50		0.637	1.16
39#1				12.7	66.2	6.62	0.0590	1.21	3.91		0.632	0.842
36#4				13.0	69.2	6.47	0.0598	1.35	3.99		0.754	0.712
40#5				12.3	72.9	7.13	0.0661	0.966	3.76		0.782	0.825
40#6				12.3	78.8	7.38	0.0716	0.763	3.98		0.712	0.545
39#6				12.2	87.9	7.50	0.0777	0.679	4.03		0.565	0.413
39#2				11.8	87.9	6.89	0.0748	0.703	3.96		0.348	0.553
39#3				12.4	93.3	7.50	0.0773	0.664	4.20		0.311	0.500
36#5				12.8	97.1	7.80	0.0828	0.713	4.27		0.597	0.428
39#4				9.53	98.1	5.99	0.0774	0.366	3.35		0.125	0.169

Source: McCaffrey et al. 1987, Tables 1 through 3.

NOTE: ^a density of sample.

^b degree of evaporation (equivalent to concentration factor, relative to seawater).

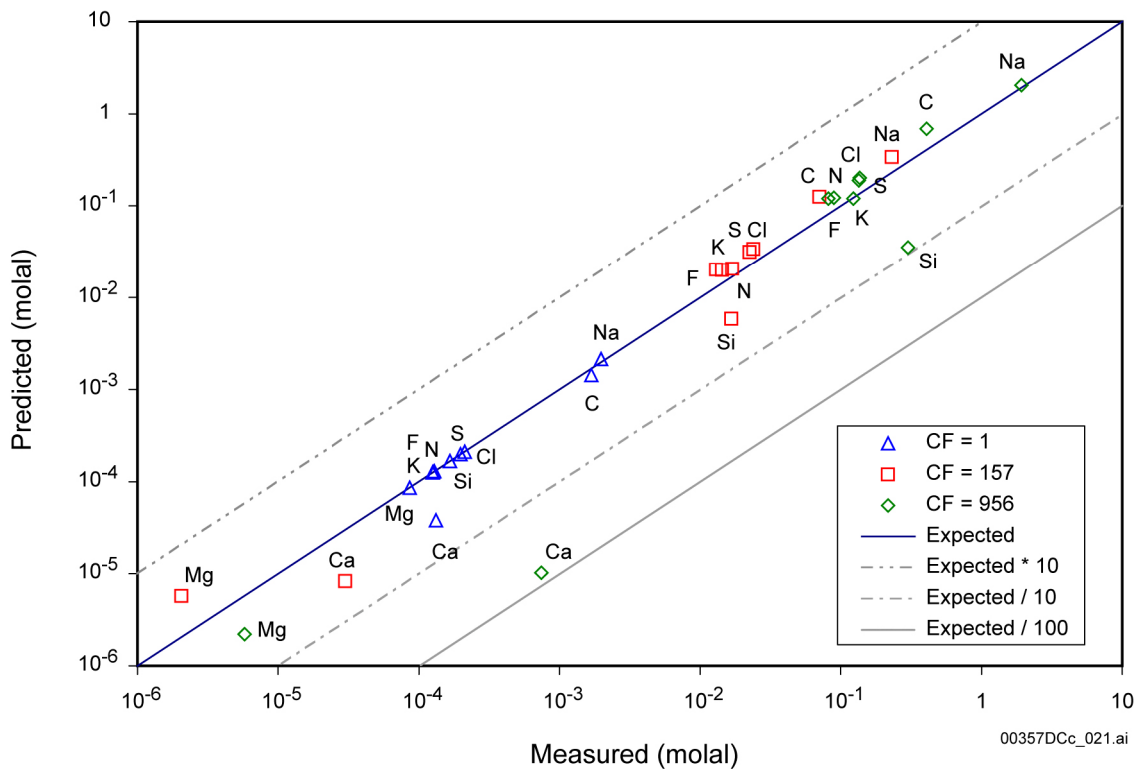
K.4.2.1 Evaporation of Average J-13 Well Water at 85°C

Rosenberg et al. (1999a) document results of an experiment in which synthetic J-13 well water was evaporated in a beaker that was open to the atmosphere and maintained at a constant temperature of 85°C. In the experiment, synthetic average J-13 well water was evaporated without contact with tuff or other rock material. The experiment began with 30 L of synthetic average J-13 well water with a measured composition (BSC 2003b). A peristaltic pump was used to pump this water into a 1-L Pyrex beaker at a constant rate while a hot plate was used to maintain a water temperature of 85°C to evaporate the water. Water samples were collected after the 30 L had been evaporated to approximately 30 mL. Results of this experiment are shown in Table K-3. The solids that had accumulated at this stage were identified by x-ray diffraction to be amorphous silica, aragonite, and calcite. Analysis of solids after complete evaporation indicated the additional presence of halite, niter, thermonatrite, and possibly gypsum, anhydrite, and hectorite.

In a similar evaporation experiment using synthetic J-13 well water, the pH of the evaporating water was monitored (Rosenberg et al. 1999a). The experiment used approximately the same J-13 starting solution as evap1 (Table K-3). The pH measurements are presented in Table K-4 as a function of concentration factor. The concentration factor was measured as the ratio of the initial water mass divided by the measured water mass at the time of analysis.

The results of these evaporation experiments were modeled using the in-drift precipitates and salts model and Pitzer database. Total aqueous concentrations, pH, ionic strength, and mineral precipitation predictions were produced (BSC 2003b, Figures 14 and 15). Comparisons of measurements and predictions are plotted in Figures K-5 and K-6.

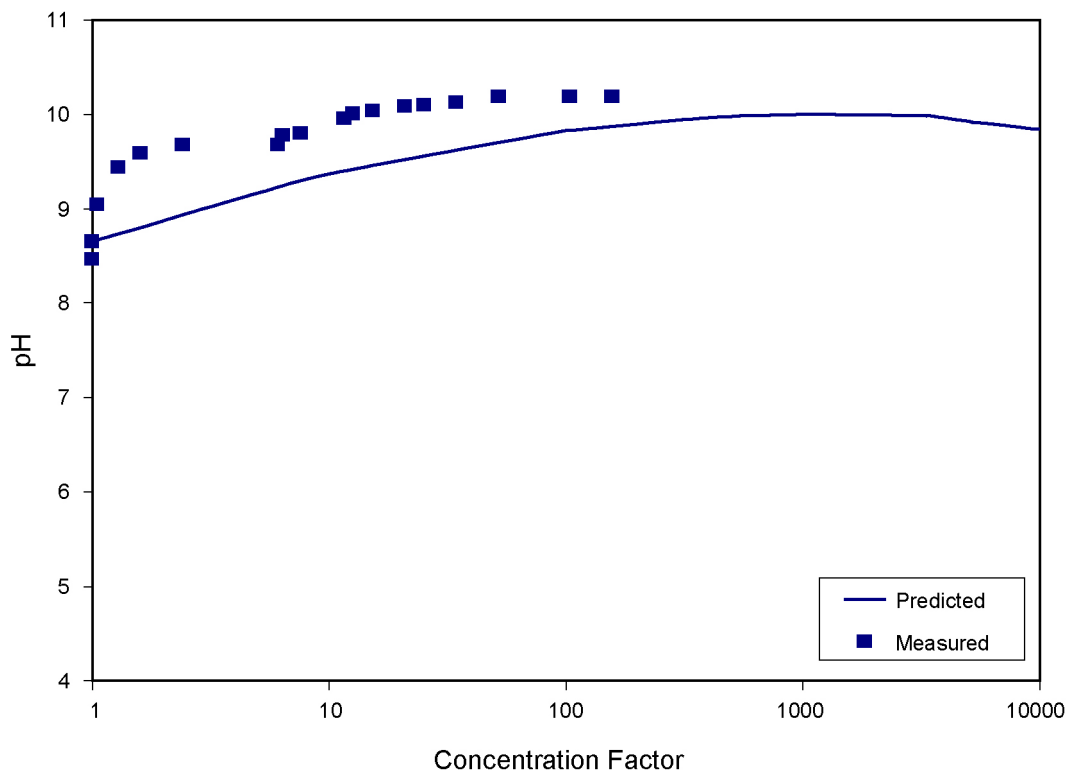
As shown in Figure K-5, the modeled evaporation results approximate the Na^+ , F^- , HCO_3^- , Cl^- , K^+ , Mg^{2+} , NO_3^- , SO_4^{2-} , and SiO_2 concentrations within a factor of 10 or less when compared to the laboratory measurements. Ca^{2+} predictions are within a factor of 100 of the measurements. The gray dashed and solid lines in Figure K-5 indicate factors of 10 and 100 from the measured values (i.e., they are not uncertainty bands) to assess the precision of model validation. Figure K-6 shows general agreement between the laboratory measured pH and modeled pH. The predicted pH is largely controlled by the fugacity of carbon dioxide, which in the model is fixed at $10^{-3.4}$ bar to approximate the laboratory condition of a beaker open to the atmosphere. Water in evap4 was concentrated to 157 times the original solution. A comparison between the predicted and measured compositions is discussed in *In-Drift Precipitates/Salts Model* (BSC 2003b).



Source: DTN MO0303MWDJ13RB.000; Rosenberg et al. 1999a.

NOTE: CF = concentration factor.

Figure K-5. Predicted versus Measured Concentrations for Synthetic J-13 Water Evaporation Experiments



00357DCc_022.ai

Source: DTN MO0303MWDJ13RB.000; Rosenberg et al. 1999a.

Figure K-6. Predicted versus Measured pH Values for Synthetic J-13 Water Evaporation Experiments

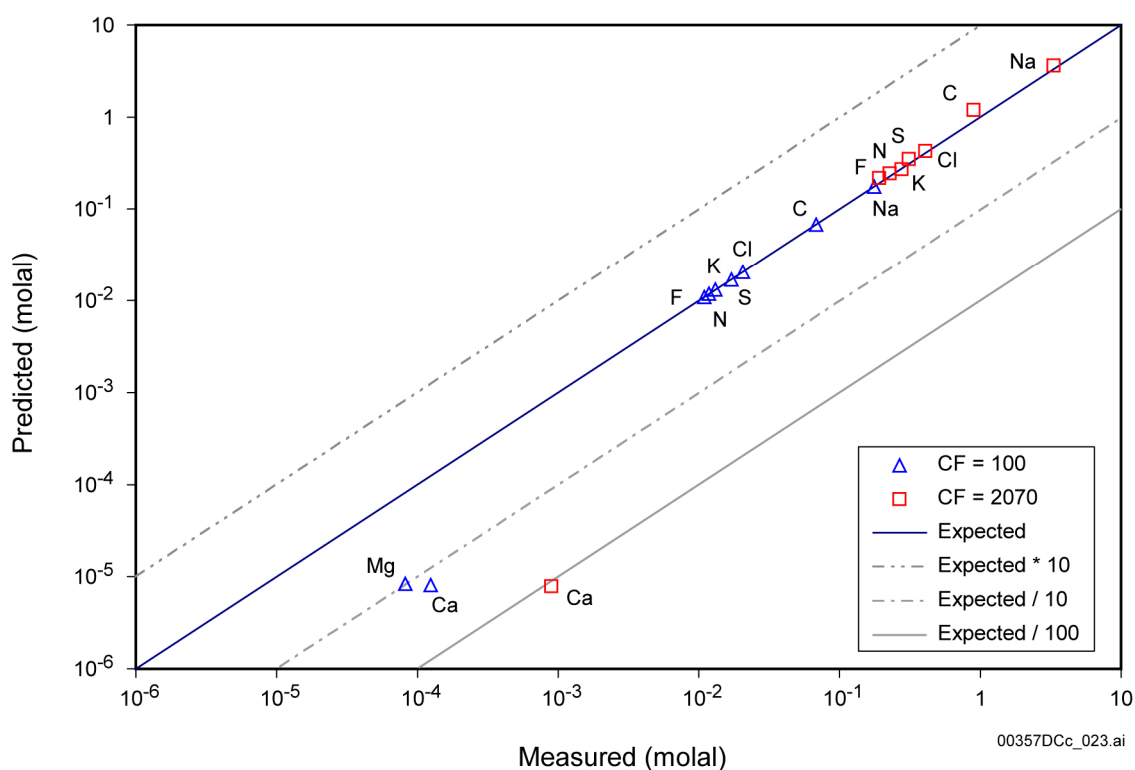
K.4.2.2 Evaporation of 100× Average J-13 Well Water at 90°C and 85 Percent Relative Humidity

In another synthetic J-13 well water evaporation experiment, a synthetic 100-times concentrated (100×) average J-13 well water was dripped through a column of heated tuff into a Teflon[®] beaker (CRWMS M&O 2000b, p. 6-16). In this experiment, the beaker was open to the atmosphere and maintained at a constant temperature of 90°C and relative humidity of 85 percent. The solution was then allowed to evaporate to a volume of approximately 5 percent of the original volume, based on the concentration factors reported. The actual volume or mass decrease in the solution was not reported. The starting and final solution compositions are displayed in Table K-5. The recipe for the synthetic 100× J-13 well water did not include silicon, aluminum, or iron, likely because these components have limited solubility or are minor constituents (aluminum and iron). A 100× concentration of these components cannot be prepared without making adjustments, such as raising the pH to an unrealistic value. A true 100× J-13 water can only be realistically derived by evaporating unconcentrated J-13 in a container open to a fixed fugacity of carbon dioxide and allowing supersaturated minerals to precipitate from solution during the process (as was done in Rosenberg et al. 1999a).

The results of these evaporation experiments were modeled using the in-drift precipitates and salts model and the Pitzer database. Predictions of total aqueous concentrations, pH, ionic strength, and mineral precipitation upon evaporation were determined (BSC 2003b, Figures 18

and 19). Measurements and predictions are compared in Figure K-7. The gray dashed and solid lines are not uncertainty bands; they indicate factors of 10 and 100 from the measured values to assess the precision of model validation. No pH measurements were reported.

Figure K-7 shows that the predictions closely approximate the Na^+ , F^- , Cl^- , K^+ , NO_3^- , HCO_3^- , and SO_4^{2-} concentrations when compared to the laboratory measurements. To compare the results to the data, the reported nitrate concentration factor of 20.7 is used to represent the concentration factor of the solution. However, because the original concentration factor of the synthesized 100× J-13 water is defined as 100, the final concentration factor is represented here as 2,070 (100×20.7). As shown in the figures, the agreement between the Na^+ , F^- , Cl^- , K^+ , HCO_3^- , and SO_4^{2-} measurements and predictions indicate that the concentration factor of the solution is well represented by the nitrate concentration factor. A comparison between the predicted and measured compositions is given in *In-Drift Precipitates/Salts Model* (BSC 2003b).



Source: DTN MO0303MWDJ13GD.000; CRWMS M&O 2000b.

NOTE: CF = concentration factor.

Figure K-7. Predicted versus Measured Concentrations for 100x Synthetic J-13 Water Evaporation Experiments

K.4.2.3 Evaporation of Topopah Spring Tuff Pore Water at 75°C

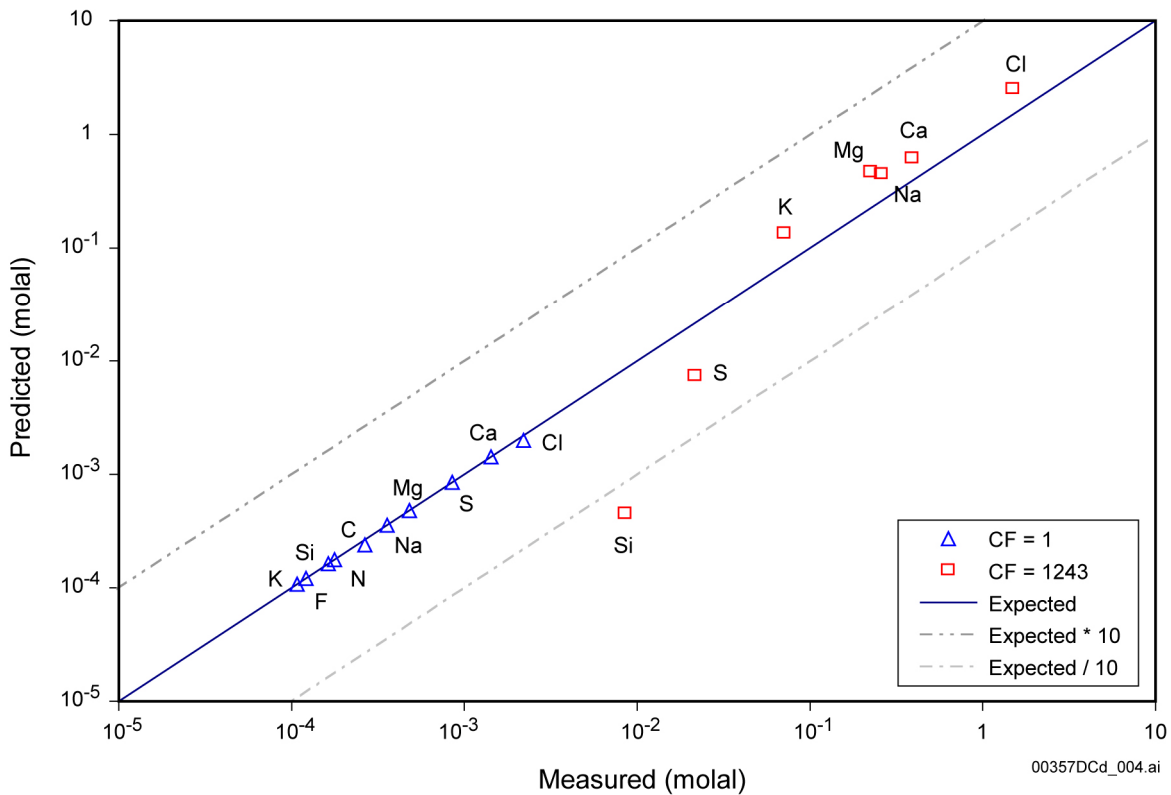
Synthetic Topopah Spring Tuff pore water was evaporated in an experiment reported in Rosenberg et al. (1999b). The experiment was performed following the same procedures as in Rosenberg et al. (1999a; see also BSC 2003b, Section 7.1.1), except that the temperature was maintained at 75°C. Both the starting and final solutions are provided in Table K-6. The final

solution was reported to have an approximate concentration factor of 1,243 plus or minus 10 percent. X-ray diffraction analysis at this concentration factor detected gypsum. After complete evaporation, tachyhydrite was also detected.

These evaporation experiments were simulated using the in-drift precipitates and salts model and the Pitzer database. Predictions of total aqueous concentrations, pH, ionic strength, and mineral precipitation upon evaporation were determined (BSC 2003b, Figures 21 and 22). These predictions are compared to the measurements in Figures K-8 and K-9. Figure K-8 shows that the modeled results closely approximate the measured Na^+ , Mg^{2+} , Ca^{2+} , Cl^- , and K^+ concentrations. The dashed lines indicate factors of 10 from the measured values to assess the precision of model validation and do not represent uncertainty. A comparison between the predicted and measured compositions is given in *In-Drift Precipitates/Salts Model* (BSC 2003b).

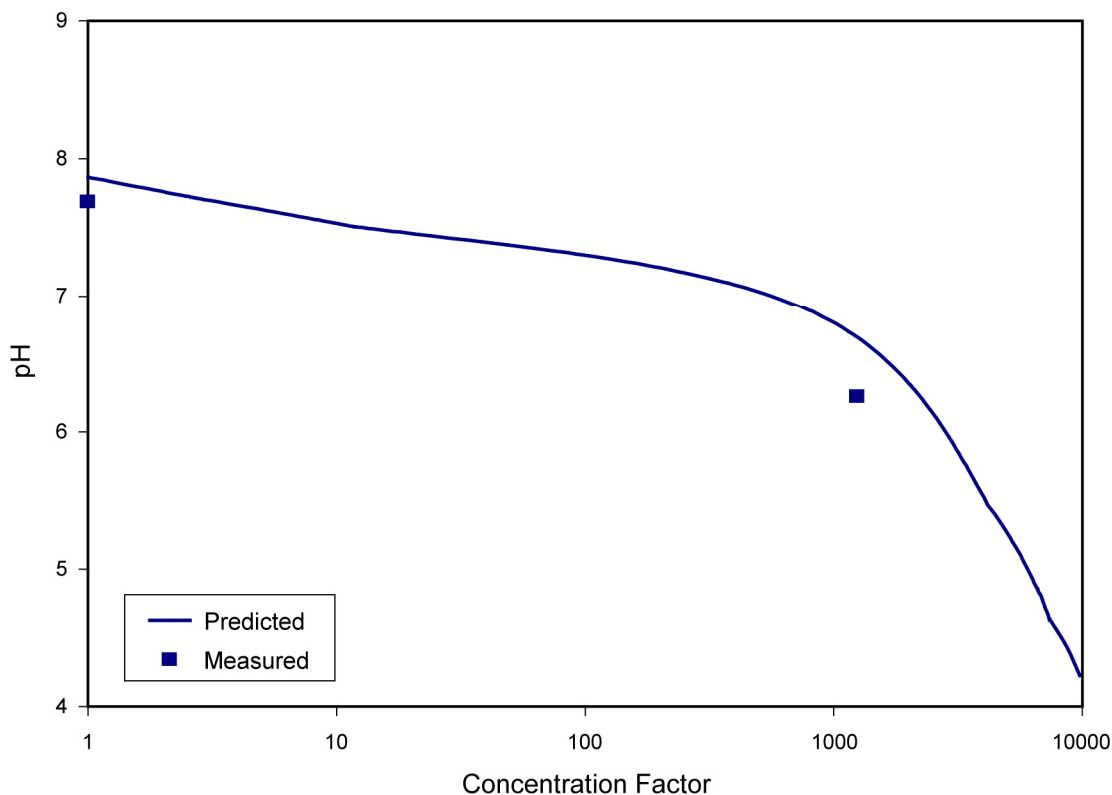
Gypsum was identified by x-ray diffraction in the laboratory experiment at the 1,243 concentration factor.

Upon complete evaporation, the only other mineral identified to precipitate was tachyhydrite. The relative amounts of gypsum and tachyhydrite in the final mineral assemblage were not measured. No precipitate was identified in the experiment that contained Na^+ , K^+ , CO_3^{2-} , F^- , silicon, or NO_3^- . As in the average J-13 well water evaporation experiment (BSC 2003b, Section 7.1.1), the reported concentration factor in the Topopah Spring Tuff pore water evaporation experiment (Table K-6) was overestimated. Cl^- and NO_3^- should have concentrated conservatively. No Cl^- and NO_3^- minerals were identified by x-ray diffraction at the reported 1,243 concentration factor. The overestimate is substantiated by the measured concentrations of Na^+ , K^+ , Ca^{2+} , and Mg^{2+} , which also should have concentrated conservatively (or nearly conservatively in the case of Ca^{2+}) (BSC 2003b, Figure 21). The NO_3^- concentration was not measured in the evaporatively concentrated sample because the sample was mistakenly preserved with nitric acid. However, if the Cl^- concentration had been used to determine the concentration factor in the experiment (instead of indirectly estimating the concentration factor from measurements of amounts of water evaporated), then the measured concentration factor would have been around 680, not 1,243.



Source: DTN MO0303MWDTSWRB.000; Rosenberg et al. 1999b.

Figure K-8. Predicted versus Measured Concentrations for Synthetic Topopah Spring Tuff Pore Water from Evaporation Experiments



00357DCd_005.ai

Source: DTN MO0303MWDTSWRB.000; Rosenberg et al. 1999b.

Figure K-9. Predicted versus Measured pH Values for Synthetic Topopah Spring Tuff Pore Water from Evaporation Experiments

K.4.2.4 Seawater Evaporation

The Morton Bahamas solar salt production facility on Great Inagua Island in the Bahamas provides an excellent example of the evaporative chemical evolution of a natural multicomponent water. At this plant, seawater is evaporatively concentrated in a sequence of reservoirs to precipitate table salt (halite). This production process results in a final brine with a concentration factor near 40 with respect to seawater. One of the primary advantages of this data set compared to samples taken from saline lakes is that these reservoirs are not subject to large mixing effects from streams and rivers. In addition, the reservoirs are shallow and open to the atmosphere, facilitating equilibrium conditions with respect to atmospheric partial pressures of carbon dioxide and oxygen. Thus, the major processes affecting the evolution of seawater at the plant are the same processes incorporated in the in-drift precipitates and salts model.

McCaffrey et al. (1987) sampled and analyzed the chemical compositions of the evolving seawater at the plant. Three of the most concentrated samples were evaporated even further in the laboratory. The data for both the reservoir samples and the laboratory evaporation experiments are presented in Table K-7. The samples in the table that start with a "w" were collected directly from the plant reservoirs while the remainders were artificially evaporated from samples w36, w39, and w40. The reported degree of evaporation is equivalent to the concentration factors of conservative components. For degrees of evaporation up to 70, the

concentration factor for magnesium was used to determine degree of evaporation. Beyond 70, the concentration factor of lithium was used.

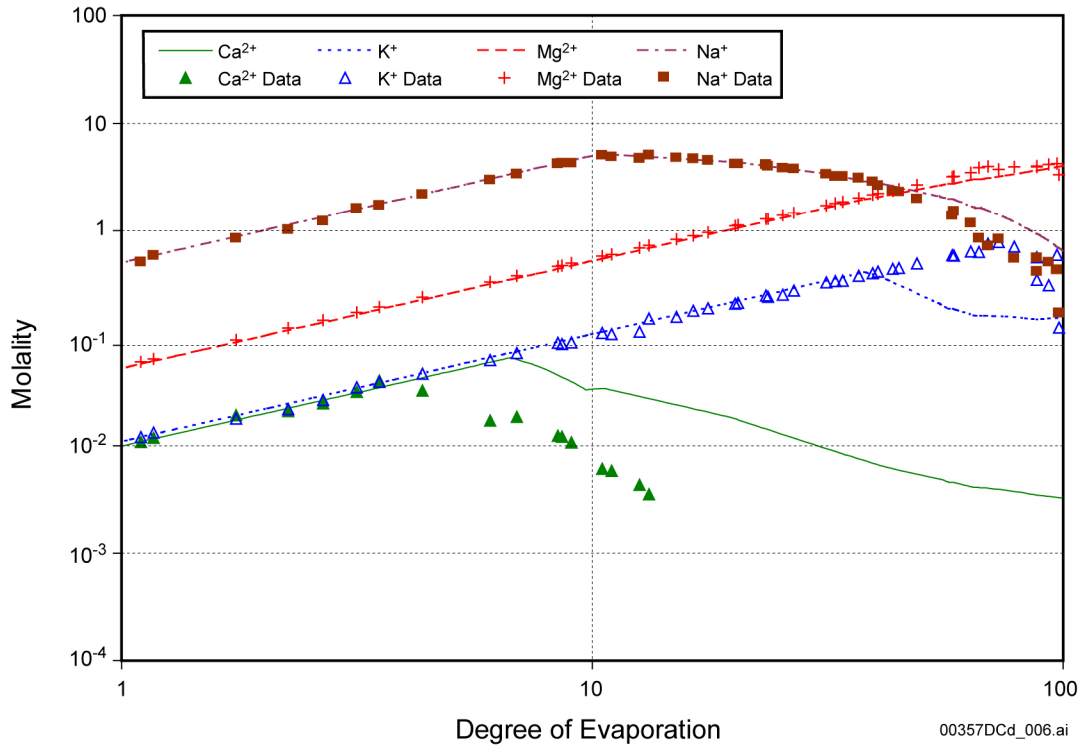
It is important to note that the laboratory evaporation experiments were closed to the atmosphere. These experiments resulted in the samples in Table K-7 that have degrees of evaporation greater than 40. These samples were derived by placing samples of w36, w39, and w40 in uncovered Teflon[®] vials and sealing them in desiccation chambers containing CaCl₂ crystals, a desiccant (McCaffrey et al. 1987, p. 931). Sealing the desiccation chambers does not allow for exchange of oxygen and carbon dioxide with the atmosphere. This could have caused partial pressure deviations from atmospheric values. Changes in carbon dioxide partial pressure affects pH, which in turn has the potential to affect which minerals precipitate. No pH values were measured for these samples.

The in-drift precipitates and salts model predictions are compared to sample measurements in Figures K-10, K-11, and K-12. These figures show that the in-drift precipitates and salts model predictions are highly accurate in reproducing the validation cases. Degree of evaporation relative to seawater was calculated from the in-drift precipitates and salts model output by multiplying the in-drift precipitates and salts concentration factor by 0.95, the degree of evaporation of the sea intake water used as the starting water for the evaporation. The concentration factor calculated by the in-drift precipitates and salts model reflects the degree of evaporation relative to the intake water.

Like halite, other minerals that control the evaporative concentration of the dissolved components are revealed by the trajectories of their concentrations in the figures. For example, McCaffrey et al. (1987, p. 935) found that gypsum (CaSO₄·2H₂O) begins to precipitate at a degree of evaporation around 3.8. This explains the decrease in Ca concentrations at this degree of evaporation.

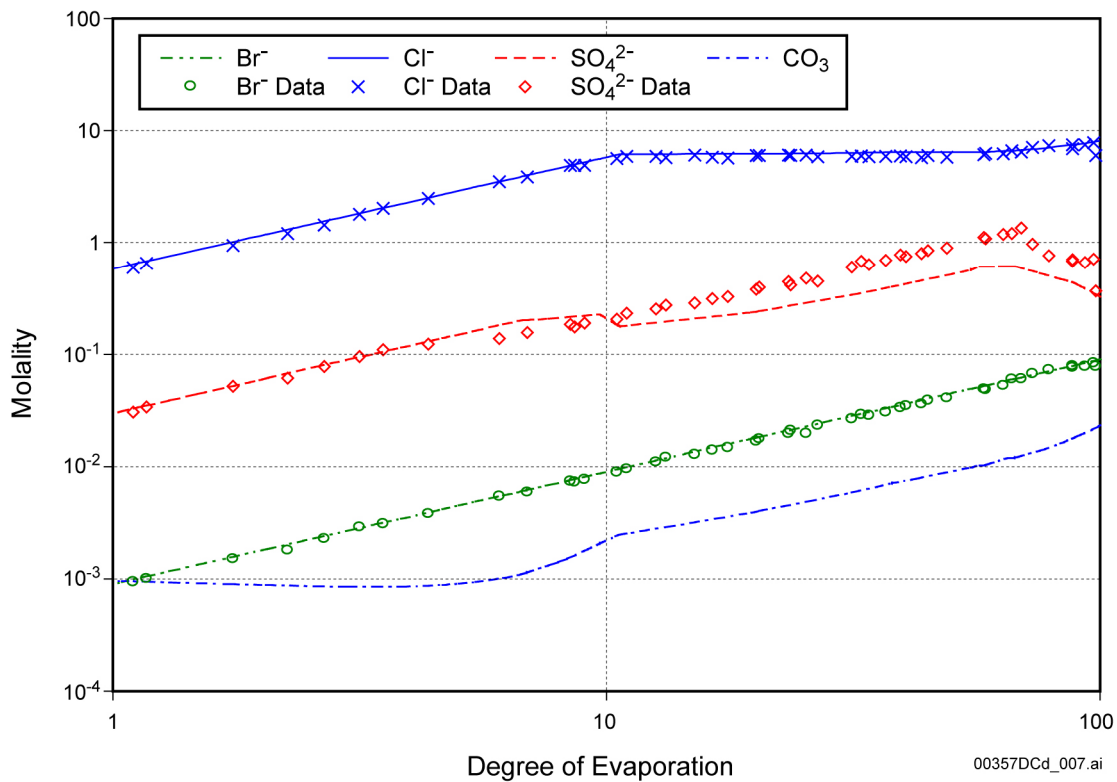
Figure K-10 shows that measured K⁺ concentrations begin to decrease sharply after concentrations reach approximately 80 times that of seawater. McCaffrey et al. (1987, p. 935) did not determine the potassium-bearing phases precipitating at this degree of evaporation.

Figure K-12 shows good agreement between measurements and predictions for pH and ionic strength. The largest difference observed for pH is approximately 0.76 pH units. For ionic strength, the largest difference is approximately 15 percent, except for the sample at the highest degree of evaporation, which is suspect because it is an outlier. This point does not agree with the other measurements made by McCaffrey et al. (1987) or measurements made by others and plotted by McCaffrey et al. (1987). The predicted activity of water is also plotted in this figure to show how it changes as a function of the degree of evaporation.



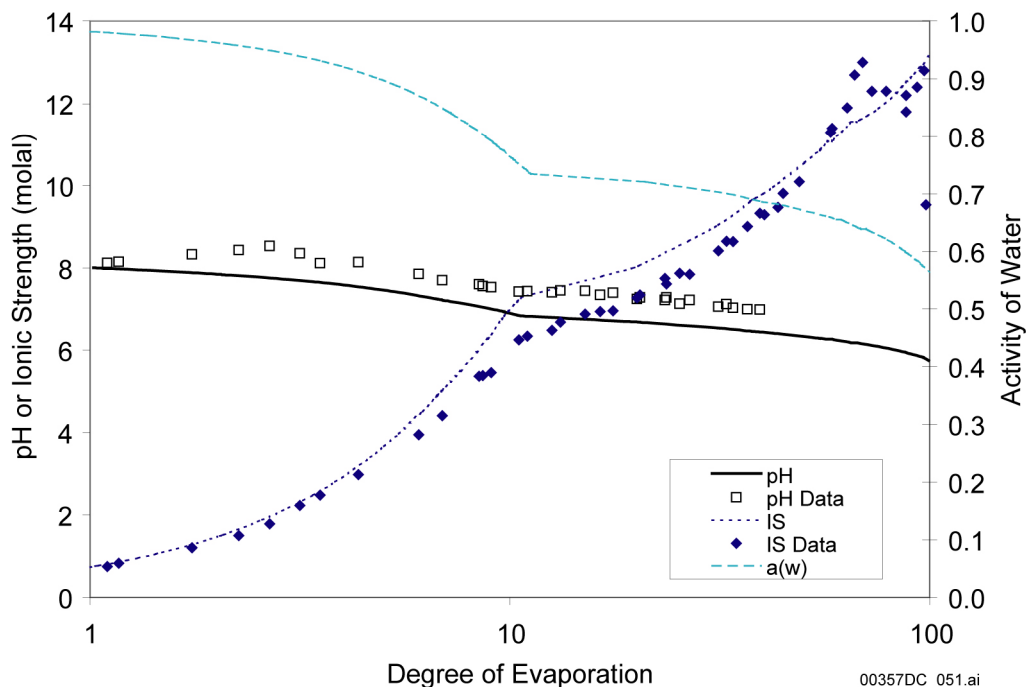
Source: DTN MO0307MWDSEAEV.000.

Figure K-10. Predicted versus Measured Ca²⁺, K⁺, Mg²⁺, and Na⁺ Concentrations from Evaporation of Inagua Seawater



Source: DTN MO0307MWDSEAEV.000.

Figure K-11 Predicted versus Measured Br⁻, Cl⁻, and SO₄²⁻ Concentrations from Evaporation of Inagua Seawater



Source: BSC 2003b, Figure 27.

Figure K-12. Predicted versus Measured pH and Ionic Strength from Evaporation of Inagua Seawater

K.4.2.5 Uncertainty in Evaporation Tests

The error in initial water compositions estimated by Rosenberg et al. (1999a, 1999b) is presented in Table K-8. This error provides an estimate of the analytical error for each of the analytes and is assumed to be representative throughout the tests. This error is also assumed to be representative for the 100× J-13 water evaporation tests, as these tests were performed similarly at the same location. Additional error is introduced in dilution of the concentrated samples prior to analysis; however, this error is small. Studies of measurement error using similar or identical techniques (ion chromatography for anions, inductively coupled plasma atomic emission spectrometry for cations) have been performed by the EPA (1998, pp. 9,056-12, 6,010B-23) and the American Public Health Association (APHA 1998, pp. 3-41 to 3-42). In these studies, samples with known concentrations of analytes of interest were sent to a number of laboratories, and results were used to quantify method uncertainty. For anions, the results were reported for the four types of waters; reagent water, drinking water, surface water, and wastewater. Table K-8 presents the mean recovery error (absolute value of the mean recovery in percent minus 100) for the drinking water and wastewater. These waters were assumed to compare most reasonably with the waters analyzed in the evaporation experiments. For cations, the American Public Health Association (APHA 1998) present precision and bias data for total and recoverable digestion. The recoverable digestion data are presented in Table K-8 because they are more applicable to the work of Rosenberg et al. (1999a, 1999b) and *Environment on the Surfaces of the Drip Shield and Waste Package Outer Barrier* (CRWMS M&O 2000b). Uncertainties in column 4 of Table K-8 are estimated by comparing uncertainty in the initial measurements with the uncertainties in the EPA studies. The estimated uncertainties compare favorably to the

uncertainties allowed in the in-drift precipitates and salts model. Error in the concentration factor assessed using the analytical chemistry information is discussed above.

McCaffrey et al. (1987) present a discussion and quantification of their analytical error. Analytical errors for Cl^- , Br^- , SO_4^{2-} , Mg^{2+} , Ca^{2+} , Na^+ , K^+ , and Li^+ were less than 2 percent. Error in charge balance is less than 3 percent. McCaffrey et al. (1987) do not present a discussion of error associated with the measurement of temperature, density, pH, and degree of evaporation. Temperature was measured to 0.1°C, pH to 0.01 pH units, and density to 0.001 mg/cm³ or calculated using the magnesium or lithium concentration. Errors in measured temperature and density are expected to be small (less than 0.5°C, less than 0.005 mg/cm³), with errors in the calculated density corresponding to the error in magnesium concentration and regression error. From the data presented in McCaffrey et al. (1987), correlation coefficients for linear fits through the density-magnesium data are greater than 0.99, resulting in a calculated density error of about 2.2 percent. The pH measurements may be affected by the ionic composition and strength of the brines and the high concentration of sodium. The differences in junction potentials from low ionic strength calibration buffers and the brines measured by McCaffrey et al. (1987) could result in estimated pH errors of 0.5 pH units. High sodium concentration is known to decrease apparent pH readings with the severity depending on the type of glass used in the electrode (Harris 2003, p. 329). Based on these errors, the total pH uncertainty is expected to be in the range of 1 pH unit.

The in-drift precipitates and salts model output parameters that will be directly used in the TSPA for the license application are pH, ionic strength, concentrations of Cl^- and NO_3^- , the $\text{Cl}^-/\text{NO}_3^-$ ratio, and deliquescence relative humidity (RH_d) (BSC 2003c, Section 6.13). These outputs are important for predicting corrosion, colloid stability, and radionuclide mobility. Thus, these parameters are the focus of the model uncertainties (see Appendix D for specific discussion). Table K-9 compares the maximum differences between predictions and measurements for the required outputs. For parameters not strongly affected by the uncertainty in concentration factor in Rosenberg et al. (1999a; 1999b), the differences are within the expected uncertainty range. For parameters affected by the uncertainty in concentration factor, consideration of that uncertainty helps to explain the magnitude of the differences.

The estimated model uncertainties associated with concentrations of Cl^- and NO_3^- and the $\text{Cl}^-/\text{NO}_3^-$ ratio outputs of the in-drift precipitates and salts model are based on professional judgment and are reasonable compared to the differences observed between experimental measurements and model predictions. Although much of the differences observed between experimental measurements and model predictions may be attributed to experimental uncertainty instead of model uncertainty, the estimated uncertainty of ± 30 percent for these parameters is small compared to the uncertainty related to bin discretization (this is discussed further in Appendix D).

Table K-8. Uncertainty Evaluation for Rosenberg et al. (1999a and 1999b) and McCaffrey et al. (1987) Evaporation Data

Analyte	Initial Uncertainty in Water Composition (%) (Rosenberg et al. 1999a, 1999b)	Typical Technique Uncertainty (Mean Recovery Error ^a , Relative Standard Deviation, %)	Estimated Uncertainty for Rosenberg et al. (1999a and 1999b) data (%)	Uncertainty for Seawater Evaporation (%) (McCaffrey et al. 1987)	IDPS Model Uncertainty Range (%)
Ca ²⁺	10.3, 3.1	(1, 7.4) ^b , (3.4, 9) ^d	11	1.3	Not established
Mg ²⁺	4.7, 1.7	(4, 6.5) ^b , (1.2, 5.6) ^d	5	1.3	Not established
K ⁺	3.8, 6.8	(5, 6.6) ^b , (6.5, 5) ^d	7	1.3	Not established
Na ⁺	1.8, 3.7	(5, 4.2) ^b , (5.3, 14.7) ^d	5	1.3	Not established
Cl ⁻	4.2, 1.7	(2-17.3, 2.9-5.9) ^c	5	1.3	30
F ⁻	4.3, 4.2	(8-13, 0.8-1.1) ^c	5	Not measured	Not established
NO ₃ ⁻	1.2, 2.7	(1-6, 1.1-1.5) ^c	3	Not measured	30
SO ₄ ²⁻	2.7, 2.3	(4-35, 1.5-3.7) ^c	4	1.3	Not established
SiO ₂	8.6, 9.2	-	10	Not measured	Not established
CO ₂	1.9, 21.2	Up to 0.2 ppm, Typically 1% of Full Scale Range ^f	22	Not measured	Not established
pH	0.25, 0.12 pH units	0.02 pH units ^e	0.25 pH units	1 pH unit	1 pH unit
Concentration factor	10	16 – 33 ^g	16 - 33	Not established	Not established
Ionic strength	Calculated	Calculated	30 ^h	Not established	30
Relative humidity	nm	1.5-5 ⁱ	5	Not established	5

NOTE: ^a Absolute value of the mean recovery (%) –100.

^b EPA 1998, Inductively coupled plasma-atomic emission spectrometry, p. 6,010B-23.

^c EPA 1998, Determination of inorganic anions by ion chromatography, p. 9,056-12.

^d APHA 1998, Method 3120, Metals by plasma emission spectroscopy, pp. 3-37 to 3-43.

^e Liptak 1994, p. 312.

^f Liptak 1994, p. 76.

^g BSC 2003b, p. 85.

^h Calculated as the square root of the sum of the squares of the uncertainties for the analytes listed.

ⁱ A variety of devices measure relative humidity with this accuracy (ASHRAE 2001).

IDPS = in-drift precipitates and salts.

Table K-9. Maximum Differences between Predictions and Measurements for pH, Ionic Strength, Cl⁻, NO₃⁻, and the Cl⁻/NO₃⁻ Ratio

Evaporation Simulation	pH (pH units)	Ionic Strength (RPD ^a)	Cl ⁻ (RPD)	NO ₃ ⁻ (RPD)	Cl ⁻ /NO ₃ ⁻ Ratio (RPD)
J-13 Evaporation Experiment	0.78	47% ^b	48% ^b	38% ^b	16%
100x J-13 Evaporation Experiment	nm ^c	ne ^d	5%	7%	-3%
Topopah Spring Tuff Pore Water Evaporation Experiment	0.46	67% ^b	66% ^b	nm ^c	nm ^c
Seawater Evaporation	0.76	15% ^e	10% ^e	nm ^c	nm ^c

DTN: MO0308SPAUCIMV.000.

NOTE: ^a RPD (relative percent difference) = 100% * ([predicted concentration] - [measured concentration]) / [measured concentration]

^b Most of the difference is likely due to overestimation in the concentration factor reported in the data source.

^c nm = not measured

^d ne = not estimated, pH needed for estimate

^e This value ignores the sample with the highest degree of evaporation because it is an outlier. It does not agree with other measurements by McCaffrey et al. (1987) or those of other researchers (also presented by McCaffrey et al. (1987)).

K.5 REFERENCES

K.5.1 Documents Cited

APHA (American Public Health Association) 1998. *Standard Methods for the Examination of Water and Wastewater*. 20th Edition. Franson, M.A.H., ed. Washington, D.C.: American Public Health Association. TIC: 242959.

ASHRAE (American Society of Heating, Refrigerating & Air-Conditioning Engineers) 2001. *2001 ASHRAE Handbook, Fundamentals*. Inch-Pound Edition. Atlanta, Georgia: American Society of Heating, Refrigerating and Air-Conditioning Engineers. TIC: 249910.

BSC (Bechtel SAIC Company) 2001. *FY 01 Supplemental Science and Performance Analyses, Volume 1: Scientific Bases and Analyses*. TDR-MGR-MD-000007 REV 00 ICN 01.

Las Vegas, Nevada: Bechtel SAIC Company. ACC: MOL.20010801.0404; MOL.20010712.0062; MOL.20010815.0001.

BSC 2002. *Thermal Testing Measurements Report*. ANL-NBS-HS-000041 REV 00.

Las Vegas, Nevada: Bechtel SAIC Company. ACC: MOL.20021004.0314.

BSC 2003a. *Drift-Scale Coupled Processes (DST and THC Seepage) Models*. MDL-NBS-HS-000001 REV 02. Las Vegas, Nevada: Bechtel SAIC Company. ACC: DOC.20030804.0004.

BSC 2003b. *In-Drift Precipitates/Salts Model*. ANL-EBS-MD-000045 REV 01. Las Vegas, Nevada: Bechtel SAIC Company. ACC: DOC.20031028.0003.

BSC 2003c. *Engineered Barrier System: Physical and Chemical Environment Model*. ANL-EBS-MD-000033 REV 02C. Las Vegas, Nevada: Bechtel SAIC Company. ACC: MOL.20031029.0034.

CRWMS M&O (Civilian Radioactive Waste Management System Management and Operating Contractor) 2000a. *Drift-Scale Coupled Processes (DST and THC Seepage) Models*. MDL-NBS-HS-000001 REV 00. Las Vegas, Nevada: CRWMS M&O. ACC: MOL.19990721.0523.

CRWMS M&O 2000b. *Environment on the Surfaces of the Drip Shield and Waste Package Outer Barrier*. ANL-EBS-MD-000001 REV 00. Las Vegas, Nevada: CRWMS M&O. ACC: MOL.20000328.0590.

CRWMS M&O 2001. *In-Drift Precipitates/Salts Analysis*. ANL-EBS-MD-000045 REV 00 ICN 02. Las Vegas, Nevada: CRWMS M&O. ACC: MOL.20010220.0008.

EPA (U.S. Environmental Protection Agency) 1998. *Test Methods for Evaluating Solid Waste, Physical/Chemical Methods*. EPA SW-846. Third Edition, Revision 5. Washington, D.C.: U.S. Environmental Protection Agency. TIC: On Order.

Harris, D.C. 2003. *Quantitative Chemical Analysis*. 6th edition. New York, New York: W.H. Freeman and Company. TIC: 255155.

Horita, J. and Wesolowski, D.J. 1994. "Liquid-Vapor Fractionation of Oxygen and Hydrogen Isotopes of Water from the Freezing to the Critical Temperature." *Geochimica et Cosmochimica Acta*, 58, (16), 3425-3437. New York, New York: Elsevier. TIC: 240153.

Liptak, B.G. 1994. *Analytical Instrumentation*. Radnor, Pennsylvania: Chilton Book Company. TIC: On Order.

McCaffrey, M.A.; Lazar, B.; and Holland, H.D. 1987. "The Evaporation Path of Seawater and the Coprecipitation of Br^- and K^+ with Halite." *Journal of Sedimentary Petrology*, 57, (5), 928-937. Tulsa, Oklahoma: Society of Economic Paleontologists and Mineralogists. TIC: 254627.

NRC (U.S. Nuclear Regulatory Commission) 2002. *Integrated Issue Resolution Status Report*. NUREG-1762. Washington, D.C.: U.S. Nuclear Regulatory Commission, Office of Nuclear Material Safety and Safeguards. TIC: 253064.

Reamer, C.W. 2001. U.S. Nuclear Regulatory Commission/U.S. Department of Energy Technical Exchange and Management Meeting on Evolution of the Near-Field Environment (January 9–12, 2001). Letter from C.W. Reamer (NRC) to S. Brocoum (DOE/YMSCO), January 26, 2001, with enclosure. ACC: MOL.20010810.0033.

Reamer, C.W. and Gil, A.V. 2001. Summary Highlights of NRC/DOE Technical Exchange and Management Meeting on Range of Thermal Operating Temperatures, September 18-19, 2001. Washington, D.C.: U.S. Nuclear Regulatory Commission. ACC: MOL.20020107.0162.

Rosenberg, N.D.; Knauss, K.G.; and Dibley, M.J. 1999a. *Evaporation of J13 Water: Laboratory Experiments and Geochemical Modeling*. UCRL-ID-134852. Livermore, California: Lawrence Livermore National Laboratory. TIC: 246322.

Rosenberg, N.D.; Knauss, K.G.; and Dibley, M.J. 1999b. *Evaporation of Topopah Spring Tuff Pore Water*. UCRL-ID-135765. Livermore, California: Lawrence Livermore National Laboratory. TIC: 246231.

Wang, J.S. 2003. "Scientific Notebooks Referenced in Model Report N0120/U0110, Drift-Scale Coupled Processes (DST and THC Seepage) Models MDL-NBS-HS-000001 REV 02." Interoffice correspondence from J.S. Wang (BSC) to File, June 6, 2003, with attachments. ACC: MOL.20030611.0079.

Williams, N.H. 2003. "Contract No. DE-AC28-01RW1210 – Transmittal of White Paper, Effects of Neoprene on Water in the Drift Scale Test." Letter from N.H. Williams (BSC) to J.D. Ziegler (DOE/ORD), February 4, 2003, 0129035843, with enclosure. ACC: MOL.20030206.0211.

YMP (Yucca Mountain Site Characterization Project) 2002. *Effects of Introduced Materials in the Drift Scale Test*. North Las Vegas, Nevada: Yucca Mountain Site Characterization Office. ACC: MOL.20020304.0044.

K.5.2 Codes, Standards, and Procedures

TIP-AC-03, Rev. 0. *Determination of Inorganic Anions by Ion Chromatography (EPA Method 300.00)*. Livermore, California: Lawrence Livermore National Laboratory. ACC: MOL.20010315.0345.

TIP-NF-33, Rev. 0. *Collection and Field Analysis of Water Samples from Boreholes in the Exploratory Studies Facility*. Livermore, California: Lawrence Livermore National Laboratory. ACC: MOL.20010110.0463.

YMP-LBNL-TIP/TT-7.0, Rev. 0, Mod. 0. *Extraction and Analysis of the Stable Isotope Components of CO₂ in Gas Samples*. Berkeley, California: Lawrence Berkeley National Laboratory. ACC: MOL.19990205.0145.

YMP-LBNL-TIP/TT-9.0, Rev. 0, Mod. 0. *Hydrogen Isotope Analyses of Waters*. Berkeley, California: Lawrence Berkeley National Laboratory. ACC: MOL.19990318.0083.

YMP-LBNL-TIP/TT-10.0, Rev. 0, Mod. 0. *Analysis of the Oxygen Isotopic Composition of Water Samples using the ISOPREP 18*. Berkeley, California: Lawrence Berkeley National Laboratory. ACC: MOL.19990224.0638.

K.5.3 Data, Listed by Data Tracking Number

LB000121123142.003. Isotope Data for CO₂ Gas Samples Collected from the Hydrology Holes of the ESF Drift Scale Test for the Period August 9, 1999 through November 30, 1999. Submittal date: 01/21/2000.

LB000718123142.003. Isotope Data for CO₂ Gas Samples Collected from the Hydrology Holes of the ESF Drift Scale Test for the Period April 18, 2000 through April 19, 2000. Submittal date: 07/18/2000.

LB0011CO₂DST08.001. Isotope Data for CO₂ from Gas Samples Collected from Hydrology Holes in Drift-Scale Test. Submittal date: 12/09/2000.

LB0102CO₂DST98.001. Concentration Data for CO₂ from Gas Samples Collected from Hydrology Holes in Drift-Scale Test. Submittal date: 02/28/2001.

LB0108CO₂DST05.001. Concentration and Isotope Data for CO₂ and H₂O from Gas Samples Collected from Hydrology Holes in Drift-Scale Test - May and August 1999, April 2000, January and April 2001. Submittal date: 08/27/2001.

LB0203CO₂DSTEH.001. Concentration/Isotope Data for CO₂/H₂O from Gas Samples Collected from Hydrology Holes in DST up to End of Heating. Submittal date: 03/13/2002.

LB0206C¹⁴DSTEH.001. Carbon 14 Isotope Data from CO₂ Gas Samples Collected from DST. Submittal date: 06/17/2002.

LB0208ISODSTHP.001. Isotope Data and CO₂ Analysis for the Heating Phase of the DST. Submittal date: 08/09/2002.

LB0307DSTTHCR2.001. Drift-Scale Coupled Processes (DST Seepage) Model: Simulations. Submittal date: 07/24/2003.

LB980420123142.005. Isotope Data for CO₂ from Gas Samples Collected from Drift Scale Test February 1998 in First Quarter TDIF Submission for the Drift Scale Test. Submittal date: 11/12/1998.

LB980715123142.003. Isotope Data for CO₂ from Gas Samples Collected from Drift Scale Test June 4, 1998 in 2nd Quarter TDIF Submission of the Drift Scale Test Heating Phase. Submittal date: 07/15/1998.

LB981016123142.004. Isotope Data for CO₂ from Gas and Water Samples Taken from June 1998 to September 1998 for the Third Quarter TDIF Submission for the Drift Scale Test. Submittal date: 10/16/1998.

LB990630123142.003. Fourth, Fifth, and Sixth Quarters TDIF Submission for the Drift Scale Test, September 1998 to May 1999. Submittal date: 06/30/1999.

LL000202905924.117. Environment on the Surfaces of the Drip Shield and Waste Package Outer Barrier. Submittal date: 02/18/2000.

LL001100931031.008. Aqueous Chemistry of Water Sampled from Boreholes of the Drift Scale Test (DST). Submittal date: 11/10/2000.

LL001200231031.009. Aqueous Chemistry of Water Sampled from Boreholes of the Drift Scale Test (DST). Submittal date: 12/04/2000.

LL020302223142.015. Aqueous Geochemistry of DST Samples Collected from HYD Boreholes. Submittal date: 03/07/2002.

LL020405123142.019. Aqueous Geochemistry of Condensed Fluids Collected During Studies of Introduced Materials. Submittal date: 05/22/2002.

LL990702804244.100. Borehole and Pore Water Data. Submittal date: 07/13/1999.

LL991008004241.041. Evaporation of Topopah Spring Tuff Pore Water. Submittal date: 10/21/1999.

LL991008104241.042. Evaporation of J13 Water: Laboratory Experiments and Geochemical Modeling. Submittal date: 10/21/1999.

MO0005PORWATER.000. Perm-Sample Pore Water Data. Submittal date: 05/04/2000.

MO0101SEPFDDST.000. Field Measured Data of Water Samples from the Drift Scale Test. Submittal date: 01/03/2001.

MO0207AL5WATER.001. Water Sampling in Alcove 5 (Results from 2/4/1997 through 4/20/1999). Submittal date: 07/11/2002.

MO0303MWDJ13GD.000. In-Drift Precipitates/Salts Model Simulation of Synthetic J-13 Water Evaporation Experiments Documented in ANL-EBS-MD-000001. Submittal date: 03/04/2003.

MO0303MWDJ13RB.000. In-Drift Precipitates/Salts Model Simulation of Synthetic J-13 Water Evaporation Experiments Documented in Rosenberg et al. 1999. Submittal date: 03/04/2003.

MO0303MWDTSWRB.000. In-Drift Precipitates/Salts Model Simulation of Synthetic Topopah Spring Tuff Pore Water Evaporation Experiments Documented in Rosenberg et al. 1999. Submittal date: 03/04/2003.

MO0307MWDSEAEV.000. Seawater Evaporation Predictions Using the IDPS Model. Submittal date: 7/31/2003.

MO0308SPAUCIMV.000. Uncertainty Comparisons in IDPS Model Validation Cases. Submittal date: 08/08/2003.

SN0203F3903102.001. Drift Scale Test Water Sampling (with Results from 4/17/2001 through 1/14/2002). Submittal date: 03/29/2002.

INTENTIONALLY LEFT BLANK

APPENDIX L
MULTISCALE THERMAL-HYDROLOGIC MODEL
(RESPONSE TO TEF 2.04)

Note Regarding the Status of Supporting Technical Information

This document was prepared using the most current information available at the time of its development. This Technical Basis Document and its appendices providing Key Technical Issue Agreement responses that were prepared using preliminary or draft information reflect the status of the Yucca Mountain Project's scientific and design bases at the time of submittal. In some cases this involved the use of draft Analysis and Model Reports (AMRs) and other draft references whose contents may change with time. Information that evolves through subsequent revisions of the AMRs and other references will be reflected in the License Application (LA) as the approved analyses of record at the time of LA submittal. Consequently, the Project will not routinely update either this Technical Basis Document or its Key Technical Issue Agreement appendices to reflect changes in the supporting references prior to submittal of the LA.

APPENDIX L

MULTISCALE THERMAL-HYDROLOGIC MODEL (RESPONSE TO TEF 2.04)

This appendix provides a response for Key Technical Issue (KTI) agreement Thermal Effects on Flow (TEF) 2.04. This agreement relates to provision of the multiscale analysis and model report.

L.1 KEY TECHNICAL ISSUE AGREEMENT

L.1.1 TEF 2.04

Agreement TEF 2.04 was reached during the U.S. Nuclear Regulatory Commission (NRC)/U.S. Department of Energy (DOE) Technical Exchange and Management Meeting on Thermal Effects on Flow held January 8 to 9, 2001, in Pleasanton, California. TEF subissues 1 and 2 were discussed at the meeting (Reamer 2001).

There has been no submittal related to this KTI Agreement to the NRC since the original meeting. Agreement TEF 2.04 simply requests the provision of the multiscale analysis and model report. From the original meeting and ensuing discussions from the presentation materials, the specific interest in this agreement is believed to center on how both potential drift-scale and waste-package-to-waste-package cold trap effects were to be addressed in revisions to the multiscale model. The current model addresses waste-package-to-waste-package variability but does not include cold trap effects. The technical basis for the treatment of cold trap effects is now currently planned to be addressed primarily through the *In-Drift Natural Convection and Condensation Model Report* (BSC 2003a). Toward this end, the response to TEF 2.04 is structured to provide an overview of the current multiscale model. TEF 2.05 will address cold trap effects in their entirety.

The wording of the agreement is as follows:

TEF 2.04

Provide the Multi-Scale Thermohydrologic Model AMR, Rev. 01. The DOE will provide the Multi-Scale Thermohydrologic Model AMR (ANL-EBS-MD-00049) Rev 01 to the NRC. Expected availability is FY 02.

L.1.2 Related Key Technical Issue Agreements

Agreement TEF 2.05 relates to TEF 2.04. It pertains specifically to the cold trap effect and how it is modeled in the multiscale model or the technical basis for excluding these effects from the model. Agreement TEF 2.05 is currently scheduled to be addressed in June 2004.

L.2 RELEVANCE TO REPOSITORY PERFORMANCE

Temperature and relative humidity are fundamental parameters of importance to repository performance. Performance of the waste package and drip shield are strong functions of these

parameters affecting both the degradation of these primary engineering barriers and the quantity and chemistry of the water contacting these engineering barriers and waste forms.

L.3 RESPONSE

The purpose of the multiscale thermal-hydrologic model is to predict the evolution of thermal-hydrologic conditions in the repository emplacement drifts, also called the engineered barrier system, and in the adjoining host rock for the repository at Yucca Mountain. *Multiscale Thermohydrologic Model Report* (BSC 2003b) documents the model.

The multiscale thermal-hydrologic model calculates the following thermal-hydrologic variables: temperature, relative humidity, liquid-phase saturation, evaporation rate, and liquid- and gas-phase fluxes (Table L-1). These thermal-hydrologic variables are required to support the total system performance assessment. The thermal-hydrologic variables are determined as a function of position along each of the emplacement drifts in the repository and as a function of waste package type. These variables are determined at various generic locations within the emplacement drifts, including the waste package and drip shield surfaces and in the invert; they are also determined at various generic locations in the adjoining host rock; these variables are determined every 20 m for each emplacement drift in the repository. Each emplacement drift is represented with its precise coordinate location. The multiscale thermal-hydrologic model also accounts for the manner in which the emplacement drifts are to be ventilated during the preclosure period, including how heat-removal efficiency from drift ventilation varies as a function of time and distance along each of the emplacement drifts.

Table L-1. Thermal-Hydrologic Variables Predicted with the Multiscale Thermal-Hydrologic Model

Thermal-Hydrologic Variable	Drift-Scale Location
Temperature	Near-field environment host rock (5 m above crown of drift)
	Near-field environment host rock (mid-pillar at repository horizon)
	Maximum lateral extent of boiling
	Drift wall (perimeter average)
	Drip shield (perimeter average)
	Drip shield (upper surface)
	Waste package (surface average)
	Invert (average)
Relative humidity	Drift wall (perimeter average)
	Drip shield (perimeter average)
	Waste package
	Invert (average)
Liquid-phase saturation (matrix)	Drift wall (perimeter average)
	Drip shield (perimeter average)
	Invert (average)
Liquid-phase flux	Near-field environment host rock (5 m above crown of drift)
	Near-field environment host rock (3 m above crown of drift)
	Drift wall (upper surface)
	Drift wall (lower surface below invert)
	Drip shield (crown)
	Drip shield (upper surface average)
	Drip shield (lower side at the base)
	Invert (average)
Gas-phase air-mass fraction	Drip shield (perimeter average)
Gas-phase pressure	Drip shield (perimeter average)
Capillary pressure	Drip shield (perimeter average)
	Invert (average)
	Drift wall (crown, in matrix)
	Drift wall (crown, in fractures)
Gas-phase (water vapor) flux	Drift wall (perimeter average)
Gas-phase (air) flux	Drift wall (perimeter average)
Evaporation rate	Drip shield (crown)
	Drip shield (perimeter total)
	Drift wall (upper surface)
	Drift wall (lower surface below invert)
	Invert (total)

The multiscale thermal-hydrologic model accounts for three-dimensional drift-scale and mountain-scale heat flow and captures the influence of the key engineering-design variables and natural-system factors affecting thermal-hydrologic conditions in the emplacement drifts and adjoining host rock:

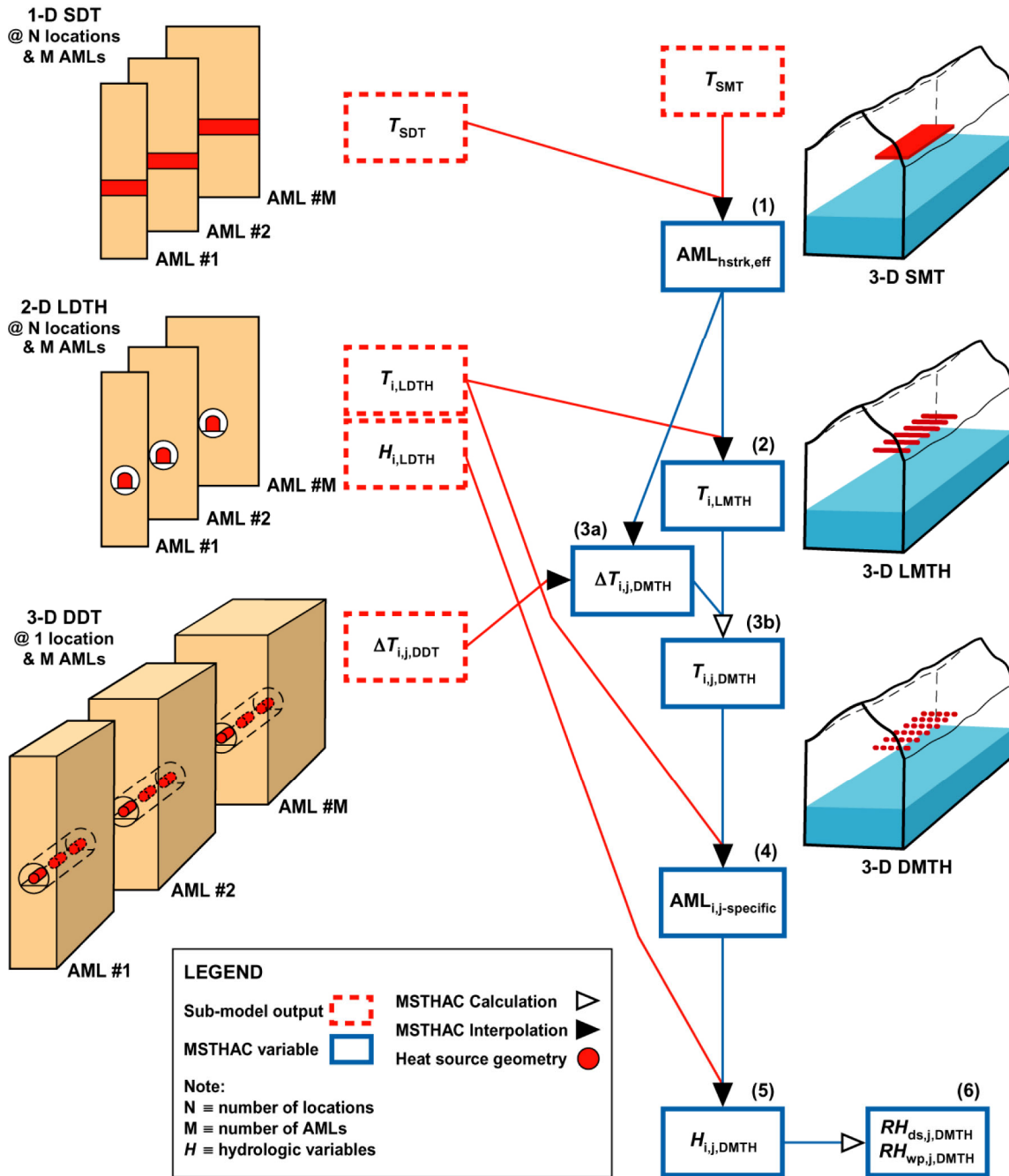
- Repository-scale variability of percolation flux
- Temporal variability of percolation flux (as influenced by climate change)
- Uncertainty in percolation flux (as addressed by the mean, high, and low flux scenarios)
- Uncertainty in percolation flux (resulting from flow focusing and flow diversion)
- Repository-scale variability of thermal conductivity (notably in host rock)
- Uncertainty in host-rock thermal conductivity
- Repository-scale variability of bulk rock density and specific heat
- Repository-scale variability of hydrologic properties of the rock matrix
- Repository-scale variability of hydrologic properties of fractures
- Repository-scale variability in overburden thickness
- Overall areal heat-generation density of the waste inventory, which is quantified by the areal mass loading (AML, expressed in MTU/acre)
- Line-averaged thermal load along emplacement drifts, which is quantified by the lineal power density (expressed in kW/m)
- Distance between emplacement drifts (also called drift spacing)
- Age of spent nuclear fuel at time of emplacement
- Location of the repository with respect to the stratigraphy
- Repository footprint shape, which influences the evolution of the edge-cooling effect that increases with proximity to the repository edges
- Dimensions of the in-drift design (waste packages, drip shield, and invert)
- Properties of the in-drift engineered barrier system components
- Waste package spacing along the drift (line-load versus point-load spacing)
- Waste package sequencing (particularly with respect to the heat output from the respective waste packages)
- Time- and distance-dependent heat-removal efficiency of preclosure drift ventilation
- Duration and heat-removal efficiency of drift ventilation.

The multiscale thermal-hydrologic model consists of four submodels, all of which are run using the NUFT computer code (Nitao 1998). The NUFT simulation code is a flexible multipurpose computer code for modeling fluid flow and transport in porous media under both nonisothermal and isothermal conditions. It solves continuum equations for the conservation of mass and energy. An integrated finite-difference spatial discretization is used to solve the balance equations. The resulting nonlinear equations are solved each time step by the Newton-Raphson method. Options for solving the linear equations are direct-banded solution and preconditioned conjugate gradient methods with various preconditioning schemes. The code can solve one-, two-, and three-dimensional problems.

The multiscale thermal-hydrologic model couples the smeared-heat-source drift-scale thermal-conduction, line-average-heat-source drift-scale thermal-hydrologic, discrete-heat-source drift-scale thermal-conduction, and smeared-heat-source mountain-scale thermal-conduction submodels such that the flow of water, water vapor, air, and heat through partially saturated fractured porous rock is adequately addressed. A visual depiction of the multiscale thermal-hydrologic model is presented in Figure L-1, with additional descriptions provided in Tables L-2 and L-3.

The fundamental concept in the multiscale thermal-hydrologic model is that the results from the two-dimensional line-averaged-heat-source drift-scale thermal-hydrologic submodels can be modified to account for the influence of three-dimensional mountain-scale heat flow as well as for local deviations arising from waste-package-to-waste-package variability in heat output. Output from the smeared-heat-source mountain-scale thermal-conduction submodel, together with the line-averaged-heat-source drift-scale thermal-hydrologic–smeared-heat-source drift-scale thermal-conduction submodel pairs, is integrated to create the line-averaged-heat-source mountain-scale thermal-hydrologic model (Figure L-1). The discrete-heat-source drift-scale thermal-conduction submodel is then used to further modify the line-averaged-heat-source mountain-scale thermal-hydrologic model to account for waste-package-specific deviations from average waste package behavior.

The multiscale model calculates the in-drift thermal-hydrologic environment—primarily, the temperature of the in-drift components and the relative humidity of the in-drift air. The impact of condensation from cold trap effects on cooler waste packages (the local effect) as well as at the repository edges (the drift-scale effect) on the predicted temperature and relative humidity is smaller than that caused by parametric uncertainty. Therefore, the cold trap effect does not play a significant role in the evolution of temperature and relative humidity within the emplacement drifts and in the adjoining host rock and has not been incorporated directly in the multiscale model. The technical basis for the treatment of cold trap effects, however, is being addressed primarily through the *In-Drift Natural Convection and Condensation Model Report* (BSC 2003a), which will support addressing the cold trap effect in response to agreement TEF 2.05.



00357DCd_010.ai

NOTE: Smeared-heat-source drift-scale thermal-conduction, line-average-heat-source drift-scale thermal-hydrologic, and discrete-heat-source drift-scale thermal-conduction submodels are run at different AMLs (left side); smeared-heat-source mountain-scale thermal-conduction, LMTH and DMTH are the series of three-dimensional mountain-scale models of increasing complexity (right side). The six stages illustrate the process of constructing intermediate variables ($AML_{hstrk,eff}$, $\Delta T_{i,j,DMTH}$, $T_{i,LMTH}$ and $AML_{i,j-specific}$) and final multiscale thermal-hydrologic model variables ($T_{i,j,DMTH}$, $RH_{i,j,DMTH}$, and $H_{i,j,DMTH}$) from NUFT submodel output (T_{SDT} , T_{SMT} , $T_{i,LDTH}$, $H_{i,LDTH}$ and $\Delta T_{i,j,DDT}$). The model types are defined in Table L-2. The variables are defined in Table L-3.

Figure L-1. Six-Stage Flow Chart Diagram of the Multiscale Thermal-Hydrologic Model

Table L-2. The Model and Submodel Types Used in the Multiscale Thermal-Hydrologic Model

Model Type	Description
MSTHM	Multiscale Thermal-Hydrologic Model
SMT	Smearred-heat-source, Mountain-scale, Thermal-conduction: three-dimensional NUFT submodel
SDT	Smearred-heat-source, Drift-scale, Thermal-conduction: one-dimensional NUFT submodel
LDTH	Line-averaged-heat-source, Drift-scale, Thermal-hydrologic: two-dimensional NUFT submodel
DDT	Discrete-heat-source, Drift-scale, Thermal-conduction: a three-dimensional NUFT submodel
LMTH	Line-averaged-heat-source, Mountain-scale, Thermal-hydrologic: three-dimensional multiscale thermal-hydrologic model intermediate result
DMTH	Discrete-heat-source, Mountain-scale, Thermal-hydrologic: three-dimensional multiscale thermal-hydrologic model final result
D/LMTH	Discrete/Line-averaged-heat-source, Mountain-scale, Thermal-hydrologic: the nested monolithic three-dimensional NUFT model used in the multiscale thermal-hydrologic model validation

Table L-3. The Variables Used in the Multiscale Thermal-Hydrologic Model Methodology

Variable Name	Description	Stage (see Figure L-1)
T_{SDT}	Host-rock temperature output from the one-dimensional Smearred-heat-source drift-scale thermal-conduction submodel.	Stage 1 (NUFT output)
T_{SMT}	Host-rock temperature output from the three-dimensional mountain-scale Smearred-heat-source, Mountain-scale, Thermal-conduction submodel.	Stage 1 (NUFT output)
$\Delta T_{i,j,DDT}$	Temperature deviation of individual waste package from averaged drift-wall temperature for generic drift location i and waste package j .	Stage 3a (NUFT output)
$\Delta T_{i,j,DMTH}$	Temperature deviation of individual waste package from averaged drift-wall temperature for generic drift location i and waste package j , adjusting for three-dimensional mountain-scale heat loss.	Stages 3a, 3b
$T_{i,LDTH}$	Temperature output from two-dimensional Line-averaged-heat-source, Drift-scale, Thermal-hydrologic drift-scale submodel.	Stages 2, 4 (NUFT output)
$T_{i,LMTH}$	Temperature for generic location i adjusted for the three-dimensional mountain-scale heat loss.	Stages 2, 3b
$T_{i,j,DMTH}$	Temperature for generic drift location i and waste package j adjusted for the three-dimensional mountain-scale heat loss and for waste package variation.	Stages 3b, 4
$H_{i,LDTH}$	Set of hydrologic variables for generic drift location i . This set includes $RH_{i,LDTH}$ and $S_{i,LDTH}$.	Stage 5 (NUFT output)
$H_{i,j,DMTH}$	Set of hydrologic variables for generic drift location i and waste package j adjusted for three-dimensional mountain-scale heat loss and for waste package variation. This set includes $RH_{i,j,DMTH}$ and $S_{i,j,DMTH}$.	Stages 5, 6
$RH_{i,j,DMTH}$	Relative humidity of the generic drift location i and waste package j for the Discrete-heat-source, Mountain-scale, Thermal-hydrologic model.	Stage 5, 6

Table L-3. The Variables Used in the Multiscale Thermal-Hydrologic Model Methodology (Continued)

Variable Name	Description	Stage (see Figure L-1)
$S_{i,j,DMTH}$	Liquid-phase saturation of the generic drift location i and waste package j for the Discrete-heat-source, Mountain-scale, Thermal-hydrologic model.	Stage 5, 6
$T_{dw,cav}$ $RH_{dw,cav}$	Perimeter averages of surfaces adjoining the open cavity outside of the drip-shield only for the Discrete-heat-source, Mountain-scale, Thermal-hydrologic model.	Stage 6
$AML_{hstrk,eff}$	Time-varying areal mass loading that translates three-dimensional mountain-scale heat-loss from Smeared-heat-source, Mountain-scale, Thermal-conduction to other submodels.	Stages 1, 2, 3a
$AML_{i,j-specific}$	Time-varying areal mass loading that translates waste package variation of DMTH-modeled temperatures to $H_{i,j,DMTH}$ variables for generic drift location i and waste package j .	Stages 4, 5
P_{sat}	Saturated vapor pressure, function of temperature.	Stage 6

NOTE: Subscript i refers to a generic location in the drift; $i=dw$ refers to drift-wall, $i=ds$ refers to drip-shield, $i=in$ refers to invert, and $i=wp$ refers to waste package. Subscript j refers to the waste package, $j=HLW$ or $PWR1$ or $PWR2$ or BWR . The multiscale thermal-hydrologic model methodology is described in detail in BSC 2003b, Section 6.2.4.

The information in this report is responsive to agreement TEF 2.04 made between the DOE and NRC. The report contains the information that the DOE considers necessary for NRC review for closure of this agreement.

L.4 BASIS FOR THE RESPONSE

The multiscale modeling approach undertaken was motivated by the need for a modeling tool that simultaneously accounts for processes occurring at a scale of a few tens of centimeters around individual waste packages and emplacement drifts and also at the scale of the mountain. Currently, a single numerical model cannot do this because it requires too large a computational time to be a viable simulation tool for performance assessment and engineering design. Note that performance assessment and design analysis both require the ability to conduct a relatively large number of realizations.

Conceptually, the approach is simple. Thermal-hydrologic behavior is directly simulated for an “average” waste package using a two-dimensional drift-scale cross section for a variety of areal-heat-generation densities at numerous locations throughout the repository footprint. In these simulations the flow of liquid and gas (water vapor and air) through variably saturated fractured porous media is represented with a dual-permeability description of permeability. This model also accounts for two-phase behavior (i.e., evaporation, boiling, and condensation). Open drifts are modeled as porous media with very high permeability and porosity. The model represents thermal conduction and convection in rock and thermal conduction, limited convection, and radiation in the open cavities in the emplacement drifts.

These two-dimensional thermal-hydrologic model results are then modified with three-dimensional thermal model results to account for three-dimensional heat flow at the mountain scale and for three-dimensional heat flow at the drift scale, which account for waste-package-to-waste-package variability in heat output. Some waste packages will generate much less heat than other waste packages. The assumption is made that any mountain-scale movement

of water and water vapor along the drift axes or between drifts can be neglected (i.e., all fluid flow is confined to a two-dimensional vertical cross section orthogonal to the drift axis, with no fluid flow across the vertical midplane in the rock pillar between the drifts). The model does not include changes in rock properties due to coupled thermal-hydrologic-chemical-mechanical processes and the effect of dissolved solutes on the thermal-hydrologic properties of water, because the effects are negligible.

The multiscale modeling approach considers the influence of the following variables as a function of geographic location in the repository: local stratigraphy, overburden thickness (i.e., distance between the repository and ground surface, which varies by about 150 m across the repository), thermal boundary conditions, and infiltration flux. It also considers the influence of the proximity to the edge of the repository, which is important because a waste package close to the repository edge will cool more quickly than one at the repository center. The differences in temperature that arise as a result of proximity to the repository edges are assumed to be governed by thermal conduction in the rock. This assumption is equivalent to saying that convective heat transfer mechanisms (notably, buoyant gas-phase convection and the heat pipe effect) have a negligible influence on lateral mountain-scale heat flow at Yucca Mountain. This assumption tends to preserve temperature differences that arise as a result of differences in proximity to the repository edges, which preserves the “tails” of the distribution of boiling-period duration across the entire repository.

The multiscale thermal-hydrologic model represents the waste packages emplaced in the repository by four major types: commercial spent nuclear fuel from pressurized-water reactors (PWRs), commercial spent nuclear fuel from boiling water reactors), high-level radioactive waste, and DOE spent nuclear fuel. The relevant point here is that the heat-generation-rate-versus-time relationships for these four waste package types are different. It is assumed that waste packages will be sequenced in such a way as to minimize the heating variability along the drift (i.e., placing hot waste packages next to cold waste packages). The model effectively considers a narrow range of possible waste package sequencing that results in eight distinct local heating conditions for waste packages. For example, the model distinguishes between a BWR placed between a PWR and a high-level radioactive waste and a BWR placed between two PWRs. The differences in temperature between relatively hotter waste package locations and cooler waste package locations are assumed to be governed by thermal conduction in the host rock and emplacement drift and thermal radiation in the open cavities in the drift. This assumption is equivalent to saying that convective heat transfer mechanisms (notably, buoyant gas-phase convection in the drift) do not significantly contribute to the attenuation of temperature variations along the axis of the drift. This assumption tends to preserve temperature variability along the drifts.

The *Multiscale Thermohydrologic Model Report* (BSC 2003b) addresses the development, validation, use, limitations, and uncertainties of the model. These considerations include the adequacy of the system description and model integration; sufficiency of data for model justification; characterization and propagation of data and model uncertainty through the model abstraction; and support of model abstraction output through objective comparison.

Through the use of the multiscale model in generating output for use in total system performance assessment license application, it was identified that percolation flux and host-rock thermal

conductivity are the two most important natural-system parameters influencing peak temperatures and the time that the drift wall remains above the boiling point. It is found that the combined influence of percolation-flux uncertainty and host-rock thermal conductivity on peak temperatures is simply the sum of the individual contributions to peak-temperature uncertainty. It is also found that the combined influence of percolation-flux uncertainty and host-rock thermal conductivity on the duration of boiling at the drift wall is simply the sum of the individual contributions to drift-wall-boiling-duration uncertainty. Thus, the concept of superposition can be utilized relative to the uncertainty associated with these two parameters. This aspect is very useful relative to the engineered barrier system considerations in performance assessments.

Multiple approaches were taken in the validation of the multiscale model. Results from the multiscale thermal-hydrologic model are compared against those from a mountain-scale thermal-hydrologic model, developed by Lawrence Berkeley National Laboratory (Haukwa et al. 1998), which represents an alternative conceptual model (BSC 2003b, Section 8.2). Three-dimensional NUFT thermal-hydrologic-model simulations are compared with temperatures and liquid-phase saturations measured in the Large Block Test. The resulting good agreement between the simulated and measured temperatures in the Large Block Test demonstrates that the NUFT thermal-hydrologic model provides a valid representation of heat flow in partially saturated fractured porous rock. Three-dimensional NUFT thermal-hydrologic model simulations were also compared with temperatures and liquid-phase saturations measured in the Drift Scale Test, and the overall agreement between simulated and measured temperatures are reasonable. Additionally, the multiscale thermal-hydrologic model methodology was compared to another model, a nested monolithic mountain/drift-scale thermal-hydrologic model, for a test case of three 243-m long drifts, representative of a scaled-down repository (BSC 2003b, Section 8.2). This three-drift test case discretely represented 15 waste packages: 7 at the center of the central drift and 4 at either end of the central drift. The results showed almost identical predictions of the thermal-hydrologic conditions at the waste package locations at the center of the repository. At the edge of the repository, the multiscale thermal-hydrologic model and nested monolithic thermal-hydrologic model predict similar conditions, with differences between the two models being the largest for the last two waste packages at the edge.

L.5 REFERENCES

BSC (Bechtel SAIC Company) 2003a. *In-Drift Natural Convection and Condensation Model Report*. MDL-EBS-MD-000001 REV00A. Las Vegas, Nevada: Bechtel SAIC Company. ACC: MOL.20030912.0050.

BSC 2003b. *Multiscale Thermohydrologic Model Report*. ANL-EBS-MD-000049 REV 01C. Las Vegas, Nevada: Bechtel SAIC Company. ACC: MOL.20030910.0158.

Haukwa, C.; Wu, Y.S.; Hinds, J.J.; Zhang, W.; Ritcey, A.C.; Pan, L.H.; Simmons, A.M.; and Bodvarsson, G.S. 1998. *Results of Sensitivity Studies of Thermo-Hydrologic Behavior Conducted on Hydrologic Parameter Sets*. Milestone SP3CK5M4. Berkeley, California: Lawrence Berkeley National Laboratory. ACC: MOL.19980918.0001.

Nitao, J.J. 1998. *Reference Manual for the NUFT Flow and Transport Code, Version 2.0*. UCRL-MA-130651. Livermore, California: Lawrence Livermore National Laboratory. ACC: MOL.19980810.0391.

Reamer, C.W. 2001. "U.S. Nuclear Regulatory Commission/U.S. Department of Energy Technical Exchange and Management Meeting on Thermal Effects on Flow (January 8 through 9, 2001)." Letter from C.W. Reamer (NRC) to S. Brocoum (DOE/YMSCO), January 26, 2001, with enclosure. ACC: MOL.20010810.0046.

INTENTIONALLY LEFT BLANK